South Coast AQMD

2022 AIR QUALITY MANAGEMENT PLAN

Appendix V

Modeling and Attainment Demonstrations

2022 AQMP
APPENDIX V

MODELING AND ATTAINMENT DEMONSTRATIONS

ADOPTED DECEMBER 2, 2022

SOUTH COAST AIR QUALITY MANAGEMENT DISTRICT

GOVERNING BOARD

Chair: BEN J. BENOIT
Mayor, Wildomar
Cities of Riverside County

Vice Chair: VANESSA DELGADO
Senator (Ret.)
Senate Rules Committee Appointee

MEMBERS:

MICHAEL A. CACCIOTTI
Mayor, South Pasadena
Cities of Los Angeles County/Eastern Region

ANDREW DO
Supervisor, First District
County of Orange

GIDEON KRACOV
Governor's Appointee

SHEILA KUEHL
Supervisor, Third District
County of Los Angeles

LARRY MCCALLON
Mayor, Highland
Cities of San Bernardino County

VERONICA PADILLA-CAMPOS
Speaker of the Assembly Appointee

V. MANUEL PEREZ
Supervisor, Fourth District
County of Riverside

NITHYA RAMAN
Council Member, Fourth District
City of Los Angeles Representative

REX RICHARDSON
Vice Mayor, City of Long Beach
Cities of Los Angeles County/Western Region

CARLOS RODRIGUEZ
Mayor, Yorba Linda
Cities of Orange County

JANICE RUTHERFORD
Supervisor, Second District
County of San Bernardino

EXECUTIVE OFFICER:

WAYNE NASTRI

CONTRIBUTORS

South Coast Air Quality Management District
(South Coast AQMD)

Wayne Nastri
Executive Officer

Susan Nakamura
Chief Operating Officer

Sarah L. Rees, Ph.D.
Deputy Executive Officer
Planning, Rule Development, and Implementation

Ian MacMillan
Assistant Deputy Executive Officer
Planning, Rule Development, and Implementation

Sang-Mi Lee, Ph.D.
Planning and Rules Manager
Planning, Rule Development, and Implementation

Authors

Eric Praske, Ph.D. – Air Quality Specialist

Elham Baranizadeh, Ph.D. – Air Quality Specialist

Cui Ge, Ph.D. – Air Quality Specialist

Marc Carreras Sospedra, Ph.D. – Program Supervisor

Rui Zhang, Ph.D. – Air Quality Specialist

Xinqiu Zhang, Ph.D. – Senior Staff Specialist

Reviewer

Barbara Baird, J.D. – Chief Deputy Counsel

Production

Rosalee Mason – Administrative Assistant I

Alex Jimenez – Graphics Arts Illustrator II

South Coast AQMD Print Shop

Table of Contents

- **Chapter 4: Modeling Emissions, Boundary Conditions, and Initial Conditions**

- **Chapter 5: 8-hour Ozone Modeling and Attainment Demonstration**

- **Chapter 6: State Air Quality Standards**

CHAPTER 1

MODELING OVERVIEW

Introduction

Air quality modeling to demonstrate future attainment of air quality standards is an integral part of the planning process to achieve clean air. Modeling provides the means to relate emission reductions from pollution sources to the resulting air quality improvements. The attainment demonstrations provided in this AQMP reflect updated emissions estimates, new technical information, enhanced air quality modeling techniques, updated attainment demonstration methodology, and the control strategies provided in Chapter 4.

This AQMP aims to develop a control strategy and corresponding attainment demonstration that: 1) ensures that the 2015 8-hour ozone National Ambient Air Quality Standard (NAAQS) is met by the established deadline in the federal Clean Air Act (CAA) and 2) achieves an expeditious rate of progress towards attaining the air quality standard.

The South Coast Air Basin is classified as an "extreme" nonattainment area for the 2015 8-hour ozone NAAQS with an attainment year of 2037. The modeling base year is 2018 and was used to derive meteorological inputs; it also served as an anchor year to project future emissions and was used in the attainment demonstration.

Modeling Methodology

Design Values

U.S. EPA guidance recommends the use of multiple year averages of design values, where appropriate, to dampen the effects of single year anomalies to the air quality trend due to factors such as adverse or favorable meteorology or radical changes in the local emissions profile. The Basin ozone design value trend is presented in Chapter 5 of the 2022 AQMP, Figure 5-1 and Chapter 2 of the 2022 AQMP, Figure 2-2. Prior to 2016, both the 1-hour and 8-hour design values had been steadily decreasing, but this progress slightly reversed in 2016 and an increase was observed through 2020. The base year design values were calculated based on 2015-2019 measurements primarily to avoid abnormal emission changes due to COVID-19 in 2020. Chapter 2 of the 2022 AQMP and Appendix 2 discuss the emission changes that occurred in 2020 in addition to the effects of atypical meteorology and wildfires on poor air quality experienced that year.

Model Selection

The attainment demonstration was developed using the U.S. Environmental Protection Agency (U.S. EPA) Community Multiscale Air Quality (CMAQ) (version 5.2.1) modeling platform with Statewide Air Pollution Research Center (SAPRC) 07 chemistry, and the Weather Research and Forecasting Model (WRF) (version 4.0.3) meteorological fields. Comprehensive descriptions of the CMAQ modeling system are provided by

U.S. EPA.[1] Additional descriptions of the SAPRC07 chemistry module are provided are available online.[2] Documentation of the National Center for Atmospheric Research (NCAR) WRF model is available from the University Corporation for Atmospheric Research (UCAR).[3]

Regional Modeling

The CMAQ air quality modeling platform with SAPRC07 chemistry and WRF meteorology was employed as the primary tool used to demonstrate future year attainment of the ozone standard. Simulations focused on the ozone season (May 1st to September 30th). Predicted daily maximum values of 8-hour ozone were calculated from the running 8-hour average simulated concentrations.

As in the 2016 AQMP, simulations were conducted using a Lambert Conformal grid projection where the western boundary of the domain is at 084 UTM, over 100 miles west of the ports of Los Angeles and Long Beach. The eastern boundary extends beyond the Colorado River, while the northern and southern boundaries of the domain extend to the southern edge of the San Joaquin Valley and the Northern portions of Mexico (3543 UTM). The grid size is 4 x 4 kilometers with 30 vertical layers. Figure V-1-1 depicts the modeling domain which includes a grid of 156 cells from west to east and 102 cells from south to north.

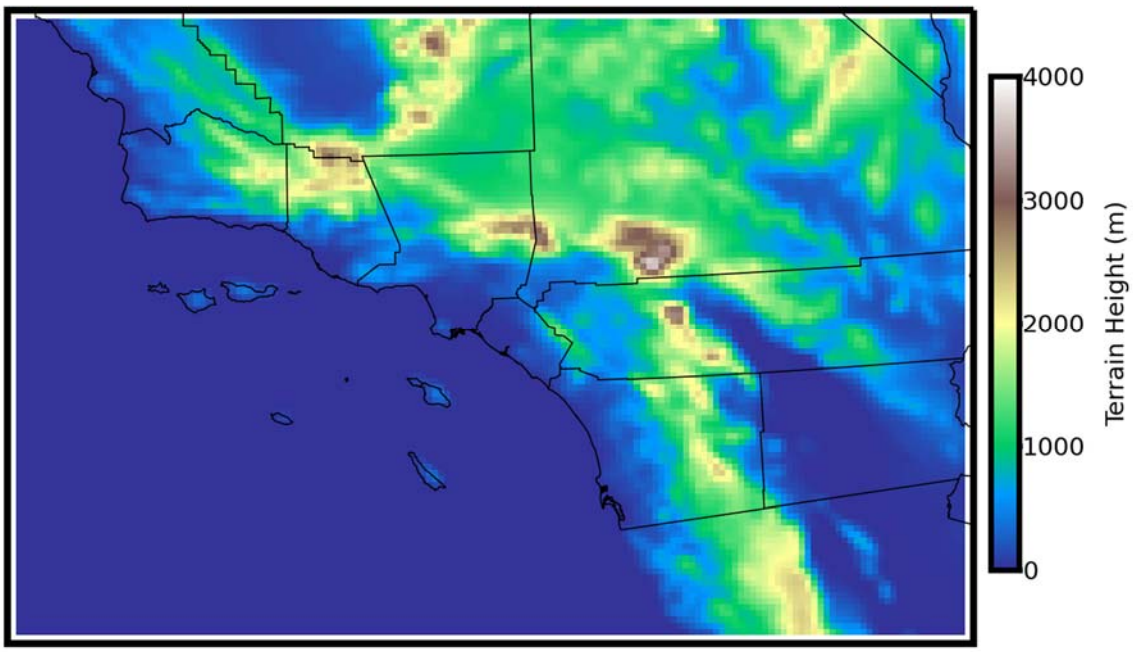

FIGURE V-1-1

2022 AQMP Regional Modeling Domain

[1] http://www.epa.gov/scram001/.
[2] http://www.engr.ucr.edu/~carter/SAPRC/.
[3] http://www.wrf-model.org/.

WRF was updated to the most recent version (version 4.0.3) available at the time of this protocol preparation and was evaluated with a set of observation data. The WRF simulations were initialized from National Centers for Environmental Prediction (NCEP) North American Regional reanalysis (NARR) Re-analysis data and run for 4-day increments with the option for four-dimensional data assimilation (FDDA). The atmospheric chemistry package used in the CMAQ simulations relied on SAPRC07 gas phase chemistry with version "c" toluene updates with the AERO6 aerosol mechanism, the Euler Backward Iterative solver, the Yamo horizontal advection scheme, the WRF vertical advection scheme, the multiscale CMAQ horizontal diffusion scheme, the ACM2 vertical diffusion scheme, in-line photolysis calculations, and clean homogeneous initial values.

Relative Response Factors and Future Year Design Values

To bridge the gap between air quality model output evaluation and applicability to the health-based air quality standards, EPA guidance has proposed the use of relative response factors (RRF). South Coast AQMD developed a tool to calculate the RRF and did not rely on EPA's MATS/SMAT software. The RRF is simply a ratio of future year predicted air quality with the control strategy fully implemented to the simulated air quality in the base year (U.S. EPA, 2018). For 8-hour ozone simulations, the top 10 days in the base-year and the corresponding days in the future year are used to determine the RRF. Only days with predictions greater than or equal to 60 ppb were considered; the RRF is undefined at sites with less than 5 days that meet this criterion. The top 10 days were chosen without regard to potential exceptional events or wildfire impacts. Finally, the maximum modelled value in the 3x3 grid surrounding each station was compared to the value in the corresponding grid position in the future year.

The future year design value is estimated by multiplying the non-dimensional RRF to the measured base year design value. Thus, the simulated improvement in air quality, based on multiple meteorological episodes, is translated to a simple metric that directly determines compliance of the standard. Equations V-1 and V-2 summarize the calculation.

Equation V-1.

$$\text{RRF} = \frac{\text{Future Year Model Prediction}}{\text{Base Year Model Prediction}}$$

Equation V-2.

$$\text{Future Design Value} = \text{RRF} \times \text{Base Design Value}$$

The modeling analyses described above use the RRF method to project future design values. A future design value less than or equal to the standard constitutes attainment. The RRF approach aims to minimize the effects of biases in the model simulations, thus providing more accurate projections of future air quality.

Weight of Evidence

Modeling guidance strongly recommends the use of corroborating evidence to support the future year attainment demonstration. The weight of evidence demonstration includes an analysis of the observed weekend ozone effect in South Coast Air Basin (SCAB), which supports the NOx-based control strategy.

Modeling Results

Air quality modeling simulations are conducted to quantify the air quality improvements resulting from the measures proposed in the AQMP, and to demonstrate that future ozone concentrations will meet the air quality standards. Modeling results show that the measures proposed in this AQMP will be able to bring ozone concentrations down and that all areas in the Basin and the Coachella Valley will be in attainment of the 2015 8-hour ozone standard by 2037.

Additional modeling was conducted to demonstrate the model ability to reproduce observed trends and to provide evidence that the model is able to predict future air quality with confidence. These additional modeling tests include analysis of the impacts of meteorology and climate on air quality, the ability of the model to predict weekday and weekend variations in ozone concentrations, the contribution of background ozone levels and the model ability to reproduce the effects COVID on air quality in the Basin.

Uncertainties Associated with the Technical Analysis

As with any attainment plan, there are uncertainties associated with the technical analysis. Uncertainties are inherent to many of the inputs used in the emissions, meteorological and air quality models. Uncertainty in emission projections stem from the uncertainties associated with the demographic and socioeconomic factors, the emission factors and the spatial distribution surrogates used in the development of emissions inventories. Modeling tools also contribute to the uncertainty as all models can only be a limited representation of the real world. Also, uncertainty in the measurements add to the uncertainty when model performance is assessed. And finally, uncertainty in future climate may also impact our understanding and ability to determine the necessary emission controls to attain the standards. While completely eliminating uncertainties is an impossible task, there are a number of features and practices built into the air quality planning process that manage and control such uncertainties and preserve the integrity of an air quality management plan. These measures include the constant revision of modeling tools and the design of contingency measures that could be enacted in the event that the measures in the AQMP do not result in the projected air quality improvements.

Document Organization

This document provides the federal attainment demonstration for ozone. Chapter 2 provides the modeling protocol which summarizes the key elements that have been revised relative to the 2016 AQMP modeling protocol. Chapter 3 provides a discussion of the meteorological modeling including a comprehensive model performance evaluation. Chapter 4 provides a brief summary of the modeling emissions, including characterization of the daily/diurnal emissions profiles and OGV emissions. Chapter 5 discusses the 8-hour ozone attainment demonstration for the 2037 attainment year. The ozone analysis includes discussions of the representativeness of the 2018 meteorological year, base-year modeling performance, and projections of future year concentrations for baseline emissions. Also provided are updated isopleth analyses and a discussion of future year carrying capacities for the current and proposed ozone standards. Weight of evidence discussions for ozone are incorporated in Chapter 5. Chapter 6 discusses state ozone standards. Table V-1-2 lists the Attachments to this document.

TABLE V-1-2

ATTACHMENTS

Number	Description
Attachment 1	WRF Model Performance Time Series
Attachment 2	CMAQ Model Performance Figures
Attachment 3	Emissions Reductions Summary for Future Control Scenarios
Attachment 4	8-hour Ozone Isopleths for 2037
Attachment 5	Performance Evaluation of VOC Species
Attachment 6	CMAQ Vertical Profiles

References

U.S. EPA (2018) Modeling Guidance for Demonstrating Air Quality Goals for Ozone, PM2.5, and Regional Haze

CHAPTER 2

MODELING PROTOCOL

Background

One of the basic requirements of a modeling attainment demonstration is the development of a comprehensive modeling protocol that defines the scope of the regional modeling analyses. This includes the attainment demonstration methodology, meteorological and chemical transport platforms, gridded and speciated emission inventories, and geographical characteristics of the modeling domains. The protocol also defines the methodology to assess model performance and the selection of the simulation periods. The 2016 AQMP provided a comprehensive discussion of the modeling protocol used for the development of the PM2.5 and ozone attainment demonstrations. The 2016 AQMP Modeling Protocol served as the prototype of the 2022 AQMP modeling protocol. This AQMP demonstrates attainment of the 2015 federal 8-hour ozone standard with 2018 as the base year and 2037 as the attainment year. Future attainment years (See Table V-2-1) are identified based on nonattainment designation, pollutant standards, and geographical area.

TABLE V-2-1

UPCOMING ATTAINMENT YEARS FOR THE 2015 8-HOUR OZONE NAAQS

Attainment Year	NAAQS	NAAQS level	Areas
2018	Base Year	Modeling Base Year	
2026	2015 ozone	70 ppb	Ventura
2032	2015 ozone	70 ppb	Coachella, W. Mojave Desert
2037	2015 ozone	70 ppb	South Coast

Attainment Demonstration

8-hour Ozone

The 8-hour attainment demonstration was performed based on the U.S. EPA guidance document, “Modeling Guidance for Demonstrating Air Quality Goals for Ozone, PM2.5, and Regional Haze”, issued on November 29, 2018. The guidance requires that a maximum concentration be determined among 9 grid cells around a monitoring station and that the specific grid location be preserved in the future year modeling scenario when calculating relative response factors (RRF). The RRF calculation is limited to the top 10 days of simulated concentrations which are higher than 60 ppb. Focusing on the top 10 days produces future-year design values that are more responsive to emission reductions.

Numerical Models

Table V-2-2 provides a side-by-side comparison of the 2012, 2016 and the current 2022 AQMP modeling protocols. In general, changes have occurred in the following categories: emissions inventories, future-year simulations, the level of the non-attainment designation and the attainment demonstration methodology. As such, these changes are expected to occur with each subsequent modeling update. Table V-2-3 highlights the main differences in CMAQ setup since the 2016 AQMP.

TABLE V-2-2

NUMERICAL MODELING PLATFORMS AND DOMAINS FOR 2022 AND PREVIOUS AQMPS

	2012 AQMP	2016 AQMP	2022 AQMP
Modeling Base Year	2008 Ozone: June – Aug PM: Annual	2012 Ozone: May – Sep PM: Annual	2018 Ozone: May - Sep
Chemical Transport Model	CMAQ as primary tool CAMx as weight of evidence	CMAQ	CMAQ
Meteorological Model	WRF version 3.3 with Updated Land Use	WRF version 3.6 with Updated Land Use	WRF version 4.0.3 Unified Noah
Emission: On-Road Off-Road	EMFAC 2011 EMFAC-LDV EMFAC-HD EMFAC-SG Category Specific Calculation	EMFAC 2014 Single package Category Specific Calculation	EMFAC 2017 Single package Category Specific Calculation
Modeling Domain	624 km by 408 km	624 km by 408 km	624 km by 408 km
Grid Resolution	4km by 4 km grid	4km by 4km grid	4km by 4km grid
Vertical Layer	18 layers with 14 layer below 2000 m Above Ground Level (AGL) and 50 hPa as top boundary	18 layers with 14 layer below 2000 m AGL and 50 hPa as top boundary	30 layers with 14 layer below 2000 m AGL and 50 hPa as top boundary

TABLE V-2-3

CHEMICAL TRANSPORT MODELING PLATFORM FOR THE 2016 AND 2012 AQMPS

Options	2016 AQMP	2022 AQMP
Numerical Model	CMAQ version 5.0.2	CMAQ version 5.2.1
Modeling Grid	156 by 102 grids with 4 km grid distance	Same
Vertical Layers	18 layers	30 layers
Gas Phase Chemical Mechanism	SAPRC07 with version "c" toluene updates	Same
Aerosol Mechanism	AERO6	Same
Chemical Solver	Euler Backward Iterative solver (EBI)	Same
Horizontal Advection	Yamo	Same
Vertical Advection	WRF	Same
Horizontal Diffusion	Multiscale CMAQ scheme	Same
Vertical Diffusion	ACM2	Same
Photolysis	In-line Calculation	Same
Initial Values	Clean Homogeneous Condition	Same
Boundary Values	Model for OZone and Related chemical Tracers (MOZART)	Nested modeling with 12km statewide CMAQ The Outer CMAQ domain used boundaries from the global model of Community Atmosphere Model with Chemistry (CAM-chem)

The Weather Research and Forecast (WRF) model remains the primary tool for meteorological modeling. WRF was updated with the most recent version (version 4.0.3) available at the time of protocol preparation and was evaluated with a set of observation data. Later WRF version 4.3 was conducted and evaluated to ensure the accuracy and reliability of meteorological predictions, while version 4.0.3 served as the primary WRF for this AQMP. WRF simulations were conducted with three nested domains with grid resolutions of 36, 12 and 4 km. The innermost domain spans 652 km by 460 km in the east–west and

north–south directions, respectively, which includes the greater Los Angeles area, its surrounding mountains, and ocean waters off the coast of the Basin (Figure V-2-1). A Lambert conformal map projection was used with reference latitudes of 30° and 60° N and the center of the modeling domain positioned at 37° N and 120° 30’ W. Details on the WRF model configuration are provided in Chapter 3.

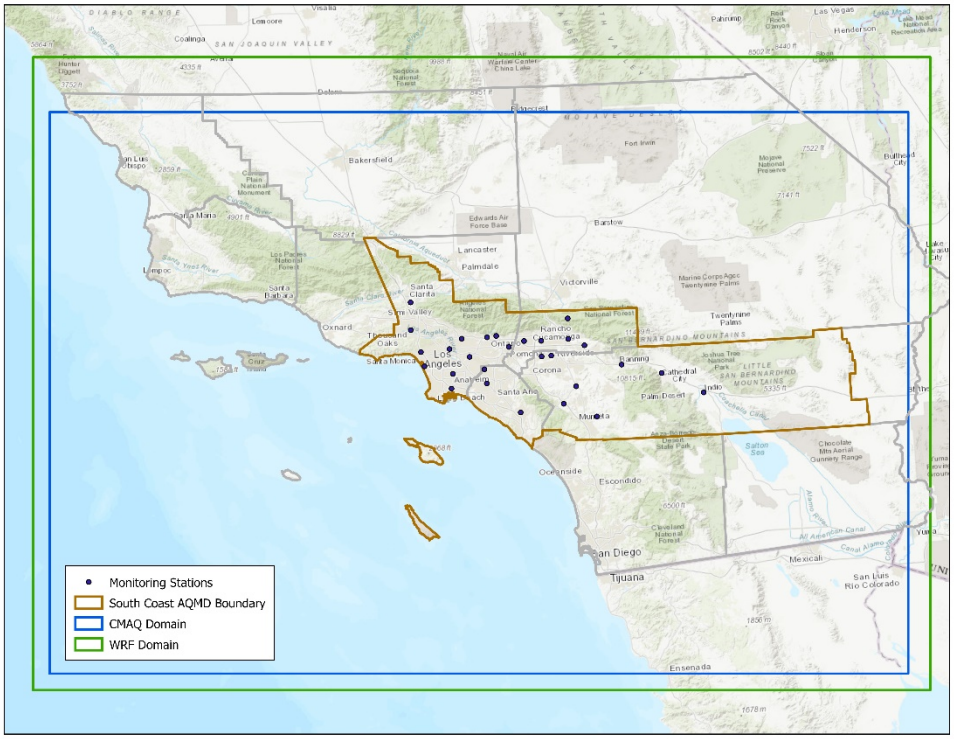

FIGURE V-2-1

THE RELATIVE LOCATIONS OF THE INNER MOST WRF DOMAIN COMPARED TO THE CMAQ DOMAIN. THE BOUNDARY OF SOUTH COAST AQMD JURISDICTION BOUNDARY AND AIR MONITORING LOCATIONS ARE OVERLAID BY A THICK SOLID LINE AND BLACK DOTS, RESPECTIVELY.

Emissions Processing

Emissions inventories are often developed on an annual basis for large geographic areas and a process must be developed to allocate the emissions to a time-dependent grid for use in chemical transport modeling. Traditionally, emissions were allocated to the modeling grid using generic or average activity patterns and profiles. These approaches did not sufficiently reflect the real-world characteristics of emissions sources. Shortcomings of previous emissions allocation methods included an inability to account for traffic flows responding to changes in weather, vessels transiting outside of well-known shipping lanes, or aircraft following airport-specific landing and takeoff trajectories. For these reasons,

new approaches were developed to spatially and temporally allocate emissions from on-road mobile sources, Ocean-Going Vessels (OGV), and aircraft. Each method used information from sensor or transponder-based datasets, which accurately reflected where and when emissions were occurring. Further details on the updated allocation methods are presented in Chapter 4 of this appendix.

TABLE V-2-4

SUMMARY OF EMISSION PROCESSING FOR 2016 AND 2022 AQMPS

Options	2016 AQMP	2022 AQMP
On-Road Emissions	EMFAC 2014 o Emissions mode to get total amount of emissions in Tons per Day o Emissions rate to estimate grams per emissions of specific vehicle category, activity, etc. Temporal allocation using Caltrans real-time Performance Measurement System (PeMS) traffic data for light and medium duty vehicles, and Weight in Motion (WIM) for heavy duty vehicles	EMFAC 2017 Temporal allocation using Caltrans real-time PeMS single loop detector-based traffic data for light, medium, and heavy-duty vehicles
Aircraft Emissions	Treated as point sources with inline emissions calculation	ACARS/GATE[1] spatial allocation
OGV Emissions	Prescribed spatial allocation following major shipping channels	AIS-based[2] spatial allocation
Vehicle Miles Traveled	2016 Regional Transportation Plan/Sustainable Communities Strategy (RTP/SCS)	2020 Regional Transportation Plan/Sustainable Communities Strategy (RTP/SCS)
Off-Road Emissions	Category Specific Calculation	Same
Mexico Emissions	CARB's Mexican emissions profile	Same

[1] Aircraft Communication Addressing and Reporting System (ACARS)/Gridded Aircraft Trajectory Emissions (GATE)

[2] Automated Identification System

TABLE V-2-5

LIST OF EMISSIONS CATEGORIES WITH AND TEMPORAL PROFILE USED

Day-Specific Profile	Generic Profile
• Wildfires[1] • Prescribed burns[1] • Biogenic and On-Road motor vehicle emissions are adjusted using day/hour-specific meteorological data.	• Agricultural burning • Residential wood combustion • Facilities • Paved road dust • Unpaved road dust • Windblown dust • Livestock dust

[1] Wildfires and prescribed burns were modeled using day-specific profiles for the model performance evaluation only. For the attainment demonstration, wildfire emissions were excluded, and prescribed burns were modeled using a generic profile.

Biogenic Emissions

Daily biogenic VOC emissions were calculated using the Model of Emissions of Gases and Aerosols from Nature version 3.0 (MEGAN3.0) using 2018 meteorology as input. MEGAN was executed in its default configuration, except for the normalized Leaf Area Index (LAIv) input. LAIv was developed by the California Air Resources Board using 2018 data from the Moderate Resolution Imaging Spectroradiometer (MODIS) on the National Aeronautical Space Administration's Terra and Aqua satellites. Because MODIS does not provide data in urban areas, LAIv in these areas was based on tree survey data from the US Forest Service. A detailed description of the biogenic inventory is provided in Chapter 4.

Computational Resources

The main computation platform employs high performance nodes. New servers, compiled to enhance computational capability, were configured with Red-Hat Enterprise Linux 7 and 64-bit operating systems. Details of the computing resources are summarized in Table V-2-6.

TABLE V-2-6

DETAILS OF COMPUTATIONAL RESOURCES USED IN THE 2012, 2016 AND 2022 AQMPS.

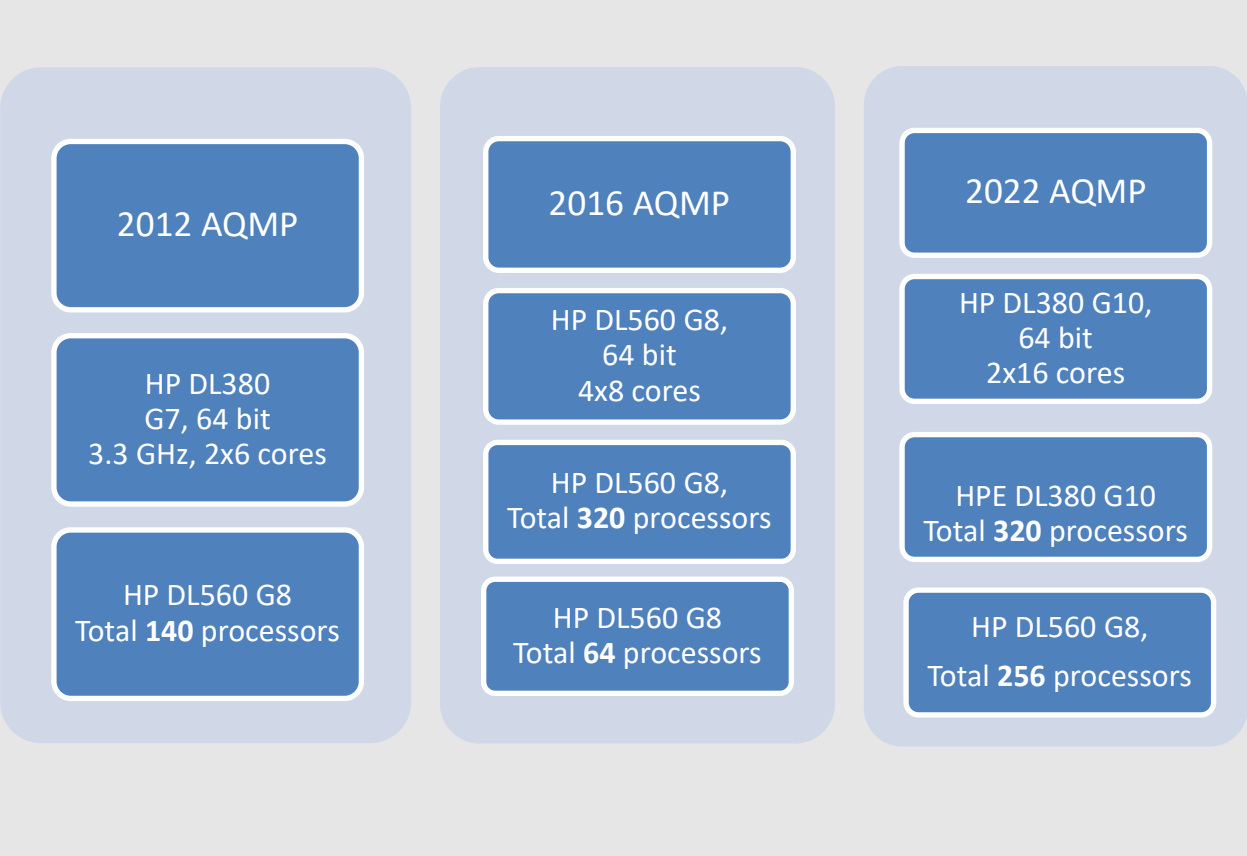

References

US EPA (2018) Modeling Guidance for Demonstrating Air Quality Goals for Ozone, PM2.5, and Regional Haze

CHAPTER 3

METEOROLOGICAL MODELING AND SENSITIVITY ANALYSES

Overview

This chapter provides a description of the meteorological modeling that serves as the foundation of the 2022 AQMP modeling analysis. As for the 2016 AQMP, the Weather Research and Forecasting (WRF) model was used to generate meteorological fields for further modeling analysis. The model offers a variety of user options to cover atmospheric boundary layer parameterizations, turbulent diffusion, cumulus parameterizations, land surface-atmosphere interactions, which can be customized to specific geographical and climatological situations. South Coast AQMD staff performed extensive sensitivity tests and developments to improve WRF performance for the South Coast Air Basin, where prediction of complex meteorological structures associated with air quality episodes is particularly challenging due to the region's unique geography and climate. This chapter describes the numerical configuration, sensitivity tests on key parameterizations, input database, and initial and boundary values used in the 2022 AQMP modeling analysis.

Comparison of 2018 observed meteorology to 2010-2019 averages

Meteorological data from airport weather stations across the Basin and the Coachella Valley were used to assess differences between regional weather patterns observed in 2018 and average conditions from 2010-2019. The 15 weather stations used for this analysis were Los Angeles International Airport (LAX), Santa Monica Municipal Airport (SMO), Hawthorne Municipal Airport (HHR), Long Beach Airport (LGB), John Wayne Airport (SNA), Fullerton Municipal Airport (FUL), Chino Airport (CNO), Ontario International Airport (ONT), Riverside Municipal Airport (RAL), March Air Reserve Base (RIV), Palm Springs International Airport (PSP), Burbank Bob Hope Airport (BUR) and Van Nuys Airport (VNY). The location of the stations is shown in Figure V-3-1. Comparisons of 2018 and 2010-2019 annual average temperature, relative humidity, and wind speed at each station are shown in Figures V-3-2 through V-3-4. On an annual basis, only the stations with > 90% valid data were used for the analysis. Torrance Municipal Airport (TOA) and San Gabriel Valley Airport (EMT) stations were not included due to insufficient valid data.

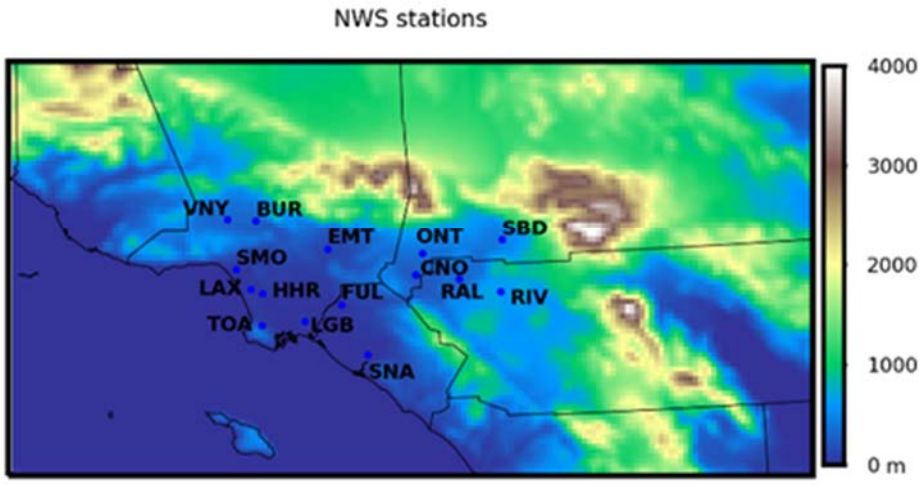

FIGURE V-3-1

15 WEATHER STATIONS DISPLAYED A TOPOGRAPHIC MAP

As shown in Figure V-3-2, all stations recorded slightly higher temperatures during 2018 compared to 10-year average levels. The largest departures from 2010-2019 average temperatures were observed at the CNO and PSP stations, where average annual temperatures in 2018 were approximately 1.18 and 0.86°C warmer than 10-year averages, respectively. The minimum difference between 2018 and 2010-2019 average temperatures was observed at the BUR station, with a marginal difference between the two datasets (0.09°C).

As shown in Figure V-3-3, annual average relative humidity (RH) in 2018 was generally close to 10-year average RH. The largest annual average RH difference was observed at the BUR station, where 2018 average RH was 4.84% higher than the 10-year average; the minimum difference was recorded at the FUL station, where 2018 average RH was 0.12% higher than the 2010-2019 average. The highest and lowest average relative humidity were recorded at the LAX and PSP stations, respectively, in both the 2018 and 2010-2019 datasets.

Average annual wind speeds were higher in 2018 at most stations (11 of 13) compared to 2010-2019 averages (see Figure V-3-4). The largest difference in average wind speed was observed at the ONT station, where wind speed was 0.30 m/s above average.

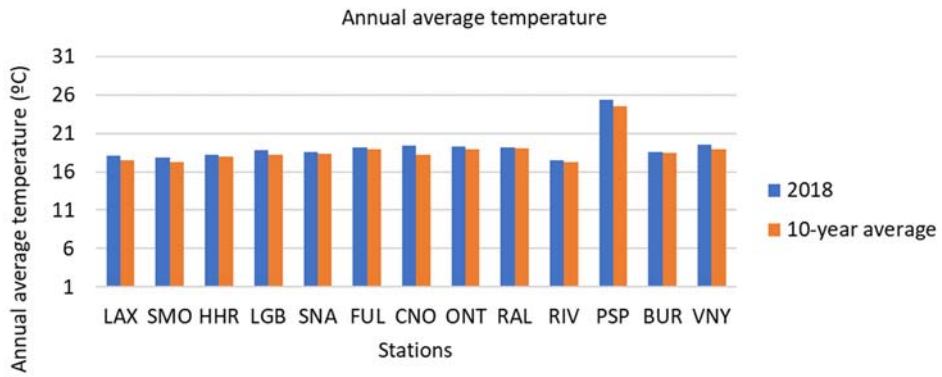

FIGURE V-3-2

ANNUAL AVERAGE TEMPERATURE AT EACH STATION IN 2018 AND THE 10-YEAR (2010-2019) AVERAGES

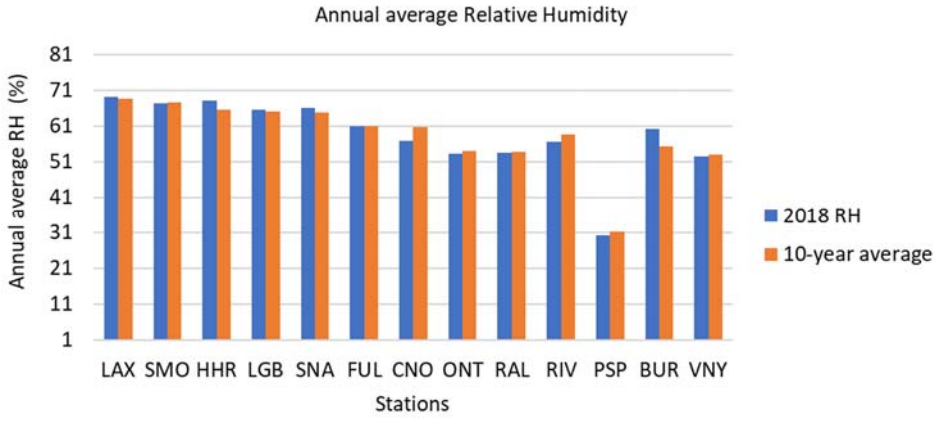

FIGURE V-3-3

ANNUAL AVERAGE RELATIVE HUMIDITY AT EACH STATION IN 2018 AND THE 10-YEAR (2010-2019) AVERAGES

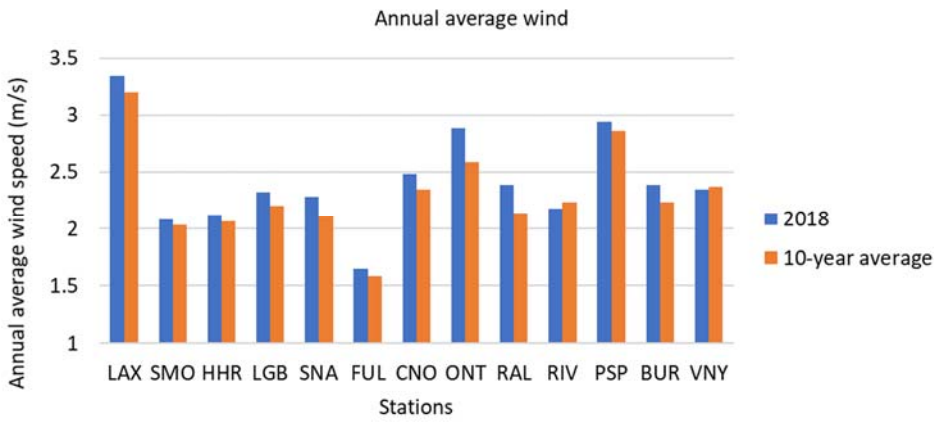

FIGURE V-3-4

ANNUAL AVERAGE WIND SPEED AT EACH STATION IN 2018 AND THE 10-YEAR (2010-2019) AVERAGES

Modeling Configuration

The WRF model is one of the most widely used meteorological models for both operational forecasting and research applications. WRF has been applied to a wide range of phenomena across geographic scales from tens of meters to thousands of kilometers, such as regional climate, monsoons, baroclinic waves, mesoscale fronts, hurricanes, deep convection, land-sea breezes, mountain-valley circulations, large eddy simulations, and fire events. The model is supported by the National Center for Atmospheric Research (NCAR) and actively developed by a worldwide user community. The WRF system contains two dynamical solvers, referred to as the ARW (Advanced Research WRF) core and the NMM (Nonhydrostatic Mesoscale Model) core. The ARW configuration was used for the 2022 AQMP modeling analysis. The ARW is primarily developed and maintained by the NCAR Mesoscale and Microscale Meteorology Laboratory.

The WRF model is a fully compressible and nonhydrostatic model (with a run-time hydrostatic option). For vertical coordinate, the model uses either a terrain-following (TF) or hybrid vertical coordinate (HVC). The grid staggering is the Arakawa C-grid. It uses a time-split small step for acoustic and gravity-wave modes. The dynamics conserve scalar variables. The WRF is designed to be a flexible, state-of-the-art atmospheric simulation system that is portable and efficient on parallel computing platforms.

The WRF simulation domain designed for the 2022 AQMP study encompasses the greater Los Angeles and suburban areas, its surrounding mountains, and ocean off the coast of the Basin, as shown in Figure V-3-5. WRF simulations were conducted with three nested domains at grid resolutions of 36 km, 12 km, and 4 km. The innermost domain has 163 by 115 grid points, which span 652km by 460km in east-west and north-south directions, respectively. Figure V-3-5 also shows the relative locations and sizes of the three nested grids. The innermost domain presented in Figure V-3-5, excluding three boundary columns and rows, served as the CMAQ (Community Multiscale Air Quality Modeling System) chemical transport modeling domain.

The WRF simulation employed 30 layers vertically with the lowest computational layer at approximately 20 m above ground level (agl) and the top layer at 50 hPa. Four-Dimensional Data Assimilation (FDDA) was conducted using grid analysis data enhanced with available surface and vertical sounding data. Sea surface temperatures (SST) are a critical control on the land-sea breeze and up-slope/down-slope flow. SST data from the Global Data Assimilation Experiment (GODAE) were used to update the WRF modeling every 6 hours to better represent the sea surface temperature. The Yon-Sei University (YSU) scheme (Hong and Pan, 1996) was used to model the planetary boundary layer (PBL). The WRF simulation with this configuration is referred as the "base" simulation. The flowchart (Figure V-3-6) of WRF simulation shows the meteorology input data, processing steps, observation nudging, and one-way nesting for high resolution inner domain.

After careful testing of different WRF physics options, the longwave radiation scheme of Rapid Radiative Transfer Model (RRTM) (Mlawer et al., 1997), the shortwave radiation scheme of Dudhia (Dudhia, J. 1989) and WRF Single-Moment 3-class scheme of micro physics were chosen for simulations. Kain-Fritsch cumulus schemes (Kain, J.S., 2004) were used in all three domains. The land surface model (LSM) scheme and the impacts of vertical resolution are evaluated in the next section.

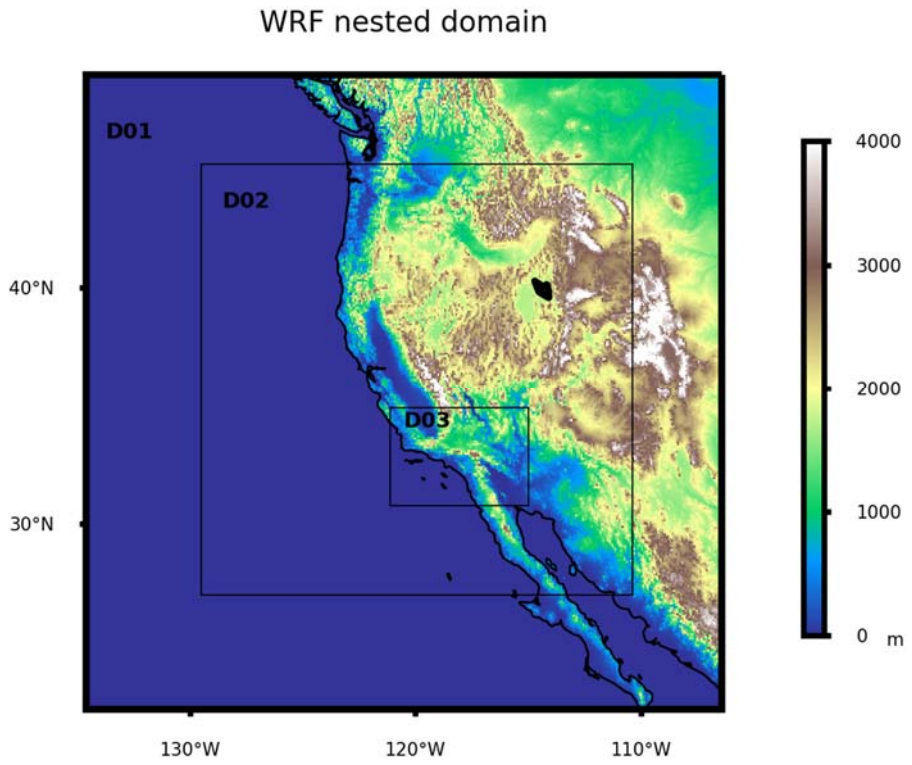

FIGURE V-3-5

THREE NESTED MODELING DOMAINS EMPLOYED IN THE WRF SIMULATIONS

Table V-3-1 below provides a summary of the WRF configuration of the major options relevant for air quality modeling used for the 2022 AQMP in comparison with the 2016 AQMP. Major parameters used for the 2022 AQMP are similar to those used for the 2016 AQMP. Sensitivity simulations were performed to evaluate land surface schemes and vertical resolutions of modeling configuration (Table V-3-2).

TABLE V-3-1

OVERVIEW OF WRF CONFIGURATION FOR 2022 AQMP IN COMPARISON WITH 2016 AQMP

Component	2016 AQMP	2022 AQMP
Numerical Platform	WRF v3.6.1	WRF v4.0.3
Number of domains	3 nested domains	
Nested Domain setting	D01: 36 km (71 X 71)	D01: 36 km (83 X 83)
	D02: 12 km (133 X 133)	D02: 12 km (169 X 169)
	D03: 4 km (163 X 115)	
Number of vertical layers	30 layers, the lowest layer is at ~ 20 m agl.	
Simulation Length	4 days with 24-hour spin-up	
Initial and boundary values	NCEP NAM[1] analysis (40 km X 40 km)	NCEP NARR[2] Re-analysis (32 km X 32 km)
Sea Surface Temperature	GHRSST[3]	
Boundary layer scheme	YSU[4] scheme	
Land Surface model	Thermal Diffusion scheme	Unified Noah
Cumulus parameterization	Kain-Fritsch for the outer three domains, explicit for the innermost domain	
Micro physics	Simple ice	WRF Single-Moment 3-class
Radiation	Cloud radiation	RRTM scheme for longwave, Dudhia scheme for shortwave
Four-dimensional data analysis	Analysis nudging with NWS surface and upper air Measurements	

[1]NAM - The North American Mesoscale Forecast System
[2]NARR - North American Regional Reanalysis
[3]GHRSST - The Group for High Resolution Sea Surface Temperature (https://www.ghrsst.org/)
[4]YSU - Yon-Sei University

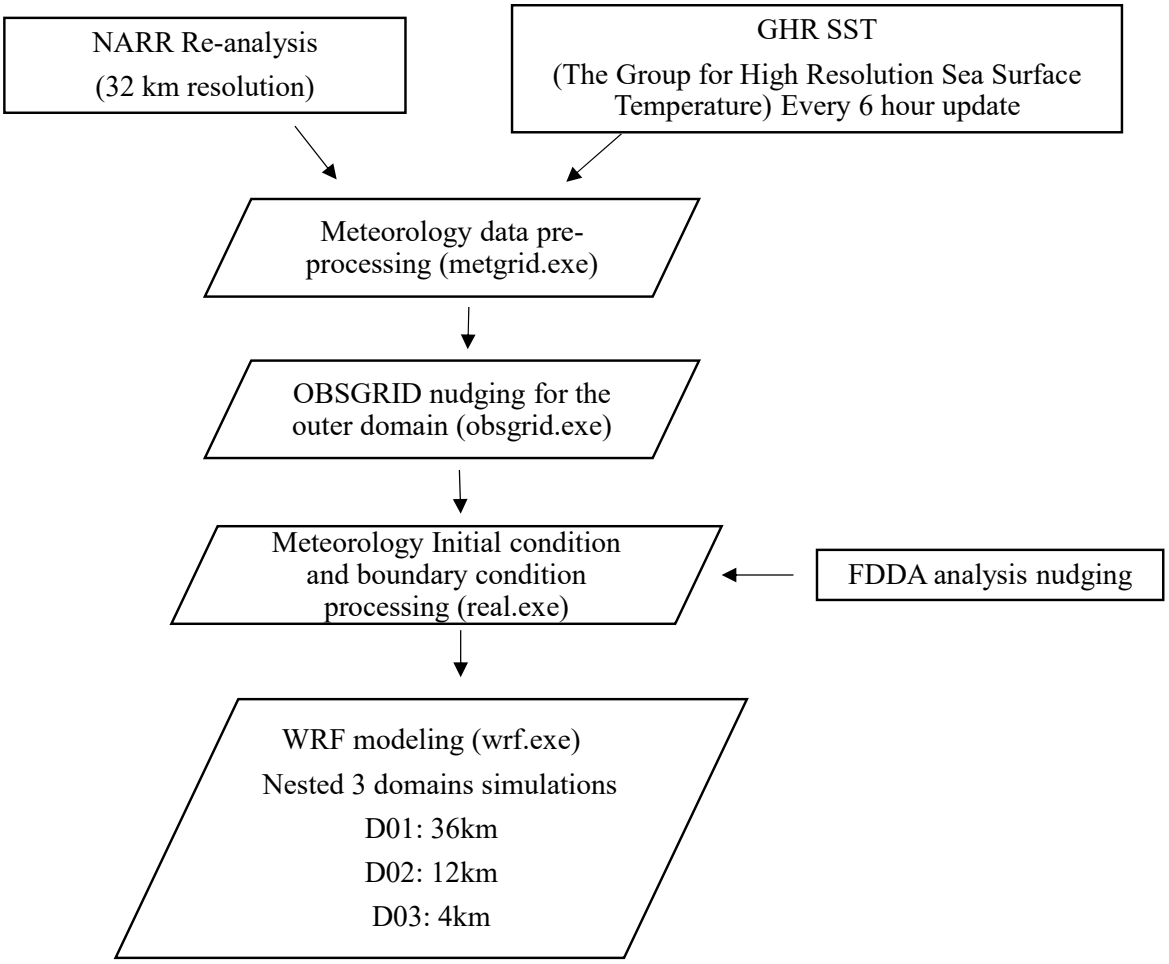

FIGURE V-3-6

FLOWCHART OF WRF SIMULATION FOR 2022 AQMP

TABLE V-3-2

WRF SENSITIVITY SIMULATIONS

#	Testing Categories	
1	Land Surface Model	Pleim-Xiu land surface model (LSM)
2	Urban Surface	Urban canopy model
3	High Vertical Resolution	35 layers in total, added 5 more layers between 0.8 km – 3 km above ground level
4	Horizontal Resolution	1km ×1km simulation
5	Version of WRF-Chem	WRF v4.3 and WRF v4.0.3

Model Performance Evaluation: Surface Level

The performance of the WRF simulations along with other sensitivity testing simulations are summarized in Table V-3-3 and Table V-3-4 for the winter season (January, November and December 2018) and summer season (June, July, and August of 2018), respectively. All the results shown in Table V-3-3 and V-3-4 are averaged values for the 15 airport weather stations. Overall, WRF simulations for summer and winter seasons provided representative meteorological fields that well characterized observed conditions in 2018. These fields were used directly in the CMAQ joint particulate and ozone simulations.

The performance of WRF simulations used as transport fields for CMAQ modeling is shown in Figure V-3-7 through Figure V-3-15. The model performance was evaluated for each month at airport stations in the model domain for January through December 2018. For simplicity, only one summer month (July) and one winter month (January) are shown in Figure V-3-7 through Figure V-3-15.

Three weather stations are carefully selected from near coastal areas (HHR, Hawthorne municipal Airport) through inland Orange County (FUL, Fullerton Municipal airport) to further east in San Bernardino County (CNO, Chino Airport) for surface level model performance evaluations. Diurnal variations of temperature, humidity and surface wind were well represented by the WRF simulations. Temperature and wind speed predictions were more accurate in the summer season than the winter months (Figure V-3-7 – Figure V-3-12). The observed temperature gradient from the coastal station of HHR to the inland station of CNO was also well characterized by the WRF model. Median observed summer temperatures in 2018 were 296.6, 298.7, and 300.9 K at HHR, FUL and CNO, respectively. The WRF model showed similar median temperature for these stations. Temperature is one of the key factors for atmospheric photochemical reactions, and high temperature is favorable for ozone formation. For the inland stations of CNO and FUL, the WRF simulations showed slight underestimation of daily high temperatures during July 2018. At the near coast station of HHR, the WRF simulation showed better performance in predicting daily high temperatures in the summer. During the winter, daily high temperature predictions were closer to observed values towards the end of January 2018 at all stations. The model tended to overpredict the daily low temperatures throughout the month.

Both observational data and WRF simulations at all stations showed distinct diurnal variations in wind speed during the summer, with a strong sea breeze in the early afternoon. Mostly, stronger wind speed indicates less accumulation of air pollutants. Daily maximum wind speeds were relatively consistent throughout July 2018, with much more variability observed during January 2018 (e.g., range of daily maximum wind speeds from ~2-13 m/s during January at CNO from both measurements and simulations). The model performance in predicting the wind speed was significantly better for July 2018 compared to January 2018 at all stations; R values for model-observation correlations were 0.84, 0.70, and 0.75 in July 2018 and 0.62, 0.50, and 0.54 in January 2018 at CNO, FUL, and HHR stations, respectively. It is noticed that the model underestimated daily maximum wind speeds at the HHR station during July 2018.

The WRF model predicted water vapor mixing ratio trends well at all stations, with model-observation correlation coefficients of 0.79, 0.81, and 0.89 in January 2018 and 0.60, 0.63, and 0.51 in July 2018 at CNO, FUL, and HHR stations, respectively. The WRF run yielded water vapor mixing ratios comparable to observed values in July. Lower water vapor mixing ratios mostly are associated with potential high ozone days. In January, the simulations showed underestimation for the water vapor mixing ratios. In both January and July, a few episodes of abrupt shifts in humidity were not captured by the WRF simulation.

TABLE V-3-3

WRF PERFORMANCE STATISTICS FOR THE SEASONAL AVERAGE OF JANUARY, FEBRUARY AND DECEMBER 2018 AT 15 NWS STATIONS

	Base	Pleim Xiu LSM	High Vertical resolution
2m Temperature Mean OBS (K)	287.7	287.7	287.7
2m Temperature Mean SIM (K)	288.0	288.0	287.0
2m Temperature Bias (K)	0.3	0.3	-0.7
2m Temperature Gross Error (K)	2.0	2.0	1.9
2m Temperature RMSE (K)	2.7	2.7	2.6
Water vapor mixing ratio Mean OBS (kg/kg)	5.5	5.5	5.5
Water vapor mixing ratio Mean SIM (kg/kg)	4.6	4.6	5.0
Water vapor mixing ratio Bias (kg/kg)	-0.9	-0.9	-0.5
Water vapor mixing ratio Gross Error (kg/kg)	1.4	1.4	1.3
Water vapor mixing ratio RMSE (kg/kg)	1.9	1.9	1.8
Wind Speed Mean OBS (m/s)	1.9	1.9	1.9
Wind Speed Mean PRD (m/s)	2.2	2.1	2.0
Wind Speed Bias (m/s)	0.3	0.3	0.1
Wind Speed Gross Error (m/s)	1.5	1.5	1.4
Wind Speed RMSE (m/s)	1.9	1.9	1.8

TABLE V-3-4

WRF PERFORMANCE STATISTICS FOR THE SEASONAL AVERAGE OF JUNE, JULY AND AUGUST 2018 AT 15 NWS STATIONS

	Base	Pleim-Xiu LSM	High Vertical Resolution
2m Temperature Mean OBS (K)	297.2	297.2	297.2
2m Temperature Mean SIM (K)	297.4	297.4	297.6
2m Temperature Bias (K)	0.2	0.2	0.4
2m Temperature Gross Error (K)	1.6	1.6	1.4
2m Temperature RMSE (K)	2.1	2.1	1.9
Water vapor mixing ratio Mean OBS (kg/kg)	10.7	10.7	10.7
Water vapor mixing ratio Mean SIM (kg/kg)	10.9	10.9	11.2
Water vapor mixing ratio Bias (kg/kg)	0.2	0.2	0.6
Water vapor mixing ratio Gross Error (kg/kg)	1.4	1.4	1.4
Water vapor mixing ratio RMSE (kg/kg)	2.4	2.4	2.4
Wind Speed Mean OBS (m/s)	2.7	2.7	2.7
Wind Speed Mean PRD (m/s)	2.5	2.5	2.5
Wind Speed Bias (m/s)	-0.2	-0.2	-0.2
Wind Speed Gross Error (m/s)	1.2	1.2	1.1
Wind Speed RMSE (m/s)	1.5	1.5	1.4

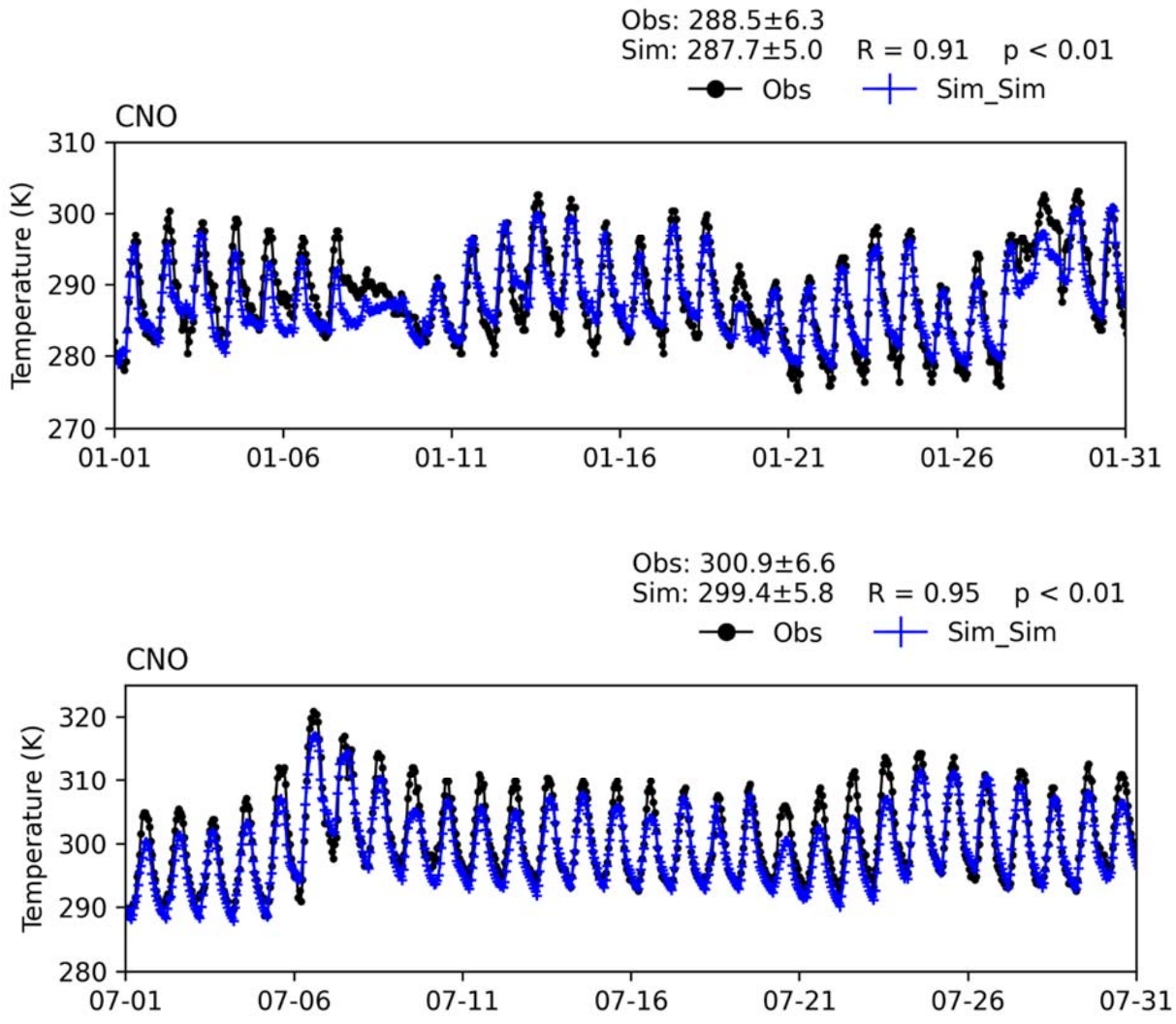

FIGURE V-3-7

TIME SERIES OF HOURLY TEMPERATURE FROM MEASUREMENT AND WRF SIMULATIONS AT CHINO (CNO) STATION FOR JANUARY 2018 AND JULY 2018

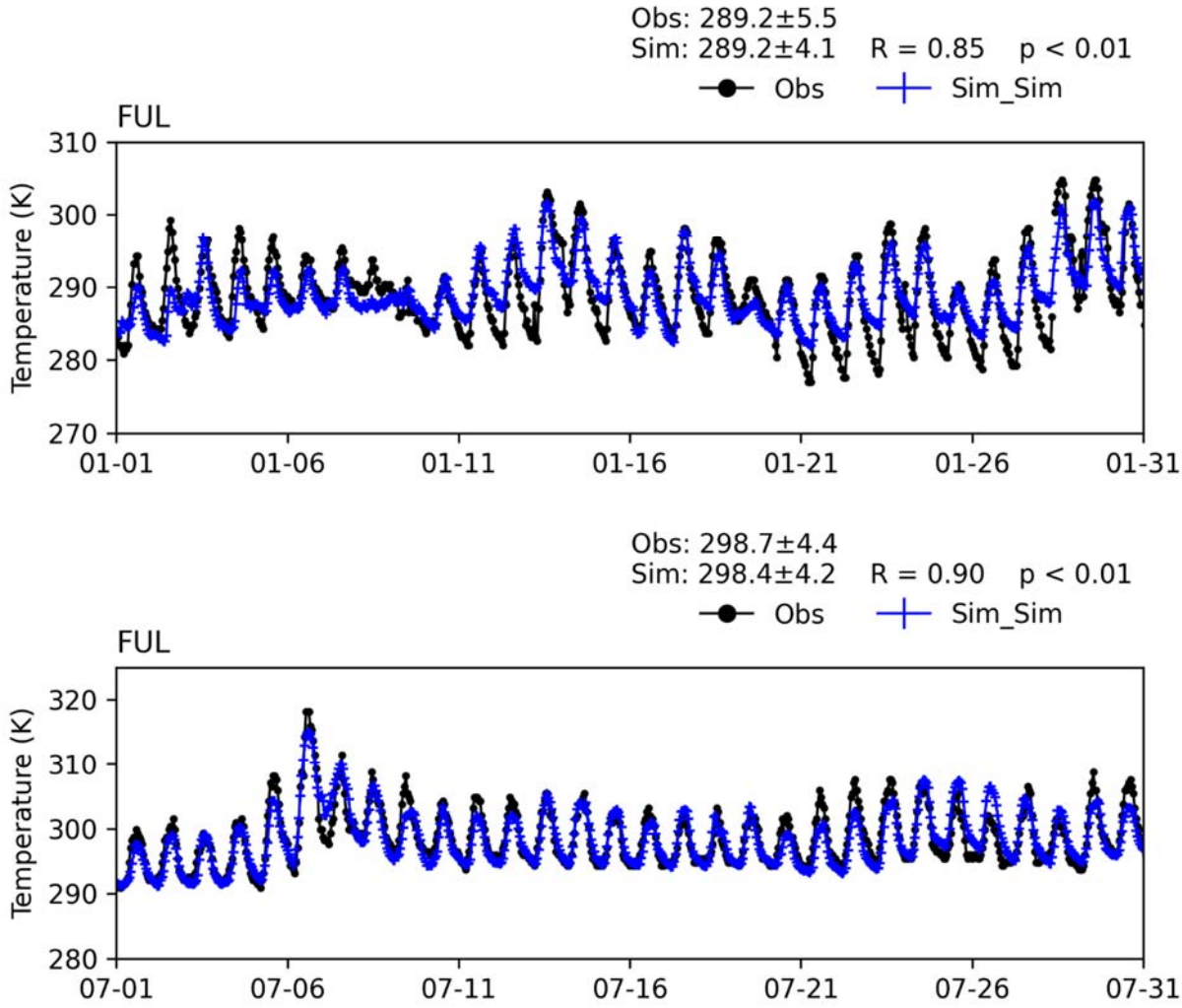

FIGURE V-3-8

TIME SERIES OF HOURLY TEMPERATURE FROM MEASUREMENTS AND WRF SIMULATIONS AT FULLERTON (FUL) STATION FOR JANUARY 2018 AND JULY 2018

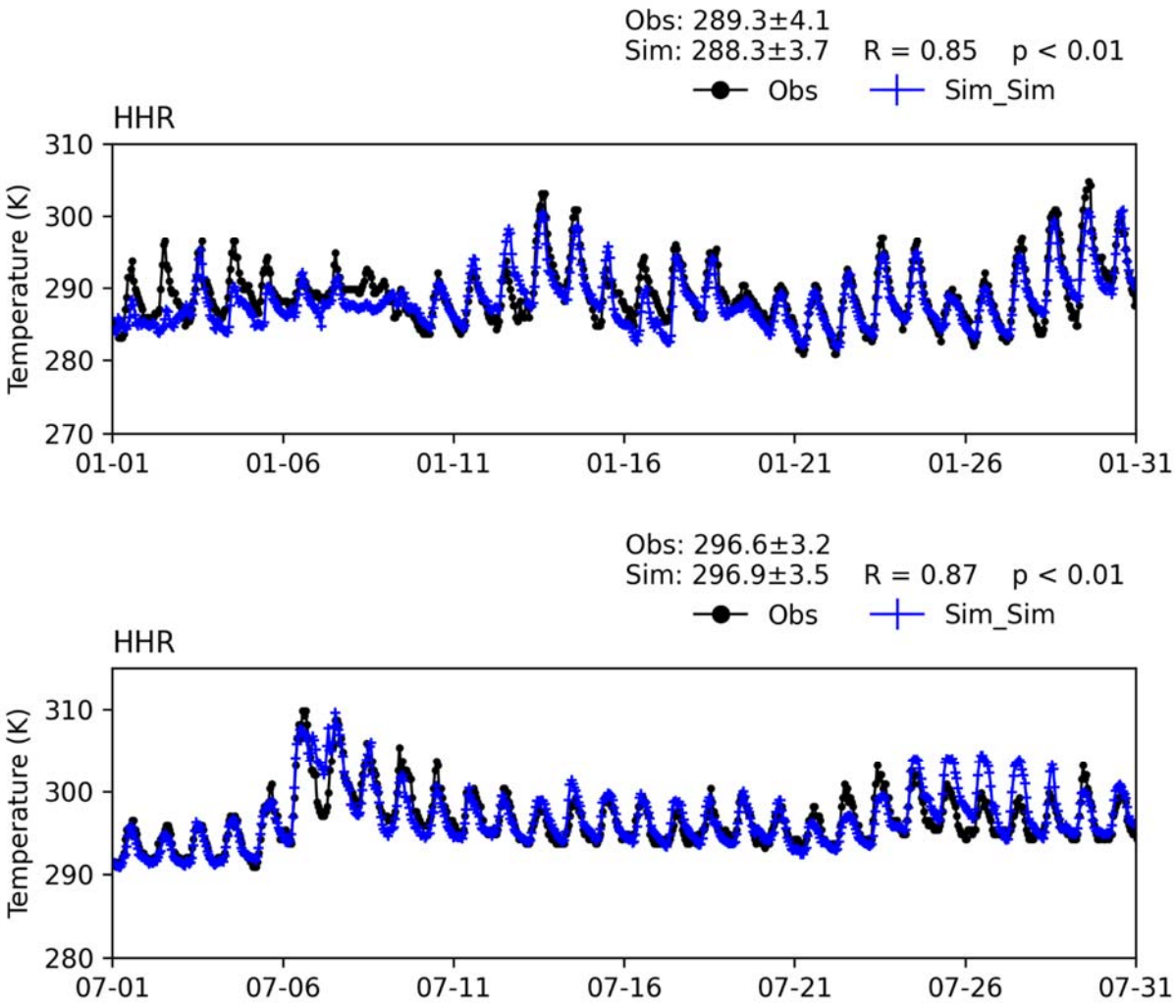

FIGURE V-3-9

TIME SERIES OF HOURLY TEMPERATURE FROM MEASUREMENTS AND WRF SIMULATIONS AT HAWTHORNE (HHR) STATION FOR JANUARY 2018 AND JULY 2018

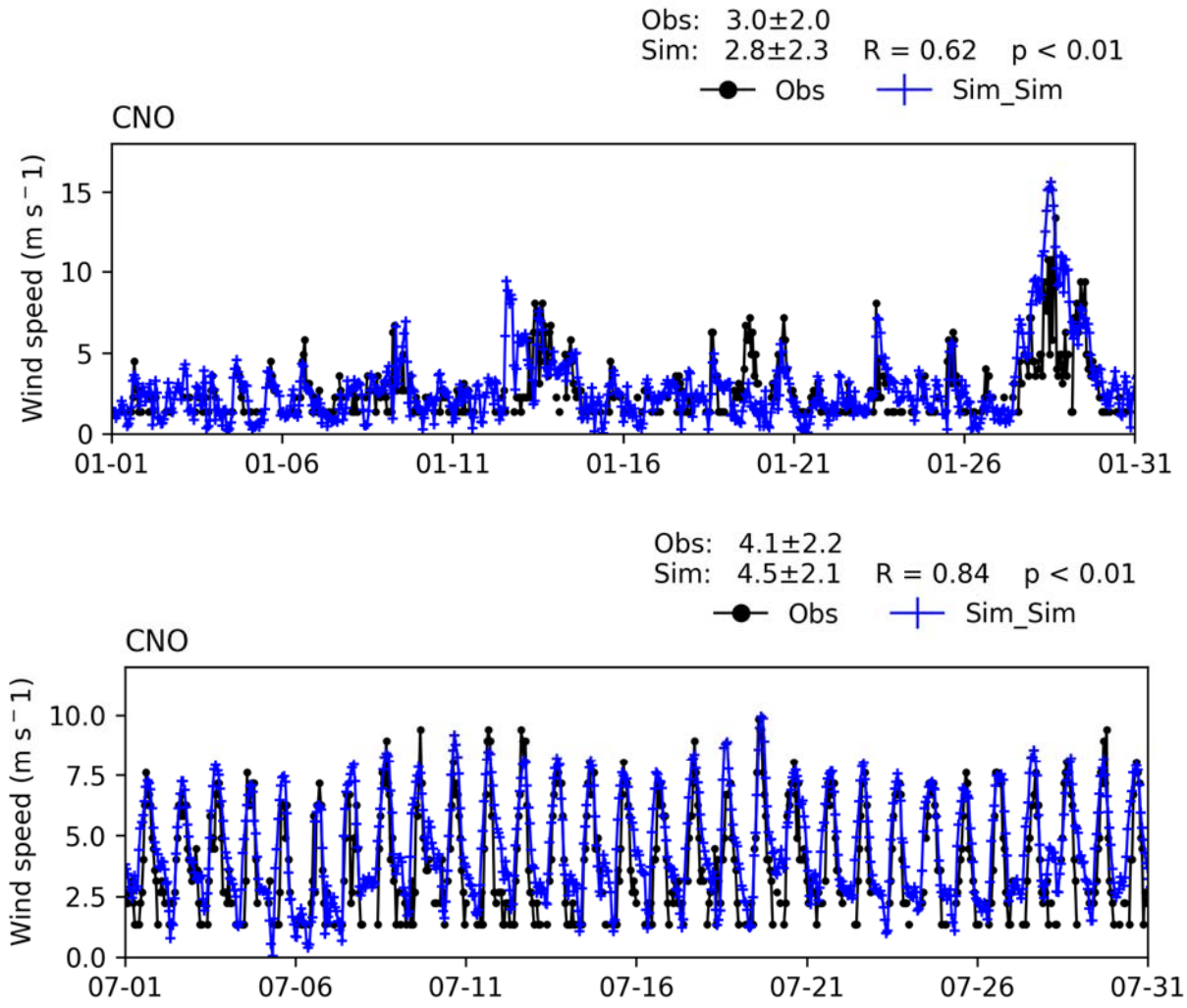

FIGURE V-3-10

TIME SERIES OF HOURLY WIND SPEED FROM MEASUREMENTS AND WRF SIMULATIONS AT CHINO (CNO) STATION FOR JANUARY 2018 AND JULY 2018

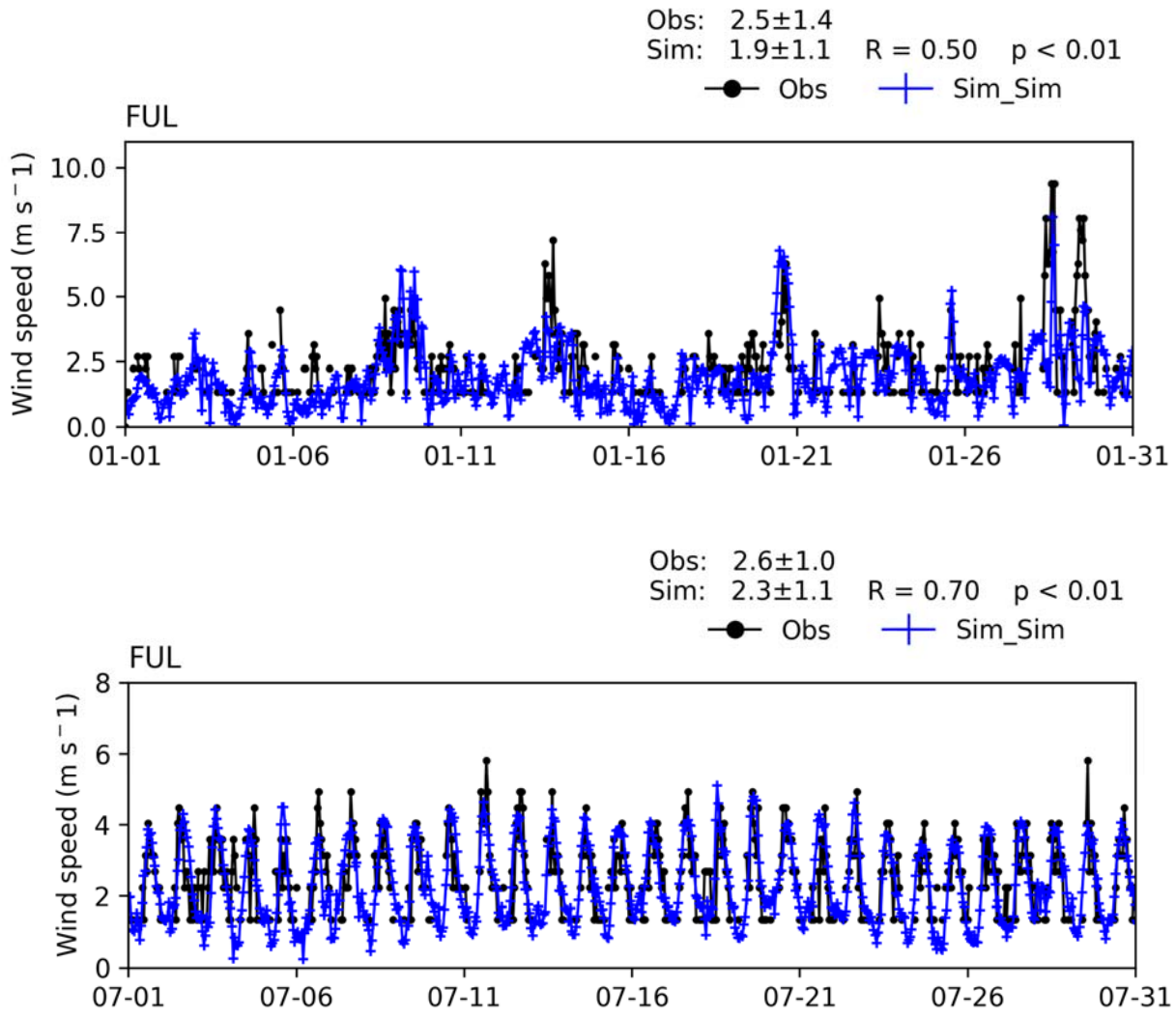

FIGURE V-3-11

TIME SERIES OF HOURLY WIND SPEED FROM MEASUREMENTS AND WRF SIMULATIONS AT FULLERTON (FUL) STATION FOR JANUARY 2018 AND JULY 2018

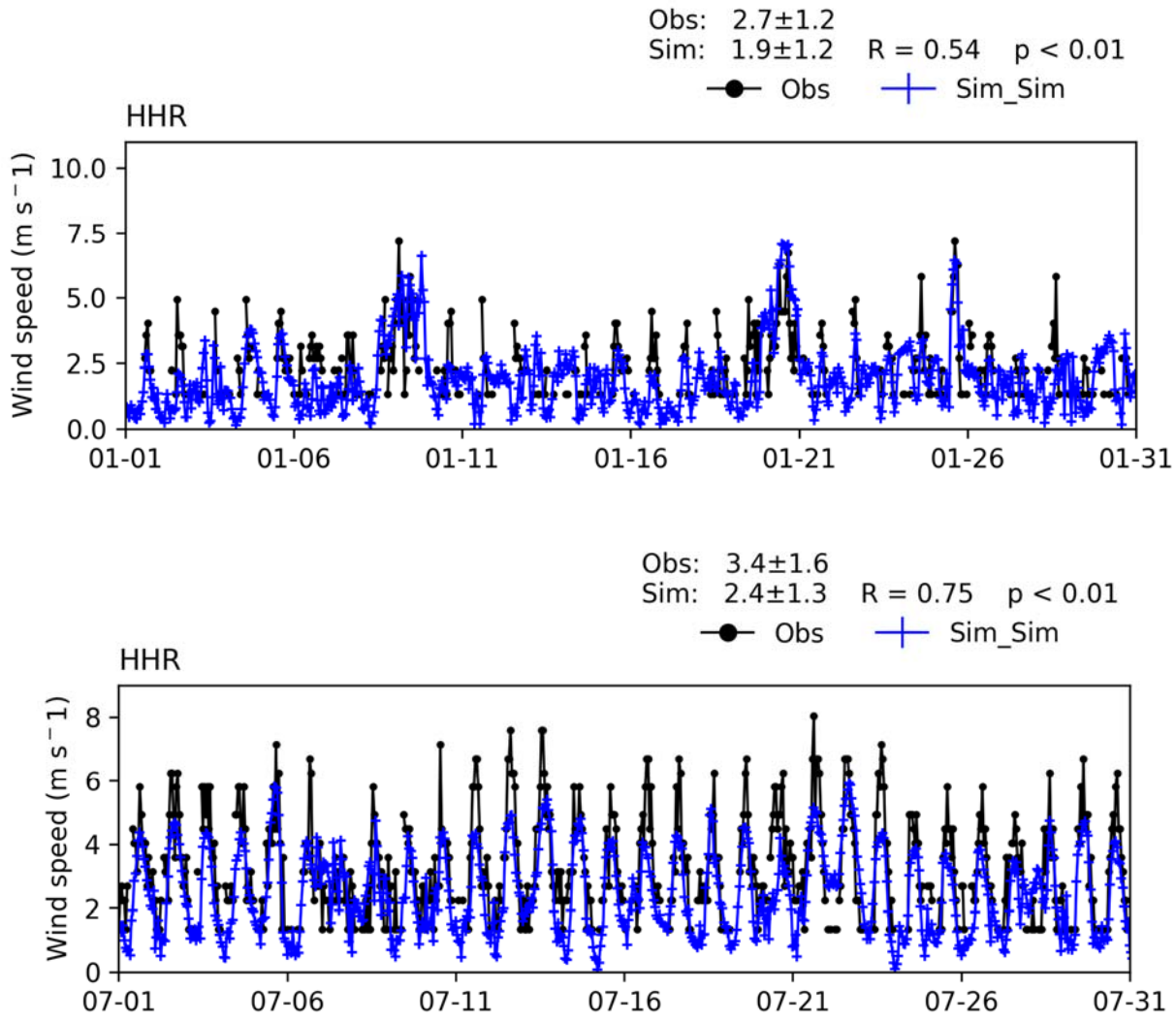

FIGURE V-3-12

TIME SERIES OF HOURLY WIND SPEED FROM MEASUREMENTS AND WRF SIMULATIONS AT HAWTHORNE (HHR) STATION FOR JANUARY 2018 AND JULY 2018

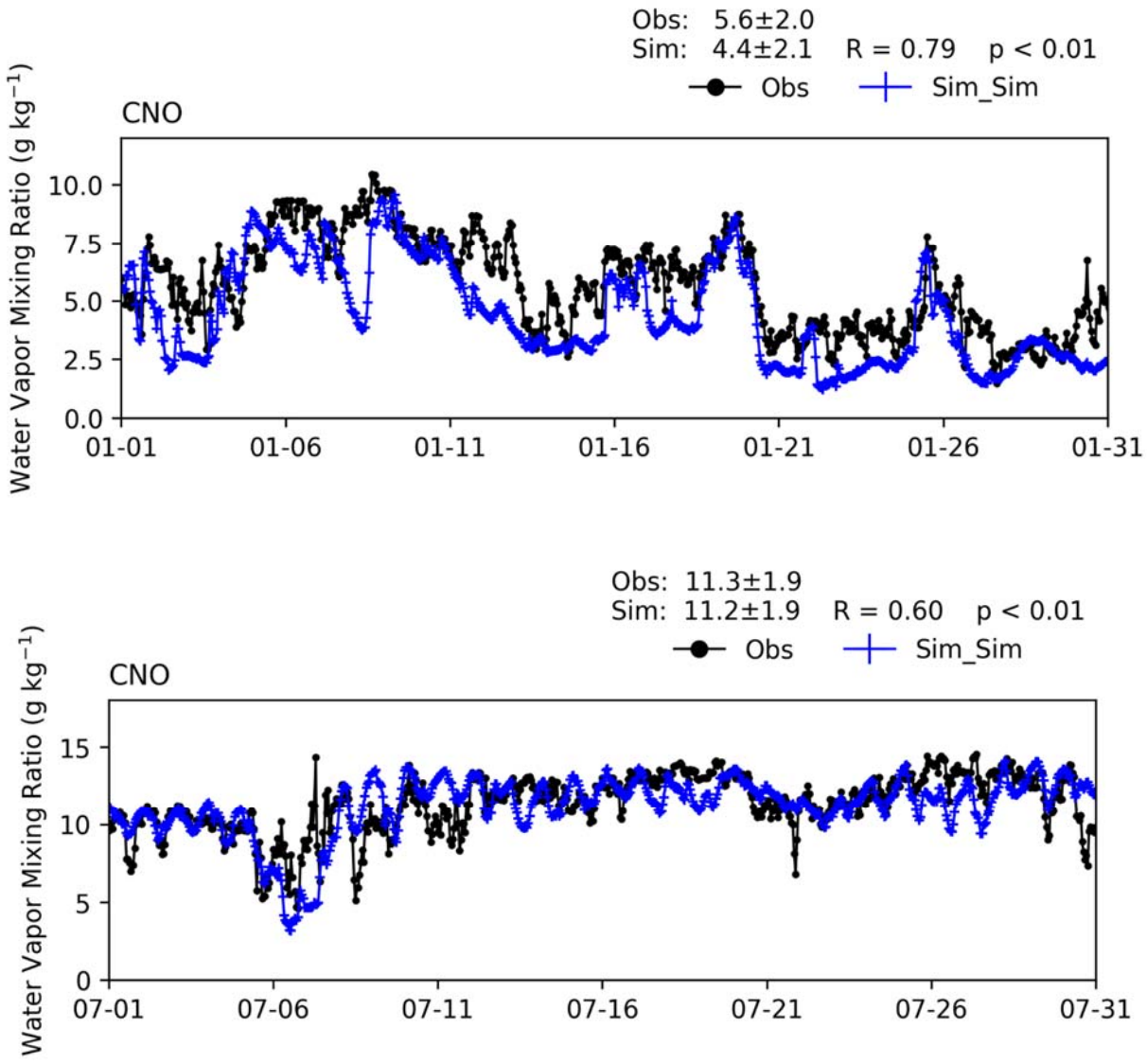

FIGURE V-3-13

TIME SERIES OF HOURLY WATER VAPOR MIXING RATIO FROM MEASUREMENTS AND WRF SIMULATIONS AT CHINO (CNO) STATION FOR JANUARY 2018 AND JULY 2018

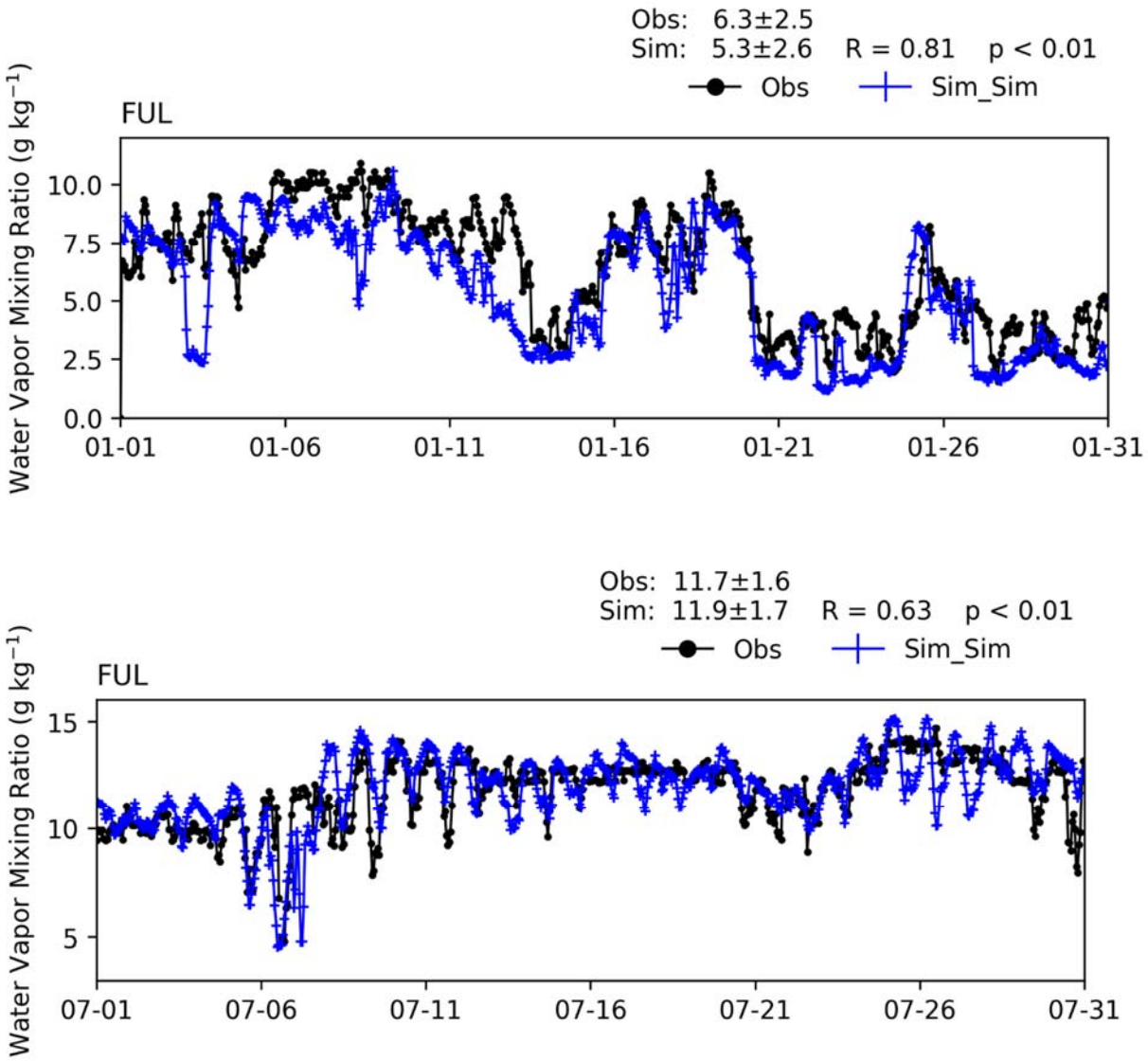

FIGURE V-3-14

TIME SERIES OF HOURLY WATER VAPOR MIXING RATIO FROM MEASUREMENTS AND WRF SIMULATIONS AT FULLERTON (FUL) STATION FOR JANUARY 2018 AND JULY 2018

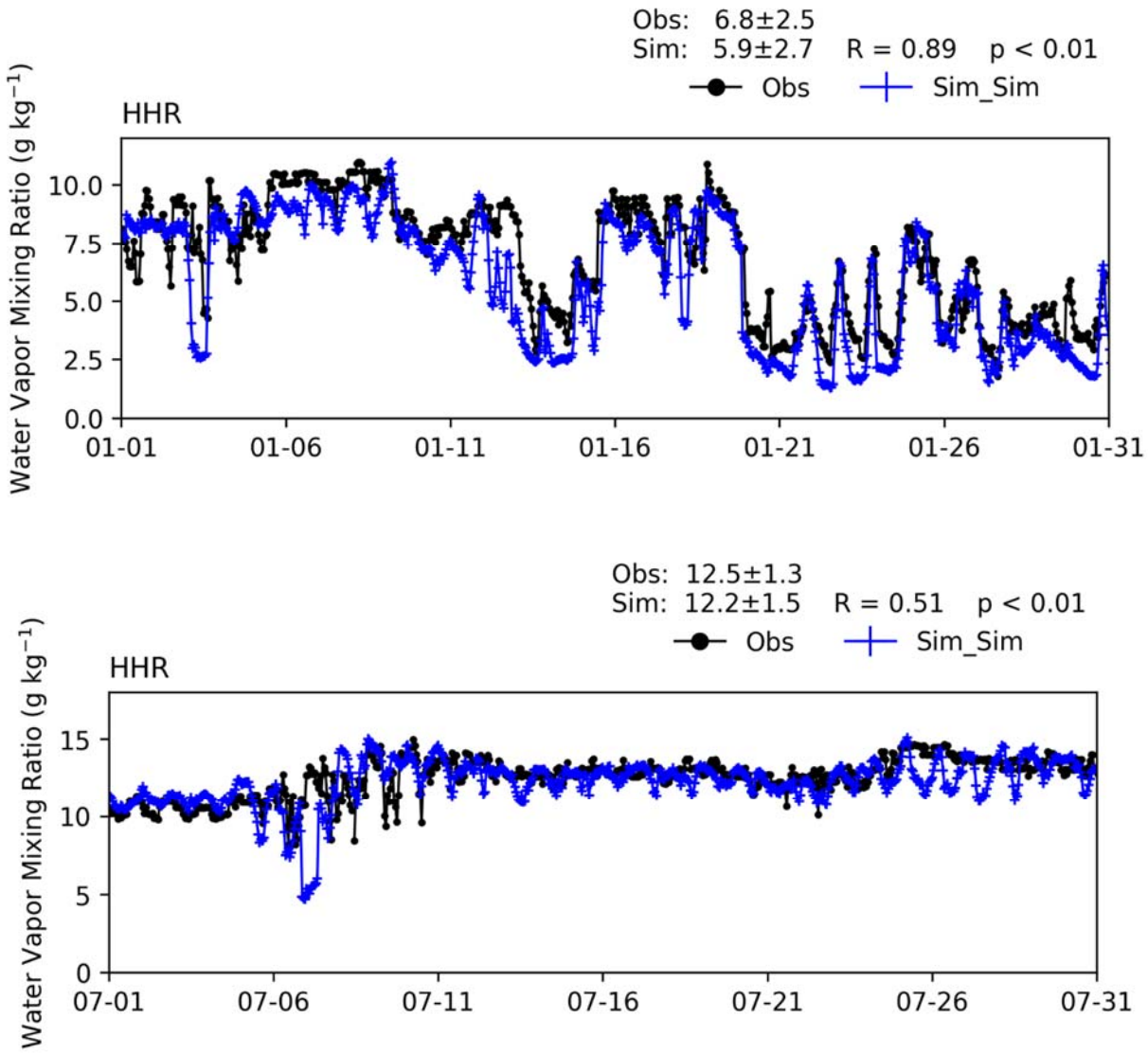

FIGURE V-3-15

TIME SERIES OF HOURLY WATER VAPOR MIXING RATIO FROM MEASUREMENTS AND WRF SIMULATIONS AT HAWTHORNE (HHR) STATION FOR JANUARY 2018 AND JULY 2018

Model Performance Evaluation: Diurnal Variations

Comparisons of simulated and measured monthly average diurnal temperature and water vapor mixing ratio variations at the Fullerton (FUL) station are shown in Figure V-3-16 and Figure V-3-17. Seasonal differences between summer and winter, as represented by July and January, respectively, and diurnal patterns were well reproduced in the WRF simulation. For example, daily temperatures in both observed and simulated diurnal profiles peaked around 14:00 local time during summer (~298 K) and winter (~292

K). Water vapor mixing ratios did not exhibit distinct diurnal variation in either observed or simulated data.

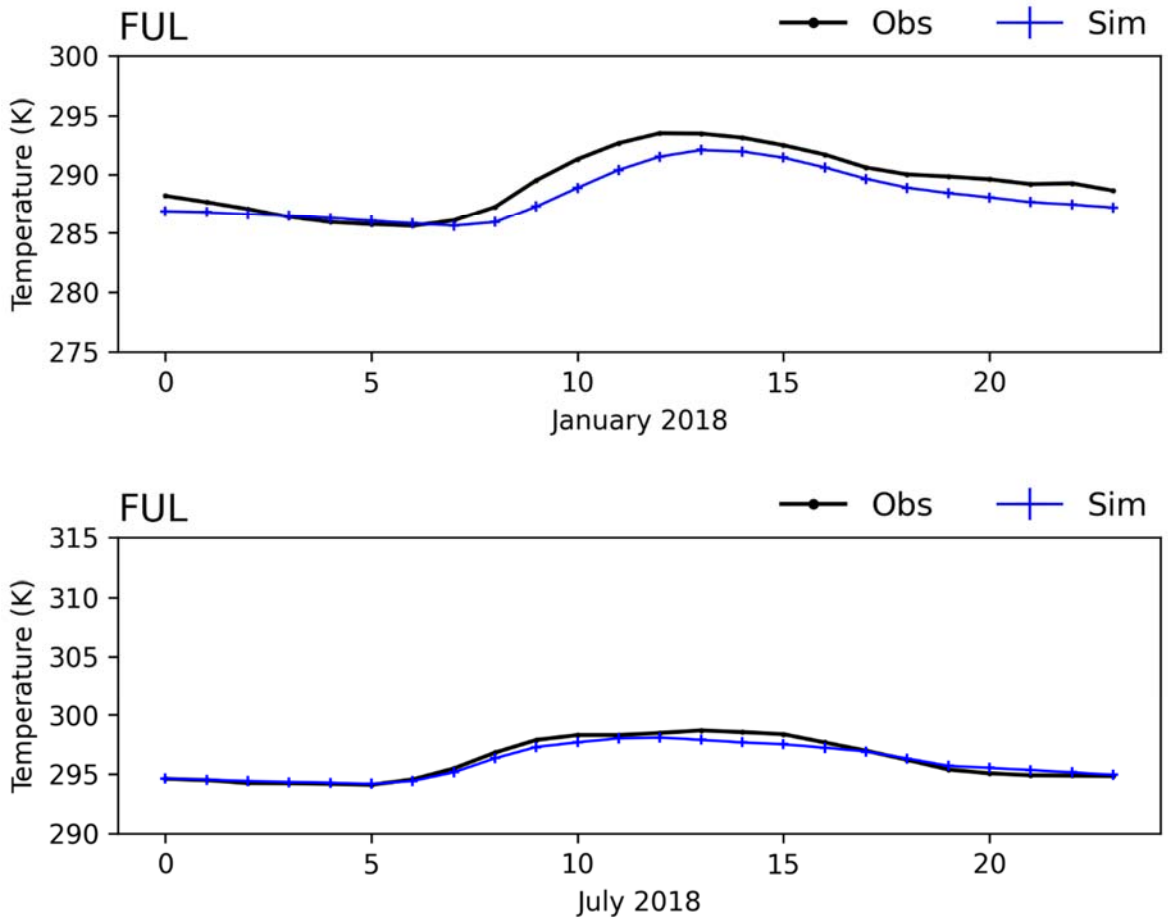

FIGURE V-3-16

MEASURED VS. SIMULATED COMPOSITE DIURNAL TEMPERATURE VARIATION AT FULLERTON (FUL) STATION FOR JULY 2018 AND JANUARY 2018

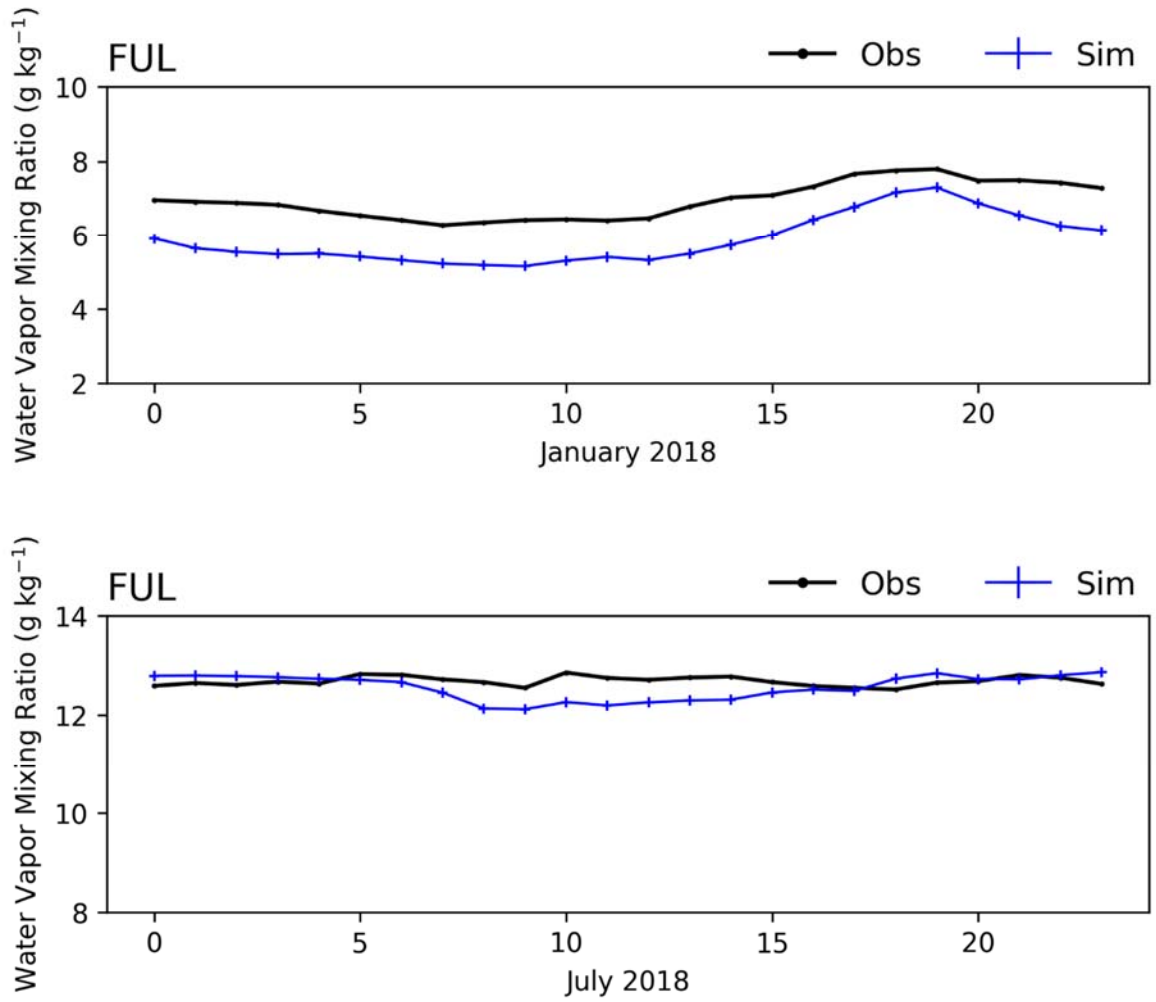

FIGURE V-3-17

WATER VAPOR MIXING RATIO AT FULLERTON (FUL) STATION FROM MEASUREMENTS AND WRF SIMULATIONS FOR JULY 2018 AND JANUARY 2018

Model Performance Evaluation: Wind Rose

The measured and WRF simulated wind rose at each station for 1-year period of January – December 2018 are shown in Figure V-3-18 – Figure V-3-22. Consistent with the sections above, HHR (near coastal areas), FUL (inland Orange County) and CNO (further east in San Bernardino County) a are presented. Another two stations: BUR (inland Los Angeles County) and ONT (San Bernardino County) are included as well to evaluate the model performance in further downwind areas. In general, the WRF simulations reproduce the dominant wind direction as the measurement at each station. For example, model and observations both show that westerly and south-westerly directions are the prevailing wind directions for the stations of CNO, FUL, HHR and ONT. The westerly or southwesterly flow is key to high ozone near the foothills. The wind direction is mostly from the southeast at the BUR station, as presented in both observations and

simulations. For the wind speed, among the five stations, the FUL and BUR stations have calm winds, mostly under 6 m/s, while other stations showed stronger wind between 6 - 8 m/s. In general, the WRF simulation underestimates the observed wind speed at HHR and ONT stations. Overall, WRF simulates surface wind speed and direction reasonably well as shown in the wind roses.

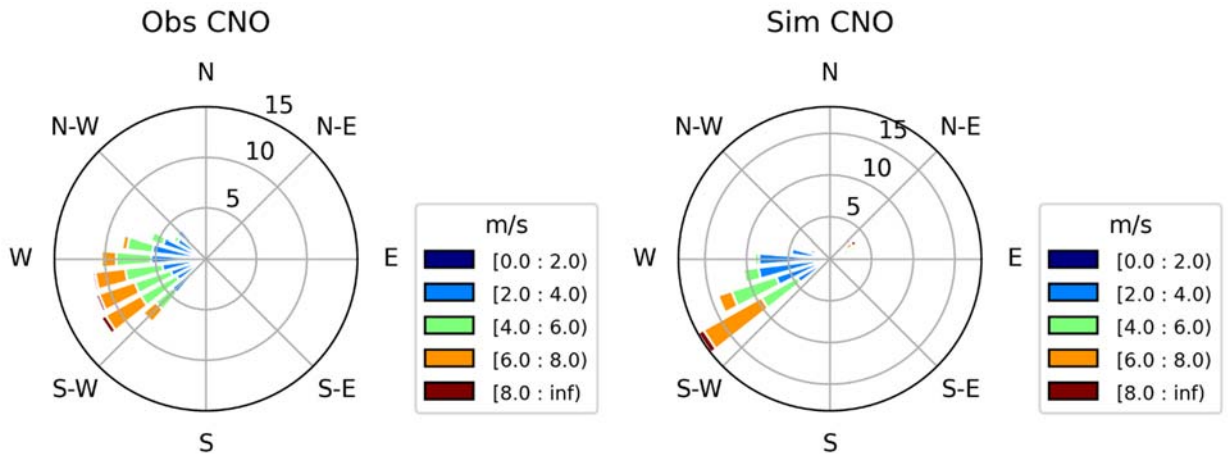

FIGURE V-3-18

WIND ROSE FROM MEASUREMENT AND WRF SIMULATION AT CHINO (CNO) STATION IN 2018

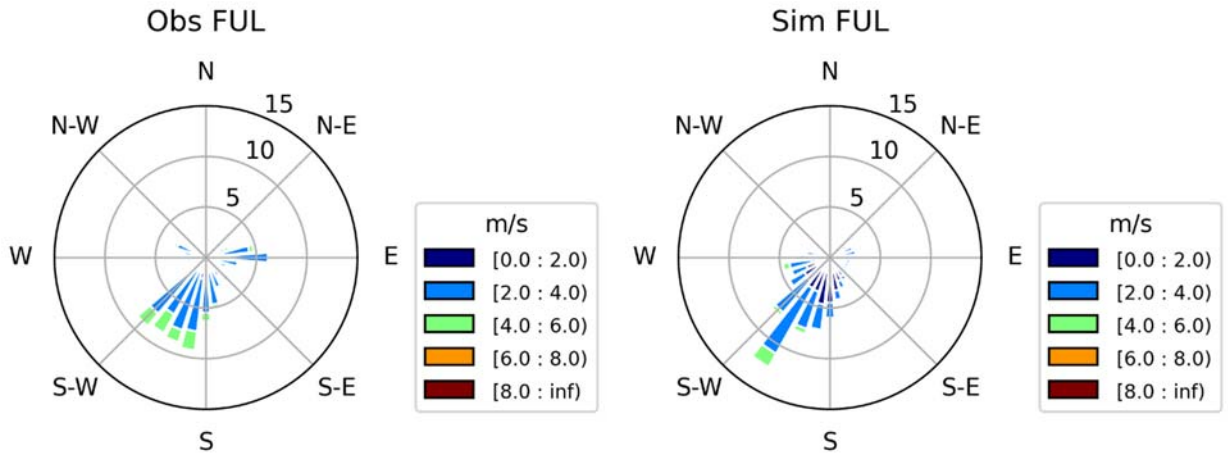

FIGURE V-3-19

WIND ROSE FROM MEASUREMENT AND WRF SIMULATION AT FULLERTON (FUL) STATION IN 2018

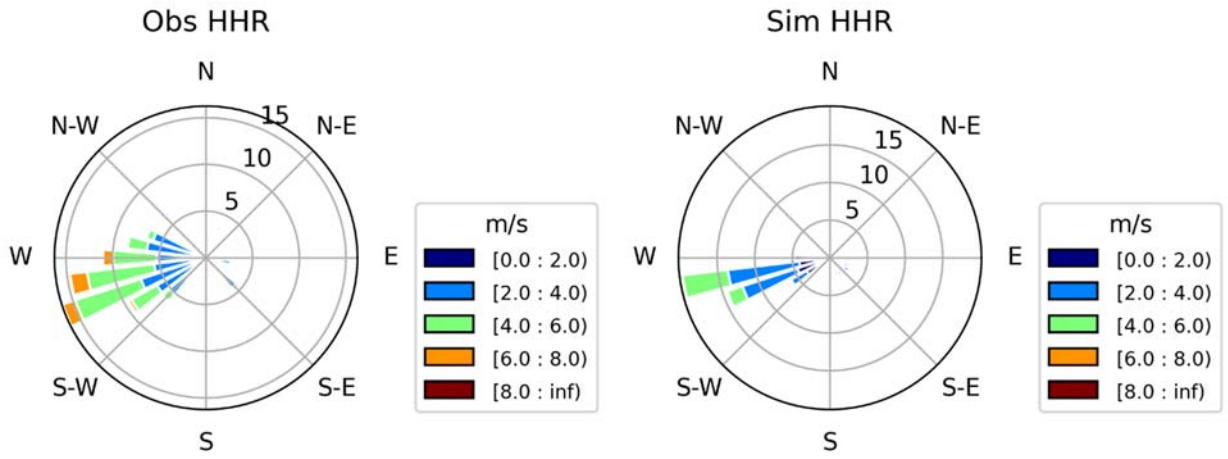

FIGURE V-3-20

WIND ROSE FROM MEASUREMENT AND WRF SIMULATION AT HAWTHORNE (HHR) STATION IN 2018

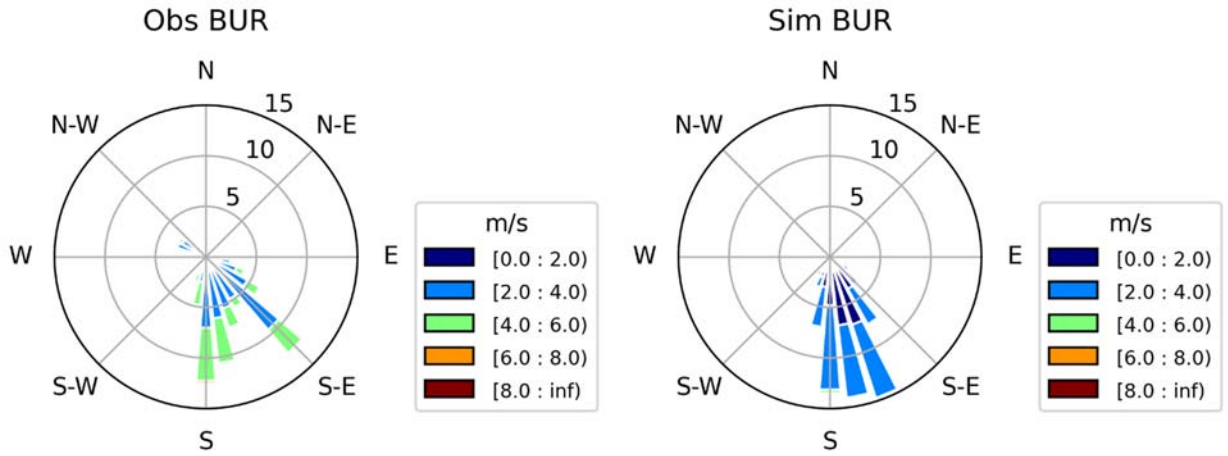

FIGURE V-3-21

WIND ROSE FROM MEASUREMENT AND WRF SIMULATION AT BURBANK (BUR) STATION IN 2018

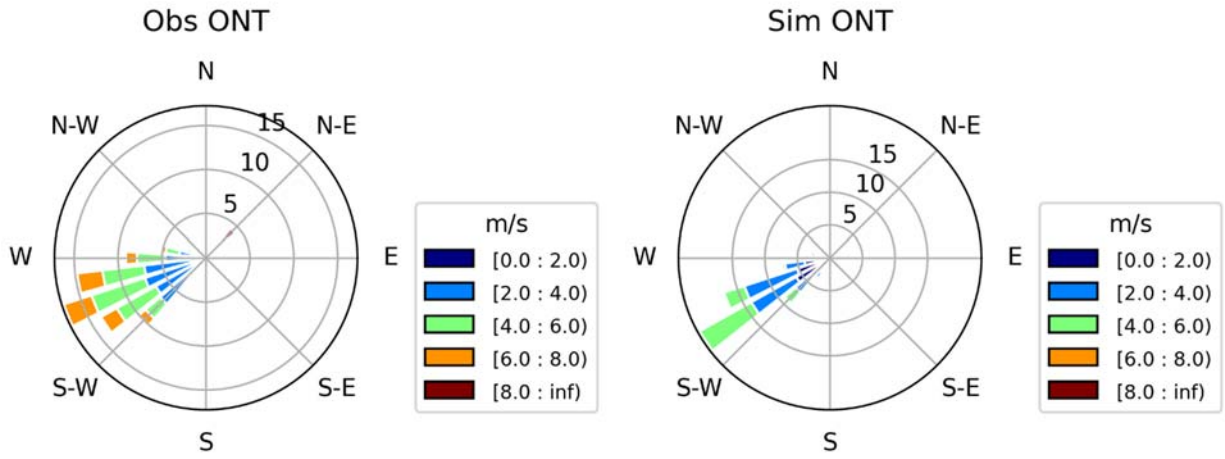

FIGURE V-3-22

WIND ROSE FROM MEASUREMENT AND WRF SIMULATION AT ONTARIO (ONT) STATION IN 2018

Model Performance: Planetary Boundary Layer Height

Time series of hourly PBLH from ceilometer measurements and WRF simulations at ONT and IRV during July 2018 are shown in Figure V-3-23. Simulated PBLHs generally showed good agreement with ceilometer derived PBLHs except for very high reported PBLH values (> 2 km). These very high PBLH measurements may have been measurements artifacts caused by cloud interference in ceilometer profiles. Time series of average PBLH diurnal variation from measurements and WRF simulations for the summer season (June-August 2018) at ONT and IRV are shown in Figure V-3-24. The diurnal cycle in PBL height was well captured by the simulations. For example, at ONT, both measured and simulated PBLHs were lowest (~200 m) during early morning, increased to maximum values of ~800m at midday due to stronger convection and vertical mixing, and then slowly decayed to lower heights during the late afternoon and early night.

Usually, the days with lower PBL height will lead to lower ventilation of air pollutions, and higher PBL height will help with dispersion of surface pollutions.

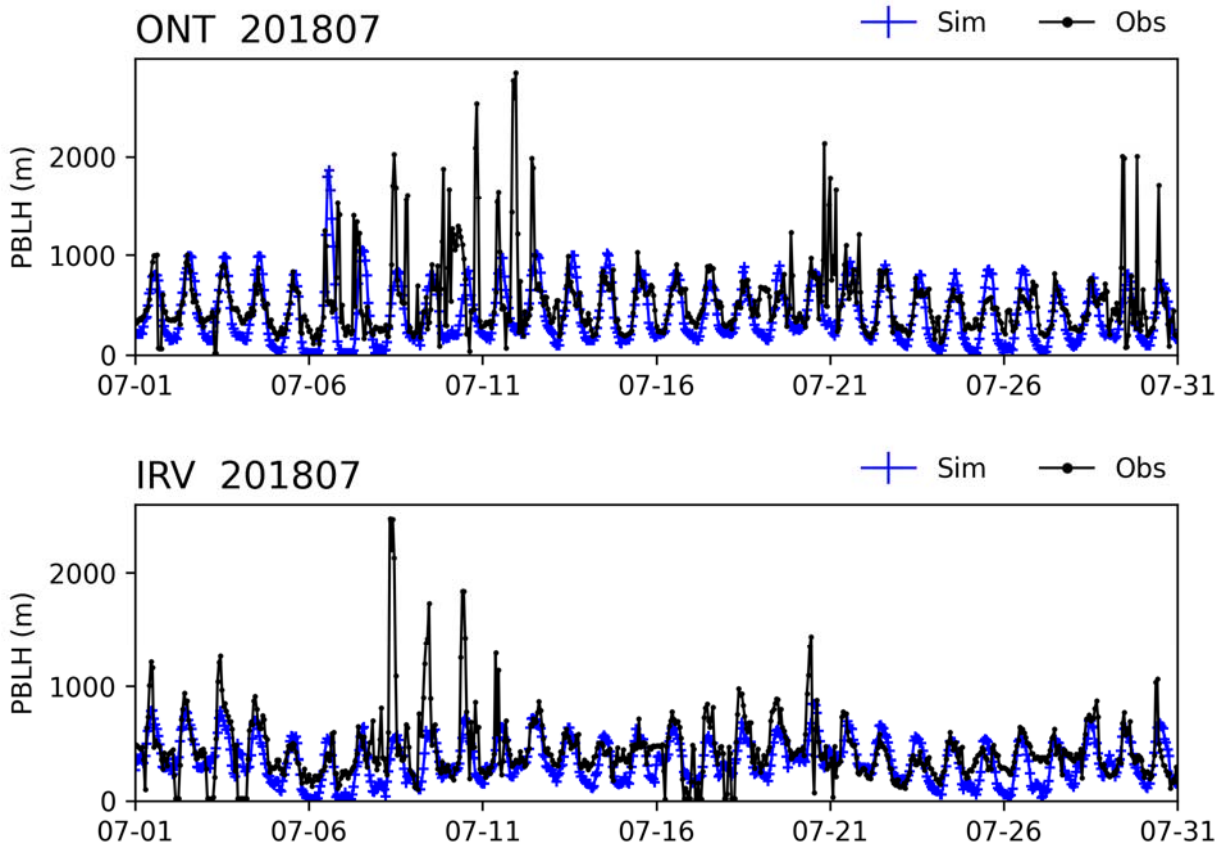

FIGURE V-3-23

TIME SERIES OF HOURLY PBLH FROM CEILOMETER MEASUREMENTS AND WRF SIMULATIONS FOR JULY 2018 AT ONTARIO (ONT) STATION AND AT IRVINE (IRV) STATION

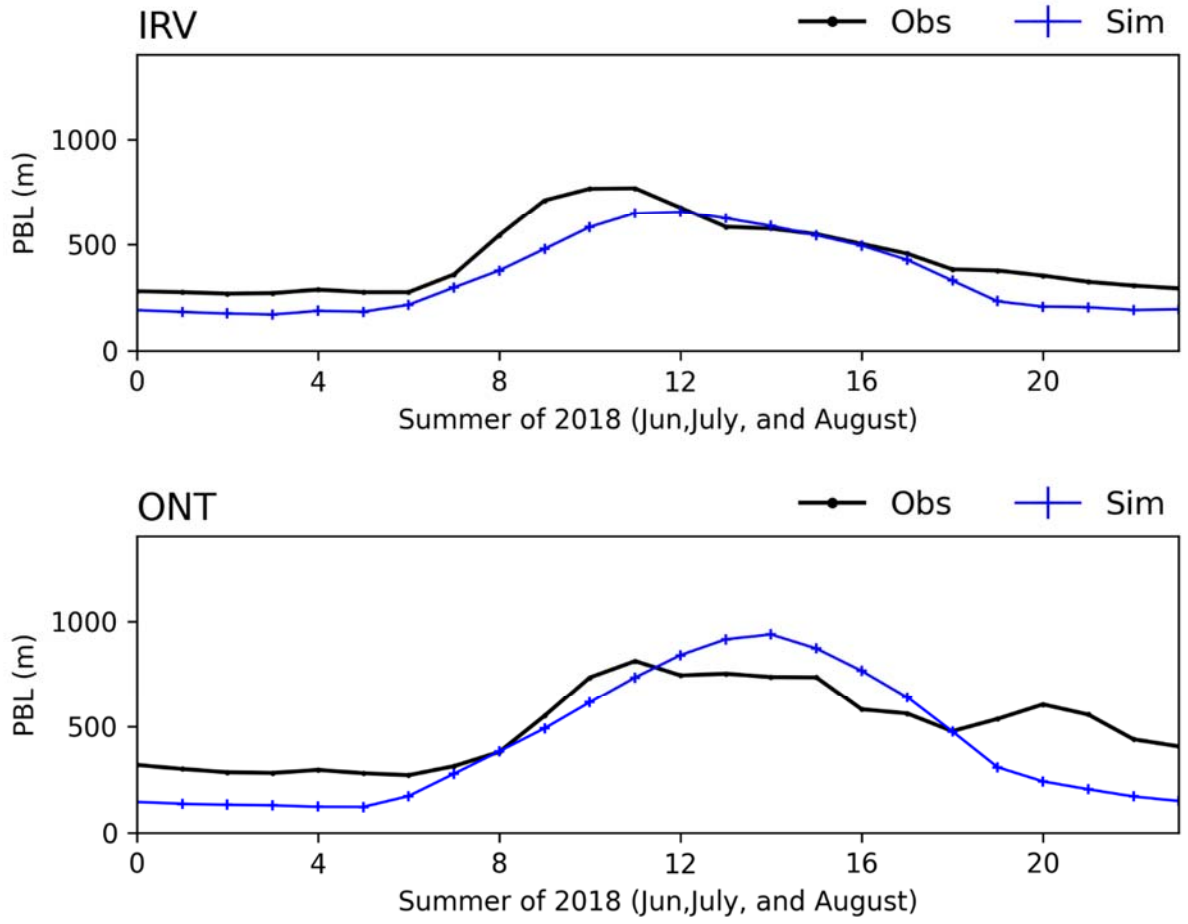

FIGURE V-3-24

TIME SERIES OF SEASONAL COMPOSED PBLH DIURNAL VARIATION FROM CEILOMETER MEASUREMENT AND WRF SIMULATIONS FOR SUMMER SEASON (JUNE-AUGUST 2018) AT ONTARIO (ONT) STATION AND IRVINE (IRV) STATION

Sensitivity Tests

Five sets of WRF sensitivity simulations were conducted, including 1) WRF simulation with Pleim-Xiu land surface scheme (Sim_PX), 2) WRF simulation with Urban canopy model, 3) WRF simulation with 35 vertical layers (Sim_35layers), 4) WRF simulation with 1km x 1km (Sim_1km) horizontal resolution, and 5) WRF v4.3. Comparing these sets of simulations, statistical results for temperature, water vapor and wind predictions were similar for both winter and summer seasons. Simulations with the Pleim-Xiu land surface scheme and urban canopy model showed slightly better performance for daily maximum temperature compared to other WRF simulations, while other WRF simulations had slightly better performance for wind speed. The sensitivity of WRF simulations to land surface features and numerical land surface schemes reflect the importance of land surface processes. Results of higher horizontal and vertical

resolution WRF simulations were generally consistent with the WRF base simulation with occasional marginal outperformance or underperformance. For future fine-scale emission inventories (e.g., 1 km or higher resolution), this evaluation of the WRF 1 km simulation provides a reliable framework for higher resolution meteorology simulations.

The performance of the WRF v4.0.3 and WRF v4.3 simulations for August 2018 are summarized in Table V-3-5. All results shown in Table V-3-5 are averaged values across the 15 airport stations. Overall, the results from WRF v4.0.3 and WRF v4.3 were very similar. Both WRF simulations provided representative meteorological fields that well characterized observed values in August 2018. Three stations were selected for surface level model performance evaluation: LAX, FUL, and CNO. They represent coastal climate, inland orange county, which frequently affected by transport from the ocean and inland climate, respectively. The observed temperature gradient from the near coastal station of LAX to the inland station of CNO was well captured by the two sets of WRF modeling. Monthly mean temperatures for August 2018 in WRF v4.0.3 and WRF v4.3 simulations were within 0.1 K at all three stations. The two sets of WRF simulations also generated similar hourly wind speeds at each station. Modeled monthly mean wind speeds at LAX (2.3 m s^{-1}) and CNO (4.1 m s^{-1}) were the same across the two simulations, while the difference between modeled monthly wind speeds at FUL was 0.1 m s^{-1}. Both WRF models predicted water vapor mixing ratio trends fairly well at all stations. The two simulations also yielded similar water vapor mixing ratio magnitudes for August 2018, with differences between simulated mean water vapor mixing ratios of 0.2, 0, and 0.1 kg/kg at CNO, FUL, and LAX stations, respectively. In all, the performance of WRF v4.0.3 is very similar to WRF v4.3 and WRF v4.0.3 was used as the primary model to generate meteorological fields for this AQMP.

TABLE V-3-5

WRF PERFORMANCE STATISTICS FOR THE MONTHLY AVERAGE OF AUGUST 2018 AT 15 NWS STATIONS

	WRF v4.0.3	WRF v4.3
2m Temperature Mean OBS (K)	296.4	296.4
2m Temperature Mean SIM (K)	298.4	298.5
2m Temperature Bias (K)	2	2.1
2m Temperature Gross Error (K)	2.8	2.8
2m Temperature RMSE (K)	3.8	3.8
Water vapor mixing ratio Mean OBS (kg/kg)	13.1	13.1
Water vapor mixing ratio Mean SIM (kg/kg)	11.8	11.8
Water vapor mixing ratio Bias (kg/kg)	-1.2	-1.3
Water vapor mixing ratio Gross Error (kg/kg)	1.8	1.9
Water vapor mixing ratio RMSE (kg/kg)	2.5	2.6
Wind Speed Mean OBS (m/s)	2.2	2.2
Wind Speed Mean PRD (m/s)	2.4	2.4
Wind Speed Bias (m/s)	0.3	0.2
Wind Speed Gross Error (m/s)	1.1	1.1
Wind Speed RMSE (m/s)	1.3	1.3

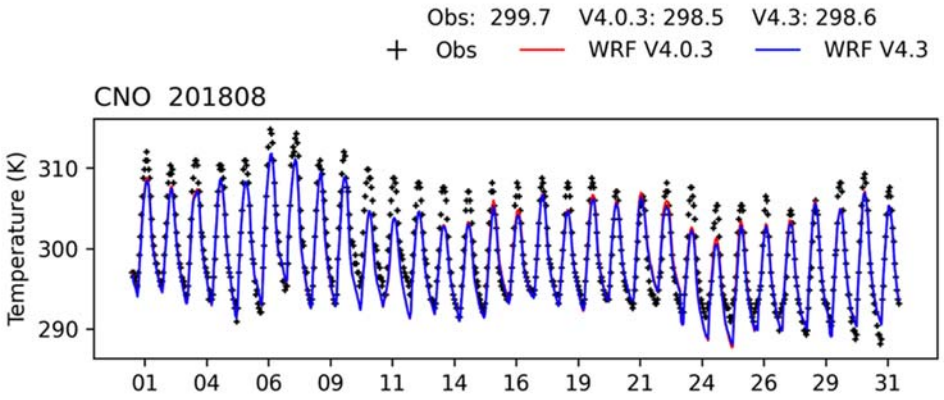

FIGURE V-3-25

TIME SERIES OF HOURLY TEMPERATURE FROM MEASUREMENTS AND WRF SIMULATIONS (V4.0.3 VS. V4.3) AT CHINO (CNO) STATION FOR AUGUST 2018

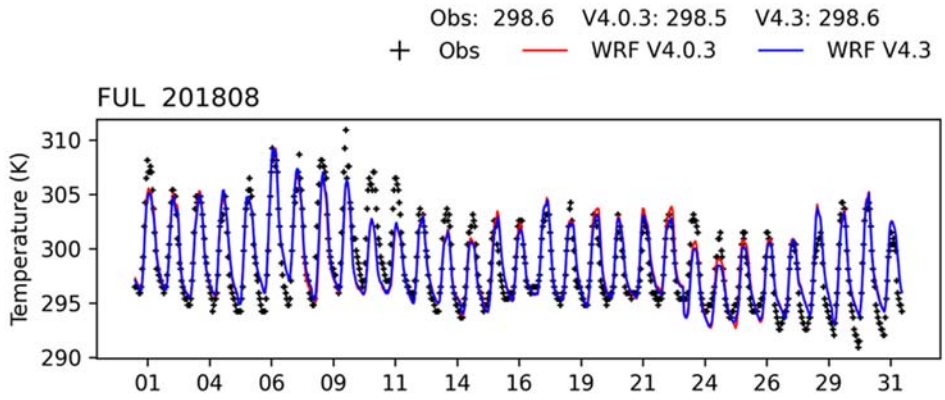

FIGURE V-3-26

TIME SERIES OF HOURLY TEMPERATURE FROM MEASUREMENTS AND WRF SIMULATIONS (V4.0.3 VS. V4.3) AT FULLERTON (FUL) STATION FOR AUGUST 2018

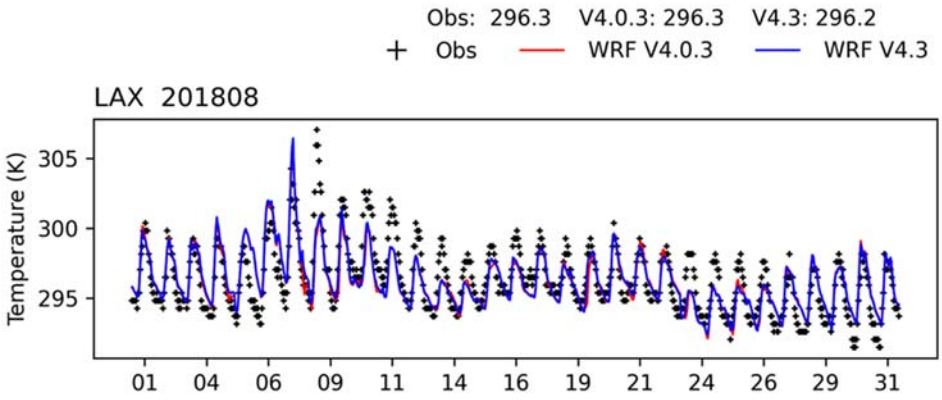

FIGURE V-3-27

TIME SERIES OF HOURLY TEMPERATURE FROM MEASUREMENTS AND WRF SIMULATIONS (V4.0.3 VS. V4.3) AT LOS ANGELES INTERNATIONAL AIRPORT (LAX) STATION FOR AUGUST 2018

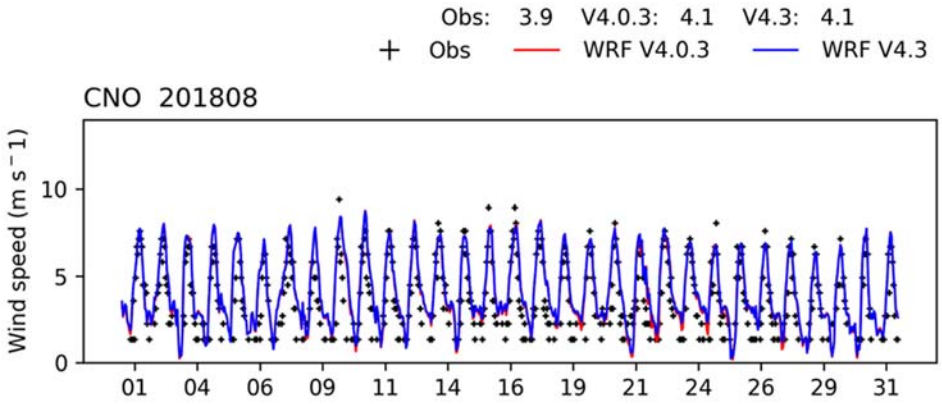

FIGURE V-3-28

TIME SERIES OF HOURLY WIND SPEED FROM MEASUREMENTS AND WRF SIMULATIONS (V4.0.3 VS. V4.3) AT CHINO (CNO) STATION FOR AUGUST 2018

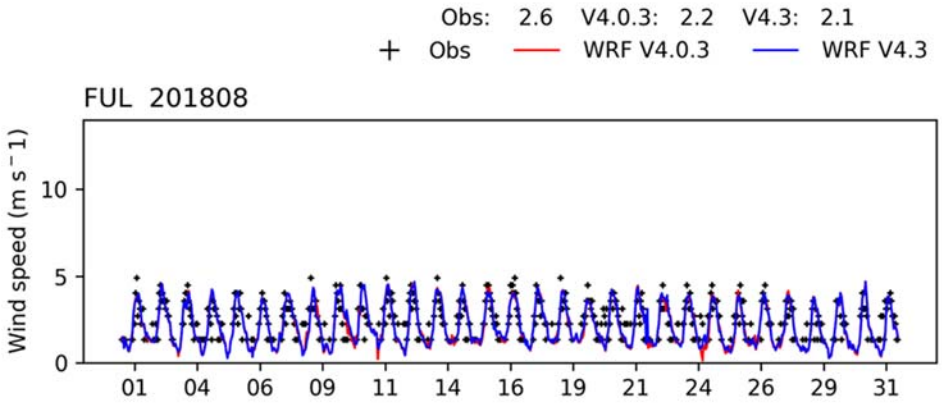

FIGURE V-3-29

TIME SERIES OF HOURLY WIND SPEED FROM MEASUREMENTS AND WRF SIMULATIONS (V4.0.3 VS. V4.3) AT FULLERTON (FUL) STATION FOR AUGUST 2018

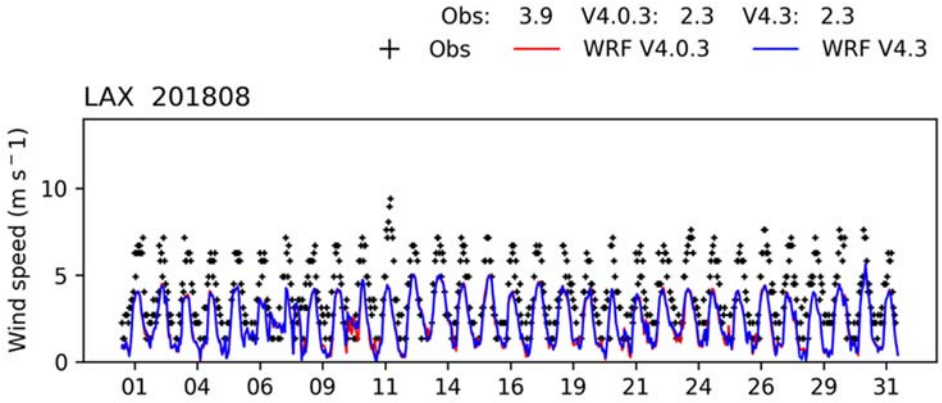

FIGURE V-3-30

TIME SERIES OF HOURLY WIND SPEED FROM MEASUREMENTS AND WRF SIMULATIONS (V4.0.3 VS. V4.3) AT LOS ANGELES INTERNATIONAL AIRPORT (LAX) STATION FOR AUGUST 2018

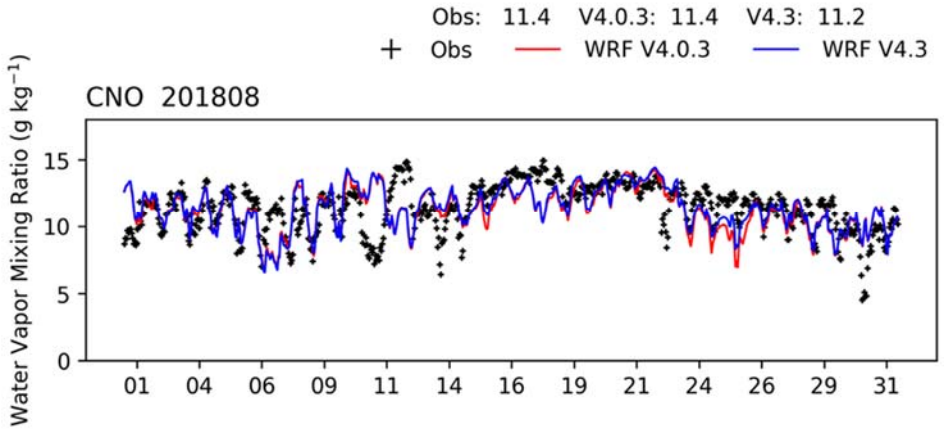

FIGURE V-3-31

TIME SERIES OF HOURLY WATER VAPOR MIXING RATIO FROM MEASUREMENTS AND WRF SIMULATIONS (V4.0.3 VS. V4.3) AT CHINO (CNO) STATION FOR AUGUST 2018

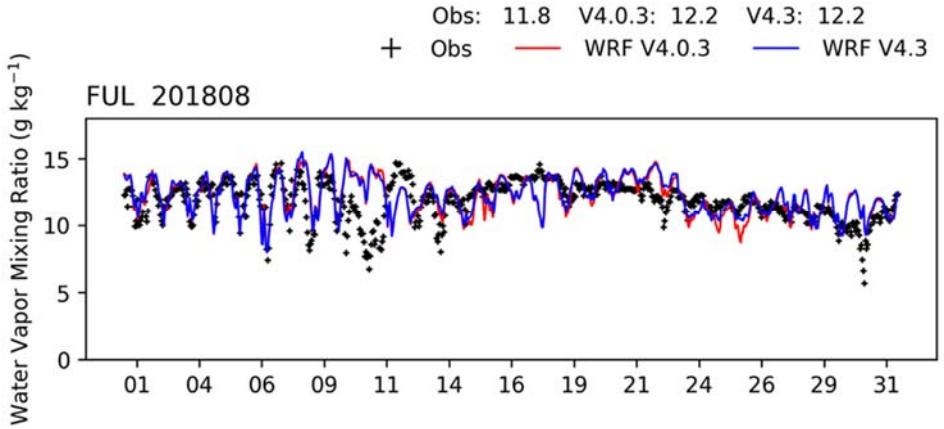

FIGURE V-3-32

TIME SERIES OF HOURLY WATER VAPOR MIXING RATIO FROM MEASUREMENTS AND WRF SIMULATIONS (V4.0.3 VS. V4.3) AT FULLERTON (FUL) STATION FOR AUGUST 2018

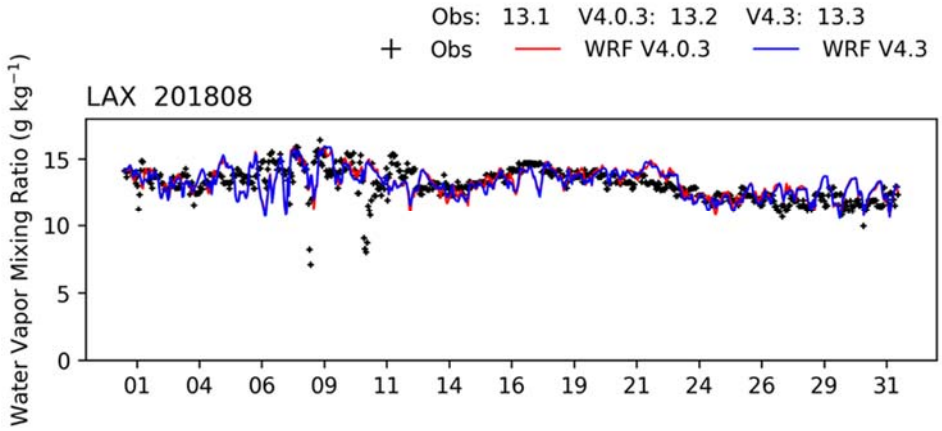

FIGURE V-3-33

TIME SERIES OF HOURLY WATER VAPOR MIXING RATIO FROM MEASUREMENTS AND WRF SIMULATIONS (V4.0.3 VS. V4.3) AT LOS ANGELES INTERNATIONAL AIRPORT (LAX) STATION FOR AUGUST 2018

References

Dudhia, J. (1989), Numerical study of convection observed during the winter monsoon experiment using a mesoscale two-dimensional model, J. Atmos. Sci, 46(20), 3077–3107, doi:10.1175/1520-046919890463C3077:NSOCOD3E2.0.CO;2. 16 682.

Hong, S.-Y., and H.-L. Pan (1996). Nonlocal boundary layer vertical diffusion in a medium-range forecast model. Mon. Wea. Rev., 124, 2322–2339, doi:10.1175/1520-0493

Kain, J.S. (2004). The Kain–Fritsch Convective Parameterization: An Update. J. Appl. Meteor., 43, 170–181.

Mlawer, E. J., S. J. Taubman, P. D. Brown, M. J. Iacono, and S. A. Clough (1997). Radiative transfer for inhomogeneous atmosphere: RRTM, a validated correlated-k model for the longwave. J. Geophys. Res., 102 (D14), 16 663 - 16 682.

Skamarock, W. C., J. B. Klemp, J. Dudhia, D. O. Gill, Z. Liu, J. Berner, W. Wang, J. G. Powers, M. G. Duda, D. M. Barker, and X.-Y. Huang (2019). A Description of the Advanced Research WRF Version 4. NCAR Tech. Note NCAR/TN-556+STR, 145 pp. doi:10.5065/1dfh-6p97

CHAPTER 4

MODELING EMISSIONS, BOUNDARY CONDITIONS, AND INITIAL CONDITIONS

Modeling Emissions Inventory

Table V-4-1 provides the summer planning baseline and controlled modeling emissions inventories that are consistent with the emissions used in the attainment demonstration and alternative analyses. The CMAQ simulations were based on the annual emissions inventory, with adjustments made for source-specific temporal profiles and daily temperature variations. An extensive discussion of the overall emissions inventory is provided in Appendix III. Approaches used in generating gridded hourly emissions for each modeling day are presented in this Chapter.

TABLE V-4-1

SUMMER PLANNING ANTHROPOGENIC EMISSIONS INVENTORY IN SOUTH COAST AIR BASIN (TONS/DAY)

	Summer Planning	
Year	VOC	NOX
(a) Baseline		
2018	406	351
2032	345	199
2037	339	184
(b) Controlled[1]		
2032	338	153
2037[2]	321	60

[1]Reflecting SCAG's 2020 RTP/SCS and implementation of the control measures relative to future baseline emissions

[2]Controlled emissions in 2037 include a SIP set-aside account of 4 tons per VOC and 0.5 tons per day NOx

Inventory Profile

Baseline modeling inventories for the base year 2018 and future years 2032 and 2037 are discussed in this section. The 2022 AQMP focuses on the attainment demonstration of the 2015 8-hour ozone National Ambient Air Quality Standard (NAAQS), 70 ppb and focuses on summer season (May 1st to September 30th) to capture high ozone episodes. The baseline emissions projection assumes no emission controls beyond already adopted measures and programs. These projections reflect the emissions resulting from increases in population and vehicle miles traveled (VMT), as well as the implementation of all adopted rules and regulations. The cut-off date for South Coast AQMD regulations is October 2020 (except Rule 1109.1 which was adopted in November 2021) and for CARB's regulations the cut-off date is December

2021. The controlled emission projections reflect the benefits of implementation of the control measures relative to future baseline emissions. Detailed descriptions of the control measures are provided in Chapter 4 and Appendix IV of the 2022 AQMP. Appendix III contains emission summary reports by source category for the base year and future baseline scenarios used in this modeling analysis. Attachment 3 of Appendix V contains detailed emissions reductions summaries by source category for the future (2032 and 2037) controlled scenarios.

Temporal and Spatial Allocations of Emissions

Day-specific point, mobile and area emissions inventories were generated for 153 days in the 2018 base year. On-road mobile source emissions were generated based on information from SCAG transportation modeling, CARB's EMFAC 2017 emissions rates, observed daily traffic variations and modeled daily temperatures.

Annual emissions are distributed into day-specific hourly emissions through using temporal profiles. For each source type, profiles for monthly throughputs, day of week variations and diurnal changes are assigned. Spatial allocations of point source emissions are according to physical locations of emitting facilities while countywide emissions (area and off-road sources) are distributed through spatial surrogates. Over 110 spatial surrogates were used in distributing area and off-road source emissions. The surrogates were developed by CARB and undergo revision during each AQMP development process. Each emissions source (by Emission Inventory Code) is assigned a surrogate profile. Example surrogates include gas stations, landfills, military bases, single family homes, and railyards. As in past AQMPs, base and future year socioeconomic data, information such as population, employment, and housing, developed by SCAG during its RTP/SCS process, were incorporated into the surrogates. The allocation of emissions from on-road vehicles, ocean-going vessels (OGV) and aircraft was performed using separate methods that are discussed below.

On-road Mobile Emissions

On-road mobile sources are responsible for a large fraction of the total VOC, NOx, and CO emissions in the modeling domain. These emission sources are highly dependent on time and location with variations up to a factor of 8 between overnight and peak traffic hours at a specific location. On-road mobile emission patterns vary significantly throughout the week and year since traffic flows are affected by special events, holidays, and weather. This variation may also be location-dependent as emissions are a function of the proximity to high-employment areas, sporting events, or seasonal activities.

Real-time traffic flow measurements from 2018 were used to apportion traffic volumes on an hourly basis throughout the five counties: Ventura, Los Angeles, Orange, Riverside and San Bernardino. Light- and heavy-duty vehicle flow data are measured at thousands of sensors throughout the Basin. Due to of the sparsity of monitoring data in the five outlying counties, San Luis Obispo, Santa Barbara, Kern, Imperial and San Diego, grid-based on-road emissions in those counties were created with generic traffic profiles that vary by day of week.

Light and medium duty vehicle emissions were distributed using the Emissions Spatial and Temporal Allocator (ESTA) with traffic profiles determined using data from the California Department of Transportation Performance Measurement System (PeMS).[1] While ESTA uses generic traffic profiles by default, the PeMS data can be used to replace the default profiles through accurate measurements of traffic volumes. The PeMS network collects traffic data at over 9,000 sensor locations within the Basin on a real-time basis at 5-minute time resolution, providing traffic profiles that reflect societal events, weather conditions, and cultural behavior. As seen in Figure V-4-1, application of the PeMS profiles resulted in a small (<1%) increase in NOx emissions during the week, but a larger (~9%) increase on weekends compared to the ESTA default profiles. The increased emissions on weekends are due to the normalization in ESTA being applied to the average of the Tuesday-Thursday traffic profiles. Additionally, weekend traffic volumes in the PeMS profiles are higher than those in the default ESTA profiles. Figure V-4-2 presents the hourly profiles during a week averaged for the entire year and shows that the hourly profiles from PeMS differ slightly from the profiles based on ESTA defaults. During weekdays, PeMS data places more emissions in the early morning and late-night hours, and less emissions during the peak hours. During weekends, the PeMS profile shows overall higher emissions than the default profiles.

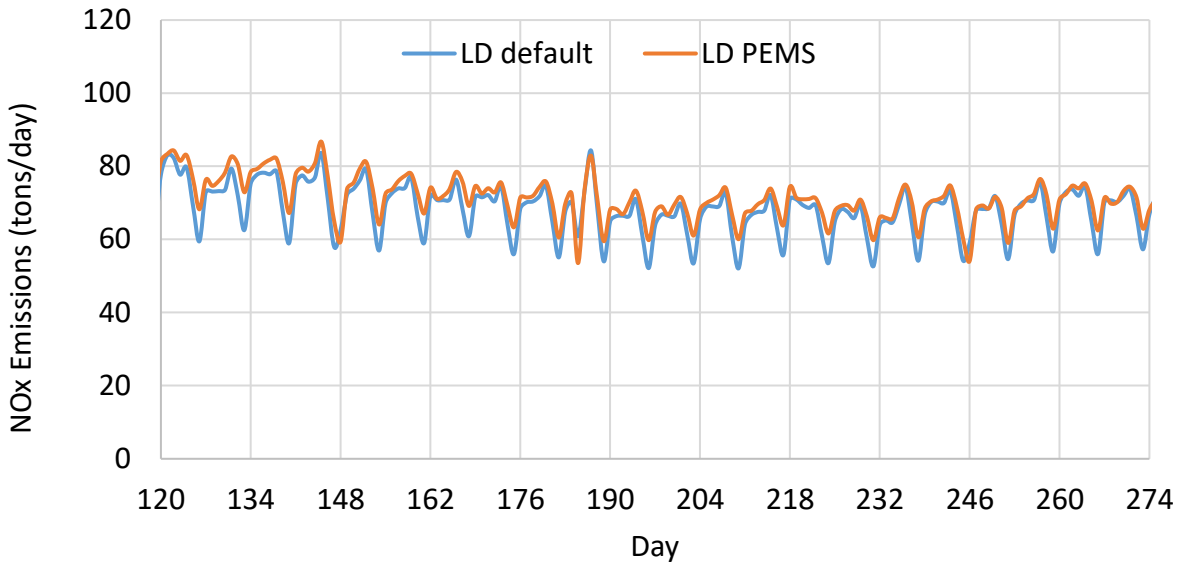

FIGURE-V-4-1

COMPARISON OF THE ESTA DEFAULT AND ESTA/PEMS METHODS FOR THE BASIN LIGHT-DUTY VEHICLE NOx EMISSIONS DURING MAY-SEPTEMBER.

[1] Emissions Spatial and Temporal Allocator. https://github.com/mmb-carb/ESTA
Caltrans Performance Measurement System. https://pems.dot.ca.gov/

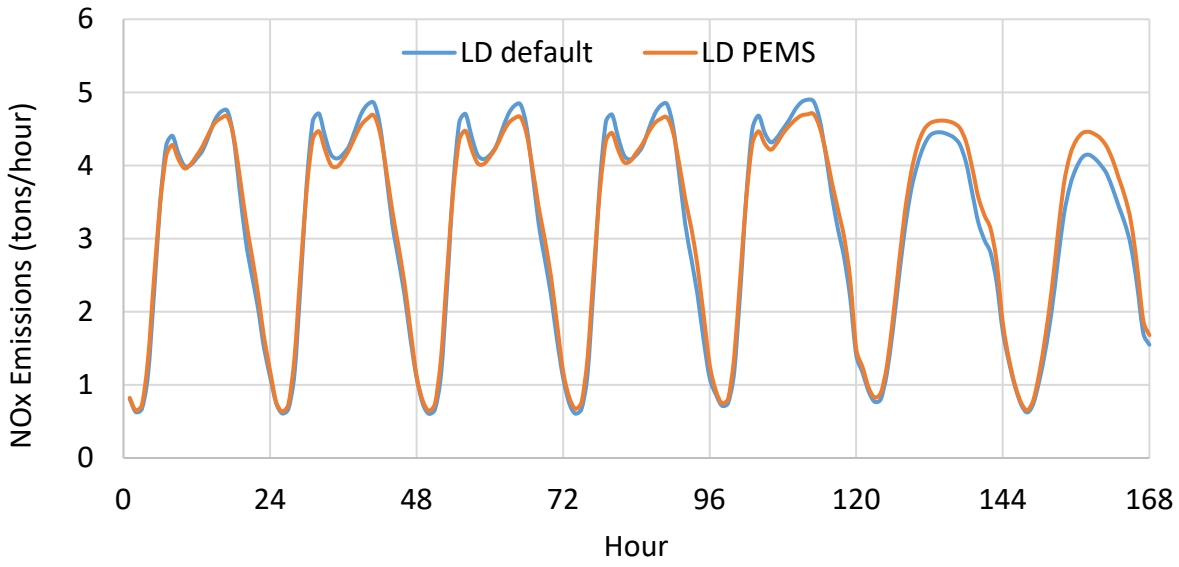

FIGURE V-4-2

A COMPARISON OF THE DEFAULT ESTA AND PEMS AVERAGE HOURLY PROFILES IN A WEEK FOR LIGHT-DUTY VEHICLES AVERAGED FOR THE ENTIRE YEAR.

Heavy-duty vehicle emissions were similarly distributed by ESTA and PeMS, using the Tuesday-Thursday average traffic flows for normalization. The heavy-duty traffic flows were derived from the same sensor network used in the light-duty analysis, with an algorithm applied to differentiate vehicle class (Kwon et al., 2003). This differed from the approach used in the 2016 AQMP which relied on a sparse network of Weight-in-Motion sensors for the heavy-duty flows. As in the case of light- and medium-duty vehicles, the heavy-duty PeMS profiles demonstrated substantially greater traffic volumes on weekends compared to the ESTA default profiles. As shown in Figure V-4-3, the PeMS profile distributes approximately 20 tons per day additional NOx emissions on weekends with respect to default profiles. As shown in Figure V-4-4, the PeMS diurnal profiles consistently demonstrated greater amplitudes compared to the default ESTA profiles.

The total on-road emissions of NOx and VOC in the Basin are shown in Figure V-4-5 and on-road emissions in the Coachella Valley are shown in Figure V-4-6.

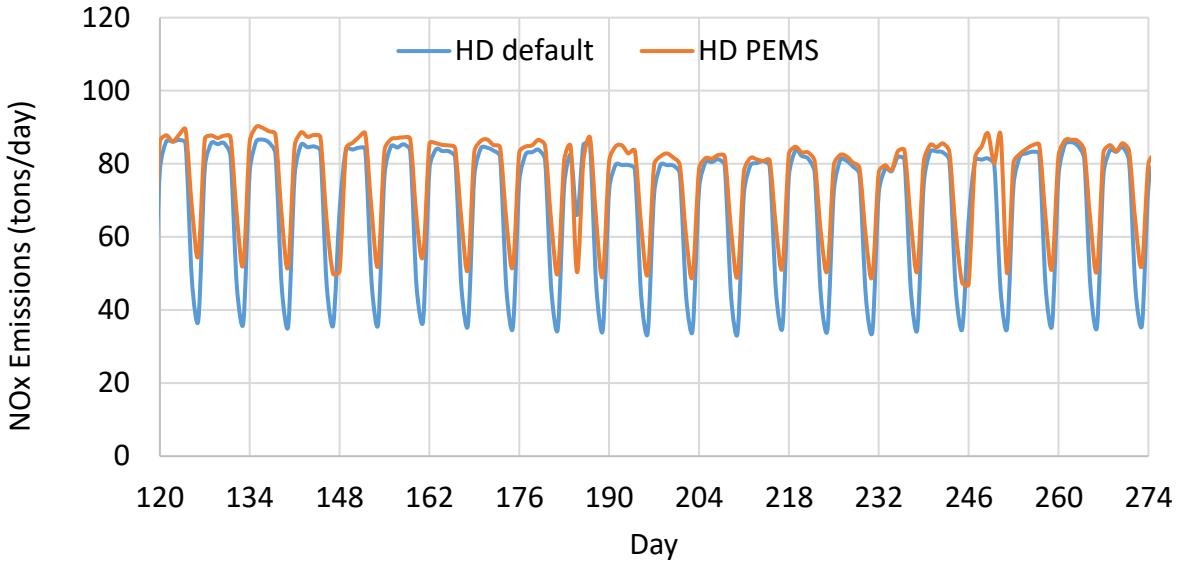

FIGURE V-4-3

SUMMER COMPARISON OF HEAVY-DUTY NOX EMISSIONS IN THE BASIN FROM THE DEFAULT ESTA AND PEMS PROFILES.

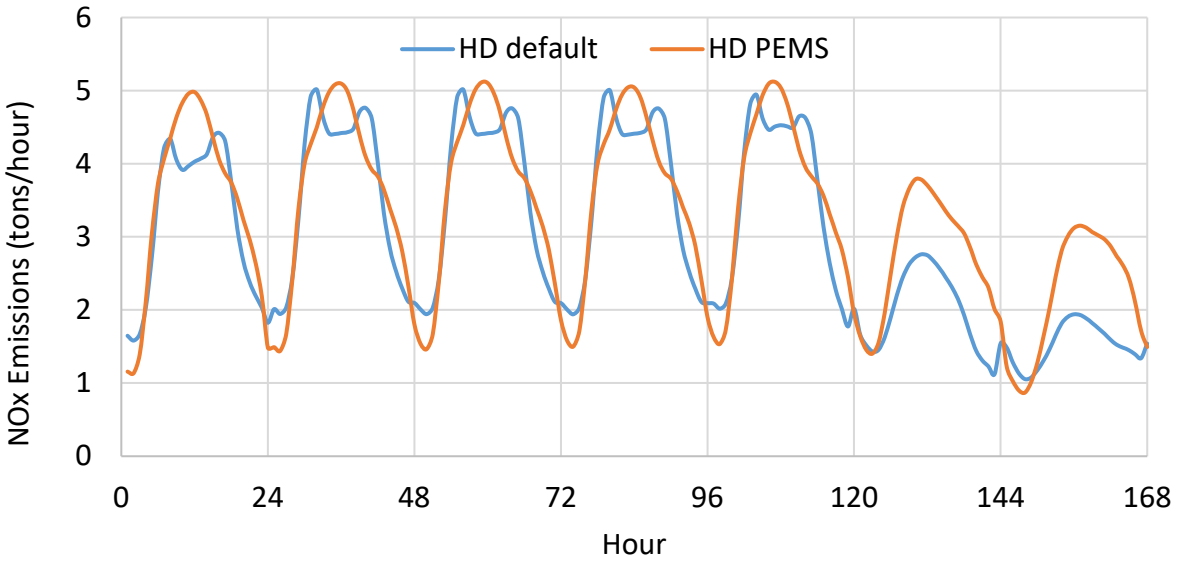

FIGURE V-4-4

A COMPARISON OF THE DEFAULT ESTA AND PEMS AVERAGE HOURLY PROFILES IN A WEEK FOR HEAVY-DUTY VEHICLES AVERAGED FOR THE ENTIRE YEAR.

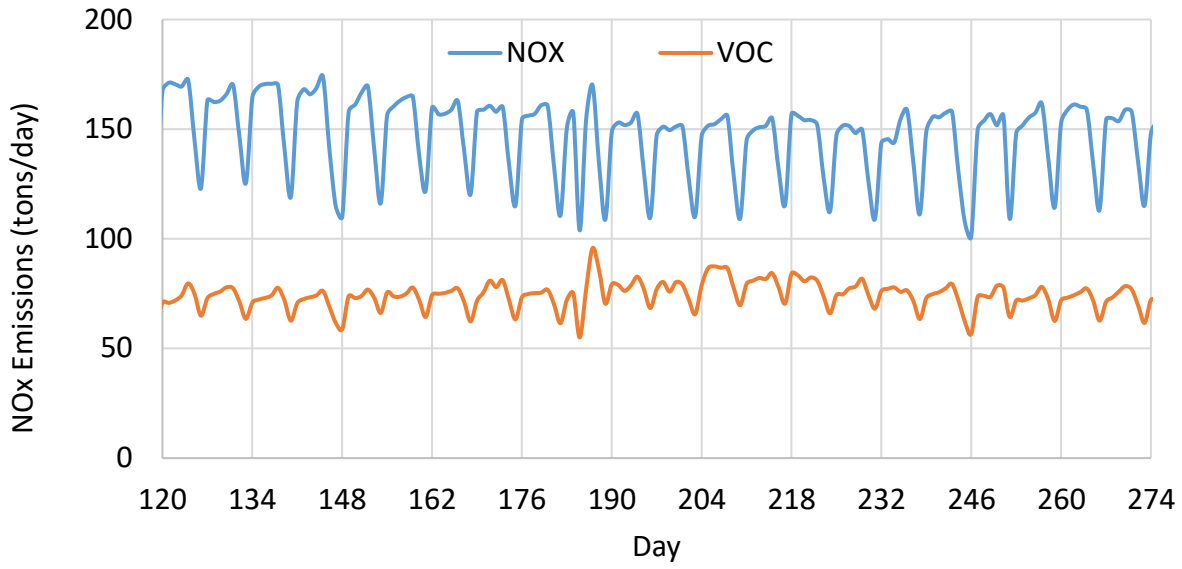

FIGURE V-4-5

SUMMER 2018 DAILY ON-ROAD NOx AND VOC EMISSIONS IN THE BASIN USED IN THE CMAQ MODELING.

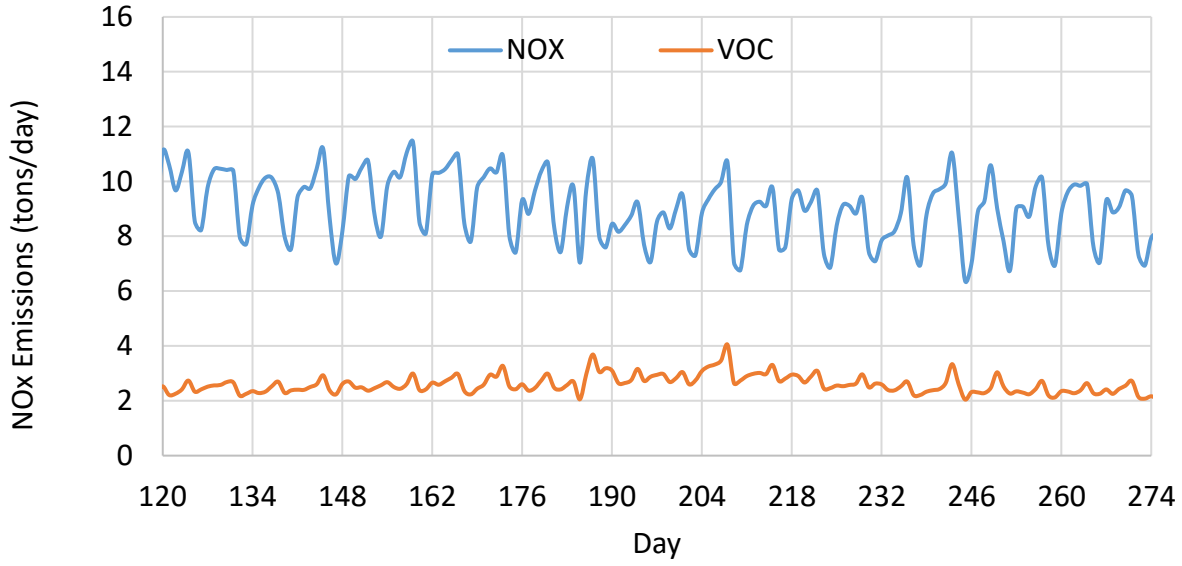

FIGURE V-4-6

SUMMER 2018 DAILY ON-ROAD NOx AND VOC EMISSIONS IN THE COACHELLA VALLEY USED IN THE CMAQ MODELING.

Ocean-Going Vessels

Data captured from the Automated Identification System (AIS) was used to allocate OGV emissions. AIS is a maritime transponder-based technology that is used to communicate vessel location, heading, speed, and operational mode. Spatial allocation factors for four vessel types and operational modes were developed using the AIS data (see Table V-4-2). Initially, day and hour-specific factors were generated; however, this produced large fluctuations in the emissions that were inconsistent with expected emission trends based on container throughput at the ports. Therefore, the allocation factors were averaged on an annual basis, thereby eliminating temporal variation. Application of the factors to the emissions inventory produced the spatial distribution displayed in Figure V-4-7. Note the logarithmic scale in this figure. While the main shipping channels are evident, the primary benefit of the AIS approach is the ability to resolve less traveled routes that have orders of magnitude lower emissions. Since these routes were previously unresolved, the AIS allocation method increased the spatial accuracy of the modeling emissions.

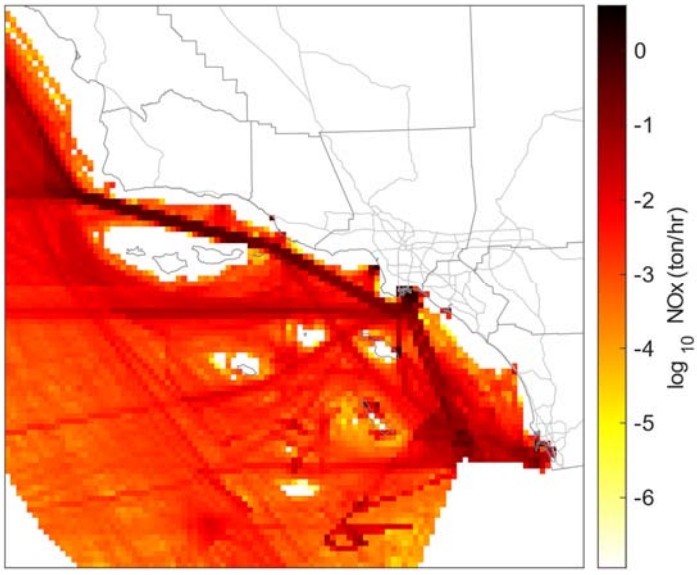

FIGURE V-4-7

SPATIAL DISTRIBUTION OF OGV NOX EMISSIONS FOLLOWING APPLICATION OF THE AIS SURROGATES.

TABLE V-4-2

VESSEL TYPES AND OPERATIONAL MODES USED TO DEVELOP SPATIAL SURROGATES.

Vessel Type	Operational Mode
Cargo Military Passenger Tanker	Transit: A vessel in motion outside of port bounds Maneuvering: A vessel in motion inside of port bounds Hoteling: A vessel at berth Anchorage: A vessel stopped outside of port bounds

Aircraft

Aircraft emissions were allocated to the modeling domain according to different methods depending on the airport type. Aircraft emissions at small general aviation airports were allocated by using the California Air Resources Board's Gridded Aircraft Trajectory Emissions (GATE) model.[2] GATE computes linear takeoff and landing trajectories at each airport and then intersects those trajectories with the modeling grid. Aircraft emissions at commercial airports were first calculated using FAA's Aviation Environmental Design Tool (AEDT).[3] AEDT resolves emissions into four vertical layers: ground level, below 1,000 feet, below mixing height, and below 10,000 feet. The mixing height corresponds to an annual average, airport-specific value assigned in AEDT. Above ground level, multiple CMAQ modeling layers exist between the AEDT layers. Thus, emissions were distributed among the corresponding modeling layers. Due to nonuniform layer thickness, emissions were weighted by the thickness of each layer. Emissions were then spatially allocated within each layer based on data derived from the Aircraft Communication Addressing and Reporting System (ACARS), a transponder system that operates on many commercial aircraft. The ACARS data stream contains aircraft latitude, longitude, and altitude. Allocation factors were developed by isolating the ACARS pings within each layer and calculating the share of the total pings within each grid cell. These factors were then multiplied by the total layer emissions to derive the spatially distributed emissions. As seen in Figures V-4-8 through V-4-9 for Los Angeles International Airport, both the vertical and horizontal emissions distribution differs significantly from the default (point/inline) profile. The default profile assumes that all emissions occur aloft in a single grid cell. This is clearly inaccurate as AEDT calculates significant ground level emissions corresponding to auxiliary power unit usage, taxiing, and takeoff and landing. The accuracy is further improved by the spatial distribution, which more accurately represents takeoff and landing trajectories at the airport.

[2] Gridded Aircraft Trajectory Emissions. https://github.com/mmb-carb/GATE_Documentation
[3] Aviation Environmental Design Tool. https://aedt.faa.gov/

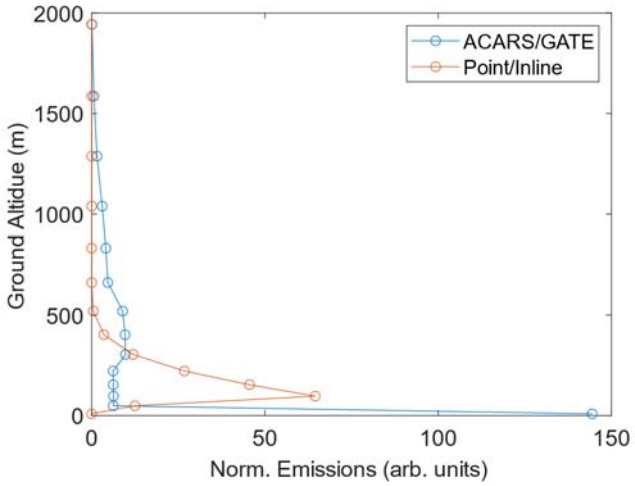

FIGURE V-4-8

COMPARISON OF THE VERTICAL PROFILE OF AIRCRAFT NOX EMISSIONS WITHIN A 5X5 GRID CELL BOX AROUND LAX.

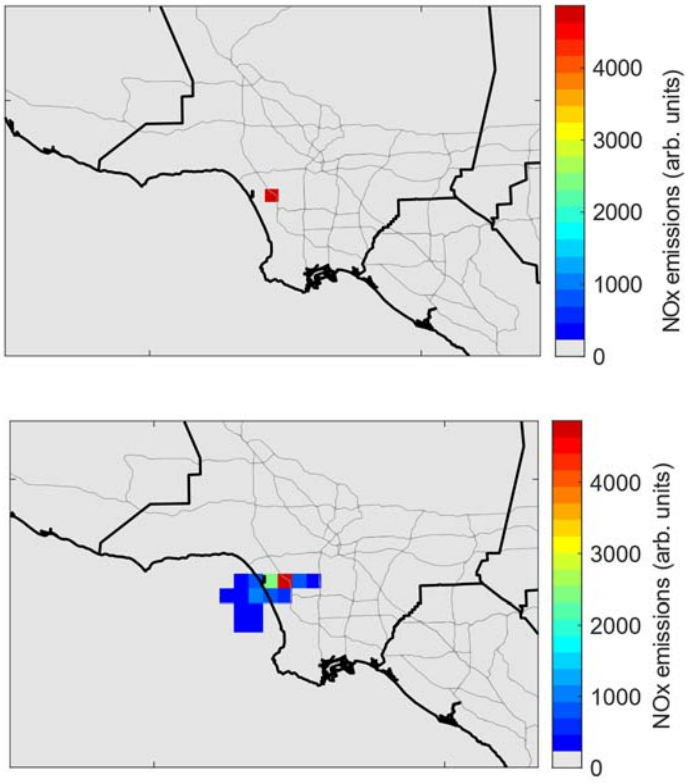

FIGURE V-4-9

VERTICALLY COLLAPSED AIRCRAFT NOx EMISSIONS WITHIN A 9X9 GRID CELL BOX CENTERED AT LAX FOR THE POINT/INLINE METHOD (TOP) AND ACARS METHOD (BOTTOM).

Effect of Emissions Allocation Methods on Ozone

The on-road PeMS, OGV AIS-based, and GATE/ACARS aircraft adjustments to the modeling emissions were evaluated based on the perturbation to the top 10 days 8-hour ozone at each station. The adjustments were analyzed separately and compared to the baseline which allocated emissions based on prescribed profiles and surrogates. The results are summarized in Figure V-4-10 and displayed in detail in Figure V-4-11. While the response varied across SCAB, the largest impact overall was observed when the GATE/ACARS aircraft emissions were used. This is primarily because the GATE/ACARS method allocated much higher emissions to modeling layer 1 compared to the default point/inline method. The on-road PeMS and OGV AIS-based adjustments produced average ozone perturbations with opposing signs. Additionally, the magnitude of the response to these changes was smaller than that observed for aircraft.

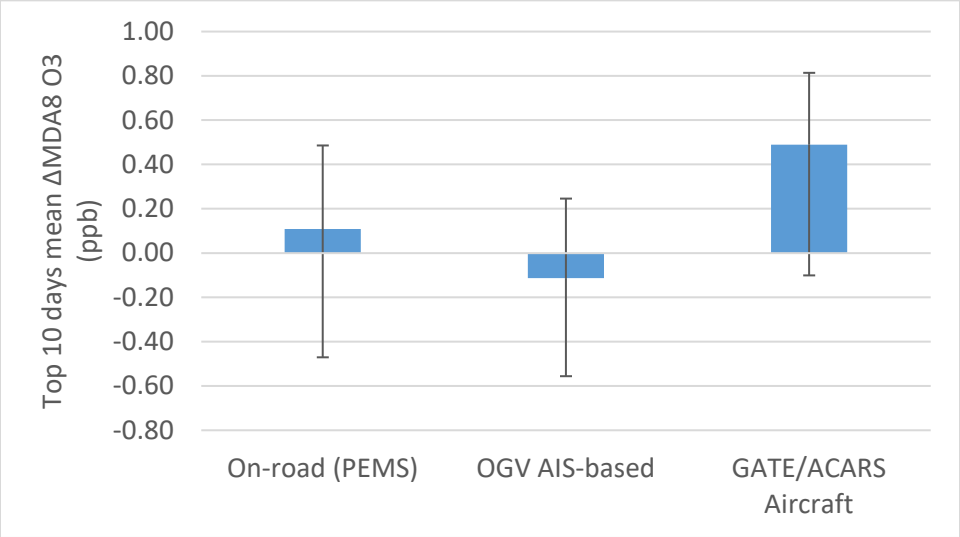

FIGURE V-4-10

AVERAGE 8-HOUR OZONE RESPONSE DUE TO EACH CHANGE TO THE MODELING EMISSIONS. BOUNDS REFLECT THE RANGE OF RESPONSES OBSERVED ACROSS BASIN MONITORING SITES.

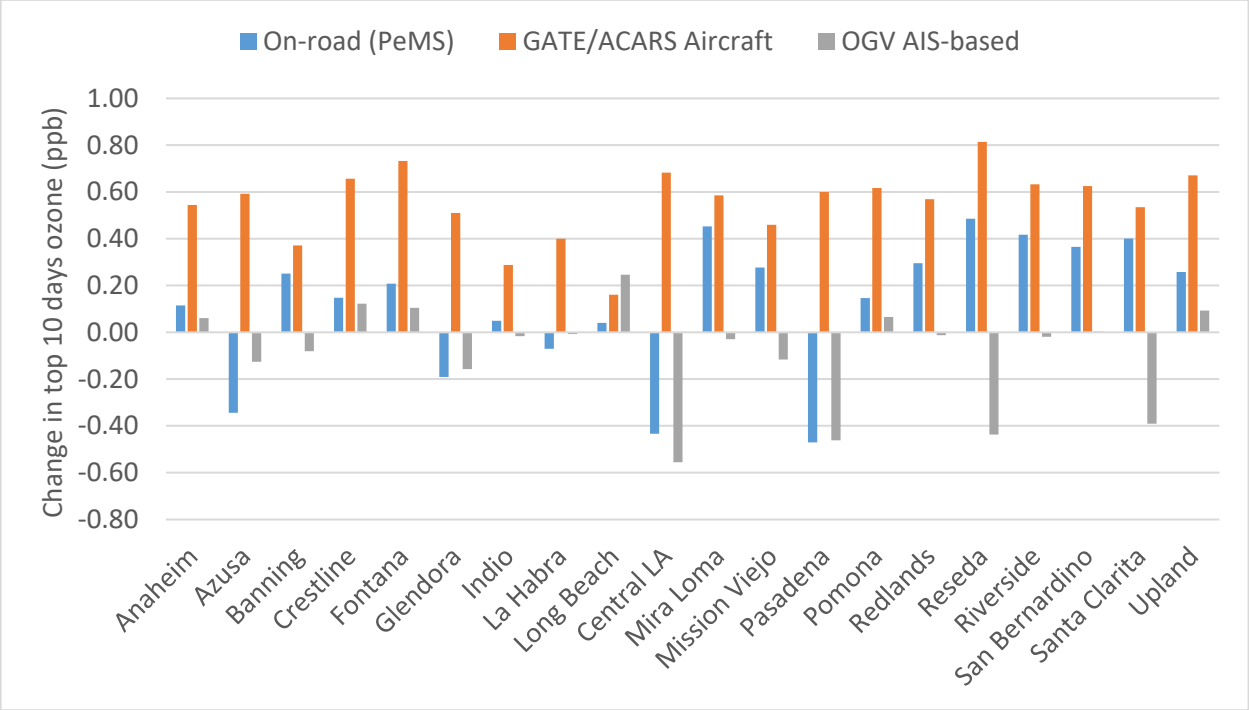

FIGURE V-4-11

8-HOUR OZONE RESPONSE AT EACH STATION DUE TO EACH CHANGE TO THE MODELING EMISSIONS

Emissions Profiles

Day specific emissions were generated for 2018. Figure V-4-12 illustrates the total CO and NOx emissions contained in the CMAQ modeling domain for May-September in 2018. Note that the emissions totals are much higher than those presented in Table V-4-1. This is because the values in Table V-4-1 represent basin-wide total emissions while those in Figure V-4-12 comprise totals from the entire modeling domain. The profile clearly depicts a changing emissions pattern with two distinct cycles represented: a weekly cycle, illustrated by Sunday through Saturday peaks and valleys, and day-to-day variations in emissions within the weekly cycle. Daily variations are primarily driven by daily vehicular activities and ambient temperature and humidity changes. Although not included in Figure V-4-12, spatially and temporally resolved emissions from prescribed fires were also included in the emissions in the modeling domain. The attainment demonstration does not include emissions from wildfires.

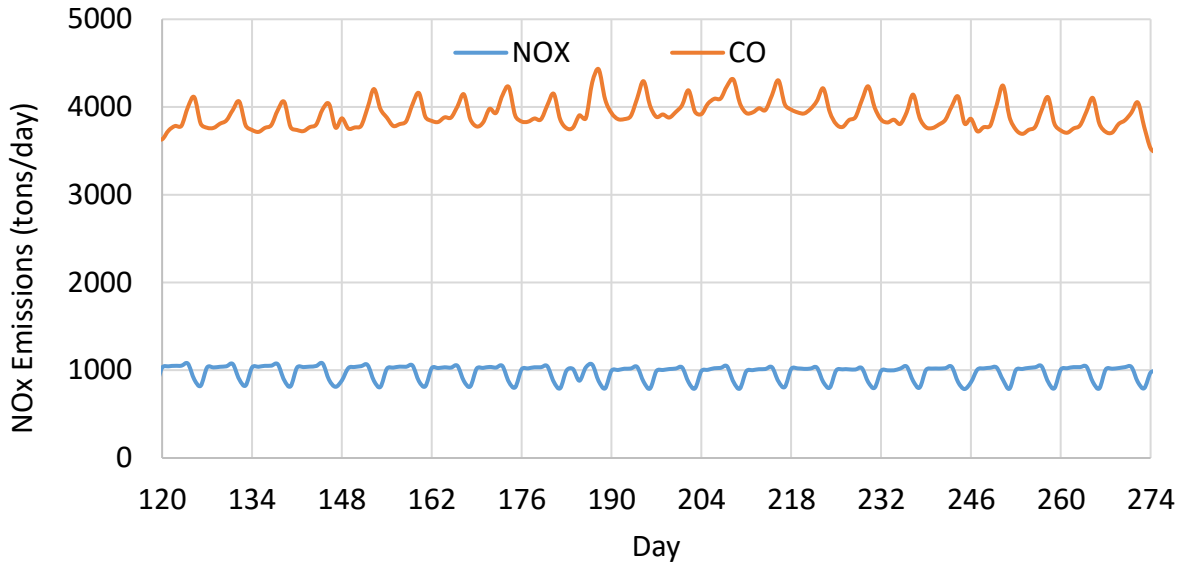

FIGURE V-4-12

2018 DAILY CO AND NOx EMISSIONS IN THE MODELING DOMAIN.

Spatial Distribution

Figures V-4-13 through V-4-17 represent the ozone season (May-September) average and provide the spatial distribution of NOx emissions for point sources, OGV, off-road, on-road and total anthropogenic categories.

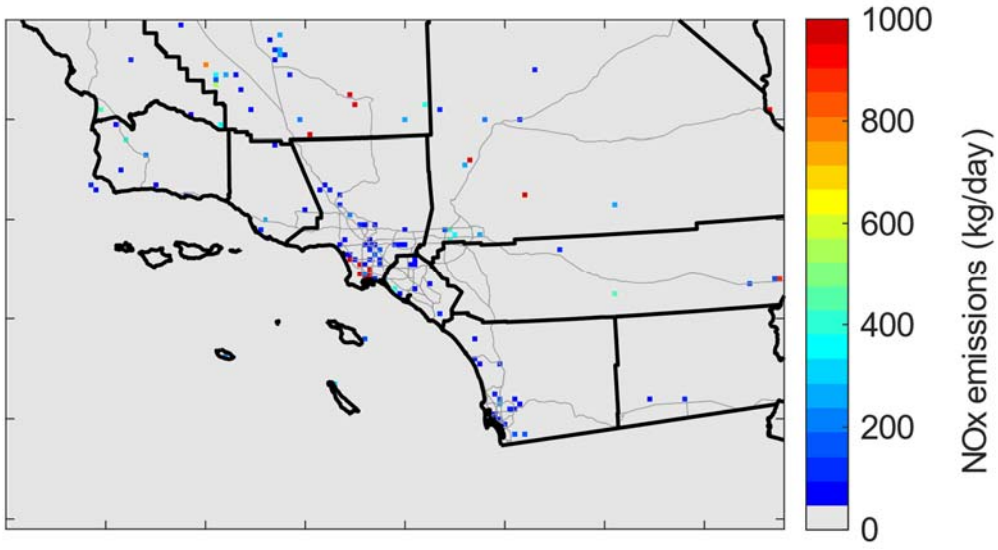

FIGURE V-4-13

STATIONARY POINT SOURCE NOx EMISSIONS IN THE MODELING DOMAIN

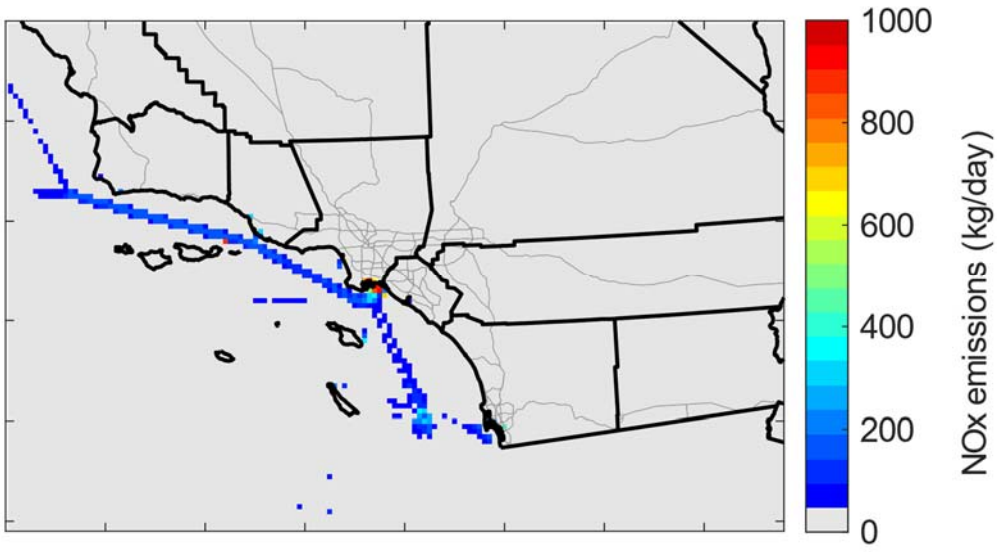

FIGURE V-4-14

OGV NOx EMISSIONS IN THE MODELING DOMAIN

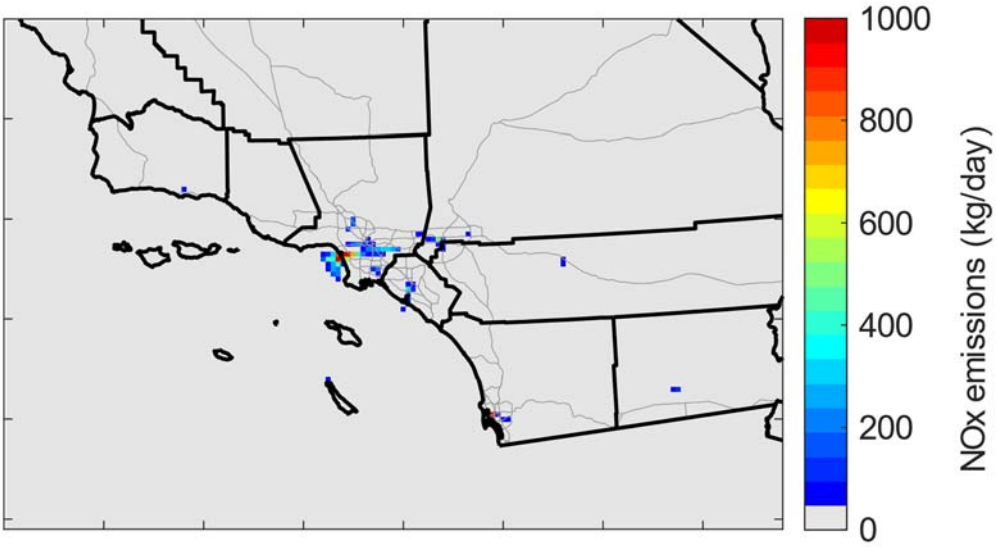

FIGURE V-4-15

AIRCRAFT NOx EMISSIONS IN THE MODELING DOMAIN

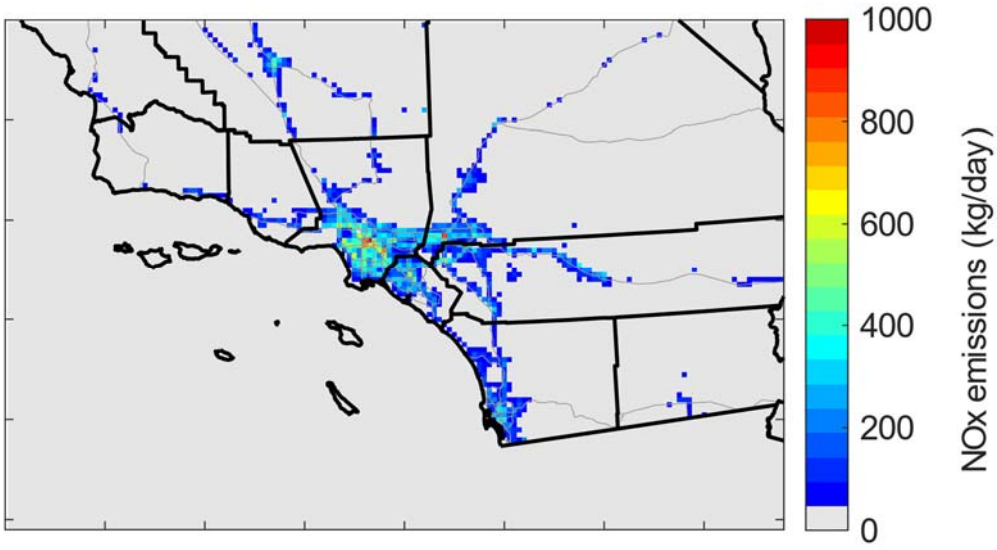

FIGURE V-4-16

ON-ROAD NOx EMISSIONS IN THE MODELING DOMAIN

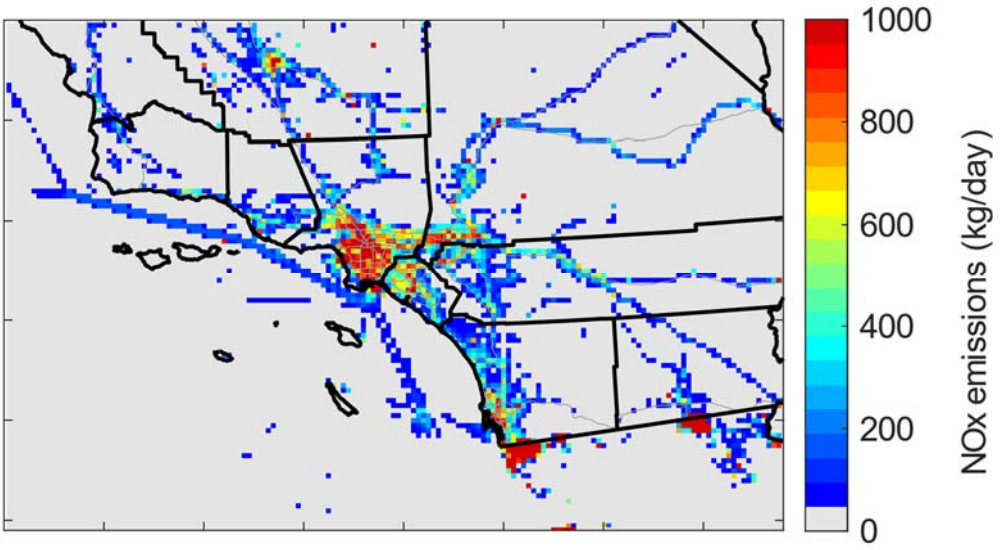

FIGURE V-4-17

SUMMER AVERAGE NOx EMISSIONS IN THE MODELING DOMAIN

Biogenic Emissions

Daily biogenic VOC emissions were calculated using the Model of Emissions of Gases and Aerosols from Nature version 3.0 (MEGAN3.0) using 2018 meteorology as input. MEGAN was executed in its default configuration, except for the normalized Leaf Area Index (LAIv) input. LAIv was developed by the California Air Resources Board using 2018 data from the Moderate Resolution Imaging Spectroradiometer (MODIS) on the National Aeronautical Space Administration's Terra and Aqua satellites. Because MODIS does not provide data in urban areas, LAIv in these areas was based on tree survey data from the US Forest Service.

Figure V-4-18 provides the daily total emissions of biogenic VOC, in tons per day, in the Basin. The trend shows higher emissions for the spring and summer months with several peaks during June through August when temperatures were highest.

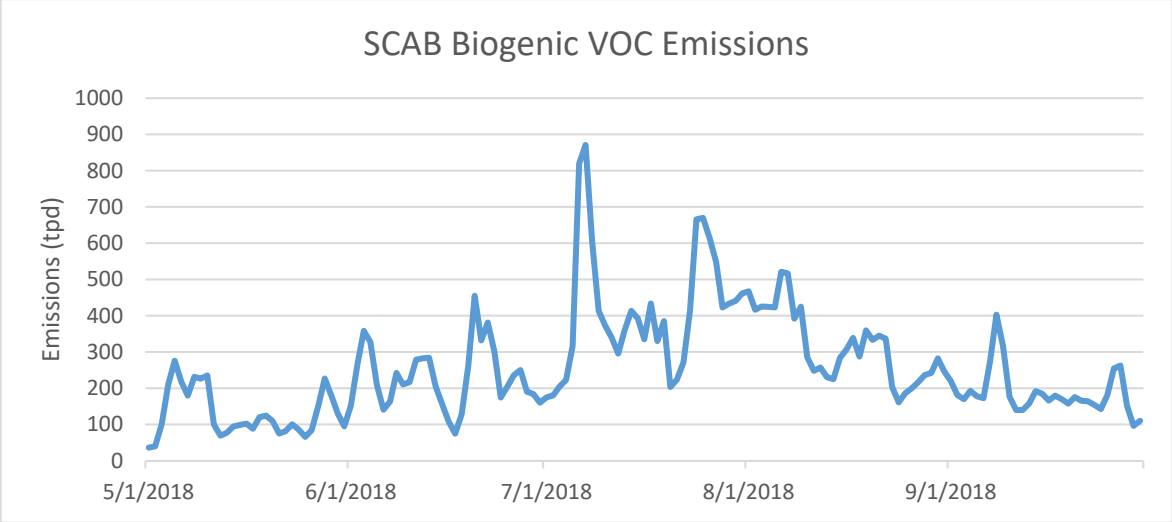

FIGURE V-4-18

2018 DAILY BIOGENIC VOC EMISSIONS IN THE BASIN

At the time of AQMP inventory development, MEGAN3.1 was released as a beta version and, thus, MEGAN3.0 served as the primary biogenic emissions model for this AQMP, while additional sensitivity tests and developmental work were conducted to improve our understanding of biogenic emissions. While MEGAN3.1 was used for internal testing and development, this version of the model was ultimately not selected for production runs. Nevertheless, a comparison of the emissions from both versions is presented in Figure V-4-19.

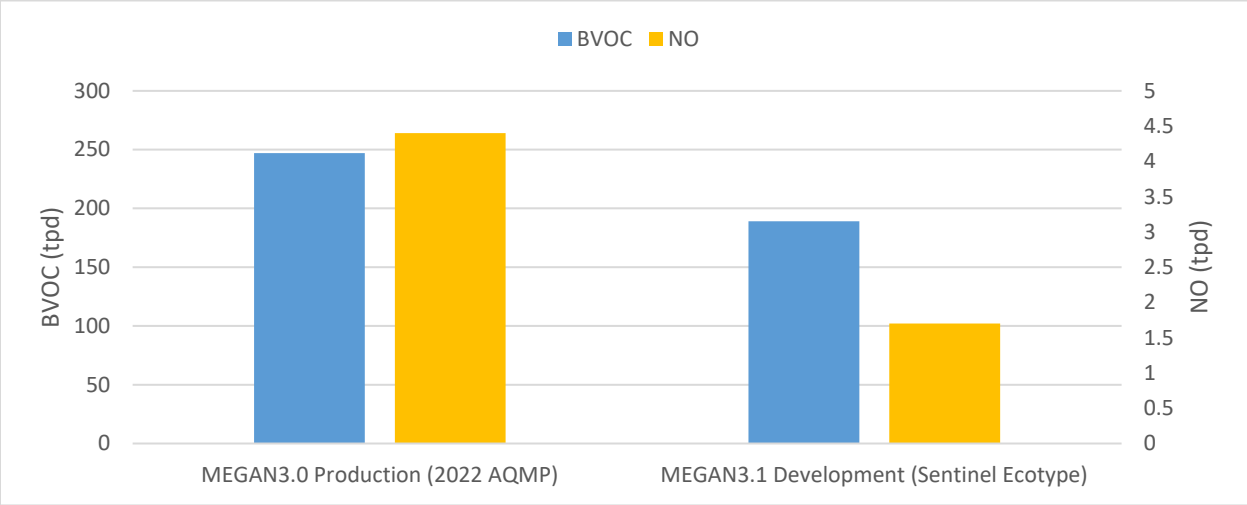

FIGURE V-4-19

MODEL VERSION COMPARISON OF SUMMER AVERAGE BIOGENIC VOC AND NO EMISSIONS IN THE BASIN

The version of MEGAN3.1 used in testing contained custom inputs for LAIv, growth forms, and ecotypes. The LAIv was developed using 2017 MODIS data augmented by 2017 monthly LAIv from the Sentinel 5-P satellite. The normalization to produce LAIv was performed using green vegetation fractions from the National Ocean and Atmospheric Administration's Visible Infrared Imaging Radiometer Suite and vegetation cover fractions from Sentinel 5-P. The default growth forms (i.e., fractional coverage of trees, shrubs, crops, and herbs) were scaled such that their sum equaled the vegetation cover fractions used in the LAIv normalization. Finally, the ecotypes were improved under a contract with the MEGAN development team. The ecotypes were adjusted to reflect the tree species composition in the Basin by using 140 municipal tree inventories as the basis for classification. MEGAN3.1 was not executed with the Berkeley Dalhousie Soil NO Processor and the default Yienger-Levy (YL) scheme was used instead.

The custom version of MEGAN3.1 employed here resulted in lower BVOC and NO emissions compared to those obtained with MEGAN3.0. This was primarily due to lower emission factors resulting from the growth form and ecotype modifications. Further refinements to the growth forms are anticipated through another contract with the MEGAN development team. In addition, this contract seeks to improve species-dependent emission factors in MEGAN. This will be accomplished by conducting enclosure measurements for tree species that are prevalent throughout the Basin.

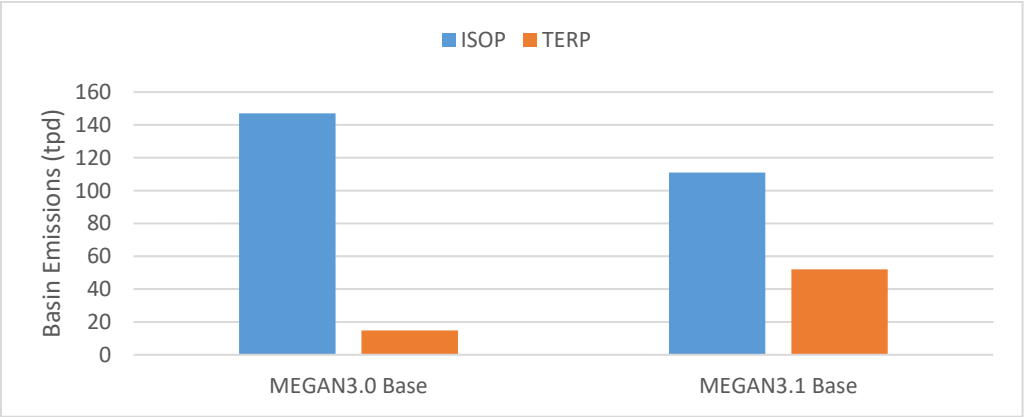

FIGURE V-4-20

2018 SUMMER AVERAGE ISOPRENE (ISOP) AND TERPENE (TERP) EMISSIONS IN THE BASIN.

In the absence of the custom inputs described, MEGAN3.1 exhibited a distinct emissions profile compared to MEGAN3.0. As seen in Figure V-4-20, executing MEGAN3.1 with default inputs resulted in a moderate decrease in isoprene emissions and a substantial increase in terpene emissions compared to MEGAN3.0 with default inputs. This was attributable to variation in the default emission factors assumed in the model.

There is considerable uncertainty in the biogenic emissions inventory as evidenced by large changes in the emissions across model versions. Preliminary analysis of the base version (i.e., using default inputs) of MEGAN3.2 indicates that isoprene emissions in the Basin are even lower than those in MEGAN3.1. This suggests that biogenic emissions inventory development is an active area of research with frequent, substantial changes likely to occur. As previously mentioned, South Coast AQMD has contracted with the MEGAN development team to improve the inventory in our region. It is expected that this improved version will be used in future AQMPs. Consistent with prior AQMPs and U.S. EPA guidance, stable releases should be used in modeling for the attainment demonstration. Out of an abundance of caution, prior AQMPs often employed model versions that were one version prior to the current stable release to avoid potential bugs. In keeping with this practice, staff determined that MEGAN3.0 was a suitable choice for attainment modeling for this AQMP.

Boundary and Initial Conditions

The initial condition for the CMAQ simulations was generated using the default profile available from the CMAQ standard package. A five day spin-up period was then introduced to offset the homogeneity in initial values. This method is consistent with the strategy implemented in previous AQMPs.

The global model of Community Atmosphere Model with Chemistry (CAM-chem) (Emmons, L. K., 2020) was used to define the boundary conditions (BCs) for the 12 km statewide CMAQ domain, while boundary

conditions for the inner South Coast 4 km domain were derived from the 12 km CMAQ output. The CAM-chem is a component of the NCAR (National Center for Atmospheric Research) Community Earth System Model (CESM) and is used for simulations of global tropospheric and stratospheric atmospheric composition. Boundary conditions were extracted for inorganic gases and VOCs along with aerosol species such as elemental carbon, organic matter, sulfate, and nitrate. CAM-Chem simulations (Buchholz, R. R., 2019) for the year 2018 were used to represent the boundary conditions in the 2022 AQMP. These simulations are publicly available and can be downloaded at https://www.acom.ucar.edu/cam-chem/cam-chem.shtml. Boundary condition data was extracted from the CAM-Chem output and processed into CMAQ model ready format using the computer program "mozart2camx" developed by the Ramboll Environ Corporation (available at http://www.camx.com/download/support-software.aspx). The program is originally made to process MOZART global model outputs, some revisions were made for CAM-Chem outputs processing. The vertical layer structure of BCON is determined by the meteorological files, and the vertical interpolation uses pressure levels of each layer interface. Horizontally, the bilinear interpolation is used to translate from the global model grid to the regional CMAQ grid. Speciation profiles are included to map CAM-Chem species to CMAQ for both trace gases (SAPRC07TC) and aerosols. The final CAM-Chem derived BCs for the CMAQ domain represent day-specific mixing ratios, which vary in both space (horizontal and vertical) and time (every 6 hour).

Figures V-4-21 and V-4-22 show surface ozone concentrations averaged along the four domain boundaries. Typically, the western boundary, located west of the Basin over the Pacific Ocean, shows the lowest concentrations followed by the southern boundary. The average ozone concentration over the entire ozone season at the western boundary is approximately 35 ppb, whereas the seasonally averaged concentration on the southern boundary is approximately 40 ppb. The average ozone concentration along the eastern boundary is approximately 53 ppb. The general circulation in Southern California is from west to east, and as a result, the eastern boundary is affected by the upwind emissions in the domain, which results in a higher boundary value over the eastern boundary. Finally, the northern boundary is affected by emissions from central California and the average surface ozone concentration is approximately 50 ppb.

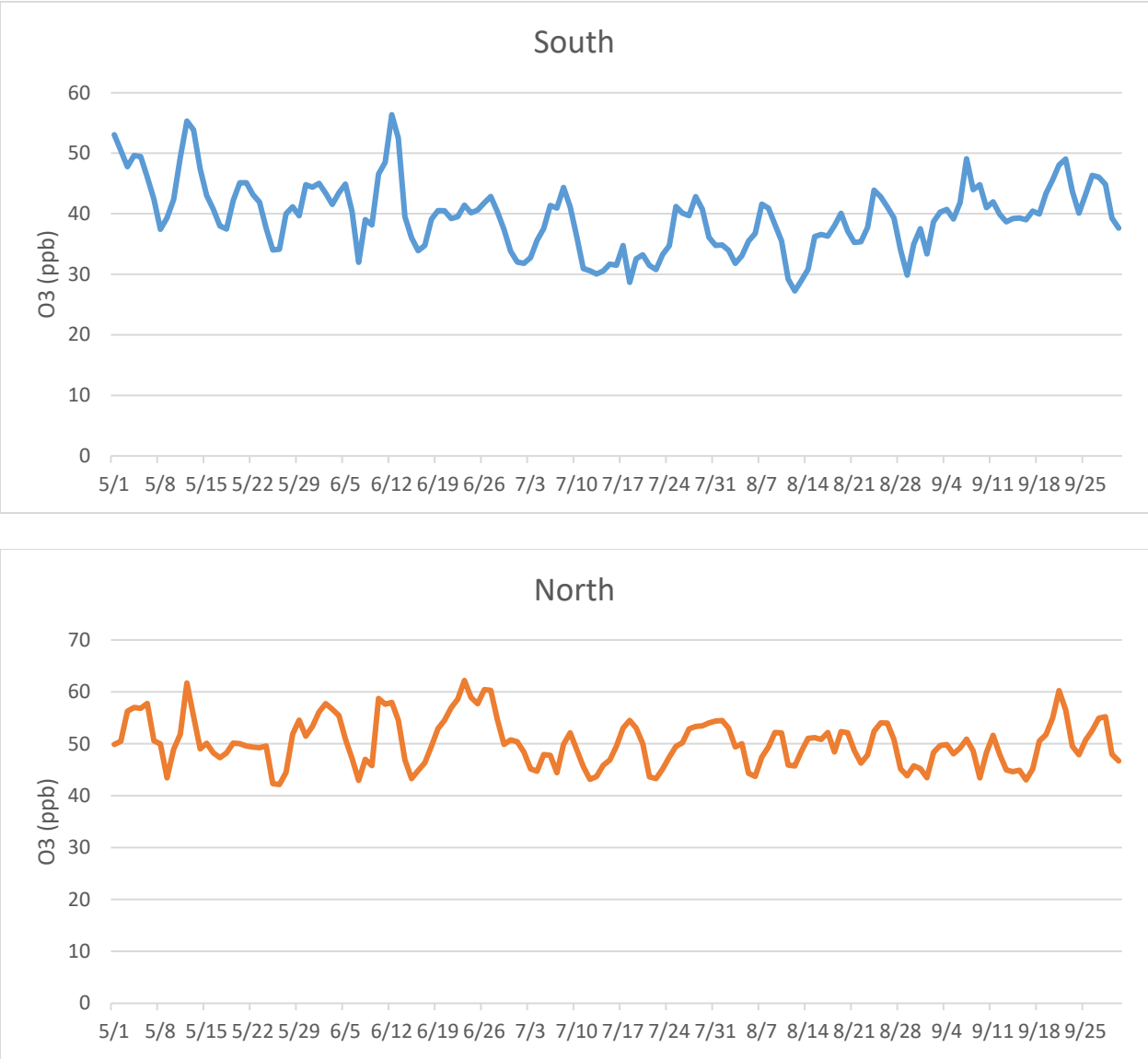

FIGURE V-4-21

SURFACE OZONE CONCENTRATION ALONG THE SOUTH AND NORTH BOUNDARIES

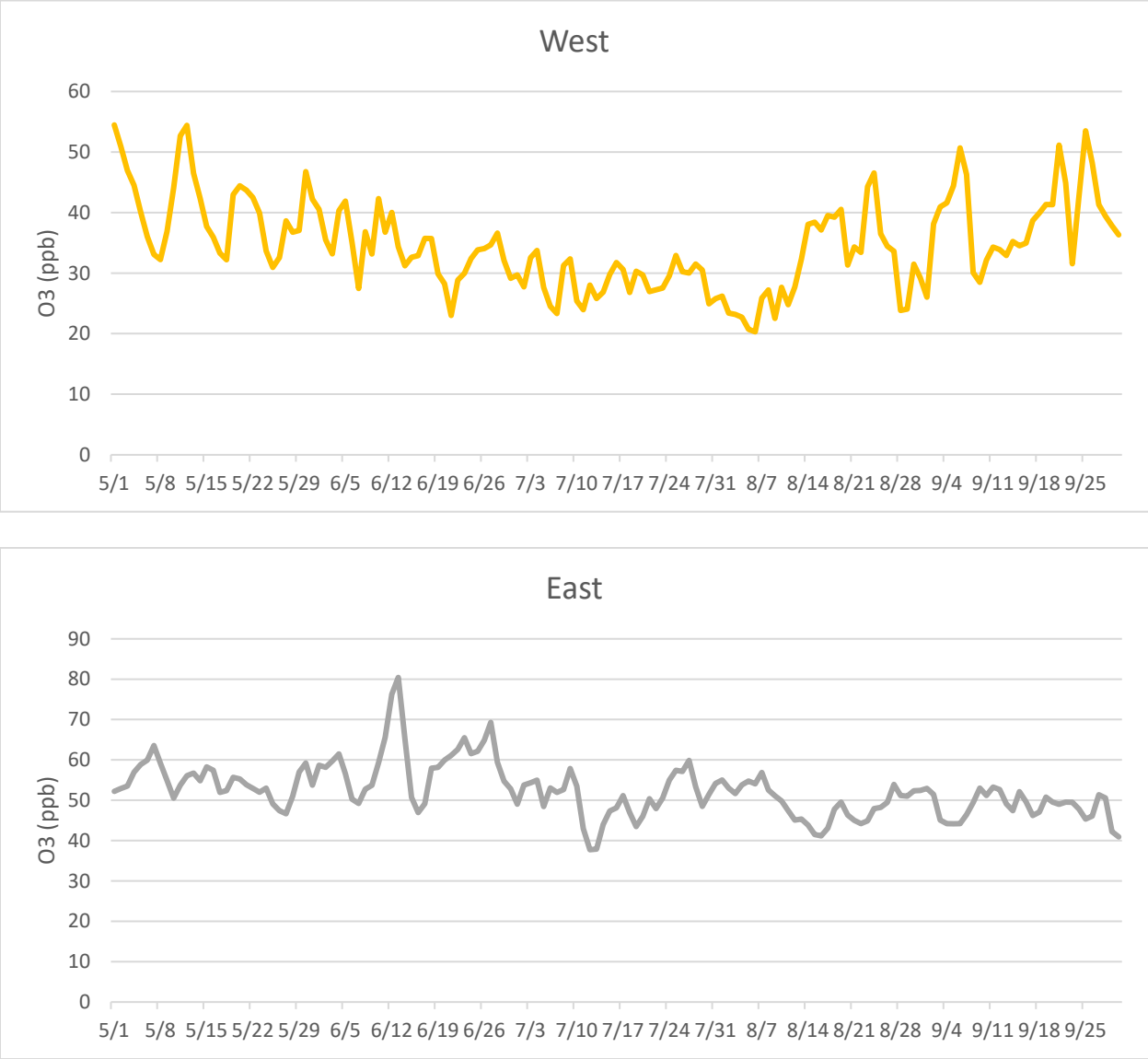

FIGURE V-4-22

SURFACE OZONE CONCENTRATION ALONG THE WEST AND EAST BOUNDARIES

Figures V-4-23 through V-4-26 present the monthly ozone vertical profiles averaged along the southern, northern, western, and eastern boundaries, respectively. Concentrations are averaged across all hours in each month. In general, ozone concentrations tend to be higher in the upper layers, especially along the cleaner boundaries. The difference between concentrations at the surface and concentrations aloft is larger along the cleaner boundaries. In particular, ozone concentrations along the western boundary exhibit the most contrast between ground level and upper levels. On the contrary, the northern and eastern boundary, which have higher ozone concentrations due to the influence of central and Southern California emissions, present a flatter vertical profile throughout the ozone season.

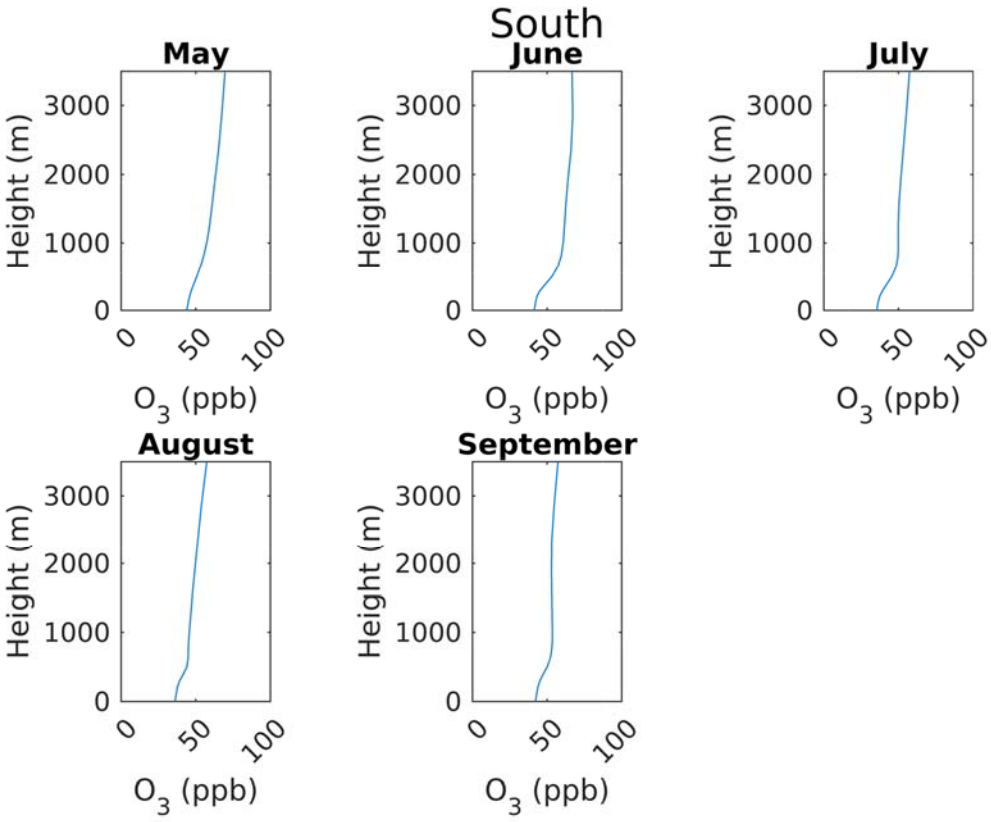

FIGURE V-4-23

OZONE VERTICAL PROFILE ALONG THE SOUTHERN BOUNDARY

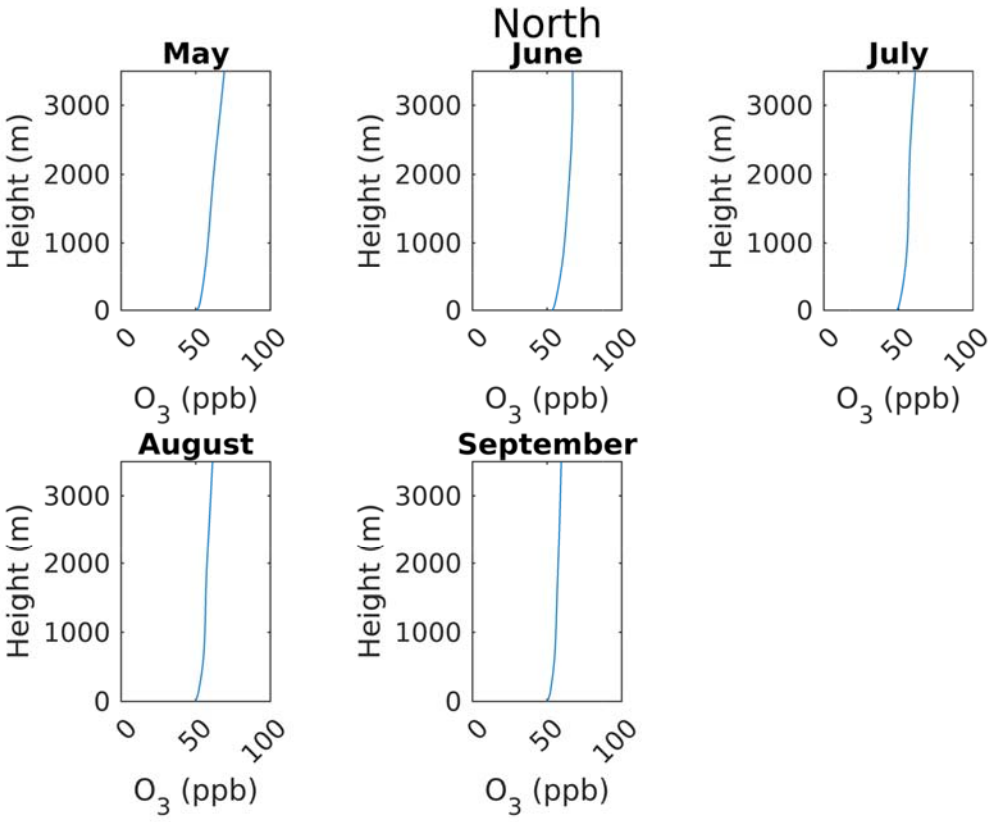

FIGURE V-4-24

OZONE VERTICAL PROFILE ALONG THE NORTHERN BOUNDARY

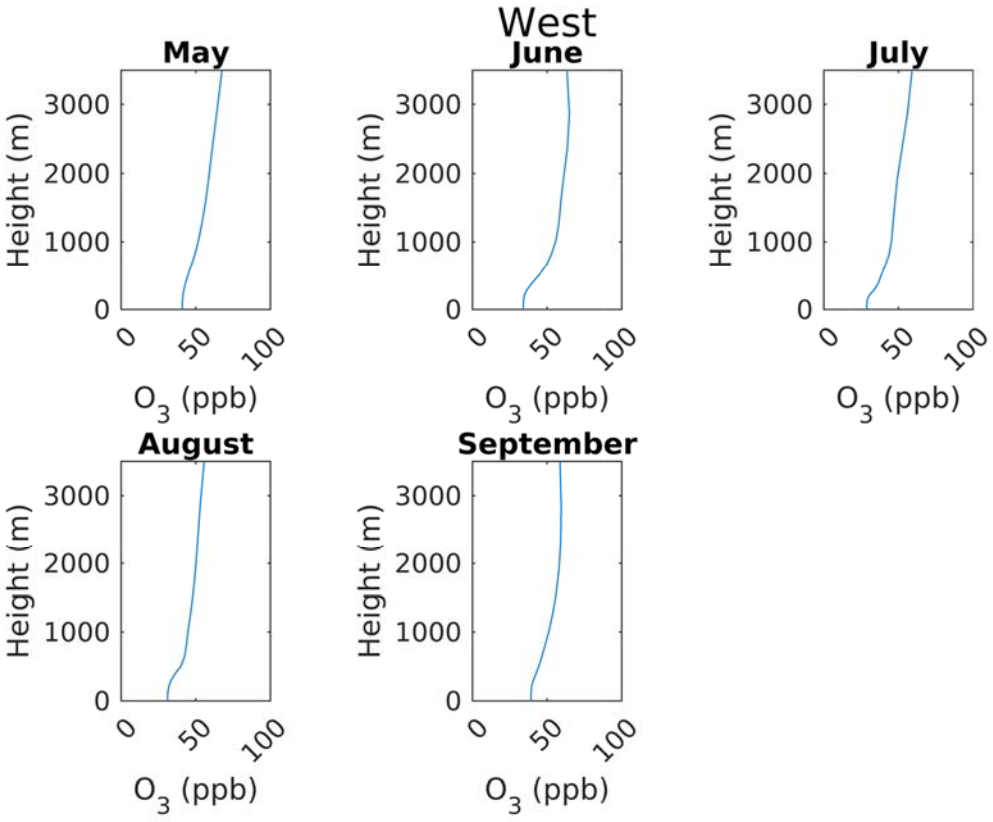

FIGURE V-4-25

OZONE VERTICAL PROFILE ALONG THE WESTERN BOUNDARY

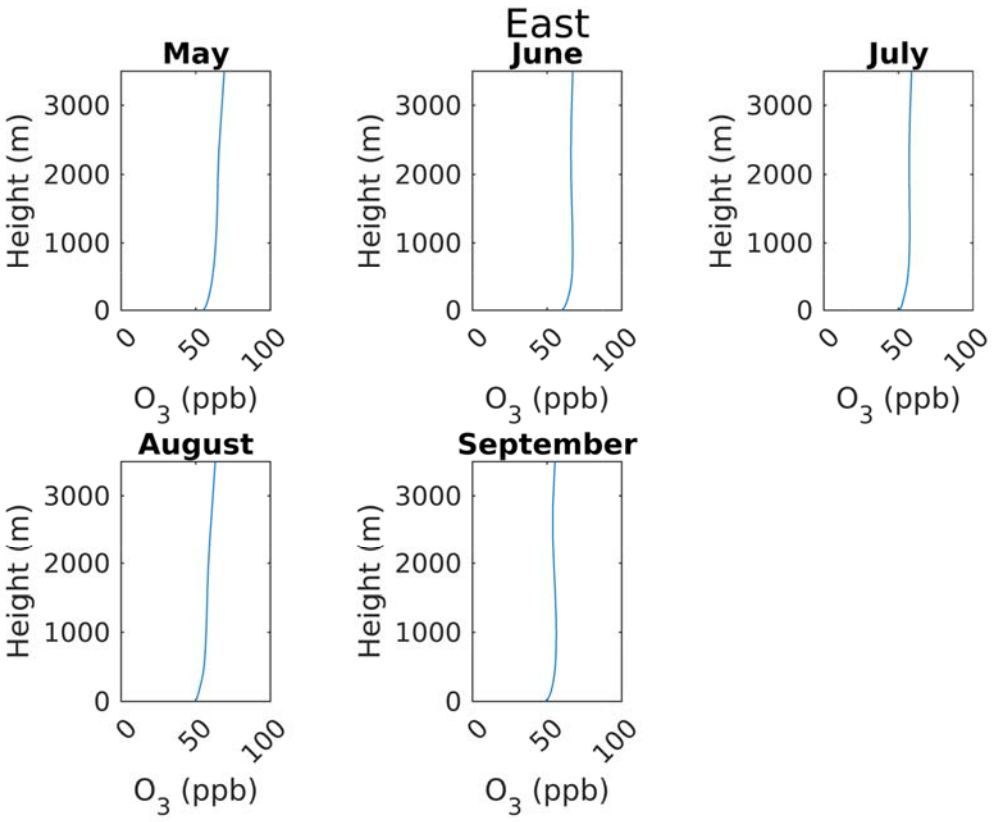

FIGURE V-4-26

OZONE VERTICAL PROFILE ALONG THE EASTERN BOUNDARY

The boundary values used in future year simulations were retrieved using the same approach as in the base year (2018), except for anthropogenic emissions, which were adjusted based on the projected future emission levels in the State. In this approach, out of state emissions were not adjusted due to the lack of accurate information, but the impact of statewide emission reductions was considered.

Boundary Condition Sensitivity

Staff conducted an analysis to determine the impact of boundary conditions on CMAQ's ability to predict ozone levels. Two independent sets of boundary conditions were used, hereafter referred to as BC1 and BC2. Both BC1 and BC2 were developed using the method described previously and BC2 corresponds to the boundary condition used in the attainment demonstration. The 12km CMAQ simulation generating BC2 was conducted by South Coast AQMD, and the 12km CMAQ simulation generating BC1 was conducted by the California Air Resources Board. These two sets of 12km CMAQ simulations used same set of 12km emission inventories, but different sets of meteorology input. The meteorology conditions are both from the Weather Research and Forecasting Model (WRF), while the configurations such as the microphysics

and land surface model were chosen differently. The comparison between BC1 and BC2 showed very similar values and patterns with slightly lower values (mostly < 1 ppbv Ozone) from BC2. The analysis focused on two aspects: 1) a comparison of 2018 baseline modeled ozone and 2) an examination of the impact to model-predicted 2037 baseline ozone levels.

CMAQ was initialized for the two sets of boundary conditions. The emissions and meteorology were identical for the baseline simulations. Figures V-4-27 through V-4-29 present a comparison of the 8-hour ozone timeseries for BC1 and BC2. Overall, BC1 and BC2 performed similarly, however, BC2 demonstrated slightly lower normalized mean bias (5-10%) at the sites with the highest base design values (Crestline, San Bernardino, and Glendora).

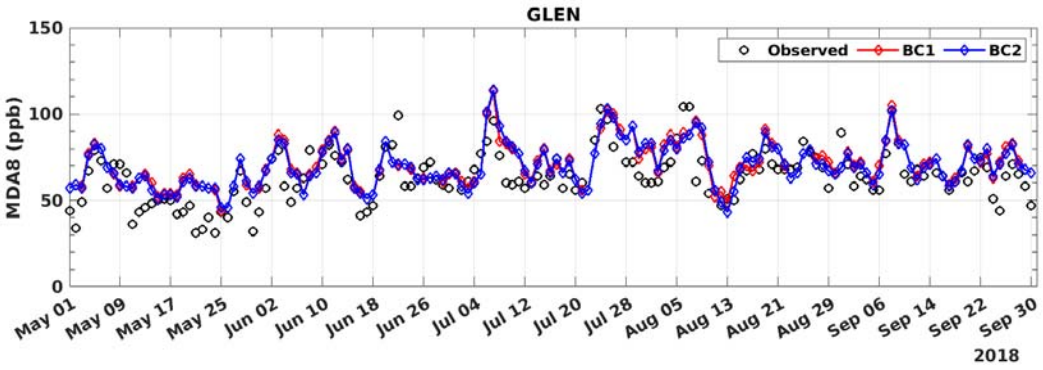

FIGURE V-4-27

GLENDORA OBSERVED VS. PREDICTED MDA8 OZONE

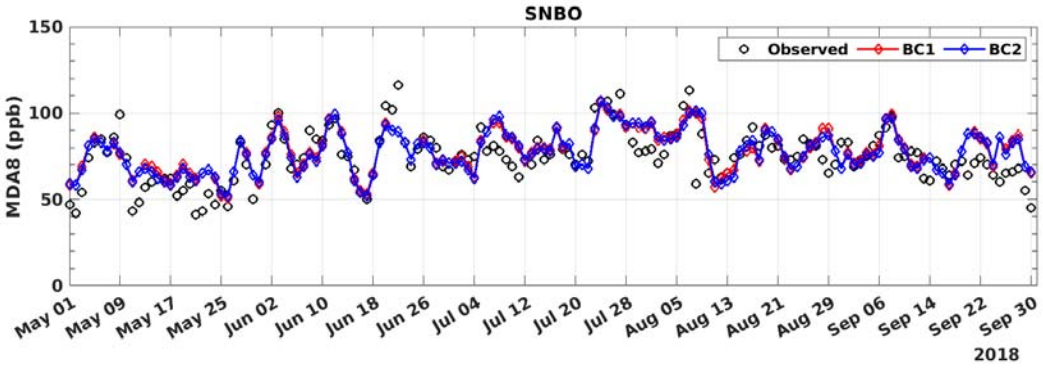

FIGURE V-4-28

SAN BERNADINO OBSERVED VS. PREDICTED MDA8 OZONE

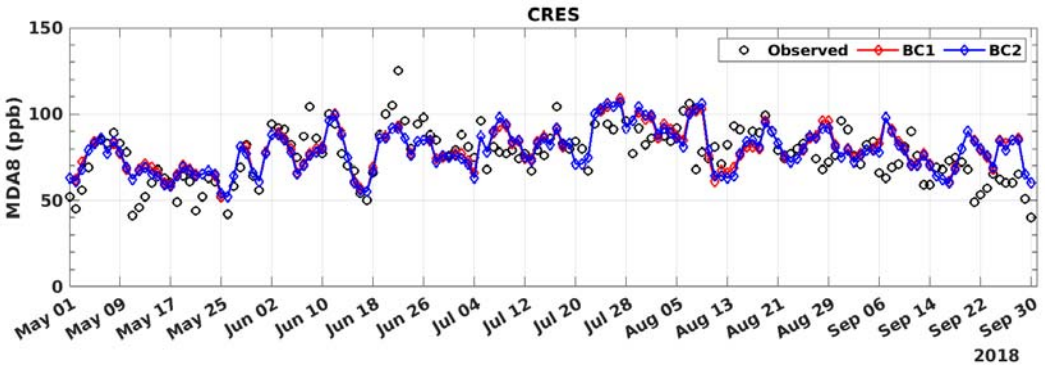

FIGURE V-4-29

CRESTLINE OBSERVED VS. PREDICTED MDA8 OZONE

In addition to 2018, the 2037 baseline scenario was simulated and the future design values are compared in Figure V-4-30. At the sites with the highest future design values (Crestline, San Bernardino, and Glendora), BC2 resulted in modest ozone design value decreases, while the response was mixed at other sites.

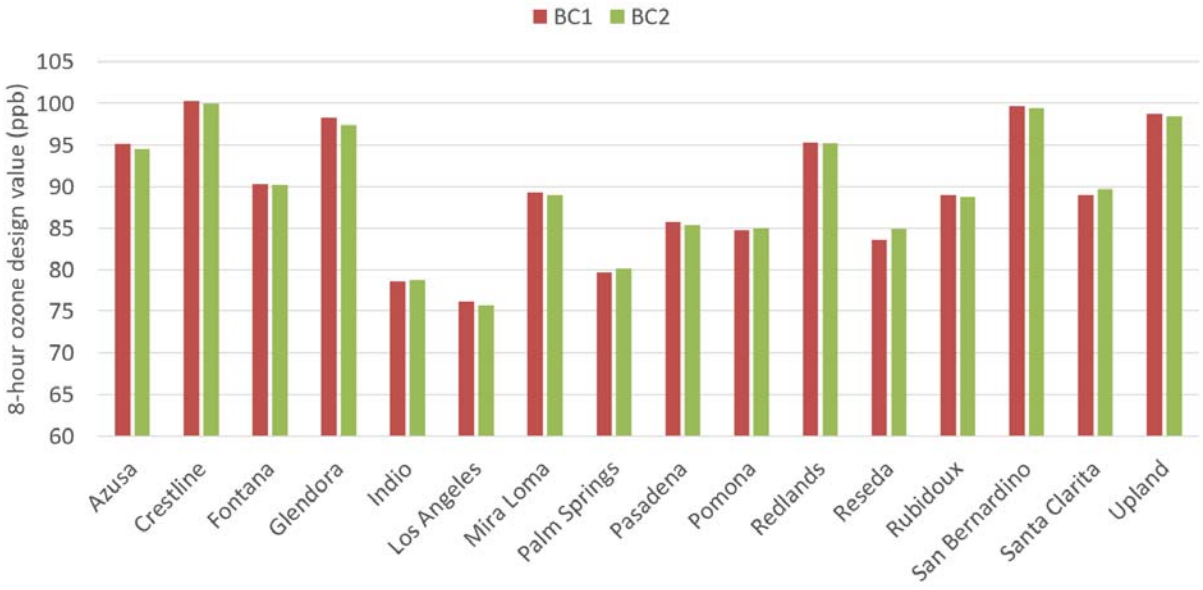

FIGURE V-4-30

FUTURE 2037 BASELINE OZONE DESIGN VALUES

In summary, two sets of boundary conditions were evaluated and their impact on ozone concentrations were assessed. The latest set of boundary conditions, BC2, resulted in lower normalized mean bias at the sites with high design values and thus it was selected for the attainment demonstration.

VOC Emissions Reactivity

The regulatory inventories presented in Chapter 3 present VOC emissions as an aggregated amount. VOC include a wide range of compounds that can react very differently in the atmosphere. One way to present the capacity of individual VOC species to produce ozone is by the Maximum Incremental Reactivity (MIR) scales, which represent the maximum potential amount of ozone that could be produced by a unit mass of a specific VOC. The average aggregate MIR values for the major source categories in the base year 2018 inventory is presented in Figure V-4-31. Industrial processes present the highest potential for ozone formation, followed by mobile sources (off-road and on-road). Diesel emissions are expected to contribute significantly to ozone reactivity because of the high carbonyl content in diesel emissions. Conversely, waste disposal and solvent evaporation (which includes consumer products) present the lowest. The air quality model used in the air quality simulations – the CMAQ model using the SAPRC-07 chemical mechanisms – accounts for these different reactivities of emission sources.

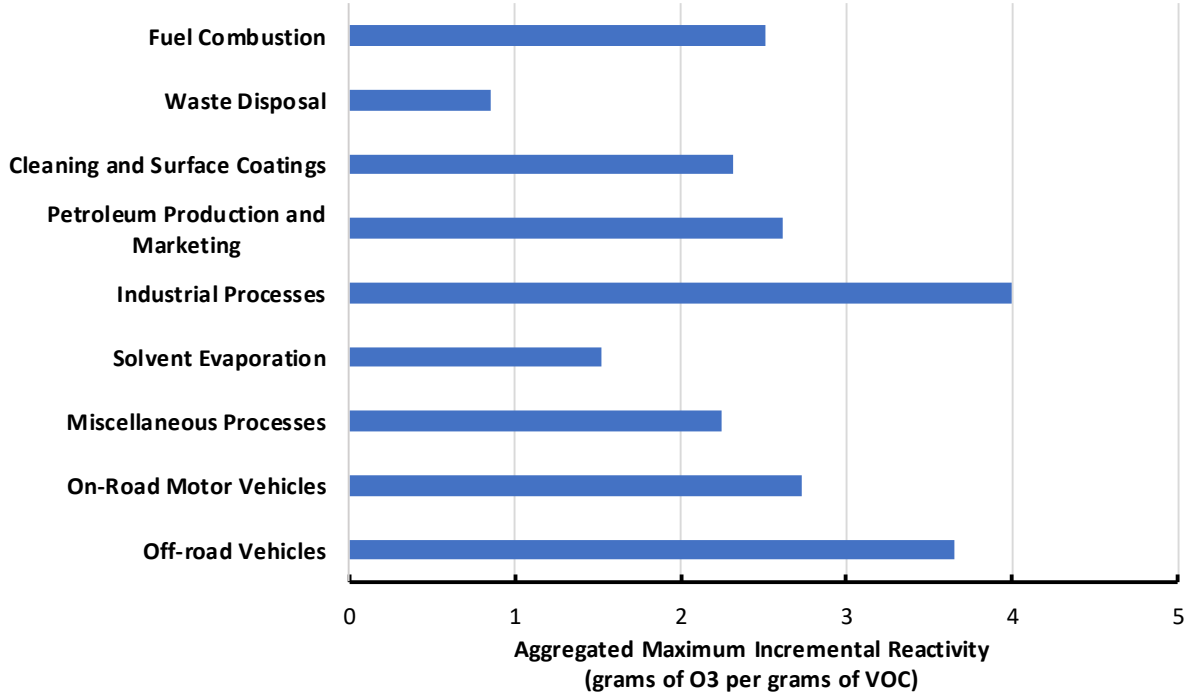

FIGURE V-4-31

AVERAGE AGGREGATED MAXIMUM INCREMENTAL REACTIVITY OF VOC EMISSIONS BY MAJOR SOURCE CATEGORY BASED ON THE BASE YEAR 2018 EMISSIONS INVENTORY

Figure V-4-32 presents the contribution to total VOC emissions by major source category, and it presents the contribution by each source with VOC emissions adjusted by reactivity. While solvent evaporation is the largest contributor to overall VOC emissions, off-road mobile sources become the largest source of VOC once the emissions are adjusted by reactivity. This illustrates that controlling mobile sources contributes effectively to reduce ozone formation potential from VOC emission reductions in conjunction with the reductions in NOx emissions.

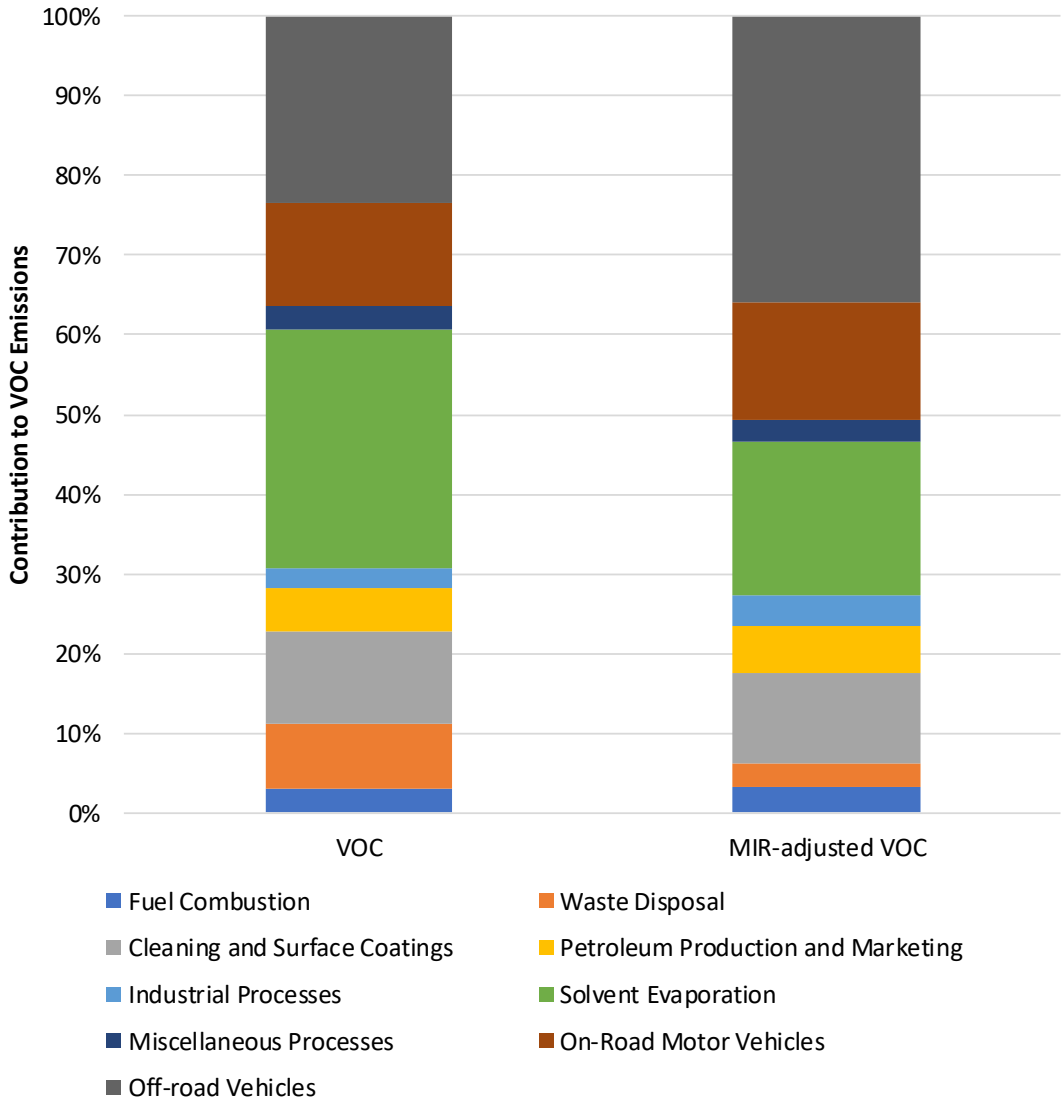

FIGURE V-4-32

CONTRIBUTION TO TOTAL VOC EMISSIONS BY MAJOR SOURCE CATEGORY WITH AND WITHOUT ADJUSTING FOR REACTIVITY, FOR THE YEAR 2018

References

Buchholz, R. R., Emmons, L. K., Tilmes, S., & The CESM2 Development Team, (2019). CESM2.1/CAM-chem Instantaneous Output for Boundary Conditions. UCAR/NCAR - Atmospheric Chemistry Observations and Modeling Laboratory. https://doi.org/10.5065/NMP7-EP60.

Emmons, L. K., Schwantes, R. H., Orlando, J. J., Tyndall, G., Kinnison, D., Lamarque, J.-F., et al., (2020). The Chemistry Mechanism in the Community Earth System Model version 2 (CESM2). Journal of Advances in Modeling Earth Systems, 12, e2019MS001882, https://doi.org/10.1029/2019MS001882

Kwon J, Varaiya P, Skabardonis A. Estimation of Truck Traffic Volume from Single Loop Detectors with Lane-to-Lane Speed Correlation. Transportation Research Record. 2003;1856(1):106-117, https://doi.org/10.3141%2F1856-11

CHAPTER 5

8-HOUR OZONE MODELING AND ATTAINMENT DEMONSTRATION

Introduction

The 2022 AQMP demonstrates attainment of the 2015 8-hour ozone standard of 70 ppb by 2037. The design values used in the attainment demonstration are based on a 5-year weighted average centered on 2017, whereas the base year for emissions and meteorology selected for the 2022 AQMP attainment demonstration is 2018. The year 2018 was selected as the base year for emissions and meteorology because that was the year of designation of the Basin as an extreme non-attainment area. In addition, the Multiple Air Toxics Exposure Study (MATES V) was conducted during 2018 and involved a comprehensive campaign of monitoring and modeling that allowed for the development of a robust and extensively validated modeling framework. However, the period for the 5-year weighted average design value (2015-2019) was centered on 2017 to discard the anomalies caused by the effects of COVID-19 on emissions and resulting air quality in 2020.

Ozone Representativeness

The CMAQ modeling provided Basin-wide ozone air quality simulations for each hour in 2018. It included 153 days from May 1st to September 30th of 2018.

The approach used in this AQMP is similar to the approach used in the 2016 AQMP and is consistent with U.S. EPA guidance (U.S. EPA, 2018).[1] Air quality simulations were conducted for each hour in the 2018 ozone season (May 1st to September 30th). Only the top 10 days were used to calculate the Relative Response Factor (RRF) provided that modeled maximum daily 8-hr (MDA8) ozone exceeded 60 ppb. Some stations did not have 10 days with MDA8 ozone exceeding 60 ppb; these stations were used provided that there were at least 5 days. The same top 10 dates in the base year corresponded to those in the future year and the maximum modeled value in the 3 by 3 grid surrounding each station was compared to the corresponding grid position in the future year.

While Redlands was the base design site in the 2016 AQMP, Crestline had the highest base design value for the five-year period in the current analysis. During this period, several well-defined multi-day ozone episodes occurred in the Basin, with 122 days having maximum daily 8-hour concentrations of 70 ppb or higher. Stations located in San Bernardino and Riverside counties show similar levels of elevated ozone as Crestline and Redlands, highlighting the influence of similar transport and chemistry patterns. Note that U.S. EPA recommends that 5-year weighted design values for the attainment demonstration retain the tenths (of a ppb) digit in all documentation. However, compliance with the NAAQS is determined by truncating the design values to the integer ppb unit, i.e., 70.9 ppb becomes 70 ppb and meets the 2015 ozone standard. Table V-5-1 lists the 2015 to 2019 5-year weighted design values used in the future year ozone projections. Stations are color coded according to their performance evaluation zone defined in the Model Performance Evaluation section below.

[1] https://www.epa.gov/sites/default/files/2020-10/documents/o3-pm-rh-modeling_guidance-2018.pdf

TABLE V-5-1

2015–2019 WEIGHTED 8-HOUR OZONE DESIGN VALUES

Station	2015–2019 8-hr Design Value	Performance Evaluation Zone
LAX	68.3	Coastal
Long Beach	56.3	Coastal
Mission Viejo	78.3	Coastal
West Los Angeles	67.3	Coastal
Reseda	90.3	SanFernando
Santa Clarita	99.3	SanFernando
Azusa	97.6	Foothills
Glendora	102.3	Foothills
Pasadena	86.3	Foothills
Anaheim	68.3	UrbanSource
Central Los Angeles	73.3	UrbanSource
La Habra	75.6	UrbanSource
Pico Rivera	75.3	UrbanSource
Pomona	91.3	UrbanSource
Banning	97.0	UrbanReceptor
Crestline	110.3	UrbanReceptor
Fontana	98.3	UrbanReceptor
Lake Elsinore	89.0	UrbanReceptor
Mira Loma	97.3	UrbanReceptor
Perris	93.0	UrbanReceptor
Redlands	106.3	UrbanReceptor
Rubidoux	97.3	UrbanReceptor
San Bernardino	110.0	UrbanReceptor
Upland	107.0	UrbanReceptor
Indio	84.3	CoachellaValley
Palm Springs	89.3	CoachellaValley

Ozone Modeling Configuration

The 2022 AQMP ozone attainment demonstration framework is an upgrade from the modeling platform used in the 2016 AQMP and more recent SIP revisions. It is built using the U.S. EPA-supported Community Multiscale Air Quality (CMAQ) (version 5.2.1) modeling platform with Statewide Air Pollution Research Center (SAPRC) 07 chemistry, and the Weather Research and Forecasting Model (WRF) (version 4.0.3) meteorological fields. The modeling platform tracks primary pollutants directly emitted that includes precursors of ozone and particulate matter and the formation of secondary pollutants like ozone and

particles formed from the chemical reactions that occur in the atmosphere. The ozone attainment demonstration focused on the period from May through September. The simulations were conducted over an area with a western boundary over 100 miles west of the Ports of Los Angeles and Long Beach. The eastern boundary extends slightly beyond the Colorado River while the northern and southern boundaries of the domain extend to the San Joaquin Valley and the Northern portions of Mexico, respectively. CMAQ was simulated with a 4-kilometer grid resolution.

For the 2022 AQMP, WRF was updated with the most recent version (version 4.0.3) available at the time of protocol preparation. The WRF simulations were initialized using National Centers for Environmental Prediction (NCEP) re-analysis data and run for three-day increments with four-dimensional data assimilation (FDDA). The inner-most modeling domain of the WRF simulation overlaps the CMAQ modeling domain, except that the WRF domain contains an extra 3 grid cells along the western, southern, and eastern boundary and an extra 9 grid cells along the northern boundary. The CMAQ domain contains 156 cells in the east/west direction and 102 cells in the N-S direction. The vertical coordinate and each computational layer are identical to those used by WRF.

Base-Year Ozone Model Performance Evaluation

For the CMAQ performance evaluation, the modeling domain is separated into several sub-regions or zones as shown in Tables V-5-1 and V-5-2. Figure V-5-1 depicts the sub-regional zones used for base-year simulation performance. The six different zones present unique air quality profiles: “Coastal” zone representing monitoring areas 2-4 and 18-21, “SanFernando” zone representing monitoring areas 6,7, and 13 within the San Fernando Valley, “Foothills” zone representing monitoring areas 8 and 9, “UrbanSource” zone representing monitoring areas 1, 5, 10-12, 16, and 17, “UrbanReceptor” zone representing monitoring areas 22-29 and 33-38, and “CoachellaValley” zone representing monitoring areas 30 and 31. Of the six areas, the “UrbanReceptor” region represents the Basin maximum ozone concentrations and the primary downwind impact zone. Table V-5-2 contains additional information regarding each station used in the analysis.

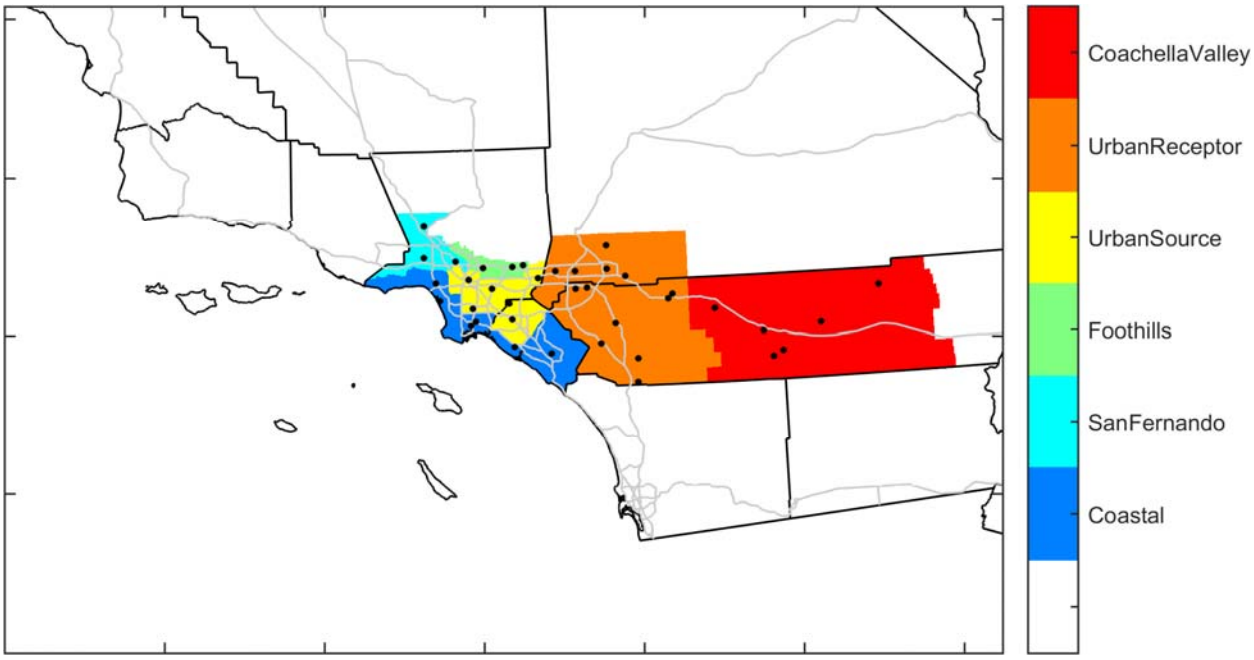

FIGURE V-5-1

PERFORMANCE EVALUATION ZONES

TABLE V-5-2

STATION INFORMATION

Location	Abbreviation	County	EPA Site Number	Monitoring Area	Performance Evaluation Zone
LAX	LAXH	Los Angeles	5005	3	Coastal
Long Beach Hudson	HDSN	Los Angeles	4006	4	Coastal
Mission Viejo	MSVJ	Orange	2022	19	Coastal
West Los Angeles	WSLA	Los Angeles	113	2	Coastal
Reseda	RESE	Los Angeles	1201	6	SanFernando
Santa Clarita	SCLR	Los Angeles	6012	13	SanFernando
Azusa	AZUS	Los Angeles	2	9	Foothills
Glendora	GLEN	Los Angeles	16	9	Foothills
Pasadena	PASA	Los Angeles	2005	8	Foothills
Anaheim	ANAH	Orange	7	17	UrbanSource
Central Los Angeles	CELA	Los Angeles	1103	1	UrbanSource
Compton	CMPT	Los Angeles	1302	12	UrbanSource
La Habra	LAHB	Orange	5001	16	UrbanSource

TABLE V-5-2 (CONCLUDED)

STATION INFORMATION

Location	Abbreviation	County	EPA Site Number	Monitoring Area	Performance Evaluation Zone
Pico Rivera	PICO	Los Angeles	1602	11	UrbanSource
Pomona	POMA	Los Angeles	1701	10	UrbanSource
Banning	BNAP	Riverside	12/1016	29	UrbanReceptor
Crestline	CRES	San Bernardino	5	37	UrbanReceptor
Fontana	FONT	San Bernardino	2002	34	UrbanReceptor
Lake Elsinore	ELSI	Riverside	9001	25	UrbanReceptor
Mira Loma	MLVB	Riverside	8005	23	UrbanReceptor
Perris	PERI	Riverside	6001	24	UrbanReceptor
Redlands	RDLD	San Bernardino	4003	35	UrbanReceptor
Riverside	RIVR	Riverside	8001	23	UrbanReceptor
San Bernardino	SNBO	San Bernardino	9004	34	UrbanReceptor
Temecula	TMCA	Riverside	9	26	UrbanReceptor
Upland	UPLA	San Bernardino	1004	32	UrbanReceptor
Indio	INDI	Riverside	1999/2002	30	CoachellaValley
Palm Springs	PLSP	Riverside	5001	30	CoachellaValley

Statistical Evaluation

The statistics used to evaluate 8-hour average CMAQ ozone performance include the following:

Statistic for O_3	Definition
MDA8 Bias Error Unpaired	Average of the differences in observed and predicted MDA8 values. Negative values indicate under-prediction. $BiasError = \frac{1}{N}\sum(Obs - Pred)$
MDA8 Bias Error Paired	Average of the differences in MDA8 observed value and the corresponding predicted concentration at the hour that the observational maximum was reached. Negative values indicate under-prediction. $BiasError = \frac{1}{N}\sum(Obs - Pred)$

MDA8 Gross Error Unpaired	Average of the absolute differences in observed and predicted MDA8 values $GrossError = \frac{1}{N}\sum\lvert Obs - Pred\rvert$
MDA8 Gross Error Paired	Average of the absolute differences in MDA8 observed value and the corresponding predicted concentration at the hour that the observational maximum was reached. $GrossError = \frac{1}{N}\sum\lvert Obs - Pred\rvert$
Normalized MDA8 Bias Error Unpaired	Average of the quantity: difference in observed and predicted MDA8 values normalized by the observed MDA8 values. Negative values indicate under-prediction. $NormBiasError = \frac{1}{N}\sum\left(\frac{Obs-Pred}{Obs}\right)\cdot 100$
Normalized MDA8 Bias Error Paired	Average of the quantity: difference in MDA8 observed value and the corresponding predicted concentration at the hour that the observational maximum was reached normalized by the observed MDA8 concentration. Negative values indicate under-prediction. $NormBiasError = \frac{1}{N}\sum\left(\frac{Obs-Pred}{Obs}\right)\cdot 100$
Normalized MDA8 Gross Error Unpaired	Average of the quantity: absolute difference in observed and predicted MDA8 values normalized by the observed MDA8 concentration $NormGrossError = \frac{1}{N}\sum\left\lvert\frac{Obs-Pred}{Obs}\right\rvert\cdot 100$
Normalized MDA8 Gross Error Paired	Average of the quantity: absolute difference in MDA8 observed value and the corresponding predicted concentration at the hour that the observational maximum was reached normalized by the observed MDA8 concentration $NormGrossError = \frac{1}{N}\sum\left\lvert\frac{Obs-Pred}{Obs}\right\rvert\cdot 100$
Peak Prediction Accuracy Unpaired	Difference in the maximum of the observed MDA8 and the maximum of the predicted MDA8

normalized by the maximum of the observed MDA8

$$PPA = \frac{(maximum(Pred) - \text{maximum}\ (Obs))}{\text{maximum}(Pred)}$$

Predicted concentrations are extracted from model output in the grid cell that each monitoring station resides.

The base year average regional model performance for May through September 2018 for each of the six regions within the Basin are presented in Tables V-5-3 to V-5-8 for days when regional maximum 8-hour ozone levels were at least 60 ppb. Only stations with more than 75% of the hourly measurements during each month of the ozone season were included in the analysis.

In general, the model over-predicts maximum daily average 8-hr (MDA8) ozone concentrations in the "Coastal", "UrbanSource", and "UrbanReceptor" regions. Conversely, the model underestimates MDA8 ozone concentrations in the "SanFernando" and "Foothills" regions. For example, the predicted paired MDA8 Mean is 56.7 ppb in September in Coastal region, 57.9 ppb in August for UrbanSource region, 73.2 in August for UrbanReceptor region, 64.5 ppb ppb in August for SanFernando region, and 68.8 ppb in August for Foothills region, versus corresponding observed values of 54.3 ppb, 57.5 ppb, 70.3 ppb, 71.6 ppb, and 69.3 ppb, respectively; the statistics in Tables V-5-3 to V-5-8 are given for the days with MDA8 > 60 ppb in each month during ozone season.

The U.S. EPA guidance describes four types of analyses for the evaluation of model performance: operational, diagnostic, dynamic and probabilistic. The operational evaluation techniques include statistical and graphical analyses aimed at determining whether the modeled simulated variables are comparable to measurements and the diagnostic evaluation focuses on process-oriented analyses that determine whether the individual processes and components of the model system are working correctly, both independently and in combination.

The dynamic evaluation assesses the ability of the air quality model to predict changes in air quality given changes in emissions or meteorology, the principal forces that drive the air quality model. A form of dynamic evaluations can be historical (i.e., retrospective) or it can employ the base year simulation provided that there are sufficient changes in emissions (i.e., by day of week). If the evaluation is historical, it is important to account for differences in meteorology. This chapter includes an extensive discussion of ozone sensitivity toward historical meteorology which can be considered a form of dynamic evaluation. Importantly, the model captured high ozone levels in 2020, as compared to the 2016-2019 period, without considering changes in emissions. This trend agreed well with observations. The U.S. EPA guidance states that a dynamic evaluation can also assess operational performance under varying conditions (e.g., by day of the week, by season, and by region). The mix of pollutants vary by day of the week and from city to city so when a model shows good operational performance across these different chemical environments, this supports the assertion that it will respond appropriately to changes in emissions. The AQMP attainment modeling includes a five-month simulation period from May to September, which includes various meteorological conditions, emissions variability, seasonal changes, etc. The ozone "weekend effect" can

be exploited to perform a dynamic evaluation. The weekend effect is explained in detail as part of the weight of evidence discussion presented later in this chapter. Briefly, NOx emissions are substantially lower on weekends compared to weekdays while VOC emissions remain similar assuming similar meteorology. This has the effect of moving from right to left in Figure V-5-2, which can either result in an ozone increase or decrease depending on the chemical environment.

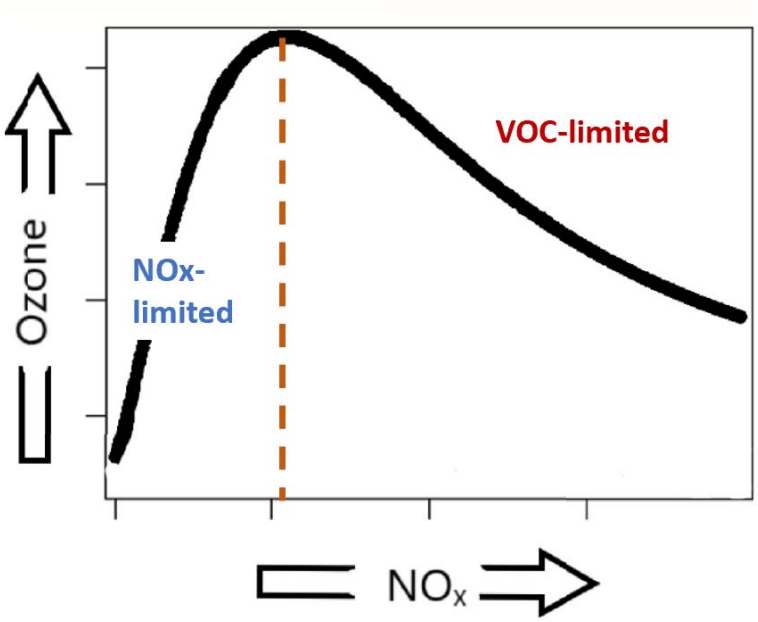

FIGURE V-5-2

OZONE VS. NOX RELATIONSHIP ASSUMING CONSTANT VOC REACTIVITY

CMAQ model performance was evaluated independently on weekends and weekdays and robust model performance across the different chemical environments was observed. Figure V-5-3 includes scatter plots of 2018 MDA8 ozone predictions versus observations color-coded by weekends versus weekdays; both the MDA8 data points and a generalized linear model fit (line) with 95 percent confidence interval (shaded area) along with 1:1 line are shown in the scatter plots. Supplemental scatter plots of observed versus predicted MDA8 ozone and daily averages of its precursors (i.e., NO, NO2, NOx, and NOy) on weekends versus weekdays for each specific station (including stations outside the Basin within model domain such as Phelan, Simi Valley, and Hesperia) are provided as Attachment 2 to this appendix. As shown on the plots, weekend and weekday data points show a distinct separation for those stations with a more pronounced weekend effect such that the slope fitted to weekend data points is larger than that for weekdays, supporting the assertion that the model responds appropriately to changes in emissions; the model performance is almost identical on other stations such as those in Coachella Valley region (see attachment 2), West Los Angles, and Redlands.

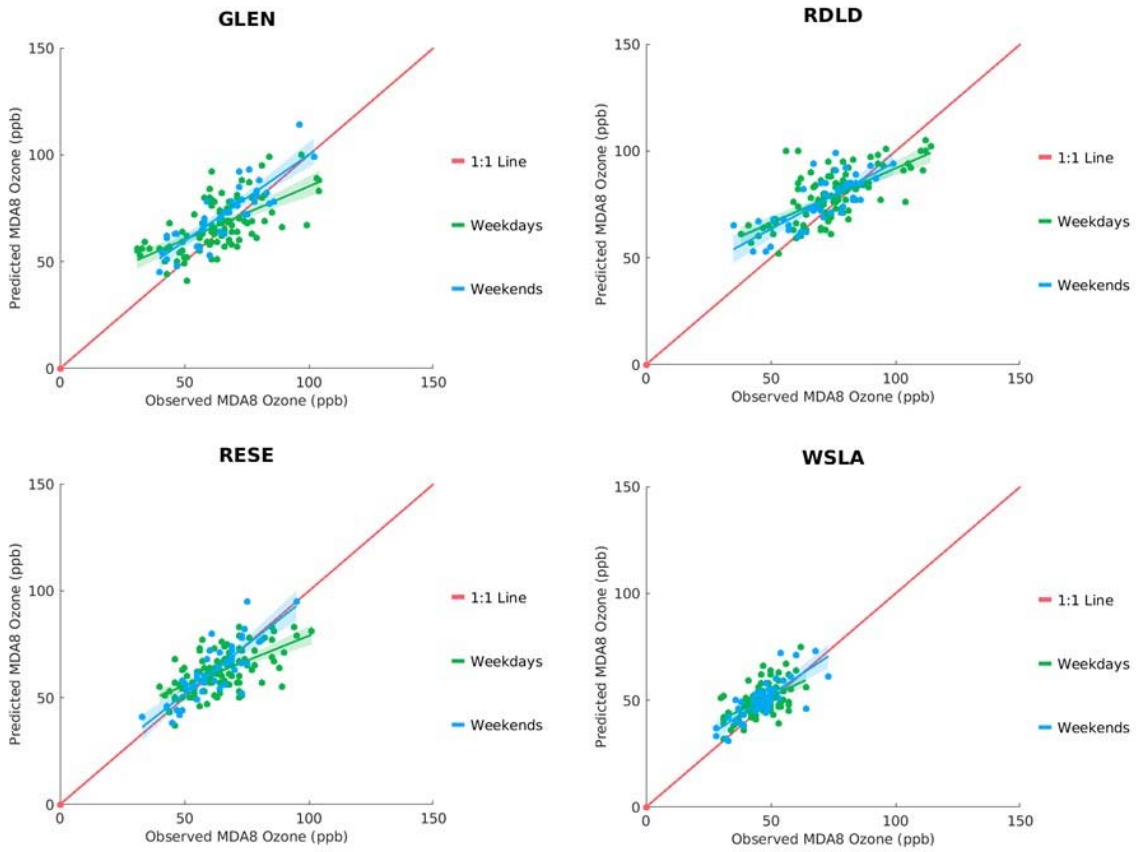

FIGURE V-5-3

OBSERVED VS. PREDICTED MDA8 OZONE COLOR-CODED BY WEEKDAYS VS. WEEKENDS FOR GLENDORA (GLEN), REDLANDS (RDLD), RESEDA (RESE), AND WEST LA (WSLA). GREEN AND BLUE LINES INDICATE GENERAL LINEAR MODEL FIT WITH 95% CONFIDENCE INTERVAL (SHADED AREA). THE RED LINE INDICATES 1:1 LINE.

Lastly, the probabilistic evaluation attempts to assess the level of confidence in the model predictions through techniques such as ensemble model simulations. While not presented in this AQMP, the CAMx model was tested extensively as part of Multiple Air Toxics Exposure Studies (MATES) and these tests serve as form of ensemble analysis. CAMx has previously been demonstrated to yield results comparable to those of CMAQ for the modeling cases (not presented), which supports the use of CMAQ as the primary modeling platform. The Weather Research and Forecasting (WRF) model coupled with Chemistry (WRF-Chem) was used to evaluate the CMAQ model performance. CMAQ predictions of air pollutants concentrations and their temporal/spatial variations generally agree well with WRF-Chem predictions (not presented in this AQMP). In all, the 2022 AQMP covers all four types of model performance evaluation methods as recommended by the U.S. EPA.

TABLE V-5-3

2018 BASE YEAR MDA8 OZONE PERFORMANCE FOR DAYS WHEN REGIONAL MDA8 ≥ 60 PPB IN THE "COASTAL" REGION

Month	Mean*Pred. [ppb]	Mean * Obs. [ppb]	Number of Days with regional MDA8>= 60 ppb	MDA8 Mean Pred. Unpaired [ppb]	MDA8 Mean Pred. Paired [ppb]	MDA8 Mean Obs. [ppb]	MDA8 Bias Err. Unpaired [ppb]	MDA8 Bias Err. Paired [ppb]	MDA8 Gross Err. Unpaired [ppb]	MDA8 Gross Err. Paired [ppb]	Norm MDA8 Bias Err. Unpaired [%]	Norm MDA8 Bias Err. Paired [%]	Norm MDA8 Gross Err. Unpaired [%]	Norm MDA8 Gross Err. Paired [%]	Peak Prediction Accuracy Unpaired [%]
May	49.7	45.8	2	68.0	67.3	60.5	7.5	6.8	7.5	6.8	13.0	11.8	13.0	11.8	7.5
Jun	50.4	46.5	4	53.3	52.3	55.4	-2.2	-3.1	6.8	6.8	-3.0	-4.8	12.1	11.9	-2.8
Jul	48.9	42.4	4	61.5	60.2	57.3	4.2	2.8	8.5	7.7	7.2	4.9	14.1	12.9	8.3
Aug	48.9	43.4	2	56.0	55.0	55.5	0.5	-0.5	5.2	5.2	1.7	-0.2	9.3	8.9	-1.4
Sep	55.4	51.3	8	59.1	58.4	58.3	0.8	0.1	7.3	7.3	2.8	1.6	12.7	12.7	-3.7

*monthly mean of MDA8 ozone including days with regional MDA8 < 60 ppb

TABLE V-5-4

2018 BASE YEAR MDA8 OZONE PERFORMANCE FOR DAYS WHEN REGIONAL MDA8 ≥ 60 PPB IN THE "SANFERNANDO" REGION

Month	Mean* Pred. [ppb]	Mean* Obs. [ppb]	Number of Days with regional MDA8 >= 60 ppb	MDA8 Mean Pred. Unpaired [ppb]	MDA8 Mean Pred. Paired [ppb]	MDA8 Mean Obs. [ppb]	MDA8 Bias Err. Unpaired [ppb]	MDA8 Bias Err. Paired [ppb]	MDA8 Gross Err. Unpaired [ppb]	MDA8 Gross Err. Paired [ppb]	Norm MDA8 Bias Err. Unpaired [%]	Norm MDA8 Bias Err. Paired [%]	Norm MDA8 Gross Err. Unpaired [%]	Norm MDA8 Gross Err. Paired [%]	Peak Prediction Accuracy Unpaired [%]
May	58.159.2	54.0	8	67.5	67.0	70.8	-3.3	-3.8	9.8	10.1	-3.4	-4.1	13.2	13.7	-15.2
Jun	65.8	67.3	23	67.7	66.9	69.9	-2.2	-2.9	7.7	7.9	-2.2	-3.3	10.7	11.0	-12.8
Jul	67.4	67.1	23	71.0	70.5	72.3	-1.3	-1.8	8.6	8.7	-1.1	-1.7	12.0	12.2	-5.2
Aug	62.3	67.7	24	64.9	64.4	71.6	-6.7	-7.3	12.1	12.0	-7.1	-7.9	16.0	15.7	-27.7
Sep	68.1	65.7	23	69.0	68.5	69.2	-0.3	-0.8	6.1	6.0	0.2	-0.6	8.8	8.6	4.5

*monthly mean of MDA8 ozone including days with regional MDA8 < 60 ppb

TABLE V-5-5

2018 BASE YEAR MDA8 OZONE PERFORMANCE FOR DAYS WHEN REGIONAL MDA8 ≥ 60 PPB IN THE "FOOTHILLS" REGION

Month	Mean* Pred. [ppb]	Mean* Obs. [ppb]	Number of Days with regional MDA8 >= 60 ppb	MDA8 Mean Pred. Unpaired [ppb]	MDA8 Mean Pred. Paired [ppb]	MDA8 Mean Obs. [ppb]	MDA8 Bias Err. Unpaired [ppb]	MDA8 Bias Err. Paired [ppb]	MDA8 Gross Err. Unpaired [ppb]	MDA8 Gross Err. Paired [ppb]	Norm MDA8 Bias Err. Unpaired [%]	Norm MDA8 Bias Err. Paired [%]	Norm MDA8 Gross Err. Unpaired [%]	Norm MDA8 Gross Err. Paired [%]	Peak Prediction Accuracy Unpaired [%]
May	55.9	48.9	7	66.0	65.7	68.2	-2.2	-2.5	5.4	5.3	-3.5	-4.0	8.1	8.1	1.2
Jun	62.3	62.1	18	64.8	64.5	69.0	-4.2	-4.5	8.1	8.1	-5.6	-5.9	11.4	11.3	-13.8
Jul	69.0	65.7	21	70.5	69.6	68.3	2.3	1.3	10.1	9.6	3.6	2.3	14.7	14.1	9.6
Aug	65.3	65.4	24	68.6	68.2	69.3	-0.7	-1.1	9.3	9.2	0.7	0.0	13.4	13.1	-13.0
Sep	66.1	62.7	21	68.3	67.9	66.3	2.0	1.7	5.5	5.5	3.4	2.9	8.5	8.5	-3.0

*monthly mean of MDA8 ozone including days with regional MDA8 < 60 ppb

TABLE V-5-6

2018 BASE YEAR MDA8 OZONE PERFORMANCE FOR DAYS WHEN REGIONAL MDA8 ≥ 60 PPB IN THE "URBANSOURCE" REGION

Month	Mean* Pred. [ppb]	Mean* Obs. [ppb]	Number of Days with regional MDA8 >= 60 ppb	MDA8 Mean Pred. Unpaired [ppb]	MDA8 Mean Pred. Paired [ppb]	MDA8 Mean Obs. [ppb]	MDA8 Bias Err. Unpaired [ppb]	MDA8 Bias Err. Paired [ppb]	MDA8 Gross Err. Unpaired [ppb]	MDA8 Gross Err. Paired [ppb]	Norm MDA8 Bias Err. Unpaired [%]	Norm MDA8 Bias Err. Paired [%]	Norm MDA8 Gross Err. Unpaired [%]	Norm MDA8 Gross Err. Paired [%]	Peak Prediction Accuracy Unpaired [%]
May	51.9	43.6	2	70.3	69.8	60.2	10.1	9.6	10.5	10.0	17.0	16.2	17.6	16.8	18.3
Jun	55.6	49.3	8	59.9	59.4	56.9	3.0	2.5	8.0	7.9	5.5	4.6	14.0	13.8	10.5
Jul	57.1	48.6	12	66.1	65.5	55.8	10.4	9.8	12.7	12.2	19.9	18.7	23.9	22.9	15.2
Aug	55.9	49.2	13	58.6	58.2	57.5	1.2	0.8	6.3	6.2	2.7	1.9	11.2	10.9	-4.5
Sep	59.3	51.2	9	62.5	62.1	57.5	5.0	4.6	7.5	7.2	9.1	8.4	13.3	12.7	10.0

*monthly mean of MDA8 ozone including days with regional MDA8 < 60 ppb

TABLE V-5-7

2018 BASE YEAR MDA8 OZONE PERFORMANCE FOR DAYS WHEN REGIONAL MDA8 ≥ 60 PPB IN THE "URBANRECEPTOR" REGION

Month	Mean* Pred. [ppb]	Mean* Obs. [ppb]	Number of Days with regional MDA8 >= 60 ppb	MDA8 Mean Pred. Unpaired [ppb]	MDA8 Mean Pred. Paired [ppb]	MDA8 Mean Obs. [ppb]	MDA8 Bias Err. Unpaired [ppb]	MDA8 Bias Err. Paired [ppb]	MDA8 Gross Err. Unpaired [ppb]	MDA8 Gross Err. Paired [ppb]	Norm MDA8 Bias Err. Unpaired [%]	Norm MDA8 Bias Err. Paired [%]	Norm MDA8 Gross Err. Unpaired [%]	Norm MDA8 Gross Err. Paired [%]	Peak Prediction Accuracy Unpaired [%]
May	64.4	57.5	20	68.0	67.5	63.6	4.4	3.9	7.1	7.0	9.1	8.2	12.3	12.0	-11.8
Jun	73.8	73.1	28	75.6	75.2	75.1	0.4	0.0	8.1	8.2	2.5	1.9	11.2	11.2	-23.8
Jul	79.3	74.4	31	79.3	78.4	74.4	4.9	4.0	9.4	9.1	7.8	6.6	13.3	12.8	-5.6
Aug	75.3	70.6	31		74.6	70.6	4.7	4.0	10.1	9.9	8.4	7.4	15.3	15.0	-6.6
Sep	72.4	65.1	28	73.1	72.3		6.5	5.7	9.4	9.1	11.1	9.9	15.2	14.6	1.0

*monthly mean of MDA8 ozone including days with regional MDA8 < 60 ppb

TABLE V-5-8

2018 BASE YEAR MDA8 OZONE PERFORMANCE FOR DAYS WHEN REGIONAL MDA8 ≥ 60 PPB IN THE "COACHELLAVALLEY" REGION

Month	Mean* Pred. [ppb]	Mean* Obs. [ppb]	Number of Days with regional MDA8 >= 60 ppb	MDA8 Mean Pred. Unpaired [ppb]	MDA8 Mean Pred. Paired [ppb]	MDA8 Mean Obs. [ppb]	MDA8 Bias Err. Unpaired [ppb]	MDA8 Bias Err. Paired [ppb]	MDA8 Gross Err. Unpaired [ppb]	MDA8 Gross Err. Paired [ppb]	Norm MDA8 Bias Err. Unpaired [%]	Norm MDA8 Bias Err. Paired [%]	Norm MDA8 Gross Err. Unpaired [%]	Norm MDA8 Gross Err. Paired [%]	Peak Prediction Accuracy Unpaired [%
May	67.0	64.1	21	69.5	68.9	68.8	0.8	0.2	4.3	4.3	2.1	1.2	6.3	6.4	-11.2
Jun	74.1	74.0	27	75.5	74.2	76.4	-0.9	-2.2	8.2	8.1	-0.1	-1.9	11.0	10.7	0.0
Jul	70.4	63.1	22	70.9	69.3	69.0	1.9	0.3	7.2	6.9	3.5	1.0	10.5	10.1	3.4
Aug	70.5	65.9	26	70.8	69.1	68.3	2.4	0.7	9.5	9.6	4.6	2.1	14.5	14.6	12.2
Sep	65.3	54.3	9	64.9	62.1	65.8	-0.9	-3.7	4.7	5.8	-0.8	-5.3	7.1	8.8	-6.5

*monthly mean of MDA8 ozone including days with regional MDA8 < 60 ppb

Model performance can be evaluated graphically with scatter plots. Figure V-5-4 compares the measured and modeled MDA8 ozone concentrations for 2018 in each region.

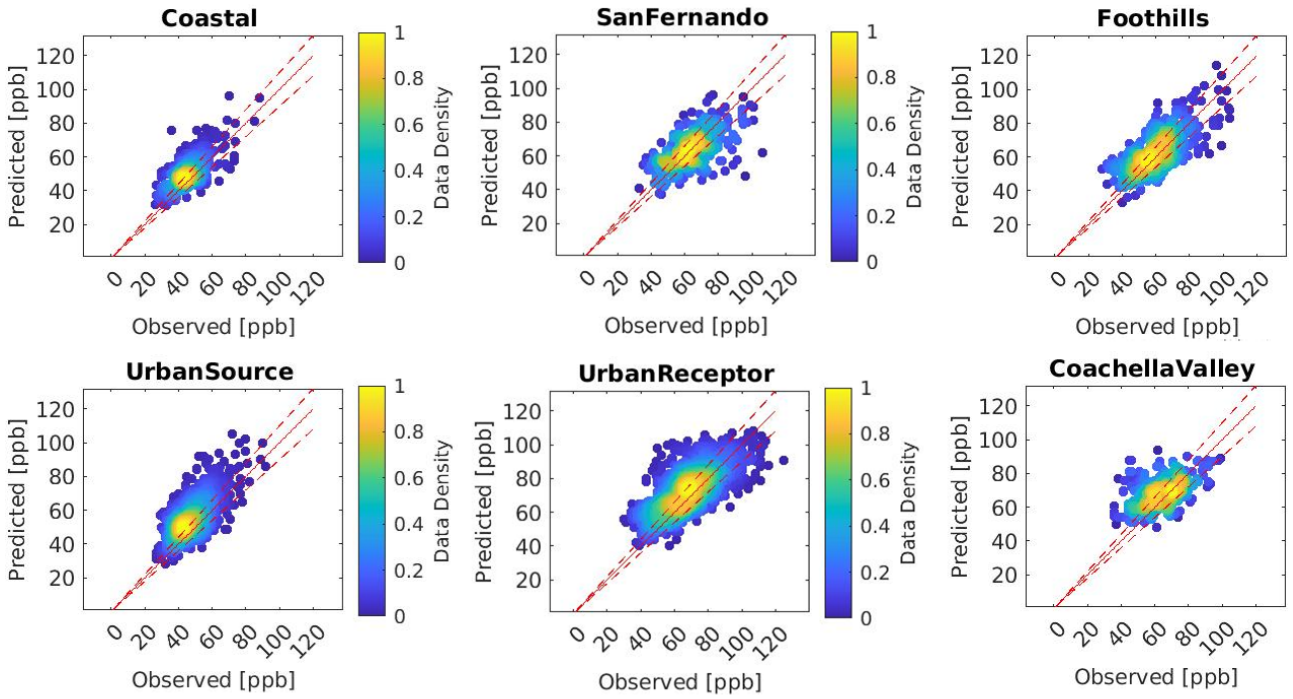

FIGURE V-5-4

OBSERVED VS. PREDICTED MAXIMUM DAILY AVERAGE 8-HOUR (MDA8) OZONE. DASHED LINES INDICATE 10% ERROR BOUNDS.

The scatter and density scatter plots show consistent results: low bias in the high concentration cases and high bias in the low concentration regime with larger deviations at low concentrations. Geographical bias is also evident, with over-prediction in the coastal zone and 'UrbunSource' zones and under-prediction in the 'San Fernando' zone. Still, predictions in the 'UrbanReceptor' zone, in where the design site and most of traditional receptor stations are located, agrees reasonably well with the measurements. While the model deviation is more noticeable at low concentrations, the latest U.S. EPA guidance requires the use of only the top 10 days greater than 60 ppb in the RRF calculation, indicating that the modeling capability to predict high concentrations is more important than the prediction of low concentrations.

Time Series and Hourly Boxplots of Observed and Predicted Ozone

Figures V-5-5 through V-5-10 show the diurnal trends of observed and predicted maximum daily average 8-hour (MDA8) ozone concentrations for each day from May 1st through September 30th, 2018, for six stations

following a transport route from the coastal area of the Basin to inland Crestline and Redlands. Supplemental diurnal observed and predicted MDA8 ozone and daily averages of its precursors (i.e., NO, NO2, NOx, and NOy) for all remaining air quality sites (including stations outside the Basin within model domain such as Phelan, Simi Valley, and Hesperia) are provided as Attachment 2 to this appendix.

The geographical bias is clearly present in the MDA8 ozone time series – over-prediction in West Los Angeles, and under-prediction in the inland area. However, the under-prediction of peak concentration is not rare in photochemical modeling. In fact, South Coast AQMD has successfully demonstrated its capability to predict episodic events better than other agencies in the nation, including the National Oceanic and Atmospheric Administration (NOAA)/EPA, the official air quality forecast agency.

Overall, it is important to note that the effects of prediction biases or errors are mitigated by the use of relative response factors for the attainment analysis.

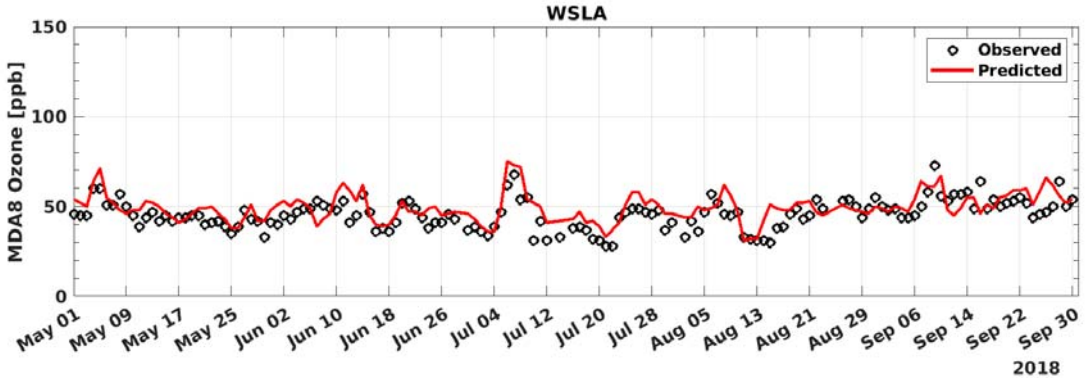

FIGURE V-5-5

TIME SERIES OF OBSERVED VS. PREDICTED MAXIMUM DAILY AVERAGE 8-HOUR (MDA8) WEST LOS ANGELES OZONE

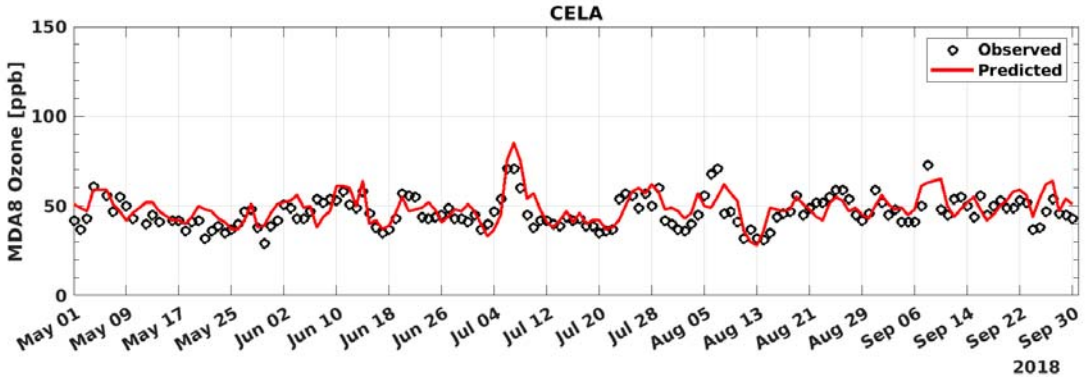

FIGURE V-5-6

TIME SERIES OF OBSERVED VS. PREDICTED MAXIMUM DAILY AVERAGE 8-HOUR (MDA8) CENTRAL LOS ANGELES OZONE

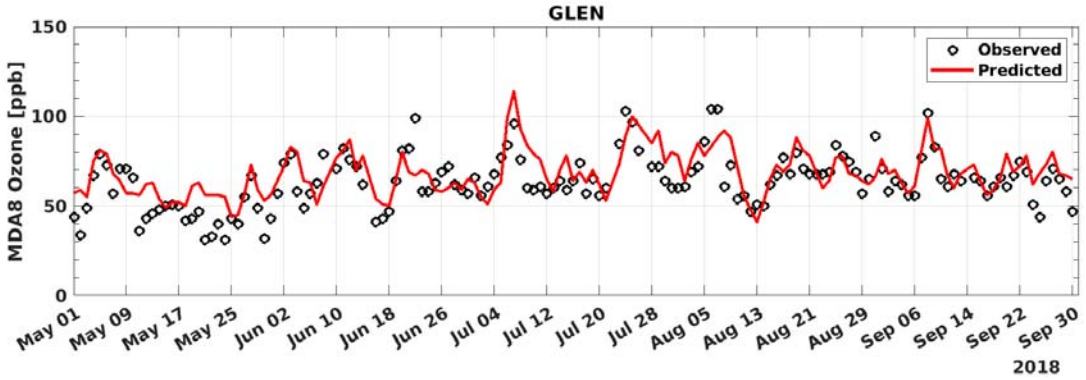

FIGURE V-5-7

TIME SERIES OF OBSERVED VS. PREDICTED MAXIMUM DAILY AVERAGE 8-HOUR (MDA8) GLENDORA OZONE

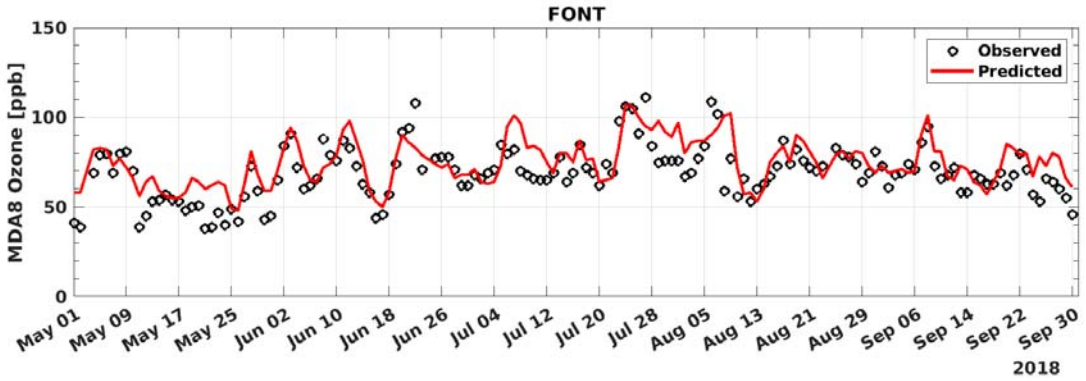

FIGURE V-5-8

TIME SERIES OF OBSERVED VS. PREDICTED MAXIMUM DAILY AVERAGE 8-HOUR (MDA8) FONTANA OZONE

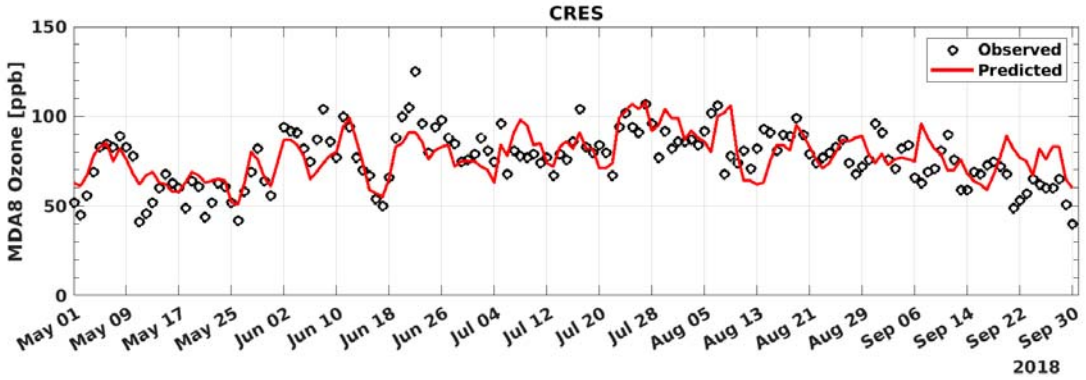

FIGURE V-5-9

TIME SERIES OF OBSERVED VS. PREDICTED MAXIMUM DAILY AVERAGE 8-HOUR (MDA8) CRESTLINE OZONE

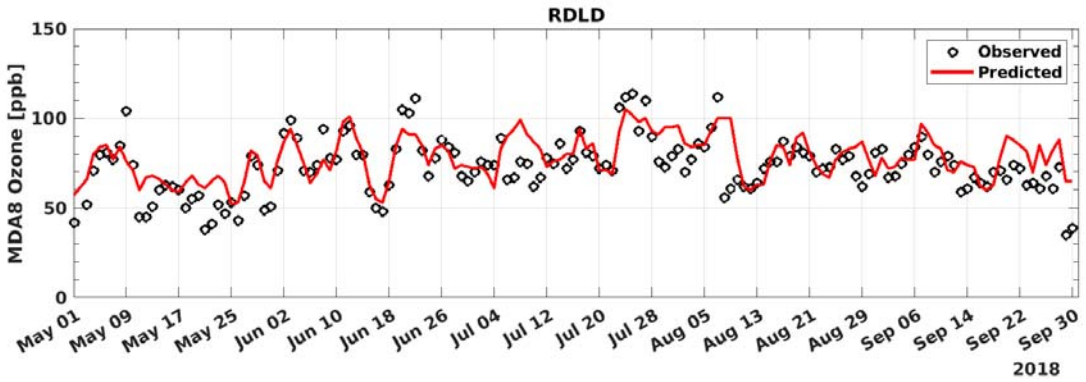

FIGURE V-5-10

TIME SERIES OF OBSERVED VS. PREDICTED MAXIMUM DAILY AVERAGE 8-HOUR (MDA8) REDLANDS OZONE

Figures V-5-11 through V-5-16 show the box-and-whisker plots (boxplots hereafter) of hourly profiles of observed and predicted 1-hour ozone concentrations during May 1st through September 30th, 2018 for the same stations as in previous sections. Included in Attachment 2 to this appendix are observed and predicted hourly profiles of 1-hour ozone and its precursors (i.e., NO, NO2, NOx, and NOy) for all remaining air quality sites. The box is drawn between the 25th (Q_1) and 75th (Q_3) percentiles, with a horizontal line drawn in the middle indicating the median. The whiskers extend above and below the box to the most extreme data points that are within a distance to the box equal to 1.5 times the interquartile range ($1.5\times(Q_3 - Q_1)$; Tukey boxplot). Points outside the whiskers' ranges indicating outliers are plotted too. As shown on the boxplots, model is in agreement with observations in prediction of hourly changes of ozone concentrations throughout the day indicating lower ozone medians at night and higher values during day-time. The model tends to over-predict the ozone medians at West LA and Central LA throughout the day, however, day-time predictions agree well with observations at inland stations. The time and magnitude of the ozone peaks are well-captured by the model; for example, the model correctly predicts that ozone concentrations peak at 13:00 in West LA, Central LA, and Glendora stations.

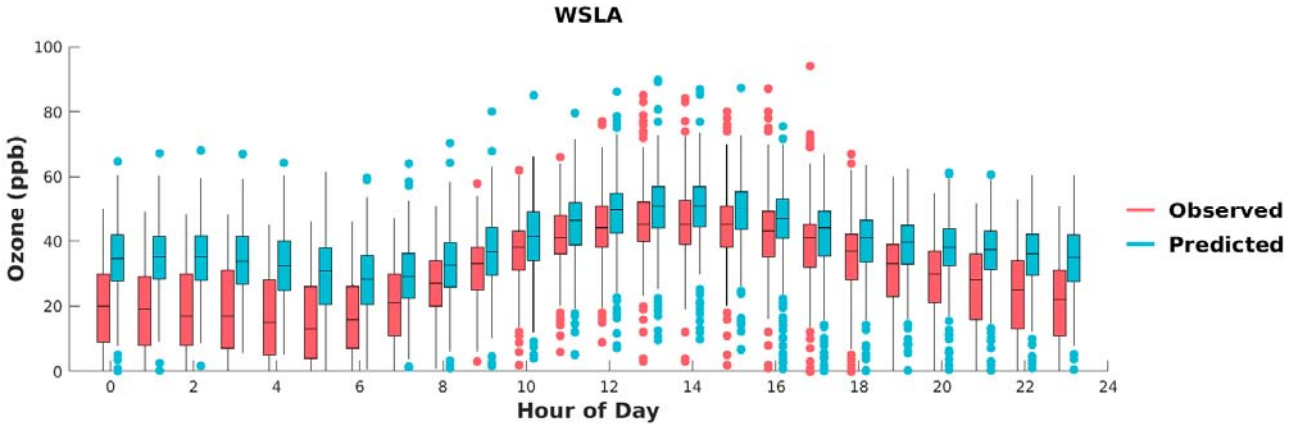

FIGURE V-5-11

BOX PLOTS OF OBSERVED VS. PREDICTED HOURLY OZONE IN WEST LOS ANGELES. HORIZONTAL LINES INDICATE 25TH, 50TH (MEDIAN; MIDDLE LINE), AND 75TH PERCENTILES.

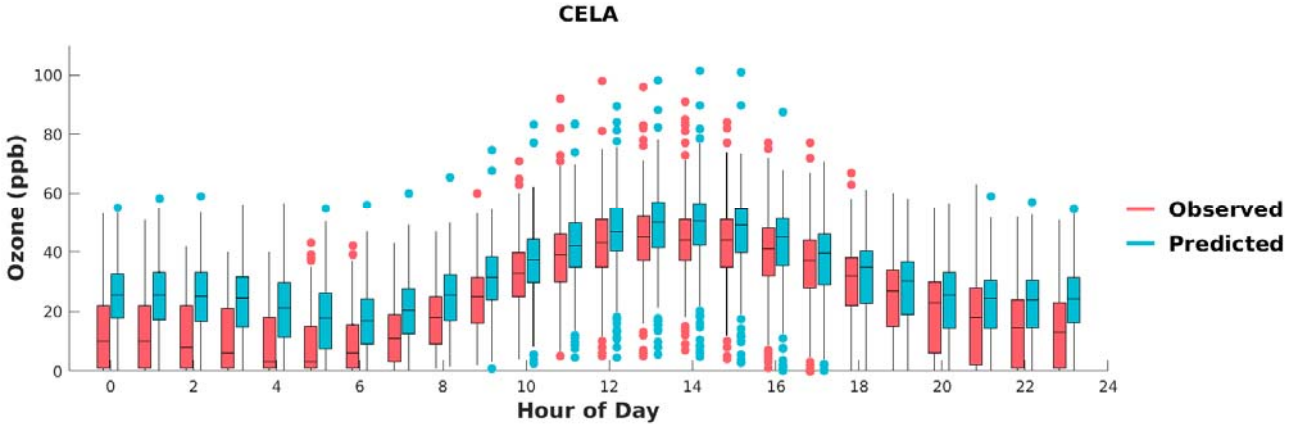

FIGURE V-5-12

BOX PLOTS OF OBSERVED VS. PREDICTED HOURLY OZONE IN CENTRAL LOS ANGELES. HORIZONTAL LINES INDICATE 25TH, 50TH (MEDIAN; MIDDLE LINE), AND 75TH PERCENTILES.

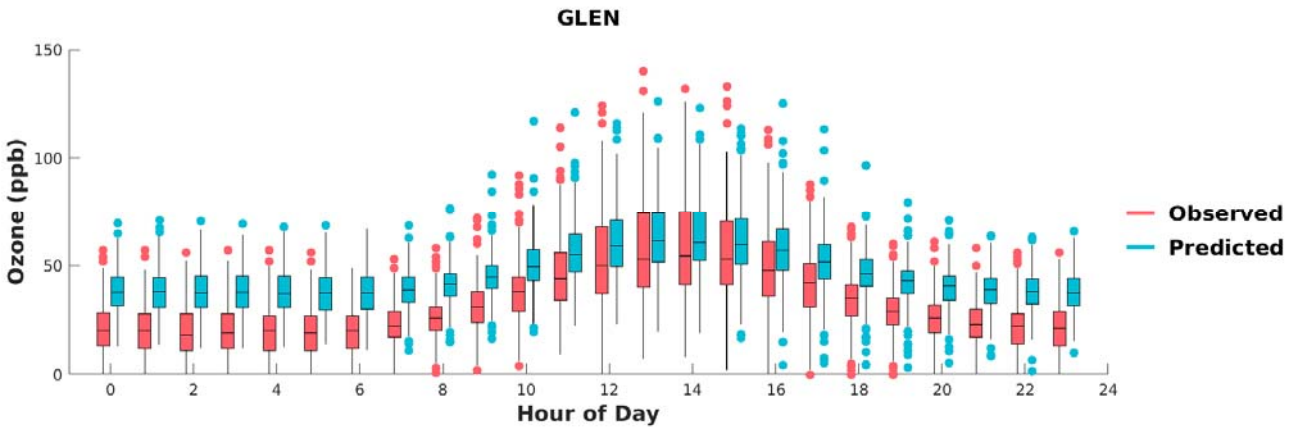

FIGURE V-5-13

BOX PLOTS OF OBSERVED VS. PREDICTED HOURLY OZONE IN GLENDORA. HORIZONTAL LINES INDICATE 25TH, 50TH (MEDIAN; MIDDLE LINE), AND 75TH PERCENTILES.

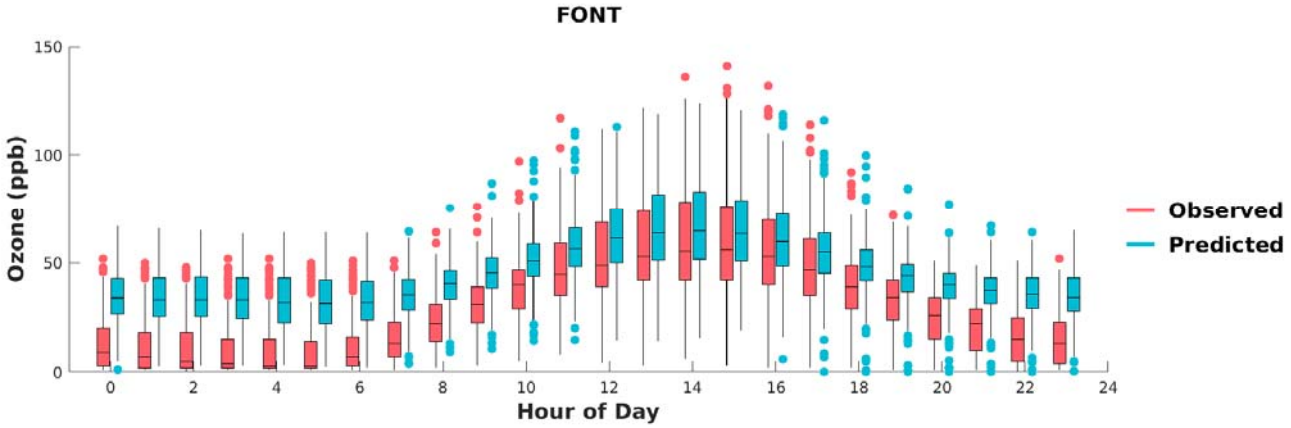

FIGURE V-5-14

BOX PLOTS OF OBSERVED VS. PREDICTED HOURLY OZONE IN FONTANA. HORIZONTAL LINES INDICATE 25TH, 50TH (MEDIAN; MIDDLE LINE), AND 75TH PERCENTILES.

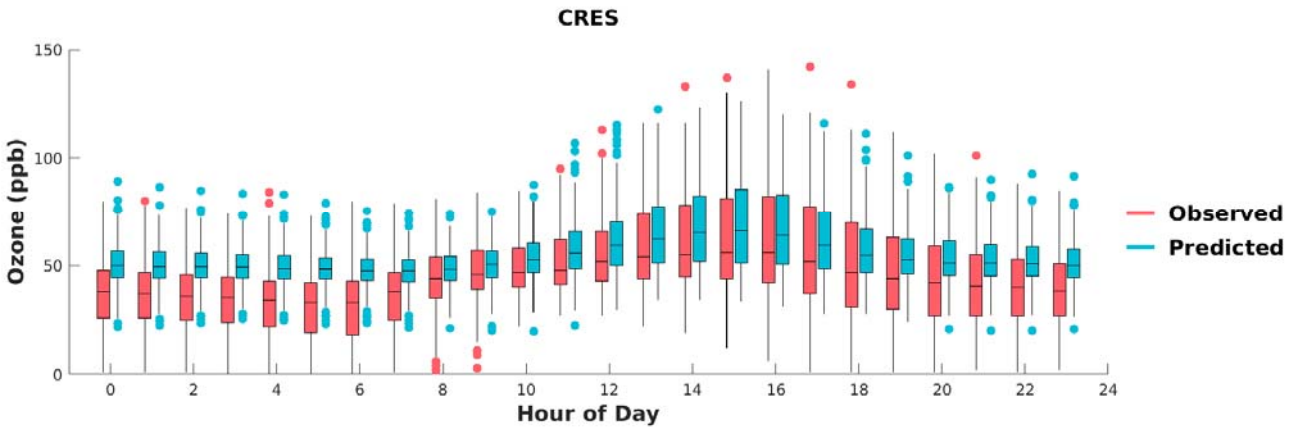

FIGURE V-5-15

BOX PLOTS OF OBSERVED VS. PREDICTED HOURLY OZONE IN CRESTLINE. HORIZONTAL LINES INDICATE 25TH, 50TH (MEDIAN; MIDDLE LINE), AND 75TH PERCENTILES.

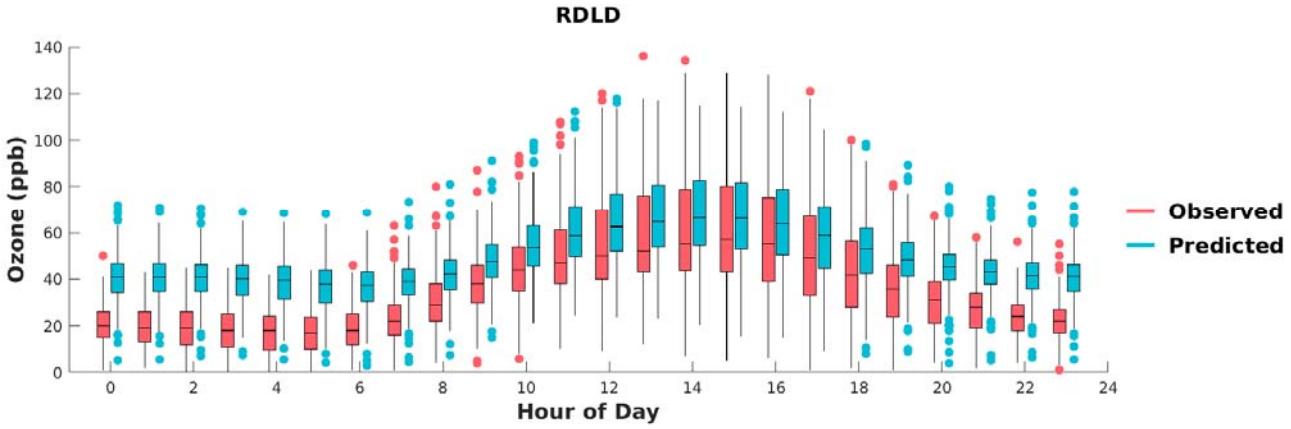

FIGURE V-5-16

BOX PLOTS OF OBSERVED VS. PREDICTED HOURLY OZONE IN REDLANDS. HORIZONTAL LINES INDICATE 25TH, 50TH (MEDIAN; MIDDLE LINE), AND 75TH PERCENTILES.

Base-Year VOC Model Performance Evaluation

A VOC performance evaluation is presented in Attachment 5. VOC measurements used for this analysis included measurements of toxic VOC species at seven stations as part of the Multiple Air Toxics Exposure Study V (MATES V) monitoring campaign[2] and measurements of carbonyl and hydrocarbon species at five

[2] The MATES V monitoring campaign was conducted from May 2018-April 2019, although measurements at some stations began several months earlier. All available data was included in this analysis.

stations in the Photochemical Assessment Monitoring Stations (PAMS) network. In 2018, both programs collected 24-hour VOC samples on a 1-in-6 day schedule. Scatter plots (predicted vs. observed) of several VOCs are presented in addition to quarterly average comparisons by monitoring site. Overall, reasonable model performance is demonstrated, although the model underpredicted concentrations for most VOCs.

Base-Year Vertical Profiles

Vertical profiles are presented in Attachment 6 for several species including NO, NO2, HNO3, O3, and select VOCs. The profiles represent Basin averages for the month of July (i.e., all hours in July and all grid cells within the Basin were averaged) and extend from ground-level up to the highest modeling layer at approximately 16 km. Vertical cross-sections up to approximately 1 km are also presented.

July was chosen as it exhibited a combination of moderate and high ozone events. In the profiles, the tropopause is denoted by a dashed line and assumes a height of 11 km. The lack of vertically resolved measurements for these species precludes a comprehensive model performance evaluation. However, the profiles are consistent with a qualitative understanding of the atmosphere. For example, NOx emissions primarily occur at ground-level where the highest concentrations are expected, yet NOx also exists in higher concentrations in the stratosphere due to photolysis of N2O and commercial aircraft emissions. VOCs, which are also emitted at ground-level, are reactive species and therefore are unable to survive long enough to be transported to the stratosphere. Thus, their concentrations taper off rapidly. The profiles are consistent with these trends, demonstrating that CMAQ performs as expected.

Ozone Modeling – Developing Ozone Isopleths

The set of 153 days from May 1st through September 30th, 2018, was simulated and analyzed to determine daily 8-hour average maximum ozone for the 2018 and 2037 emissions inventories. A set of simulations with incremental VOC and NOx emission reductions from the 2037 baseline emissions was generated to create ozone isopleths for each station in the Basin. The ozone isopleths, included in Attachment 4 of Appendix 5, provide updated guidance for the formulation of the future control strategies. They represent the projected design values under NOx and VOC control scenarios using RRFs. Ozone RRFs were calculated using the ratio methodology described in detail in Chapter 1 of Appendix V. A sample of the RRF calculation is provided in the next section.

The isopleths approximate the expected ozone design value for a given level of VOC and NOx emissions. Thus, the isopleths can be used to guide the attainment strategy. The isopleth for Glendora (GLEN), the site with the highest predicted design value in the attainment scenario, and Crestline (CRES) are depicted in Figure V-5-17. The NOx and VOC emissions correspond to the Basin total. Attainment occurs for design values less than or equal to 70.9 ppb, which is denoted by the white contour in the isopleth. With VOC emissions greater than 300 tons per day, the corresponding NOx emissions along the white contour are approximately 60-70 tons per day at GLEN and 70-80 tons per day at CRES. The isopleth further demonstrates that VOC reductions alone are insufficient to demonstrate attainment; NOx reductions are the only pathway to attainment. Ozone chemistry depends on location specific emissions and meteorology. Therefore, the NOx emission meeting the

70.9 ppb varies from station to station. Additionally, the isopleths were developed using across-the-board emission reduction percentage, not category specific reductions, therefore, the estimated NOx amount to meet the standard from the isopleths is different from the attainment scenario presented in the 2022 AQMP and later chapter of this Appendix.

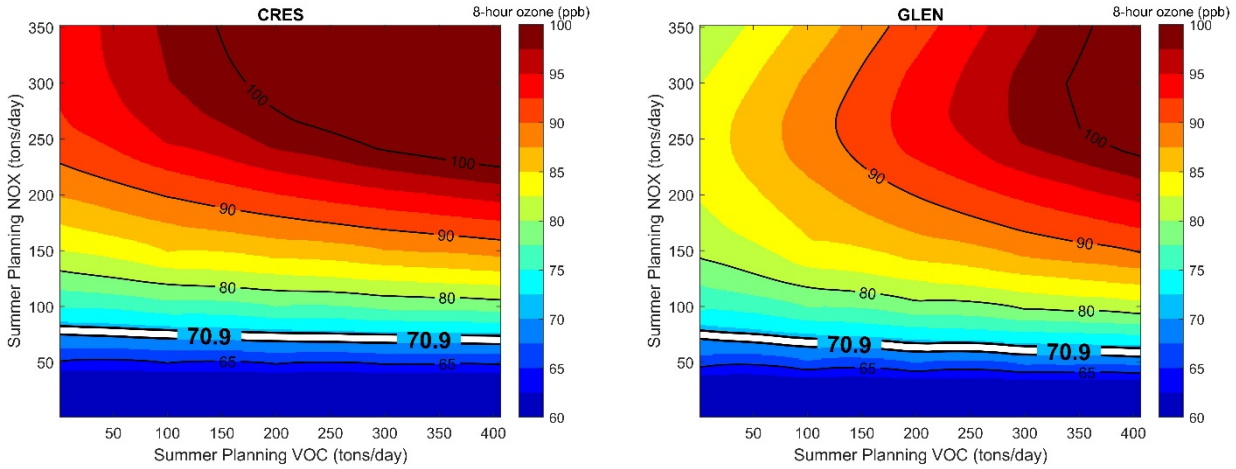

FIGURE V-5-17

ISOPLETH FOR CRESTLINE AND GLENDORA DEPICTING BASIN TOTAL NOX AND VOC EMISSIONS AND CORRESPONDING OZONE DESIGN VALUE

Consistent with previous AQMPs, attainment demonstration simulations do not include emissions from wildfires in either base year simulations or future year simulations. While wildfire smoke can have a significant impact on particulate matter concentrations and wildfire events pending the exceptional event demonstration can be discarded for the determination of PM2.5 standards attainment, wildfire emissions have very limited effect on ozone design values. In particular, wildfire events had very limited impact on ozone concentrations during the entire modeling period in 2018, and in particular, on the top-10 days that are used for the RRF calculation. High ozone days in the Basin are typically driven by photochemical reactions from NOx and VOC under abundance of sunlight and stagnant meteorological conditions. Figure V-5-18 shows the difference in modeled ozone between baseline 2018 with and without wildfire emissions in Azusa and Glendora, which are the stations with the highest design values projected in the attainment simulation. As a result, the impact of wildfires on the attainment demonstration is expected to be negligible. Still, day-specific wildfire emissions were included in the base year model performance evaluation.

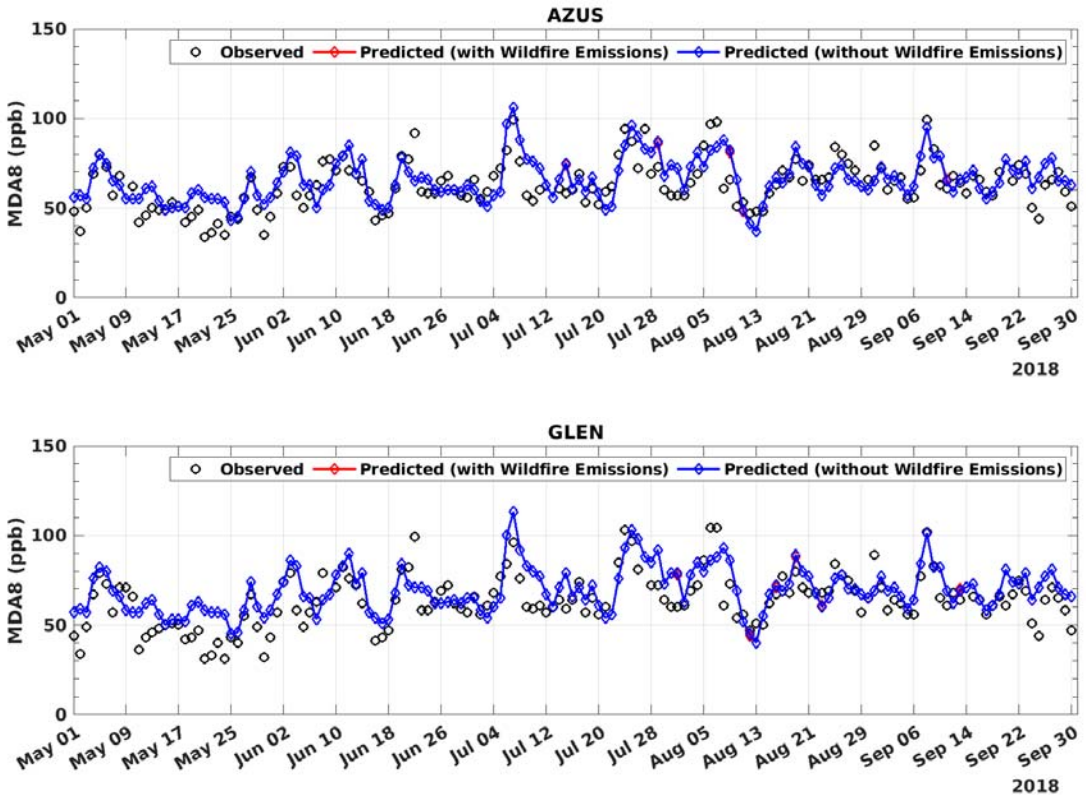

FIGURE V-5-18

COMPARISON OF MODELED MDA8 OZONE CONCENTRATIONS WITH (RED SOLID LINE) AND WITHOUT (BLUE SOLID LINE) INCLUDING WILDFIRE EMISSIONS DURING MAY TO SEPTEMBER 2018 IN AZUSA (TOP) AND GLENDORA (BOTTOM); OBSERVATIONS ARE PRESENTED WITH CIRCLE MARKERS.

Future Ozone Air Quality

Chapter 5 summarizes the results of the ozone simulations. Table V-5-9 shows the 2018 base year, 2037 baseline, and 2037 attainment ozone design values. The 2037 baseline scenario without any additional reduction beyond already adopted measures does not lead to attainment, indicating additional emission reductions are necessary to meet the standards. NOx emissions must be reduced by about 67% beyond the 2037 baseline. With the proposed controls in place, the updated analysis shows the highest design value at the Glendora monitoring site.

TABLE V-5-9

MEASURED AND PREDICTED OZONE DESIGN VALUES

Station	5-year Weighted Base	2037 Baseline	2037 Controlled
Azusa	97.6	90.3	68.8
Banning	97.0	79.7	60.6
Crestline	110.3	93.4	67.0
Fontana	98.3	85.0	61.9
Glendora	102.3	93.3	70.3
Indio	84.3	75.5	66.0
La Habra	75.6	72.4	59.2
Los Angeles	73.3	7.35	63.4
Lake Elsinore	89.0	72.4	55.2
Mira Loma	97.3	84.0	63.8
Mission Viejo	78.3	74.8	61.9
Palm Springs	89.3	75.3	61.3
Pasadena	86.3	81.8	64.6
Perris	93.0	76.0	57.7
Pico Rivera	75.3	74.2	60.4
Pomona	91.3	80.6	59.3
Redlands	106.3	89.2	65.3
Reseda	90.3	81.8	64.5
Rubidoux	97.3	83.7	63.6
San Bernardino	110.0	93.2	67.3
Santa Clarita	99.3	85.0	63.8
Temecula	79.6	69.3	59.7
Upland	107.0	92.9	68.1

The detailed RRF calculation demonstrating attainment is shown below. Table V-5-10 shows the modeled maximum daily average 8-hour ozone concentrations at Glendora for the top 10 days in the baseline 2018 simulation and the corresponding values for the 2037 attainment demonstration simulation.

TABLE V-5-10

DAILY MAX 8-HOUR AVERAGE OZONE CONCENTRATIONS IN THE TOP-10 DAYS MODELED IN THE BASE YEAR 2018 SIMULATION AND CORRESPONDING MODELED CONCENTRATIONS FOR THE 2037 ATTAINMENT SIMULATION

Date	Base Year 2018	Attainment 2037
7/7/2018	120.1	72.2
7/25/2018	106.3	68.9
7/26/2018	102.1	67.5
9/8/2018	102.0	73.0
7/6/2018	101.1	70.5
7/24/2018	97.0	66.0
8/8/2018	96.7	70.0
7/8/2018	96.3	71.6
7/29/2018	95.9	66.2
8/9/2018	92.9	68.8
Top-10 Day average	101.0	69.5

The RRF is calculated using the average of the top-10 days in the base year and attainment simulations:

RRF = 69.5 /101.0 = 0.6874

With the 5-year weighted base year design value for Glendora at 102.3 ppb, the projected design value for the 2037 attainment simulation is:

Future Design Value = 102.3 ppb × 0.6874 = 70.3 ppb

Based on EPA's modeling guidance, the future design value is truncated at the decimal point, and as a result, the future design value is 70 ppb, which passes the modeled attainment test.

Spatial Projections of 8-Hour Ozone Design Values

The spatial distribution of ozone design values for the 2018 base year and 2037 baseline and controlled scenarios are shown in Chapter 5 (main body).

Unmonitored Area Analysis

An unmonitored area analysis was conducted to estimate the design values at unmonitored locations. This analysis uses both the measurement design values and the modeled ozone profiles throughout the modeling domain to estimate 8-hour daily max ozone design values at unmonitored locations.

Five-year weighted design values were calculated for all monitoring stations within and in the vicinity of the modeling domain for the 2015 to 2019 period. Only stations that met the data completeness requirement for each of the 5 years were included in the analysis. A model gradient adjustment method was implemented to

determine base year ozone in unmonitored locations. The adjustment method selected the nearest monitors and calculated the ratio of the top five modeled 8-hour ozone values during July-September at unmonitored and monitored locations. It then multiplied the ratio by the measured design values while applying an inverse distance weight; thus, monitors nearest to the unmonitored location carried the greatest weight. Figure V-5-19 illustrates the spatial distribution of 8-hour ozone 5-year weighted design values calculated using the model gradient adjustment method.

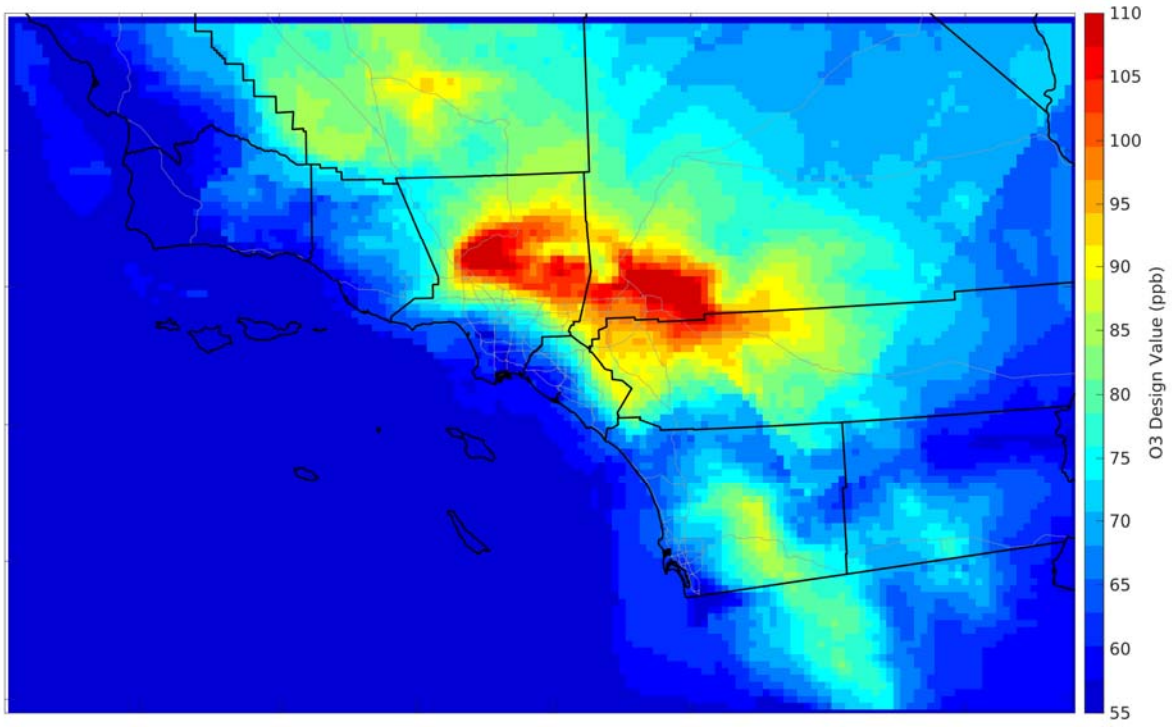

FIGURE V-5-19

MODEL GRADIENT ADJUSTED 8-HOUR OZONE DESIGN VALUES IN 2018

Domain-wide relative response factors (RRFs) can be calculated to forecast ozone design values in future years. The 10 highest maximum daily 8-hour ozone concentrations in the model data are averaged in the base and future years. The RRF is the quotient of this average in the future year and this average in the base year. Only ten maximum daily 8-hour concentrations that are greater than or equal to 60 ppb are used in the RRF. RRFs are still calculated if at least 5 daily measurements in the top ten values are greater than or equal to 60 ppb. However, the RRF cannot be calculated if there are less than 5 daily measurements exceeding 60 ppb in either the base or future years. SCAB RRFs for the 2037 model simulation are presented in Figure V-5-20.

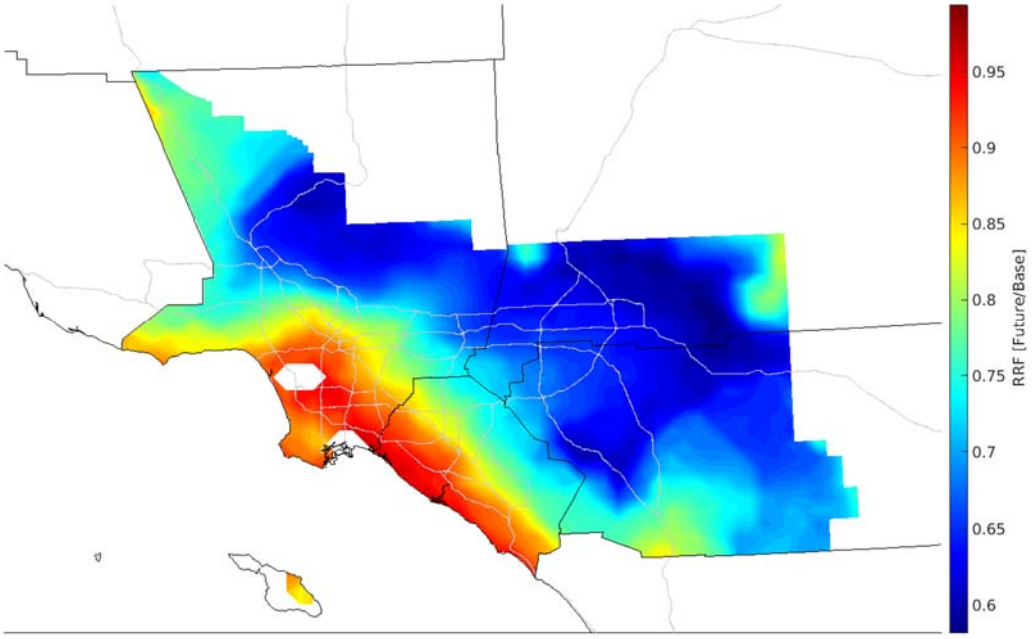

FIGURE V-5-20

2037 RRFS IN THE BASIN

The calculated RRFs are then used to project the interpolated measurement field to simulate future year concentrations. An illustration of the future ozone predictions for the 2037 control scenario is presented below in Figure V-5-21.

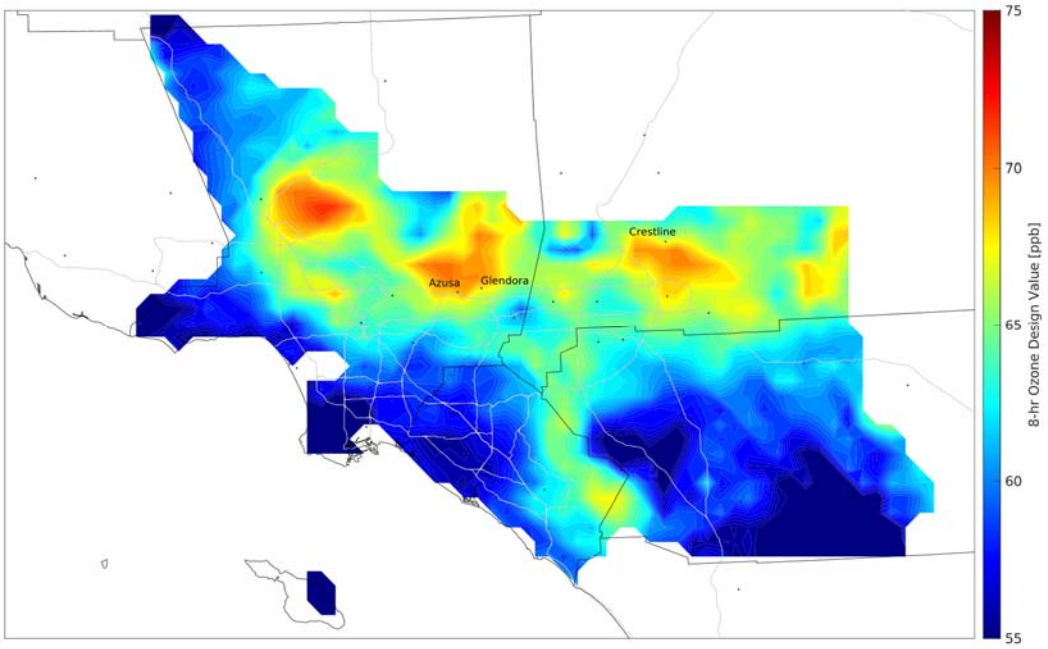

FIGURE V-5-21

2037 CONTROLLED OZONE PREDICTIONS

Controls do not reduce ozone concentrations uniformly and therefore, the location with the highest ozone concentration shifts in future years. Crestline has the highest 2018 5-year weighted design value. In 2037, the unmonitored area analysis predicts that the mountains east of Santa Clarita will have the highest design value in the Basin with a maximum design value of 71.8 ppb. This is a relatively uninhabited area with a population of less than 50 people per square mile according to the 2020 Census (see Figure V-5-22). All other areas are projected to be in attainment.

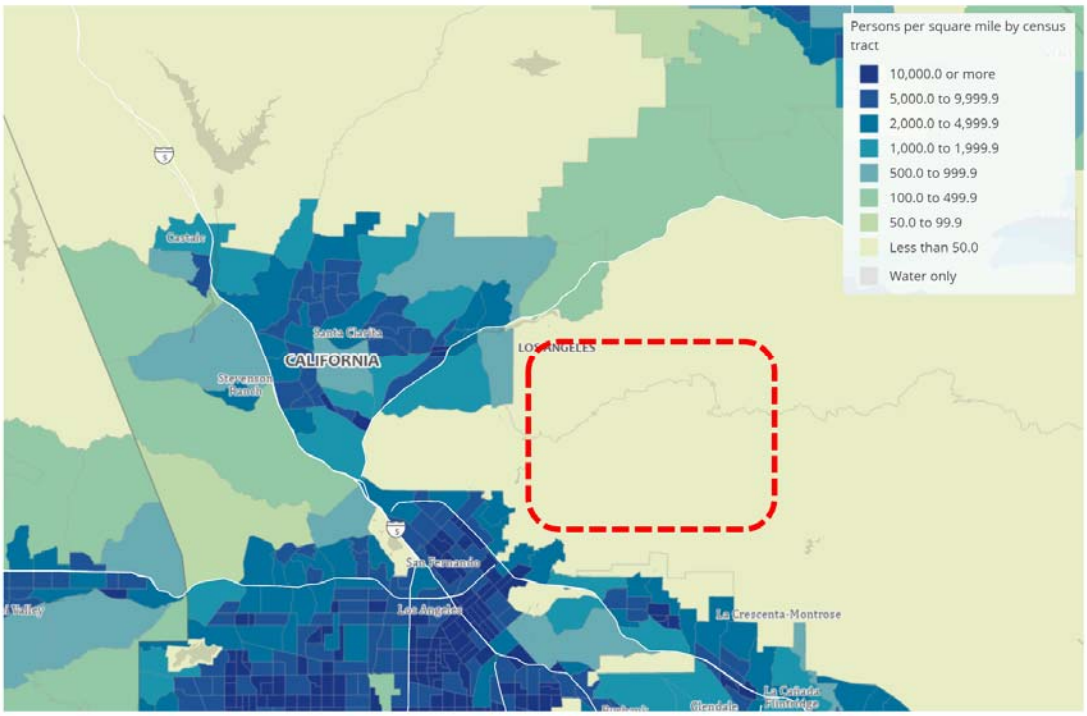

FIGURE V-5-22

2020 CENSUS POPULATION BY CENSUS TRACT.[3] AREA OF OZONE EXCEEDENCE INDICATED BY DASHED BOX

Coachella Valley

The unmonitored area analysis was extended to the Coachella Valley to ensure attainment of the 2015 8-hour ozone standard in 2037. The same model gradient adjustment method used for SCAB was applied to the Coachella Valley unmonitored area analysis; 8-hour ozone design values in 2018 are depicted in Figure V-5-19.

The declining effectiveness of Basin emission reductions in the Coachella Valley is evident upon examining the 2037 model-calculated RRFs in Figure V-5-23. While the RRFs are low (i.e., emission reductions are more effective) in the Palm Springs area, the RRFs gradually increase and approach unity in the southern and eastern portions of the Coachella Valley. This is expected since these areas are distant from the Basin and are therefore less sensitive to emission reductions in the Basin.

[3] Source: 2020 Census Demographic Data Map Viewer

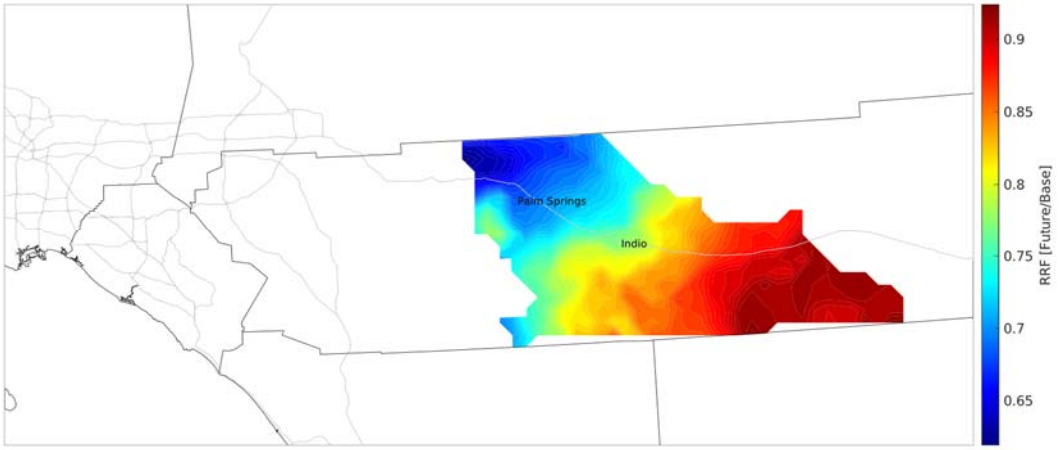

FIGURE V-5-23

2037 RRFS IN COACHELLA VALLEY

The unmonitored area analysis was conducted in the same manner as for the Basin. The analysis demonstrated attainment of the 2015 8-hour ozone standard in Coachella Valley with a maximum design value of 68.6 ppb east of Indio (Figure V-5-24).

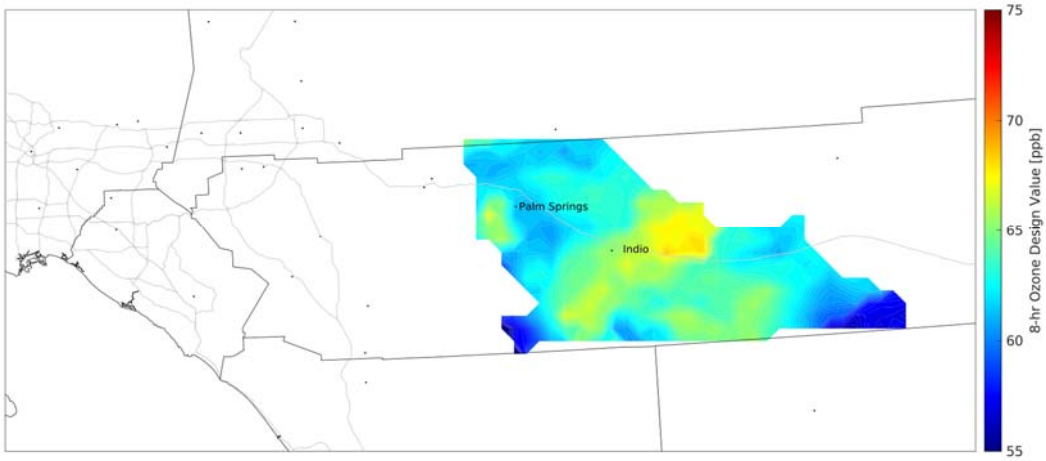

FIGURE V-5-24

2037 CONTROLLED OZONE PREDICTIONS IN COACHELLA VALLEY

Weight of Evidence Analysis

Weekend Ozone Effect

The weekend ozone effect is a well-studied phenomenon in the Basin whereby NOx emission decreases on weekends, primarily due to lower heavy-duty traffic volumes, produce increases in ozone (Pollack et al., 2012; Nussbaumer and Cohen, 2020; Kim et al., 2022; Schroeder et al., 2022). The NOx emission decrease on weekends is reflected in the NOx concentrations at the Central Los Angeles monitoring site (see Figure V-5-26). Assuming that meteorology on weekends and weekdays is similar, the ozone increase is attributable to differences in the VOC:NOx ratio as VOC emissions do not significantly decline on weekends. As the Basin transitions toward NOx-limited ozone formation, it is expected that the weekend ozone effect will decline and eventually reverse (i.e., weekend ozone will be lower than weekday ozone). Thus, the weekend ozone effect can be used to explore the dominant ozone formation regime in the Basin.

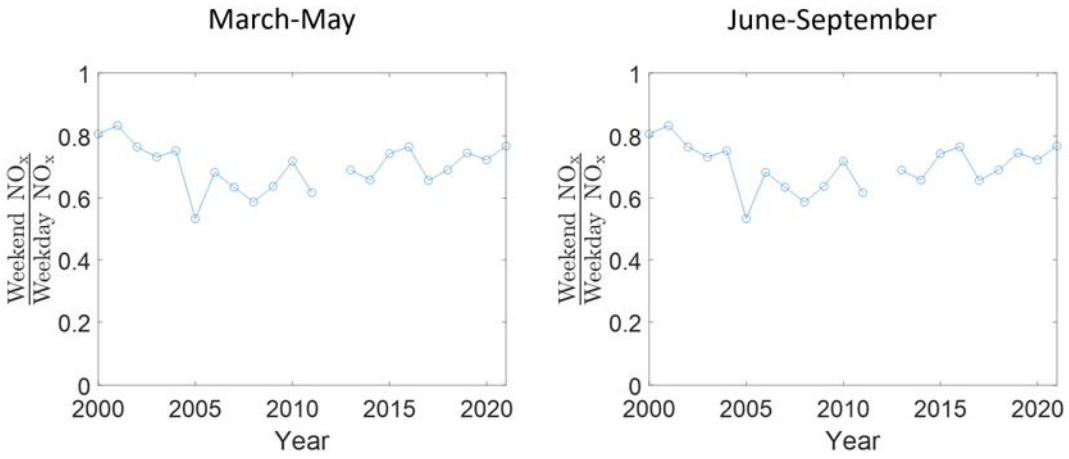

FIGURE V-5-26

MEAN RATIO OF WEEKEND TO WEEKDAY NOX IN LOS ANGELES

The weekend ozone effect differs depending on season and location. The seasonality is explained by higher VOC emissions during summer, largely due to biogenic emissions, causing the ozone formation regime to shift towards NOx-limited. Additionally, NOx-limited ozone formation will first become apparent in downwind locations (e.g., Crestline) before the transition occurs in emission source areas (e.g., Los Angeles) due to differences in ambient NOx levels.

The weekend ozone effect was analyzed between 2000 and 2021 using 8-hour ozone measurements during March-May and June-September in Crestline and Glendora. These sites correspond to the base year and future year design sites, respectively. Figure V-5-27 depicts the ratio of weekend to weekday 8-hour ozone; ratios greater than one indicate VOC-limited ozone formation, while ratios less than one indicate NOx-limited ozone formation. All measurement trends indicate that the region is progressing towards NOx-limited ozone formation (i.e., reduced NOx emissions lead to reduced ozone) with Crestline during June-September showing strong evidence that downwind areas have already transitioned to the NOx-limited regime. These observations support the 2022 AQMP control strategy which heavily relies on NOx over VOC controls. Substantial NOx reductions will ensure that all the Basin enters the NOx-limited regime, whereby reducing

NOx is the most effective strategy to reduce ozone. Furthermore, NOx reductions are the only viable pathway to attain the 2015 8-hour ozone NAAQS.

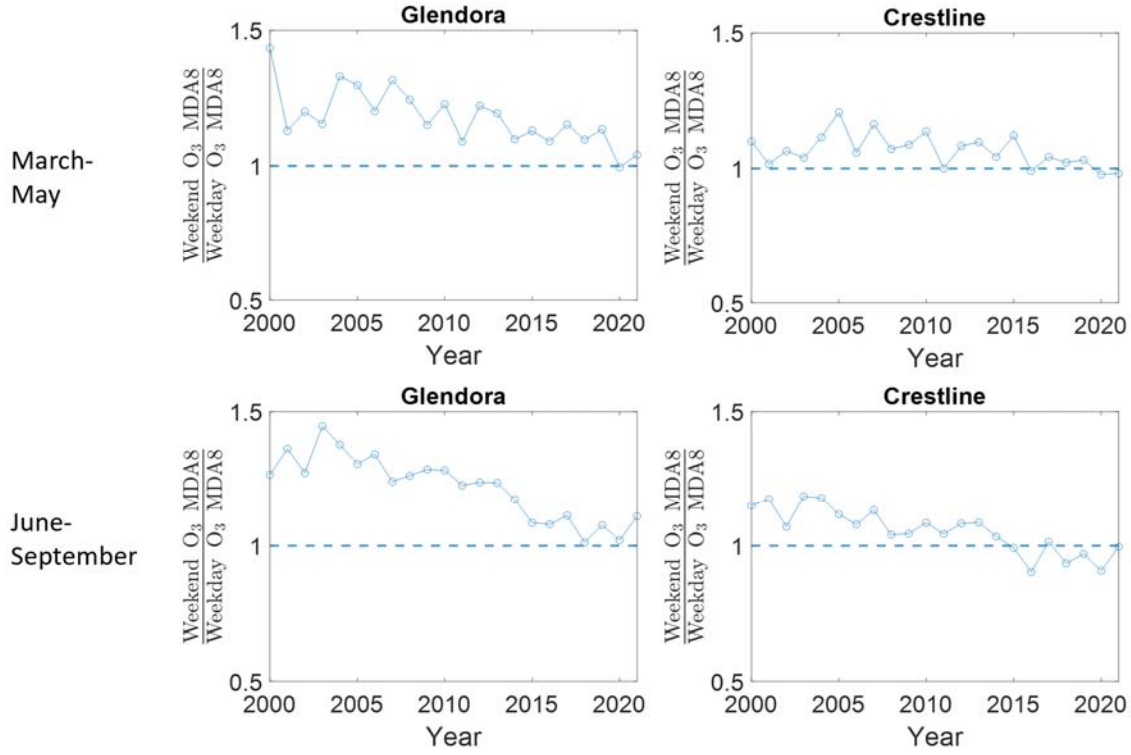

FIGURE V-5-27

MEAN RATIO OF WEEKEND TO WEEKDAY 8-HOUR OZONE IN GLENDORA AND CRESTLINE.

Long-Term Trends in Ozone Background Levels

The transport of ozone and its precursor emissions to California has important implications for air quality in the Basin. In addition to U.S. anthropogenic sources, unraveling the international anthropogenic pollution contribution of surface ozone is complicated. Several studies evaluated the influences of international ozone sources on spatial and temporal ozone distribution and trends over California, while most studies did not focus on the South Coast Air Basin. High elevation locations are more sensitive to Asian pollution because of their exposure to the free troposphere. In the study of Hudman et al. (Hudman, R. C., et al. JGR, 2004), model results indicated a mean Asian pollution enhancement of 7 ppb ozone at Sequoia National Park (mountain sites) in May 2002 on those days when the 8-hour average ozone concentration exceeded 80 ppb. From the study of Zhang et al. (Zhang, L., et al. ACP, 2008), Asian pollution enhanced surface ozone concentrations by 5–7 ppb over western North America in spring 2006. Pfister et al. (Pfister, G. G., et al. JGR, 2013) estimated that, on average, 10 ± 9 ppb of surface afternoon ozone over California during June-July 2008 was attributable to ozone and ozone precursors entering the region from outside. This contribution features significant spatial and temporal variability. Lin's study showed (Lin, M., et al. JGR, 2012) during strong episodes in May-June 20210, Asian emissions can contribute 8–15 ppbv ozone in the model on days when observed maximum daily 8-h average ozone (MDA8 O3) exceeds 60 ppbv. Asher's study (Asher, E. C.,

et al. JGR, 2018) showed ozone is elevated by 6.3 ± 0.8 ppb due to transpacific transport in a remote mountaintop site - Chews Ridge - in California, in February–September 2012. One of the studies (David D. Parrish 2022) addressed that the US background Ozone Design Value was larger than the US anthropogenic Ozone Design Value in the Los Angeles urban area in the year of 2020. Based upon EPA's air quality modeling for the Revised Cross-State Air Pollution Rule Update (https://www.epa.gov/csapr/final-cross-state-air-pollution-rule-update), it is projected that in 2021, the contribution from Canada, Mexico and offshore sources to the Basin is an average of 3.77 ppbv of ozone.

The Basin design values have decreased significantly over the past few decades (see Chapters 2 and 5). However, since 1980, an investigation of histograms (Figure V-5-28) detailing half-decadal changes in average maximum daily 8-hr ozone distributions reveals that concentrations have not decreased uniformly on all days. Figure V-5-28 reveals that the percent of days exceeding the 2008 NAAQS 8-hr Federal Standard of 75 ppb has decreased significantly since 1980 when looking at all surface measurement stations in the basin. On the other hand, the frequency of extremely clean days has decreased in the past few decades, suggesting that background concentrations have increased.

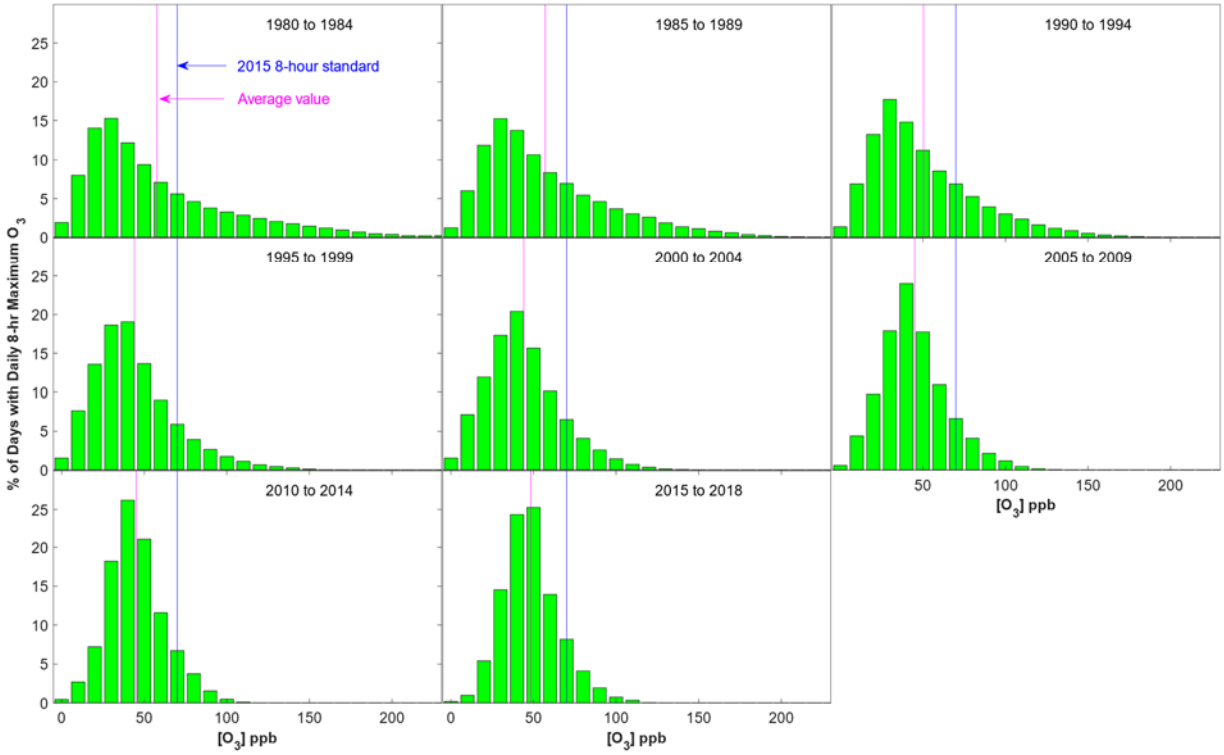

FIGURE V-5-28

HALF-DECADAL HISTOGRAMS DETAILING THE PERCENT OF DAYS WITH EACH SPECIFIC MAXIMUM DAILY 8-HOUR OZONE VALUE

Meteorology and Climate Change Impacts on Ozone

Meteorology introduces uncertainty into the attainment demonstration because it is known to affect ozone formation, resulting in substantial interannual variability in the Basin design value. Three independent analyses were undertaken to quantify the impact of this variability. Two approaches focused on the historical record to estimate the contribution of meteorology to ozone, while the third approach was designed to estimate climate-related impacts in 2037.

Following the increase in ozone design value that began in 2016, South Coast AQMD contracted with academic researchers to assess the extent to which meteorology contributed to the increase. The researchers analyzed meteorological data from 1990-2019 and found increasing trends in ambient temperature and synoptic high-pressure systems over the Basin. Both meteorological factors are known to degrade air quality in the region. Generalized Additive Modeling (GAM) was then conducted to distinguish the effects of emissions and meteorology. As shown in Figure V-5-29, in the absence of meteorological variation, the GAM predicted a rapid decline in the ozone design value due to continual emission reductions until about 2010. However, the rate of ozone decline slowed after 2010, which is consistent with the region overcoming a NOx disbenefit. The GAM also demonstrated that meteorological variability resulted in ozone fluctuations of approximately ±5 ppb from 1990-2019. Furthermore, the GAM demonstrated an ozone increase in 2017 due to meteorology, consistent with the high ozone levels observed that year.

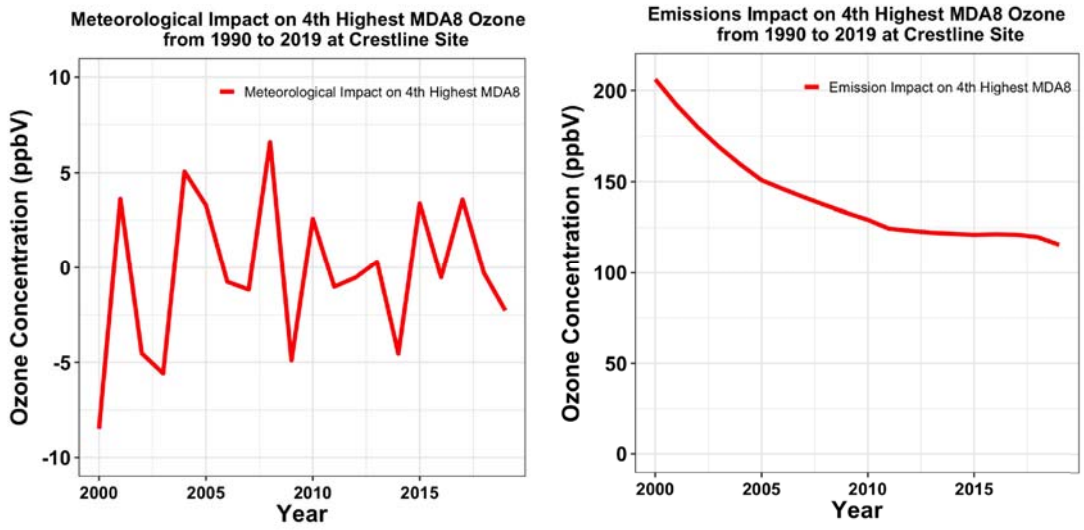

FIGURE V-5-29
STATISTICAL MODELING WAS USED TO DISTINGUISH THE EFFECTS OF EMISSIONS AND METEOROLOGY ON THE BASIN OZONE DESIGN VALUE BETWEEN 1990 AND 2019.

South Coast AQMD conducted an independent modeling analysis with the objective being to isolate the impact of meteorological variation on ozone air quality. National Center for Environmental Prediction North American Regional Reanalysis data for 2016-2020 was processed using WRF to develop gridded meteorological inputs for the South Coast domain. Anthropogenic emissions were held constant and biogenic emissions were recalculated using each year's meteorology. The RRF approach, used in the

attainment demonstration to project future air quality, was modified for this analysis. EPA's guidance for calculating RRF dictates that the top 10 dates at each monitor in the base year be carried over to the future year. Additionally, the guidance requires that the calculation be based on the highest MDA8 modeled in a 3x3 grid cell box surrounding the monitor and that the same grid cell be preserved for the future case. Since EPA's attainment demonstration guidance requires that the base and future years use the same meteorology, these are reasonable requirements. However, this analysis used distinct meteorology for each year and thus both restrictions were removed.

The results for the 2016-2020 analysis period are displayed in Figure V-5-30, which demonstrates the variation in modeled 4th highest 8-hour ozone concentrations at several monitoring sites. Meteorological variability differed by site, but was similar to that predicted by the GAM approach for the Crestline site. The highest ozone levels were predicted in 2020 for most Basin monitors, consistent with observations as explained thoroughly in Chapter 2 (main body).

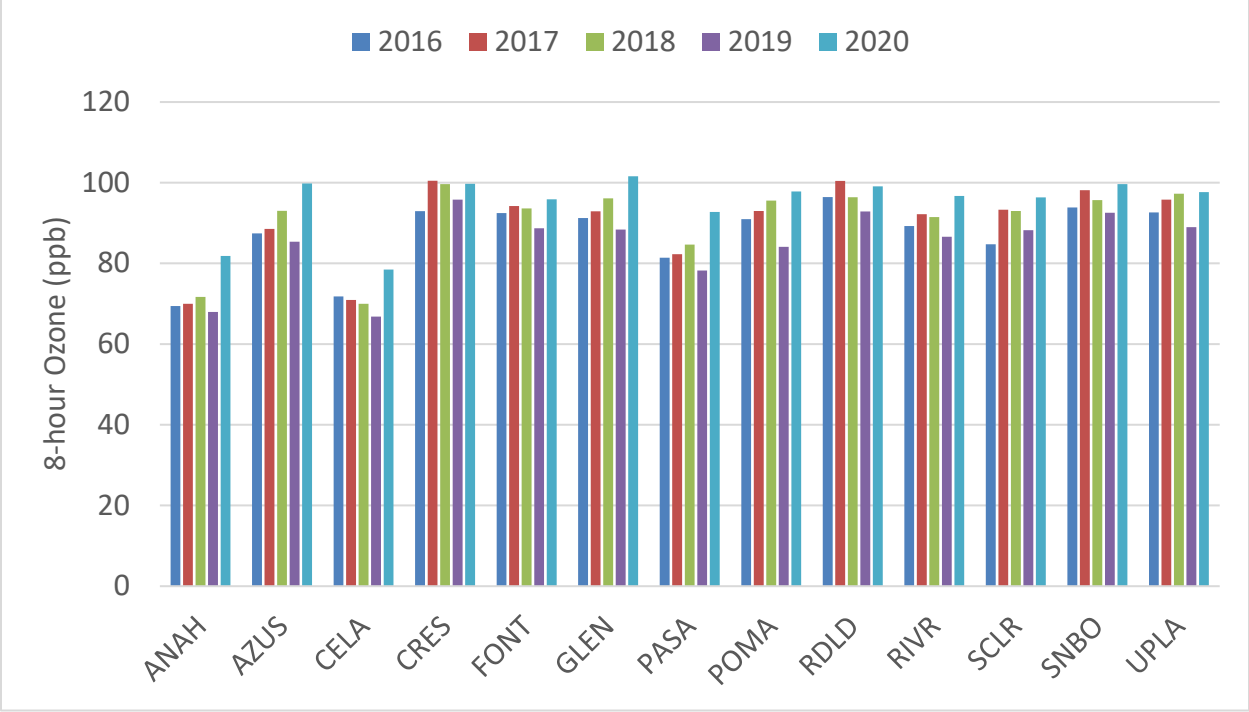

FIGURE V-5-30

4TH HIGHEST MODEL-PREDICTED 8-HOUR OZONE DURING THE 2016-2020 ANALYSIS PERIOD.

Another objective of South Coast AQMD's analysis was to examine the effect of climate change on attainment of the 2015 8-hour ozone standard of 70 ppb in 2037. This analysis employed meteorology consistent with the Representative Concentration Pathway (RCP) 8.5 modeled by the Geophysical Fluid Dynamics Laboratory's Earth System Model and downscaled to the 4 km regional domain using WRF.[4] The RCP 8.5 pathway represents unmitigated greenhouse gas emissions. The base and future simulation periods were 2016-2020 and 2035-2039, respectively. Because the objective was to isolate climate impacts,

[4] Earth System Model, Geophysical Fluid Dynamics Laboratory. https://www.gfdl.noaa.gov/earth-system-model/

anthropogenic emissions were held constant while biogenic emissions were adjusted using each year's meteorology. Simulated 8-hour ozone on the top 10 days in each of the 5-year base and future periods was extracted. The mean of the top 10 days was averaged in each year and those values were subsequently averaged across each 5-year period. The RRF was determined by the ratio of the future to base 5-year average and the RRF was multiplied by the observed base design values. As shown in Figures V-5-31 and V-5-32, this analysis predicts high variability in the climate impact, ranging from a 4.5 ppb increase in Glendora to a decrease of 0.5 ppb in Long Beach.

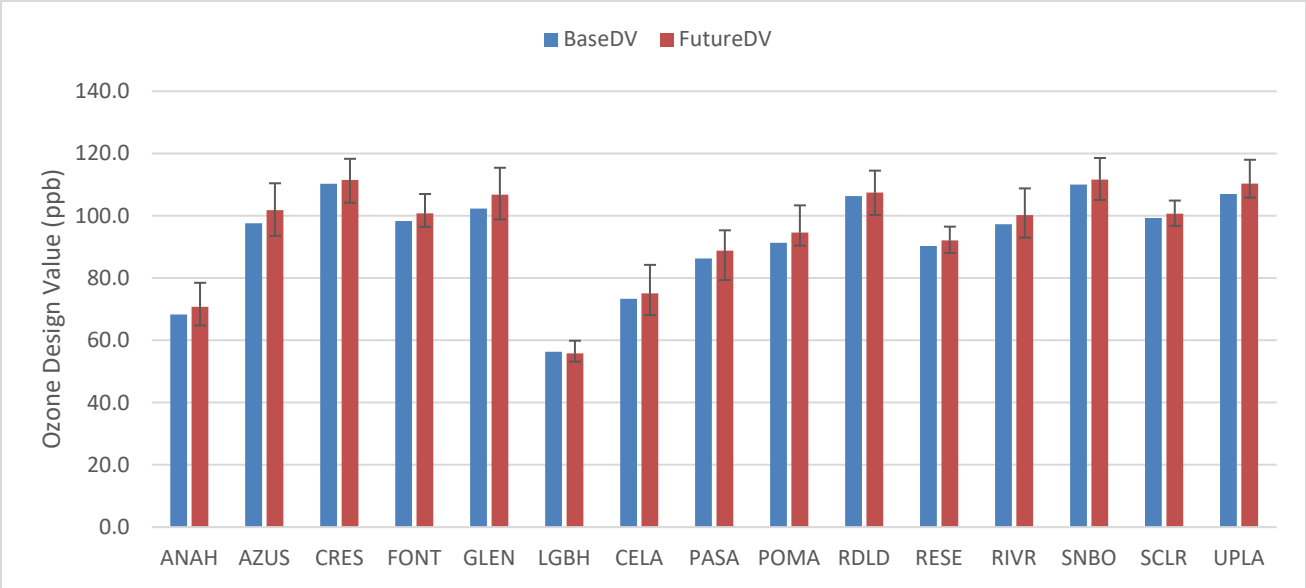

FIGURE V-5-31

PREDICTED FUTURE OZONE DESIGN VALUES USING RCP 8.5 METEOROLOGY COMPARED TO MEASURED BASELINE VALUES. UNCERTAINTY IS REFLECTED AS THE FULL RANGE OF RESPONSES SEEN IN THE FUTURE 5-YEAR PERIOD.

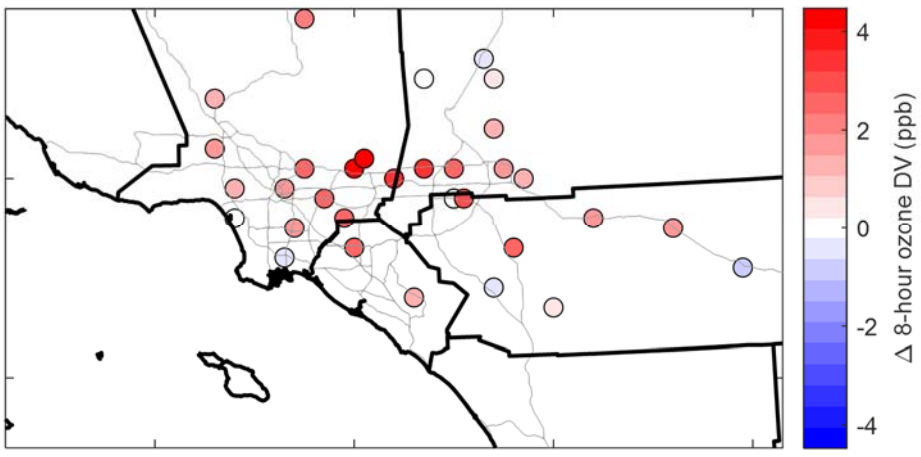

FIGURE V-5-32

MAP DISPLAYING THE CHANGE IN FUTURE OZONE DESIGN VALUES USING RCP 8.5 METEOROLOGY COMPARED TO MEASURED BASELINE VALUES.

Results from the climate impact assessment should be interpreted with caution. Significant uncertainty is introduced by the 5-year window of the base and future periods, as natural meteorological variability can obscure the climate signal. For this reason, air quality climate assessments typically employ 10 to 15-year base and future simulation periods which dampen the effects of natural variability. Furthermore, it is challenging to tease out short term (i.e., less than 30-year interval between base and future scenarios) climate impacts. However, this constraint was necessary given that the objective of the analysis was to quantify impacts on attainment of the 2015 8-hour ozone standard of 70 ppb, for which attainment must be demonstrated in 2037. Finally, meteorological downscaling from global climate models potentially introduces bias and no effort was made to correct this bias. However, since bias would presumably affect both base and future periods and climate impacts were estimated in a relative, rather than absolute sense, it is not clear that this would significantly alter the results.

Modeling the effect of the "Safer at Home" order due to COVID-19 in 2020

Air quality was modeled during March 15 - May 15, 2020, a period affected by the Governor's "Safer at Home" order,[5] with a goal of quantifying the impacts of meteorology and emissions changes on high ozone concentrations measured in the last week of April and first two weeks of May. This analysis serves to bolster confidence in the AQMP modeling platform.

The modeling analysis initially sought to determine the extent to which meteorology contributed to the high ozone episodes. Biogenic emissions were estimated using 2020 meteorology. However, anthropogenic emissions were not adjusted to account for COVID-related changes in activity. Instead, emissions projected from the 2016 AQMP baseline were used, and on-road emissions were aligned with the 2020 calendar. Figure V-5-33 shows the simulated and measured 8-hour ozone concentrations in Glendora. Even without accounting for COVID-related emission changes, the model captured the high ozone episodes at the end of April and beginning of May, indicating that meteorology was largely responsible.

[5] https://www.gov.ca.gov/wp-content/uploads/2020/03/3.19.20-EO-N-33-20-COVID-19-HEALTH-ORDER-03.19.2020-signed.pdf

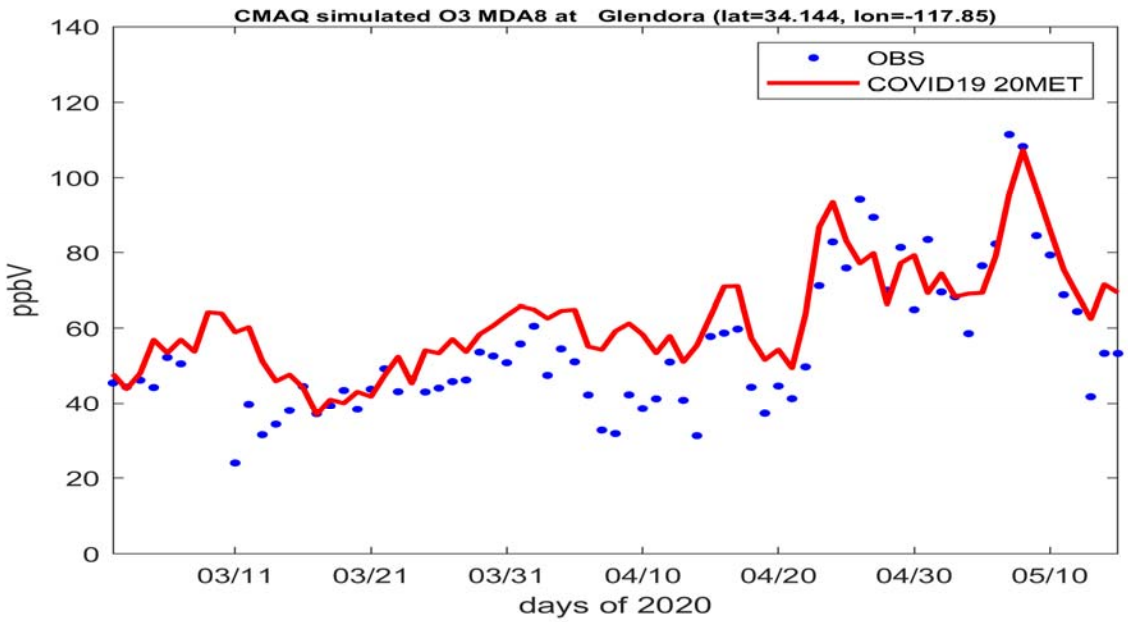

FIGURE V-5-33

MODELED AND OBSERVED 8-HOUR OZONE IN GLENDORA

The second phase of the analysis sought to quantify emission changes due to COVID-related impacts. Multiple information sources such as Caltrans PeMS, the Federal Aviation Administration's aircraft operations databases, and maritime activity records were consulted to account for decreases in transportation and goods movement. An aviation decrease of 61%, a 12-43% reduction in traffic volume, and an 11% reduction in cargo throughput at the ports were reflected in the modeling emissions. Figure V-5-34 demonstrates the change in NOx and VOC emissions compared to the baseline. Marginal VOC emission increases reflect consumer product usage over the Basin and align with population density. Fugitive VOC emissions from tankers during marine transit of crude oil and petroleum products were added to baseline emissions. Figure V-5-35 shows the model-predicted 8-hour ozone response averaged across the 10 highest days in the study period. Similar to the ozone weekend effect, the reduced NOx emissions in populated areas contributed to higher ozone in LA county, while inland downwind area was predicted to have lower ozone due to reduced NOx emissions.

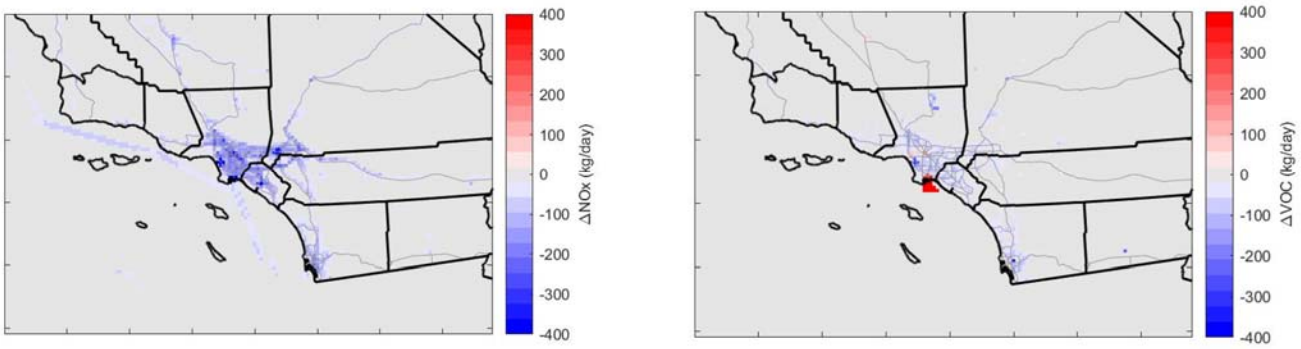

FIGURE V-5-34

NOX AND VOC EMISSION CHANGES DUE TO COVID IMPACTS DURING THE STUDY PERIOD

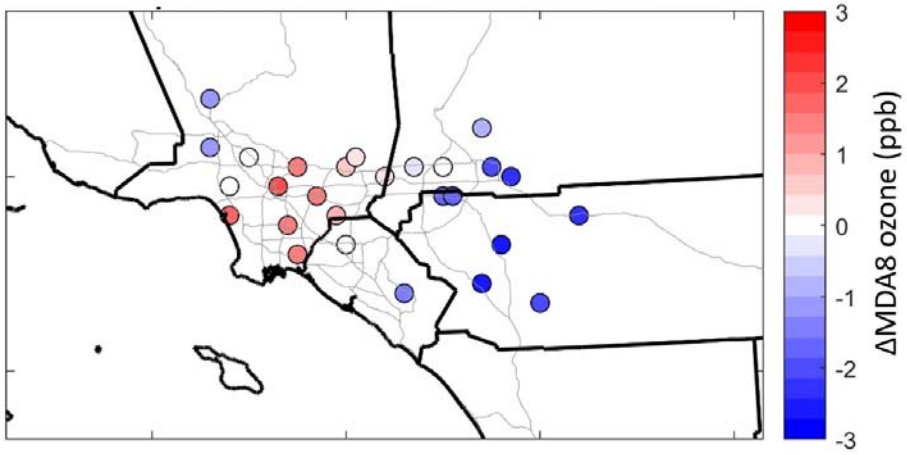

FIGURE V-5-35

MODELED TOP 10 DAYS 8-HOUR OZONE RESPONSE DUE TO EMISSION CHANGES DURING THE COVID STUDY PERIOD

In summary, modeling indicated that meteorology played a significant role in the poor air quality experienced during the study period, with a lesser impact due to emission changes. However, the model predicted that downwind areas experienced ozone decreases due to COVID-related NOx emission decreases while the urban core experienced ozone increases. This is consistent with the weekend effect analysis and therefore lends further confidence in our modeling platform. We further note that the findings in this analysis are generally consistent with those of Parker et al.

Uncertainties Associated with the Technical Analysis

As with any attainment plan, there are uncertainties associated with the technical analysis. Described herein are the primary contributors to such uncertainties as well as some of the safeguards built into the air quality planning process to manage and control such uncertainties.

Demographic and Growth Projections

Uncertainties exist in the demographic and growth projections for future years. As projections are made to longer periods (i.e., over ten or more years), the uncertainty of the projections become greater. Examples of activities that may contribute to these types of uncertainties include the growth rate and the type of new sources in the Basin and their geographic distribution, future residential construction, military base reuse, and economic conditions.

Emissions Inventory

Emissions were prepared for the 2018 base year and for the 2037 baseline and control scenarios. The baseline represents the level of emissions with no additional reductions beyond adopted measures, while the control case contains additional emission reductions proposed in this AQMP to reach attainment.

While significant improvements have been realized in mobile source emissions models, uncertainties continue to exist in the mobile source emissions inventory estimates. EMFAC on-road mobile source emission estimates have improved with each new EMFAC release. On-road mobile source emissions have inherent uncertainties with the current methodologies used to estimate vehicle miles traveled and the impacts of fuel additives such as ethanol. Stationary (or point) source emission estimates have less associated uncertainties compared to area source emission estimates. Major stationary sources report emissions annually whereas minor stationary and area source emissions are, in general, estimated based on a top down approach that relies on production, usage or activity information. Area source emissions including paved road dust and fugitive dust have significant uncertainties in the estimation of particulate ($PM_{2.5}$) emissions due to the methodologies used for estimation, temporal loading and weather impacts.

Ambient Air Quality Monitoring Data

Generally, ambient air quality measurements are accurate to within plus or minus half of a unit of measurement (e.g., for ozone usually reported in units of parts-per-hundred million (pphm) would be accurate to within ±0.5 pphm or ±5 ppb). Due to rounding conventions, the Basin's 8-hour attainment status based on ambient monitoring data would be achieved if all ozone monitors reported ozone concentrations less than or equal to 70.9 ppb.

Air Quality and Meteorological Models

The air quality models used for ozone and particulate air quality analysis are state-of-the-art, comprehensive 3-dimensional models that utilize 3-dimensional meteorological models, complex chemical mechanisms that accurately simulate ambient reactions of pollutants, and sophisticated numerical methods to solve complex mathematical equations that lead to the prediction of ambient air quality concentrations. While air quality models progressively became more sophisticated in employing improved chemical reaction modules that more accurately simulate the complex ambient chemical reaction mechanisms of the various pollutants, such improved modules are still based on limited experimental data that carry associated uncertainties. In order to predict ambient air quality concentrations, air quality models rely on the application of sophisticated

numerical methods to solve mathematical equations that govern the highly complex physical and chemical processes that also have associated uncertainties.

Meteorology and Climate Change Impacts on Ozone

Meteorology introduces uncertainty into the attainment demonstration because it is known to affect ozone formation, resulting in substantial interannual variability in the Basin design value. Three independent analyses were undertaken to quantify the impact of this variability. Two approaches focused on the historical record to estimate the contribution of meteorology to ozone, while the third approach was designed to estimate climate-related impacts in 2037. Analysis of the historical record showed that meteorology contributed to variation of about ±5 ppb in the annual 4th highest 8-hour ozone at the Crestline monitoring site. The final analysis attributed design value increases exceeding 4 ppb in 2037 to climate change, with the greatest impacts observed at foothill and inland monitoring sites. Taken together, natural meteorological variability and climate change introduce considerable uncertainty in the attainment demonstration. Nevertheless, the U.S. EPA modeling guidance states that the same meteorology must be used for base and future years.

Safeguards against Uncertainties

While completely eliminating uncertainties is an impossible task, there are a number of features and practices built into the air quality planning process that manage and control such uncertainties and preserve the integrity of an air quality management plan.

The concerns regarding future year uncertainties in the technical analysis are reduced with future AQMP revisions. Each AQMP revision employs the best available technical information. Under state law, AQMP revision is a dynamic process with revisions occurring every three years. AQMP revision represents a "snapshot in time" providing the progress achieved since the previous AQMP revision and efforts still needed in order to attain air quality standards.

Under the federal Clean Air Act, a state implementation plan (SIP) is prepared for each criteria pollutant. The SIP is not required to be updated on a routine basis under the federal Clean Air Act. However, the federal Clean Air Act recognizes that uncertainties do exist and provides a safeguard if a nonattainment area does not meet an applicable milestone or attain federal air quality standards by their applicable dates. Contingency (or backstop) measures are required in the AQMP and must be developed into regulations such that they will take effect if a nonattainment area does not meet an applicable milestone or attainment date. In addition, federal sanctions may be imposed until an area meets applicable milestone or attainment targets.

Summary and Conclusion

The attainment demonstration for the South Coast Air Basin predicts that 124 tons per day of NOx reductions from the 2037 baseline are needed to meet the 8-hour ozone standard in 2037, resulting in a carrying capacity of 60 tons per day. This equates to an approximately 67% reduction from the 2037 baseline. With the controls proposed in this AQMP, future ozone concentrations are expected to meet the federal 2015 8-hour ozone standard in 2037.

The Coachella Valley is currently a "severe-15" nonattainment area for the 2015 8-hour ozone standard. A voluntary reclassification request to "extreme" nonattainment and an attainment demonstration for Coachella was presented. With the controls proposed in this AQMP, future ozone concentrations are expected to meet the federal 2015 8-hour ozone standard in 2037.

Supporting analyses that examined the effect of meteorology and climate change were performed. The 4th highest 8-hour ozone concentration is susceptible to interannual variability of ±5 ppb due to meteorology. Climate change is expected to enhance the meteorological impact on 8-hour ozone, especially in the Glendora area which is also the area with the highest design value in the attainment demonstration. Dynamic model evaluations assessed the model's ability to predict ozone response to changes in emissions on weekends compared to weekdays and during the "Safer at Home" period in 2020. The model exhibited robust performance across these different chemical environments thereby bolstering confidence in the attainment demonstration.

References

Brown-Steiner, B. and P. Hess (2011). "Asian influence on surface ozone in the United States: A comparison of chemistry, seasonality, and transport mechanisms." Journal of Geophysical Research **116**(D17).

Hudman, R. C., D. J. Jacob, O. R. Cooper, M. J. Evans, C. L. Heald, R. J. Park, F. Fehsenfeld, et al. 2004. "Ozone Production in Transpacific Asian Pollution Plumes and Implications for Ozone Air Quality in California." Journal of Geophysical Research: Atmospheres 109 (D23) (December 8). doi:10.1029/2004jd004974

Jaffe, D. (2003). "Increasing background ozone during spring on the west coast of North America." Geophysical Research Letters **30**(12).

Levelt, P. F., G. H. J. van den Oord, M. R. Dobber, A. Malkki, V. Huib, J. de Vries, P. Stammes, J. O. V. Lundell and H. Saari (2006). "The ozone monitoring instrument." Geoscience and Remote Sensing, IEEE Transactions on **44**(5): 1093-1101.

National Oceanic and Atmospheric Administration, U. S. D. o. C. and E. S. R. L. Global Monitoring Division (2014). Ozone Sonde Vertical Profile Data. Boulder, CO.

Ohara, T., H. Akimoto, J. Kurokawa, N. Horii, K. Yamaji, X. Yan and T. Hayasaka (2007). "An Asian emission inventory of anthropogenic emission sources for the period 1980-2020." Atmos. Chem. Phys. **7**(16): 4419-4444.

Parker LK, Johnson J, Grant J, Vennam P, Parikh R, Chien C-J, Morris R. Ozone Trends and the Ability of Models to Reproduce the 2020 Ozone Concentrations in the South Coast Air Basin in Southern California under the COVID-19 Restrictions. Atmosphere. 2022; 13(4):528. https://doi.org/10.3390/atmos13040528

Pollack, et al. Airborne and ground-based observations of a weekend effect in ozone, precursors, and oxidation products in the California South Coast Air Basin, Journal of Geophysical Research Atmospheres (2012). doi:10.1029/2011JD016772

Nussbaumer and Cohen. The Role of Temperature and NOx in Ozone Trends in the Los Angeles Basin, Environmental Science and Technology (2020). doi:10.1021/acs.est.0c04910

Kim, et al. Understanding the paths of surface ozone abatement in the Los Angeles Basin, Journal of Geophysical Research Atmospheres (2022). doi:10.1029/2021JD035606

Schroeder, et al. Changing Ozone Sensitivity in the South Coast Air Basin during the COVID-19 Period, Atmospheric Chemistry and Physics Discussions (2022). doi:10.5194/acp-2022-178

Sibson, R. (1981), A brief description of natural neighbor interpolation. Interpolating multivariate data, John Wiley & Sons, New York, 1981, p. 21-36.

US EPA (2018) Modeling Guidance for Demonstrating Air Quality Goals for Ozone, PM2.5, and Regional Haze

Verstraeten, W. W., J. L. Neu, J. E. Williams, K. W. Bowman, J. R. Worden and K. F. Boersma (2015). "Rapid increases in tropospheric ozone production and export from China." Nature Geosci **8**(9): 690-695.

Volz A., Kley D. (1988) Evaluation of the Montsouris series of ozone measurements made in the nineteenth century, Nature, **332**, 240-242

Zhang, L., Jacob, D. J., Boersma, K. F., Jaffe, D. A., Olson, J. R., Bowman, K. W., Worden, J. R., Thompson, A. M., Avery, M. A., Cohen, R. C., Dibb, J. E., Flock, F. M., Fuelberg, H. E., Huey, L. G., McMillan, W. W., Singh, H. B., and Weinheimer, A. J.: Transpacific transport of ozone pollution and the effect of recent Asian emission increases on air quality in North America: an integrated analysis using satellite, aircraft, ozonesonde, and surface observations, Atmos. Chem. Phys., **8**, 6117–6136, https://doi.org/10.5194/acp-8-6117-2008, 2008.

Pfister, G. G., S. Walters, L. K. Emmons, D. P. Edwards, and J. Avise (2013), Quantifying the contribution of inflow on surface ozone over California during summer 2008, J. Geophys. Res. Atmos., **118**, 12,282–12,299, doi:10.1002/2013JD020336.

Itahashi, S., Mathur, R., Hogrefe, C., Napelenok, S. L., and Zhang, Y.: Modeling stratospheric intrusion and trans-Pacific transport on tropospheric ozone using hemispheric CMAQ during April 2010 – Part 2: Examination of emission impacts based on the higher-order decoupled direct method, Atmos. Chem. Phys., 20, 3397–3413, https://doi.org/10.5194/acp-20-3397-2020, 2020.

Meiyun Lin, Arlene M. Fiore, Larry W. Horowitz, Owen R. Cooper, Vaishali Naik, John Holloway, Bryan J. Johnson, Ann M. Middlebrook, Samuel J. Oltmans, Ilana B. Pollack, Tomas B. Ryerson, Juying X. Warner, Christine Wiedinmyer, John Wilson, and Bruce Wyman. (2012), Transport of Asian ozone pollution into surface air over the western United States in spring, J. Geophys. Res., **117**, D00V07, doi:10.1029/2011JD016961.

Asher, EC; Christensen, JN; Post, A.; Perry, K.; Cliff, SS; Zhao, Y., et al. (2018). The Transport of Asian Dust and Combustion Aerosols and Associated Ozone to North America as Observed From a Mountaintop Monitoring Site in the California Coast Range. *Journal of Geophysical Research: Atmospheres*, **123**(10), 5667-5680. doi:10.1029/2017JD028075.

David D. Parrish, Ian C. Faloona & Richard G. Derwent (2022): Observational based Assessment of Contributions to Maximum Ozone Concentrations in the western US, Journal of the Air & Waste Management Association, DOI: 10.1080/10962247.2022.2050962

CHAPTER 6

STATE AIR QUALITY STANDARDS

Comparison to State Standards

Coachella Valley

Comparison to State Standards

This section discusses future air quality in the context of the California Ambient Air Quality Standards (CAAQS), which are distinct from the National Ambient Air Quality Standards (NAAQS). The CAAQS for 1-hour and 8-hour ozone are 0.09 ppm and 0.070 ppm, respectively.

The CAAQS are based on designation values, while the NAAQS are based on design values. Designation values are calculated using Expected Peak Day Concentrations (EPDC), which represent the concentration that statistically is estimated to recur once per year. In the area designation process, measured concentrations that are higher than the calculated EPDC, after the EPDC is rounded to the precision of the relevant State standard, are identified as affected by an extreme concentration event and are not considered violations of the State standards. The designation value refers to the highest measured concentration (rounded to the precision of the relevant State standard) remaining at a given site after all measured concentrations affected by extreme concentration events are excluded. In the calculations of EPDCs, concentrations affected by exceptional events or unusual concentration events are not excluded. However, measured concentrations that are identified as affected by an exceptional event or unusual concentration event are excluded from being considered as the designation value.

As in the attainment demonstration for the 2015 federal 8-hour ozone standard, 5-year weighted designation values were determined based on 2015-2019 data. The Relative Response Factor (RRF) was then applied to the 5-year weighted designation values to predict 2037 designation values. There is no guidance on how to demonstrate attainment of the state standards, therefore EPA's guidance to demonstrate NAAQS is utilized for the state standard. Although the 70 ppb 8-hour ozone CAAQS aligns with the 70 ppb 2015 8-hour ozone NAAQS, the base year designation values are substantially higher than the base year design values. Thus, the 2037 controlled scenario does not produce attainment of the 8-hour ozone CAAQS, with a maximum designation value of 78.3 ppb in Glendora. Designation values for other stations are presented in Table V-6-1 and are spatially depicted in Figure V-6-1.

While the state does not have well-established requirements for nonattainment area, the California Health and Safety Code requires South Coast Air Basin to have an estimated carrying capacity for CAAQS. Since the 2037 controlled scenario (with 60 tons per day Basin NOx emissions) did not produce attainment for the 8-hour CAAQS, further simulations were conducted by incrementally reducing NOx emissions in the Basin by 10 tons per day until attainment was achieved. Basin carbon monoxide emissions were reduced by an equivalent ratio, while VOC emissions remained constant. The initial two simulations, with 50 and 40 tons per day of Basin NOx emissions, did not achieve attainment of the 8-hour CAAQS. However, a final simulation with 30 tons per day of NOx emissions demonstrated attainment in the Basin with a maximum designation value of 65.7 ppb in Glendora. This is a level that is 50% lower than the carrying capacity for the 8-hour NAAQS for which 2037 is the attainment year. Thus, additional time will be required to attain the 8-hour CAAQS.

TABLE V-6-1

BASE AND FUTURE DESIGNATION VALUES (PPB) FOR THE 70 PPB 8-HOUR CAAQS

Station	2017 Designation Value	2018 Designation Value	2019 Designation Value	5-year Weighted Designation Values	5-year Weighted Design Values[1]	2037 Controlled Designation Values	2037 Controlled Design Values[1]
Azusa	109	109	109	109.0	97.6	77.3	69.2
Banning	106	106	106	106.0	97.0	67.2	61.5
Crestline	122	125	122	123.0	110.3	75.9	68.1
Fontana	106	111	111	109.3	98.3	70.0	63.0
Glendora	114	114	114	114.0	102.3	78.3	70.3
La Habra	84	84	84	84.0	75.6	66.6	60.0
Los Angeles	83	85	85	84.3	73.3	72.7	63.2
Lake Elsinore	99	98	98	98.0	89.0	64.0	58.1
Mira Loma	106	108	108	107.3	97.3	72.0	65.3
Mission Viejo	89	89	88	88.7	78.3	70.0	61.8
Pasadena	96	96	96	96.0	86.3	72.2	64.9
Perris	106	106	106	106.0	93.0	70.2	61.6
Pico Rivera	83	83	83	83.0	75.3	67.8	61.5
Pomona	107	101	101	103.0	91.3	67.2	59.6
Redlands	120	120	118	119.3	106.3	75.4	67.2
Reseda	99	101	101	100.3	90.3	71.6	64.4
Rubidoux	106	114	102	107.3	97.3	71.3	64.6
San Bernardino	118	118	118	118.0	110.0	74.0	69.0
Santa Clarita	112	116	109	112.3	99.3	73.7	65.2
Upland	121	121	121	121.0	107.0	78.0	69.0

[1] NAAQS Design Values are presented for comparison

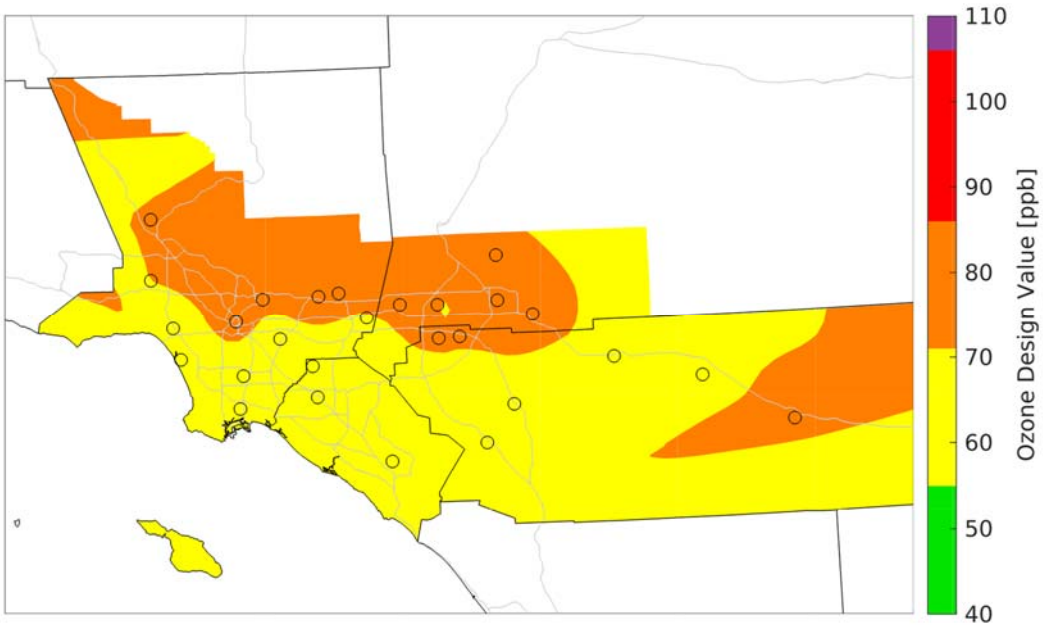

FIGURE V-6-1

INTERPOLATED 8-HOUR OZONE DESIGNATION VALUES (PPB) FOR 2037. VALUES ARE COLOR-CODED TO CORRESPOND TO THE 2015 70 PPB STANDARD AIR QUALITY INDEX.

As discussed in Chapter 5, the RRFs for 8-hour standards are determined by the ten highest 8-hour ozone concentrations at each monitoring site in the base and future scenarios. However, the RRF for the 1-hour ozone CAAQS is determined by the two highest 1-hour ozone concentrations in the base and future scenarios. Applying the RRF to the 5-year weighted 1-hour designation values results in a maximum future designation value of 100 ppb in Glendora. Thus, the 2037 controlled scenario does not lead to attainment of the 1-hour ozone CAAQS. The future designation values for other stations are presented in Table V-6-2 and are spatially depicted in Figure V-6-2.

The additional modeling analyses conducted for the 8-hour CAAQS were used to estimate the carrying capacity for the 1-hour CAAQS. The scenario with 40 tons per day NOx attained the 1-hour standard with a maximum designation value of 89.9 ppb in Glendora. The attainment threshold for this standard is 94.9 ppb, so the 40 tons per day scenario is well within attainment. This is a level about 33% lower than the carrying capacity for the 8-hour NAAQS for which 2037 is the attainment year. Thus, additional time will be required to attain the 1-hour CAAQS.

TABLE V-6-2

BASE AND FUTURE DESIGNATION VALUES (PPB) FOR THE 90 PPB 1-HOUR CAAQS

Station	2017 Designation Value	2018 Designation Value	2019 Designation Value	5-year Weighted Designation Values	5-year Weighted Design Values[1]	2037 Controlled Designation Values	2037 Controlled Design Values[1]
Azusa	140	140	140	140	139	90	93
Banning	130	130	130	130	123	70	69
Crestline	150	150	140	150	142	90	81
Fontana	130	130	130	130	135	80	82
Glendora	140	150	150	150	147	100	98
La Habra	110	100	100	100	103	70	76
Los Angeles	100	100	100	100	104	80	83
Lake Elsinore	120	120	120	120	116	70	69
Mira Loma	120	130	120	120	128	70	77
Mission Viejo	100	100	110	100	102	80	81
Pasadena	120	120	110	120	122	80	86
Perris	120	120	120	120	118	70	71
Pico Rivera	110	110	110	110	108	80	81
Pomona	130	130	120	130	135	80	85
Redlands	130	140	140	140	135	70	72
Reseda	120	120	120	120	127	70	79
Rubidoux	130	120	120	120	126	70	77
San Bernardino	150	150	140	150	141	90	83
Santa Clarita	130	130	130	130	130	70	74
Upland	150	150	140	150	146	90	92

[1] NAAQS Design Values are presented for comparison

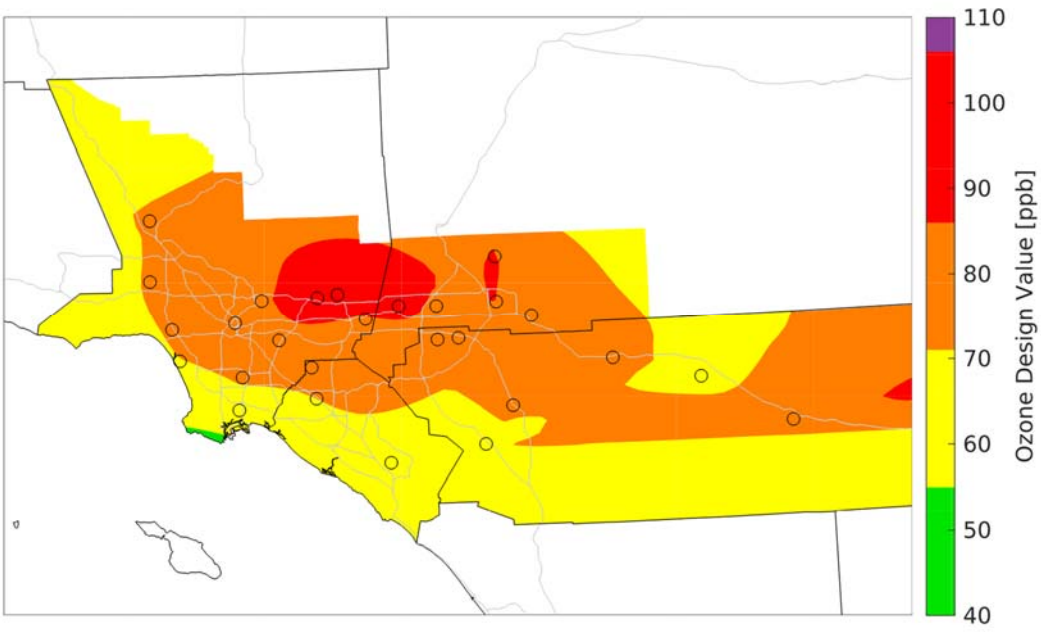

FIGURE V-6-2

INTERPOLATED 1-HOUR OZONE DESIGNATION VALUES (PPB) FOR 2037. ALTHOUGH THIS IS A 1-HOUR STANDARD, VALUES ARE COLOR-CODED TO CORRESPOND TO THE 8-HOUR AIR QUALITY INDEX SINCE COLOR-CODING TO THE 1-HOUR AIR QUALITY INDEX WOULD NOT DISPLAY DIFFERENCES.

Coachella Valley

Palm Springs has traditionally served as the design site for Coachella as it experiences the highest ozone levels. However, modeling initially demonstrated that Indio would overtake Palm Springs as the future design site. It was found that Indio's ozone levels were unduly influenced by a single episode between June 12 and 13. Examination of the modeled ozone during this episode, depicted in Figure V-6-3, demonstrated high ozone levels over the southeast corner of the modeling domain. Mexico was determined to be the origin of the high ozone, which explained why this episode remained insensitive to NOx controls in South Coast AQMD's jurisdiction. While there is no formal guidance for CAAQS, Clean Air Act Section 179B allows states to exclude ozone exceedances that preclude attainment if the exceedances were caused by international emissions. In addition, Mexico emissions contain older data vintage and high uncertainties. On this basis, the June 12-13 episode was excluded when calculating the RRF for Indio and Palm Springs remained the future design site. With Palm Springs as the design site and considering implementation of the control strategy, the Coachella Valley will be in attainment of both the 1-hour and 8-hour CAAQS in 2037.

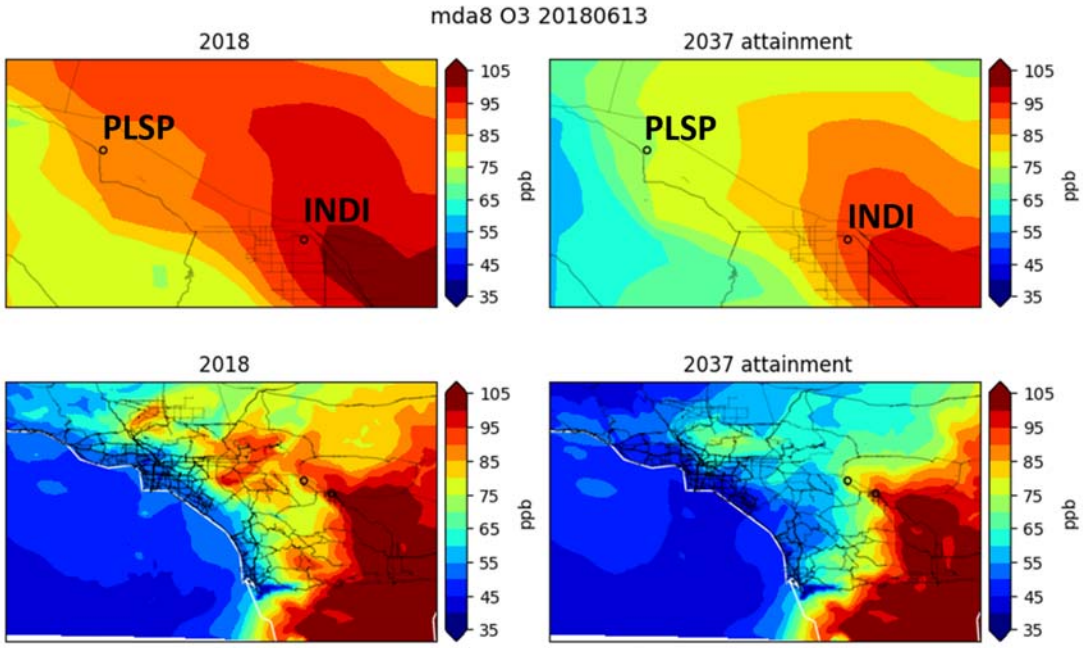

FIGURE V-6-3

MODELED OZONE CONCENTRATION ON JUNE 13 IN THE COACHELLA VALLEY (TOP) AND THE ENTIRE MODELING DOMAIN (BOTTOM). BOTH THE BASE YEAR AND 2037 CONTROLLED SCENARIOS ARE DEPICTED.

Attachment 1

WRF MODEL PERFORMANCE TIME SERIES

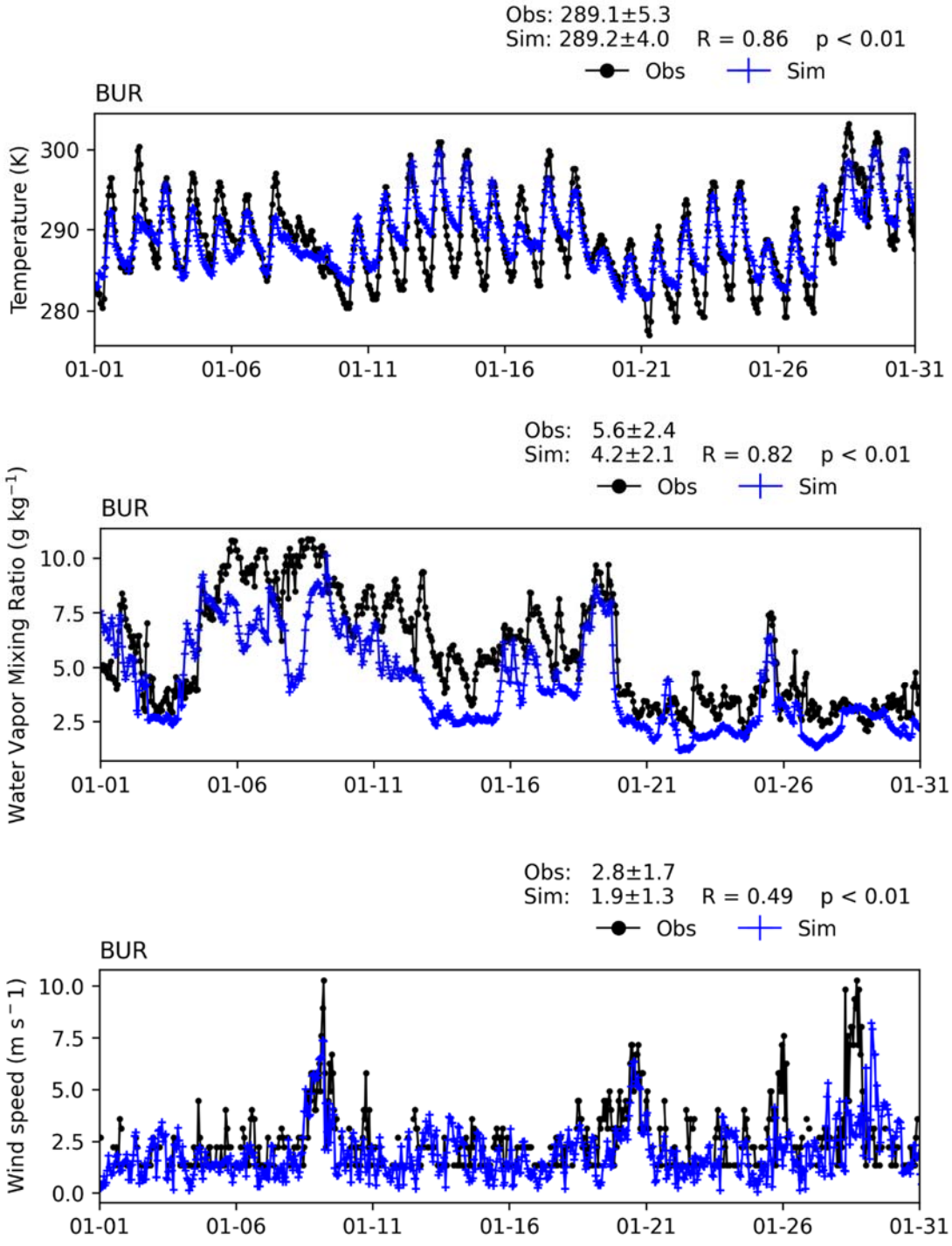

FIGURE V-A1
TIME SERIES OF HOURLY MEASUREMENTS AND WRF BASE SIMULATIONS AT BURBANK AIRPORT (BUR) FOR JANUARY 2018

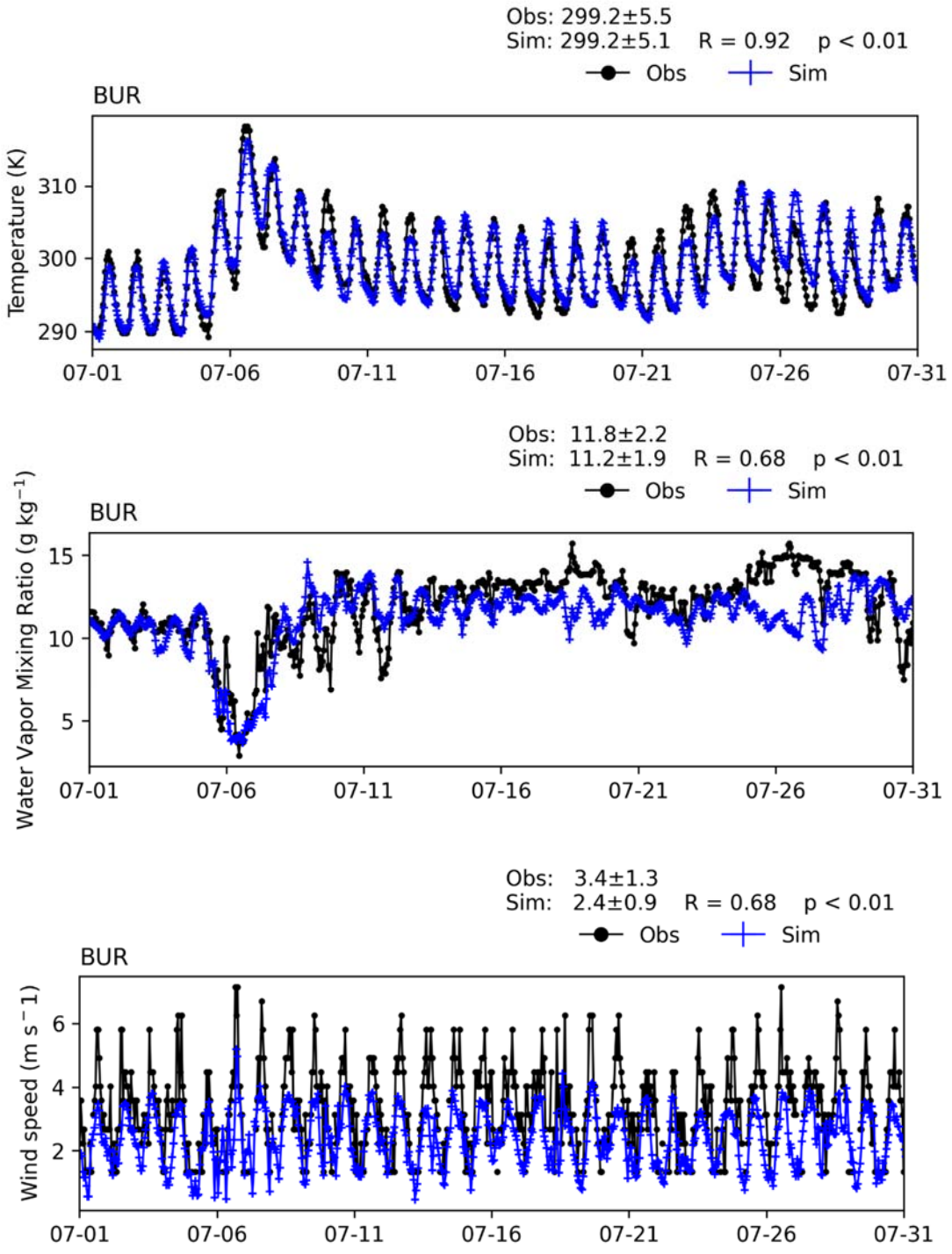

FIGURE V-A2
TIME SERIES OF HOURLY MEASUREMENTS AND WRF BASE SIMULATIONS AT BURBANK AIRPORT (BUR) FOR JULY 2018

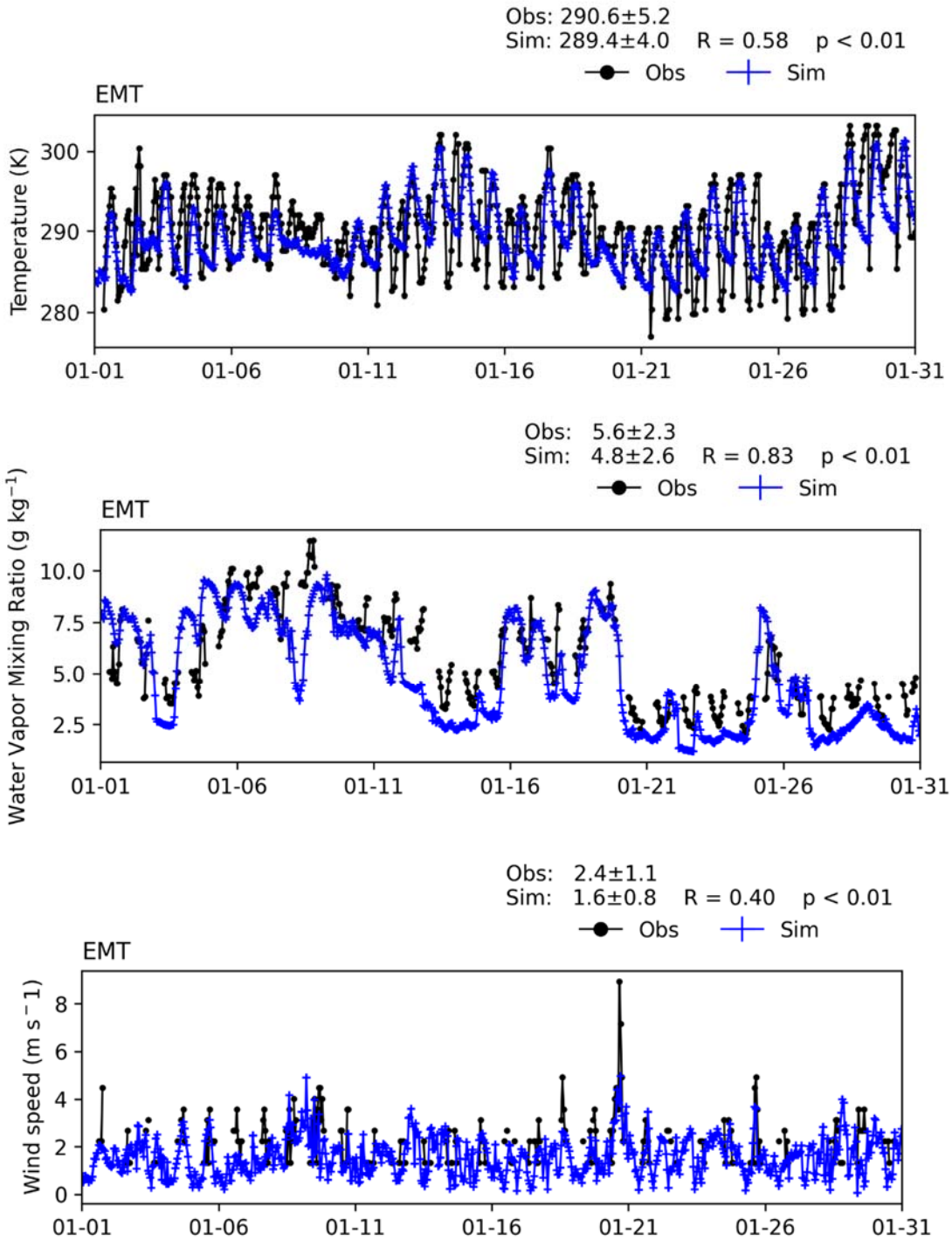

FIGURE V-A3
TIME SERIES OF HOURLY MEASUREMENTS AND WRF BASE SIMULATIONS AT EI MONTE (EMT) FOR JANUARY 2018

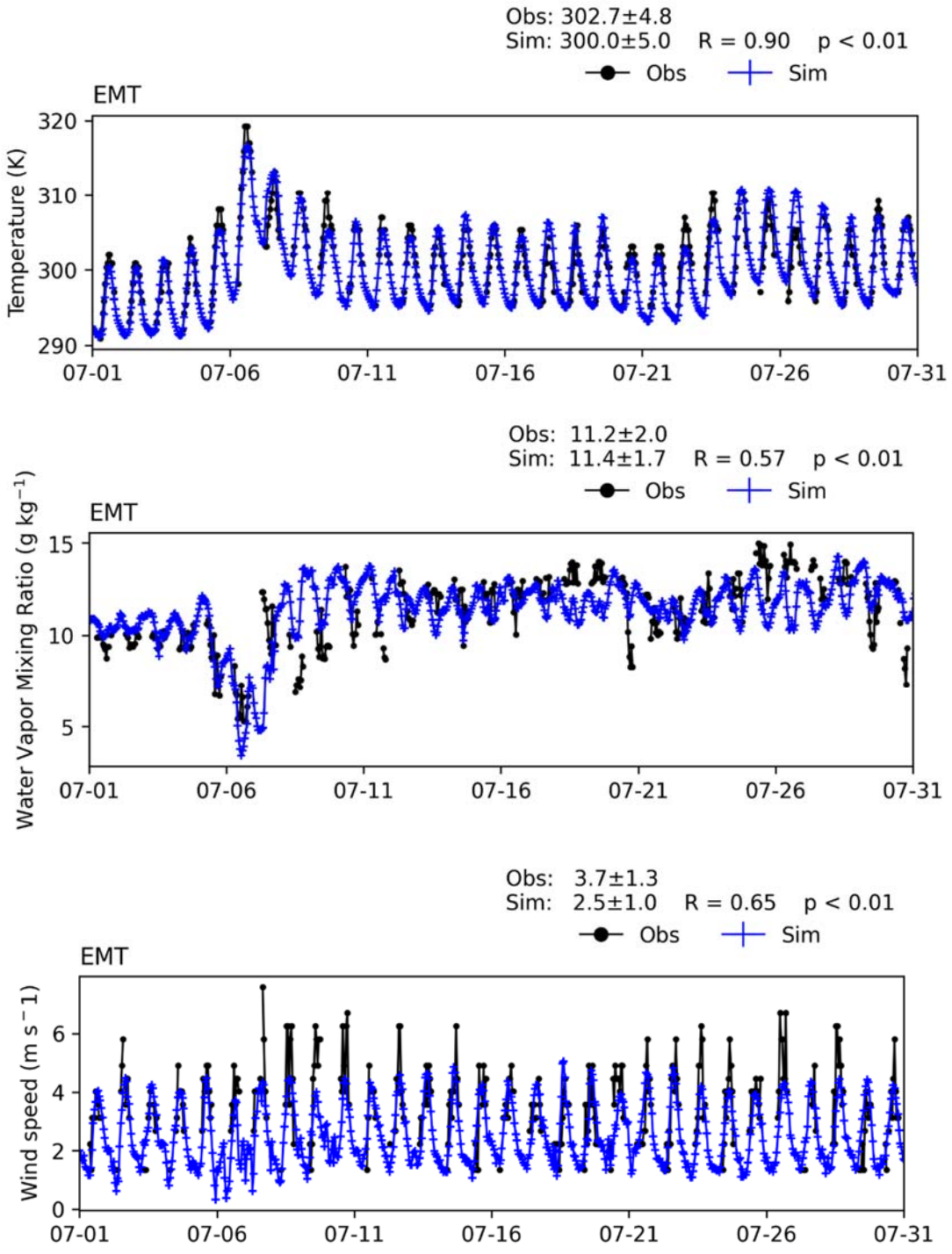

FIGURE V-A4
TIME SERIES OF HOURLY MEASUREMENTS AND WRF BASE SIMULATIONS AT EI MONTE (EMT) FOR JULY 2018

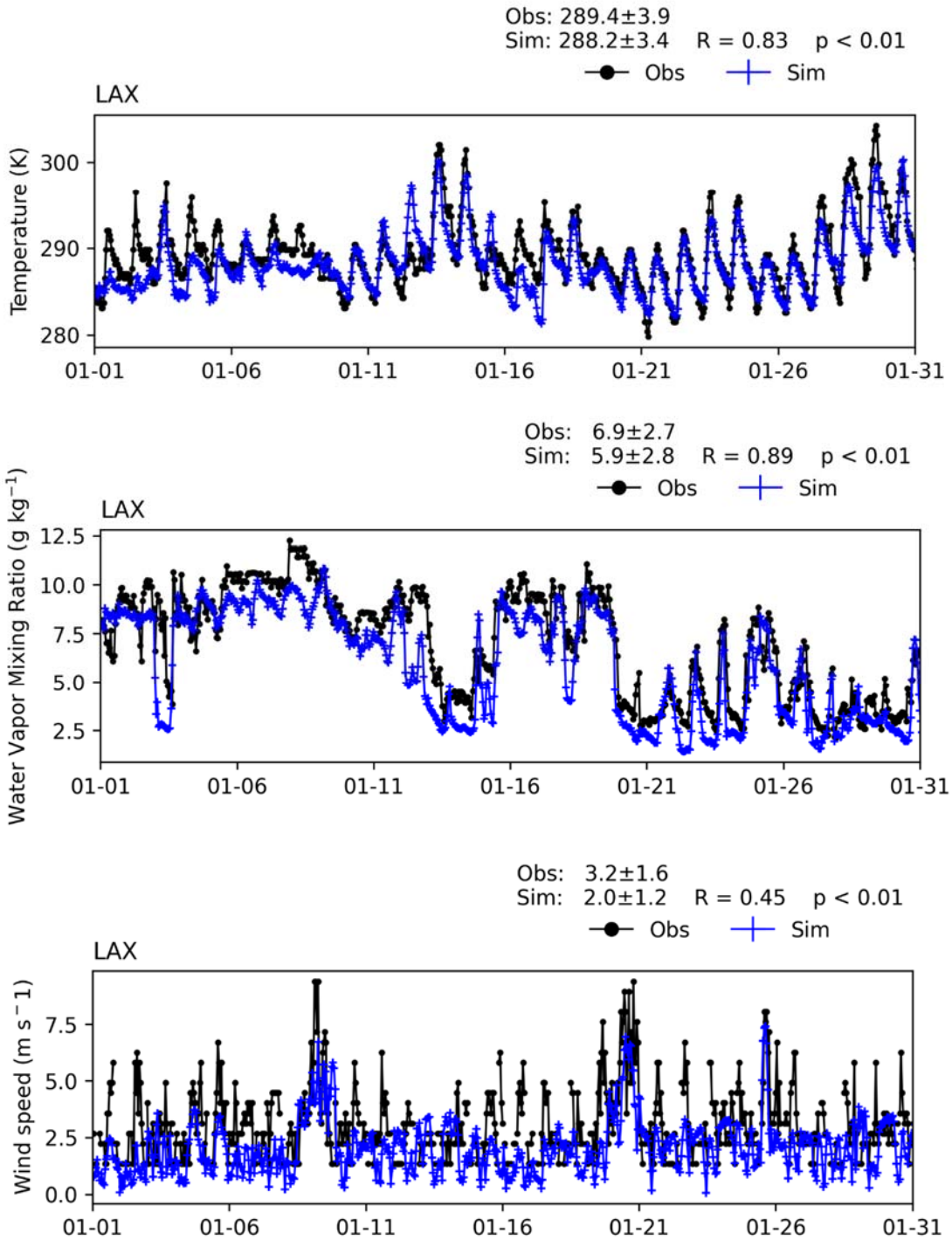

FIGURE V-A5
TIME SERIES OF HOURLY MEASUREMENTS AND WRF BASE SIMULATIONS AT LOS ANGELES AIRPORT (LAX) FOR JANUARY 2018

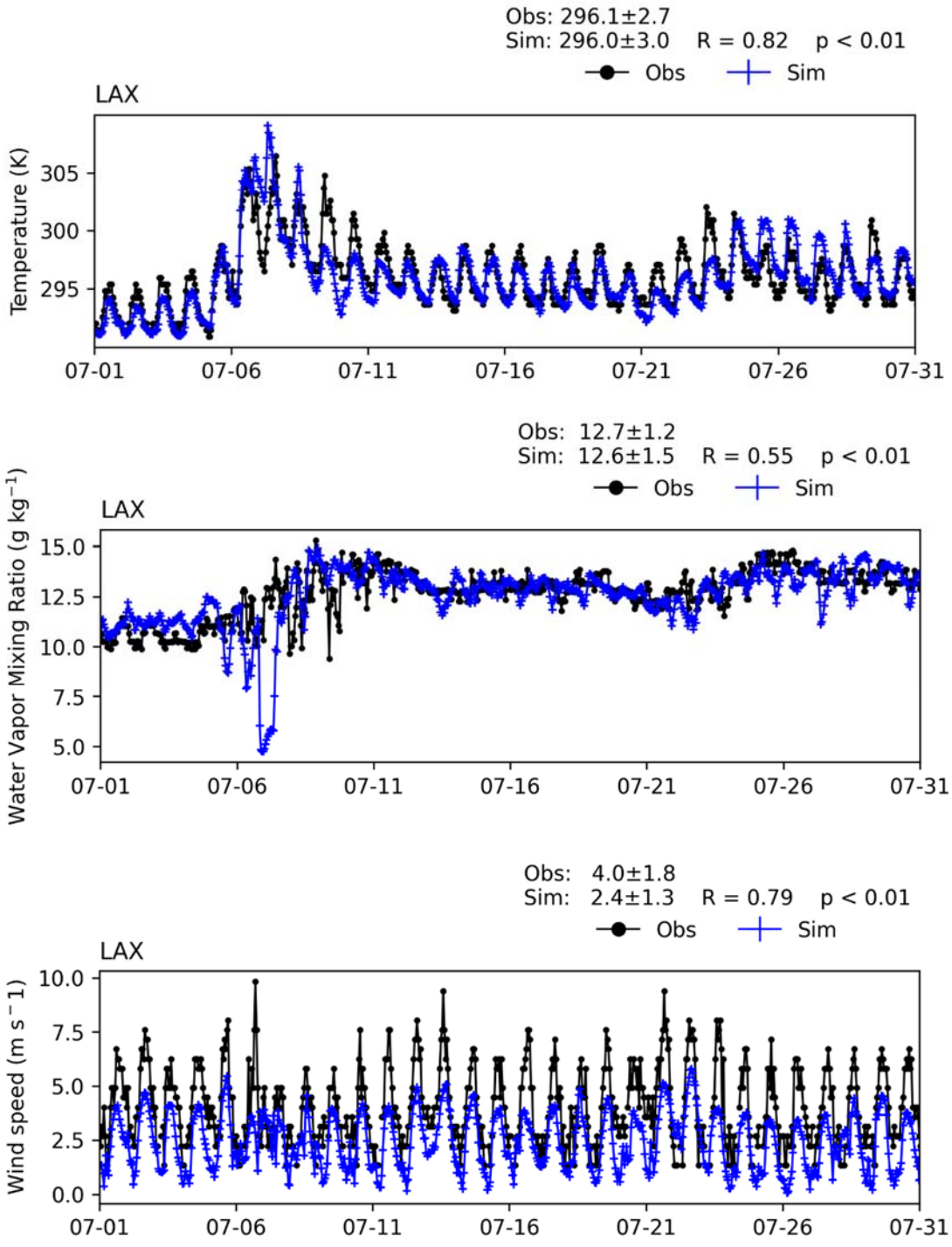

FIGURE V-A6
TIME SERIES OF HOURLY MEASUREMENTS AND WRF BASE SIMULATIONS AT LOS ANGELES AIRPORT (LAX) FOR JULY 2018

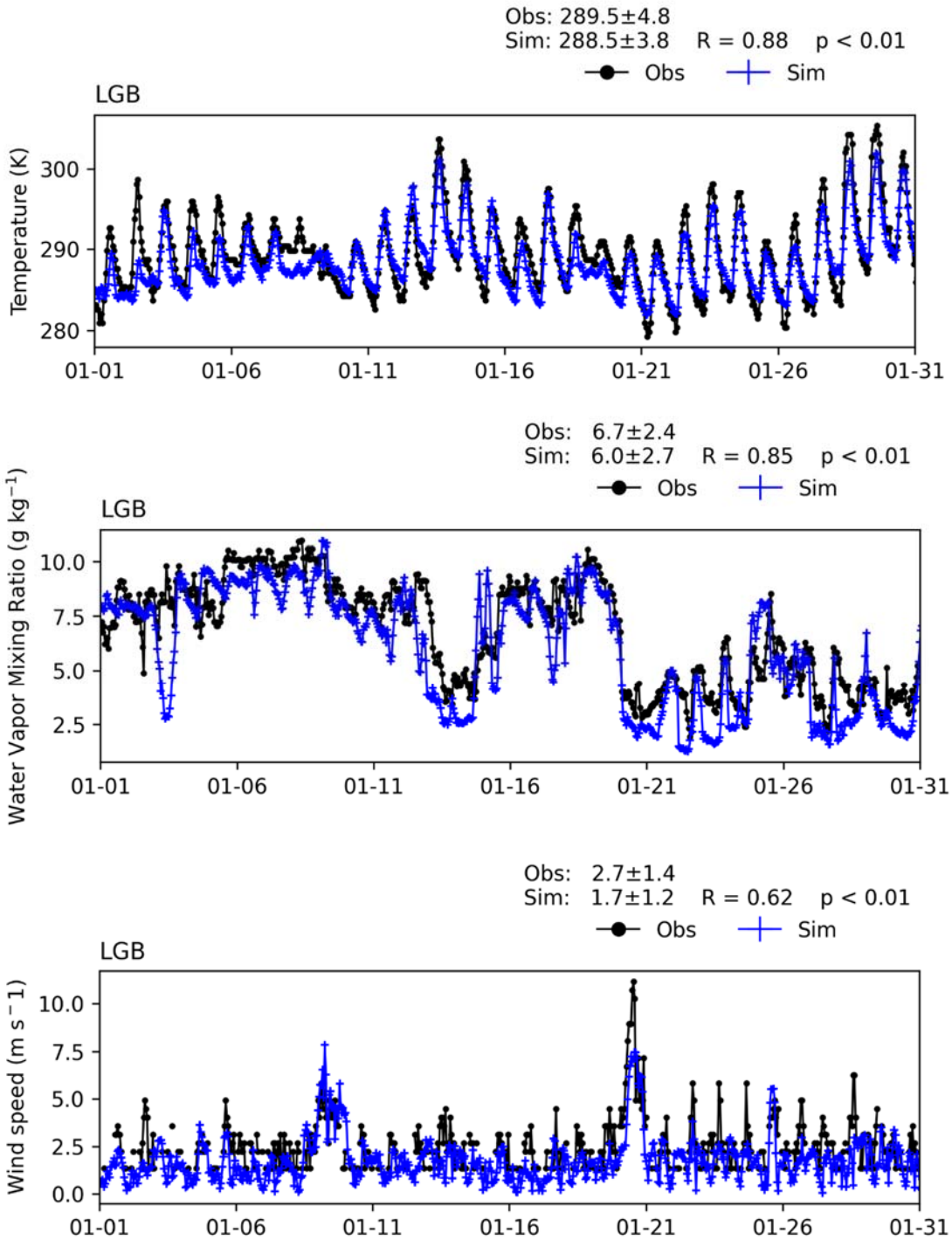

FIGURE V-A7
TIME SERIES OF HOURLY MEASUREMENTS AND WRF BASE SIMULATIONS AT LONG BEACH AIRPORT (LGB) FOR JANUARY 2018

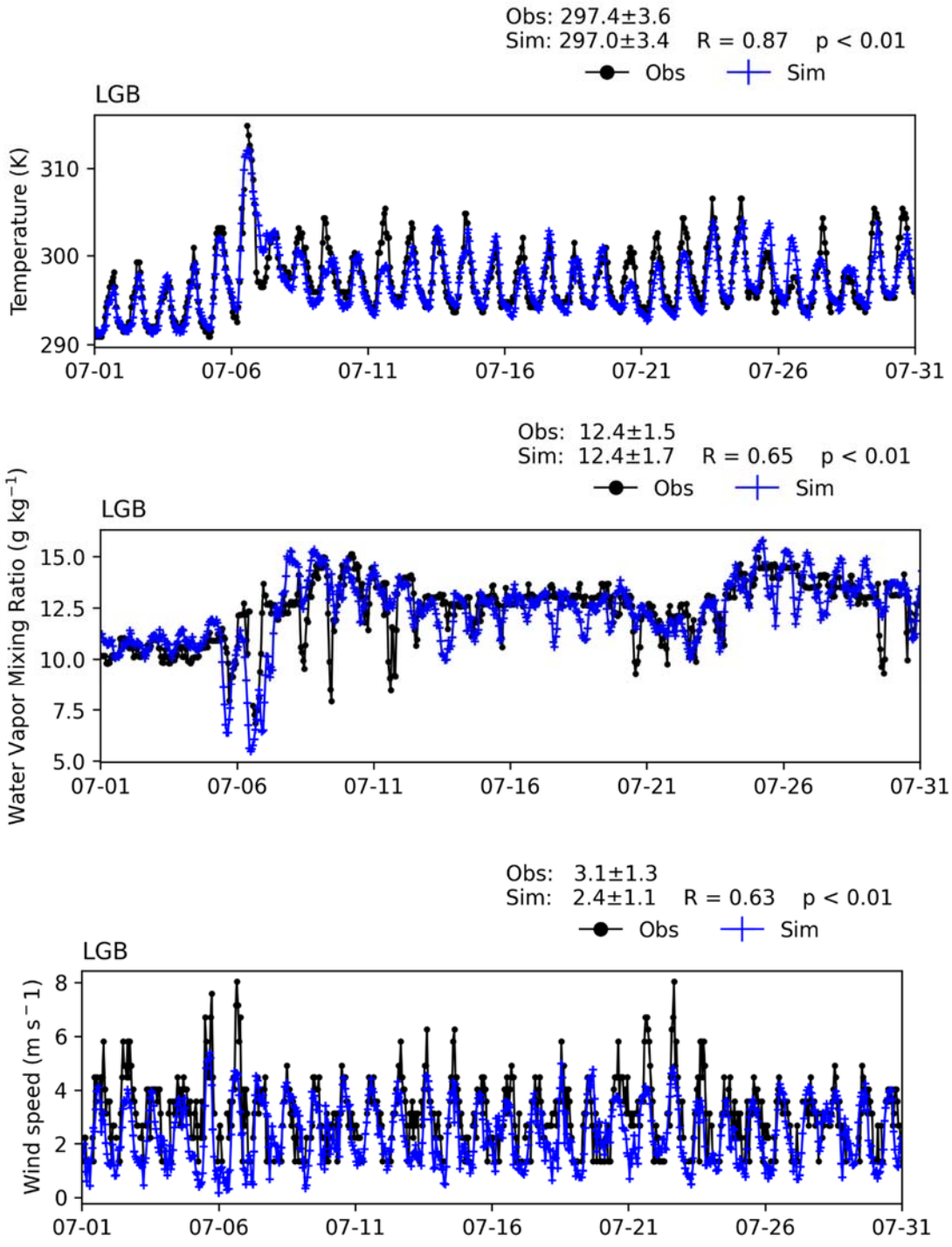

FIGURE V-A8
TIME SERIES OF HOURLY MEASUREMENTS AND WRF BASE SIMULATIONS AT LONG BEACH AIRPORT (LGB) FOR JULY 2018

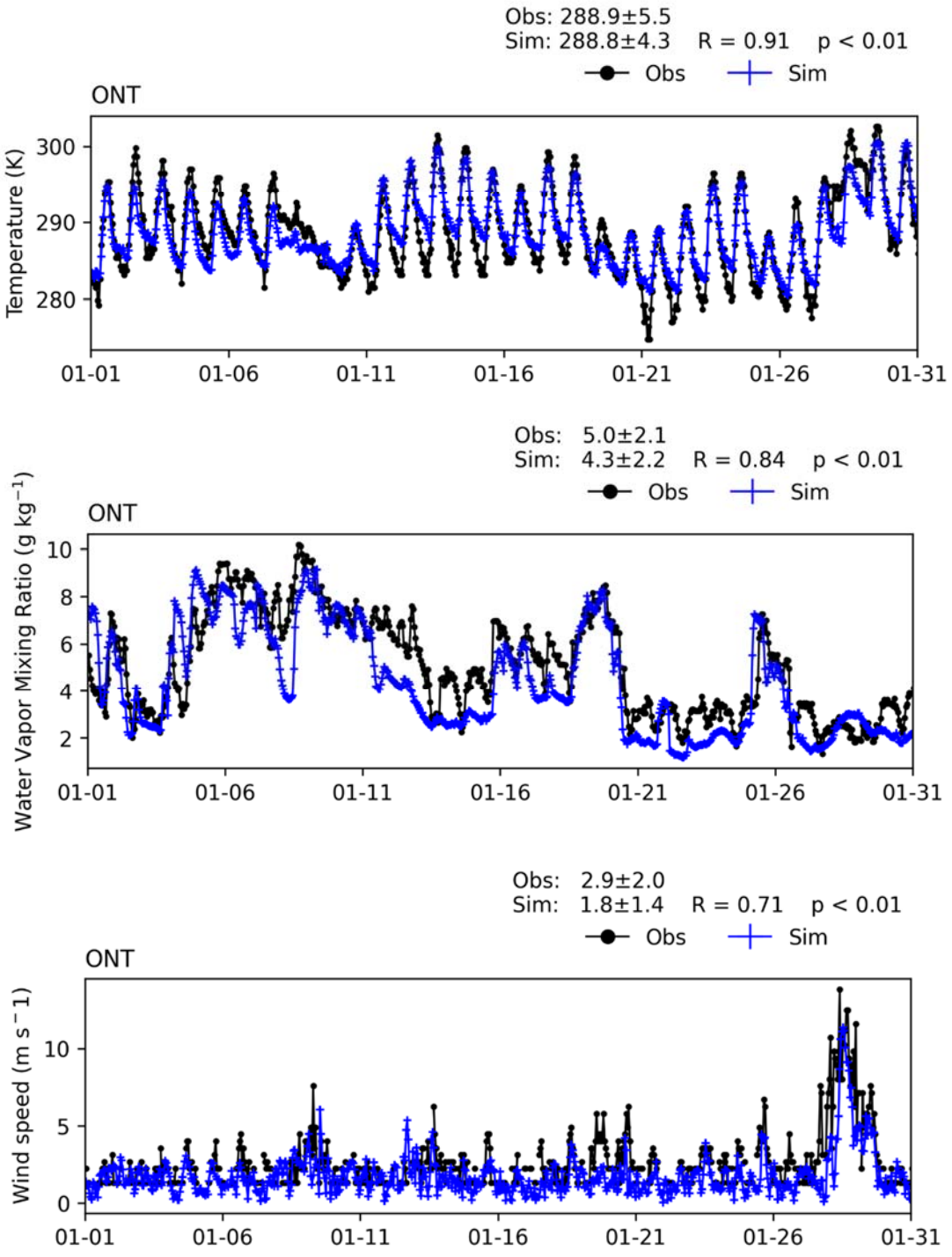

FIGURE V-A9
TIME SERIES OF HOURLY MEASUREMENTS AND WRF BASE SIMULATIONS AT ONTARIO INTERNATIONAL AIRPORT (ONT) FOR JANUARY 2018

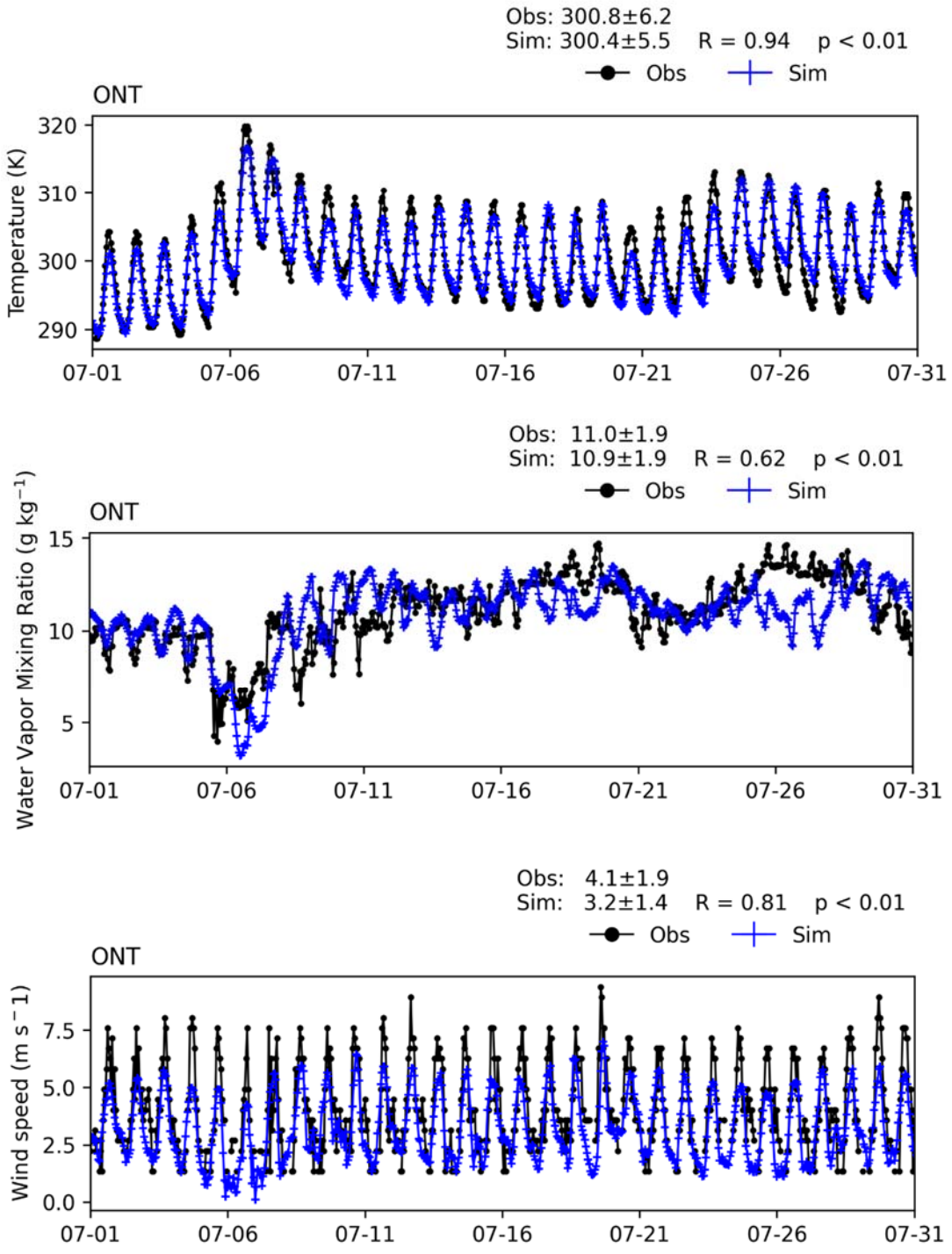

FIGURE V-A10
TIME SERIES OF HOURLY MEASUREMENTS AND WRF BASE SIMULATIONS AT ONTARIO INTERNATIONAL AIRPORT (ONT) FOR JULY 2018

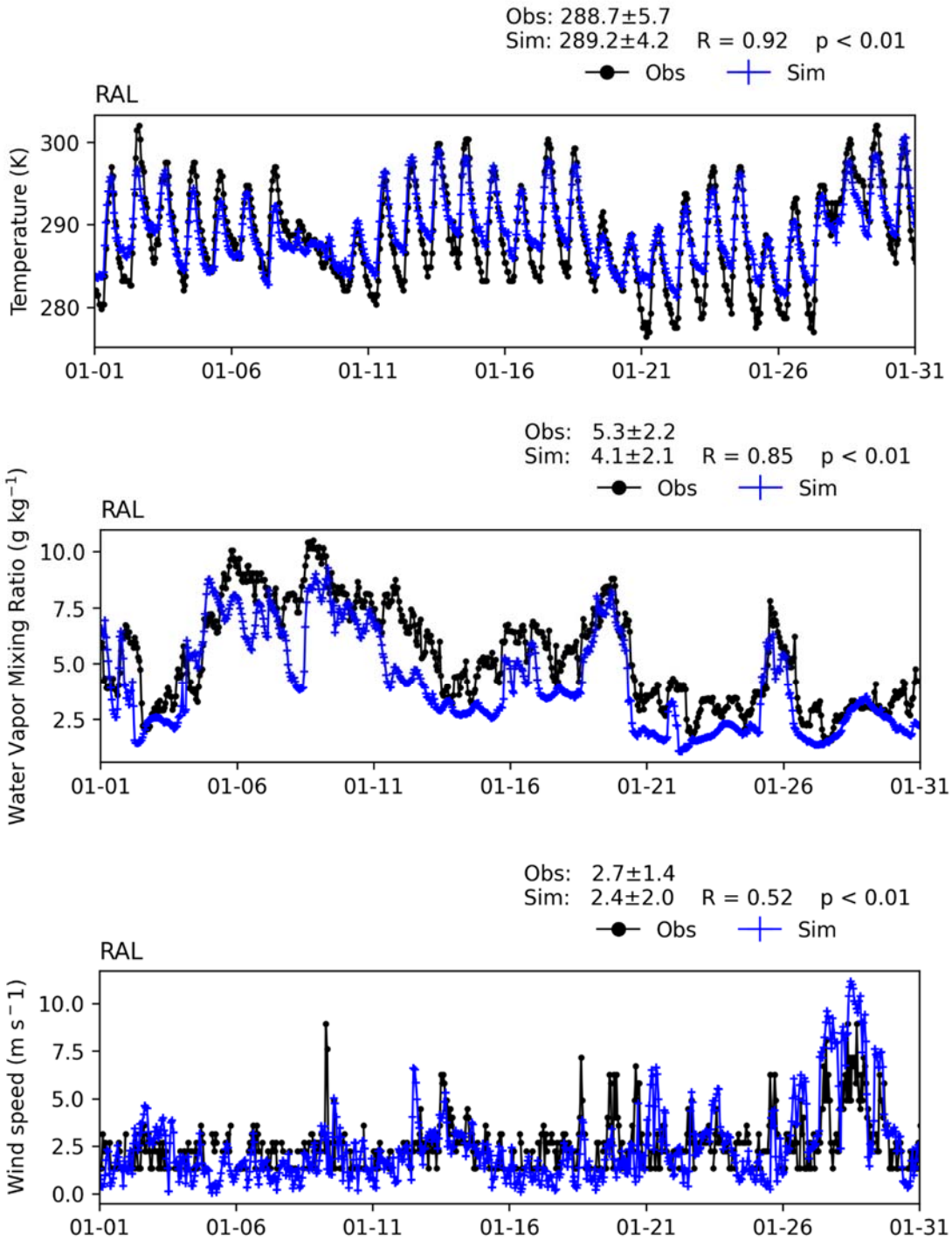

FIGURE V-A11
TIME SERIES OF HOURLY MEASUREMENTS AND WRF BASE SIMULATIONS AT RIVERSIDE MUNICIPAL AIRPORT (RAL) FOR JANUARY 2018

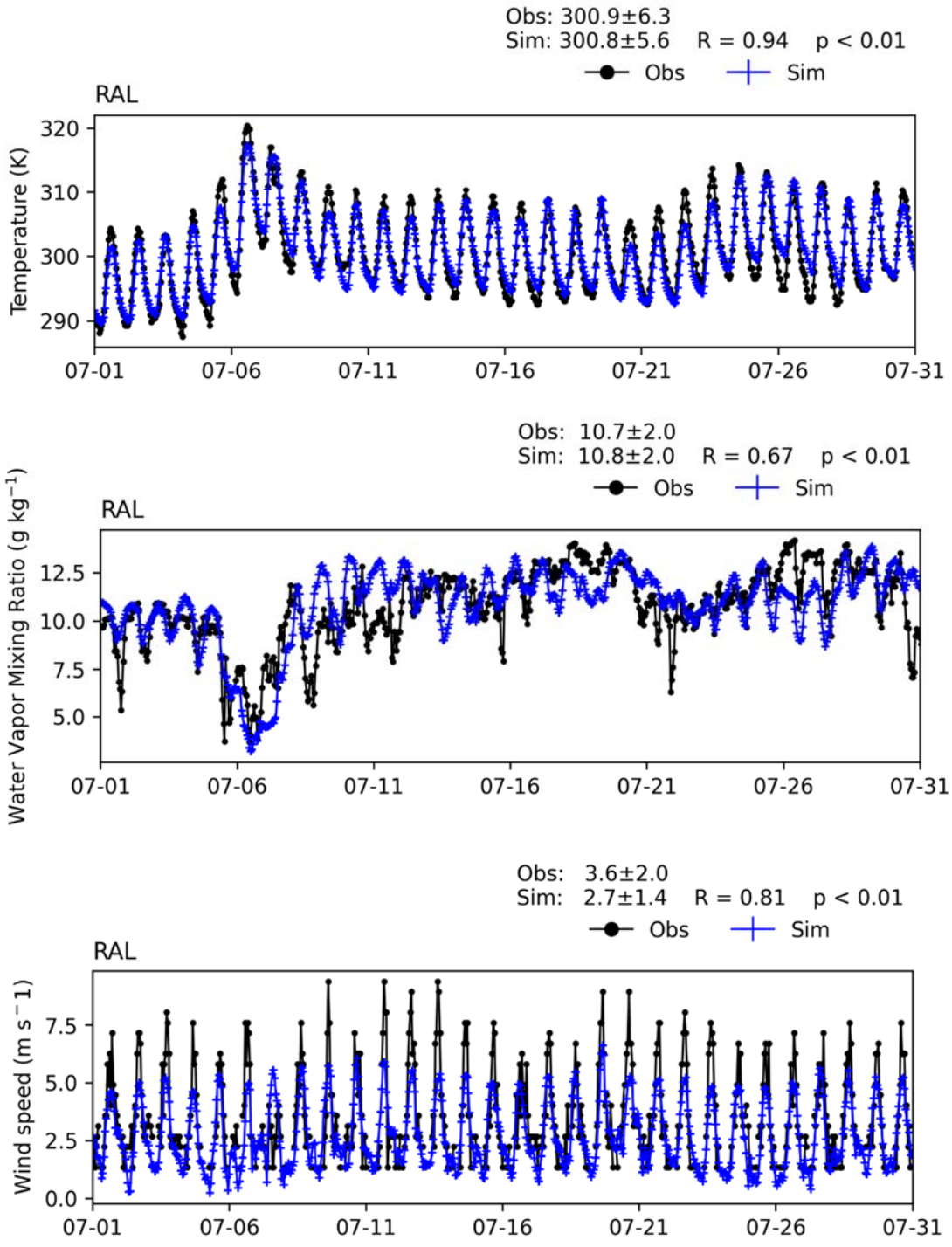

FIGURE V-A12
TIME SERIES OF HOURLY MEASUREMENTS AND WRF BASE SIMULATIONS AT RIVERSIDE MUNICIPAL AIRPORT (RAL) FOR JULY 2018

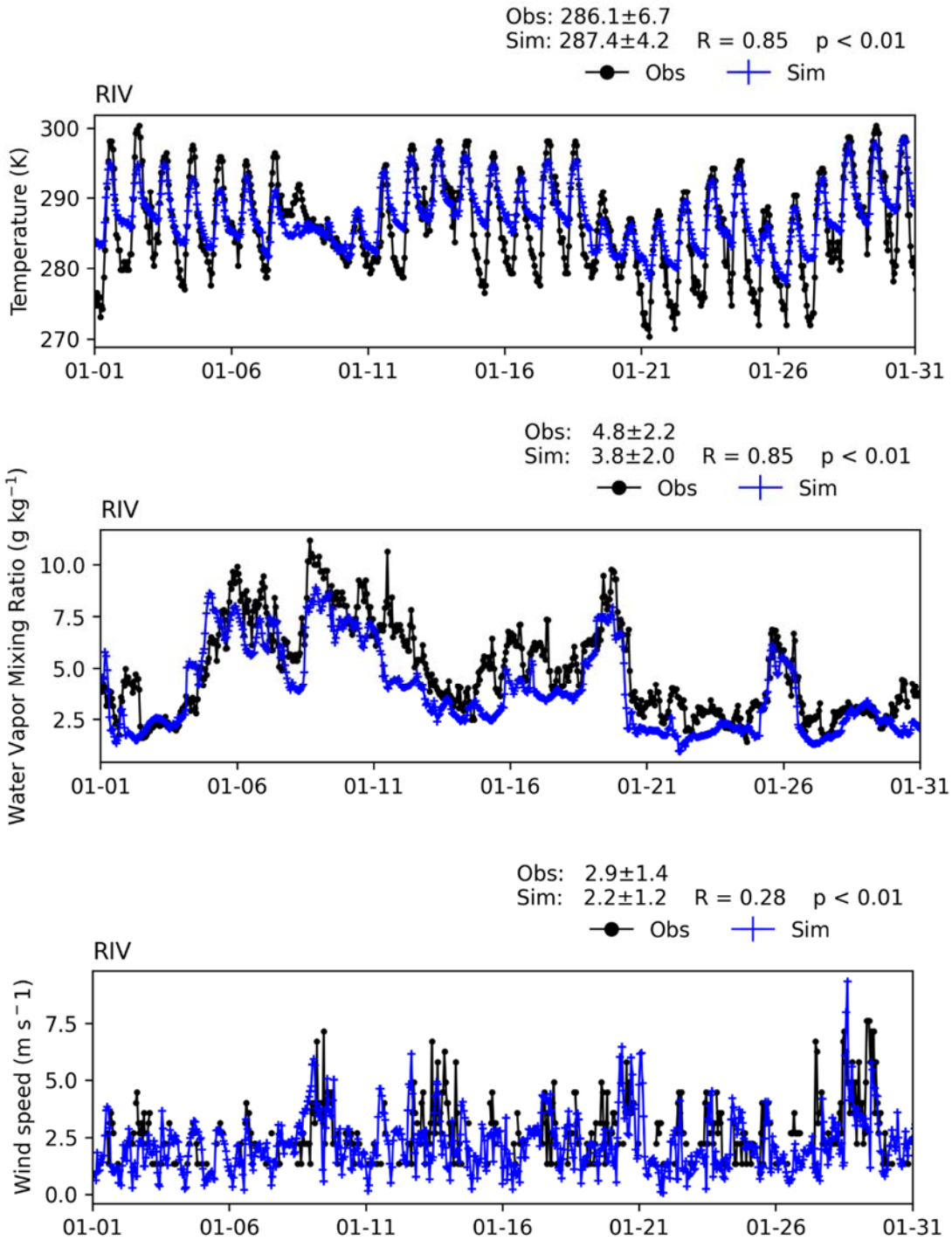

FIGURE V-A13
TIME SERIES OF HOURLY MEASUREMENTS AND WRF BASE SIMULATIONS AT MARCH AIR RESERVE AIRPORT (RIV) FOR JANUARY 2018

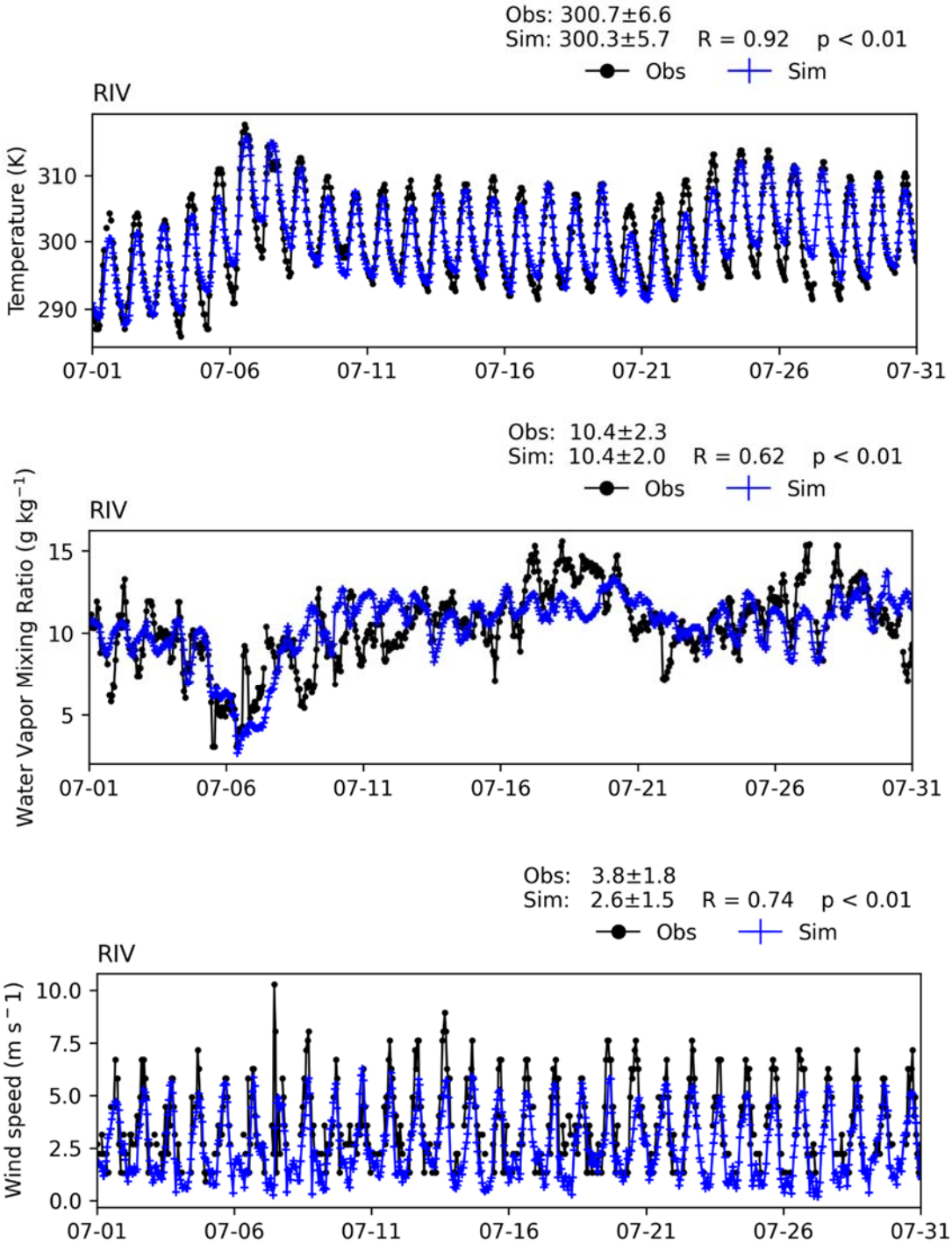

FIGURE V-A14
TIME SERIES OF HOURLY MEASUREMENTS AND WRF BASE SIMULATIONS AT MARCH AIR RESERVE AIRPORT (RIV) FOR JULY 2018

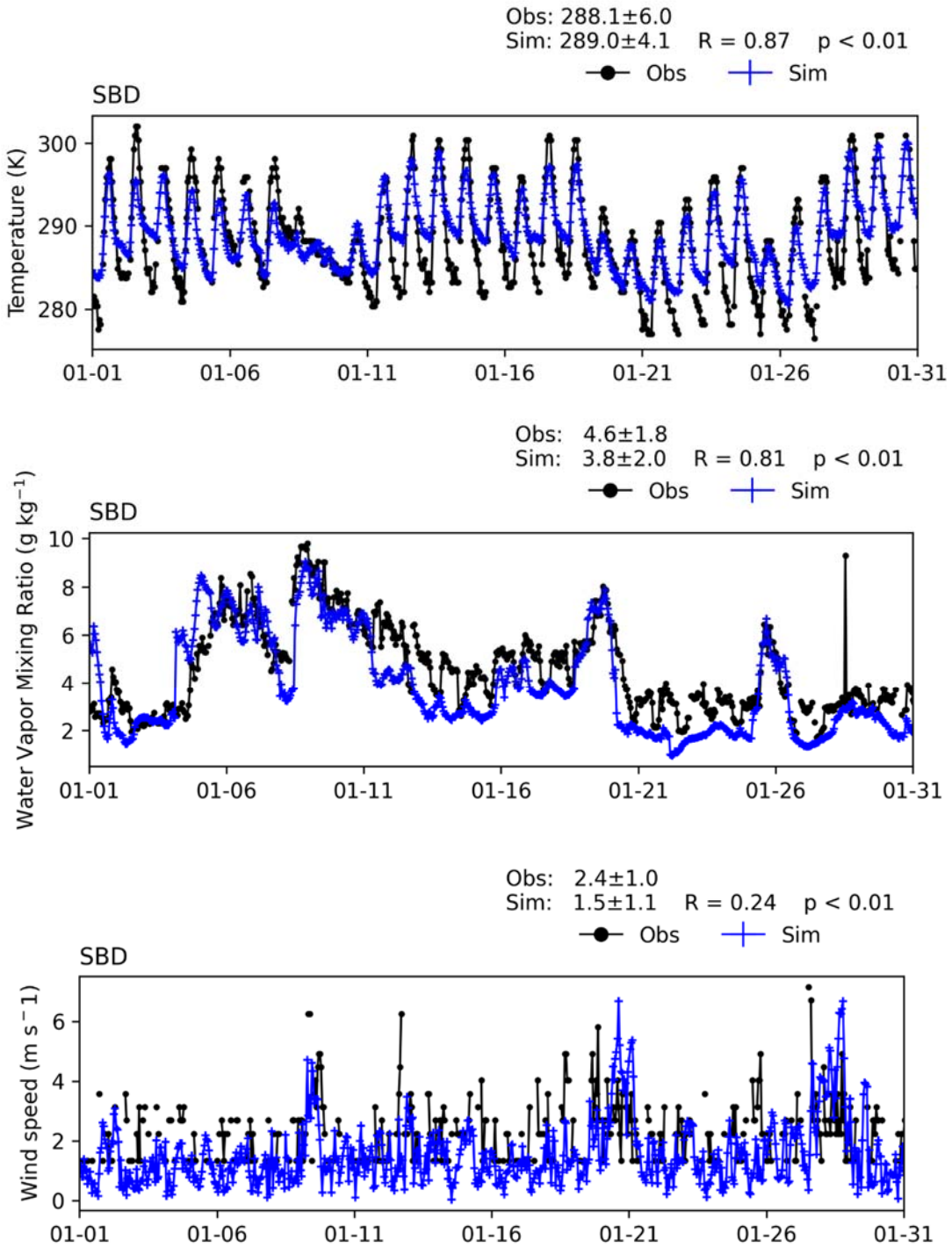

FIGURE V-A15
TIME SERIES OF HOURLY MEASUREMENTS AND WRF BASE SIMULATIONS AT SAN BERNARDINO INTERNATIONAL AIRPORT (SBD) FOR JANUARY 2018

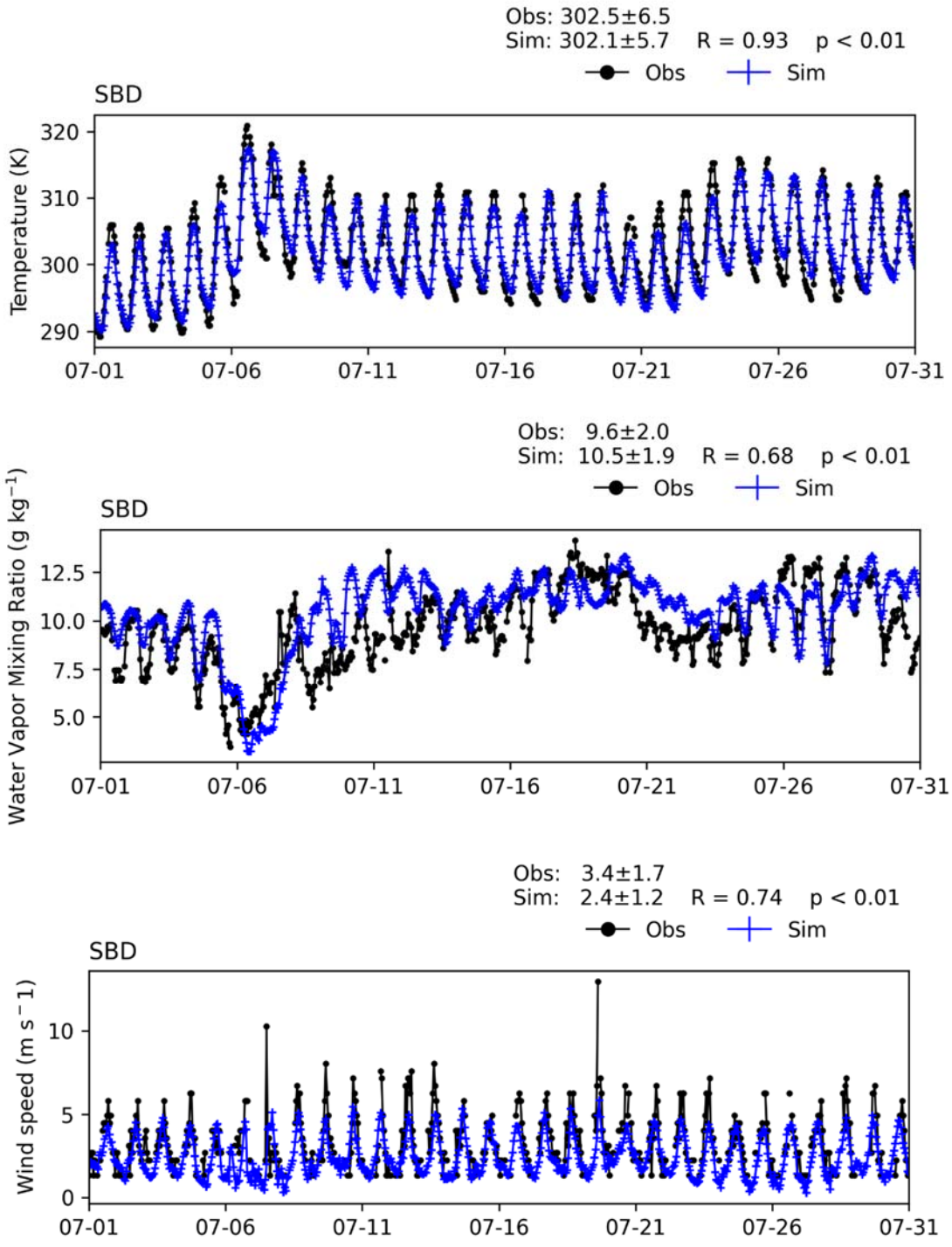

FIGURE V-A16
TIME SERIES OF HOURLY MEASUREMENTS AND WRF BASE SIMULATIONS AT SAN BERNARDINO INTERNATIONAL AIRPORT (SBD) FOR JULY 2018

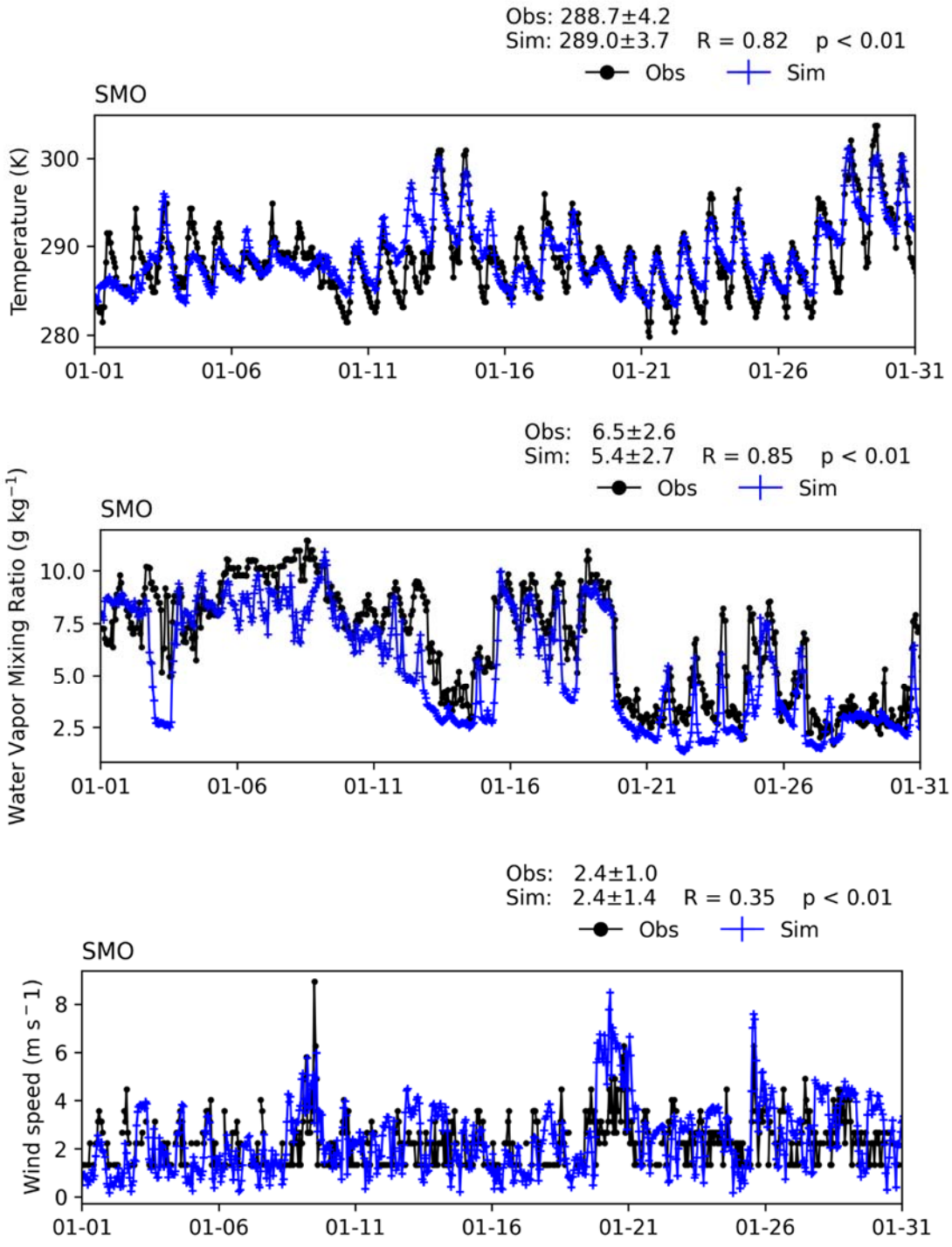

FIGURE V-A17
TIME SERIES OF HOURLY MEASUREMENTS AND WRF BASE SIMULATIONS AT SANTA MONICA AIRPORT (SMO) FOR JANUARY 2018

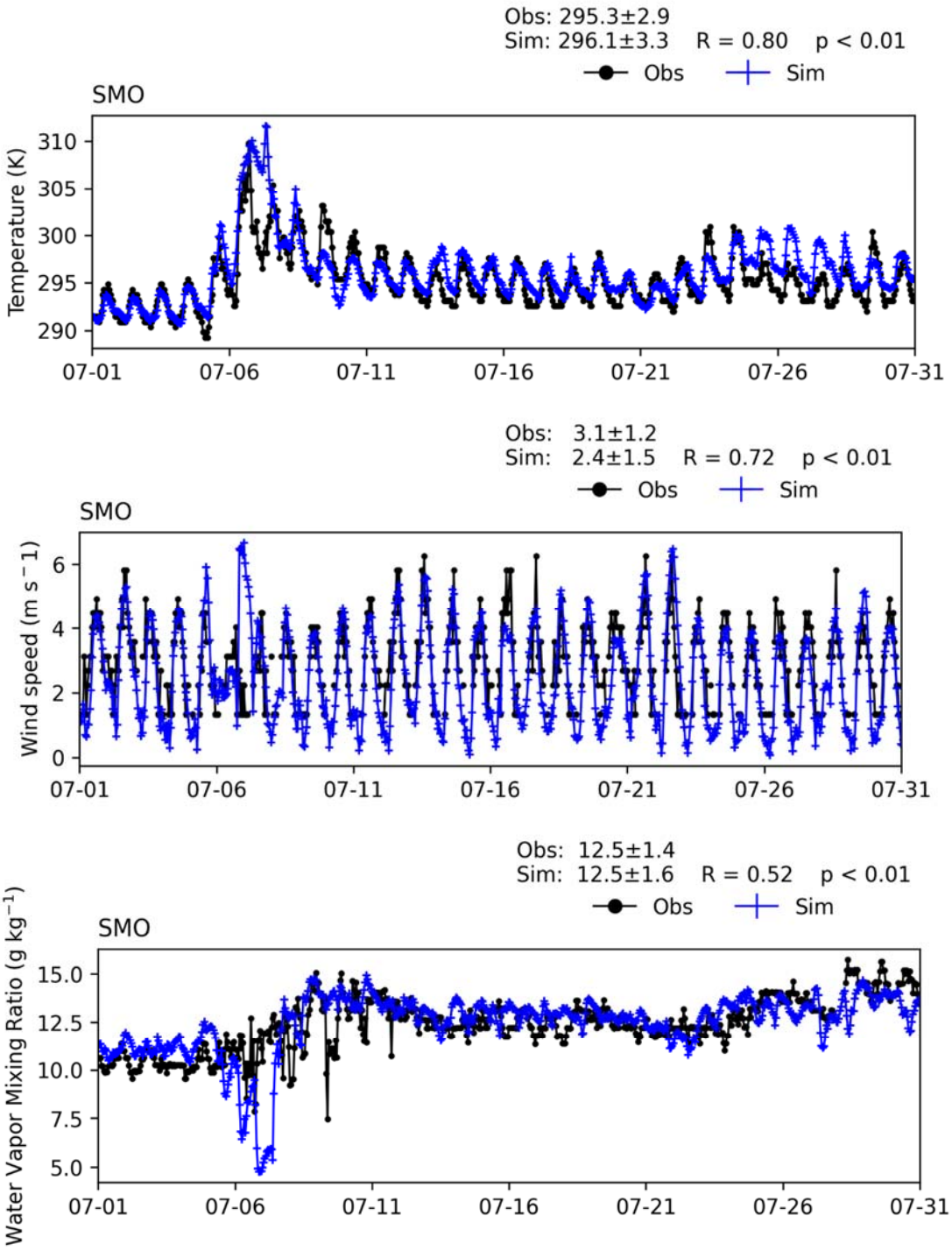

FIGURE V-A18
TIME SERIES OF HOURLY MEASUREMENTS AND WRF BASE SIMULATIONS AT SANTA MONICA AIRPORT (SMO) FOR JULY 2018

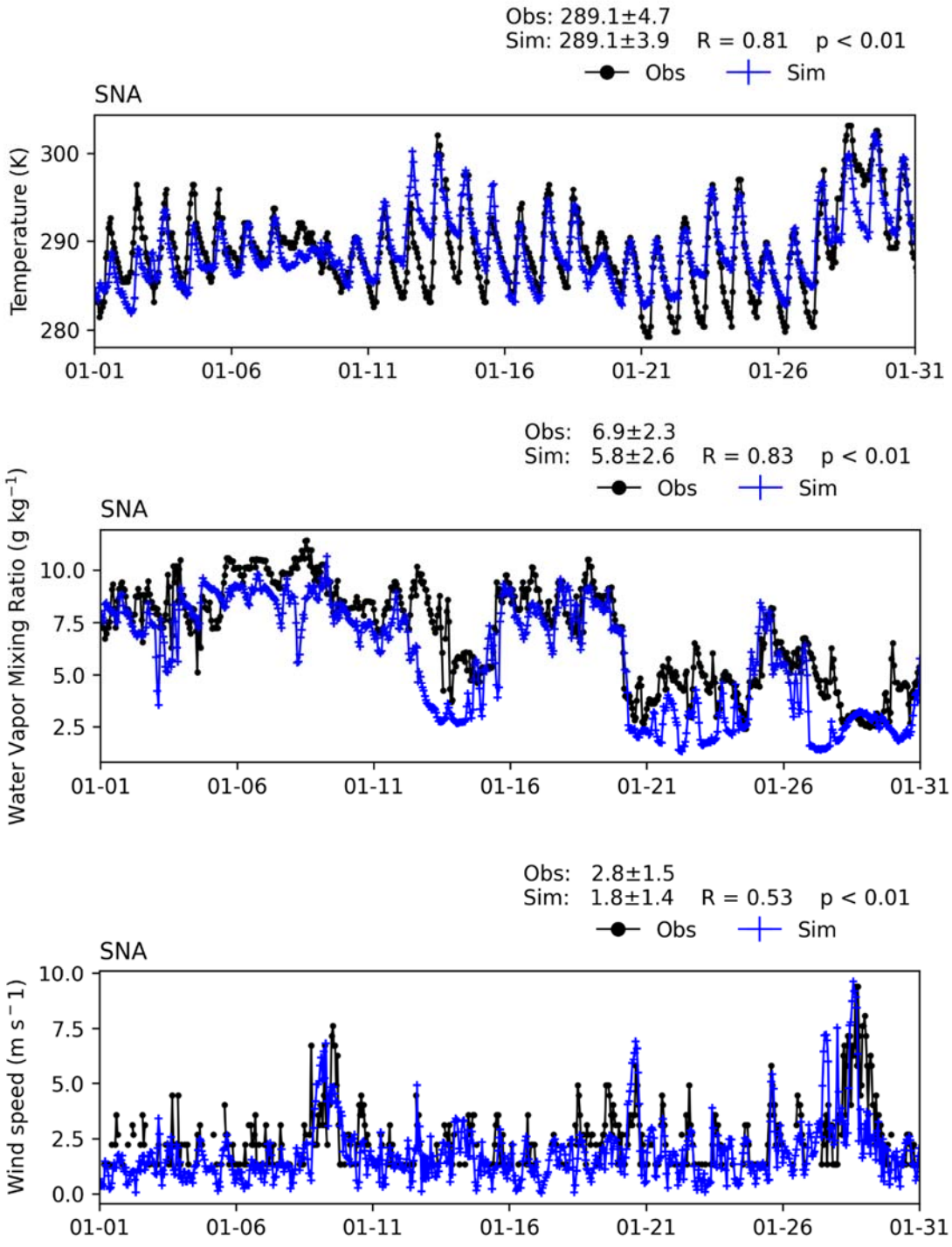

FIGURE V-A19
TIME SERIES OF HOURLY MEASUREMENTS AND WRF BASE SIMULATIONS AT SANTA ANA JOHN WAYNE AIRPORT (SNA) FOR JANUARY 2018

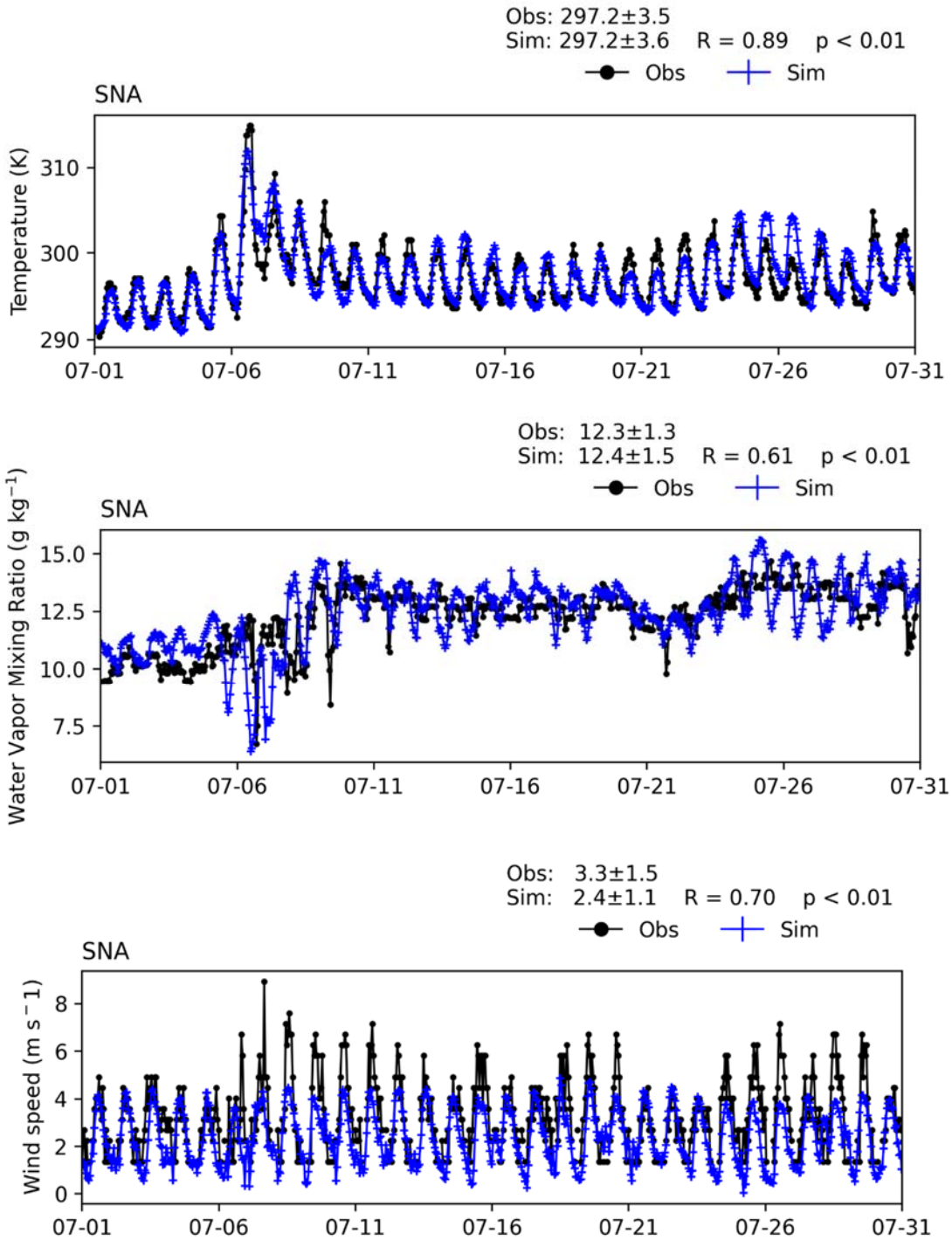

FIGURE V-A20
TIME SERIES OF HOURLY MEASUREMENTS AND WRF BASE SIMULATIONS AT SANTA ANA JOHN WAYNE AIRPORT (SNA) FOR JULY 2018

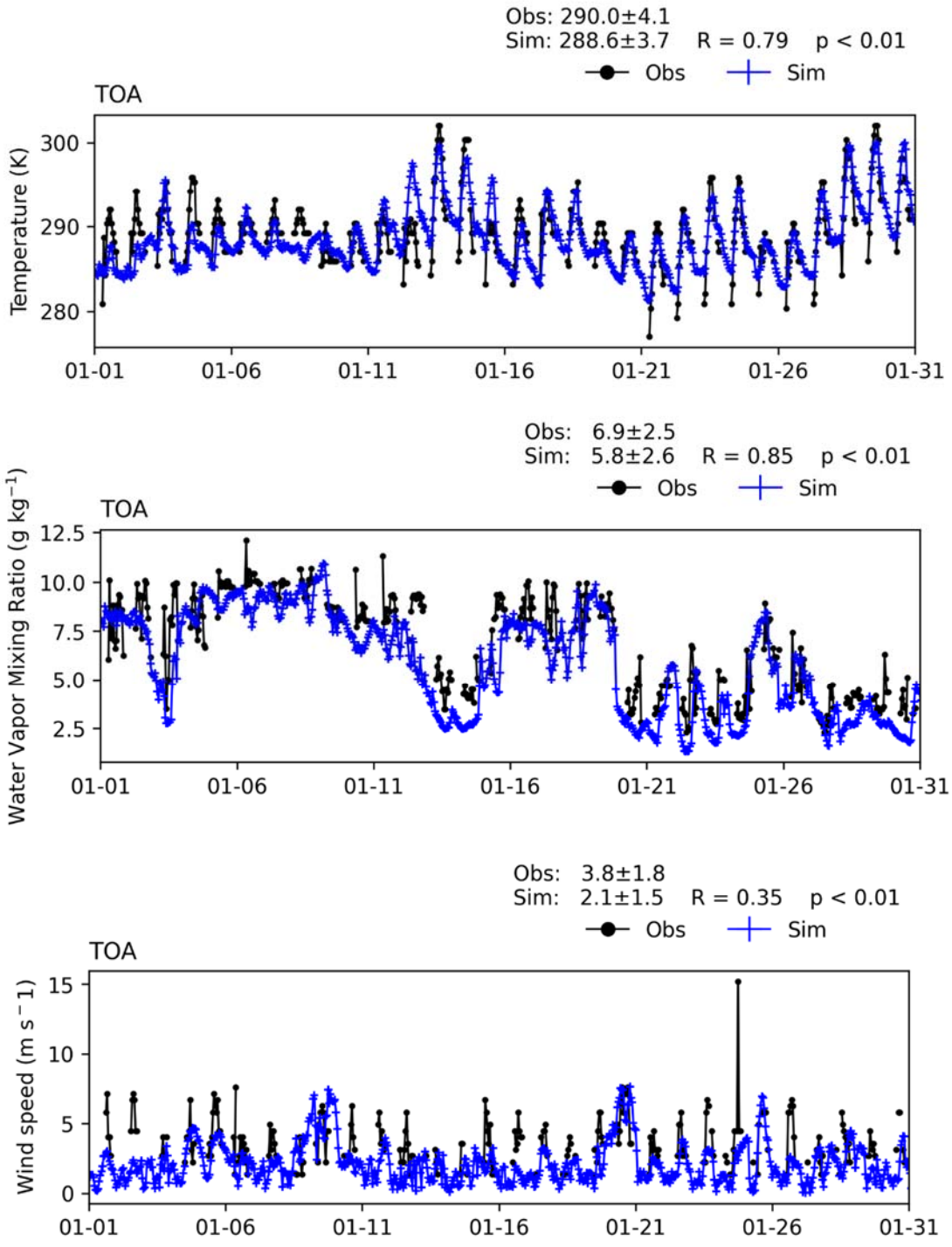

FIGURE V-A21
TIME SERIES OF HOURLY MEASUREMENTS AND WRF BASE SIMULATIONS AT TORRANCE (TOA) FOR JANUARY 2018

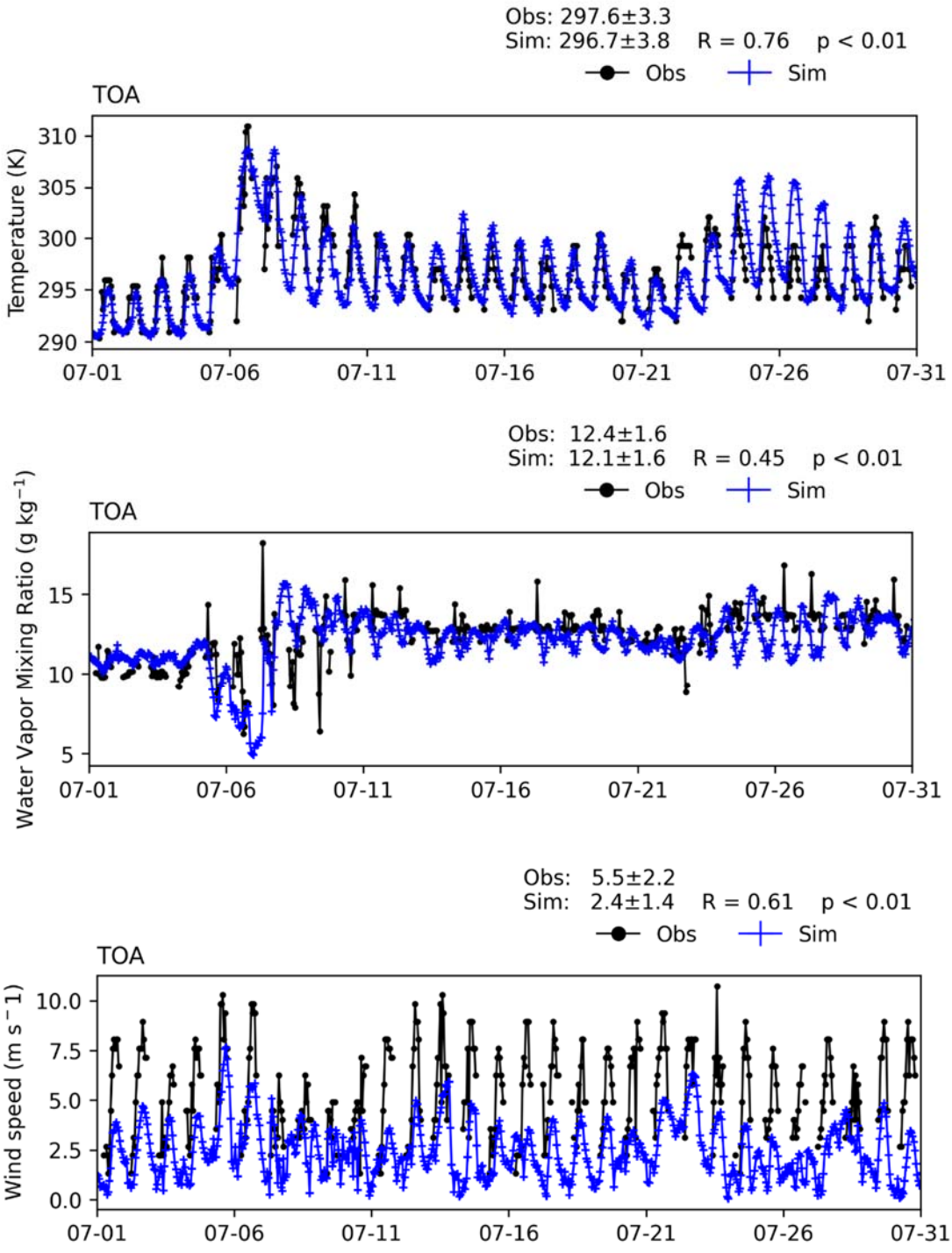

FIGURE V-A22
TIME SERIES OF HOURLY MEASUREMENTS AND WRF BASE SIMULATIONS AT TORRANCE (TOA) FOR JULY 2018

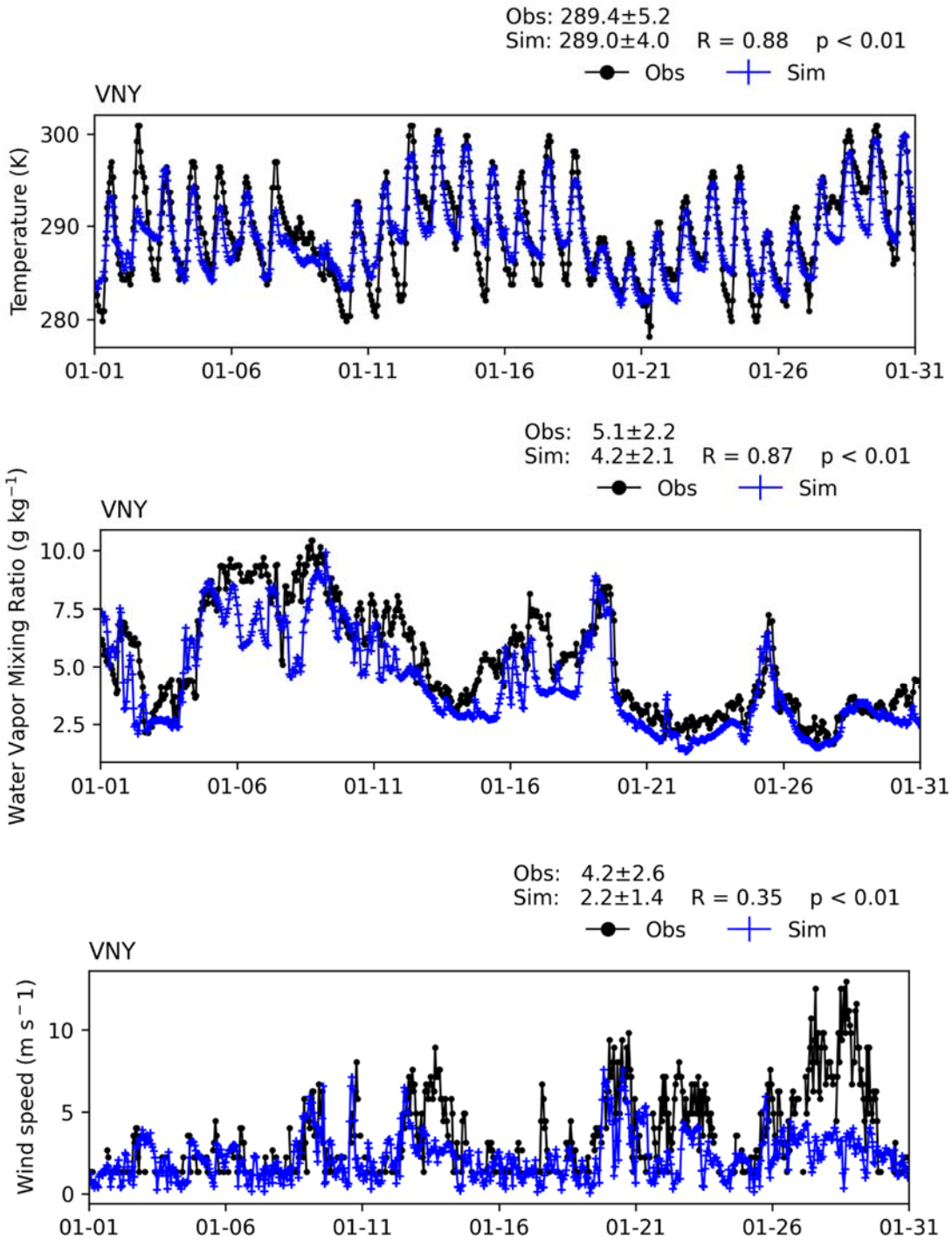

FIGURE V-A23
TIME SERIES OF HOURLY MEASUREMENTS AND WRF BASE SIMULATIONS AT VAN NUYS AIRPORT (VNY) FOR JANUARY 2018

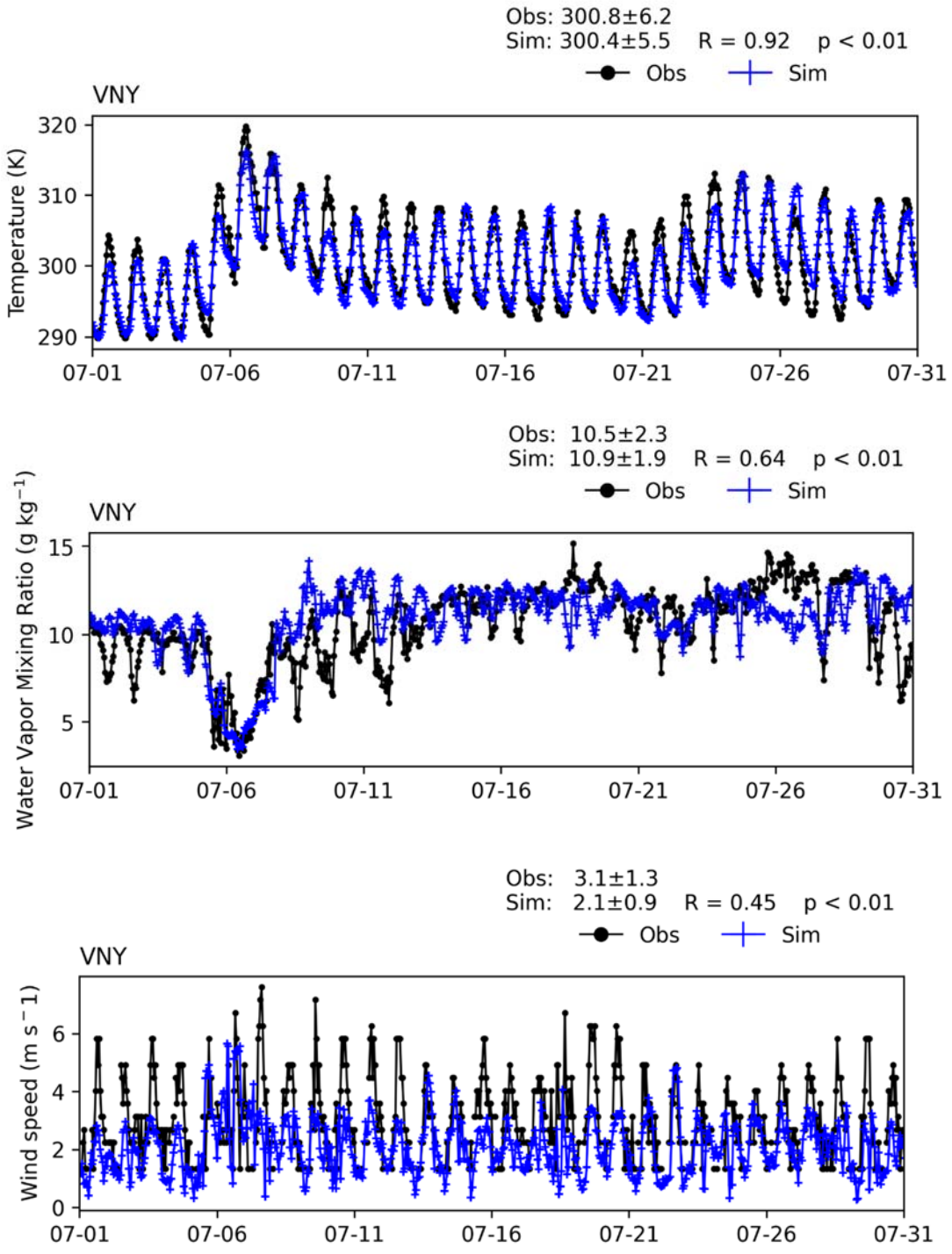

FIGURE V-A24
TIME SERIES OF HOURLY MEASUREMENTS AND WRF BASE SIMULATIONS AT VAN NUYS AIRPORT (VNY) FOR JULY 2018

Attachment 2

CMAQ MODEL PERFORMANCE TIME SERIES, BOXPLOTS, AND SCATTER PLOTS

CMAQ MODEL PERFORMANC TIME SERIES:

A: CMAQ Model Performance Time Series for Maximum Daily Average 8-Hour (MDA8) Ozone

B: CMAQ Model Performance Time Series for Daily Averaged NO Concentrations

C: CMAQ Model Performance Time Series for Daily Averaged NO2 Concentrations

D: CMAQ Model Performance Time Series for Daily Averaged NOx Concentrations

E: CMAQ Model Performance Time Series for Daily Averaged NOy Concentrations

CMAQ MODEL PERFORMANC BOXPLOTS:

F: CMAQ Model Performance Hourly Boxplots for 1-Hour Ozone Concentrations during May 1st, 2018, to September 30th, 2018

G: CMAQ Model Performance Hourly Boxplots of 1-Hour NO Concentrations during May 1st, 2018, to September 30th, 2018

H: CMAQ Model Performance Hourly Boxplots of 1-Hour NO2 Concentrations during May 1st, 2018, to September 30th, 2018

I: CMAQ Model Performance Hourly Boxplots of 1-Hour NOx Concentrations during May 1st, 2018, to September 30th, 2018

J: CMAQ Model Performance Hourly Boxplots of 1-Hour NOy Concentrations during May 1st, 2018, to September 30th, 2018

CMAQ MODEL PERFORMANC SCATTERPLOTS:

K: CMAQ Model Performance Scatter Plots for MDA8 Ozone Color-coded by Weekend vs. Weekday during May 1st, 2018, to September 30th, 2018

L: CMAQ Model Performance Scatter Plots for Daily Average NO Concentrations Color-Coded by Weekend vs. Weekday during May 1st, 2018, to September 30th, 2018

M: CMAQ Model Performance Scatter Plots for Daily Average NO2 Concentrations Color-Coded by Weekend vs. Weekday during May 1st, 2018, to September 30th, 2018

N: CMAQ Model Performance Scatter Plots for Daily Average NOx Concentrations Color-Coded by Weekend vs. Weekday during May 1st, 2018, to September 30th, 2018

O: CMAQ Model Performance Scatter Plots for Daily Average NOy Concentrations Color-Coded by Weekend vs. Weekday during May 1st, 2018, to September 30th, 2018

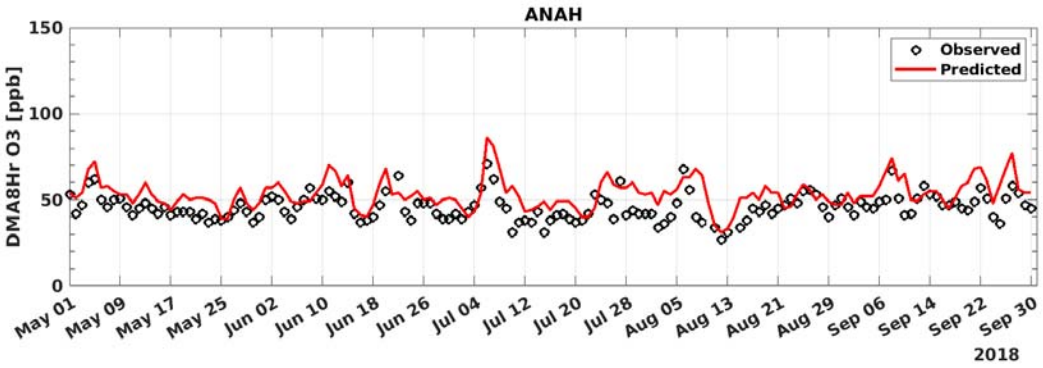

FIGURE A-1: 2018 MAXIMUM DAILY AVERAGE 8-HOUR (MDA8) OZONE MODEL PREDICTION AND MEASUREMENT COMPARISON AT ANAHEIM

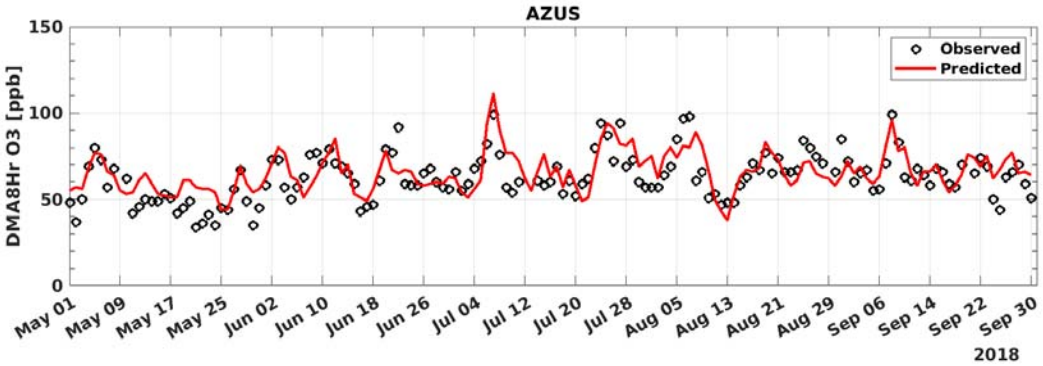

FIGURE A-2: 2018 MAXIMUM DAILY AVERAGE 8-HOUR (MDA8) OZONE MODEL PREDICTION AND MEASUREMENT COMPARISON AT AZUSA

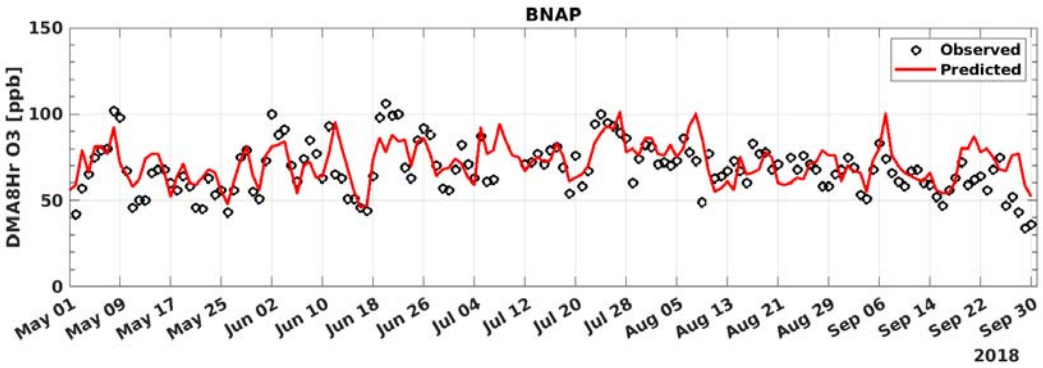

FIGURE A-3: 2018 MAXIMUM DAILY AVERAGE 8-HOUR (MDA8) OZONE MODEL PREDICTION AND MEASUREMENT COMPARISON AT BANNING

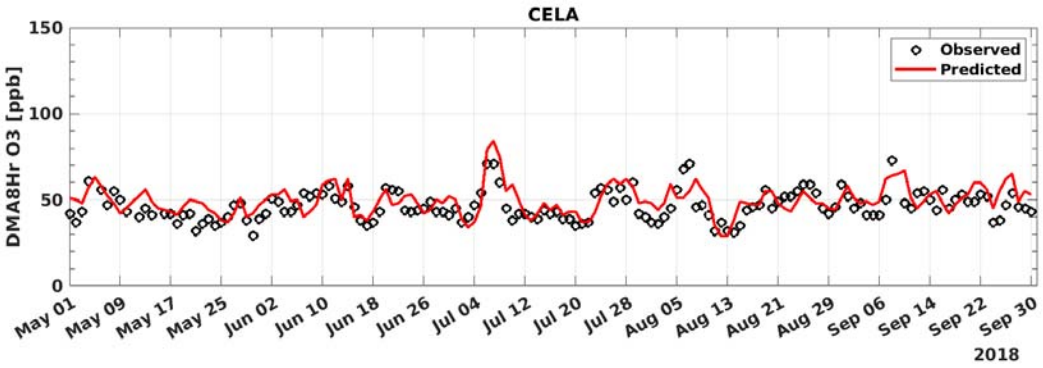

FIGURE A-4: 2018 MAXIMUM DAILY AVERAGE 8-HOUR (MDA8) OZONE MODEL PREDICTION AND MEASUREMENT COMPARISON AT CENTRAL LOS ANGELES

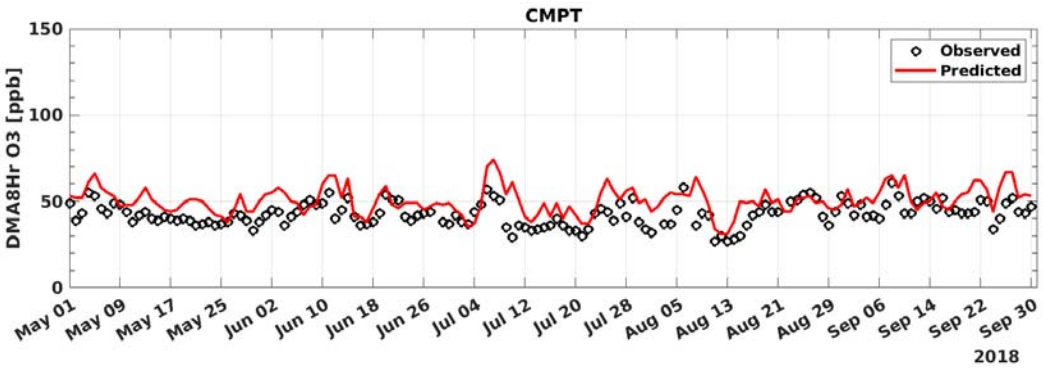

FIGURE A-5: 2018 MAXIMUM DAILY AVERAGE 8-HOUR (MDA8) OZONE MODEL PREDICTION AND MEASUREMENT COMPARISON AT COMPTON

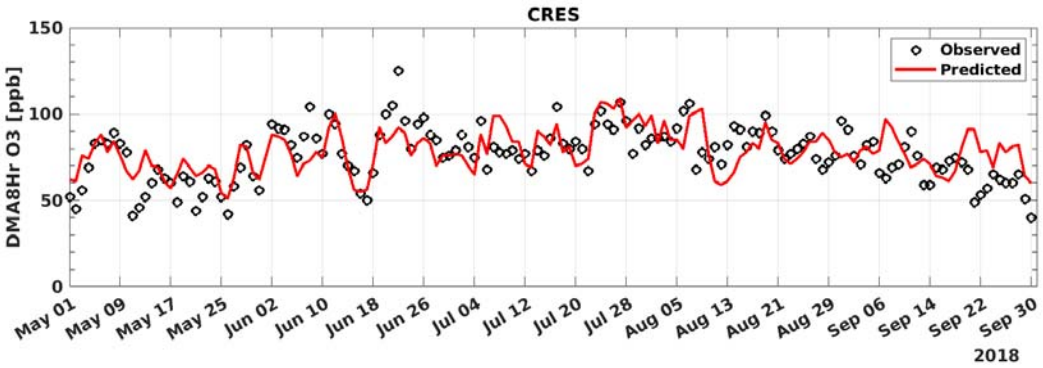

FIGURE A-6: 2018 MAXIMUM DAILY AVERAGE 8-HOUR (MDA8) OZONE MODEL PREDICTION AND MEASUREMENT COMPARISON AT CRESTLINE

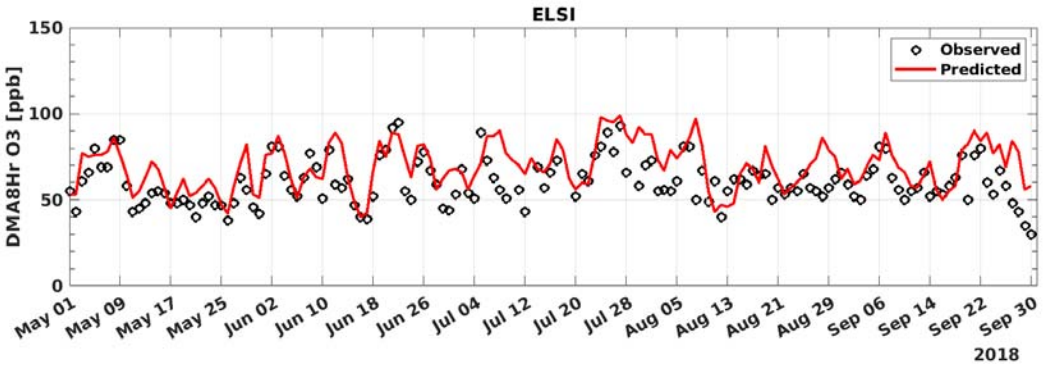

FIGURE A-7: 2018 MAXIMUM DAILY AVERAGE 8-HOUR (MDA8) OZONE MODEL PREDICTION AND MEASUREMENT COMPARISON AT LAKE ELSINORE

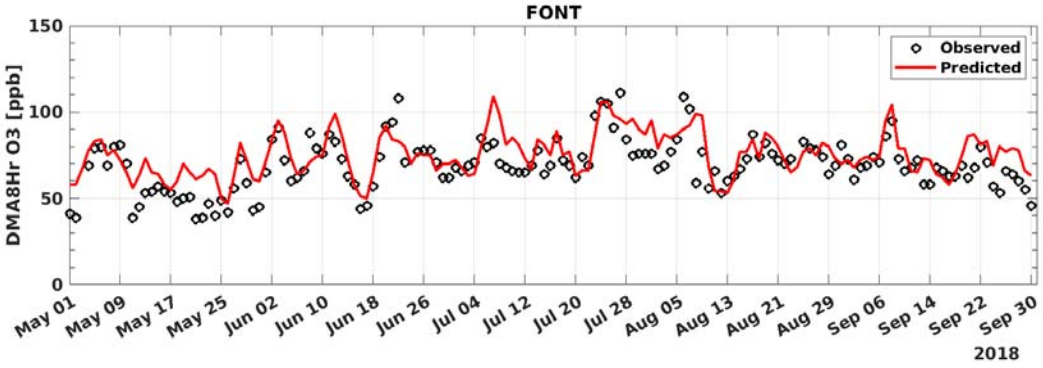

FIGURE A-8: 2018 MAXIMUM DAILY AVERAGE 8-HOUR (MDA8) OZONE MODEL PREDICTION AND MEASUREMENT COMPARISON AT FONTANA

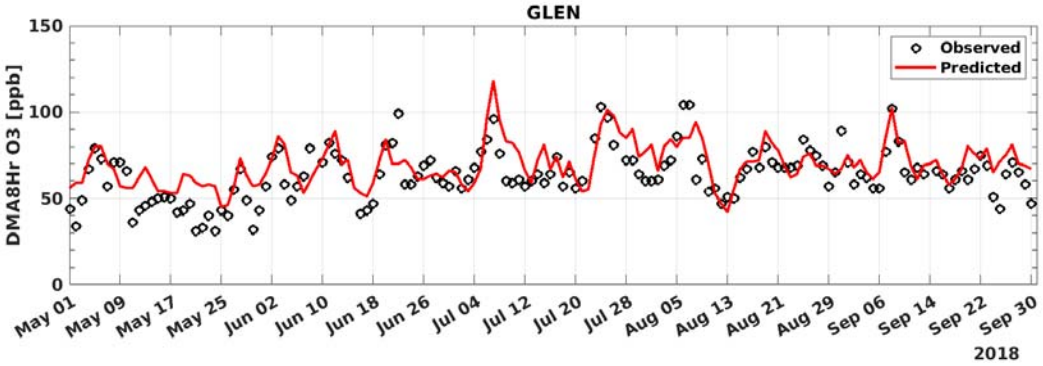

FIGURE A-9: 2018 MAXIMUM DAILY AVERAGE 8-HOUR (MDA8) OZONE MODEL PREDICTION AND MEASUREMENT COMPARISON AT GLENDORA

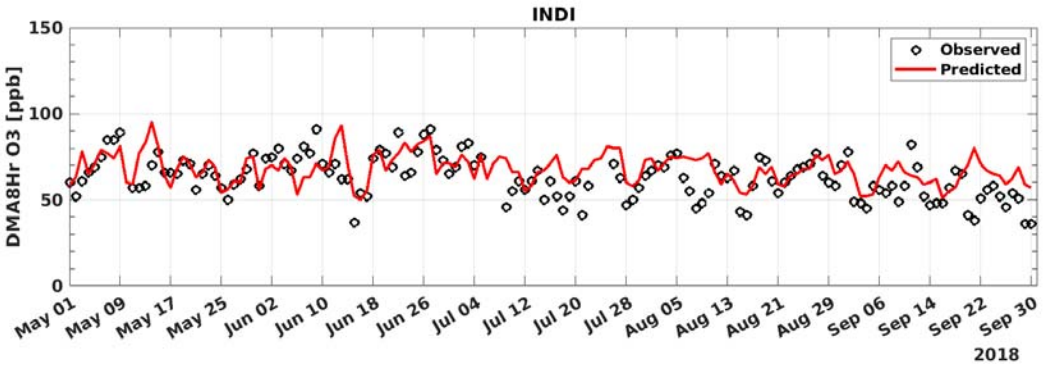

FIGURE A-10: 2018 MAXIMUM DAILY AVERAGE 8-HOUR (MDA8) OZONE MODEL PREDICTION AND MEASUREMENT COMPARISON AT INDIO

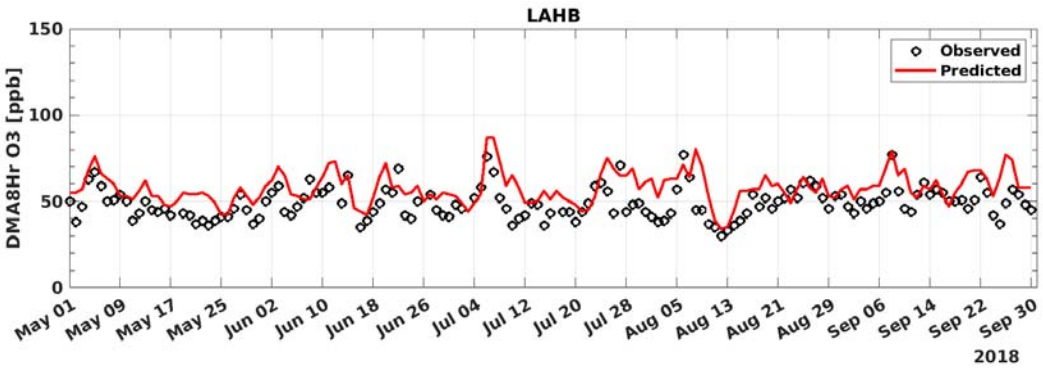

FIGURE A-11: 2018 MAXIMUM DAILY AVERAGE 8-HOUR (MDA8) OZONE MODEL PREDICTION AND MEASUREMENT COMPARISON AT LA HABRA

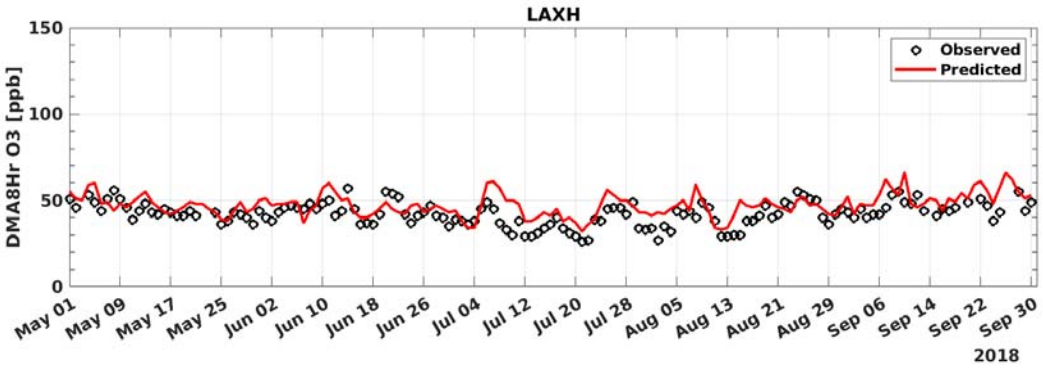

FIGURE A-12: 2018 MAXIMUM DAILY AVERAGE 8-HOUR (MDA8) OZONE MODEL PREDICTION AND MEASUREMENT COMPARISON AT LAX

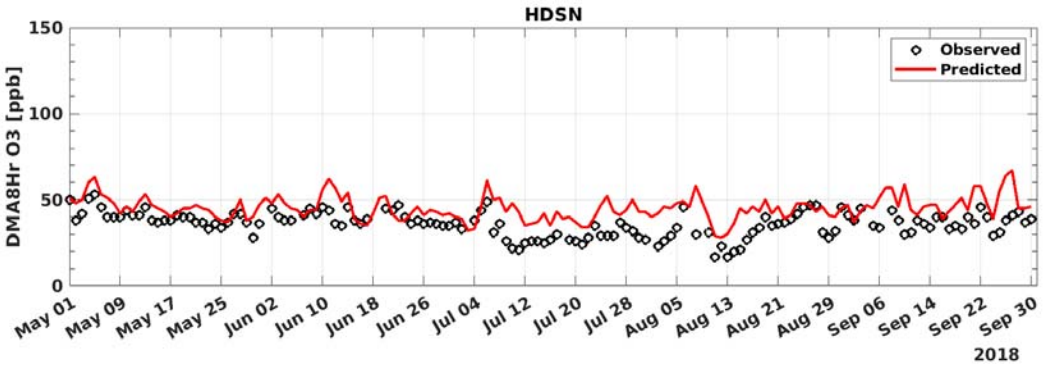

FIGURE A-13: 2018 MAXIMUM DAILY AVERAGE 8-HOUR (MDA8) OZONE MODEL PREDICTION AND MEASUREMENT COMPARISON AT LONG BEACH HUDSON

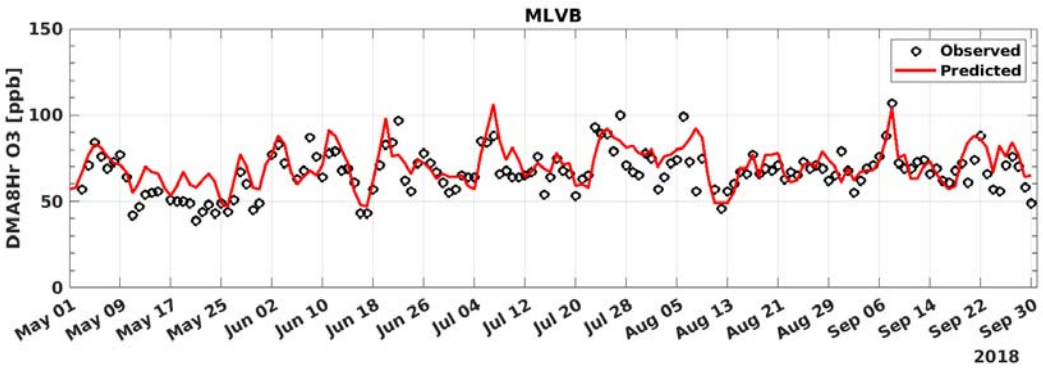

FIGURE A-142: 2018 MAXIMUM DAILY AVERAGE 8-HOUR (MDA8) OZONE MODEL PREDICTION AND MEASUREMENT COMPARISON AT MIRA LOMA

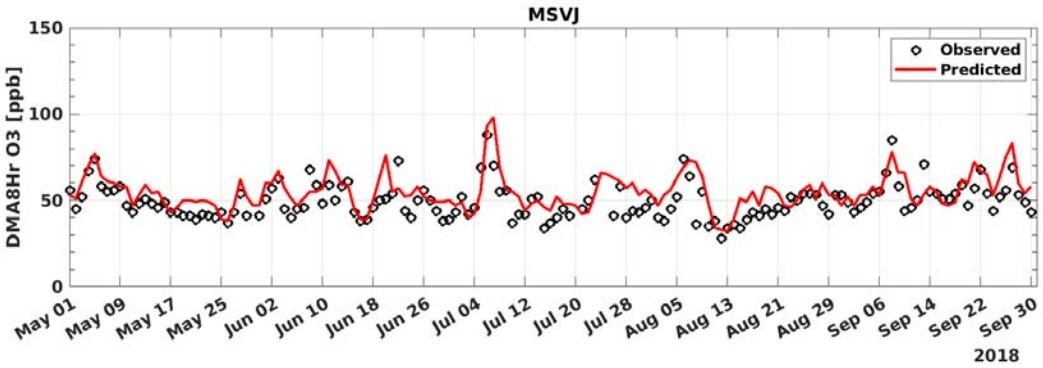

FIGURE A-15: 2018 MAXIMUM DAILY AVERAGE 8-HOUR (MDA8) OZONE MODEL PREDICTION AND MEASUREMENT COMPARISON AT MISSION VIEJO

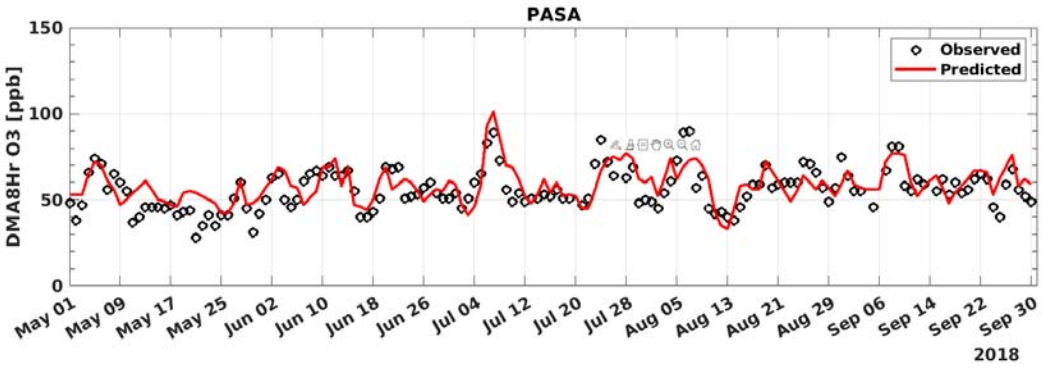

FIGURE A-16: 2018 MAXIMUM DAILY AVERAGE 8-HOUR (MDA8) OZONE MODEL PREDICTION AND MEASUREMENT COMPARISON AT PASADENA

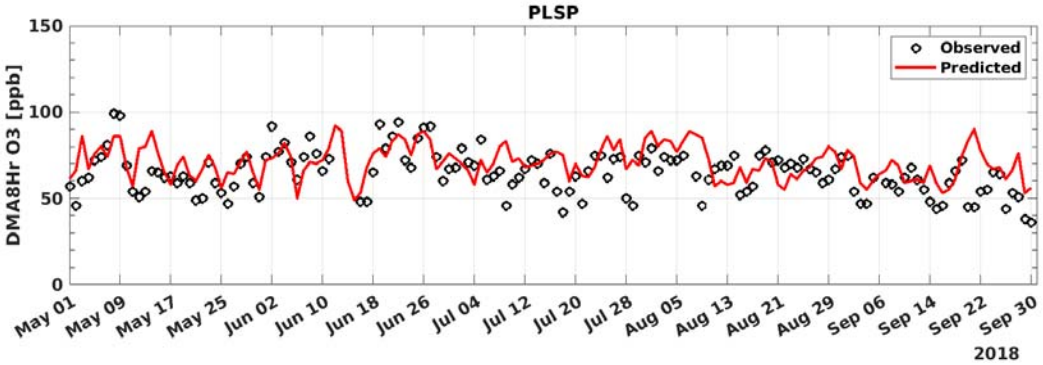

FIGURE A-17: 2018 MAXIMUM DAILY AVERAGE 8-HOUR (MDA8) OZONE MODEL PREDICTION AND MEASUREMENT COMPARISON AT PALM SPRINGS

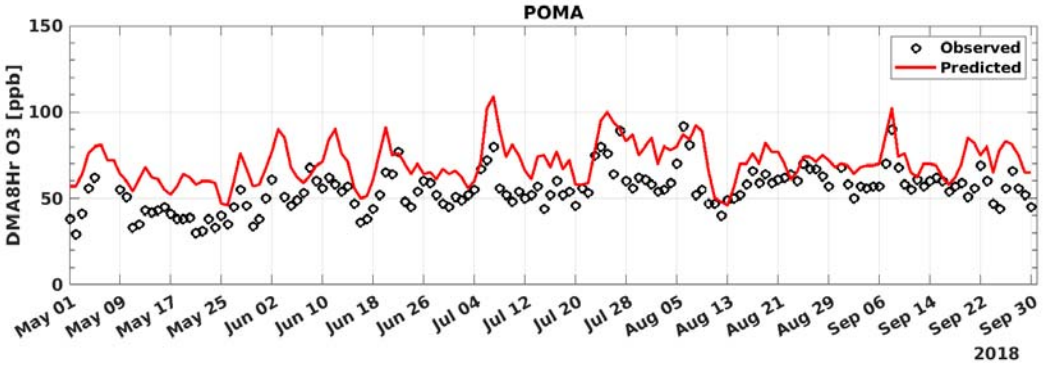

FIGURE A-18: 2018 MAXIMUM DAILY AVERAGE 8-HOUR (MDA8) OZONE MODEL PREDICTION AND MEASUREMENT COMPARISON AT POMONA

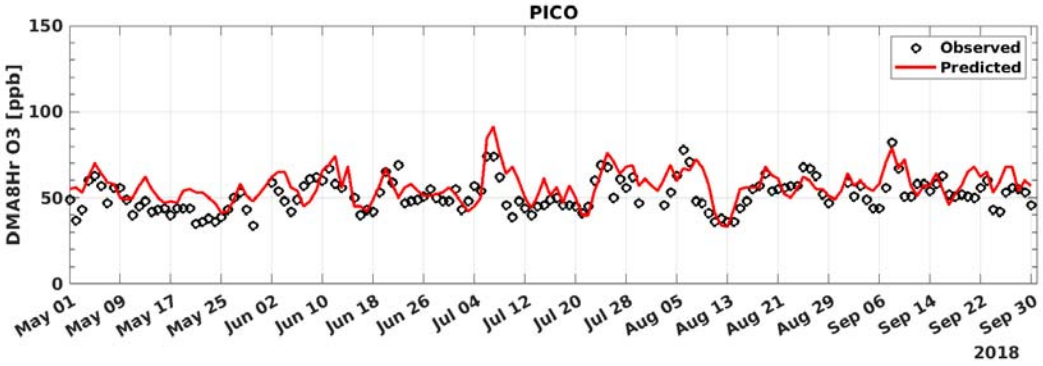

FIGURE A-19: 2018 MAXIMUM DAILY AVERAGE 8-HOUR (MDA8) OZONE MODEL PREDICTION AND MEASUREMENT COMPARISON AT PICO RIVERA

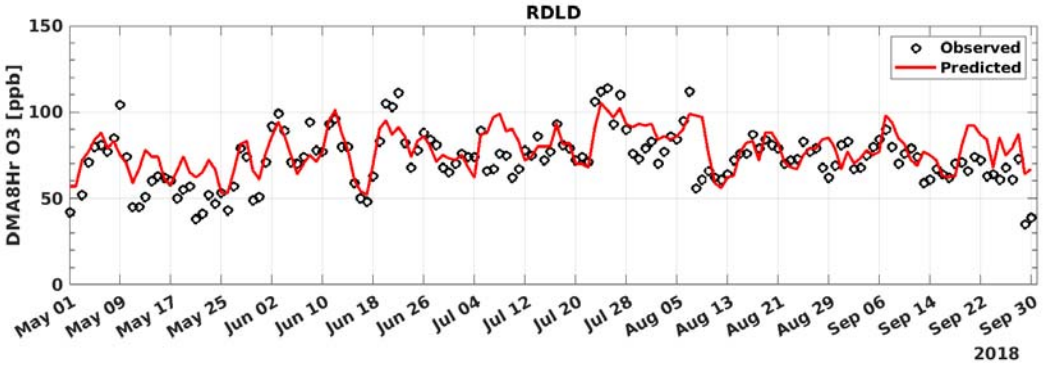

FIGURE A-20: 2018 MAXIMUM DAILY AVERAGE 8-HOUR (MDA8) OZONE MODEL PREDICTION AND MEASUREMENT COMPARISON AT REDLANDS

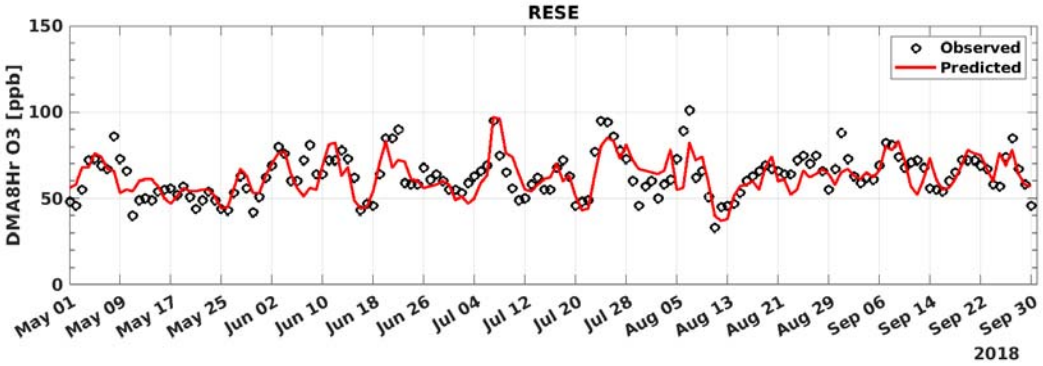

FIGURE A-21: 2018 MAXIMUM DAILY AVERAGE 8-HOUR (MDA8) OZONE MODEL PREDICTION AND MEASUREMENT COMPARISON AT RESEDA

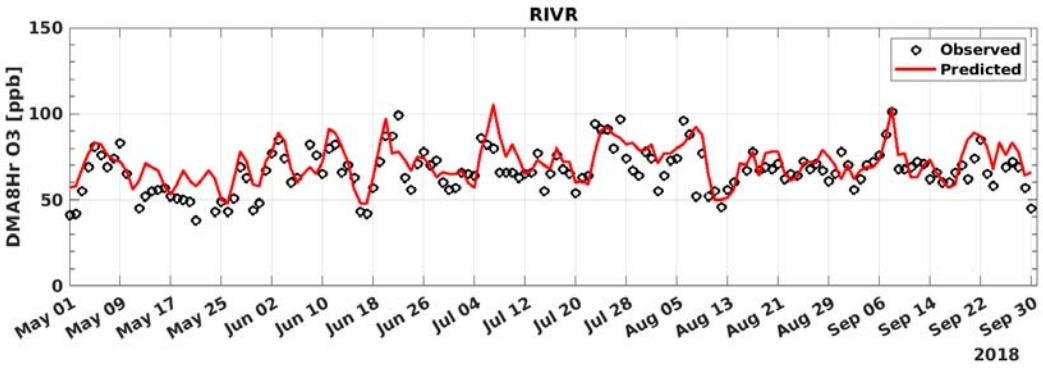

FIGURE A-22: 2018 MAXIMUM DAILY AVERAGE 8-HOUR (MDA8) OZONE MODEL PREDICTION AND MEASUREMENT COMPARISON AT RIVERSIDE

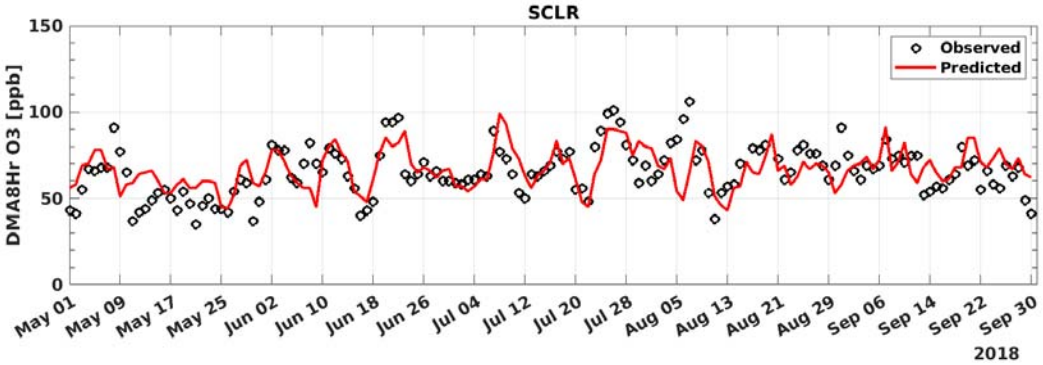

FIGURE A-23: 2018 MAXIMUM DAILY AVERAGE 8-HOUR (MDA8) OZONE MODEL PREDICTION AND MEASUREMENT COMPARISON AT SANTA CLARITA

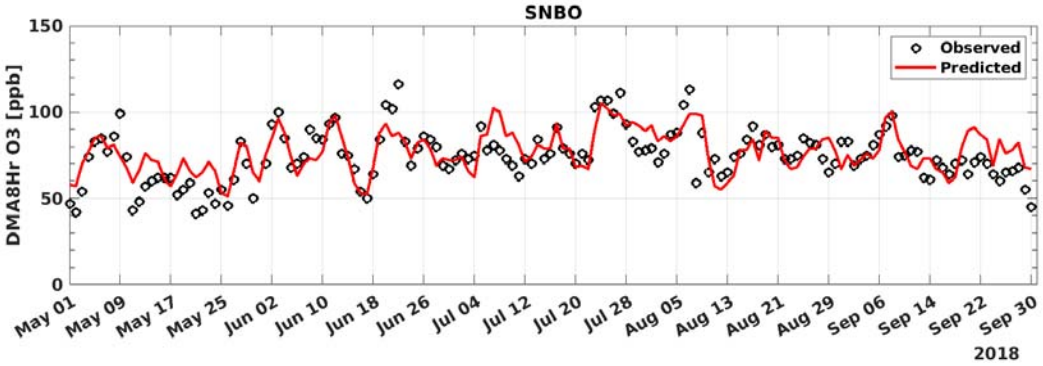

FIGURE A-24: 2018 MAXIMUM DAILY AVERAGE 8-HOUR (MDA8) OZONE MODEL PREDICTION AND MEASUREMENT COMPARISON AT SAN BERNARDINO

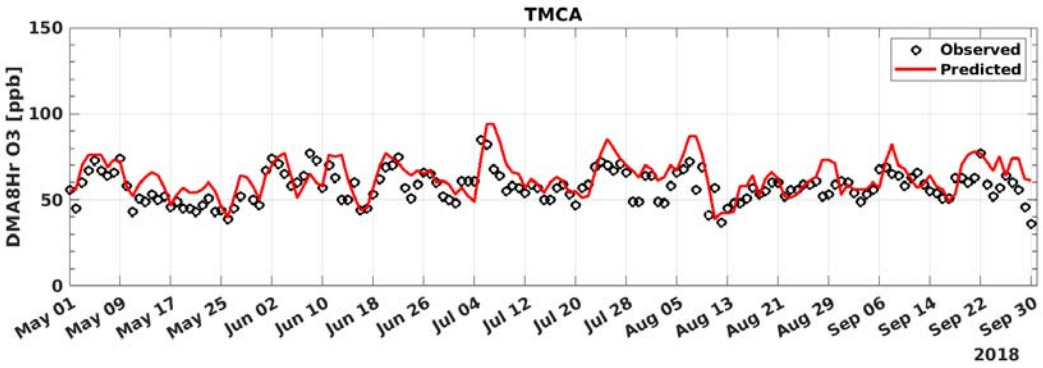

FIGURE A-25: 2018 MAXIMUM DAILY AVERAGE 8-HOUR (MDA8) OZONE MODEL PREDICTION AND MEASUREMENT COMPARISON AT TEMECULA

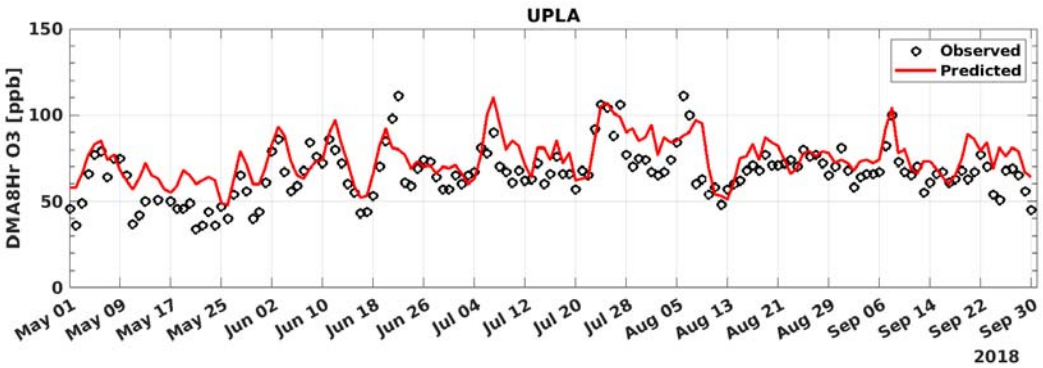

FIGURE A-26: 2018 MAXIMUM DAILY AVERAGE 8-HOUR (MDA8) OZONE MODEL PREDICTION AND MEASUREMENT COMPARISON AT UPLAND

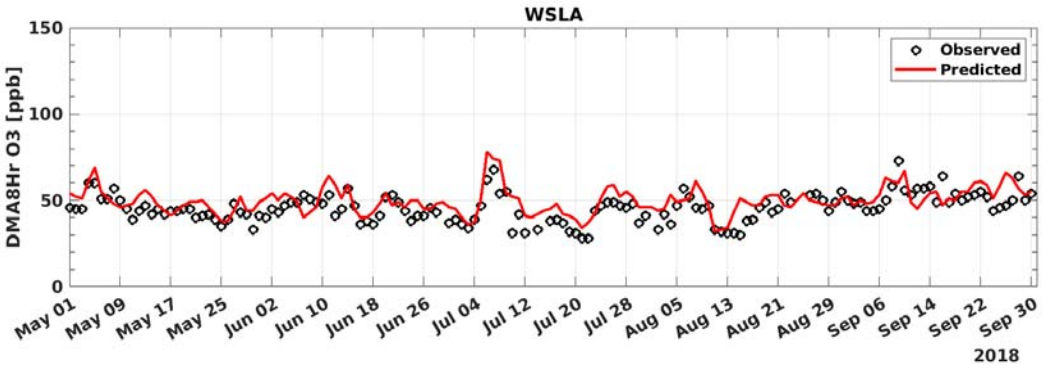

FIGURE A-27: 2018 MAXIMUM DAILY AVERAGE 8-HOUR (MDA8) OZONE MODEL PREDICTION AND MEASUREMENT COMPARISON AT WEST LOS ANGELES

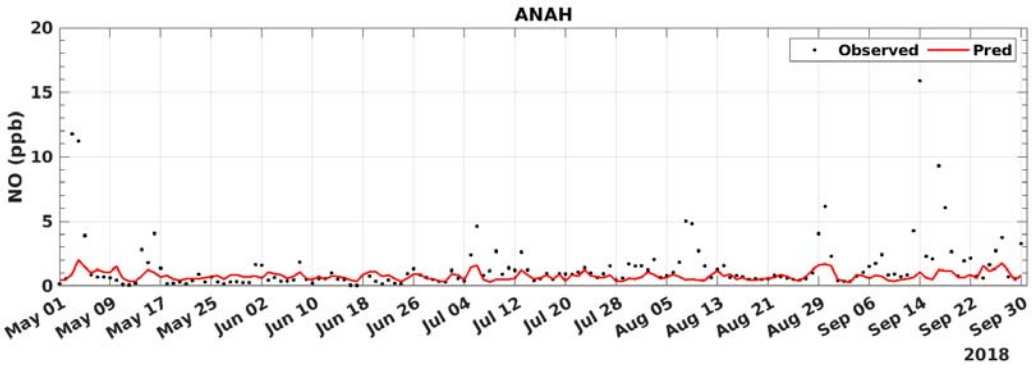

FIGURE B-1: 2018 DAILY AVERAGED NO MODEL PREDICTION AND MEASUREMENT COMPARISON AT ANAHEIM

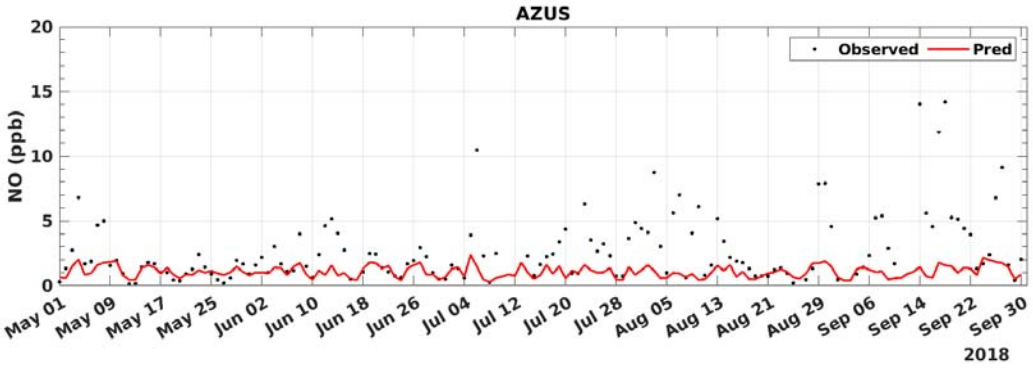

FIGURE B-2: 2018 DAILY AVERAGED NO MODEL PREDICTION AND MEASUREMENT COMPARISON AT AZUSA

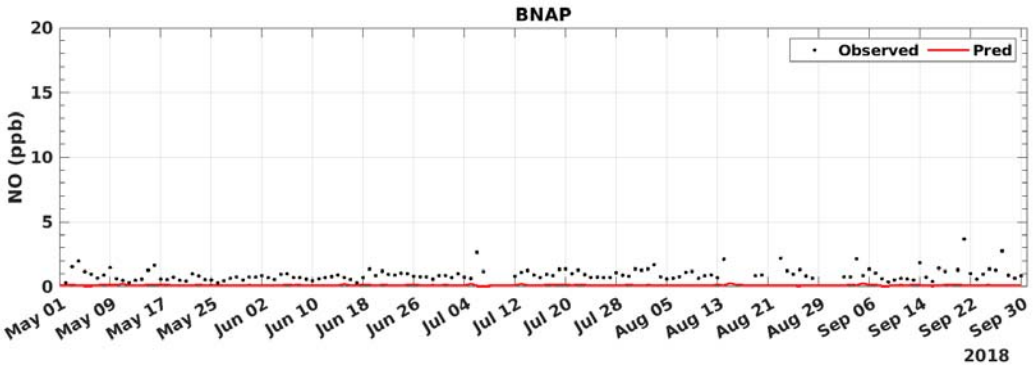

FIGURE B-3: 2018 DAILY AVERAGED NO MODEL PREDICTION AND MEASUREMENT COMPARISON AT BANNING

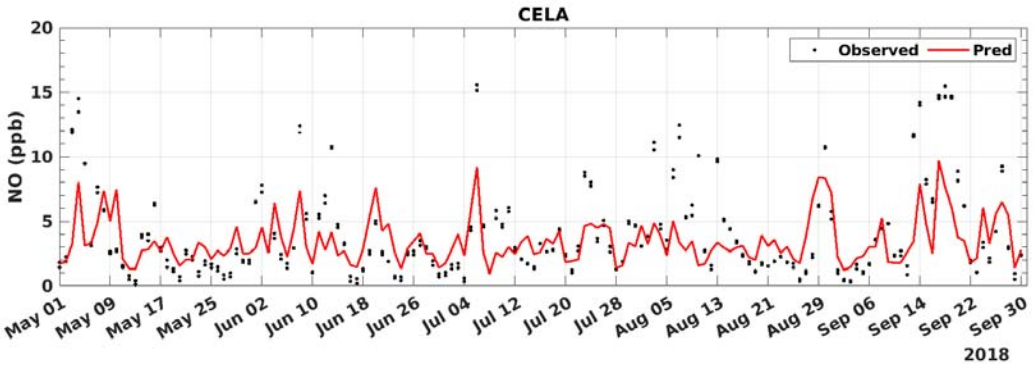

FIGURE B-4: 2018 DAILY AVERAGED NO MODEL PREDICTION AND MEASUREMENT COMPARISON AT CENTRAL LOS ANGLES

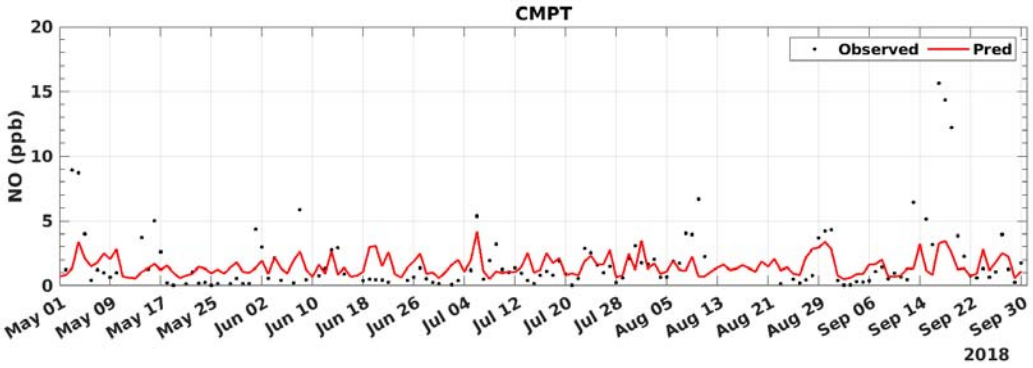

FIGURE B-5: 2018 DAILY AVERAGED NO MODEL PREDICTION AND MEASUREMENT COMPARISON AT COMPTON

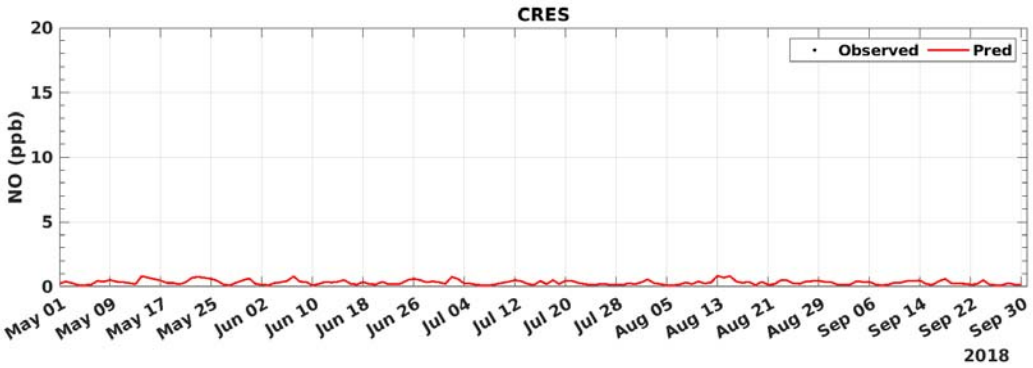

FIGURE B-6: 2018 DAILY AVERAGED NO MODEL PREDICTION AND MEASUREMENT COMPARISON AT CRESTLINE

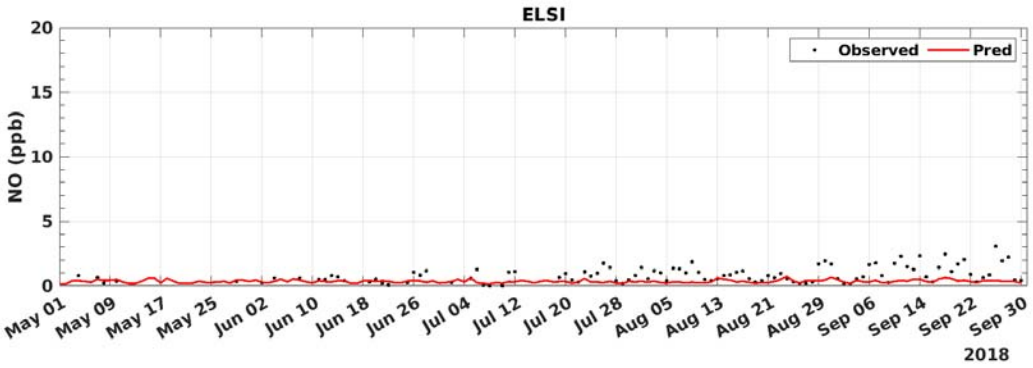

FIGURE B-7: 2018 DAILY AVERAGED NO MODEL PREDICTION AND MEASUREMENT COMPARISON AT LAKE ELSINORE

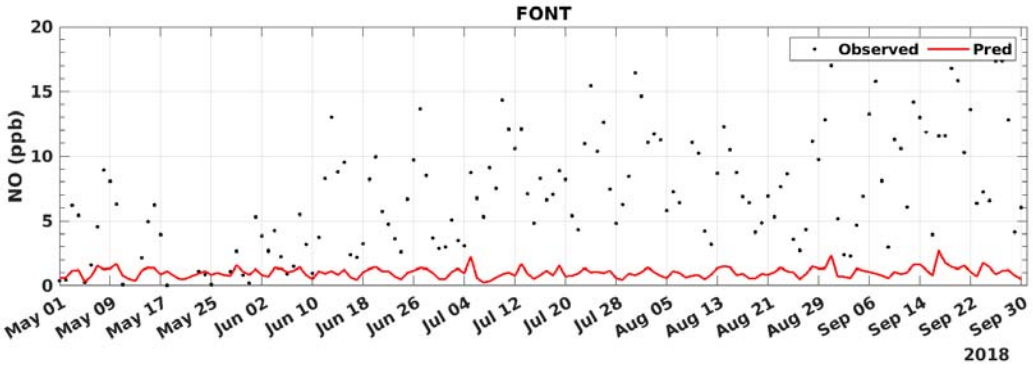

FIGURE B-8: 2018 DAILY AVERAGED NO MODEL PREDICTION AND MEASUREMENT COMPARISON AT FONTANA

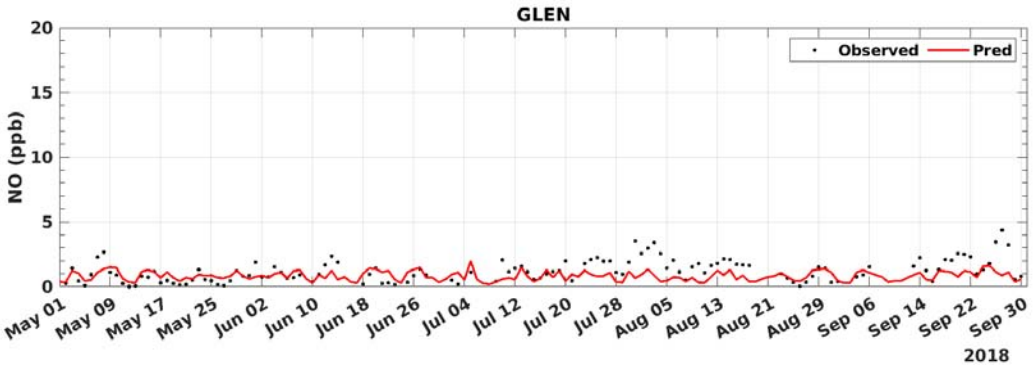

FIGURE B-9: 2018 DAILY AVERAGED NO MODEL PREDICTION AND MEASUREMENT COMPARISON AT GLENDORA

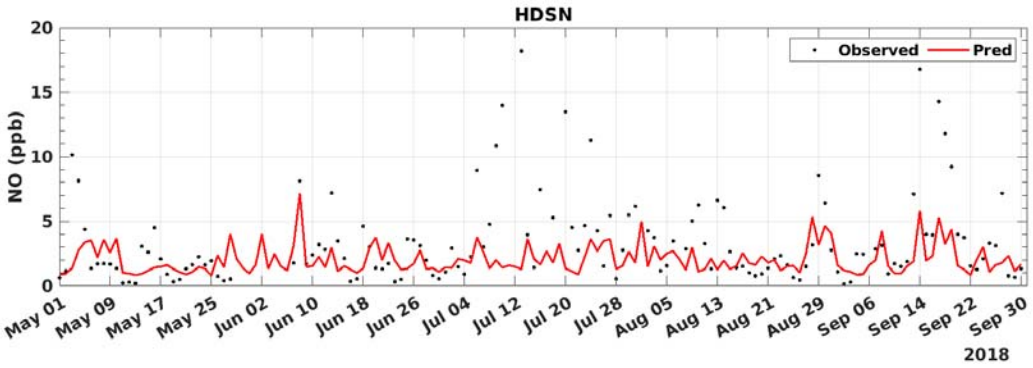

FIGURE B-10: 2018 DAILY AVERAGED NO MODEL PREDICTION AND MEASUREMENT COMPARISON AT HUDSON

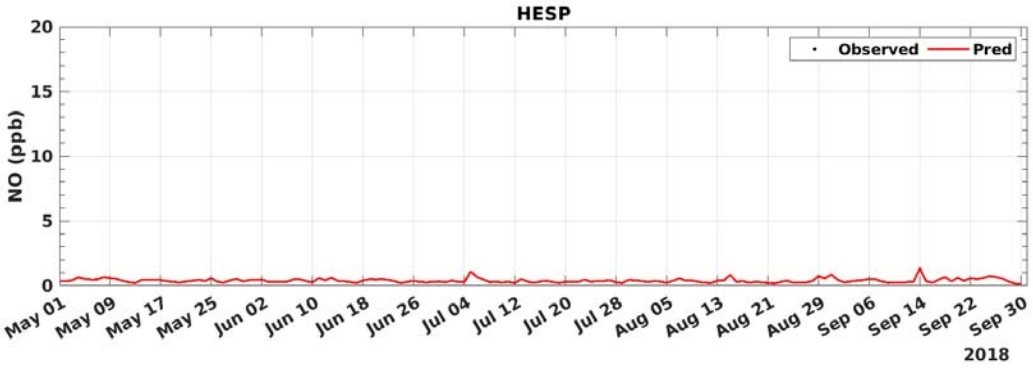

FIGURE B-11: 2018 DAILY AVERAGED NO MODEL PREDICTION AND MEASUREMENT COMPARISON AT HESPERIA

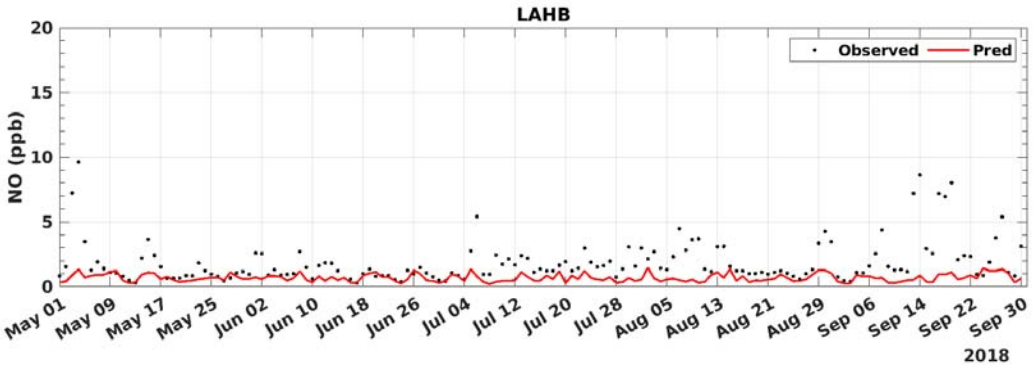

FIGURE B-12: 2018 DAILY AVERAGED NO MODEL PREDICTION AND MEASUREMENT COMPARISON AT LA HABRA

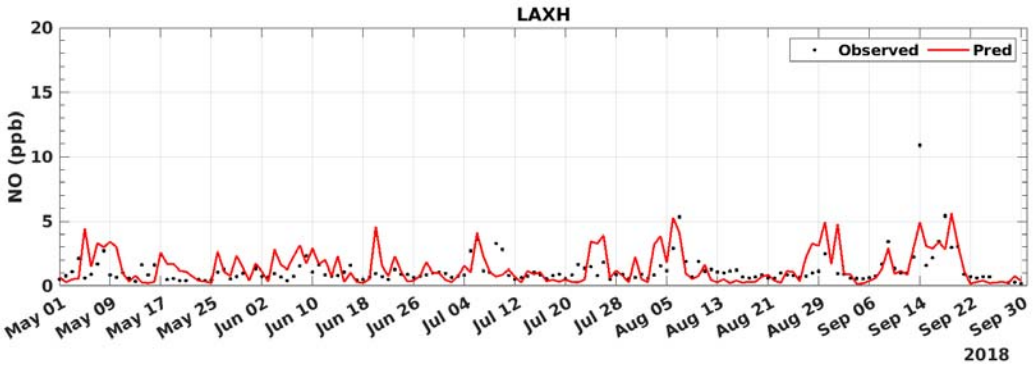

FIGURE B-13: 2018 DAILY AVERAGED NO MODEL PREDICTION AND MEASUREMENT COMPARISON AT LAX

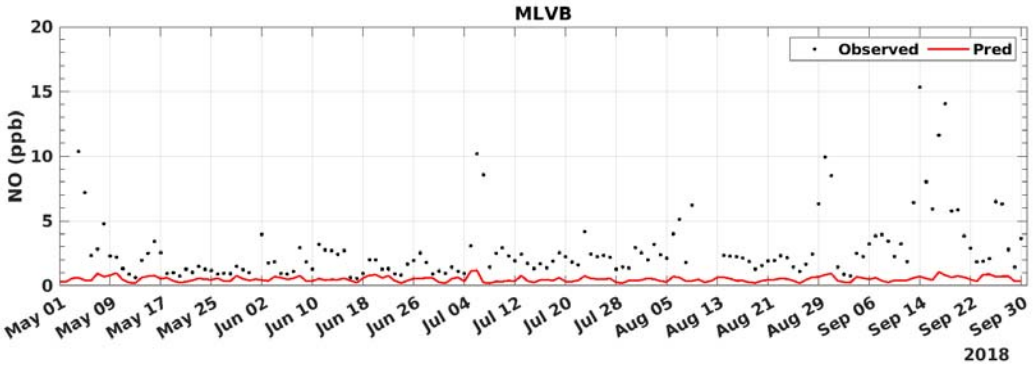

FIGURE B-14: 2018 DAILY AVERAGED NO MODEL PREDICTION AND MEASUREMENT COMPARISON AT MIRA LOMA VAN BUREN

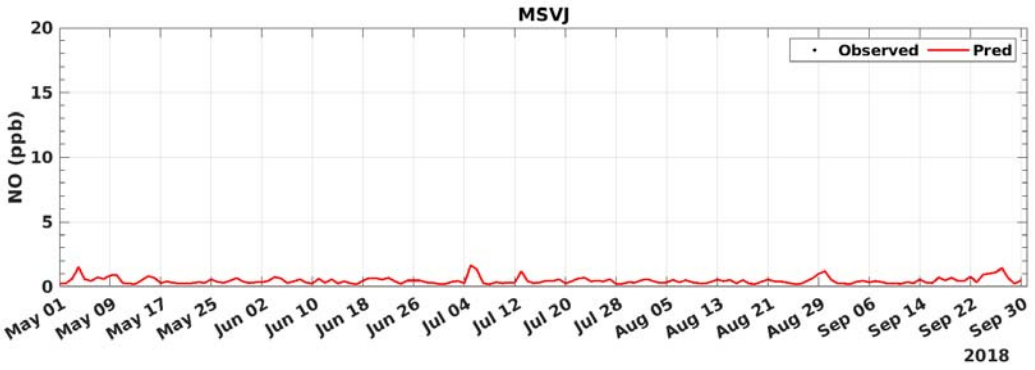

FIGURE B-15: 2018 DAILY AVERAGED NO MODEL PREDICTION AND MEASUREMENT COMPARISON AT MISSION VIEJO

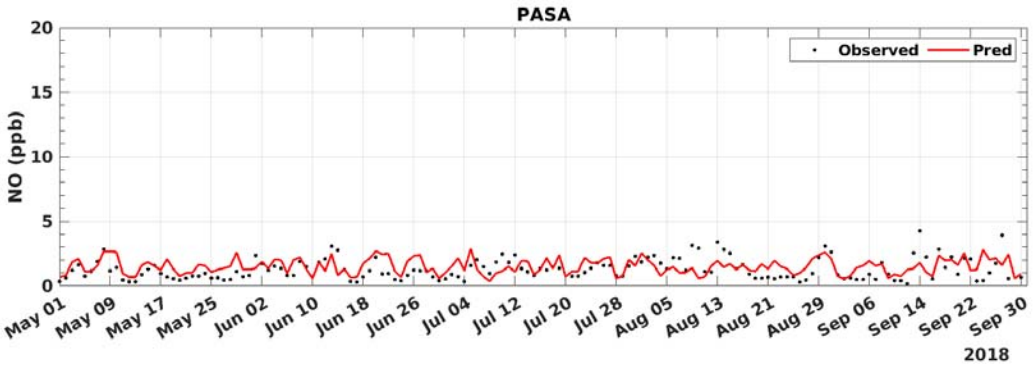

FIGURE B-16: 2018 DAILY AVERAGED NO MODEL PREDICTION AND MEASUREMENT COMPARISON AT PASADENA

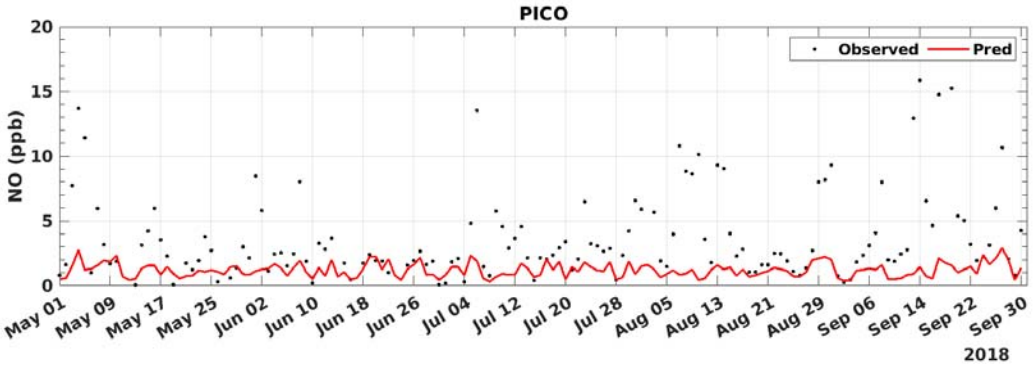

FIGURE B-17: 2018 DAILY AVERAGED NO MODEL PREDICTION AND MEASUREMENT COMPARISON AT PICO RIVERA

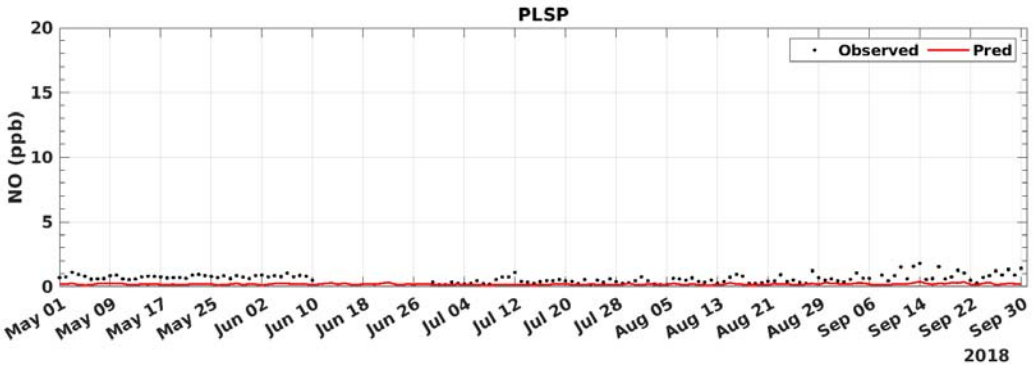

FIGURE B-18: 2018 DAILY AVERAGED NO MODEL PREDICTION AND MEASUREMENT COMPARISON AT PALM SPRINGS

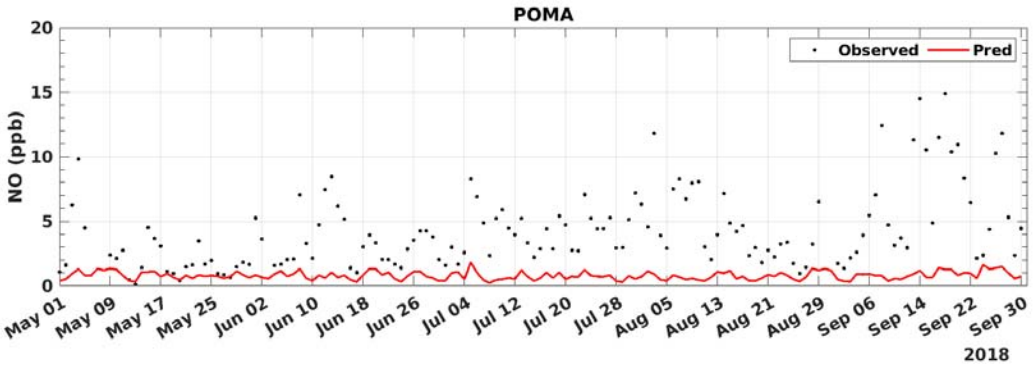

FIGURE B-19: 2018 DAILY AVERAGED NO MODEL PREDICTION AND MEASUREMENT COMPARISON AT POMONA

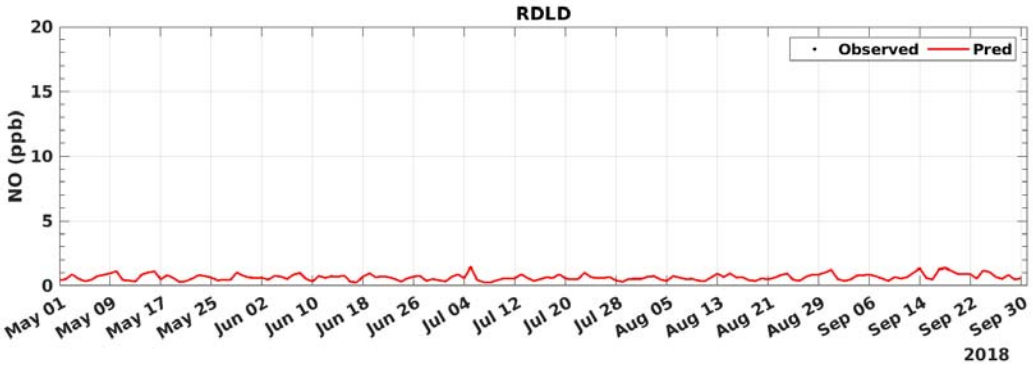

FIGURE B-20: 2018 DAILY AVERAGED NO MODEL PREDICTION AND MEASUREMENT COMPARISON AT REDLANDS

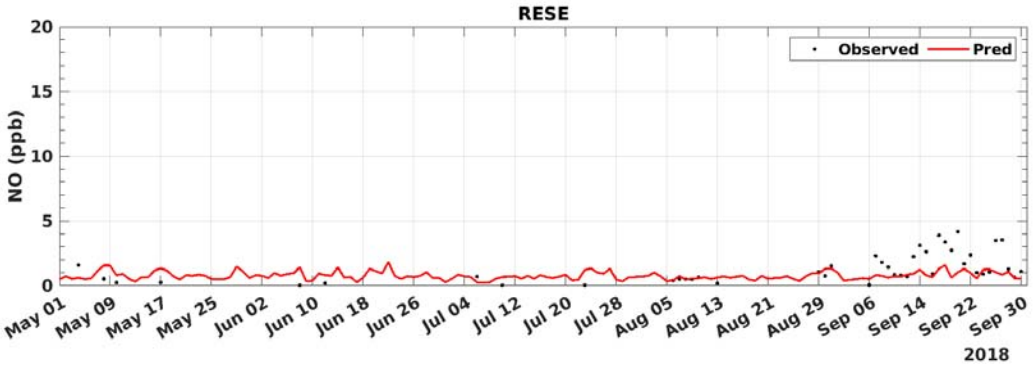

FIGURE B-21: 2018 DAILY AVERAGED NO MODEL PREDICTION AND MEASUREMENT COMPARISON AT RESEDA

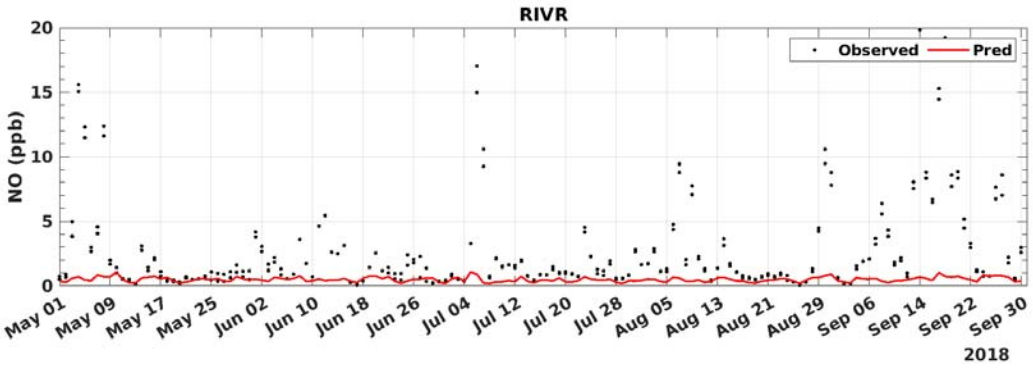

FIGURE B-22: 2018 DAILY AVERAGED NO MODEL PREDICTION AND MEASUREMENT COMPARISON AT RIVERSIDE

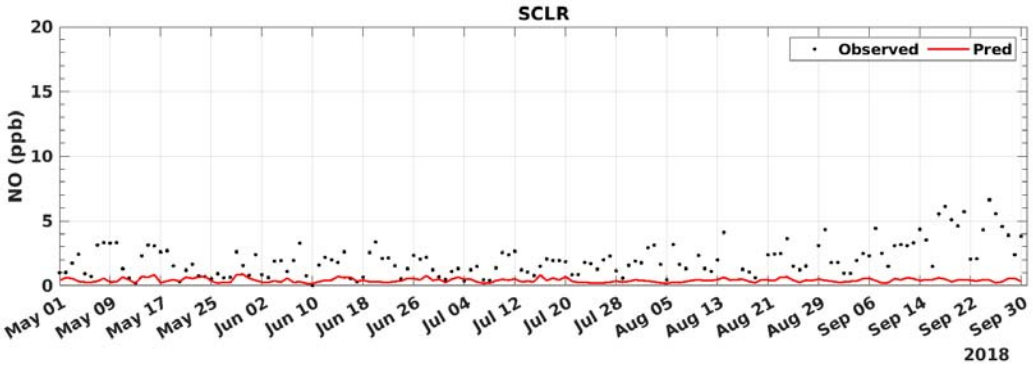

FIGURE B-23: 2018 DAILY AVERAGED NO MODEL PREDICTION AND MEASUREMENT COMPARISON AT SANTA CLARITA

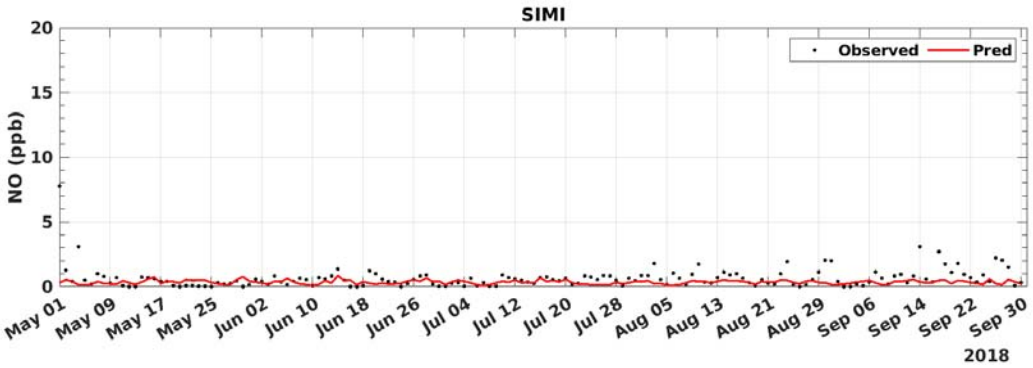

FIGURE B-24: 2018 DAILY AVERAGED NO MODEL PREDICTION AND MEASUREMENT COMPARISON AT SIMI VALLEY

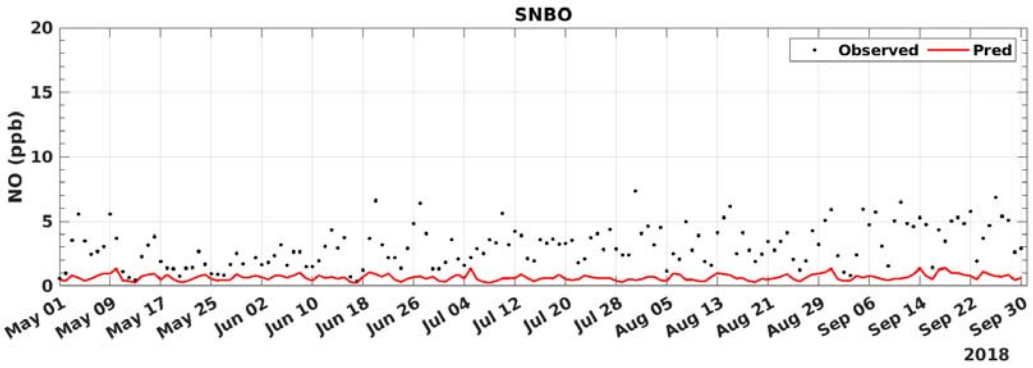

FIGURE B-25: 2018 DAILY AVERAGED NO MODEL PREDICTION AND MEASUREMENT COMPARISON AT SAN BERNARDINO

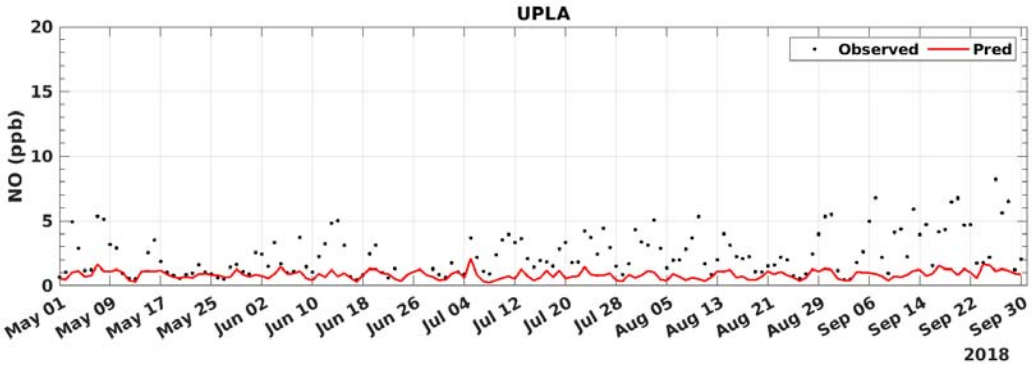

FIGURE B-26: 2018 DAILY AVERAGED NO MODEL PREDICTION AND MEASUREMENT COMPARISON AT UPLAND

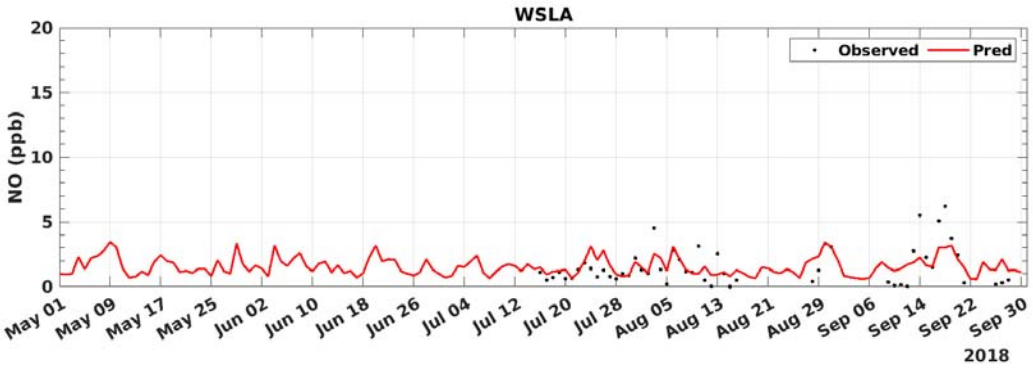

FIGURE B-27: 2018 DAILY AVERAGED NO MODEL PREDICTION AND MEASUREMENT COMPARISON AT WEST LOS ANGELES

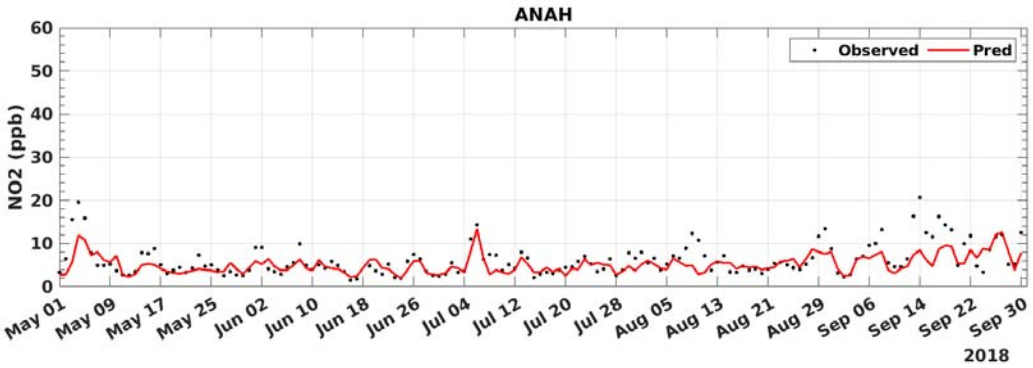

FIGURE C-1: 2018 DAILY AVERAGED NO2 MODEL PREDICTION AND MEASUREMENT COMPARISON AT ANAHEIM

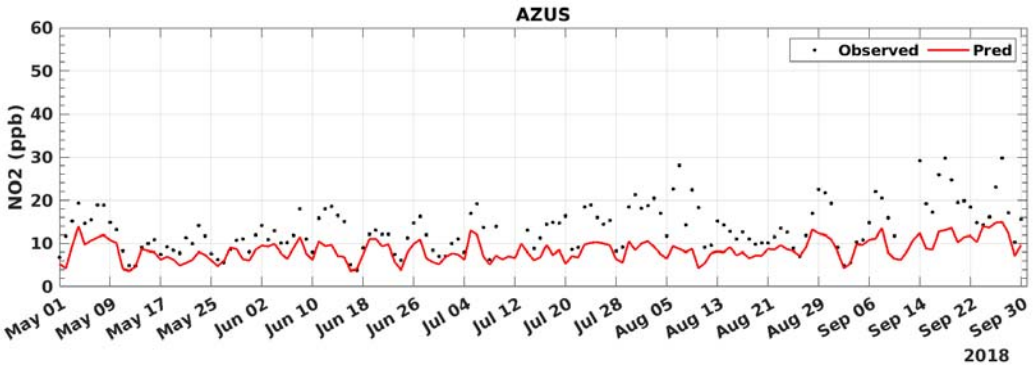

FIGURE C-2: 2018 DAILY AVERAGED NO2 MODEL PREDICTION AND MEASUREMENT COMPARISON AT AZUSA

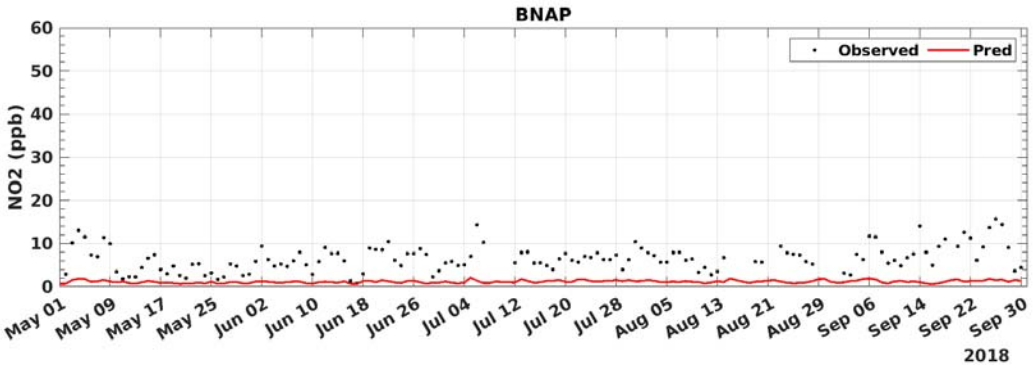

FIGURE C-3: 2018 DAILY AVERAGED NO2 MODEL PREDICTION AND MEASUREMENT COMPARISON AT BANNING

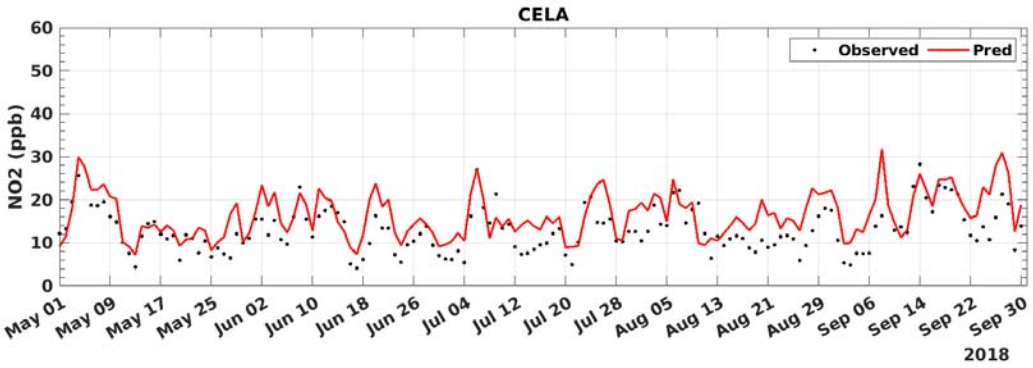

FIGURE C-4: 2018 DAILY AVERAGED NO2 MODEL PREDICTION AND MEASUREMENT COMPARISON AT CENTRAL LOS ANGELES

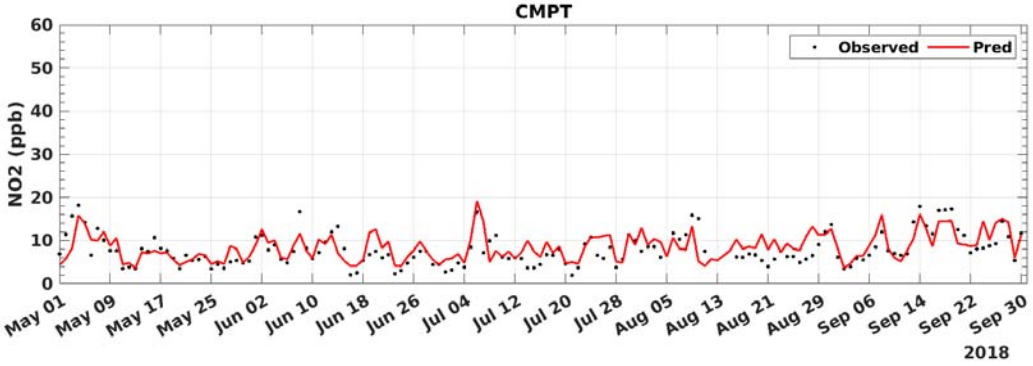

FIGURE C-5: 2018 DAILY AVERAGED NO2 MODEL PREDICTION AND MEASUREMENT COMPARISON AT COMPTON

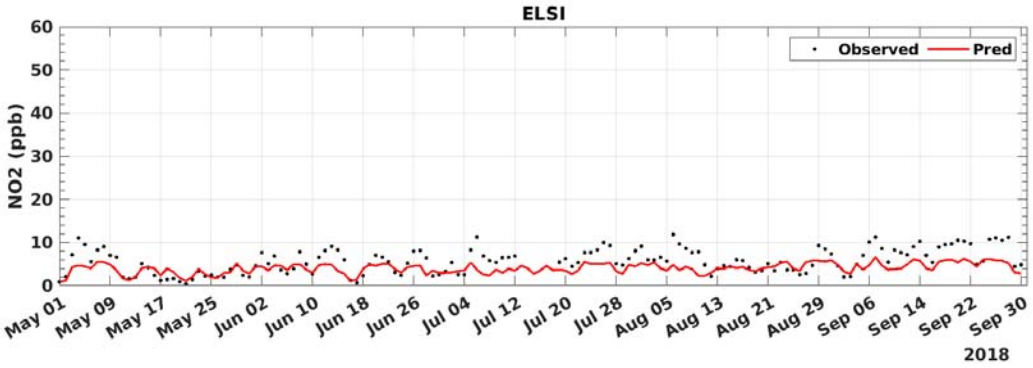

FIGURE C-6: 2018 DAILY AVERAGED NO2 MODEL PREDICTION AND MEASUREMENT COMPARISON AT LAKE ELSINORE

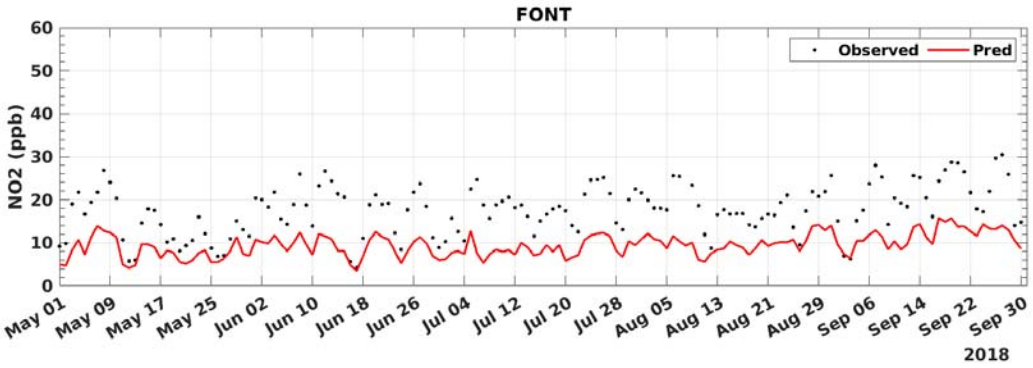

FIGURE C-7: 2018 DAILY AVERAGED NO2 MODEL PREDICTION AND MEASUREMENT COMPARISON AT FONTANA

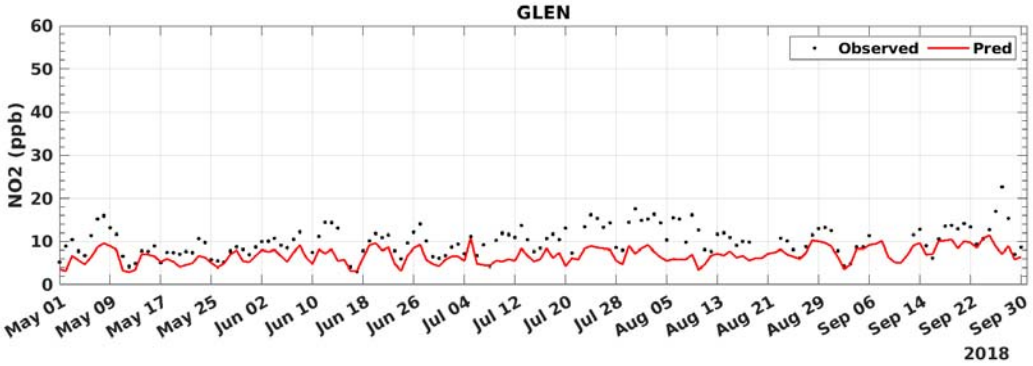

FIGURE C-8: 2018 DAILY AVERAGED NO2 MODEL PREDICTION AND MEASUREMENT COMPARISON AT GLENDORA

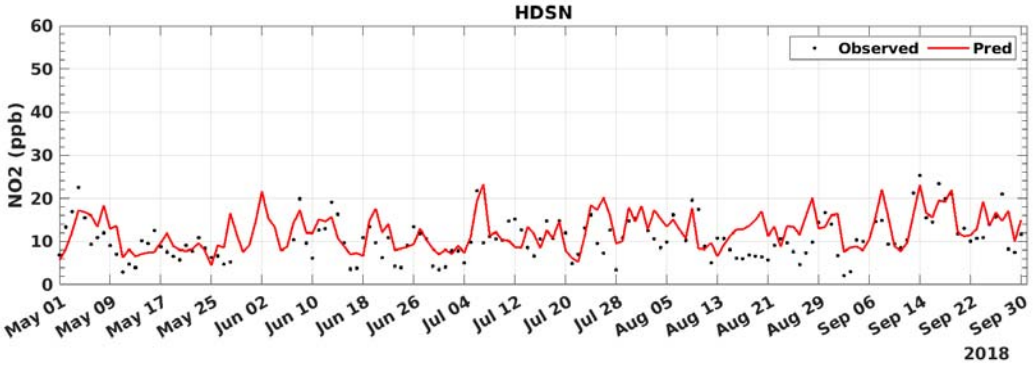

FIGURE C-9: 2018 DAILY AVERAGED NO2 MODEL PREDICTION AND MEASUREMENT COMPARISON AT HUDSON

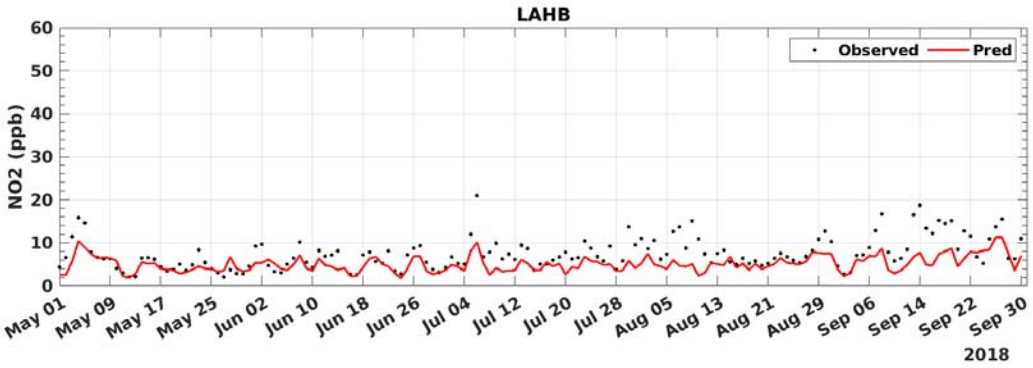

FIGURE C-10: 2018 DAILY AVERAGED NO2 MODEL PREDICTION AND MEASUREMENT COMPARISON AT LA HABRA

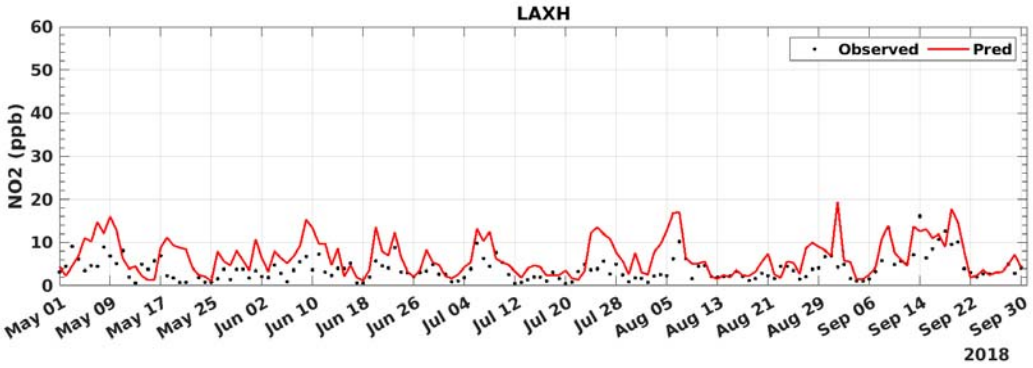

FIGURE C-11: 2018 DAILY AVERAGED NO2 MODEL PREDICTION AND MEASUREMENT COMPARISON AT LAX

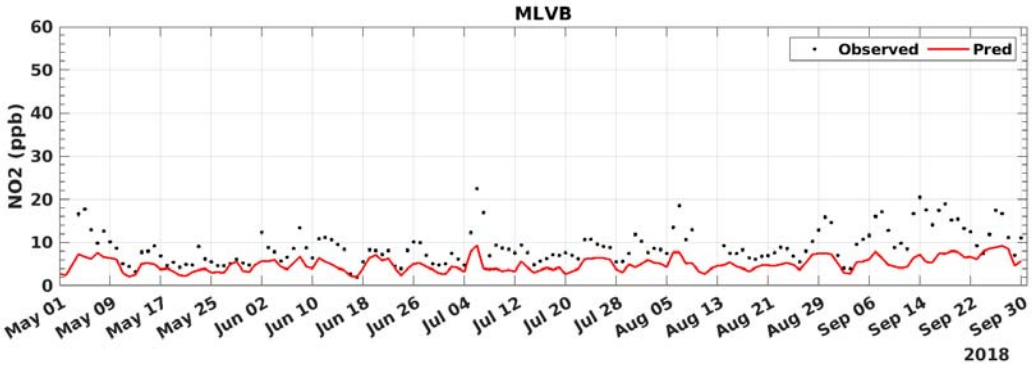

FIGURE C-12: 2018 DAILY AVERAGED NO2 MODEL PREDICTION AND MEASUREMENT COMPARISON AT MIRA LOMA VAN BUREN

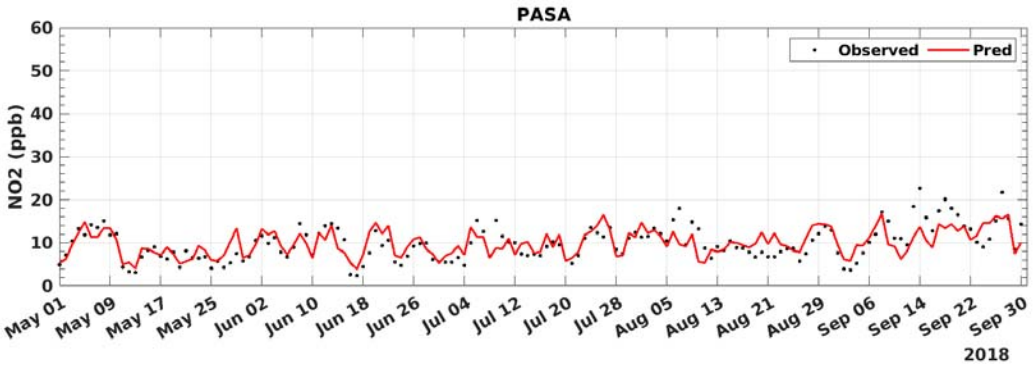

FIGURE C-13: 2018 DAILY AVERAGED NO2 MODEL PREDICTION AND MEASUREMENT COMPARISON AT PASADENA

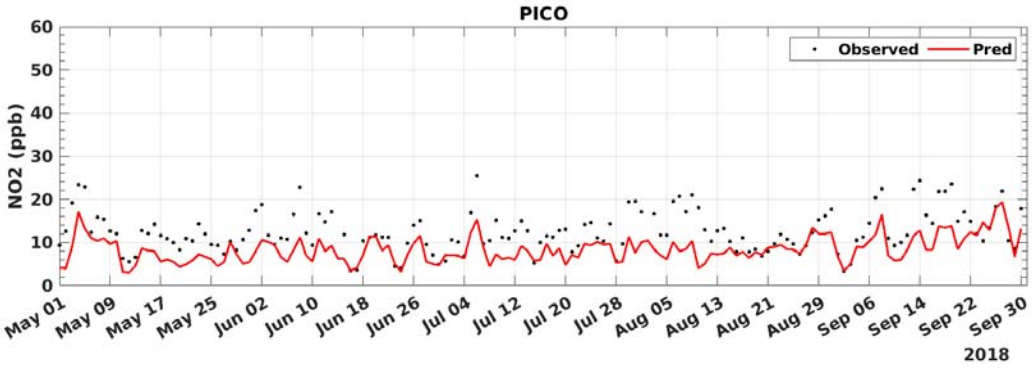

FIGURE C-14: 2018 DAILY AVERAGED NO2 MODEL PREDICTION AND MEASUREMENT COMPARISON AT PICO RIVERA

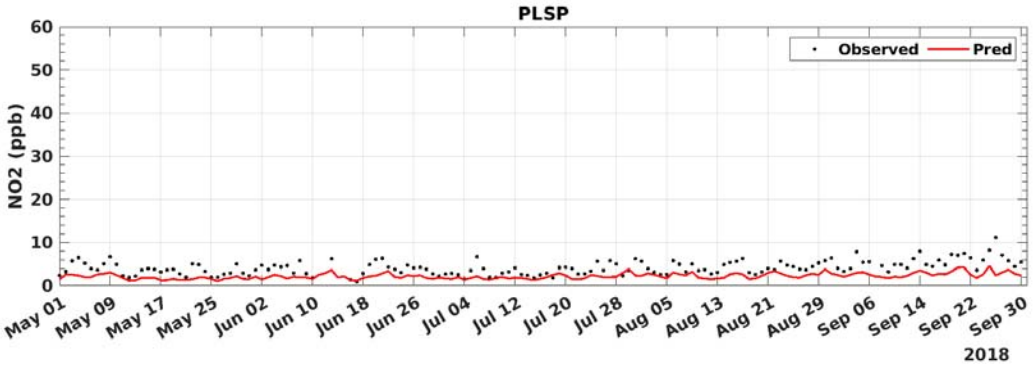

FIGURE C-15: 2018 DAILY AVERAGED NO2 MODEL PREDICTION AND MEASUREMENT COMPARISON AT PALM SPRINGS

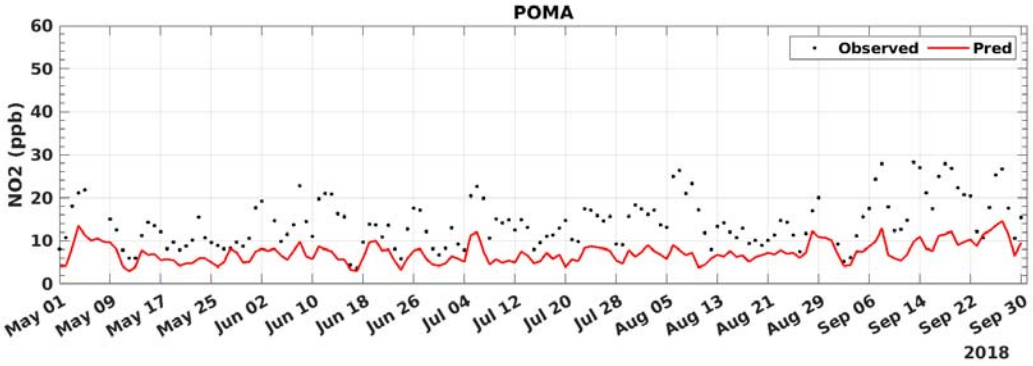

FIGURE C-16: 2018 DAILY AVERAGED NO2 MODEL PREDICTION AND MEASUREMENT COMPARISON AT POMONA

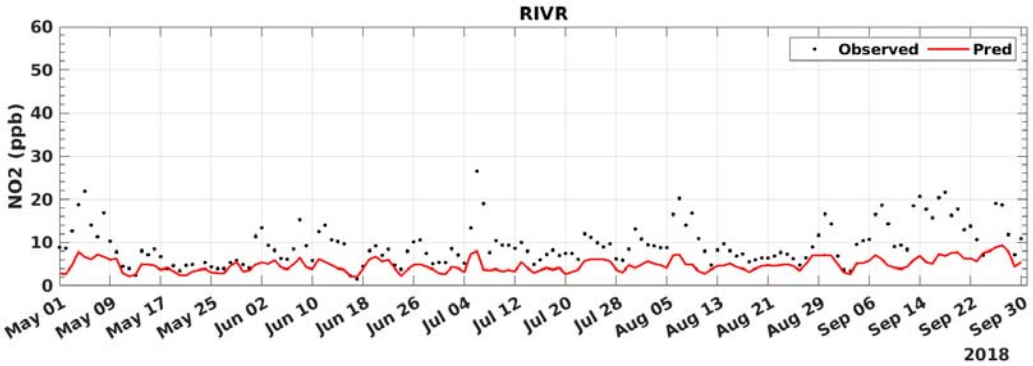

FIGURE C-17: 2018 DAILY AVERAGED NO2 MODEL PREDICTION AND MEASUREMENT COMPARISON AT RIVERSIDE

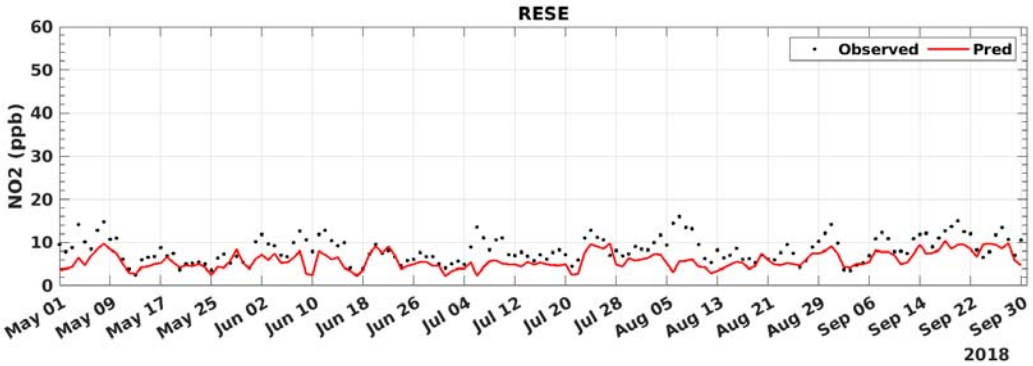

FIGURE C-18: 2018 DAILY AVERAGED NO2 MODEL PREDICTION AND MEASUREMENT COMPARISON AT RESEDA

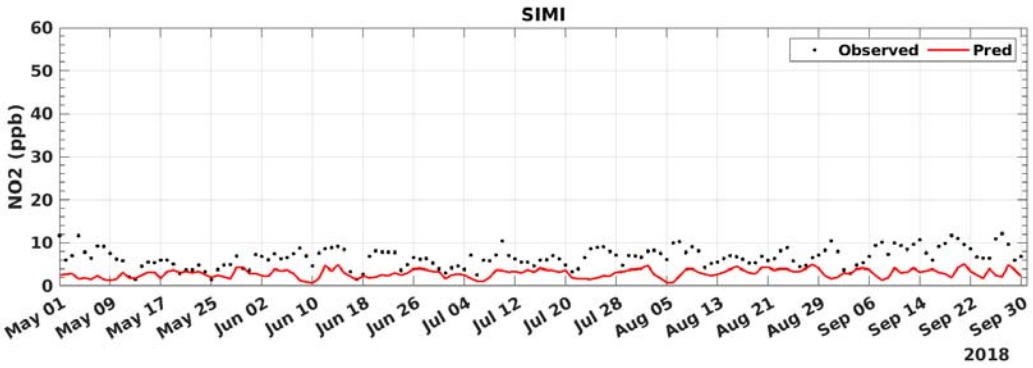

FIGURE C-19: 2018 DAILY AVERAGED NO2 MODEL PREDICTION AND MEASUREMENT COMPARISON AT SIMI VALLEY

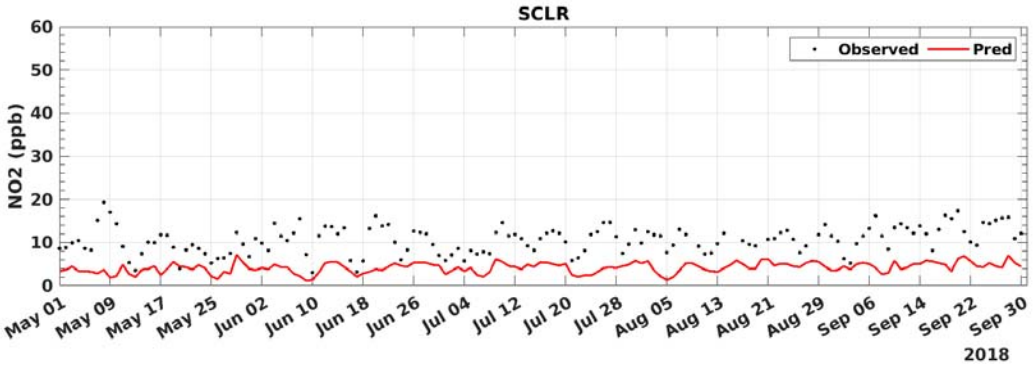

FIGURE C-20: 2018 DAILY AVERAGED NO2 MODEL PREDICTION AND MEASUREMENT COMPARISON AT SANTA CLARITA

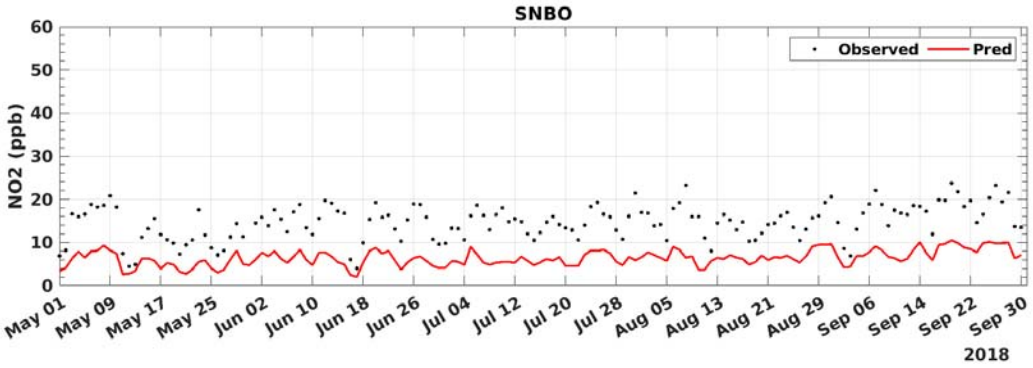

FIGURE C-21: 2018 DAILY AVERAGED NO2 MODEL PREDICTION AND MEASUREMENT COMPARISON AT SAN BERNARDINO

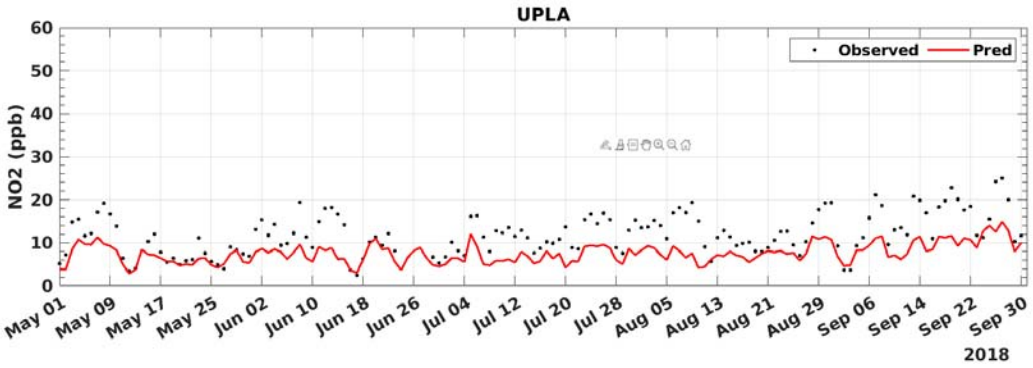

FIGURE C-22: 2018 DAILY AVERAGED NO2 MODEL PREDICTION AND MEASUREMENT COMPARISON AT UPLAND

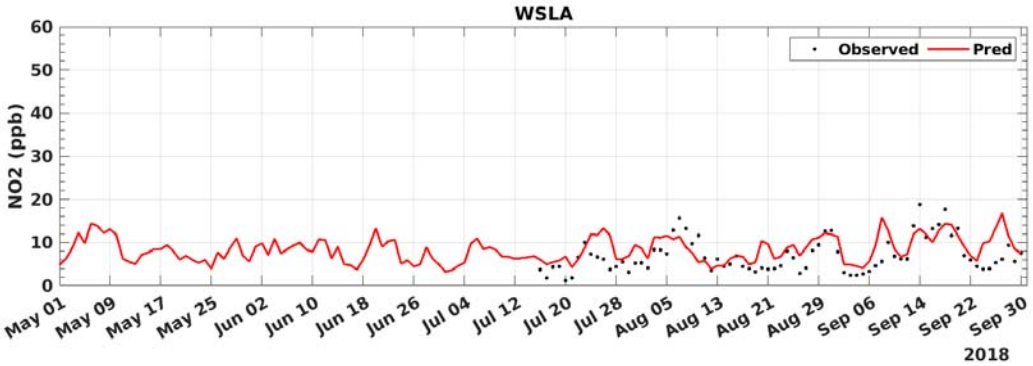

FIGURE C-23: 2018 DAILY AVERAGED NO2 MODEL PREDICTION AND MEASUREMENT COMPARISON AT WEST LOS ANGELES

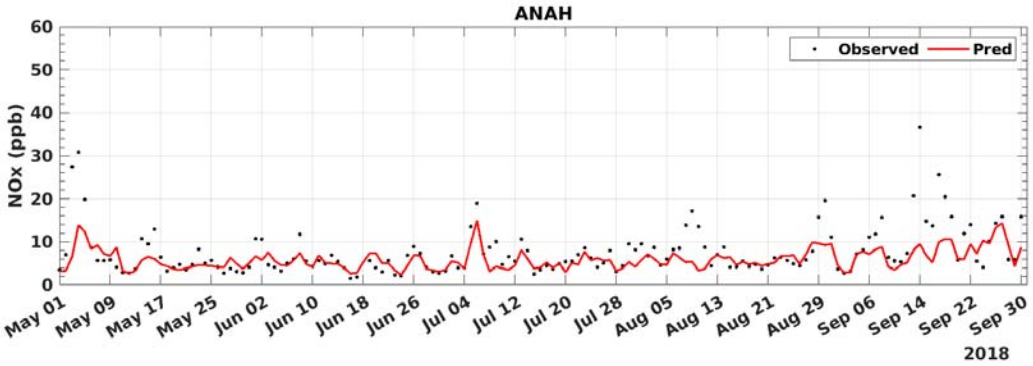

FIGURE D-1: 2018 DAILY AVERAGED NOX MODEL PREDICTION AND MEASUREMENT COMPARISON AT ANAHEIM

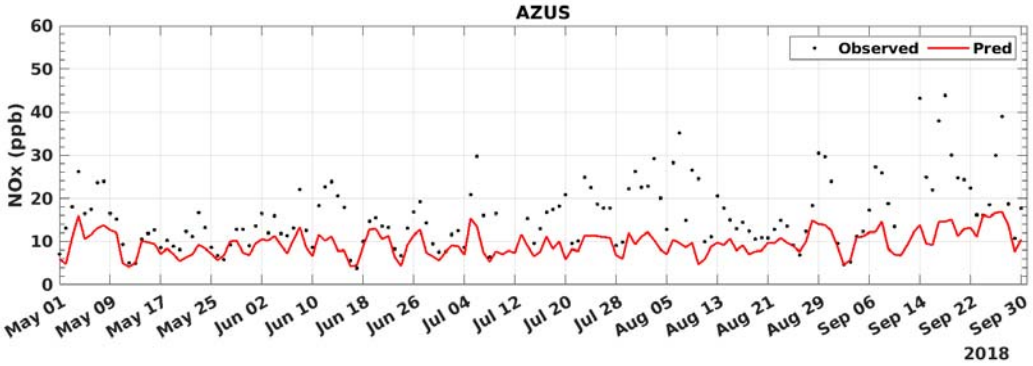

FIGURE D-2: 2018 DAILY AVERAGED NOX MODEL PREDICTION AND MEASUREMENT COMPARISON AT AZUSA

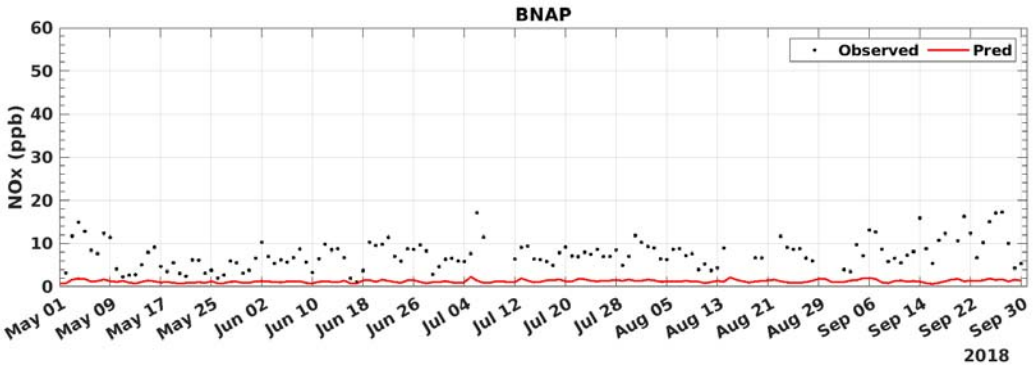

FIGURE D-3: 2018 DAILY AVERAGED NOX MODEL PREDICTION AND MEASUREMENT COMPARISON AT BANNING

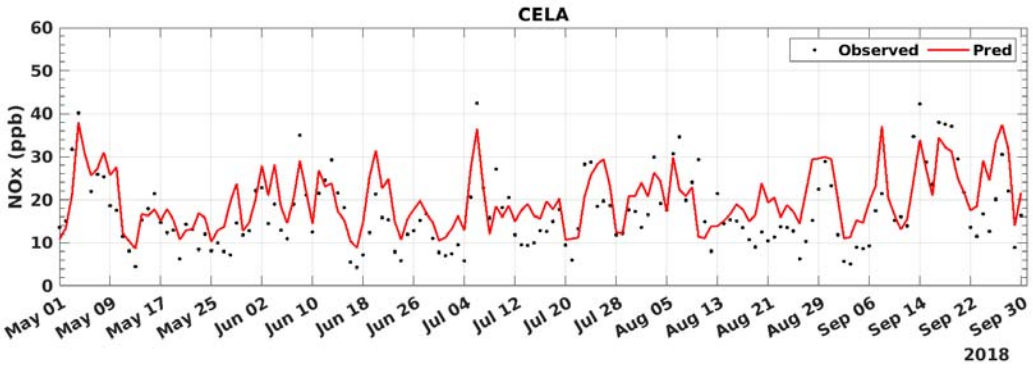

FIGURE D-4: 2018 DAILY AVERAGED NOX MODEL PREDICTION AND MEASUREMENT COMPARISON AT CENTRAL LOS ANGELES

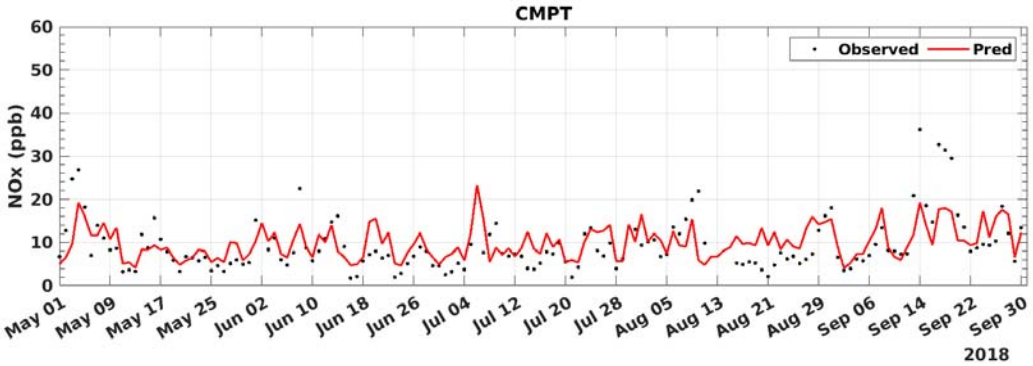

FIGURE D-5: 2018 DAILY AVERAGED NOX MODEL PREDICTION AND MEASUREMENT COMPARISON AT COMPTON

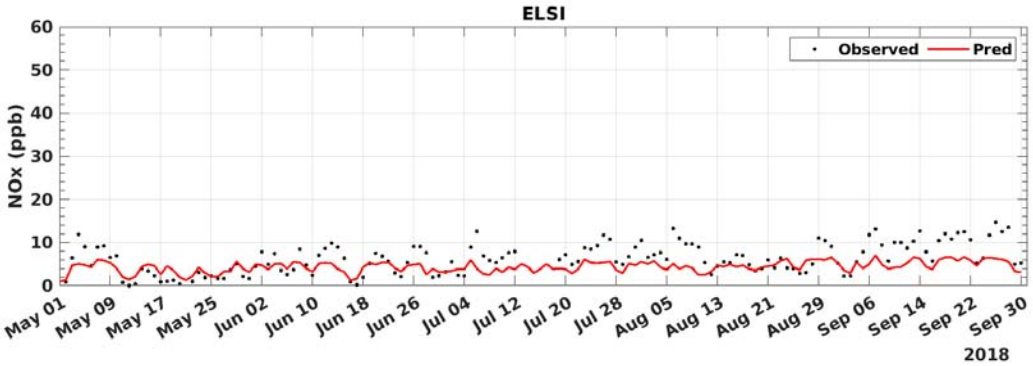

FIGURE D-6: 2018 DAILY AVERAGED NOX MODEL PREDICTION AND MEASUREMENT COMPARISON AT LAKE ELSINORE

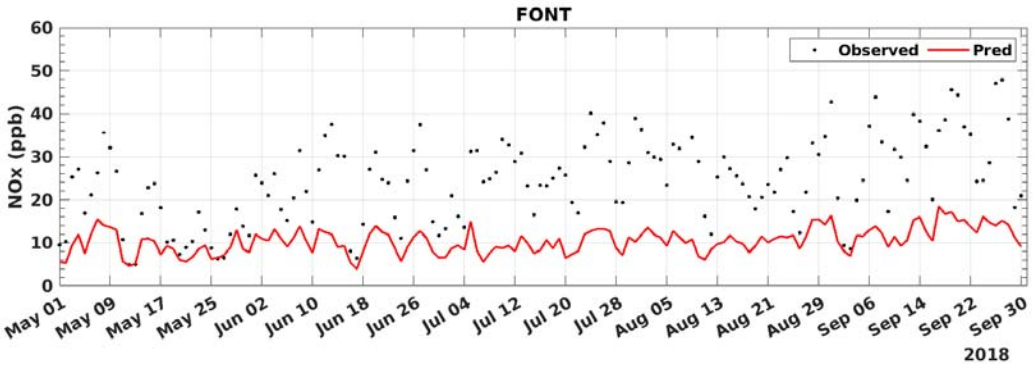

FIGURE D-7: 2018 DAILY AVERAGED NOX MODEL PREDICTION AND MEASUREMENT COMPARISON AT FONTANA

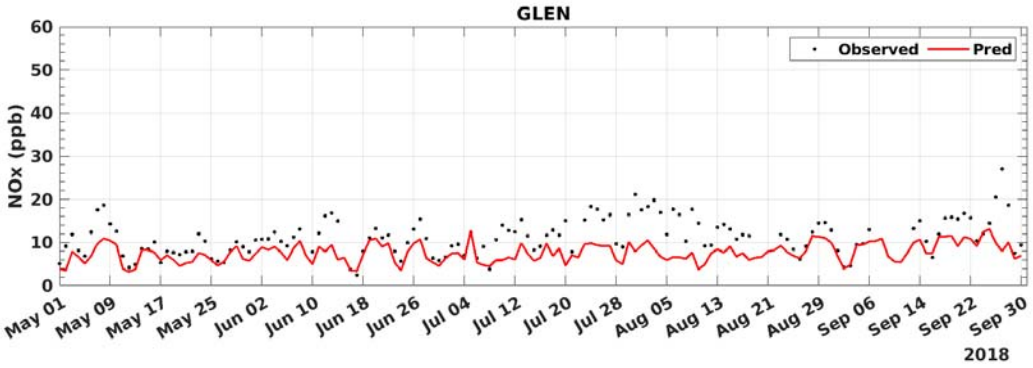

FIGURE D-8: 2018 DAILY AVERAGED NOX MODEL PREDICTION AND MEASUREMENT COMPARISON AT GLENDORA

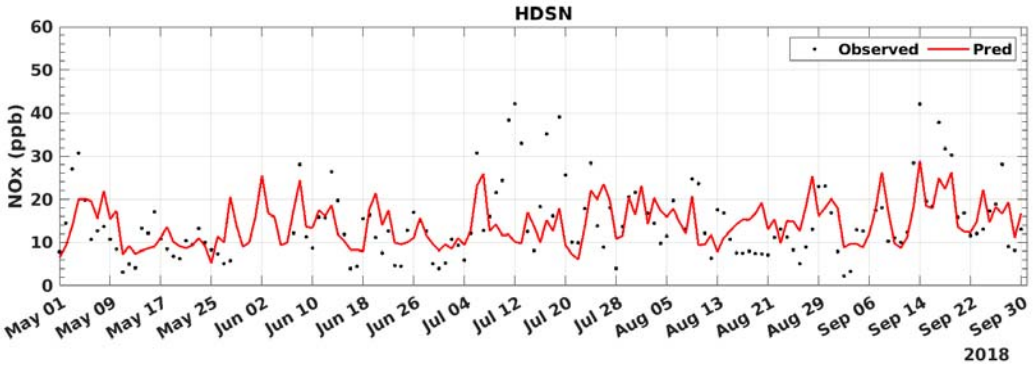

FIGURE D-9: 2018 DAILY AVERAGED NOX MODEL PREDICTION AND MEASUREMENT COMPARISON AT HUDSON

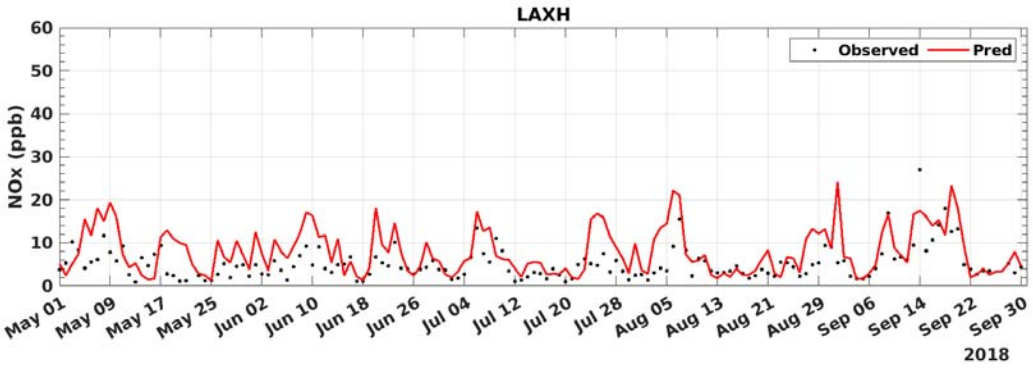

FIGURE D-10: 2018 DAILY AVERAGED NOX MODEL PREDICTION AND MEASUREMENT COMPARISON AT LAX

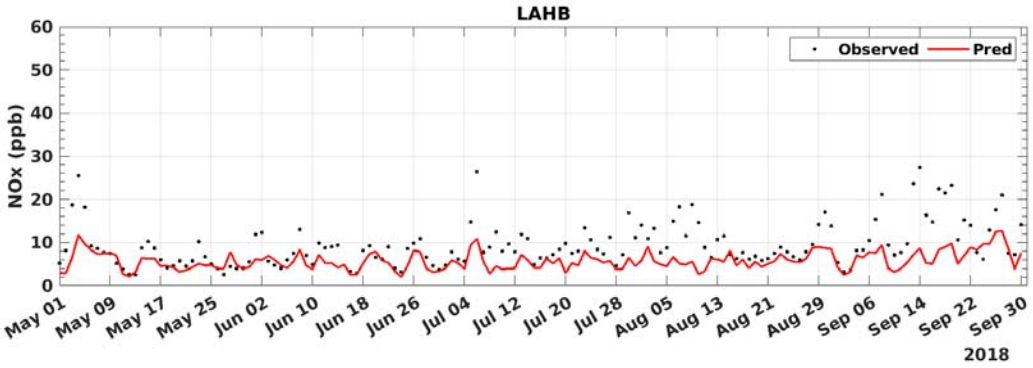

FIGURE D-11: 2018 DAILY AVERAGED NOX MODEL PREDICTION AND MEASUREMENT COMPARISON AT LA HABRA

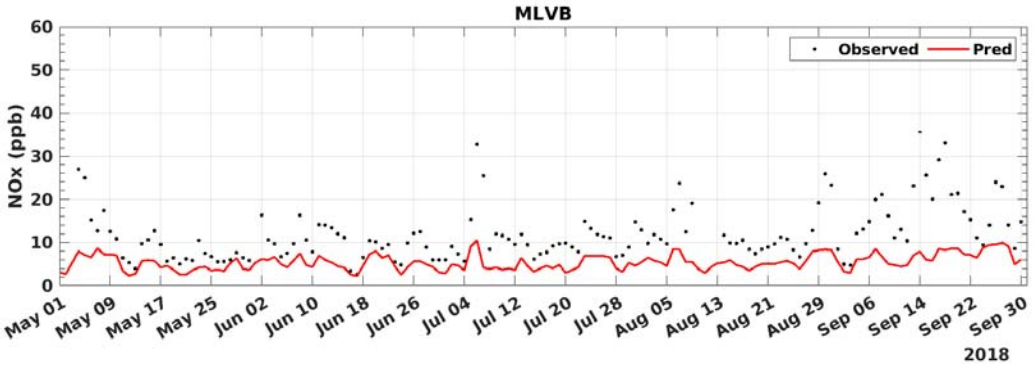

FIGURE D-12: 2018 DAILY AVERAGED NOX MODEL PREDICTION AND MEASUREMENT COMPARISON AT MIRA LOMA VAN BUREN

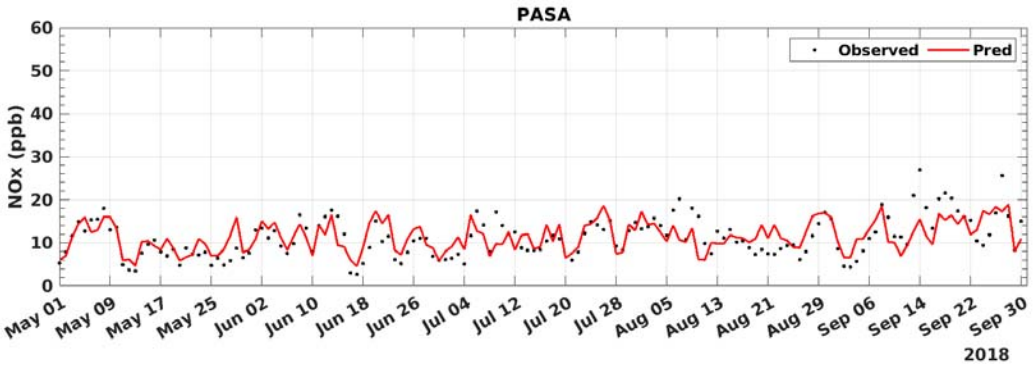

FIGURE D-13: 2018 DAILY AVERAGED NOX MODEL PREDICTION AND MEASUREMENT COMPARISON AT PASADENA

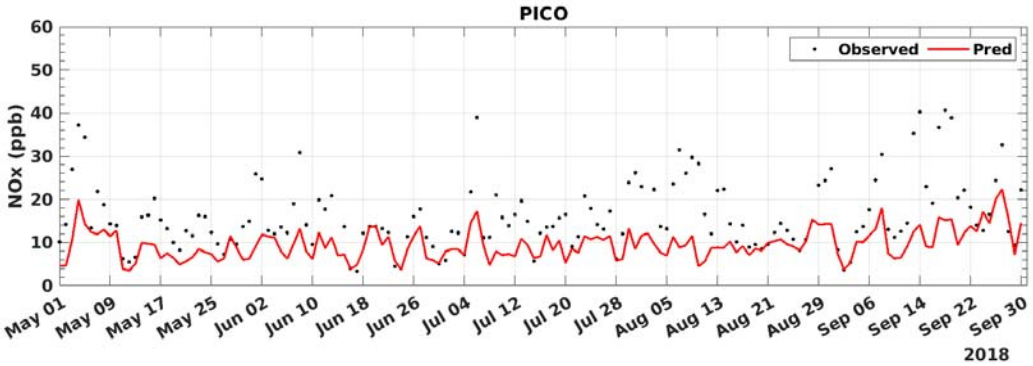

FIGURE D-14: 2018 DAILY AVERAGED NOX MODEL PREDICTION AND MEASUREMENT COMPARISON AT PICO RIVERA

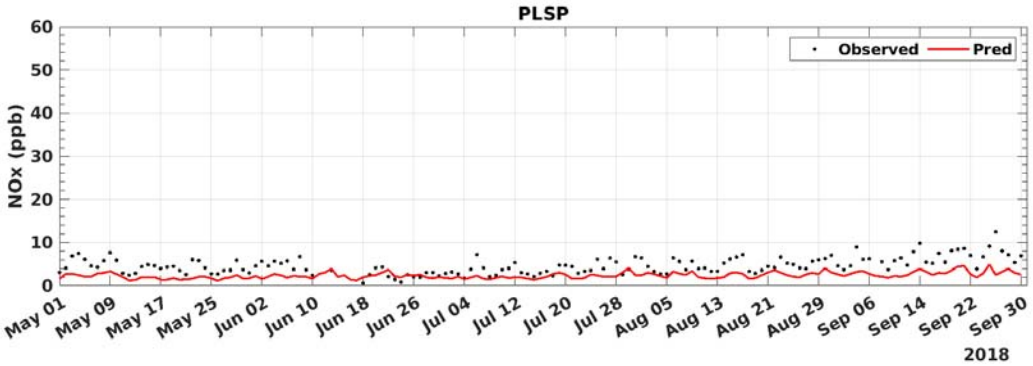

FIGURE D-15: 2018 DAILY AVERAGED NOX MODEL PREDICTION AND MEASUREMENT COMPARISON AT PALM SPRINGS

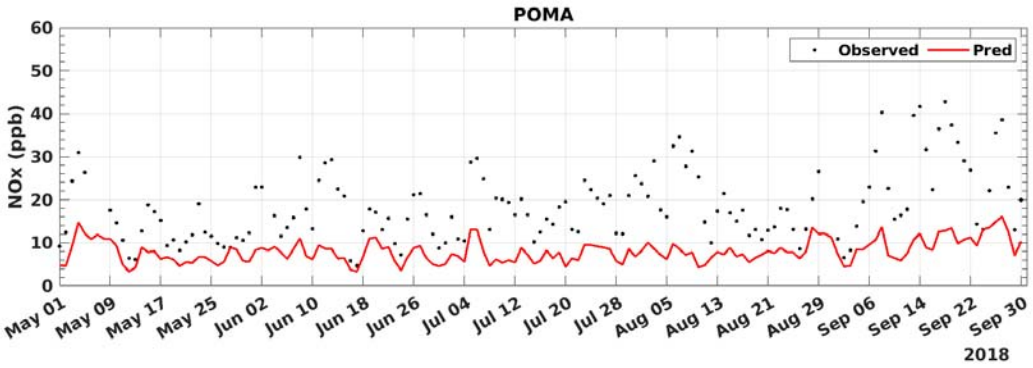

FIGURE D-16: 2018 DAILY AVERAGED NOX MODEL PREDICTION AND MEASUREMENT COMPARISON AT POMONA

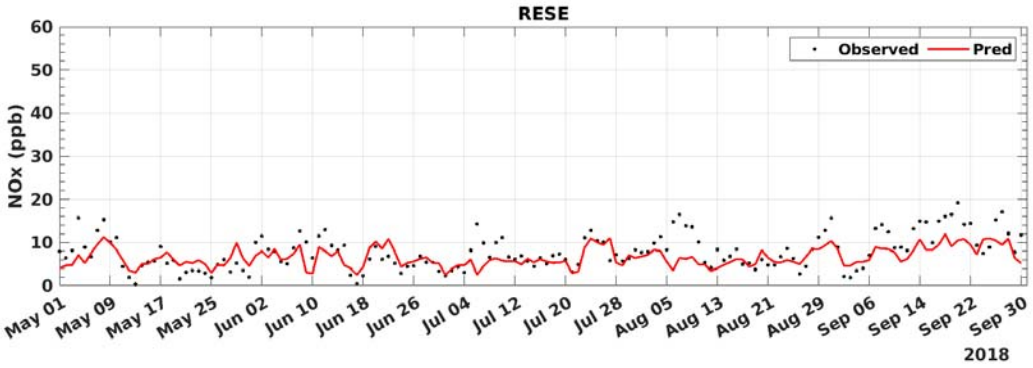

FIGURE D-17: 2018 DAILY AVERAGED NOX MODEL PREDICTION AND MEASUREMENT COMPARISON AT RESEDA

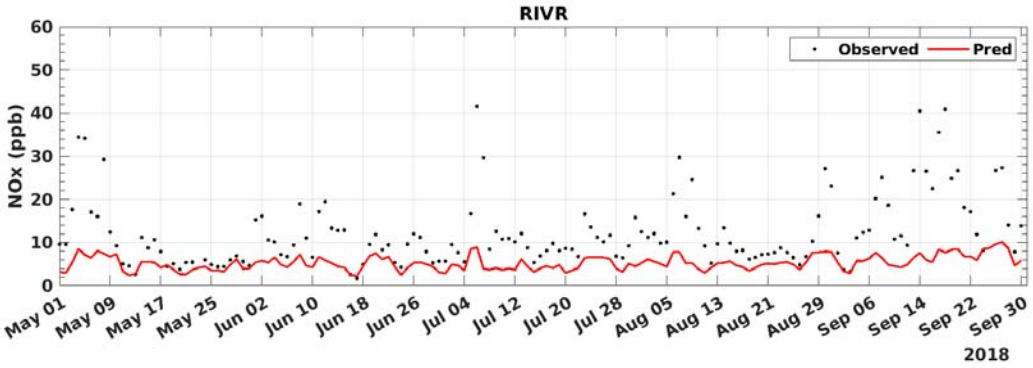

FIGURE D-18: 2018 DAILY AVERAGED NOX MODEL PREDICTION AND MEASUREMENT COMPARISON AT RIVERSIDE

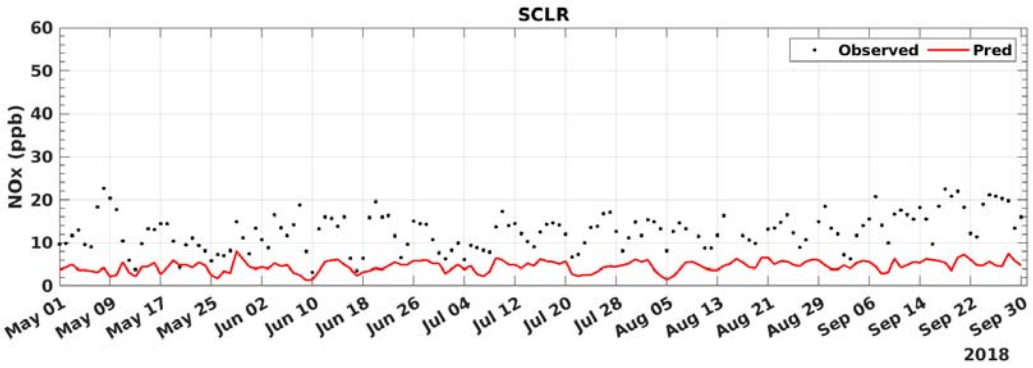

FIGURE D-19: 2018 DAILY AVERAGED NOX MODEL PREDICTION AND MEASUREMENT COMPARISON AT SANTA CLARITA

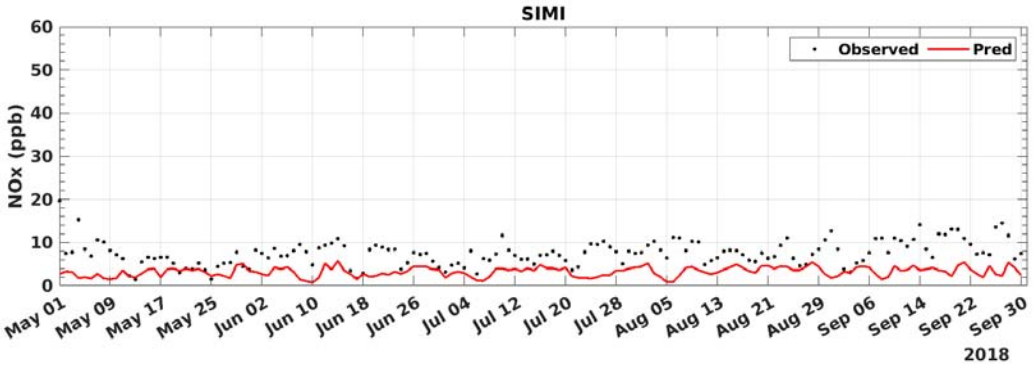

FIGURE D-20: 2018 DAILY AVERAGED NOX MODEL PREDICTION AND MEASUREMENT COMPARISON AT SIMI VALLEY

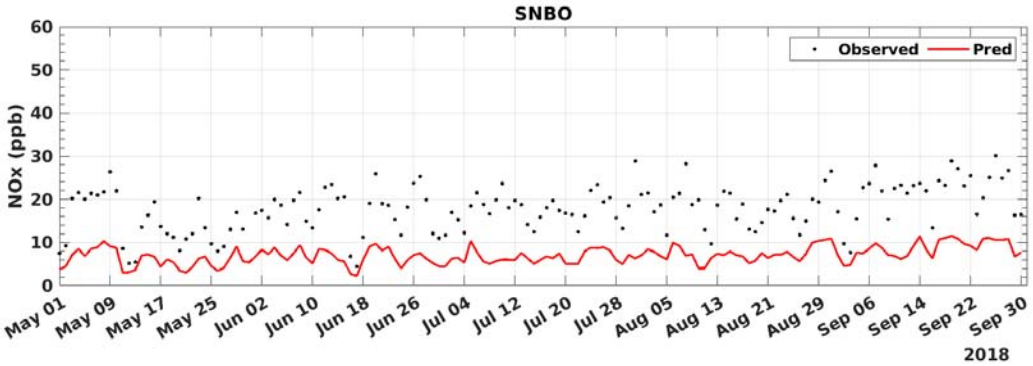

FIGURE D-21: 2018 DAILY AVERAGED NOX MODEL PREDICTION AND MEASUREMENT COMPARISON AT SAN BERNARDINO

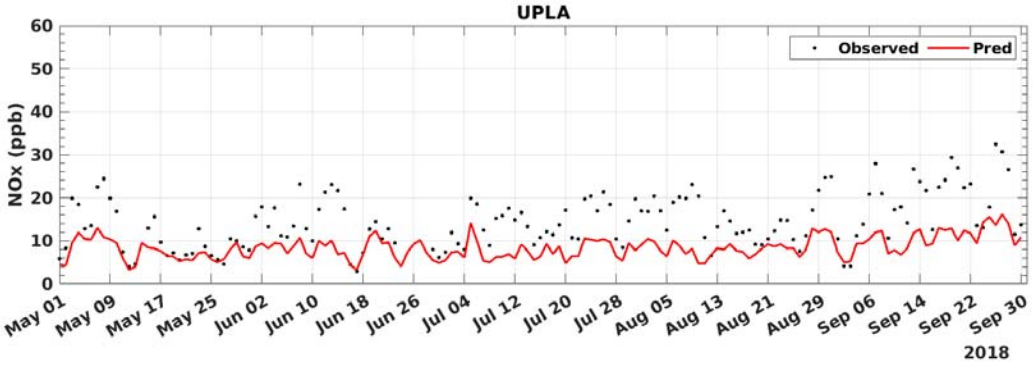

FIGURE D-22: 2018 DAILY AVERAGED NOX MODEL PREDICTION AND MEASUREMENT COMPARISON AT UPLAND

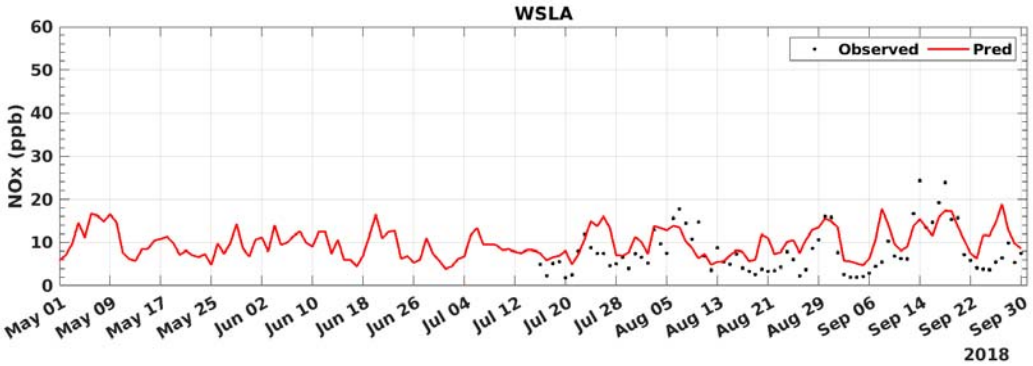

FIGURE D-23: 2018 DAILY AVERAGED NOX MODEL PREDICTION AND MEASUREMENT COMPARISON AT WEST LOS ANGELES

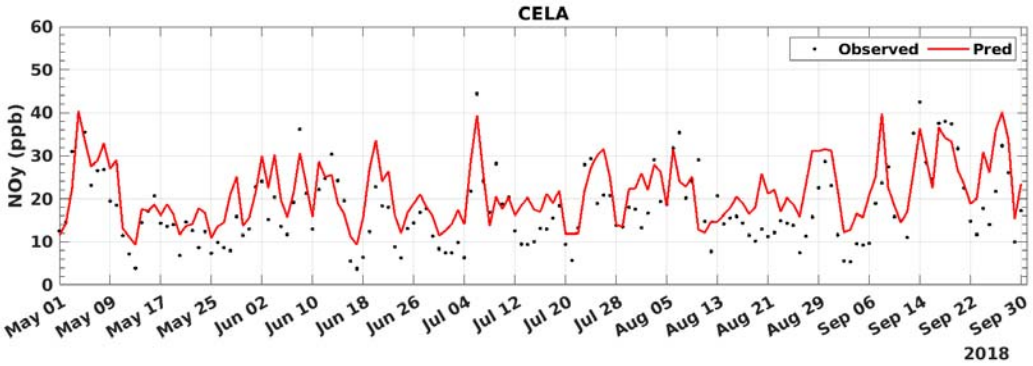

FIGURE E-1: 2018 DAILY AVERAGED NOY MODEL PREDICTION AND MEASUREMENT COMPARISON AT CENTRAL LOS ANGELES

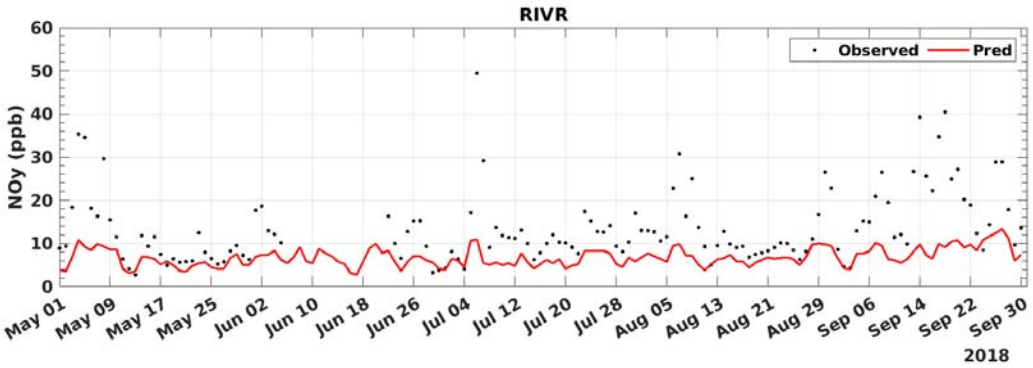

FIGURE E-2: 2018 DAILY AVERAGED NOY MODEL PREDICTION AND MEASUREMENT COMPARISON AT RIVERSIDE

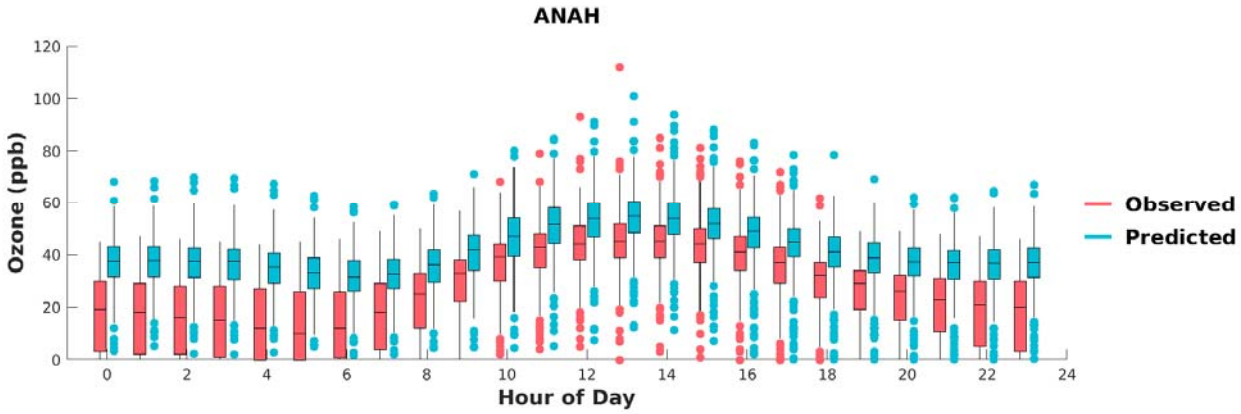

FIGURE F-1: BOX PLOTS OF OBSERVED VS. PREDICTED HOURLY OZONE DURING MAY 1ST TO SEPTEMBER 30TH, 2018, AT ANAHEIM. HORIZANTAL LINES INDICATE 25TH, 50TH (MEDIAN), AND 75TH PERCENTILES.

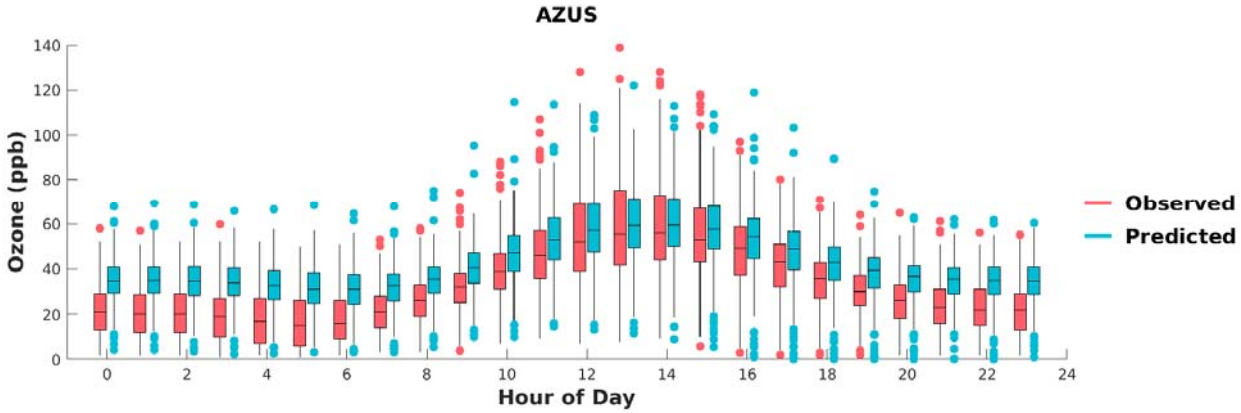

FIGURE F-2: BOX PLOTS OF OBSERVED VS. PREDICTED HOURLY OZONE DURING MAY 1ST TO SEPTEMBER 30TH, 2018, AT AZUSA. HORIZANTAL LINES INDICATE 25TH, 50TH (MEDIAN), AND 75TH PERCENTILES.

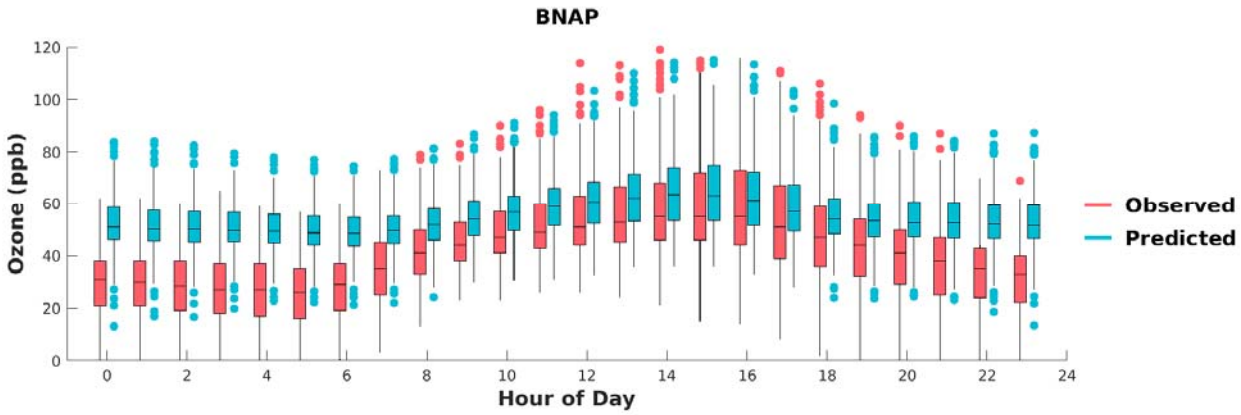

FIGURE F-3: BOX PLOTS OF OBSERVED VS. PREDICTED HOURLY OZONE DURING MAY 1ST TO SEPTEMBER 30TH, 2018, AT BANNING. HORIZANTAL LINES INDICATE 25TH, 50TH (MEDIAN), AND 75TH PERCENTILES.

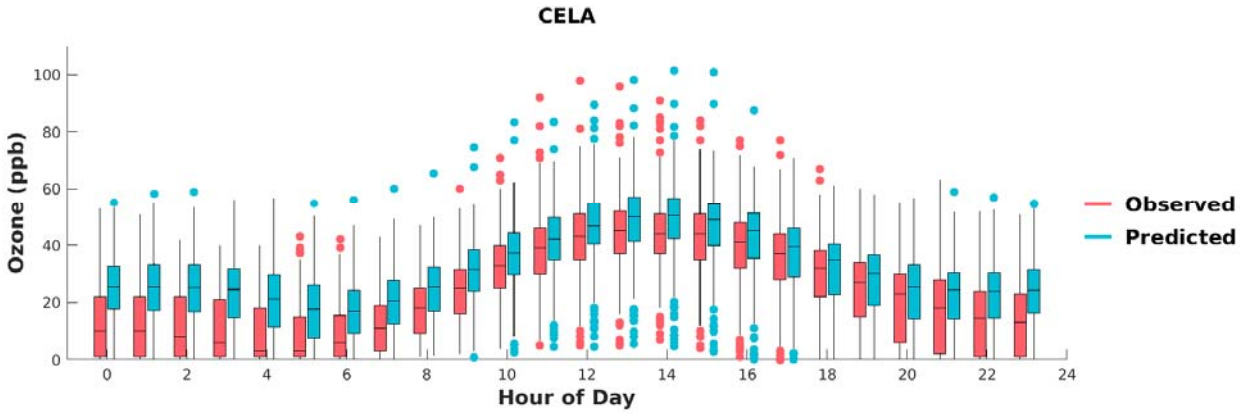

FIGURE F-4: BOX PLOTS OF OBSERVED VS. PREDICTED HOURLY OZONE DURING MAY 1ST TO SEPTEMBER 30TH, 2018, AT CENTRAL LOS ANGELES. HORIZANTAL LINES INDICATE 25TH, 50TH (MEDIAN), AND 75TH PERCENTILES.

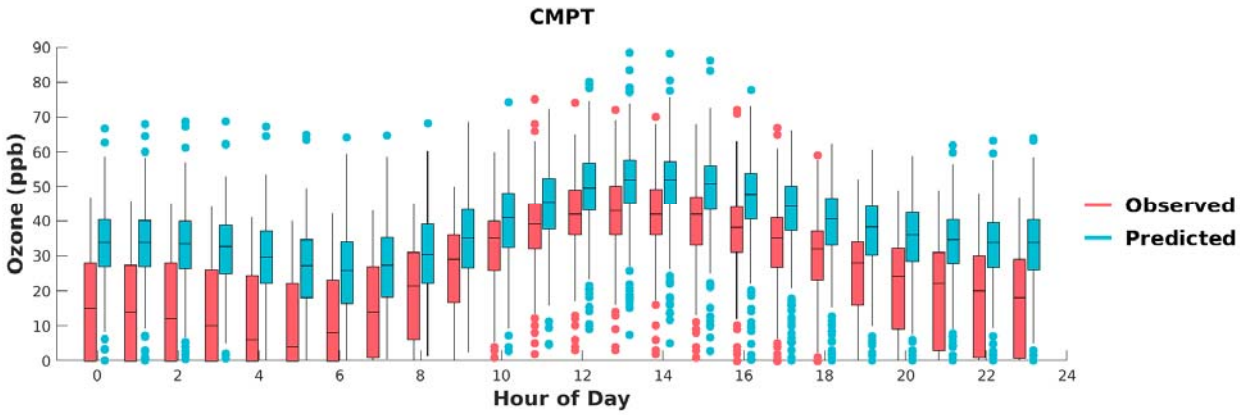

FIGURE F-5: BOX PLOTS OF OBSERVED VS. PREDICTED HOURLY OZONE DURING MAY 1ST TO SEPTEMBER 30TH, 2018, AT COMPTON. HORIZANTAL LINES INDICATE 25TH, 50TH (MEDIAN), AND 75TH PERCENTILES.

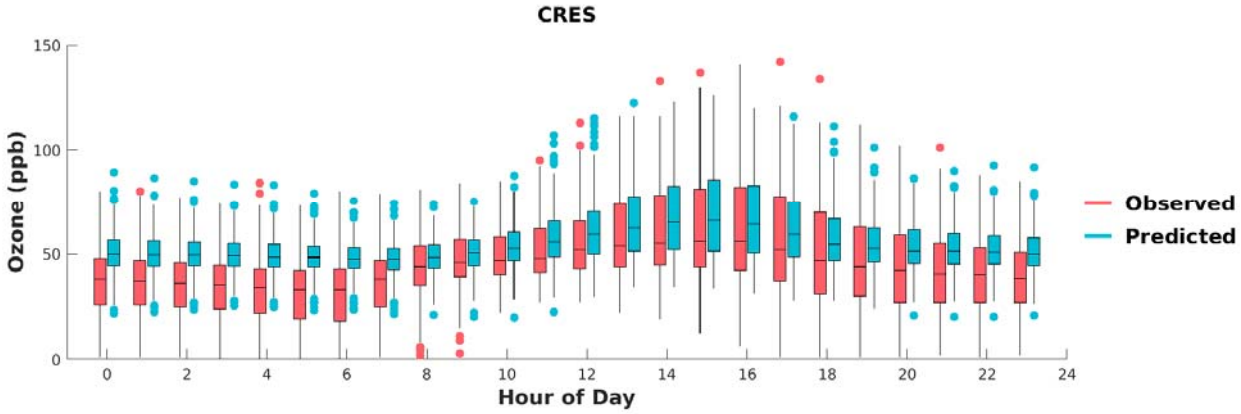

FIGURE F-6: BOX PLOTS OF OBSERVED VS. PREDICTED HOURLY OZONE DURING MAY 1ST TO SEPTEMBER 30TH, 2018, AT CRESTLINE. HORIZANTAL LINES INDICATE 25TH, 50TH (MEDIAN), AND 75TH PERCENTILES.

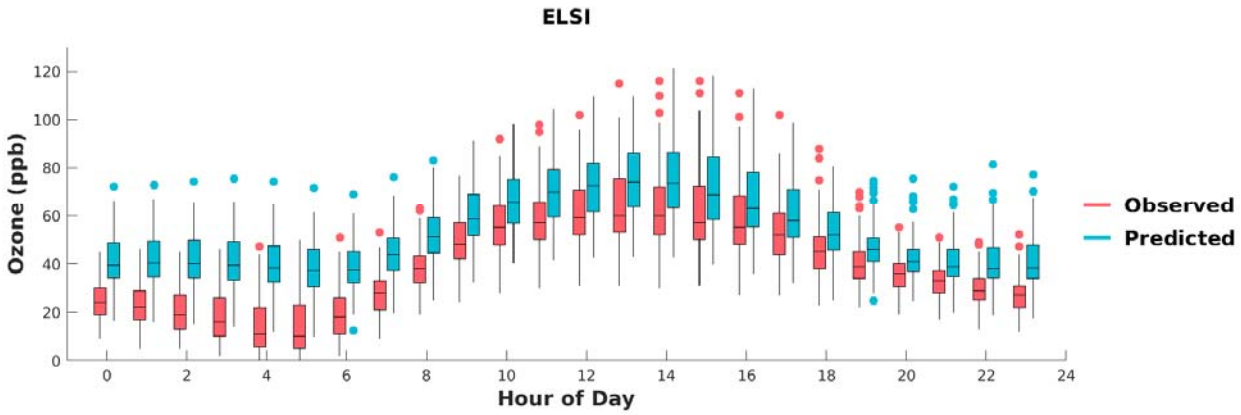

FIGURE F-7: BOX PLOTS OF OBSERVED VS. PREDICTED HOURLY OZONE DURING MAY 1ST TO SEPTEMBER 30TH, 2018, AT LAKE ELSINORE. HORIZANTAL LINES INDICATE 25TH, 50TH (MEDIAN), AND 75TH PERCENTILES.

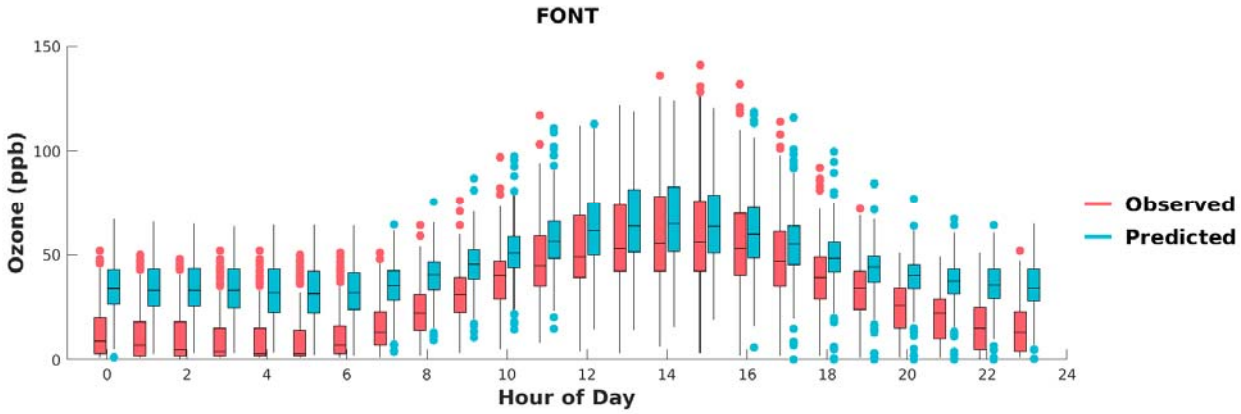

FIGURE F-8: BOX PLOTS OF OBSERVED VS. PREDICTED HOURLY OZONE DURING MAY 1ST TO SEPTEMBER 30TH, 2018, AT FONTANA. HORIZANTAL LINES INDICATE 25TH, 50TH (MEDIAN), AND 75TH PERCENTILES.

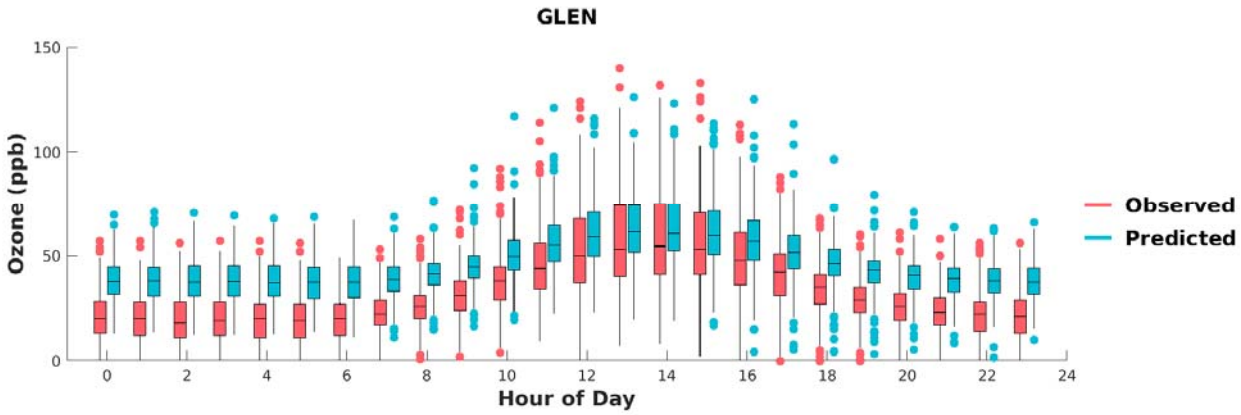

FIGURE F-9: BOX PLOTS OF OBSERVED VS. PREDICTED HOURLY OZONE DURING MAY 1ST TO SEPTEMBER 30TH, 2018, AT GLENDORA. HORIZANTAL LINES INDICATE 25TH, 50TH (MEDIAN), AND 75TH PERCENTILES.

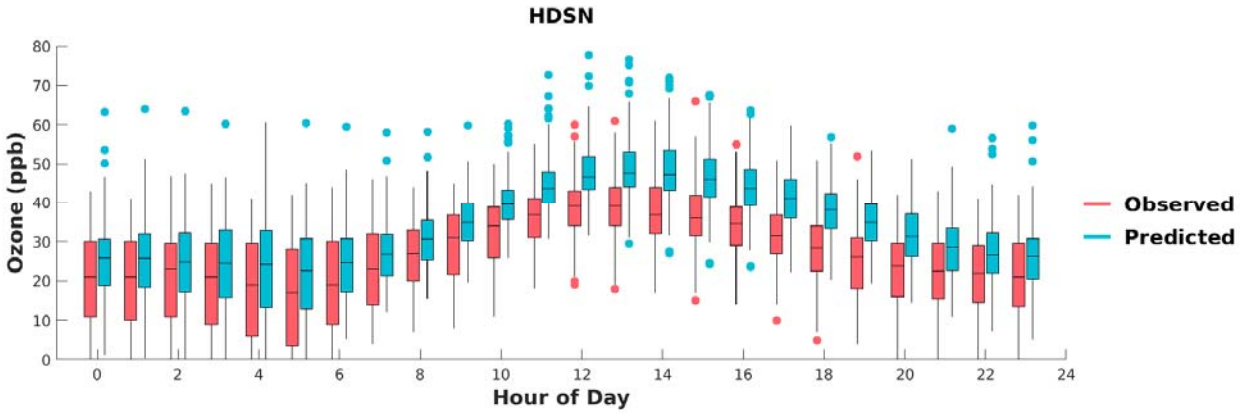

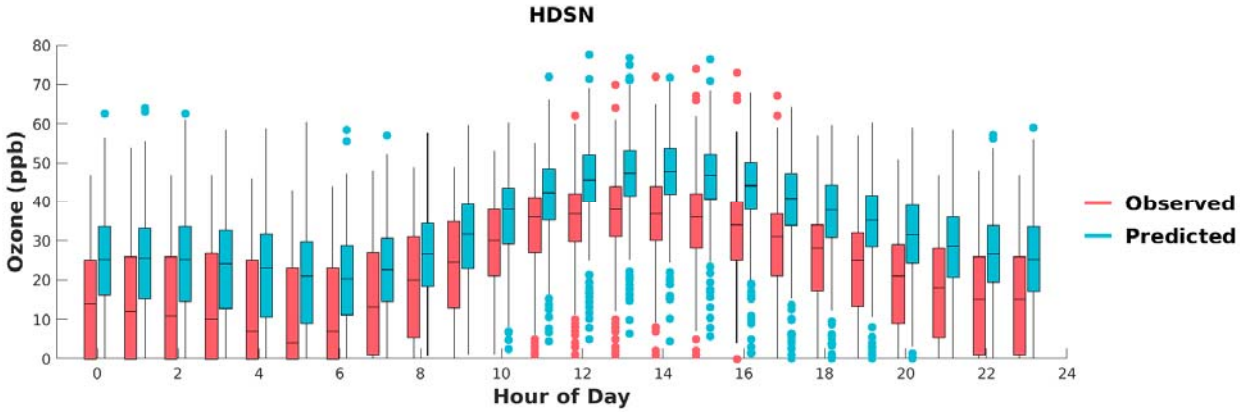

FIGURE F-10: BOX PLOTS OF OBSERVED VS. PREDICTED HOURLY OZONE DURING MAY 1ST TO SEPTEMBER 30TH, 2018, AT HUDSON. HORIZANTAL LINES INDICATE 25TH, 50TH (MEDIAN), AND 75TH PERCENTILES.

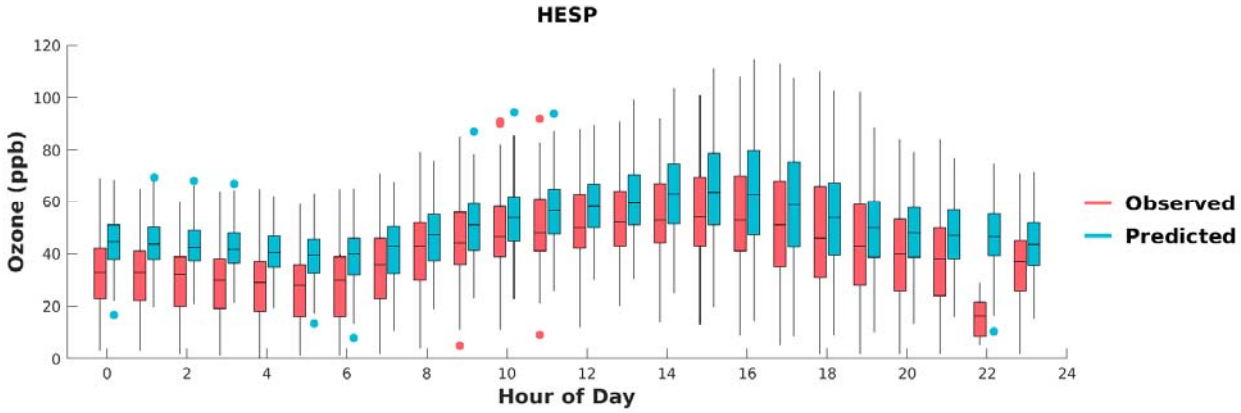

FIGURE F-11: BOX PLOTS OF OBSERVED VS. PREDICTED HOURLY OZONE DURING MAY 1ST TO SEPTEMBER 30TH, 2018, AT HESPERIA. HORIZANTAL LINES INDICATE 25TH, 50TH (MEDIAN), AND 75TH PERCENTILES.

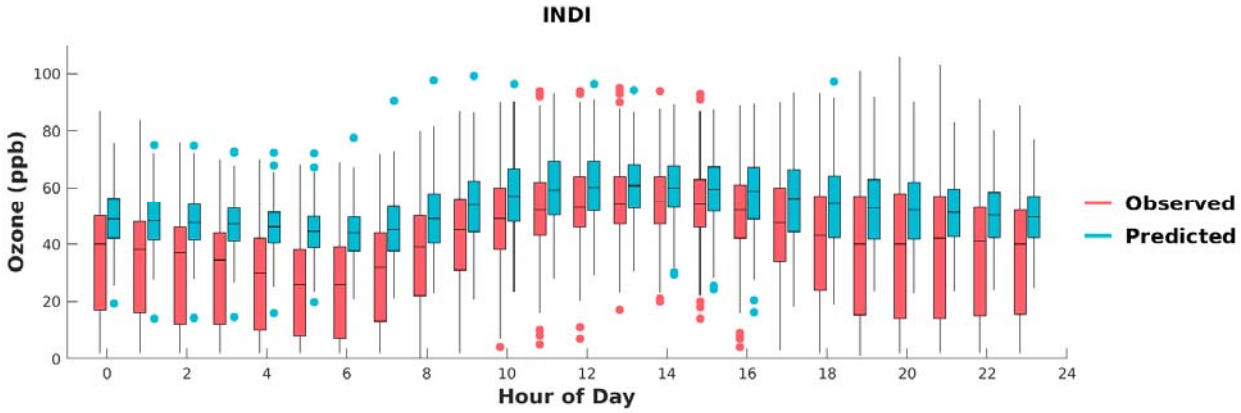

FIGURE F-12: BOX PLOTS OF OBSERVED VS. PREDICTED HOURLY OZONE DURING MAY 1ST TO SEPTEMBER 30TH, 2018, AT INDIO. HORIZANTAL LINES INDICATE 25TH, 50TH (MEDIAN), AND 75TH PERCENTILES.

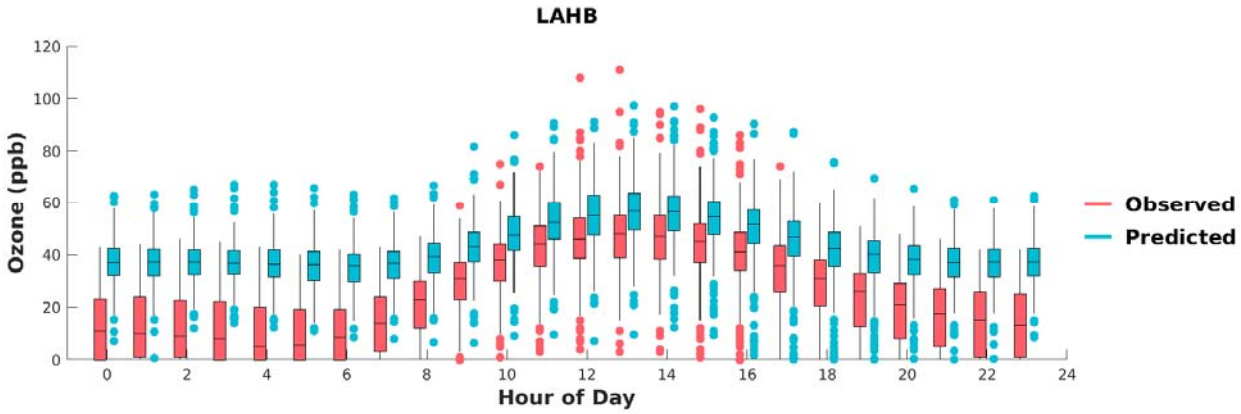

FIGURE F-13: BOX PLOTS OF OBSERVED VS. PREDICTED HOURLY OZONE DURING MAY 1ST TO SEPTEMBER 30TH, 2018, AT LA HABRA. HORIZANTAL LINES INDICATE 25TH, 50TH (MEDIAN), AND 75TH PERCENTILES.

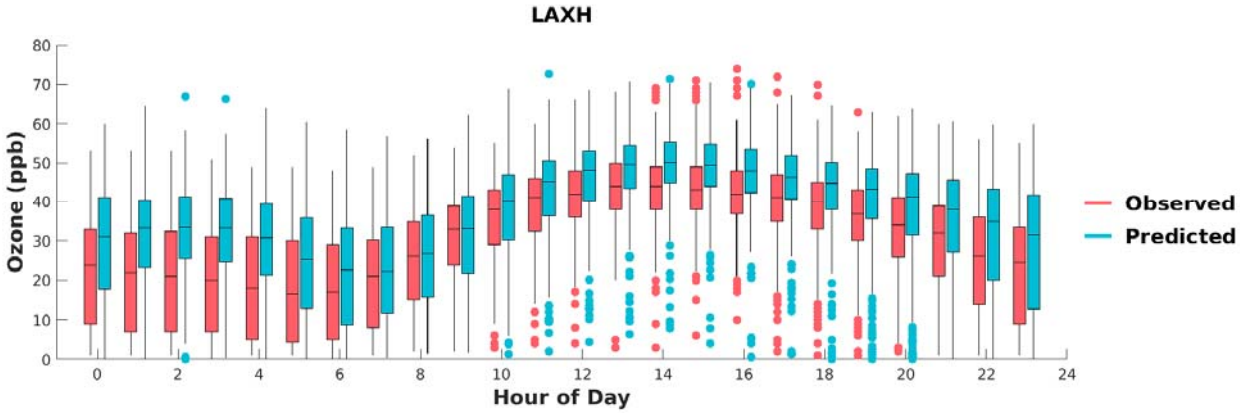

FIGURE F-14: BOX PLOTS OF OBSERVED VS. PREDICTED HOURLY OZONE DURING MAY 1ST TO SEPTEMBER 30TH, 2018, AT LAX. HORIZANTAL LINES INDICATE 25TH, 50TH (MEDIAN), AND 75TH PERCENTILES.

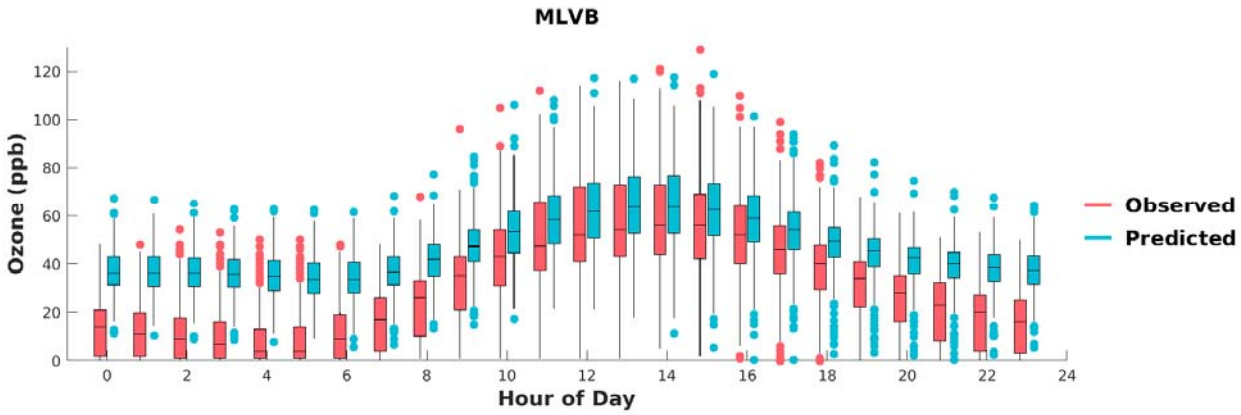

FIGURE F-15: BOX PLOTS OF OBSERVED VS. PREDICTED HOURLY OZONE DURING MAY 1ST TO SEPTEMBER 30TH, 2018, AT MIRA LOMA VAN BUREN. HORIZANTAL LINES INDICATE 25TH, 50TH (MEDIAN), AND 75TH PERCENTILES.

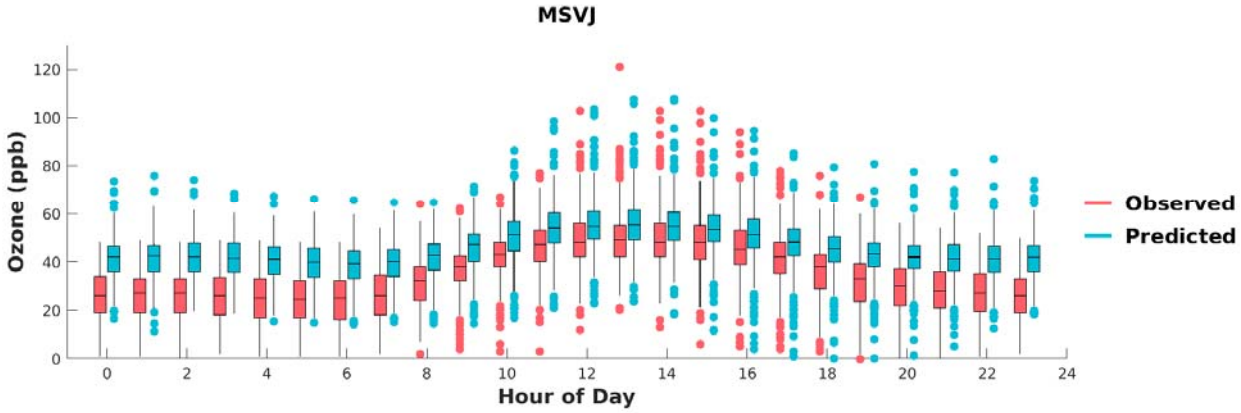

FIGURE F-16: BOX PLOTS OF OBSERVED VS. PREDICTED HOURLY OZONE DURING MAY 1ST TO SEPTEMBER 30TH, 2018, AT MISSION VIEJO. HORIZANTAL LINES INDICATE 25TH, 50TH (MEDIAN), AND 75TH PERCENTILES.

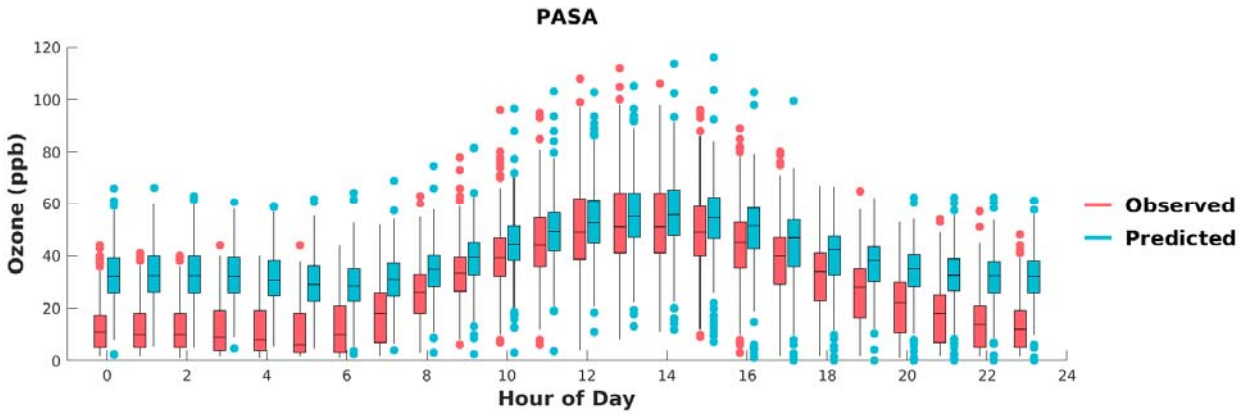

FIGURE F-17: BOX PLOTS OF OBSERVED VS. PREDICTED HOURLY OZONE DURING MAY 1ST TO SEPTEMBER 30TH, 2018, AT PASADENA. HORIZANTAL LINES INDICATE 25TH, 50TH (MEDIAN), AND 75TH PERCENTILES.

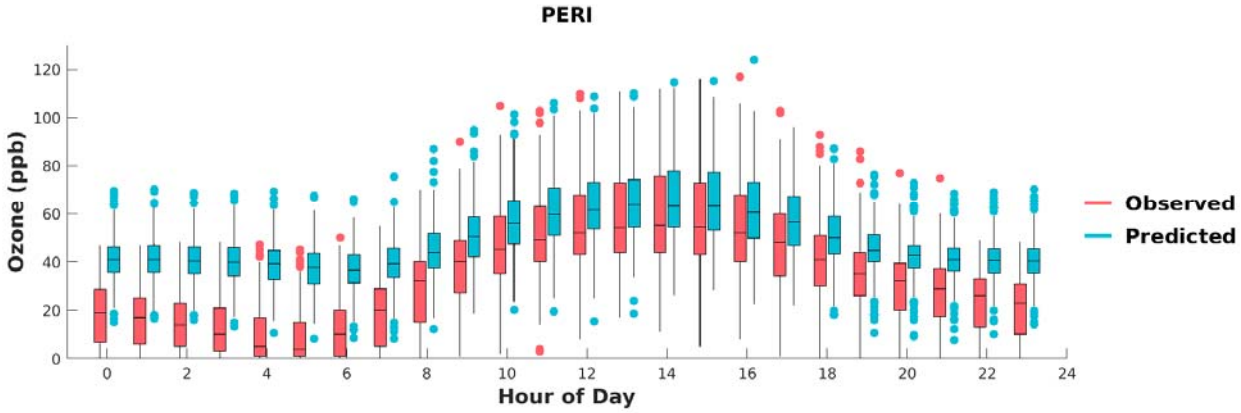

FIGURE F-18: BOX PLOTS OF OBSERVED VS. PREDICTED HOURLY OZONE DURING MAY 1ST TO SEPTEMBER 30TH, 2018, AT PERRIS. HORIZANTAL LINES INDICATE 25TH, 50TH (MEDIAN), AND 75TH PERCENTILES.

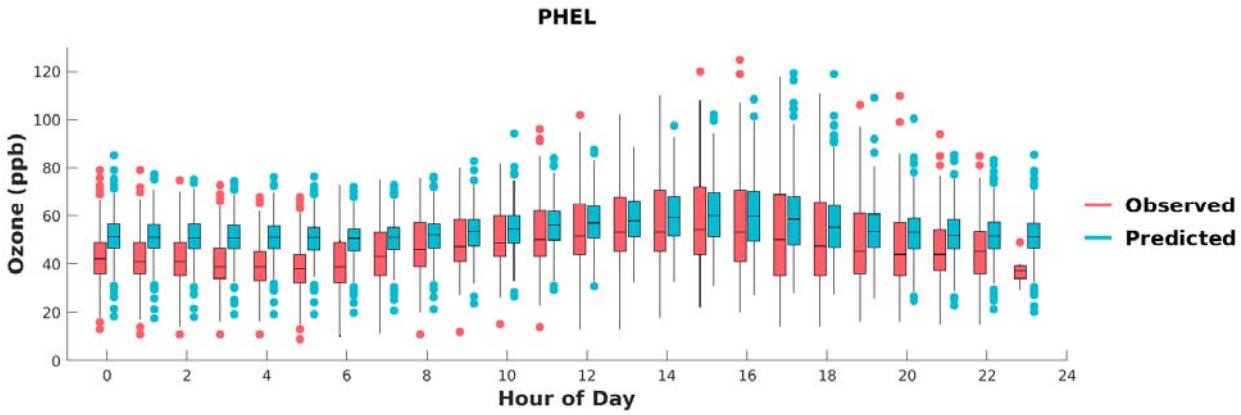

FIGURE F-19: BOX PLOTS OF OBSERVED VS. PREDICTED HOURLY OZONE DURING MAY 1ST TO SEPTEMBER 30TH, 2018, AT PHELAN. HORIZANTAL LINES INDICATE 25TH, 50TH (MEDIAN), AND 75TH PERCENTILES.

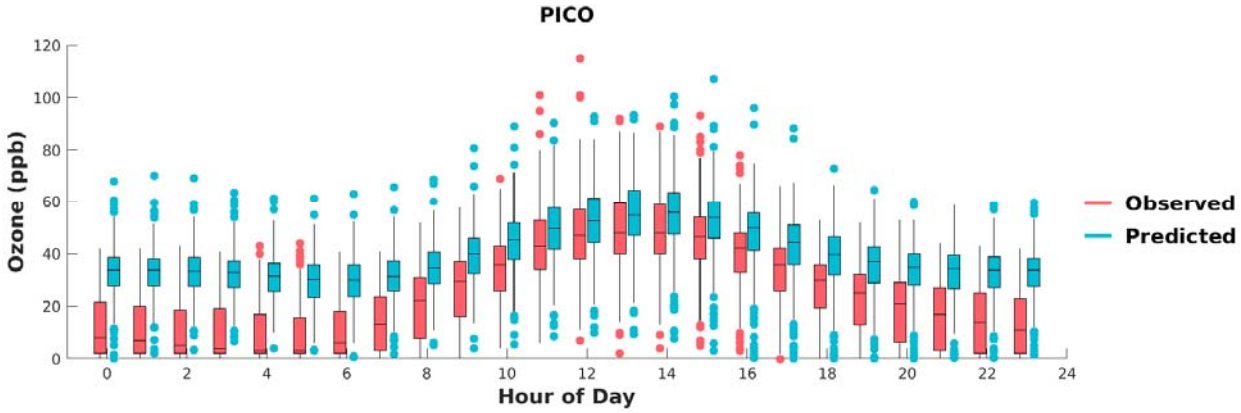

FIGURE F-20: BOX PLOTS OF OBSERVED VS. PREDICTED HOURLY OZONE DURING MAY 1ST TO SEPTEMBER 30TH, 2018, AT PICO RIVERO. HORIZANTAL LINES INDICATE 25TH, 50TH (MEDIAN), AND 75TH PERCENTILES.

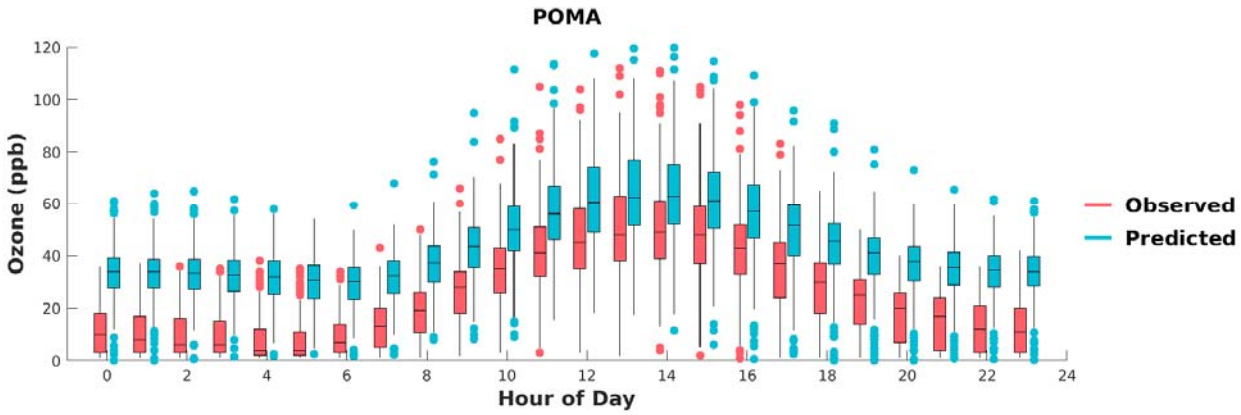

FIGURE F-21: BOX PLOTS OF OBSERVED VS. PREDICTED HOURLY OZONE DURING MAY 1ST TO SEPTEMBER 30TH, 2018, AT POMONA. HORIZANTAL LINES INDICATE 25TH, 50TH (MEDIAN), AND 75TH PERCENTILES.

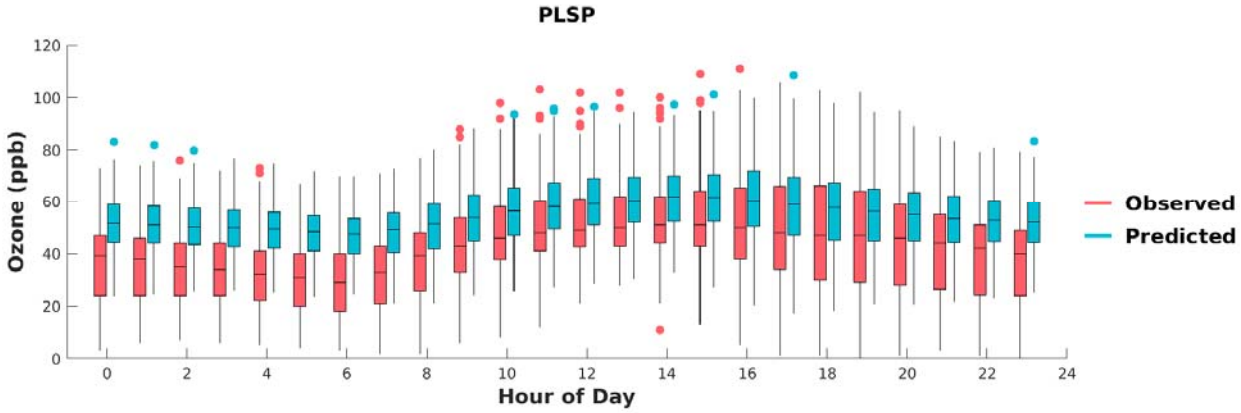

FIGURE F-22: BOX PLOTS OF OBSERVED VS. PREDICTED HOURLY OZONE DURING MAY 1ST TO SEPTEMBER 30TH, 2018, AT PALM SPRINGS. HORIZANTAL LINES INDICATE 25TH, 50TH (MEDIAN), AND 75TH PERCENTILES.

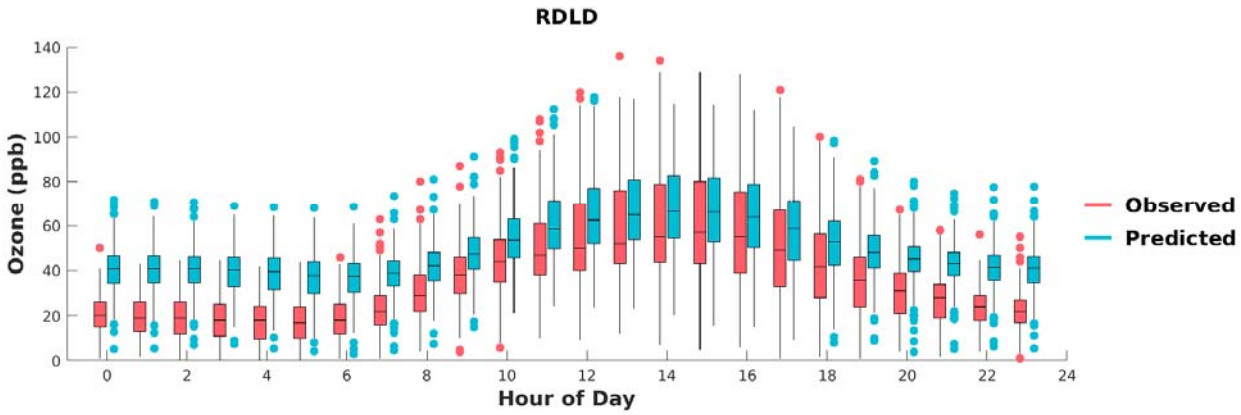

FIGURE F-23: BOX PLOTS OF OBSERVED VS. PREDICTED HOURLY OZONE DURING MAY 1ST TO SEPTEMBER 30TH, 2018, AT REDLANDS. HORIZANTAL LINES INDICATE 25TH, 50TH (MEDIAN), AND 75TH PERCENTILES.

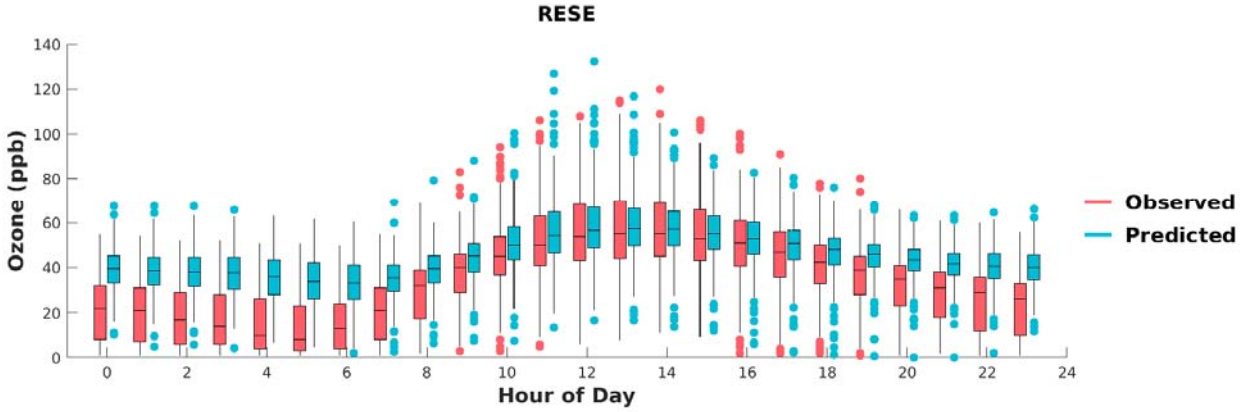

FIGURE F-24: BOX PLOTS OF OBSERVED VS. PREDICTED HOURLY OZONE DURING MAY 1ST TO SEPTEMBER 30TH, 2018, AT RESEDA. HORIZANTAL LINES INDICATE 25TH, 50TH (MEDIAN), AND 75TH PERCENTILES.

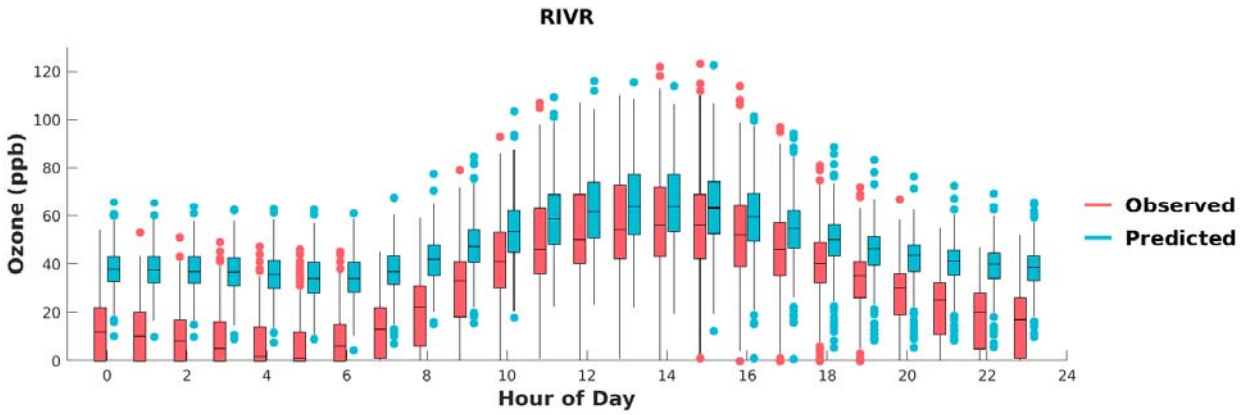

FIGURE F-25: BOX PLOTS OF OBSERVED VS. PREDICTED HOURLY OZONE DURING MAY 1ST TO SEPTEMBER 30TH, 2018, AT RIVERSIDE. HORIZANTAL LINES INDICATE 25TH, 50TH (MEDIAN), AND 75TH PERCENTILES.

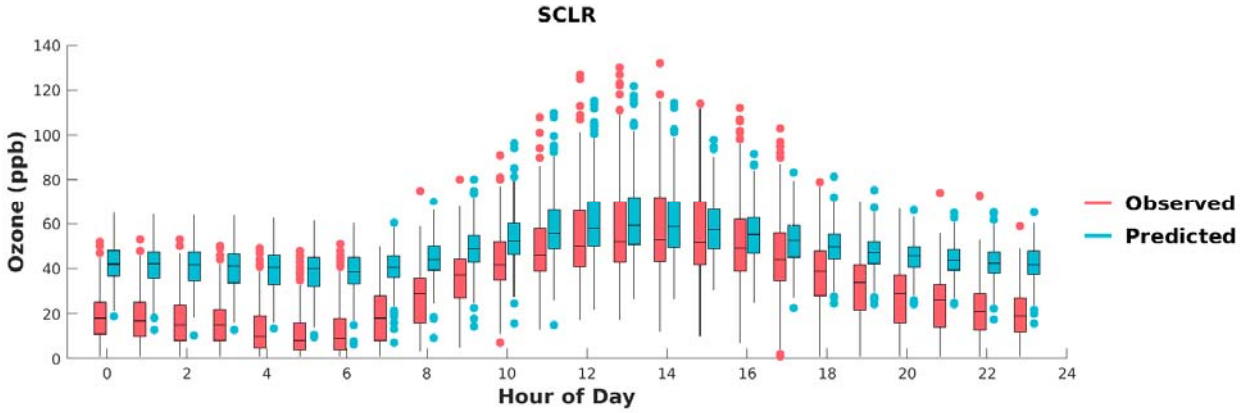

FIGURE F-26: BOX PLOTS OF OBSERVED VS. PREDICTED HOURLY OZONE DURING MAY 1ST TO SEPTEMBER 30TH, 2018, AT SANTA CLARITA. HORIZANTAL LINES INDICATE 25TH, 50TH (MEDIAN), AND 75TH PERCENTILES.

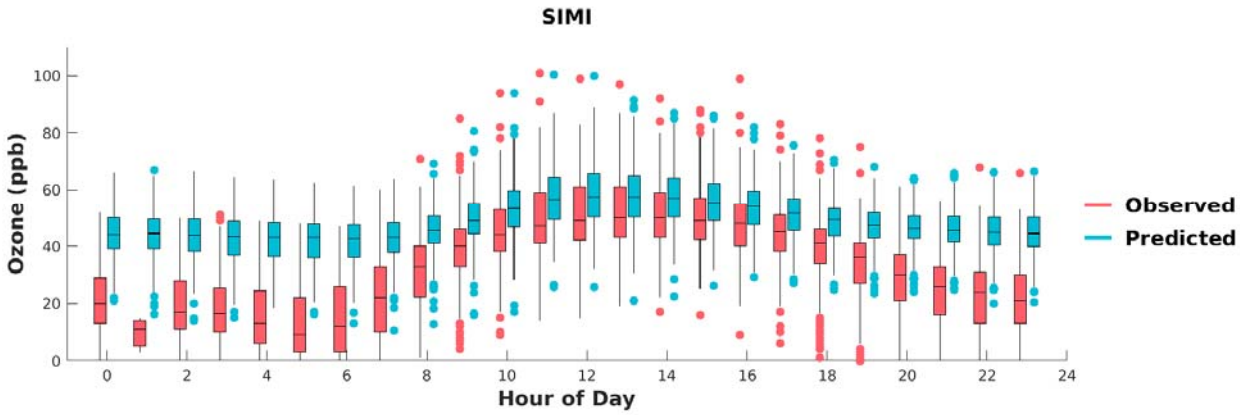

FIGURE F-27: BOX PLOTS OF OBSERVED VS. PREDICTED HOURLY OZONE DURING MAY 1ST TO SEPTEMBER 30TH, 2018, AT SIMI VALLEY. HORIZANTAL LINES INDICATE 25TH, 50TH (MEDIAN), AND 75TH PERCENTILES.

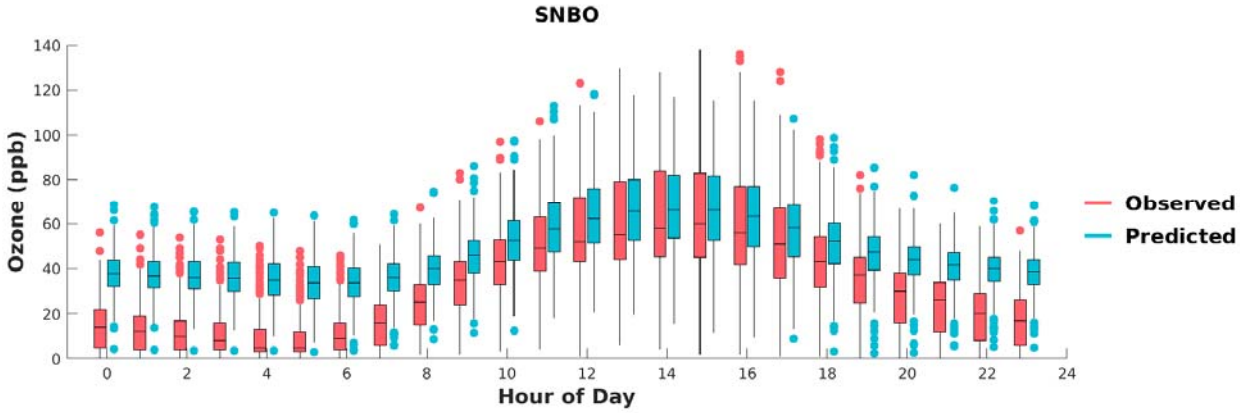

FIGURE F-28: BOX PLOTS OF OBSERVED VS. PREDICTED HOURLY OZONE DURING MAY 1ST TO SEPTEMBER 30TH, 2018, AT SAN BERNARDINO. HORIZANTAL LINES INDICATE 25TH, 50TH (MEDIAN), AND 75TH PERCENTILES.

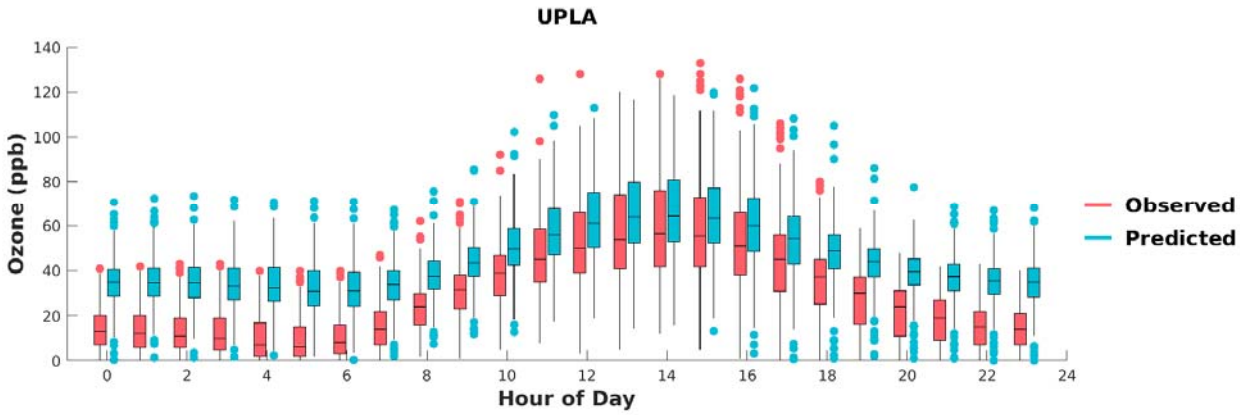

FIGURE F-29: BOX PLOTS OF OBSERVED VS. PREDICTED HOURLY OZONE DURING MAY 1ST TO SEPTEMBER 30TH, 2018, AT UPLAND. HORIZANTAL LINES INDICATE 25TH, 50TH (MEDIAN), AND 75TH PERCENTILES.

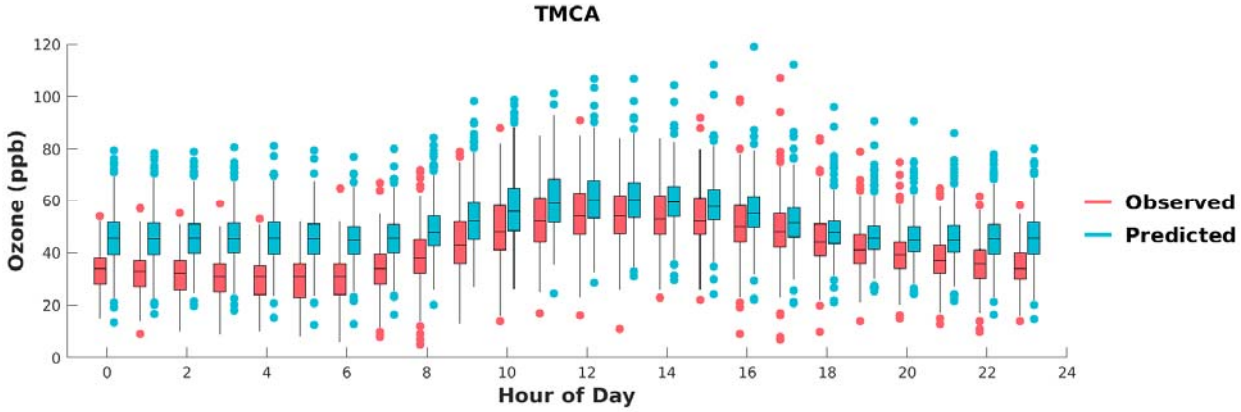

FIGURE F-30: BOX PLOTS OF OBSERVED VS. PREDICTED HOURLY OZONE DURING MAY 1ST TO SEPTEMBER 30TH, 2018, AT TEMACULA. HORIZANTAL LINES INDICATE 25TH, 50TH (MEDIAN), AND 75TH PERCENTILES.

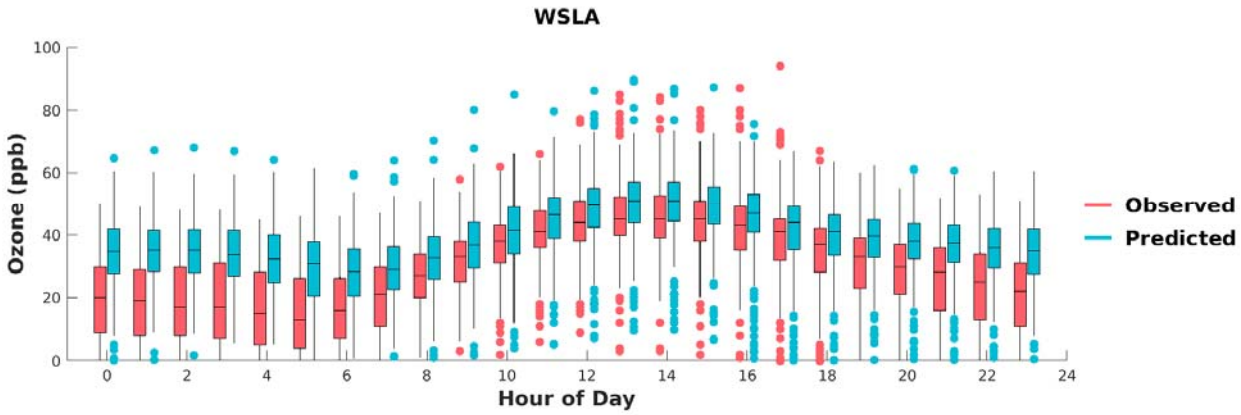

FIGURE F-31: BOX PLOTS OF OBSERVED VS. PREDICTED HOURLY OZONE DURING MAY 1ST TO SEPTEMBER 30TH, 2018, AT WEST LOS ANGELES. HORIZANTAL LINES INDICATE 25TH, 50TH (MEDIAN), AND 75TH PERCENTILES.

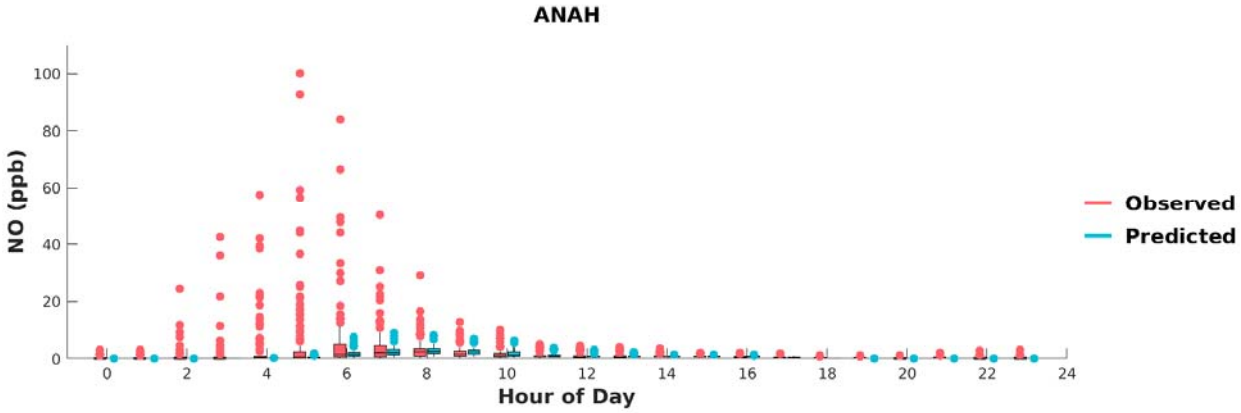

FIGURE G-1: BOX PLOTS OF OBSERVED VS. PREDICTED HOURLY NO DURING MAY 1ST TO SEPTEMBER 30TH, 2018, AT ANAHEIM. HORIZANTAL LINES INDICATE 25TH, 50TH (MEDIAN), AND 75TH PERCENTILES.

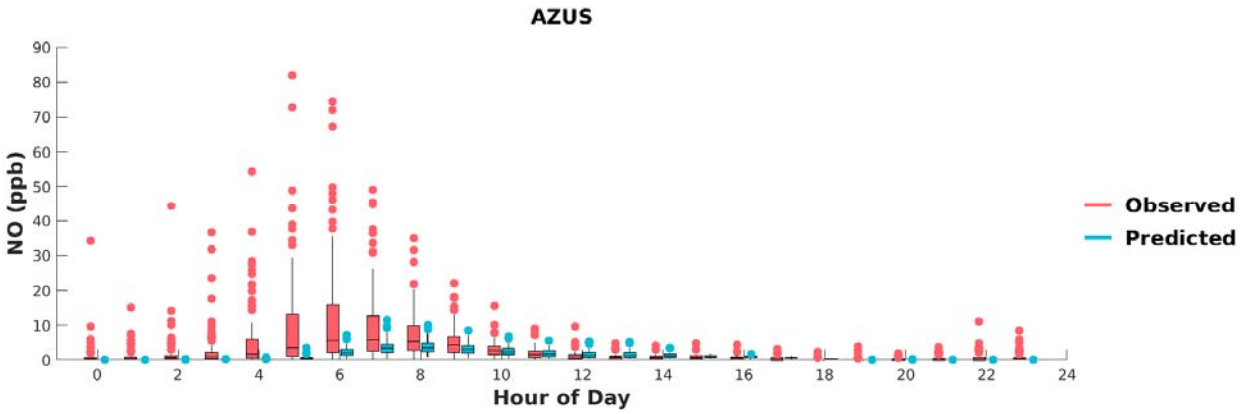

FIGURE G-2: BOX PLOTS OF OBSERVED VS. PREDICTED HOURLY NO DURING MAY 1ST TO SEPTEMBER 30TH, 2018, AT AZUSA. HORIZANTAL LINES INDICATE 25TH, 50TH (MEDIAN), AND 75TH PERCENTILES.

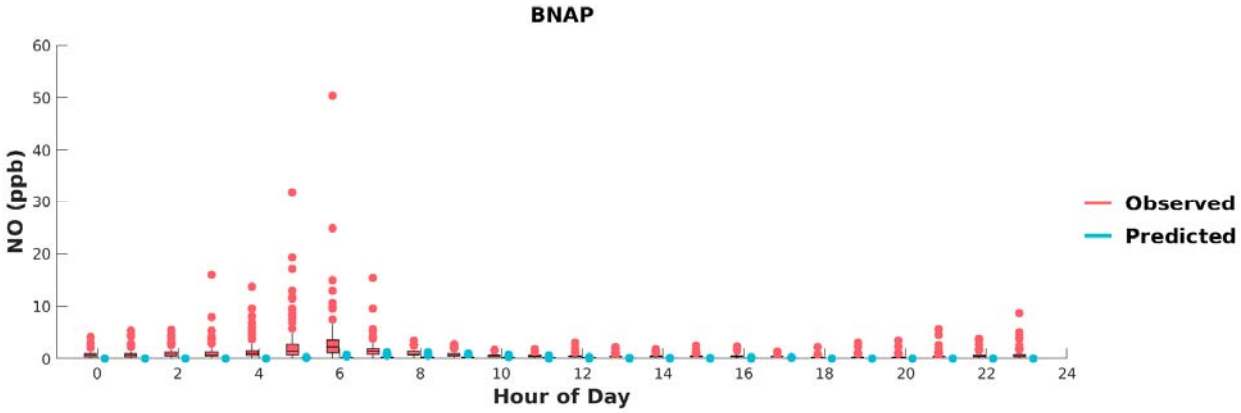

FIGURE G-3: BOX PLOTS OF OBSERVED VS. PREDICTED HOURLY NO DURING MAY 1ST TO SEPTEMBER 30TH, 2018, AT BANNING. HORIZANTAL LINES INDICATE 25TH, 50TH (MEDIAN), AND 75TH PERCENTILES.

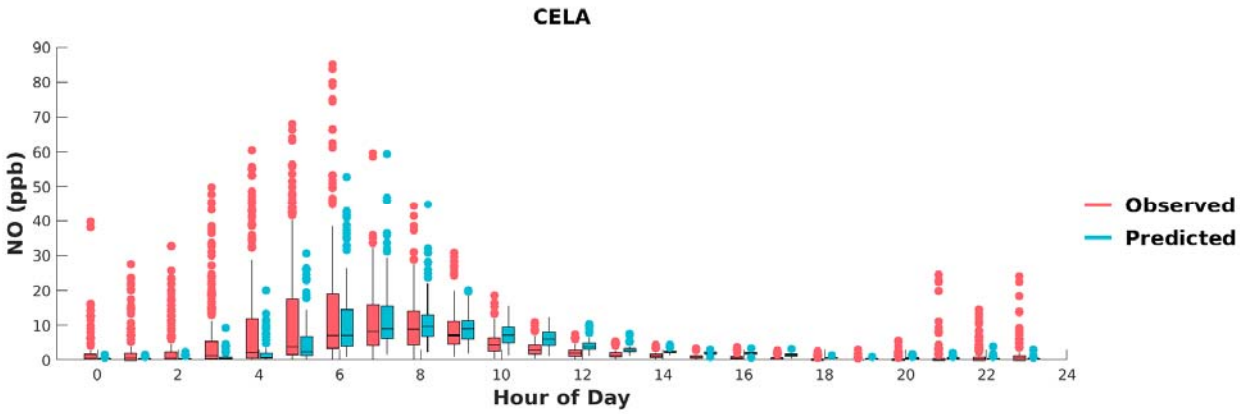

FIGURE G-4: BOX PLOTS OF OBSERVED VS. PREDICTED HOURLY NO DURING MAY 1ST TO SEPTEMBER 30TH, 2018, AT CENTRAL LOS ANGELES. HORIZANTAL LINES INDICATE 25TH, 50TH (MEDIAN), AND 75TH PERCENTILES.

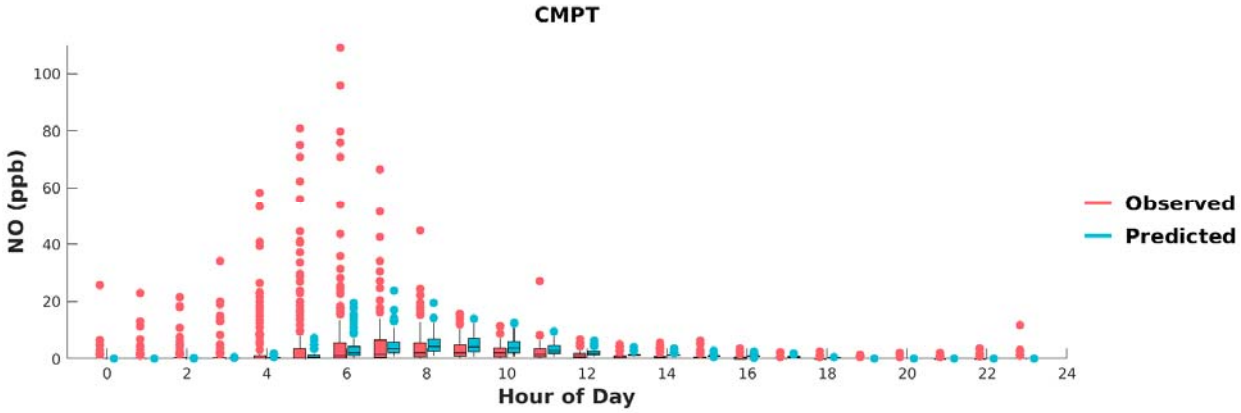

FIGURE G-5: BOX PLOTS OF OBSERVED VS. PREDICTED HOURLY NO DURING MAY 1ST TO SEPTEMBER 30TH, 2018, AT COMPTON. HORIZANTAL LINES INDICATE 25TH, 50TH (MEDIAN), AND 75TH PERCENTILES.

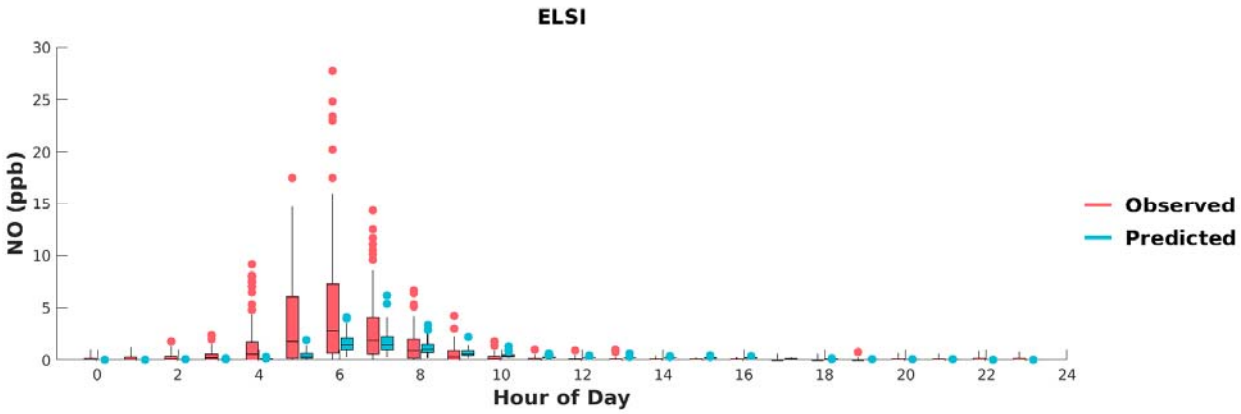

FIGURE G-6: BOX PLOTS OF OBSERVED VS. PREDICTED HOURLY NO DURING MAY 1ST TO SEPTEMBER 30TH, 2018, AT LAKE ELSINORE. HORIZANTAL LINES INDICATE 25TH, 50TH (MEDIAN), AND 75TH PERCENTILES.

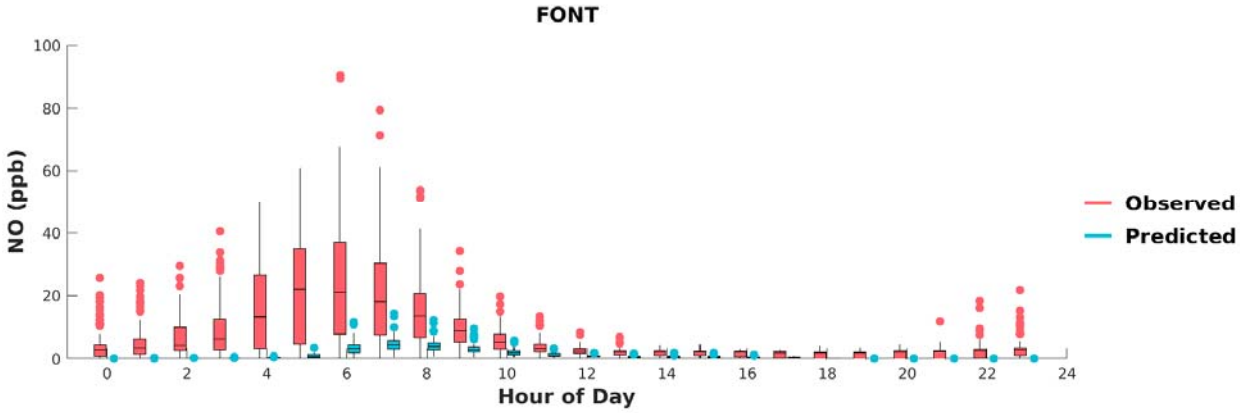

FIGURE G-7: BOX PLOTS OF OBSERVED VS. PREDICTED HOURLY NO DURING MAY 1ST TO SEPTEMBER 30TH, 2018, AT FONTANA. HORIZANTAL LINES INDICATE 25TH, 50TH (MEDIAN), AND 75TH PERCENTILES.

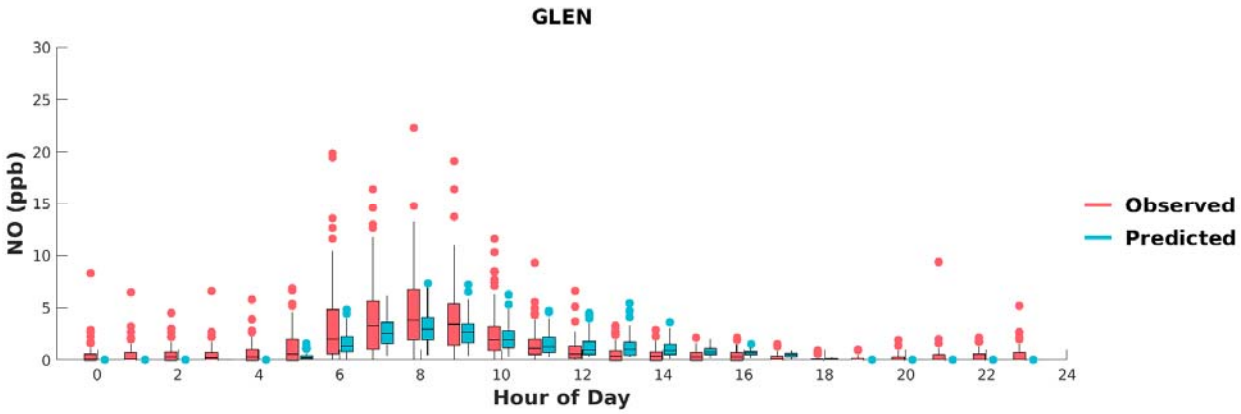

FIGURE G-8: BOX PLOTS OF OBSERVED VS. PREDICTED HOURLY NO DURING MAY 1ST TO SEPTEMBER 30TH, 2018, AT GLENDORA. HORIZANTAL LINES INDICATE 25TH, 50TH (MEDIAN), AND 75TH PERCENTILES.

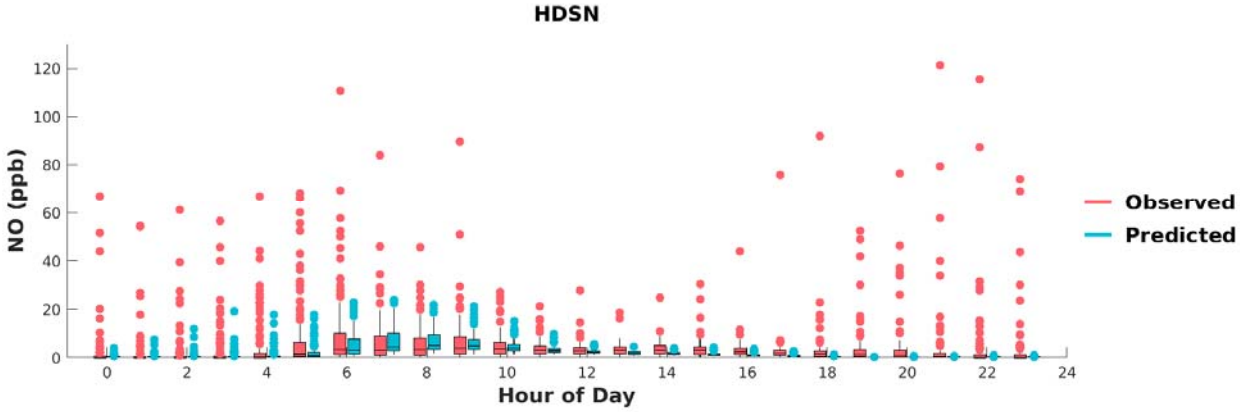

FIGURE G-9: BOX PLOTS OF OBSERVED VS. PREDICTED HOURLY NO DURING MAY 1ST TO SEPTEMBER 30TH, 2018, AT HUDSON. HORIZANTAL LINES INDICATE 25TH, 50TH (MEDIAN), AND 75TH PERCENTILES.

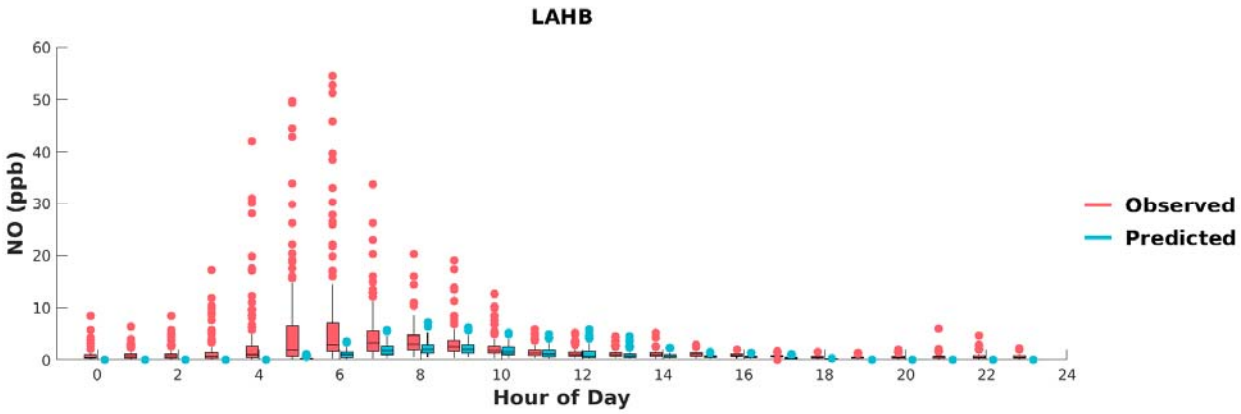

FIGURE G-10: BOX PLOTS OF OBSERVED VS. PREDICTED HOURLY NO DURING MAY 1ST TO SEPTEMBER 30TH, 2018, AT LA HABRA. HORIZANTAL LINES INDICATE 25TH, 50TH (MEDIAN), AND 75TH PERCENTILES.

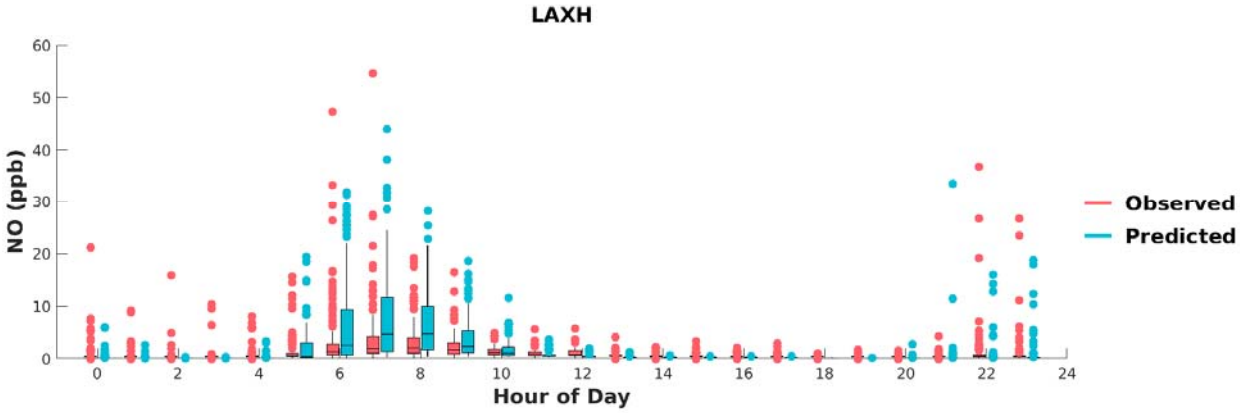

FIGURE G-11: BOX PLOTS OF OBSERVED VS. PREDICTED HOURLY NO DURING MAY 1ST TO SEPTEMBER 30TH, 2018, AT LAX. HORIZANTAL LINES INDICATE 25TH, 50TH (MEDIAN), AND 75TH PERCENTILES.

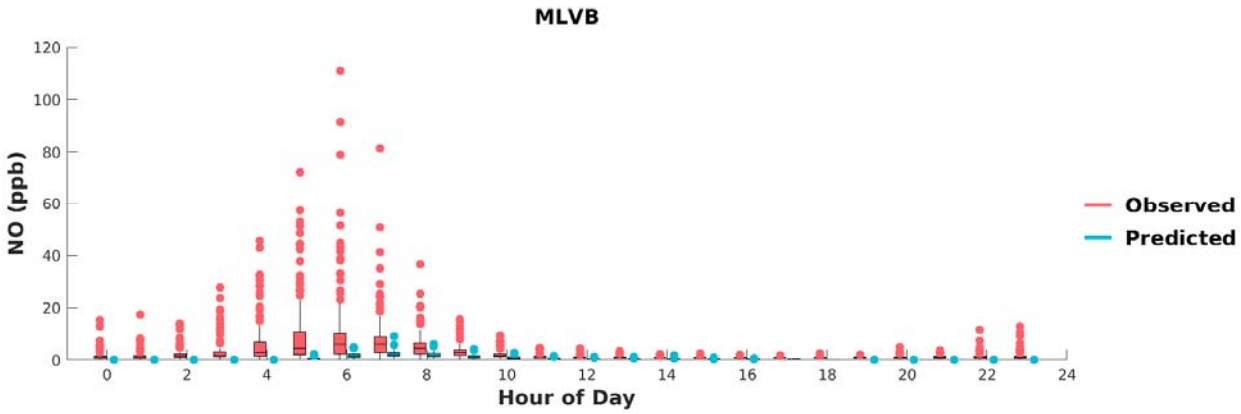

FIGURE G-12: BOX PLOTS OF OBSERVED VS. PREDICTED HOURLY NO DURING MAY 1ST TO SEPTEMBER 30TH, 2018, AT MIRA LOMA VAN BUREN. HORIZANTAL LINES INDICATE 25TH, 50TH (MEDIAN), AND 75TH PERCENTILES.

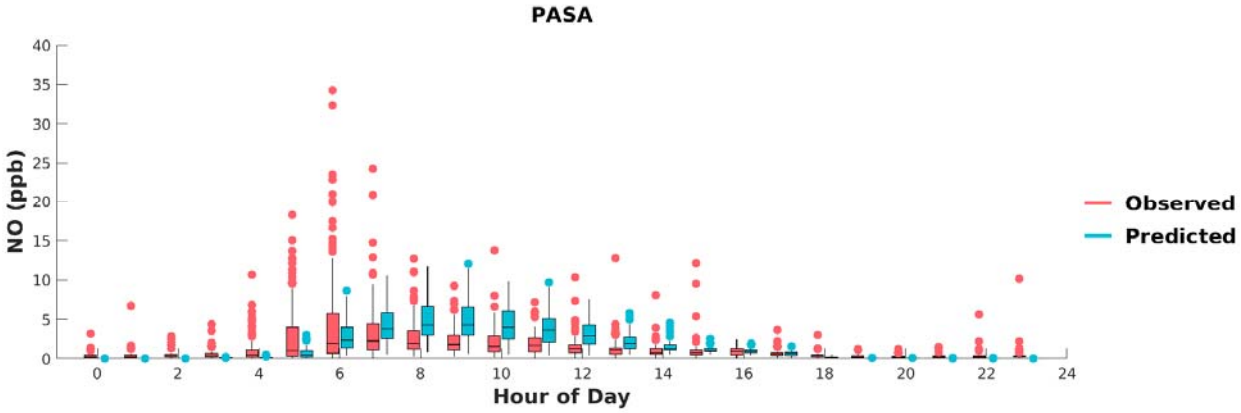

FIGURE G-13: BOX PLOTS OF OBSERVED VS. PREDICTED HOURLY NO DURING MAY 1ST TO SEPTEMBER 30TH, 2018, AT PASADENA. HORIZANTAL LINES INDICATE 25TH, 50TH (MEDIAN), AND 75TH PERCENTILES.

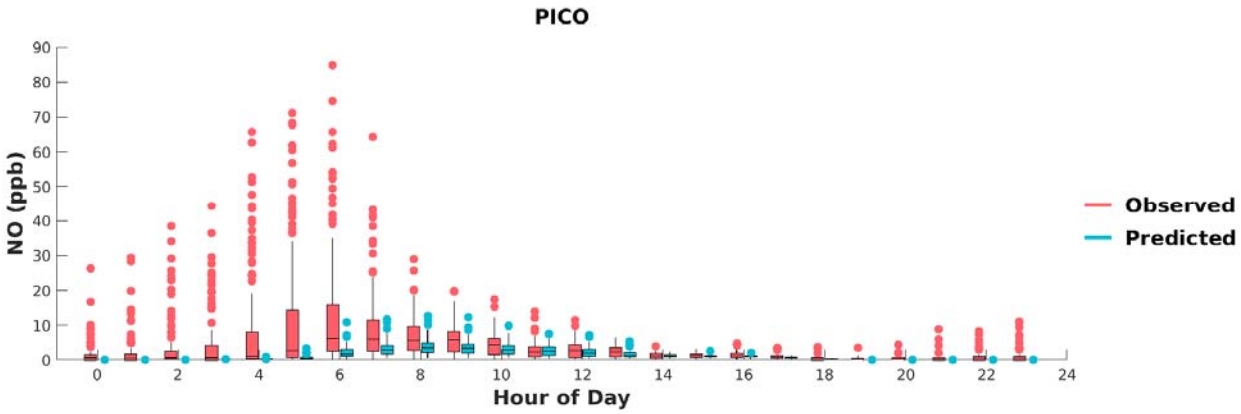

FIGURE G-14: BOX PLOTS OF OBSERVED VS. PREDICTED HOURLY NO DURING MAY 1ST TO SEPTEMBER 30TH, 2018, AT PICO RIVERO. HORIZANTAL LINES INDICATE 25TH, 50TH (MEDIAN), AND 75TH PERCENTILES.

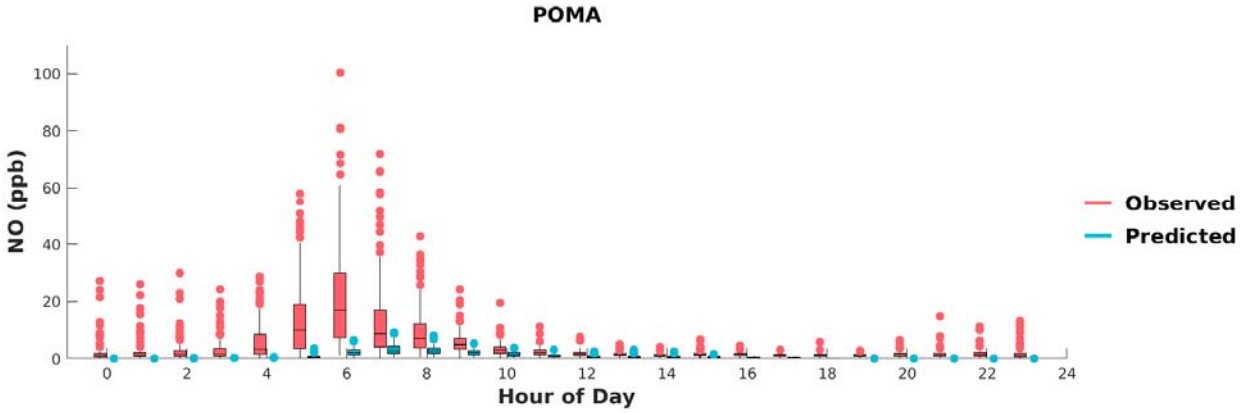

FIGURE G-15: BOX PLOTS OF OBSERVED VS. PREDICTED HOURLY NO DURING MAY 1ST TO SEPTEMBER 30TH, 2018, AT POMONA. HORIZANTAL LINES INDICATE 25TH, 50TH (MEDIAN), AND 75TH PERCENTILES.

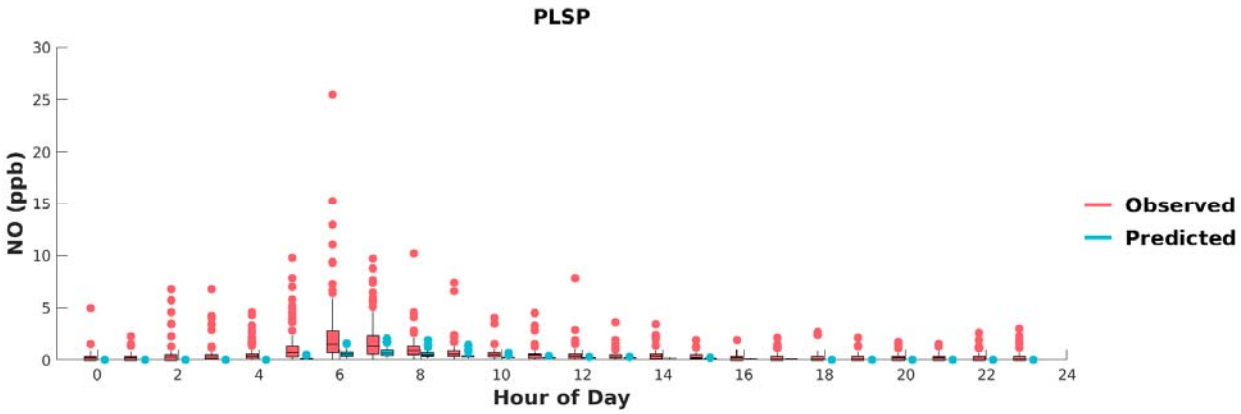

FIGURE G-16: BOX PLOTS OF OBSERVED VS. PREDICTED HOURLY NO DURING MAY 1ST TO SEPTEMBER 30TH, 2018, AT PALM SPRINGS. HORIZANTAL LINES INDICATE 25TH, 50TH (MEDIAN), AND 75TH PERCENTILES.

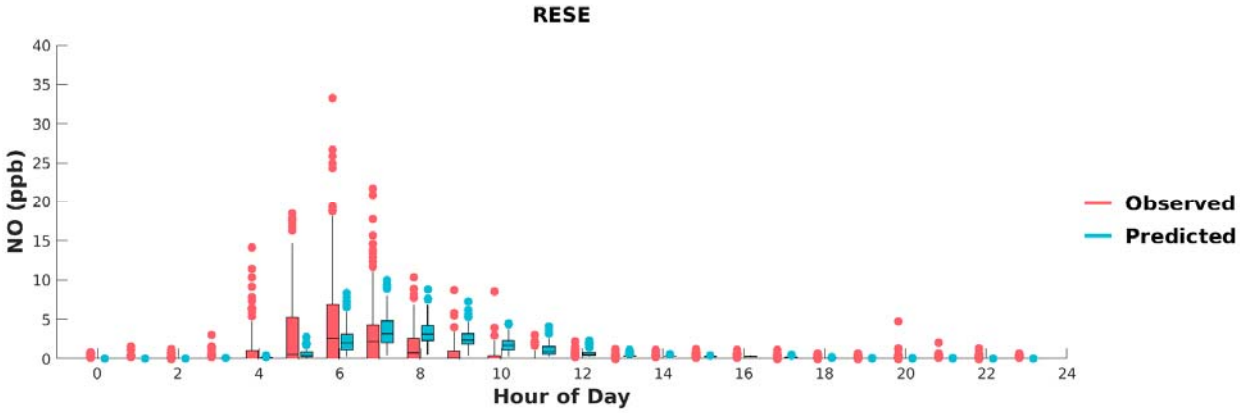

FIGURE G-17: BOX PLOTS OF OBSERVED VS. PREDICTED HOURLY NO DURING MAY 1ST TO SEPTEMBER 30TH, 2018, AT RESEDA. HORIZANTAL LINES INDICATE 25TH, 50TH (MEDIAN), AND 75TH PERCENTILES.

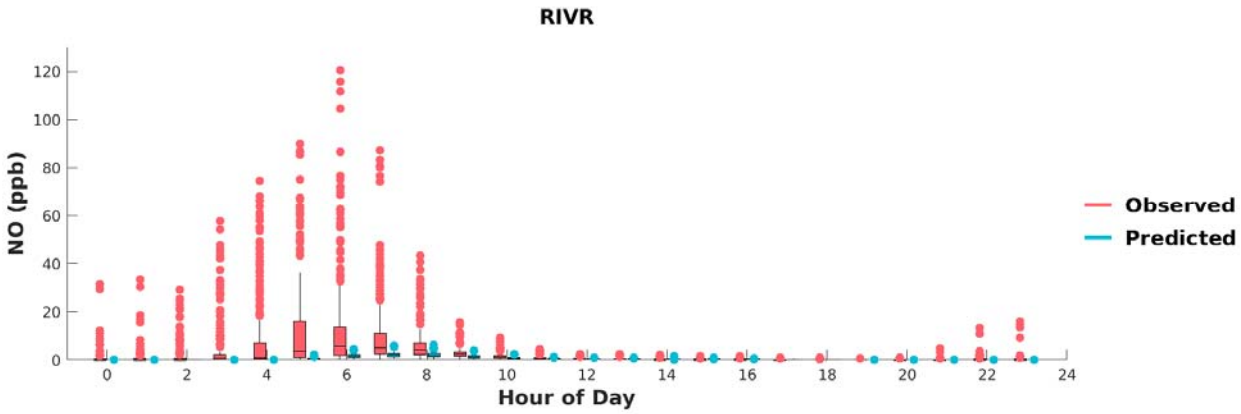

FIGURE G-18: BOX PLOTS OF OBSERVED VS. PREDICTED HOURLY NO DURING MAY 1ST TO SEPTEMBER 30TH, 2018, AT RIVERSIDE. HORIZANTAL LINES INDICATE 25TH, 50TH (MEDIAN), AND 75TH PERCENTILES.

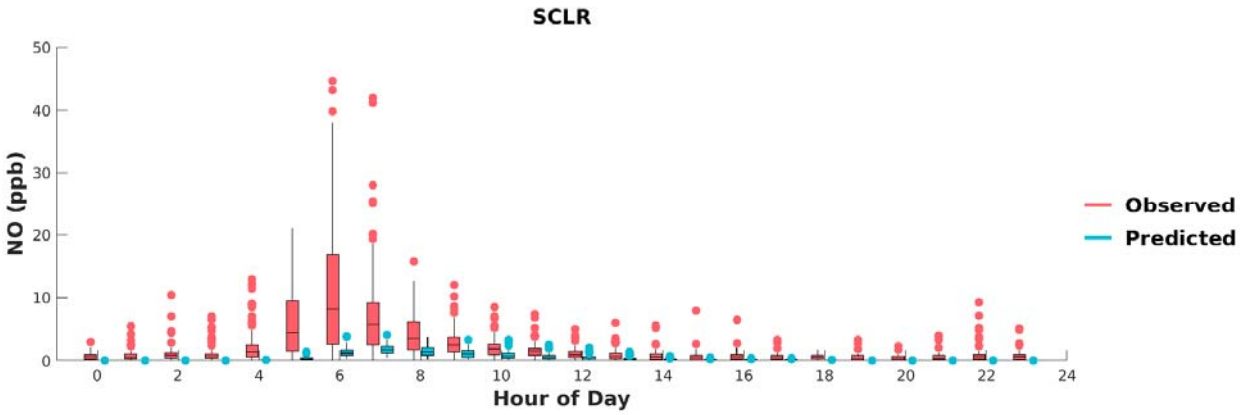

FIGURE G-19: BOX PLOTS OF OBSERVED VS. PREDICTED HOURLY NO DURING MAY 1ST TO SEPTEMBER 30TH, 2018, AT SANTA CLARITA. HORIZANTAL LINES INDICATE 25TH, 50TH (MEDIAN), AND 75TH PERCENTILES.

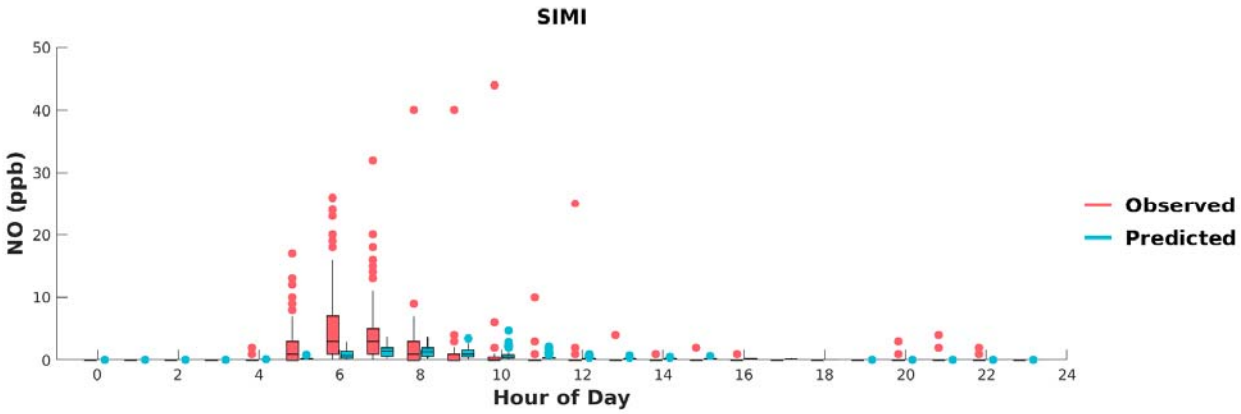

FIGURE G-20: BOX PLOTS OF OBSERVED VS. PREDICTED HOURLY NO DURING MAY 1ST TO SEPTEMBER 30TH, 2018, AT SIMI VALLEY. HORIZANTAL LINES INDICATE 25TH, 50TH (MEDIAN), AND 75TH PERCENTILES.

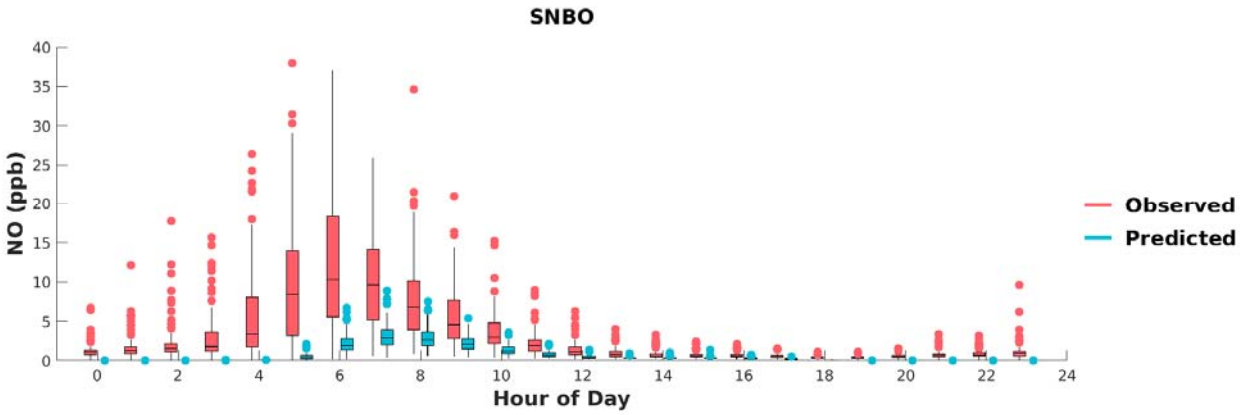

FIGURE G-21: BOX PLOTS OF OBSERVED VS. PREDICTED HOURLY NO DURING MAY 1ST TO SEPTEMBER 30TH, 2018, AT SAN BERNARDINO. HORIZANTAL LINES INDICATE 25TH, 50TH (MEDIAN), AND 75TH PERCENTILES.

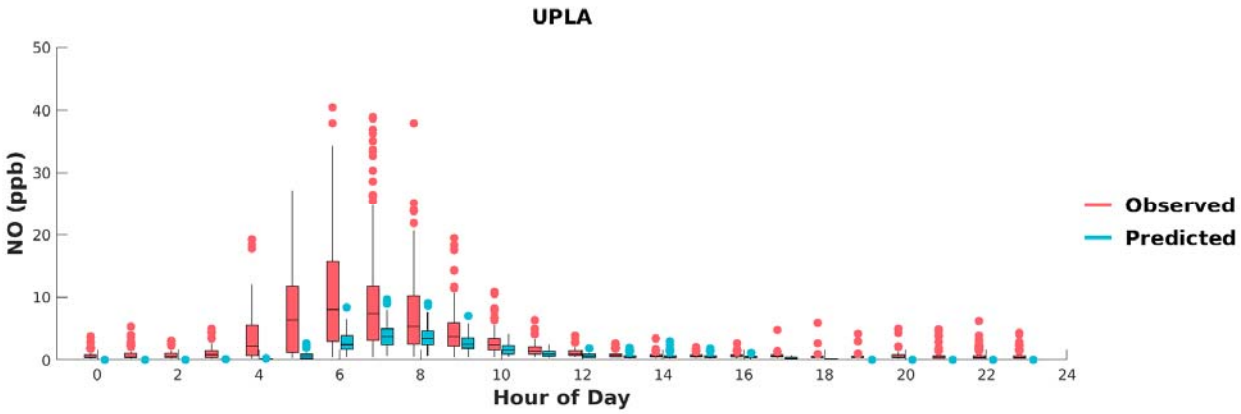

FIGURE G-22: BOX PLOTS OF OBSERVED VS. PREDICTED HOURLY NO DURING MAY 1ST TO SEPTEMBER 30TH, 2018, AT UPLAND. HORIZANTAL LINES INDICATE 25TH, 50TH (MEDIAN), AND 75TH PERCENTILES.

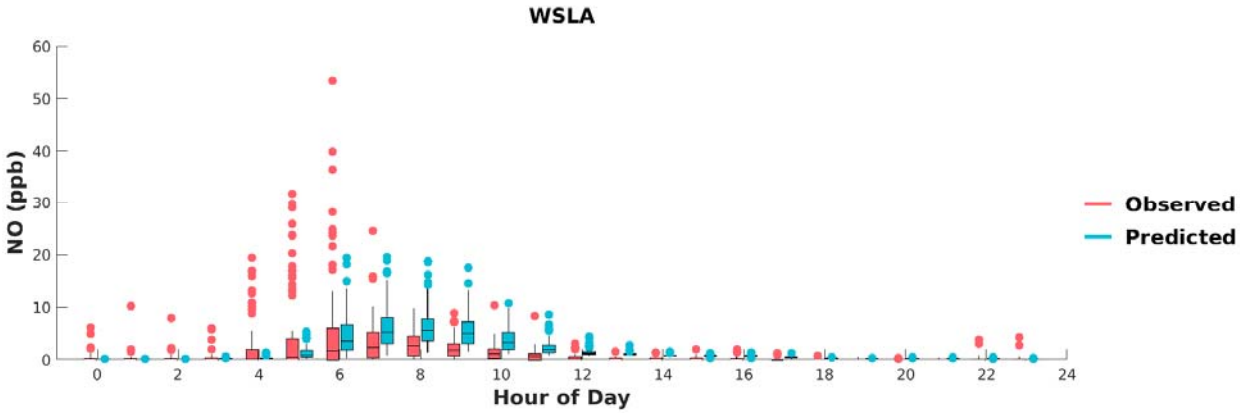

FIGURE G-23: BOX PLOTS OF OBSERVED VS. PREDICTED HOURLY NO DURING MAY 1ST TO SEPTEMBER 30TH, 2018, AT WEST LOS ANGELES. HORIZANTAL LINES INDICATE 25TH, 50TH (MEDIAN), AND 75TH PERCENTILES.

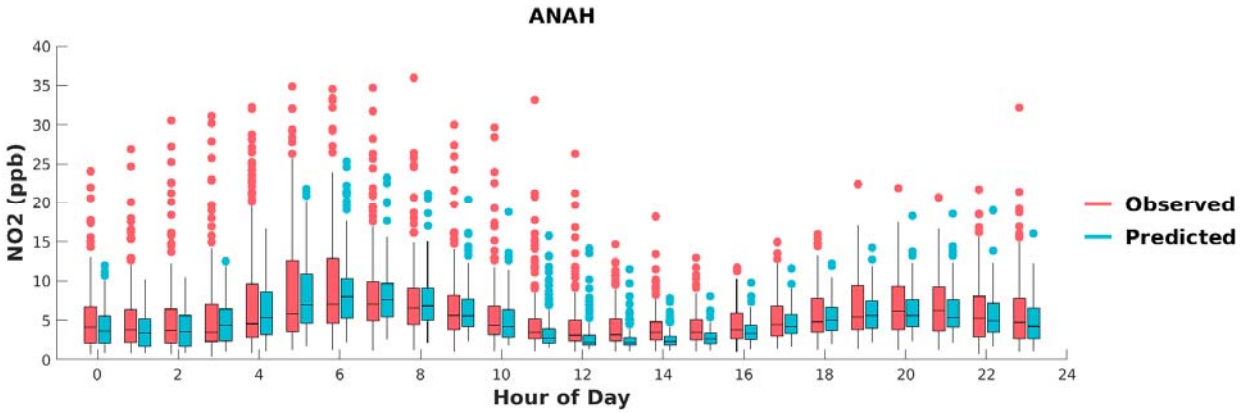

FIGURE H-1: BOX PLOTS OF OBSERVED VS. PREDICTED HOURLY NO2 DURING MAY 1ST TO SEPTEMBER 30TH, 2018, AT ANAHEIM. HORIZANTAL LINES INDICATE 25TH, 50TH (MEDIAN), AND 75TH PERCENTILES.

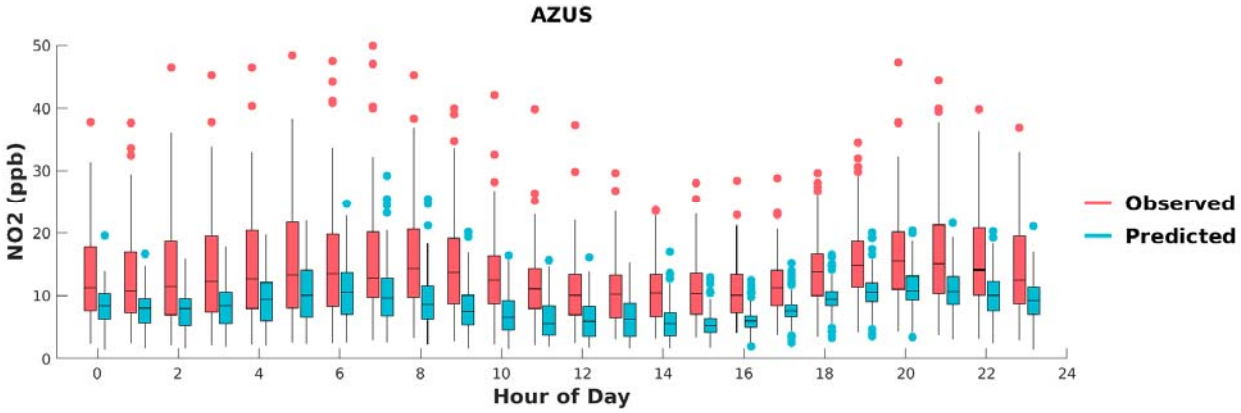

FIGURE H-2: BOX PLOTS OF OBSERVED VS. PREDICTED HOURLY NO2 DURING MAY 1ST TO SEPTEMBER 30TH, 2018, AT AZUSA. HORIZANTAL LINES INDICATE 25TH, 50TH (MEDIAN), AND 75TH PERCENTILES.

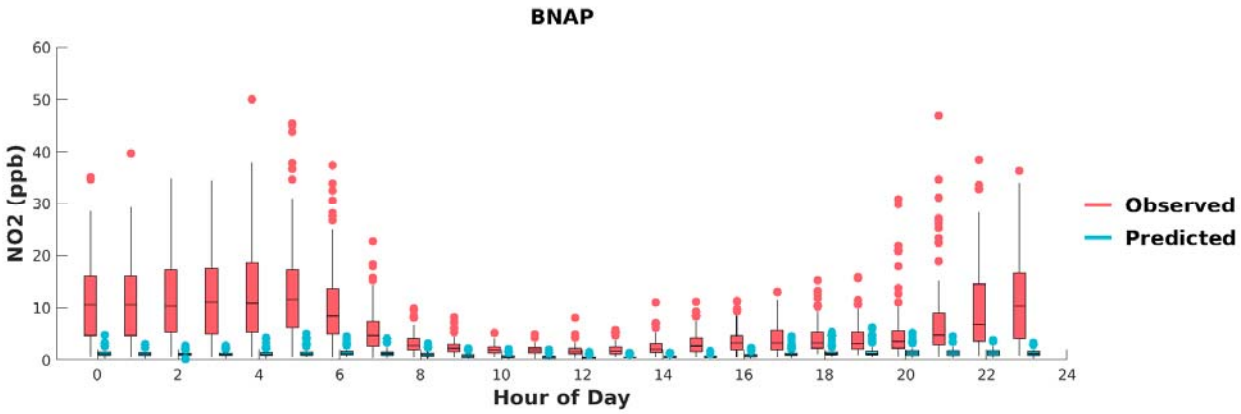

FIGURE H-3: BOX PLOTS OF OBSERVED VS. PREDICTED HOURLY NO2 DURING MAY 1ST TO SEPTEMBER 30TH, 2018, AT BANNING. HORIZANTAL LINES INDICATE 25TH, 50TH (MEDIAN), AND 75TH PERCENTILES.

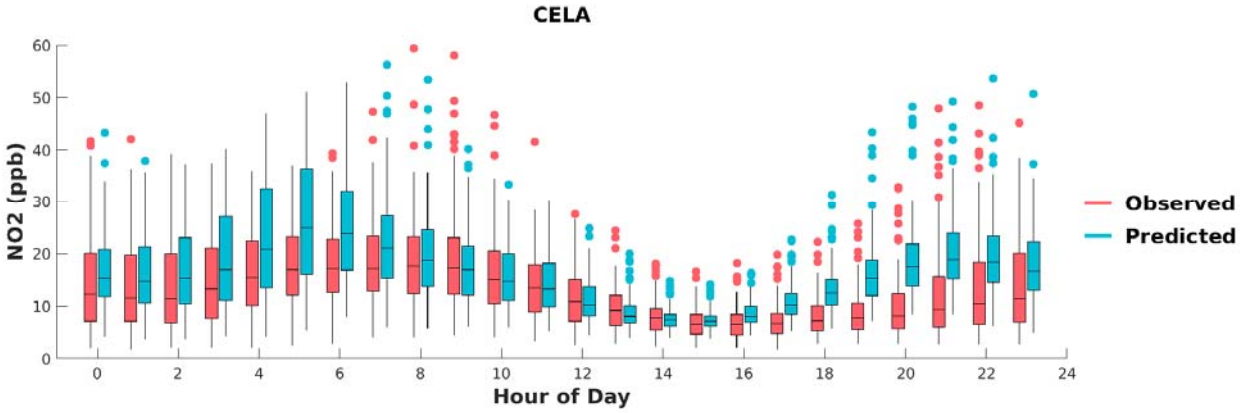

FIGURE H-4: BOX PLOTS OF OBSERVED VS. PREDICTED HOURLY NO2 DURING MAY 1ST TO SEPTEMBER 30TH, 2018, AT CENTRAL LOS ANGELES. HORIZANTAL LINES INDICATE 25TH, 50TH (MEDIAN), AND 75TH PERCENTILES.

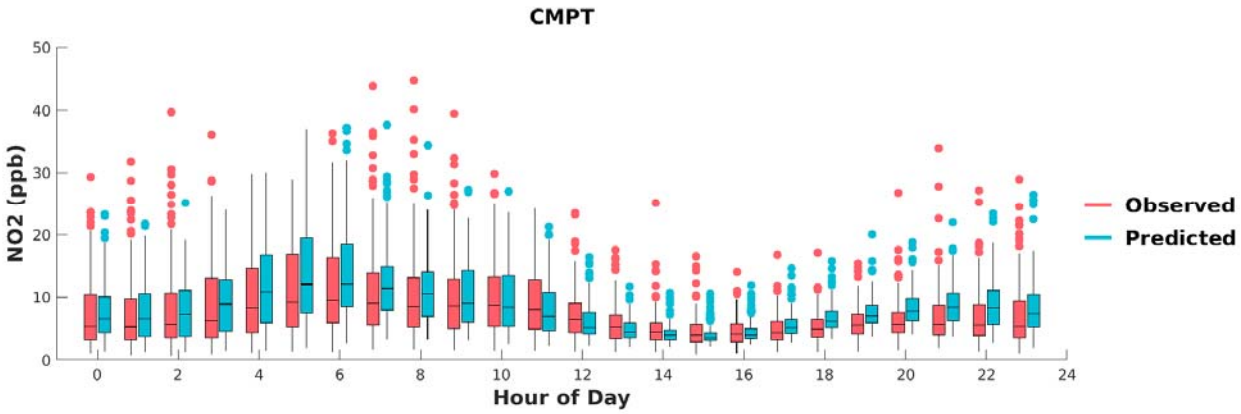

FIGURE H-5: BOX PLOTS OF OBSERVED VS. PREDICTED HOURLY NO2 DURING MAY 1ST TO SEPTEMBER 30TH, 2018, AT COMPTON. HORIZANTAL LINES INDICATE 25TH, 50TH (MEDIAN), AND 75TH PERCENTILES.

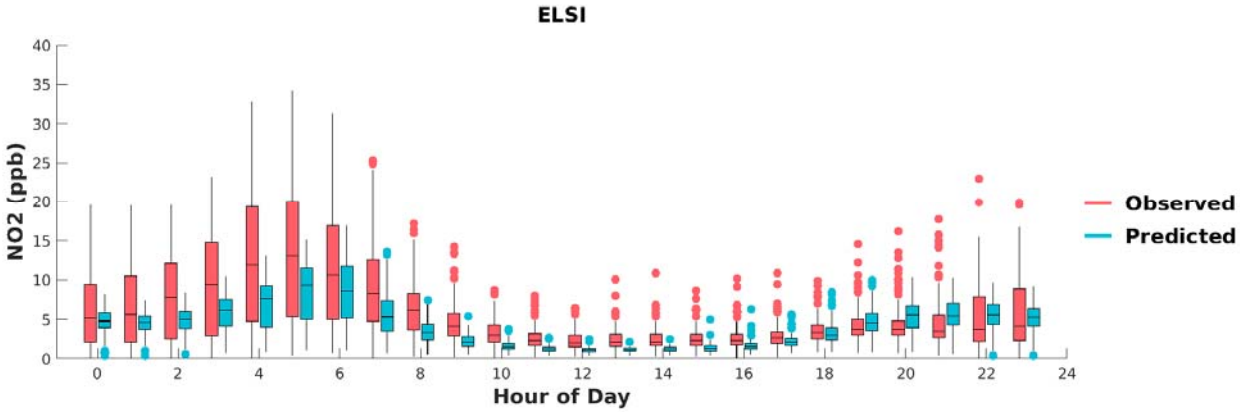

FIGURE H-6: BOX PLOTS OF OBSERVED VS. PREDICTED HOURLY NO2 DURING MAY 1ST TO SEPTEMBER 30TH, 2018, AT LAKE ELSINORE. HORIZANTAL LINES INDICATE 25TH, 50TH (MEDIAN), AND 75TH PERCENTILES.

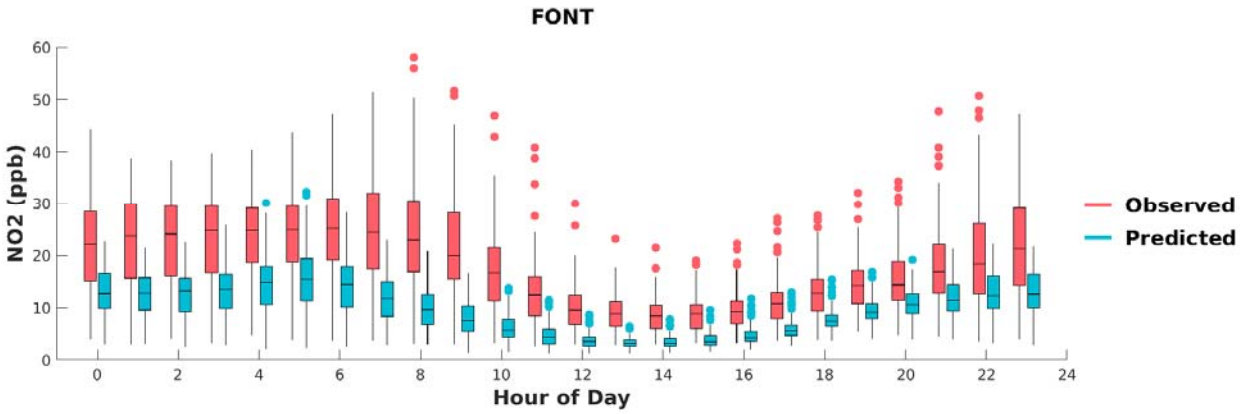

FIGURE H-7: BOX PLOTS OF OBSERVED VS. PREDICTED HOURLY NO2 DURING MAY 1ST TO SEPTEMBER 30TH, 2018, AT FONTANA. HORIZANTAL LINES INDICATE 25TH, 50TH (MEDIAN), AND 75TH PERCENTILES.

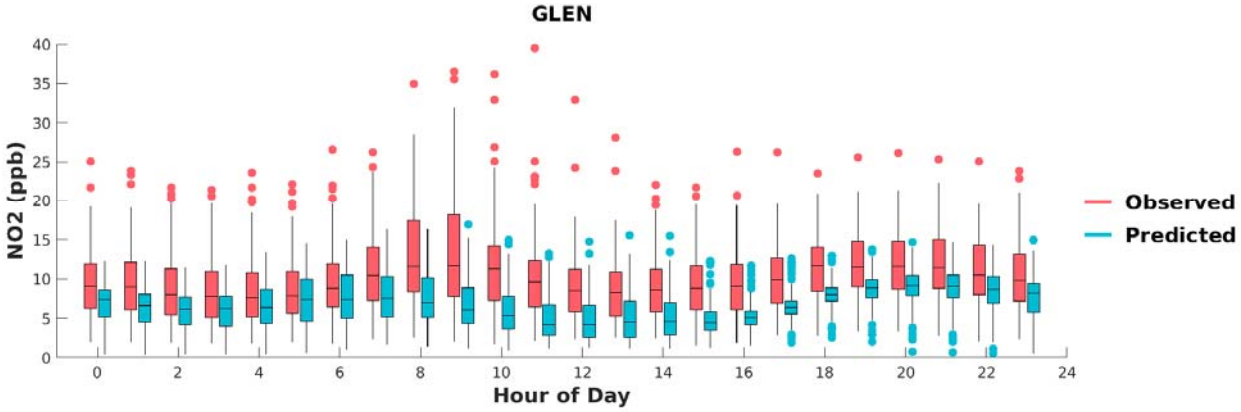

FIGURE H-8: BOX PLOTS OF OBSERVED VS. PREDICTED HOURLY NO2 DURING MAY 1ST TO SEPTEMBER 30TH, 2018, AT GLENDORA. HORIZANTAL LINES INDICATE 25TH, 50TH (MEDIAN), AND 75TH PERCENTILES.

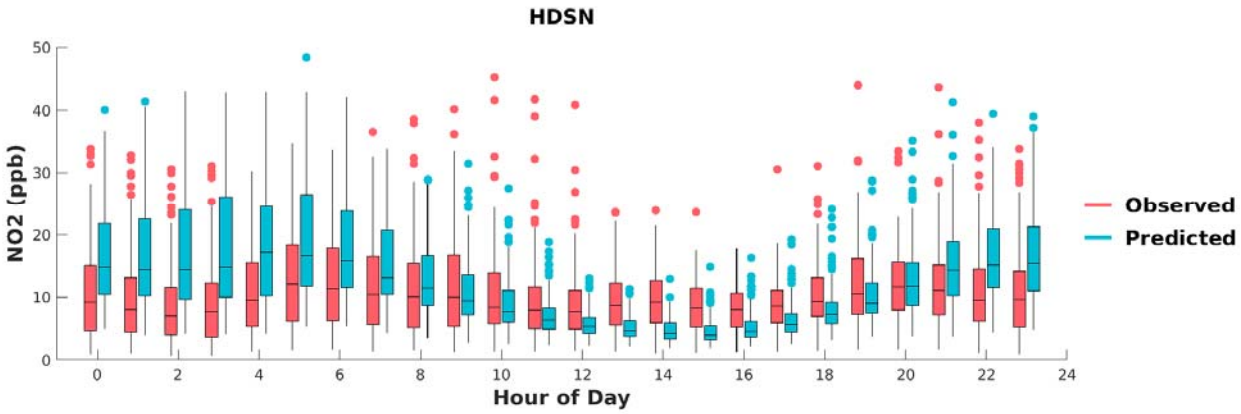

FIGURE H-9: BOX PLOTS OF OBSERVED VS. PREDICTED HOURLY NO2 DURING MAY 1ST TO SEPTEMBER 30TH, 2018, AT HUDSON. HORIZANTAL LINES INDICATE 25TH, 50TH (MEDIAN), AND 75TH PERCENTILES.

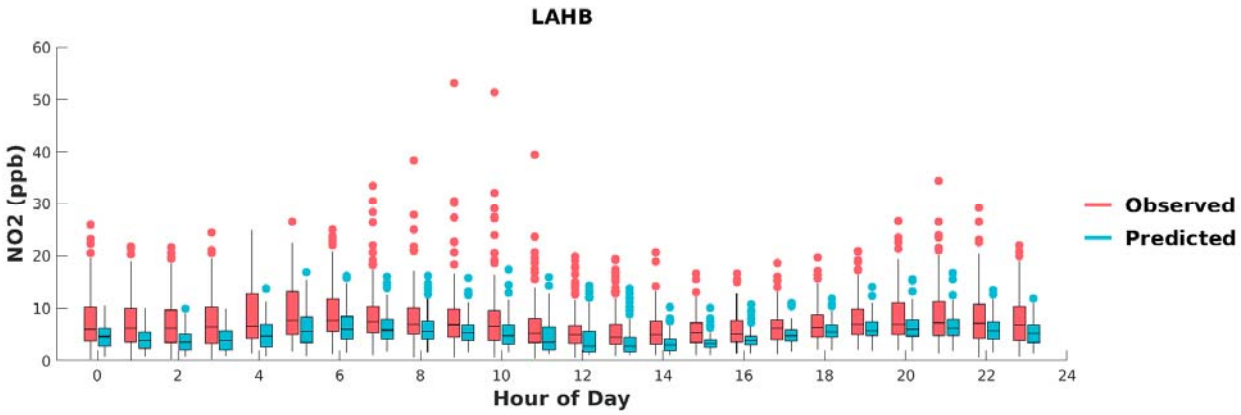

FIGURE H-10: BOX PLOTS OF OBSERVED VS. PREDICTED HOURLY NO2 DURING MAY 1ST TO SEPTEMBER 30TH, 2018, AT LA HABRA. HORIZANTAL LINES INDICATE 25TH, 50TH (MEDIAN), AND 75TH PERCENTILES.

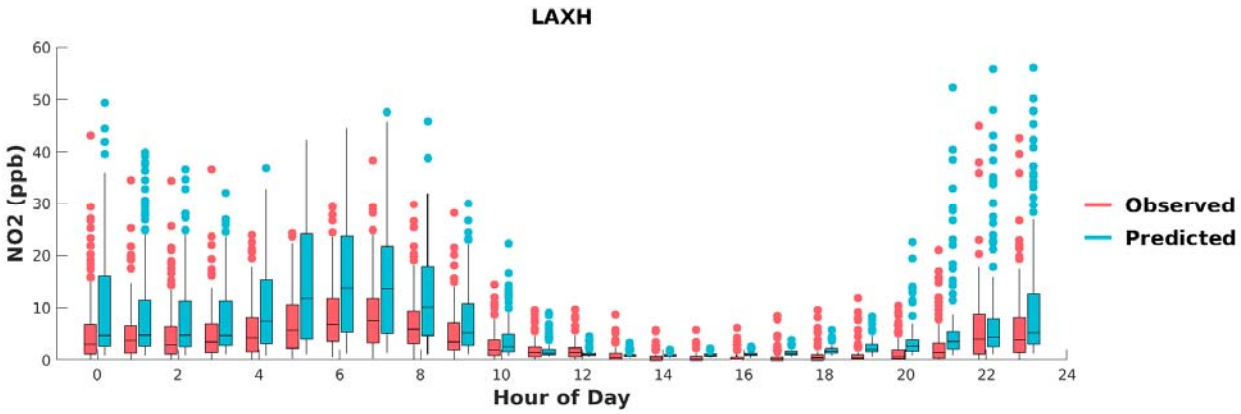

FIGURE H-11: BOX PLOTS OF OBSERVED VS. PREDICTED HOURLY NO2 DURING MAY 1ST TO SEPTEMBER 30TH, 2018, AT LAX. HORIZANTAL LINES INDICATE 25TH, 50TH (MEDIAN), AND 75TH PERCENTILES.

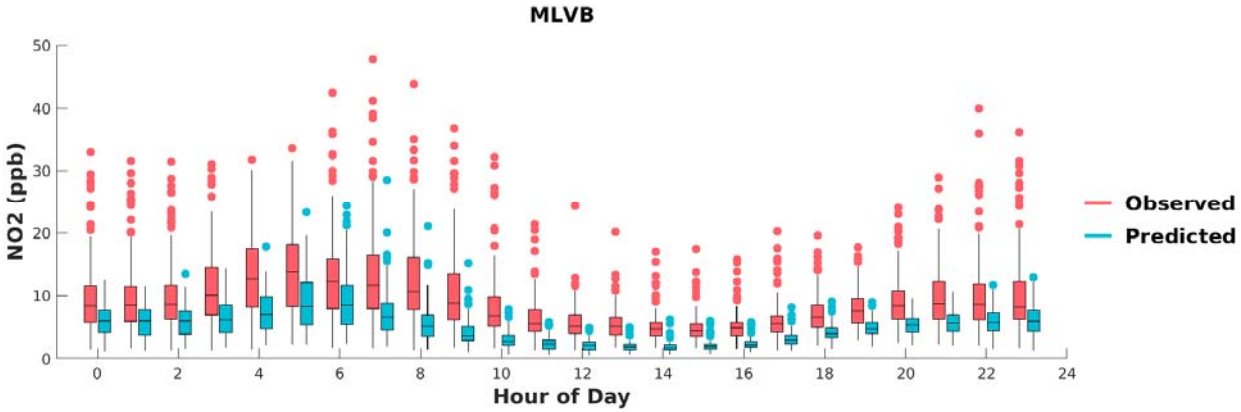

FIGURE H-12: BOX PLOTS OF OBSERVED VS. PREDICTED HOURLY NO2 DURING MAY 1ST TO SEPTEMBER 30TH, 2018, AT MIRA LOMA VAN BUREN. HORIZANTAL LINES INDICATE 25TH, 50TH (MEDIAN), AND 75TH PERCENTILES.

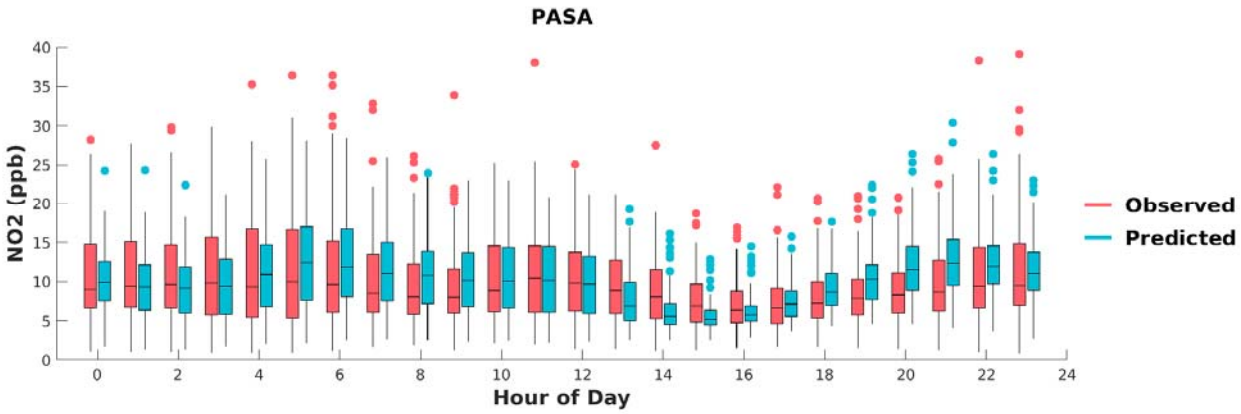

FIGURE H-13: BOX PLOTS OF OBSERVED VS. PREDICTED HOURLY NO2 DURING MAY 1ST TO SEPTEMBER 30TH, 2018, AT PASADENA. HORIZANTAL LINES INDICATE 25TH, 50TH (MEDIAN), AND 75TH PERCENTILES.

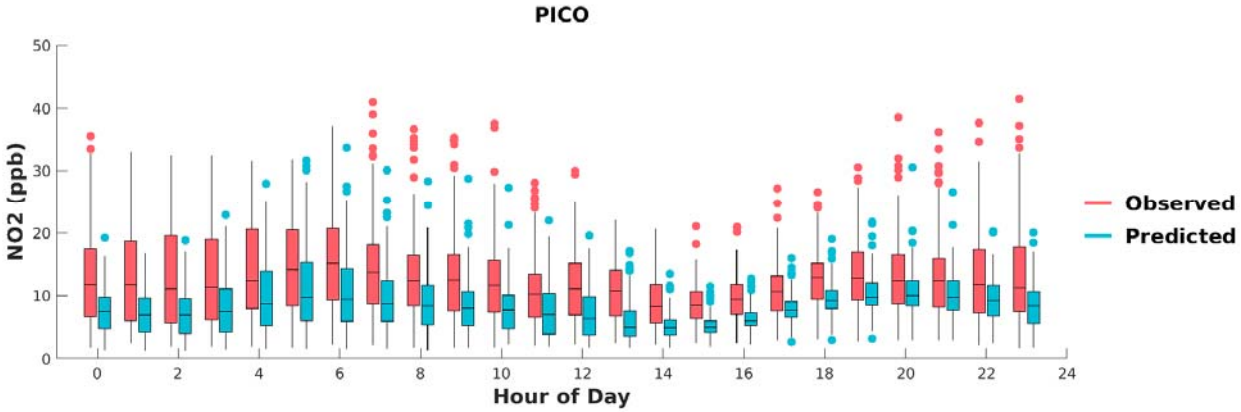

FIGURE H-14: BOX PLOTS OF OBSERVED VS. PREDICTED HOURLY NO2 DURING MAY 1ST TO SEPTEMBER 30TH, 2018, AT PICO RIVERO. HORIZANTAL LINES INDICATE 25TH, 50TH (MEDIAN), AND 75TH PERCENTILES.

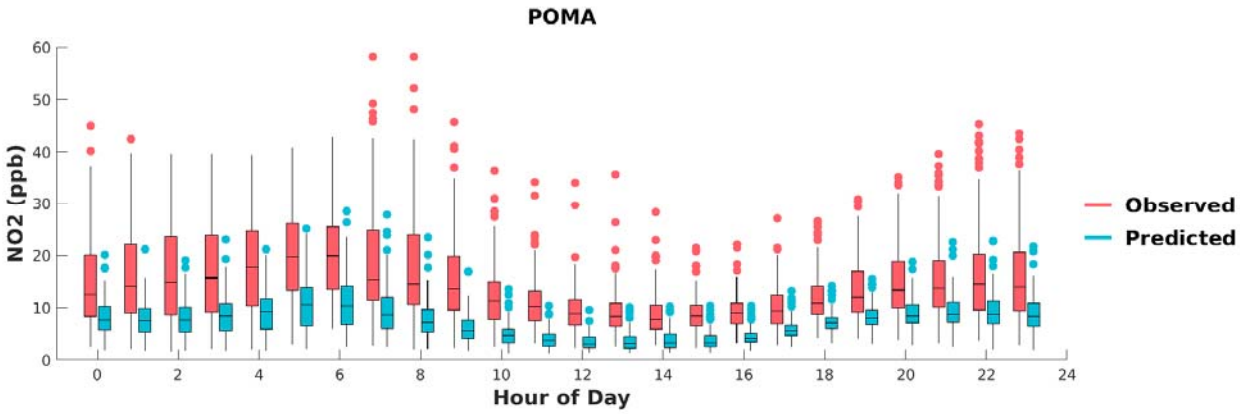

FIGURE H-15: BOX PLOTS OF OBSERVED VS. PREDICTED HOURLY NO2 DURING MAY 1ST TO SEPTEMBER 30TH, 2018, AT POMONA. HORIZANTAL LINES INDICATE 25TH, 50TH (MEDIAN), AND 75TH PERCENTILES.

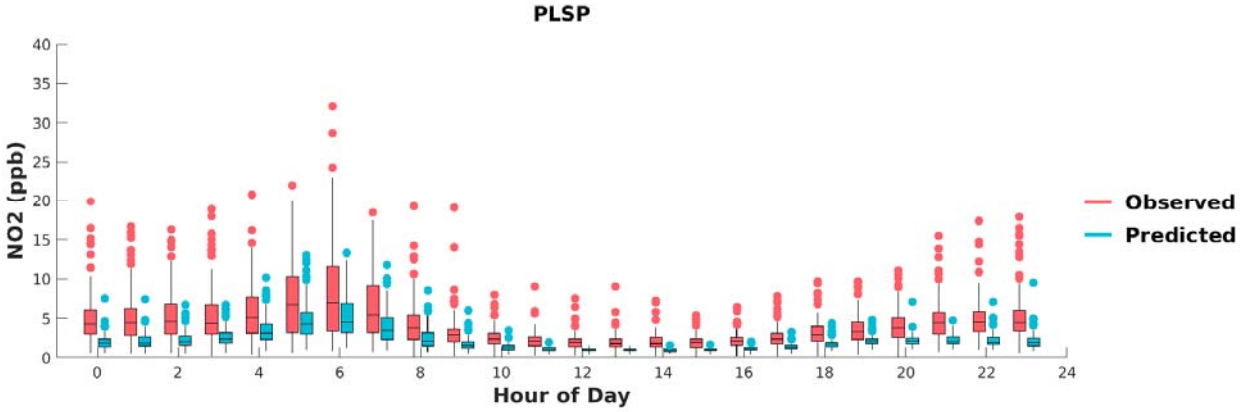

FIGURE H-16: BOX PLOTS OF OBSERVED VS. PREDICTED HOURLY NO2 DURING MAY 1ST TO SEPTEMBER 30TH, 2018, AT PALM SPRINGS. HORIZANTAL LINES INDICATE 25TH, 50TH (MEDIAN), AND 75TH PERCENTILES.

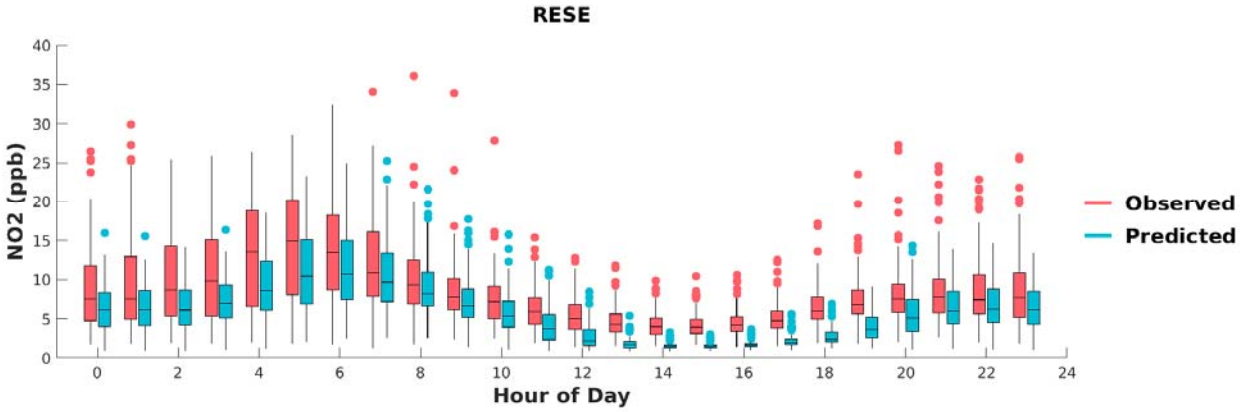

FIGURE H-17: BOX PLOTS OF OBSERVED VS. PREDICTED HOURLY NO2 DURING MAY 1ST TO SEPTEMBER 30TH, 2018, AT RESEDA. HORIZANTAL LINES INDICATE 25TH, 50TH (MEDIAN), AND 75TH PERCENTILES.

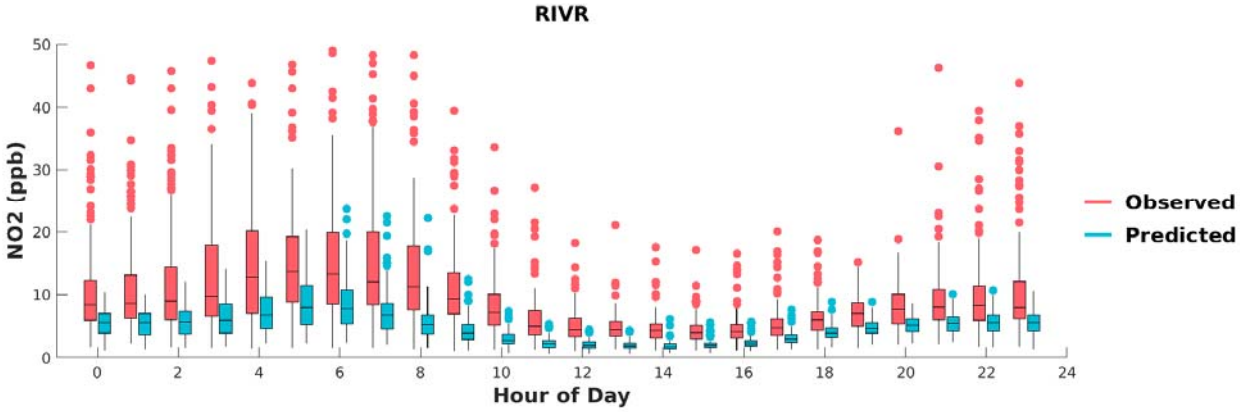

FIGURE H-18: BOX PLOTS OF OBSERVED VS. PREDICTED HOURLY NO2 DURING MAY 1ST TO SEPTEMBER 30TH, 2018, AT RIVERSIDE. HORIZANTAL LINES INDICATE 25TH, 50TH (MEDIAN), AND 75TH PERCENTILES.

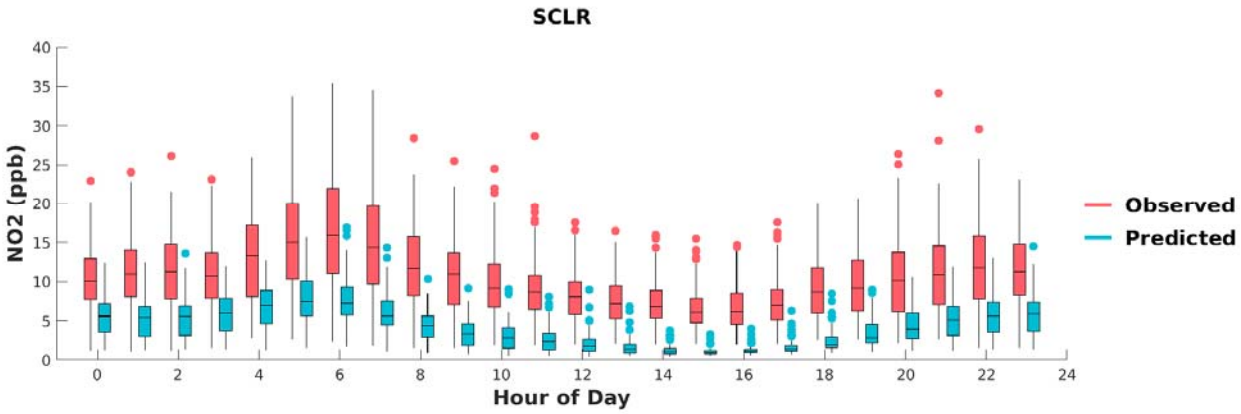

FIGURE H-19: BOX PLOTS OF OBSERVED VS. PREDICTED HOURLY NO2 DURING MAY 1ST TO SEPTEMBER 30TH, 2018, AT SANTA CLARITA. HORIZANTAL LINES INDICATE 25TH, 50TH (MEDIAN), AND 75TH PERCENTILES.

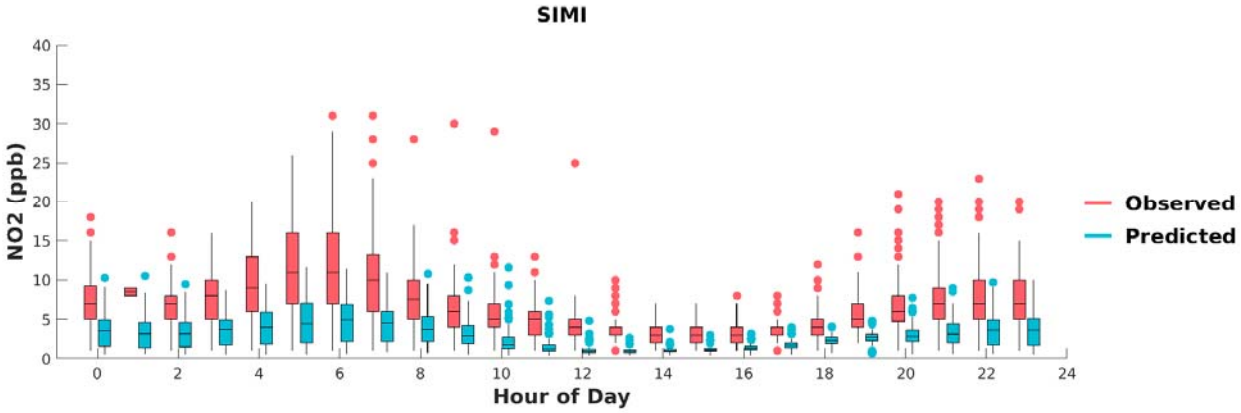

FIGURE H-20: BOX PLOTS OF OBSERVED VS. PREDICTED HOURLY NO2 DURING MAY 1ST TO SEPTEMBER 30TH, 2018, AT SIMI VALLEY. HORIZANTAL LINES INDICATE 25TH, 50TH (MEDIAN), AND 75TH PERCENTILES.

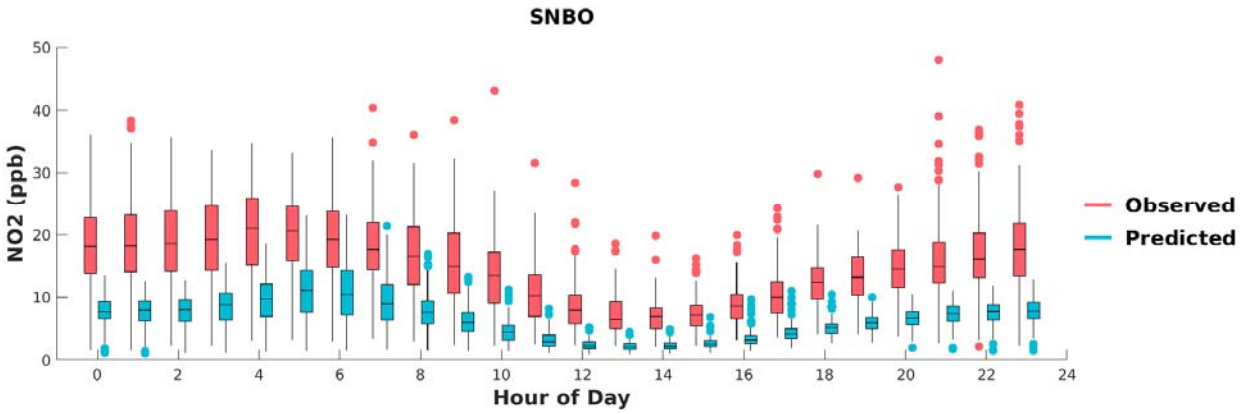

FIGURE H-21: BOX PLOTS OF OBSERVED VS. PREDICTED HOURLY NO2 DURING MAY 1ST TO SEPTEMBER 30TH, 2018, AT SAN BERNARDINO. HORIZANTAL LINES INDICATE 25TH, 50TH (MEDIAN), AND 75TH PERCENTILES.

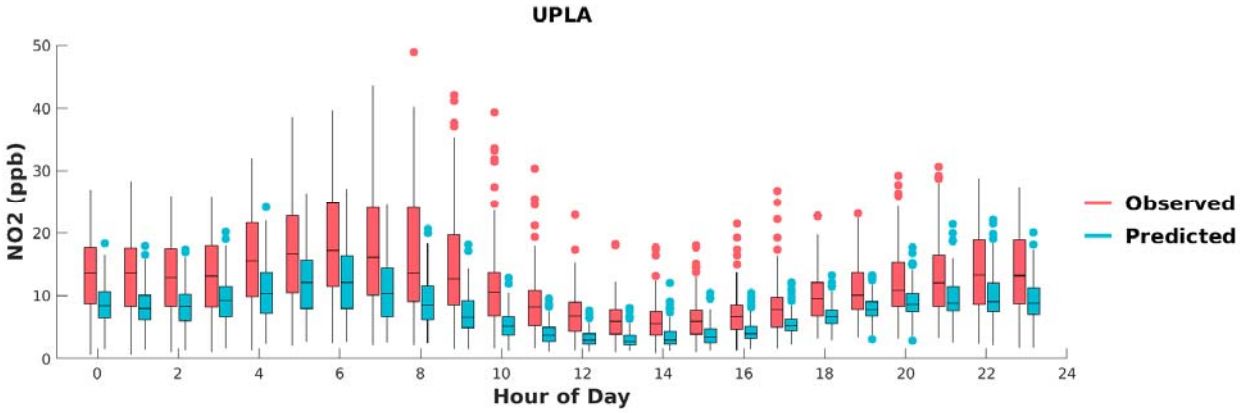

FIGURE H-22: BOX PLOTS OF OBSERVED VS. PREDICTED HOURLY NO2 DURING MAY 1ST TO SEPTEMBER 30TH, 2018, AT UPLAND. HORIZANTAL LINES INDICATE 25TH, 50TH (MEDIAN), AND 75TH PERCENTILES.

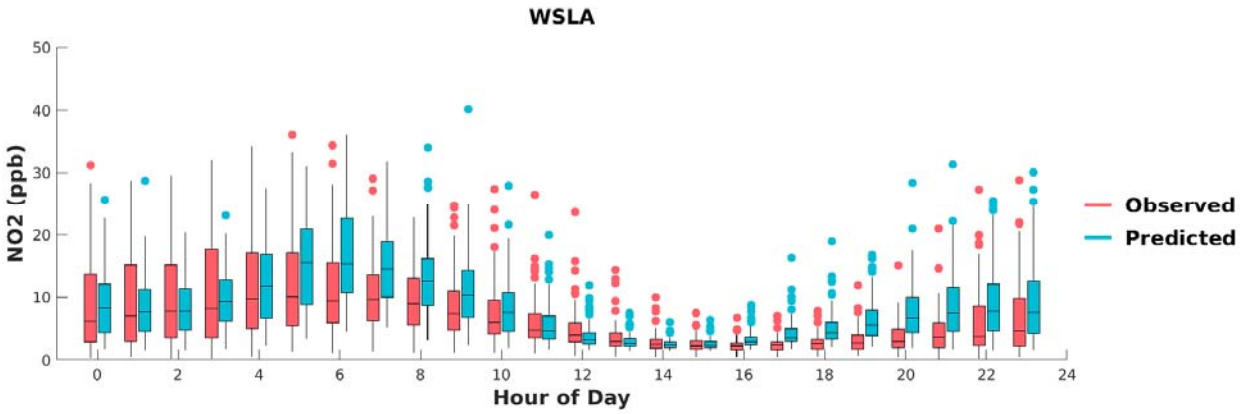

FIGURE H-23: BOX PLOTS OF OBSERVED VS. PREDICTED HOURLY NO2 DURING MAY 1ST TO SEPTEMBER 30TH, 2018, AT WEST LOS ANGELES. HORIZANTAL LINES INDICATE 25TH, 50TH (MEDIAN), AND 75TH PERCENTILES.

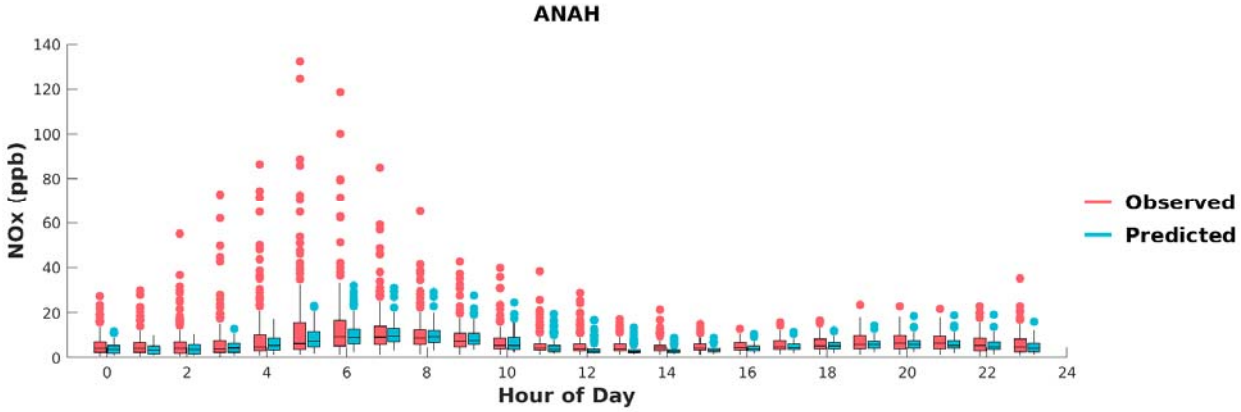

FIGURE I-1: BOX PLOTS OF OBSERVED VS. PREDICTED HOURLY NOX DURING MAY 1ST TO SEPTEMBER 30TH, 2018, AT ANAHEIM. HORIZANTAL LINES INDICATE 25TH, 50TH (MEDIAN), AND 75TH PERCENTILES.

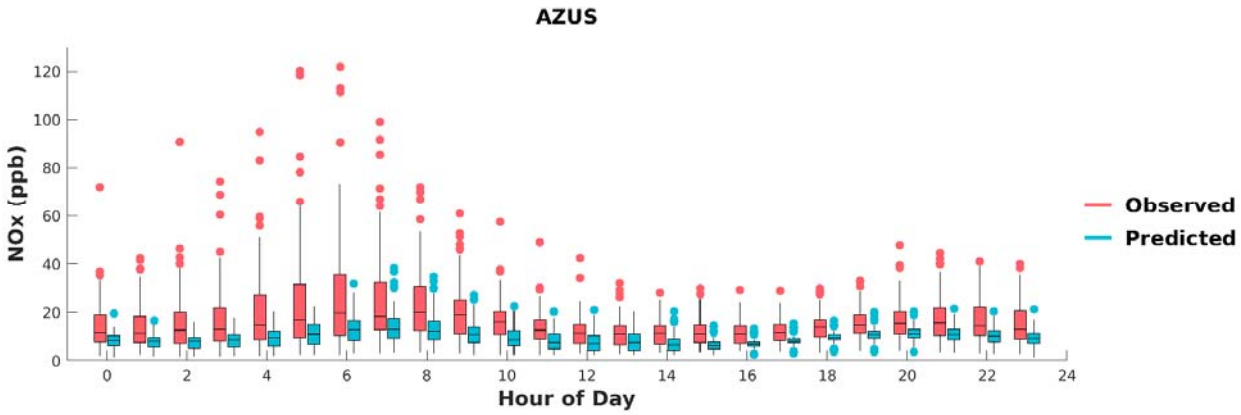

FIGURE I-2: BOX PLOTS OF OBSERVED VS. PREDICTED HOURLY NOX DURING MAY 1ST TO SEPTEMBER 30TH, 2018, AT AZUSA. HORIZANTAL LINES INDICATE 25TH, 50TH (MEDIAN), AND 75TH PERCENTILES.

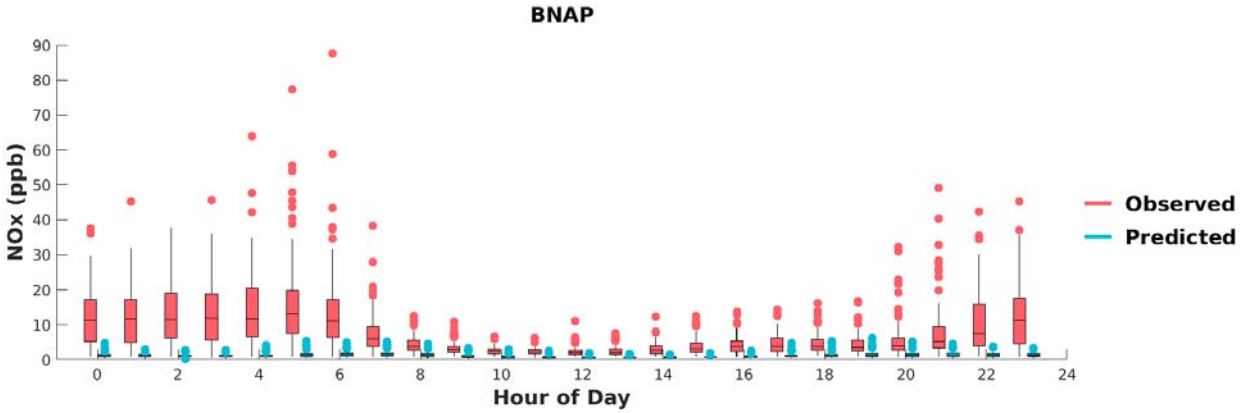

FIGURE I-3: BOX PLOTS OF OBSERVED VS. PREDICTED HOURLY NOX DURING MAY 1ST TO SEPTEMBER 30TH, 2018, AT BANNING. HORIZANTAL LINES INDICATE 25TH, 50TH (MEDIAN), AND 75TH PERCENTILES.

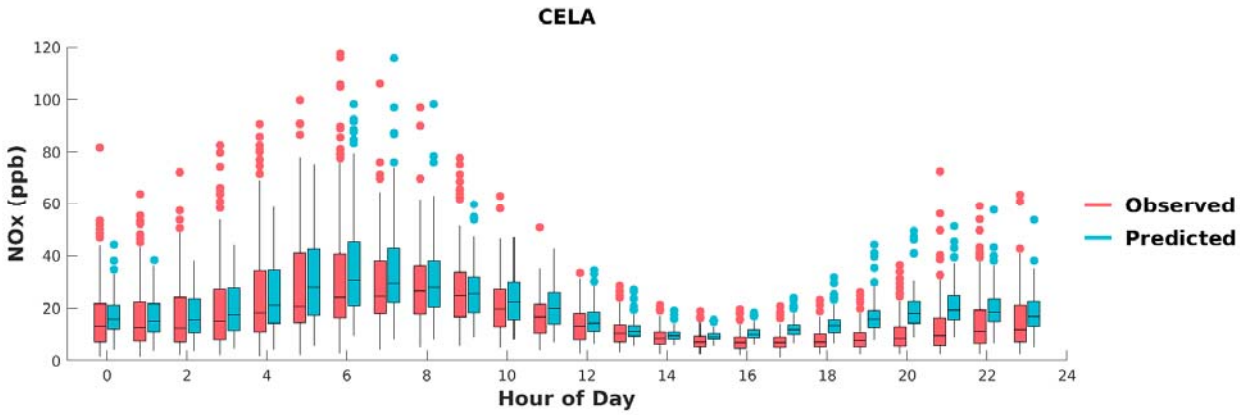

FIGURE I-4: BOX PLOTS OF OBSERVED VS. PREDICTED HOURLY NOX DURING MAY 1ST TO SEPTEMBER 30TH, 2018, AT CENTRAL LOS ANGELES. HORIZANTAL LINES INDICATE 25TH, 50TH (MEDIAN), AND 75TH PERCENTILES.

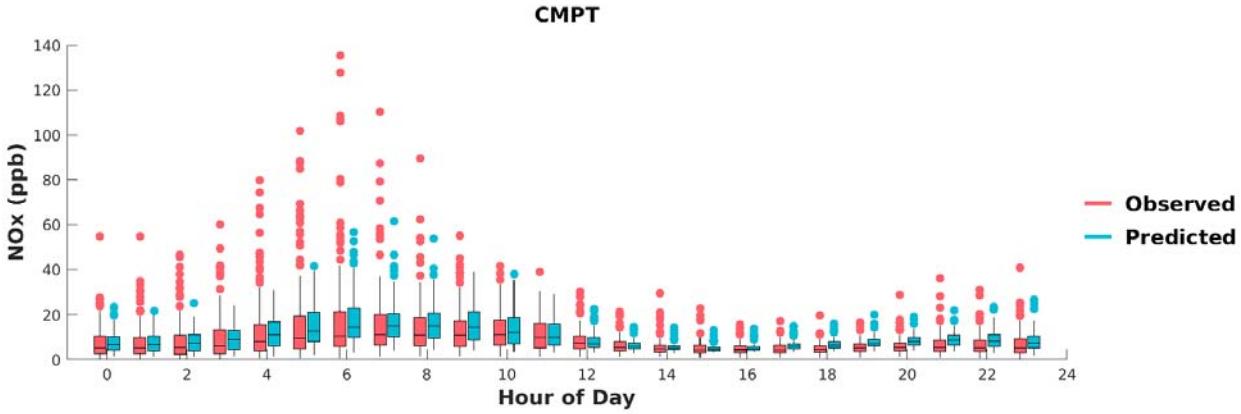

FIGURE I-5: BOX PLOTS OF OBSERVED VS. PREDICTED HOURLY NOX DURING MAY 1ST TO SEPTEMBER 30TH, 2018, AT COMPTON. HORIZANTAL LINES INDICATE 25TH, 50TH (MEDIAN), AND 75TH PERCENTILES.

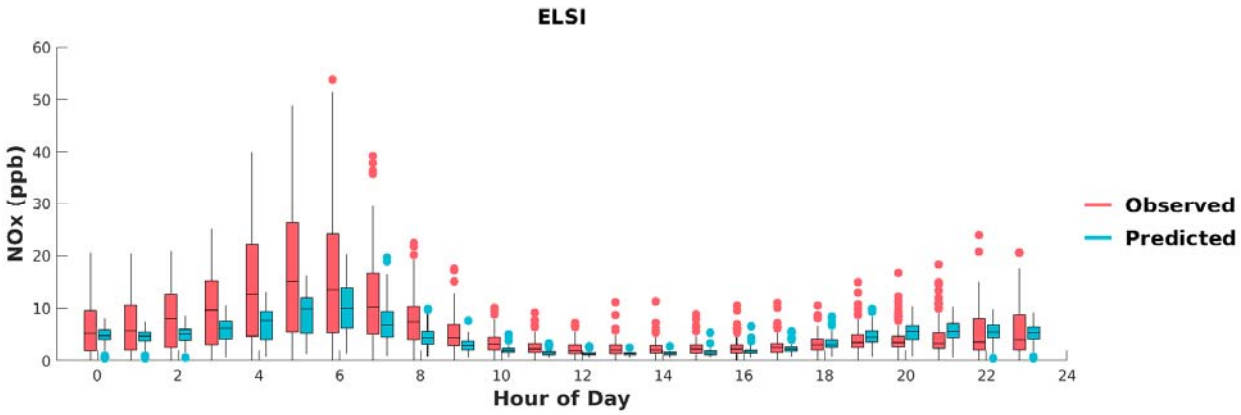

FIGURE I-6: BOX PLOTS OF OBSERVED VS. PREDICTED HOURLY NOX DURING MAY 1ST TO SEPTEMBER 30TH, 2018, AT LAKE ELSINORE. HORIZANTAL LINES INDICATE 25TH, 50TH (MEDIAN), AND 75TH PERCENTILES.

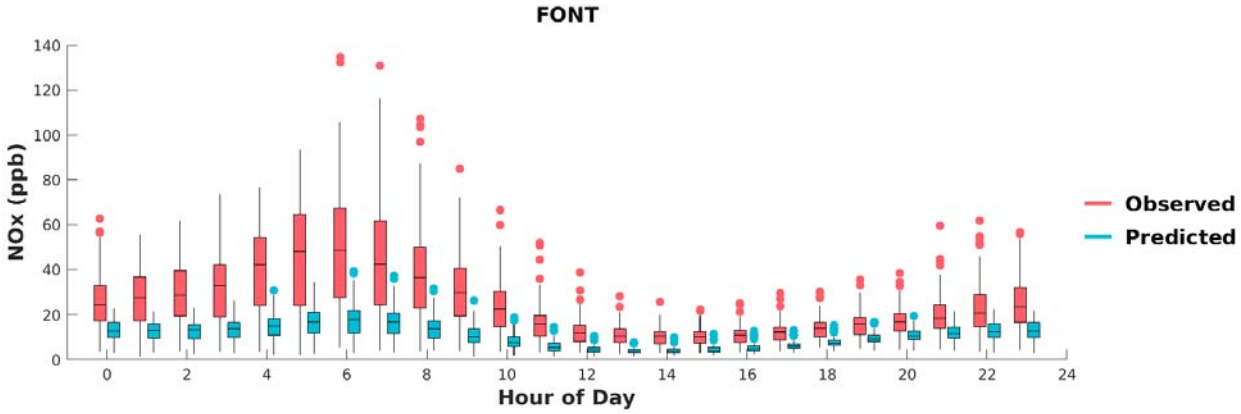

FIGURE I-7: BOX PLOTS OF OBSERVED VS. PREDICTED HOURLY NOX DURING MAY 1ST TO SEPTEMBER 30TH, 2018, AT FONTANA. HORIZANTAL LINES INDICATE 25TH, 50TH (MEDIAN), AND 75TH PERCENTILES.

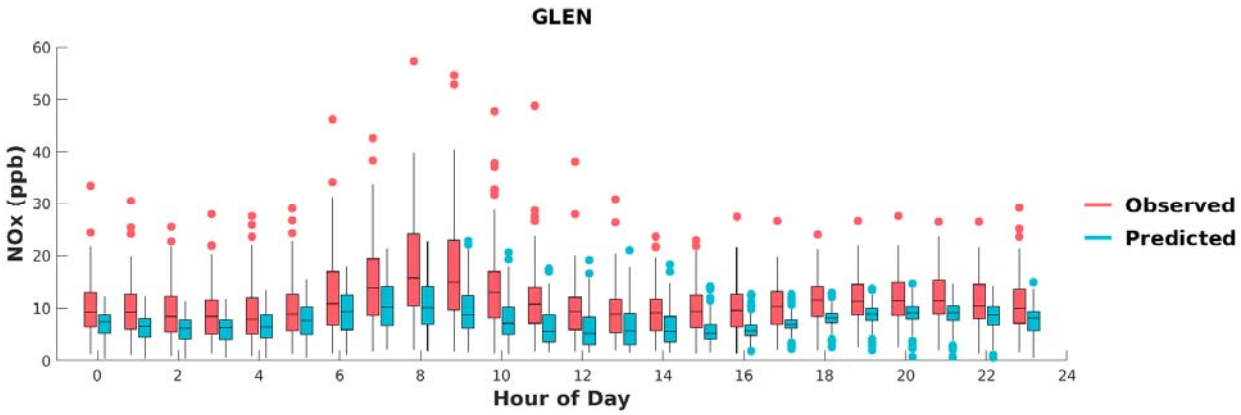

FIGURE I-8: BOX PLOTS OF OBSERVED VS. PREDICTED HOURLY NOX DURING MAY 1ST TO SEPTEMBER 30TH, 2018, AT GLENDORA. HORIZANTAL LINES INDICATE 25TH, 50TH (MEDIAN), AND 75TH PERCENTILES.

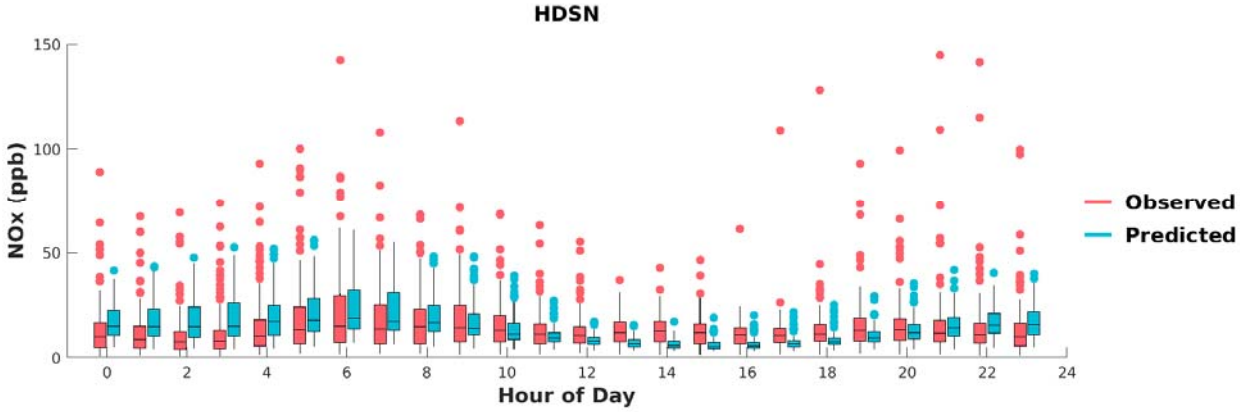

FIGURE I-9: BOX PLOTS OF OBSERVED VS. PREDICTED HOURLY NOX DURING MAY 1ST TO SEPTEMBER 30TH, 2018, AT HUDSON. HORIZANTAL LINES INDICATE 25TH, 50TH (MEDIAN), AND 75TH PERCENTILES.

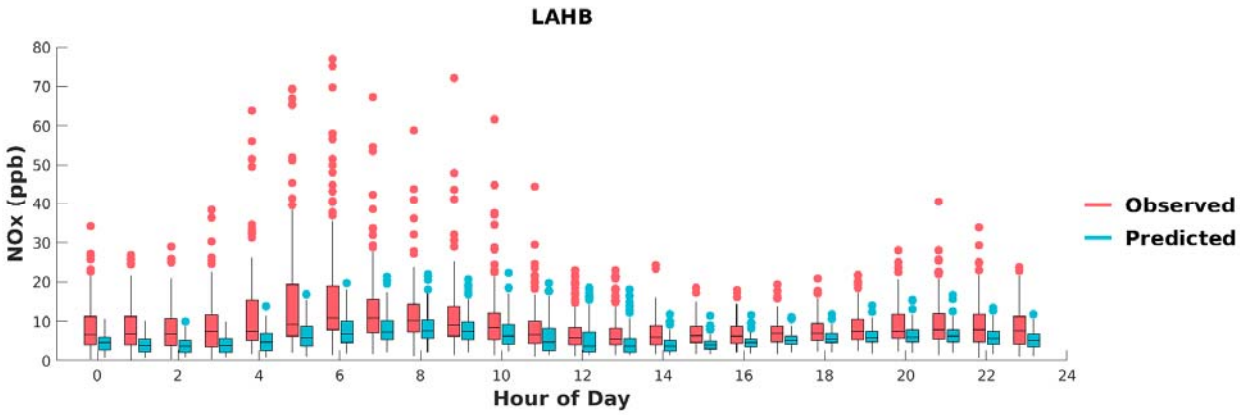

FIGURE I-10: BOX PLOTS OF OBSERVED VS. PREDICTED HOURLY NOX DURING MAY 1ST TO SEPTEMBER 30TH, 2018, AT LA HABRA. HORIZANTAL LINES INDICATE 25TH, 50TH (MEDIAN), AND 75TH PERCENTILES.

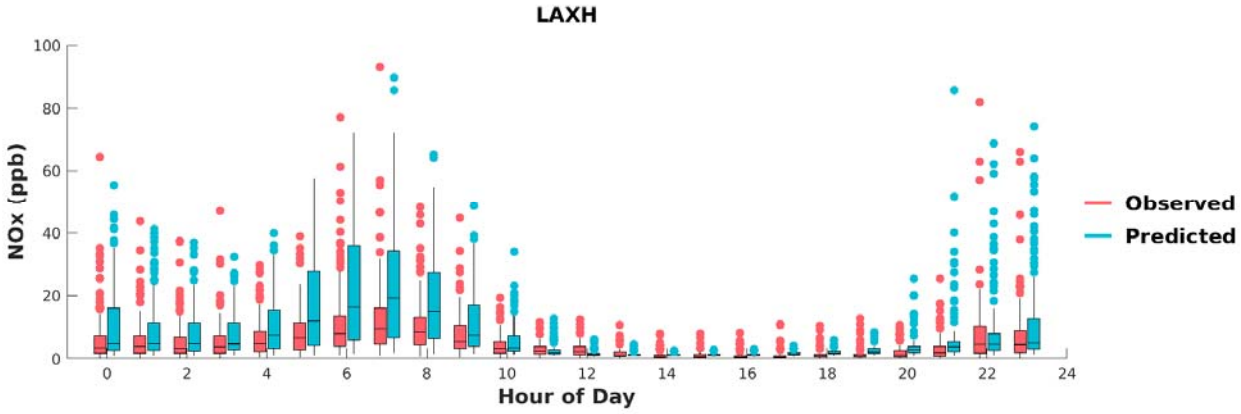

FIGURE I-11: BOX PLOTS OF OBSERVED VS. PREDICTED HOURLY NOX DURING MAY 1ST TO SEPTEMBER 30TH, 2018, AT LAX. HORIZANTAL LINES INDICATE 25TH, 50TH (MEDIAN), AND 75TH PERCENTILES.

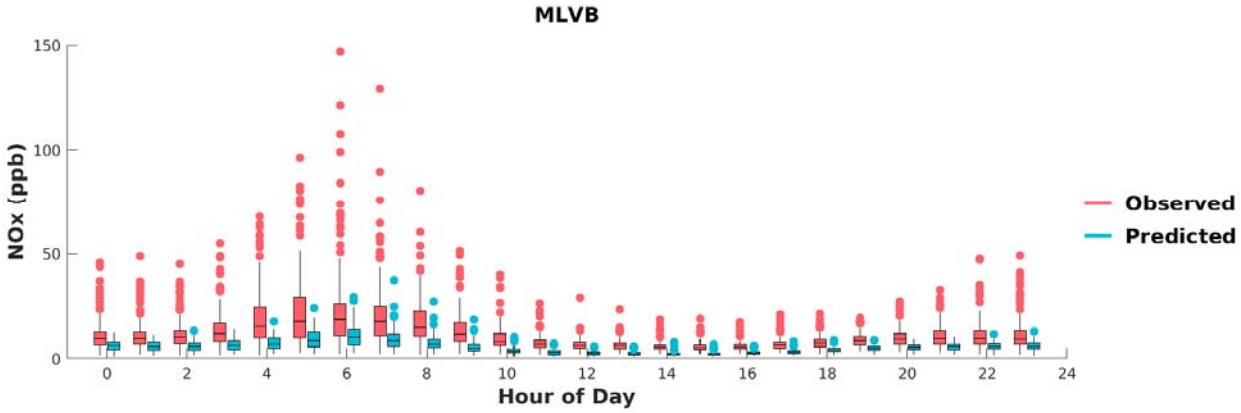

FIGURE I-12: BOX PLOTS OF OBSERVED VS. PREDICTED HOURLY NOX DURING MAY 1ST TO SEPTEMBER 30TH, 2018, AT MIRA LOMA VAN BUREN. HORIZANTAL LINES INDICATE 25TH, 50TH (MEDIAN), AND 75TH PERCENTILES.

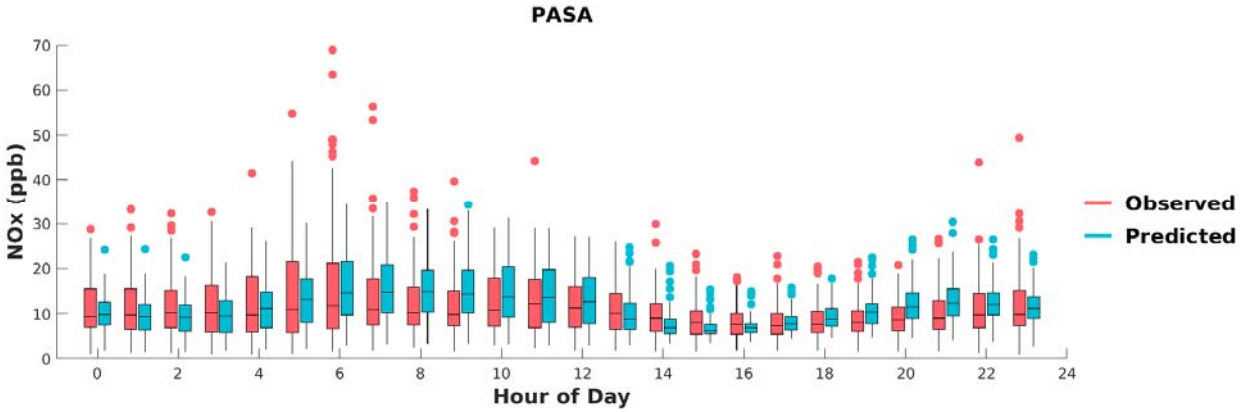

FIGURE I-13: BOX PLOTS OF OBSERVED VS. PREDICTED HOURLY NOX DURING MAY 1ST TO SEPTEMBER 30TH, 2018, AT PASADENA. HORIZANTAL LINES INDICATE 25TH, 50TH (MEDIAN), AND 75TH PERCENTILES.

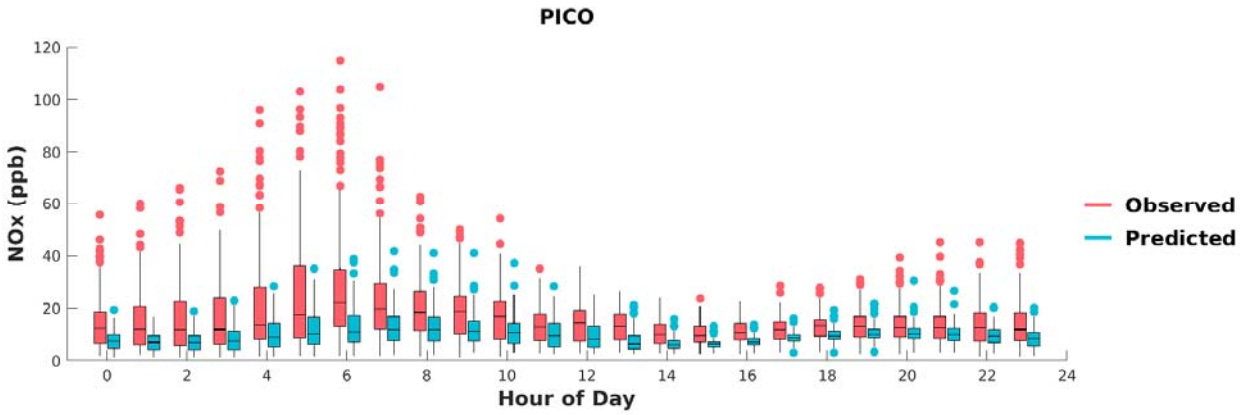

FIGURE I-14: BOX PLOTS OF OBSERVED VS. PREDICTED HOURLY NOX DURING MAY 1ST TO SEPTEMBER 30TH, 2018, AT PICO RIVERO. HORIZANTAL LINES INDICATE 25TH, 50TH (MEDIAN), AND 75TH PERCENTILES.

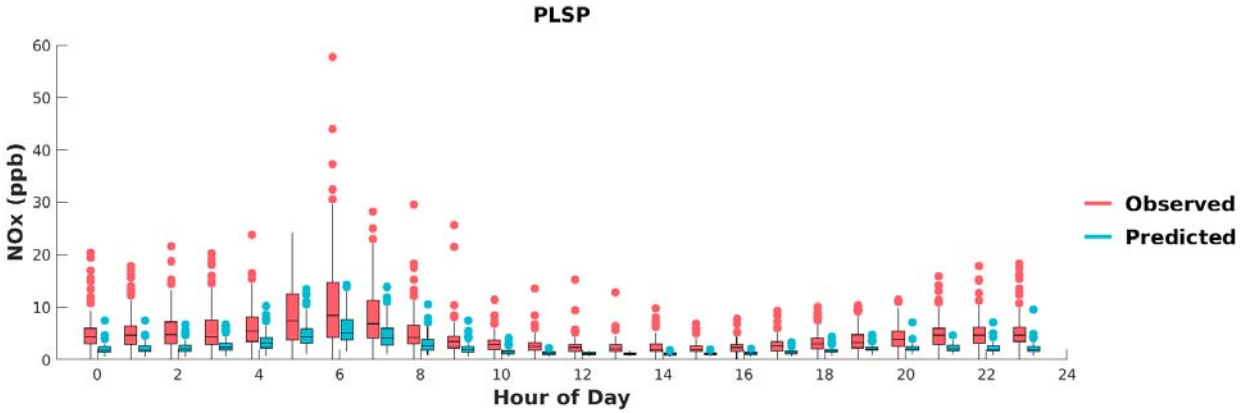

FIGURE I-15: BOX PLOTS OF OBSERVED VS. PREDICTED HOURLY NOX DURING MAY 1ST TO SEPTEMBER 30TH, 2018, AT PALM SPRINGS. HORIZANTAL LINES INDICATE 25TH, 50TH (MEDIAN), AND 75TH PERCENTILES.

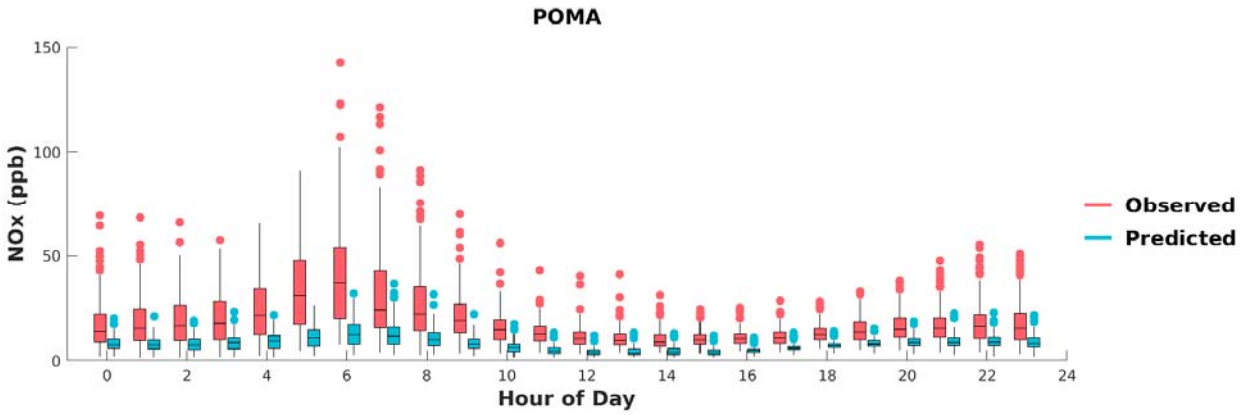

FIGURE I-16: BOX PLOTS OF OBSERVED VS. PREDICTED HOURLY NOX DURING MAY 1ST TO SEPTEMBER 30TH, 2018, AT POMONA. HORIZANTAL LINES INDICATE 25TH, 50TH (MEDIAN), AND 75TH PERCENTILES.

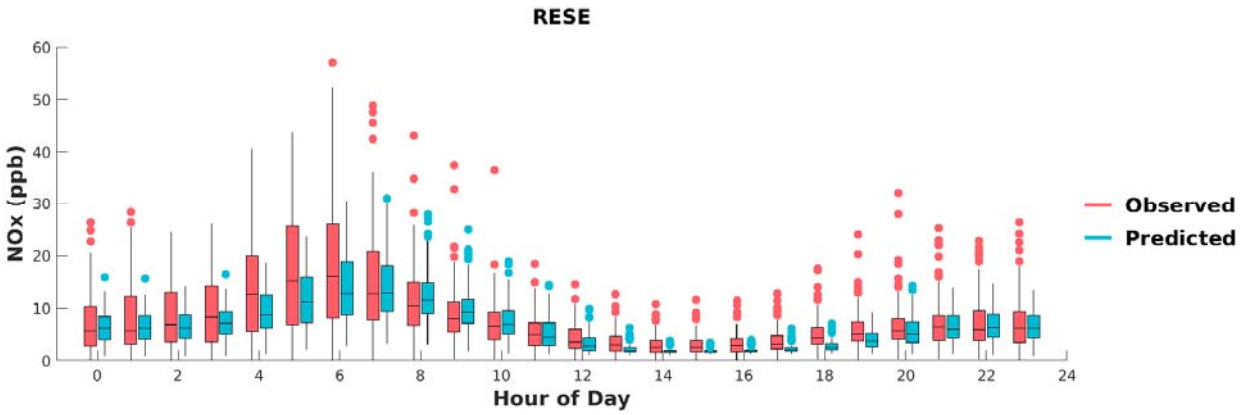

FIGURE I-17: BOX PLOTS OF OBSERVED VS. PREDICTED HOURLY NOX DURING MAY 1ST TO SEPTEMBER 30TH, 2018, AT RESEDA. HORIZANTAL LINES INDICATE 25TH, 50TH (MEDIAN), AND 75TH PERCENTILES.

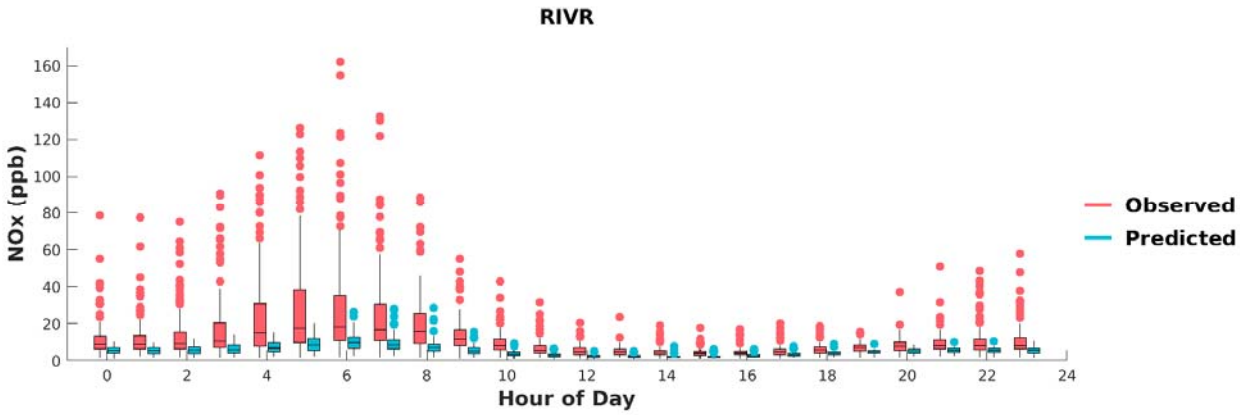

FIGURE I-18: BOX PLOTS OF OBSERVED VS. PREDICTED HOURLY NOX DURING MAY 1ST TO SEPTEMBER 30TH, 2018, AT RIVERSIDE. HORIZANTAL LINES INDICATE 25TH, 50TH (MEDIAN), AND 75TH PERCENTILES.

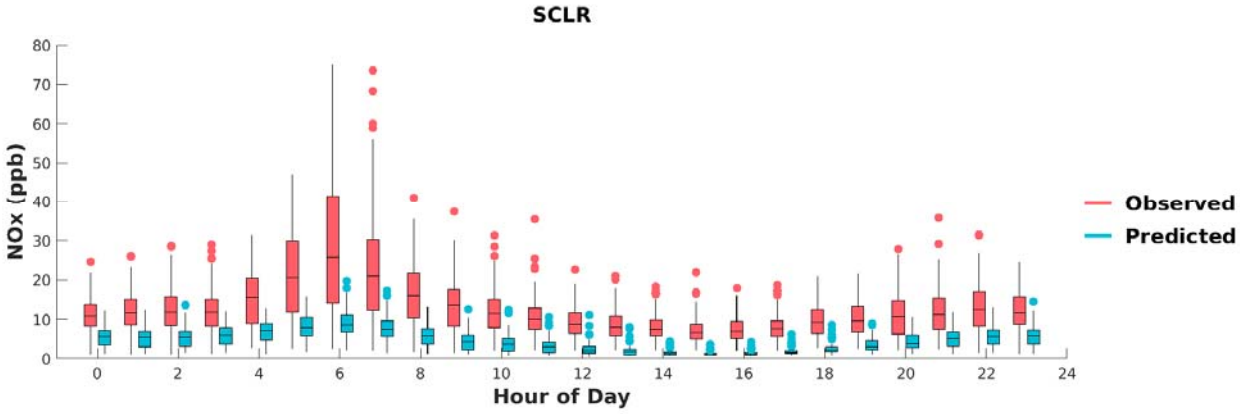

FIGURE I-19: BOX PLOTS OF OBSERVED VS. PREDICTED HOURLY NOX DURING MAY 1ST TO SEPTEMBER 30TH, 2018, AT SANTA CLARITA. HORIZANTAL LINES INDICATE 25TH, 50TH (MEDIAN), AND 75TH PERCENTILES.

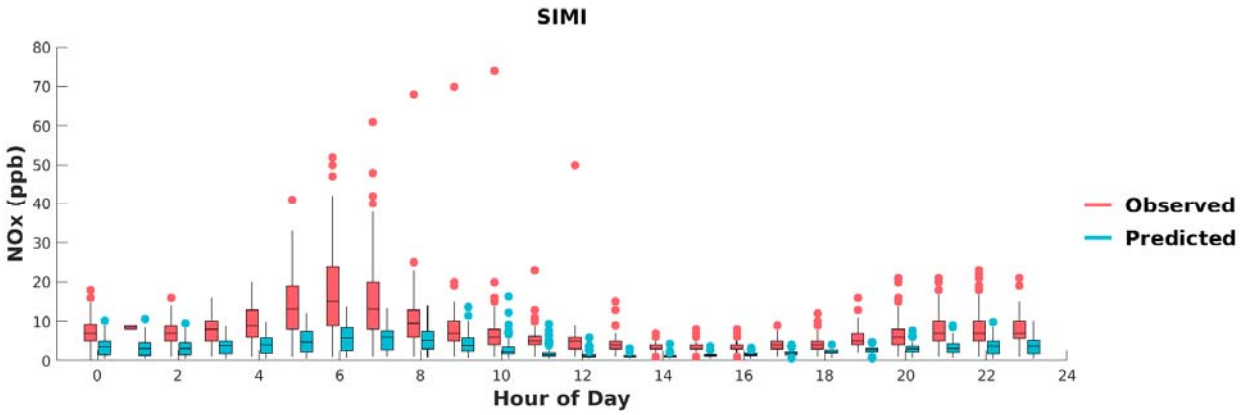

FIGURE I-20: BOX PLOTS OF OBSERVED VS. PREDICTED HOURLY NOX DURING MAY 1ST TO SEPTEMBER 30TH, 2018, AT SIMI VALLEY. HORIZANTAL LINES INDICATE 25TH, 50TH (MEDIAN), AND 75TH PERCENTILES.

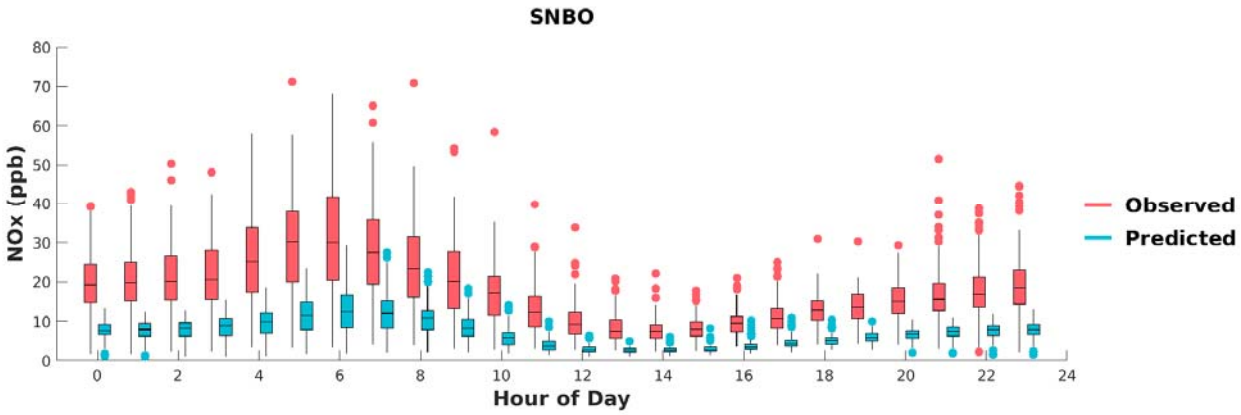

FIGURE I-21: BOX PLOTS OF OBSERVED VS. PREDICTED HOURLY NOX DURING MAY 1ST TO SEPTEMBER 30TH, 2018, AT SAN BERNARDINO. HORIZANTAL LINES INDICATE 25TH, 50TH (MEDIAN), AND 75TH PERCENTILES.

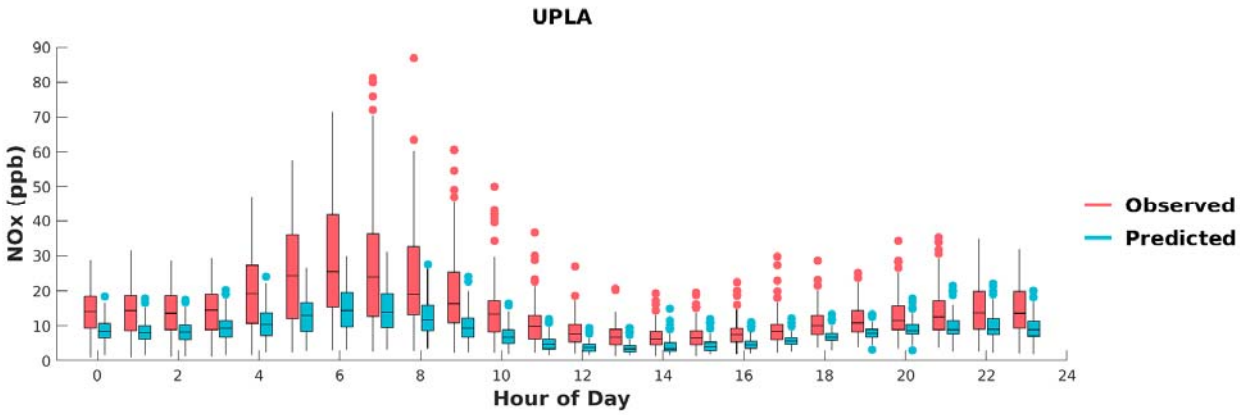

FIGURE I-22: BOX PLOTS OF OBSERVED VS. PREDICTED HOURLY NOX DURING MAY 1ST TO SEPTEMBER 30TH, 2018, AT UPLAND. HORIZANTAL LINES INDICATE 25TH, 50TH (MEDIAN), AND 75TH PERCENTILES.

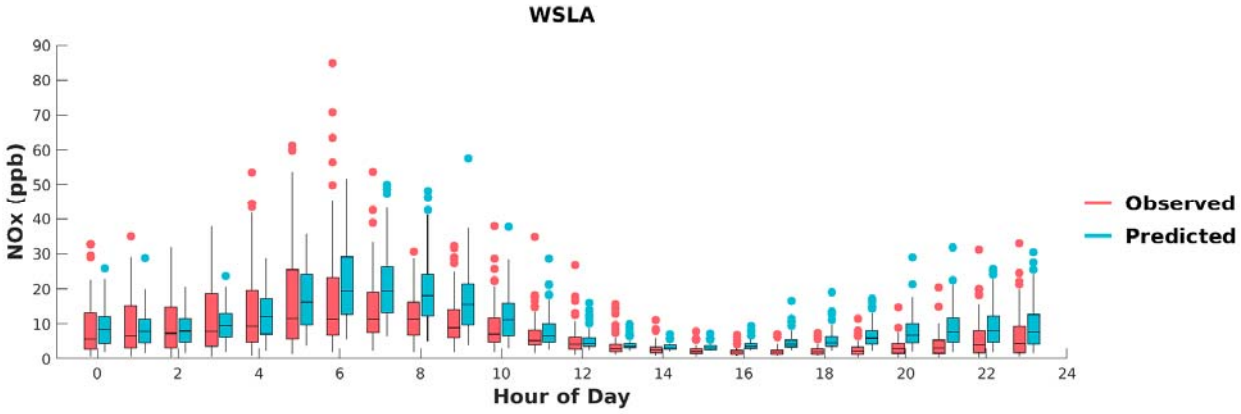

FIGURE I-23: BOX PLOTS OF OBSERVED VS. PREDICTED HOURLY NOX DURING MAY 1ST TO SEPTEMBER 30TH, 2018, AT WEST LOS ANGELES. HORIZANTAL LINES INDICATE 25TH, 50TH (MEDIAN), AND 75TH PERCENTILES.

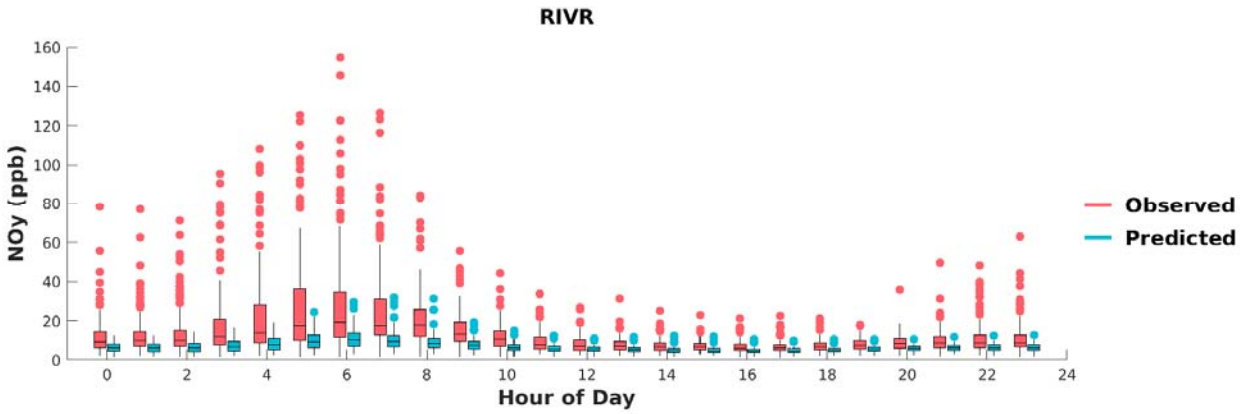

FIGURE J-1: BOX PLOTS OF OBSERVED VS. PREDICTED HOURLY NOY DURING MAY 1ST TO SEPTEMBER 30TH, 2018, AT RIVERSIDE. HORIZANTAL LINES INDICATE 25TH, 50TH (MEDIAN), AND 75TH PERCENTILES.

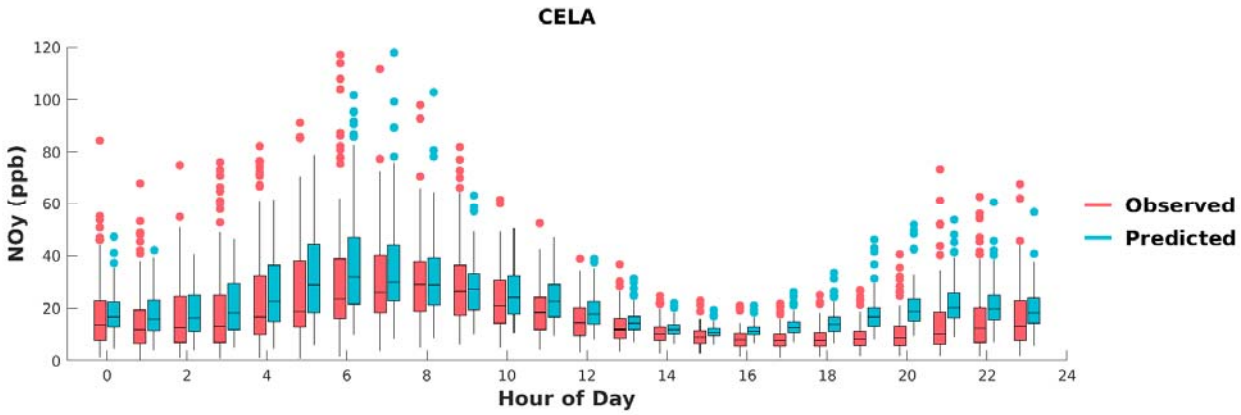

FIGURE J-2: BOX PLOTS OF OBSERVED VS. PREDICTED HOURLY NOY DURING MAY 1ST TO SEPTEMBER 30TH, 2018, AT CENTRAL LOS ANGELES. HORIZANTAL LINES INDICATE 25TH, 50TH (MEDIAN), AND 75TH PERCENTILES.

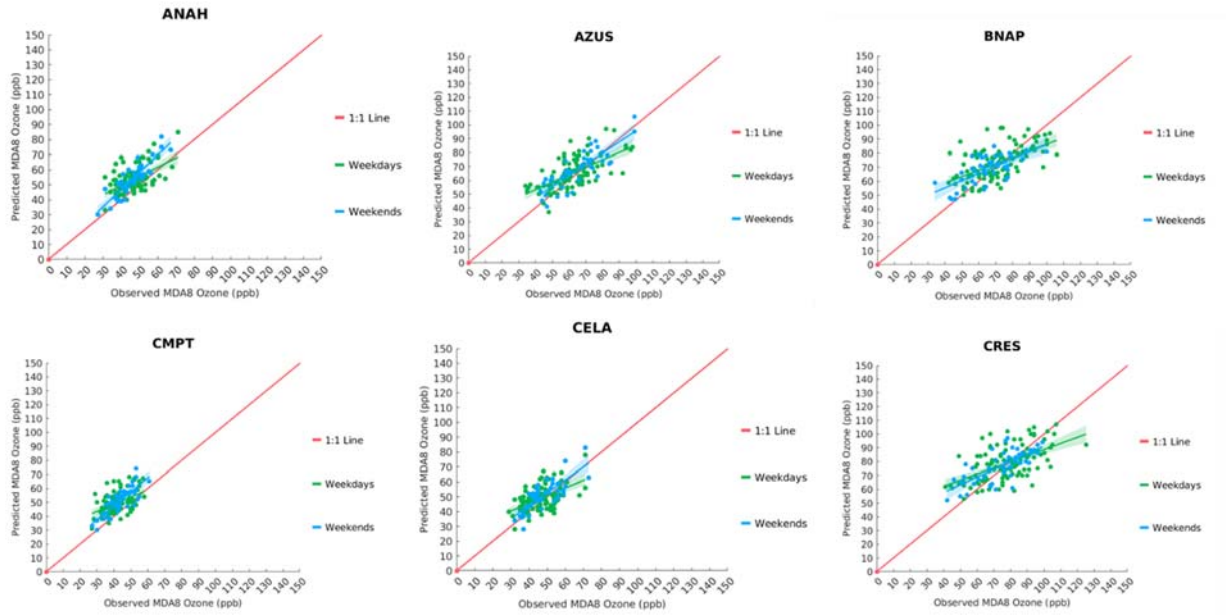

FIGURE K-1: SCATTER PLOT OF OBSERVED VS. PREDICTED MDA8 OZONE DURING MAY 1ST TO SEPTEMBER 30TH, 2018, AT ANEHIM (ANAH), AZUSA (AZUS), BANNING (BANP), COMPTON (CMPT), CENTRAL LOS ANGELES (CELA), AND CRESTLINE (CRES). GREEN AND BLUE LINES INDICATE GENERAL LINEAR MODEL FIT WITH 95% CONFIDENCE INTERVAL (SHADED AREA). THE RED LINE INDICATES 1:1 LINE.

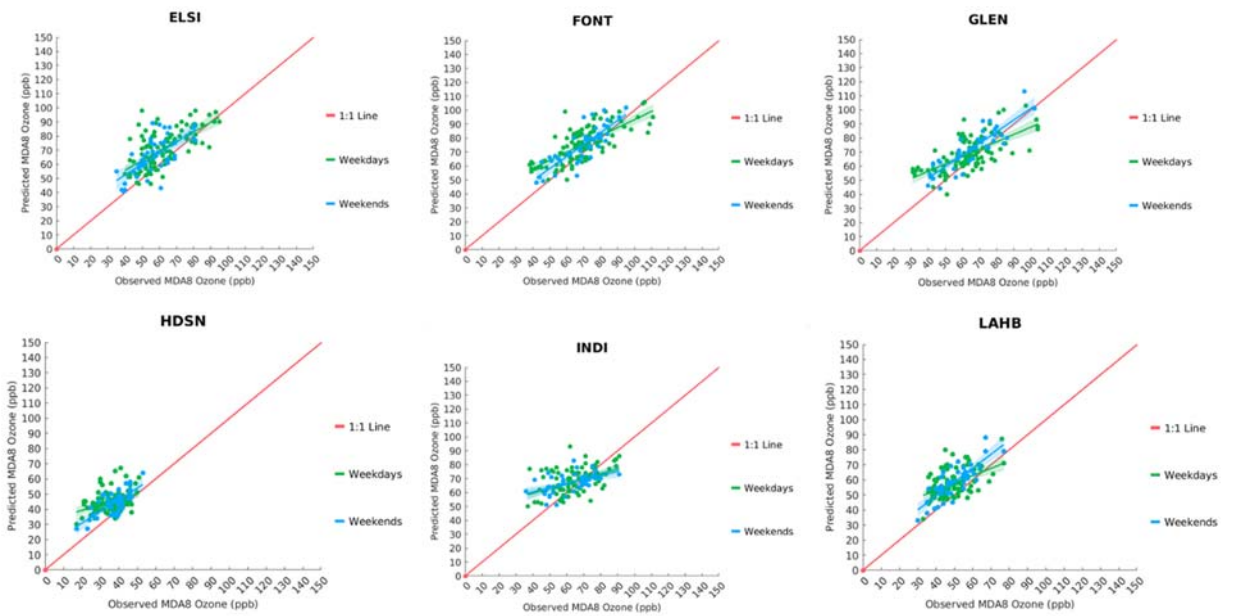

FIGURE K-2: SCATTER PLOT OF OBSERVED VS. PREDICTED MDA8 OZONE DURING MAY 1ST TO SEPTEMBER 30TH, 2018, AT LAKE ELSINORE (ELSI), FONTANA (FONT), GLENDORA (GLEN), HUDSON (HDSN), INDIO (INDI), AND LA HABRA (LAHB). GREEN AND BLUE LINES INDICATE GENERAL LINEAR MODEL FIT WITH 95% CONFIDENCE INTERVAL (SHADED AREA). THE RED LINE INDICATES 1:1 LINE.

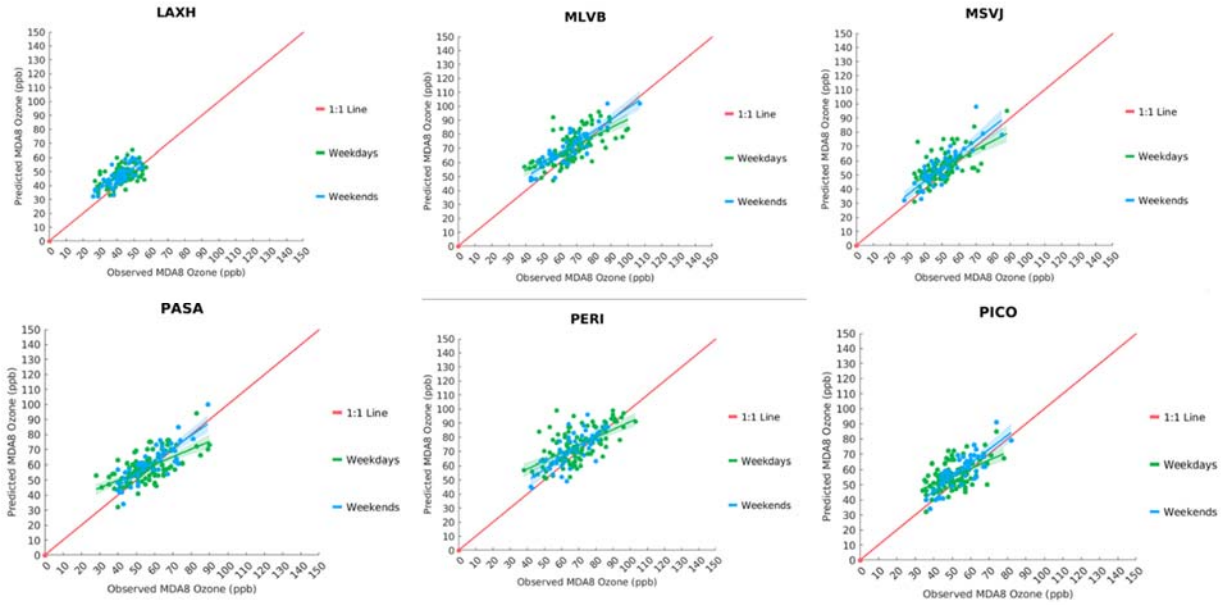

FIGURE K-3: SCATTER PLOT OF OBSERVED VS. PREDICTED MDA8 OZONE DURING MAY 1ST TO SEPTEMBER 30TH, 2018, AT LAX (LAX), MIRA LOMA VAN BUREN (MLVB), MISSION VIEJO (MSVJ), PASADENA (PASA), PERRIS (PERI), AND PICO RIVERO (PICO). GREEN AND BLUE LINES INDICATE GENERAL LINEAR MODEL FIT WITH 95% CONFIDENCE INTERVAL (SHADED AREA). THE RED LINE INDICATES 1:1 LINE.

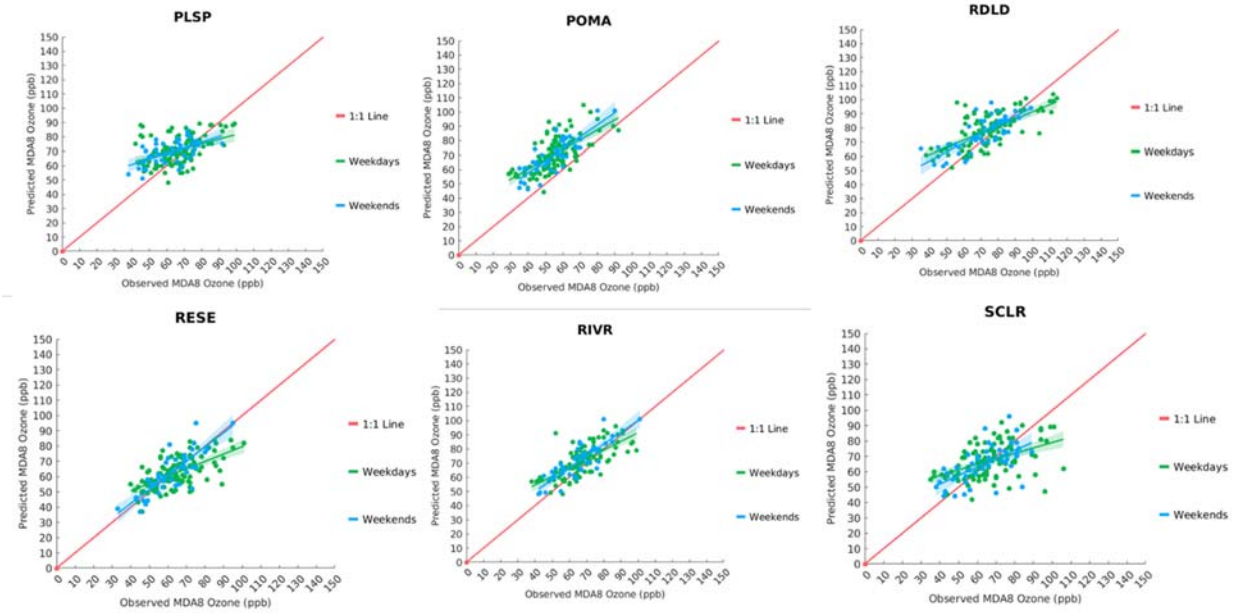

FIGURE K-4: SCATTER PLOT OF OBSERVED VS. PREDICTED MDA8 OZONE DURING MAY 1ST TO SEPTEMBER 30TH, 2018, AT PALM SPRINGS (PLSP), POMONA (POMA), RED LANDS (RDLD), RESEDA (RESE), RIVERSIDE (RIVR), AND SANTA CLARITA (SCLR). GREEN AND BLUE LINES INDICATE GENERAL LINEAR MODEL FIT WITH 95% CONFIDENCE INTERVAL (SHADED AREA). THE RED LINE INDICATES 1:1 LINE.

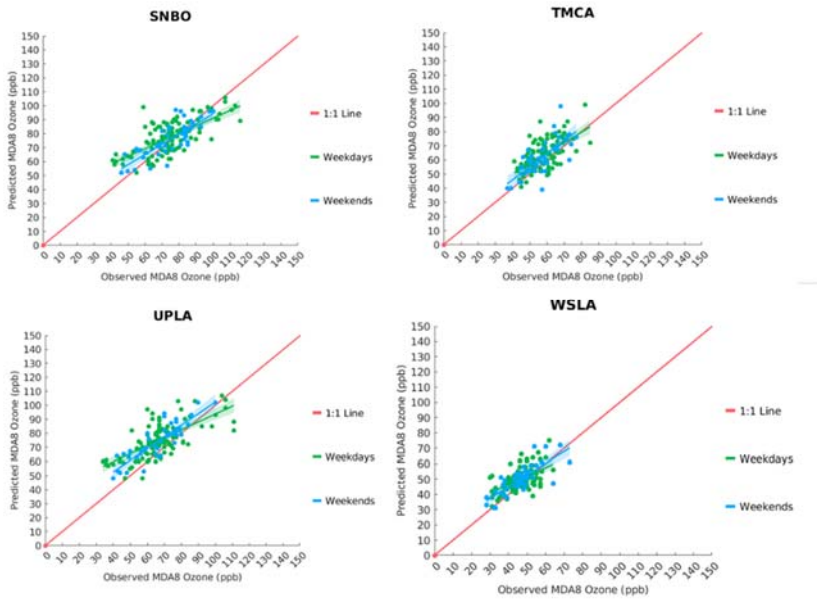

FIGURE K-5: SCATTER PLOT OF OBSERVED VS. PREDICTED MDA8 OZONE DURING MAY 1ST TO SEPTEMBER 30TH, 2018, AT SAN BERNARDION (SNBO), TEMACULA (TMCA), UPLAND (UPLA), AND WEST LOS ANGELES (WSLA). GREEN AND BLUE LINES INDICATE GENERAL LINEAR MODEL FIT WITH 95% CONFIDENCE INTERVAL (SHADED AREA). THE RED LINE INDICATES 1:1 LINE.

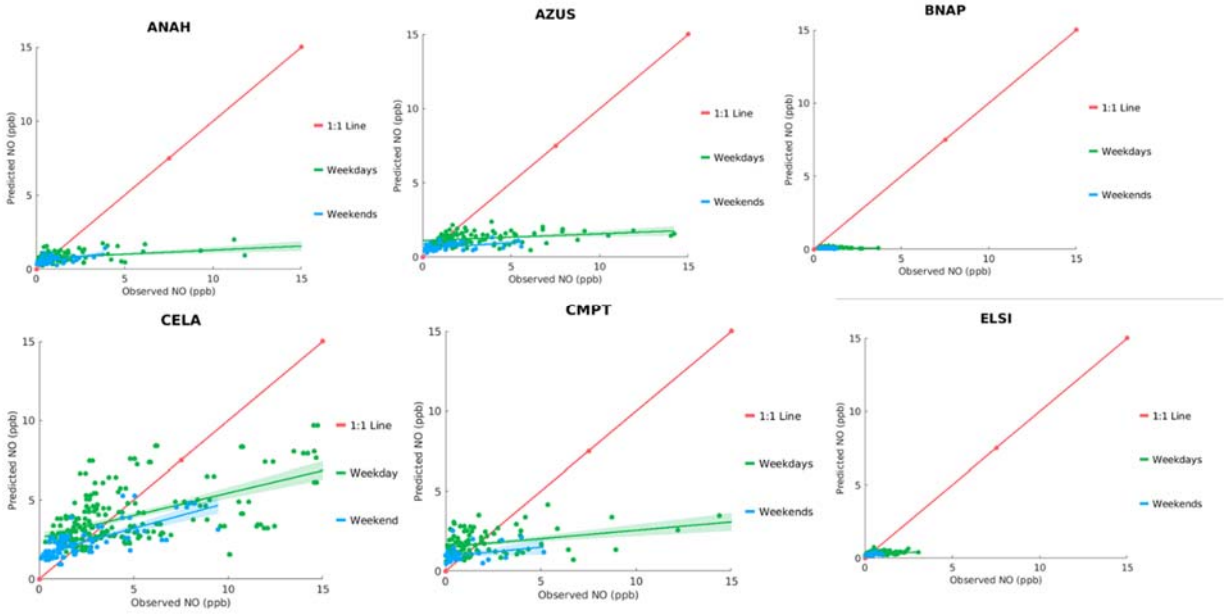

FIGURE L-1: SCATTER PLOT OF OBSERVED VS. PREDICTED DAILY AVERAGE NO DURING MAY 1ST TO SEPTEMBER 30TH, 2018, AT ANEHIM (ANAH), AZUSA (AZUS), BANNING (BANP), COMPTON (CMPT), CENTRAL LOS ANGELES (CELA), AND LAKE ELSINORE (ELSI). GREEN AND BLUE LINES INDICATE GENERAL LINEAR MODEL FIT WITH 95% CONFIDENCE INTERVAL (SHADED AREA). THE RED LINE INDICATES 1:1 LINE.

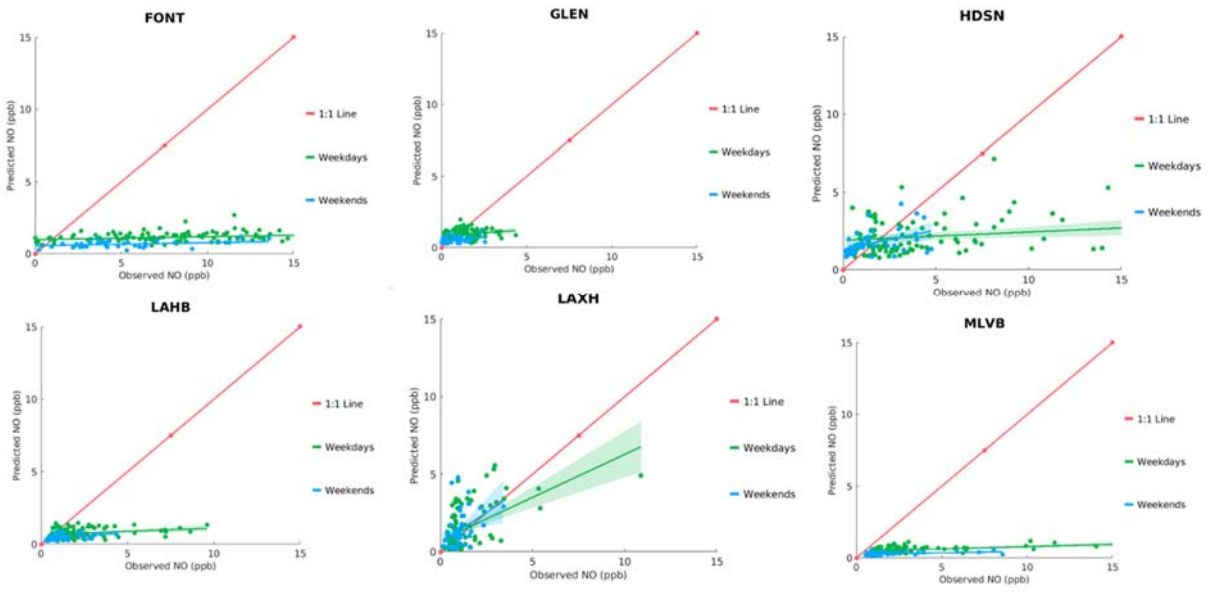

FIGURE L-2: SCATTER PLOT OF OBSERVED VS. PREDICTED DAILY AVERAGE NO DURING MAY 1ST TO SEPTEMBER 30TH, 2018, AT FONTANA (FONT), GLENDORA (GLEN), HUDSON (HDSN), LA HABRA (LAHB), LAX (LAX), AND MIRA LOMA VAN BUREN (MLVB) . GREEN AND BLUE LINES INDICATE GENERAL LINEAR MODEL FIT WITH 95% CONFIDENCE INTERVAL (SHADED AREA). THE RED LINE INDICATES 1:1 LINE.

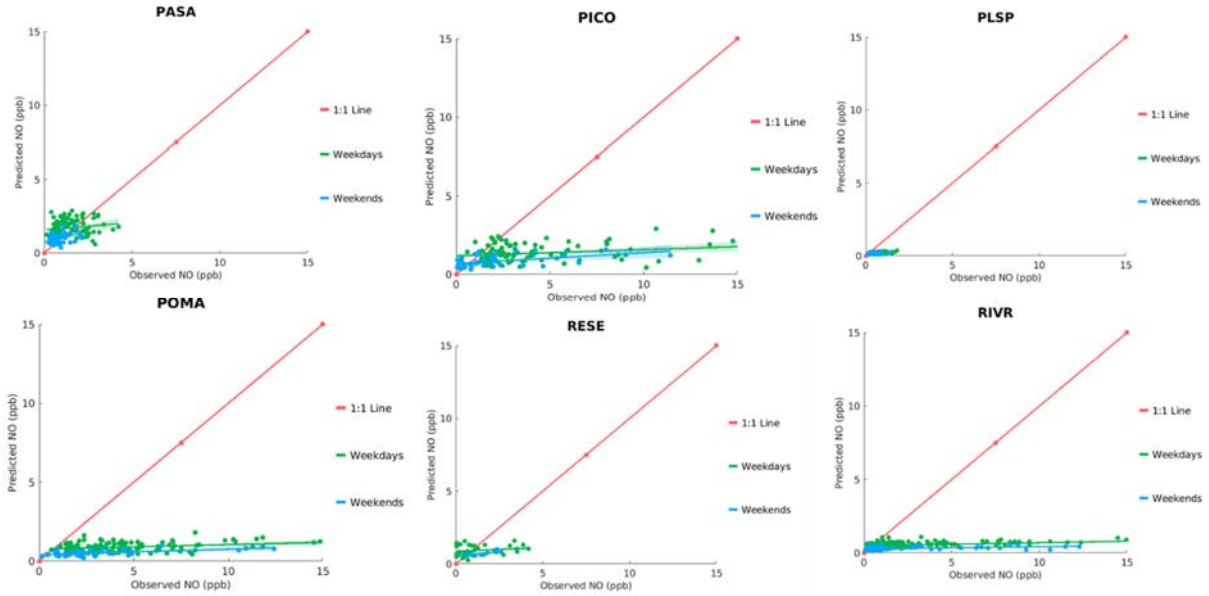

FIGURE L-3: SCATTER PLOT OF OBSERVED VS. PREDICTED DAILY AVERAGE NO DURING MAY 1ST TO SEPTEMBER 30TH, 2018, PASADENA (PASA), PICO RIVERO (PICO), PALM SPRINGS (PLSP), POMONA (POMA), RESEDA (RESE), AND RIVERSIDE (RIVR). GREEN AND BLUE LINES INDICATE GENERAL LINEAR MODEL FIT WITH 95% CONFIDENCE INTERVAL (SHADED AREA). THE RED LINE INDICATES 1:1 LINE.

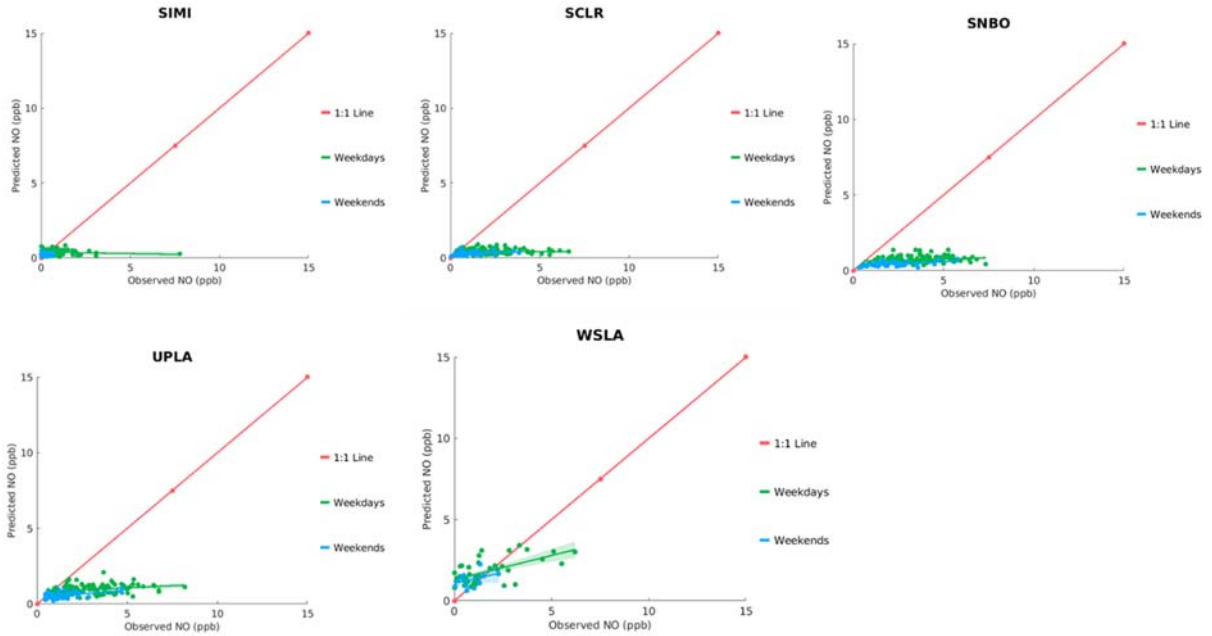

FIGURE L-4: SCATTER PLOT OF OBSERVED VS. PREDICTED DAILY AVERAGE NO DURING MAY 1ST TO SEPTEMBER 30TH, 2018, AT SIMI VALLEY (SIMI), SANTA CLARITA (SCLR), SAN BERNARDION (SNBO), UPLAND (UPLA), AND WEST LOS ANGELES (WSLA). GREEN AND BLUE LINES INDICATE GENERAL LINEAR MODEL FIT WITH 95% CONFIDENCE INTERVAL (SHADED AREA). THE RED LINE INDICATES 1:1 LINE.

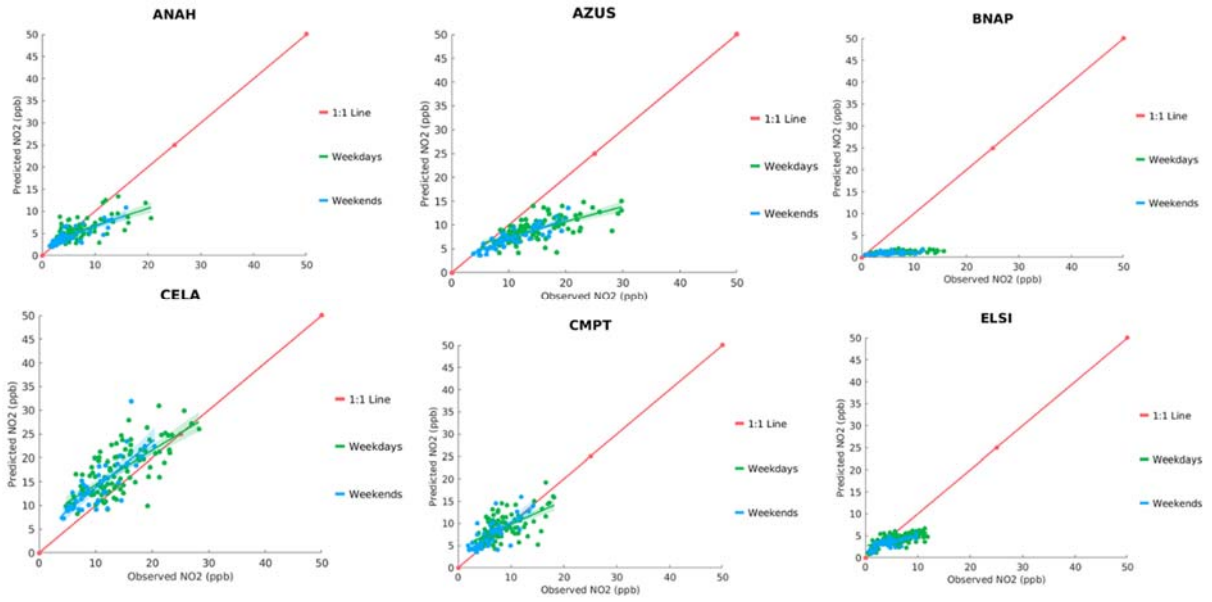

FIGURE M-1: SCATTER PLOT OF OBSERVED VS. PREDICTED DAILY AVERAGE NO2 DURING MAY 1ST TO SEPTEMBER 30TH, 2018, AT ANAHEIM (ANAH), AZUSA(AZUS), BANNING (BNAP), CENTRAL LOS ANGLES (CELA), COMPTON (CMPT), AND LAKE ELSIONOR (ELSI). GREEN AND BLUE LINES INDICATE GENERAL LINEAR MODEL FIT WITH 95% CONFIDENCE INTERVAL (SHADED AREA). THE RED LINE INDICATES 1:1 LINE.

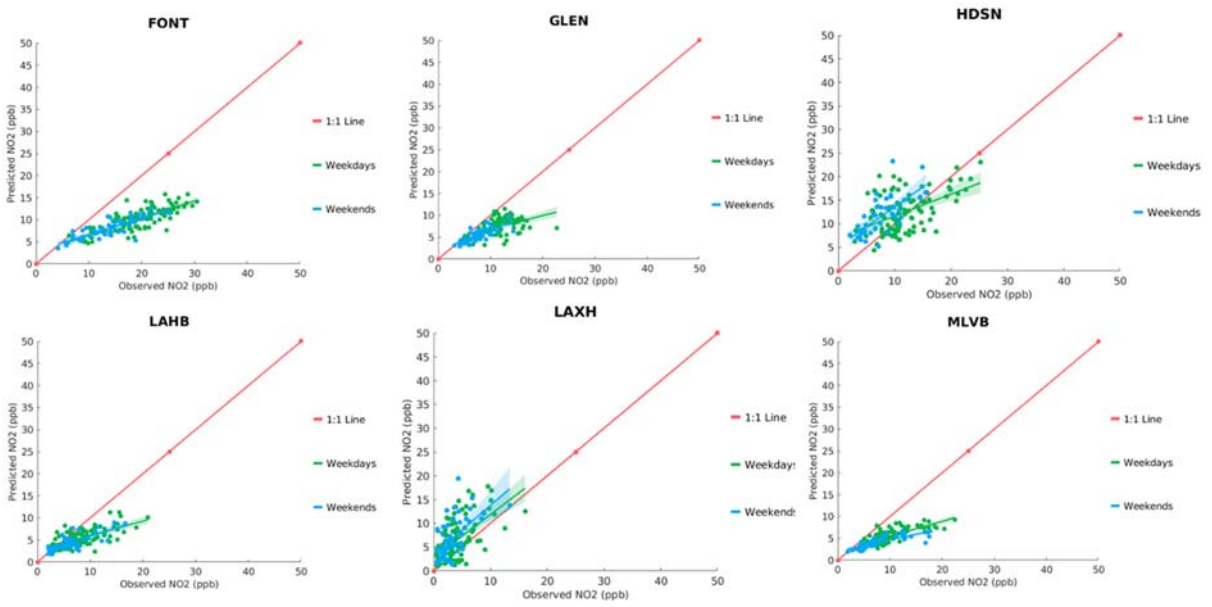

FIGURE M-2: SCATTER PLOT OF OBSERVED VS. PREDICTED DAILY AVERAGE NO2 DURING MAY 1ST TO SEPTEMBER 30TH, 2018, AT FONTANA (FONT), SANTA GLENDORA (GLEN), HUDSON (HDSN), LA HABRA (LAHB), LAX (LAX) AND MIRA LOMA (MLVB). GREEN AND BLUE LINES INDICATE GENERAL LINEAR MODEL FIT WITH 95% CONFIDENCE INTERVAL (SHADED AREA). THE RED LINE INDICATES 1:1 LINE.

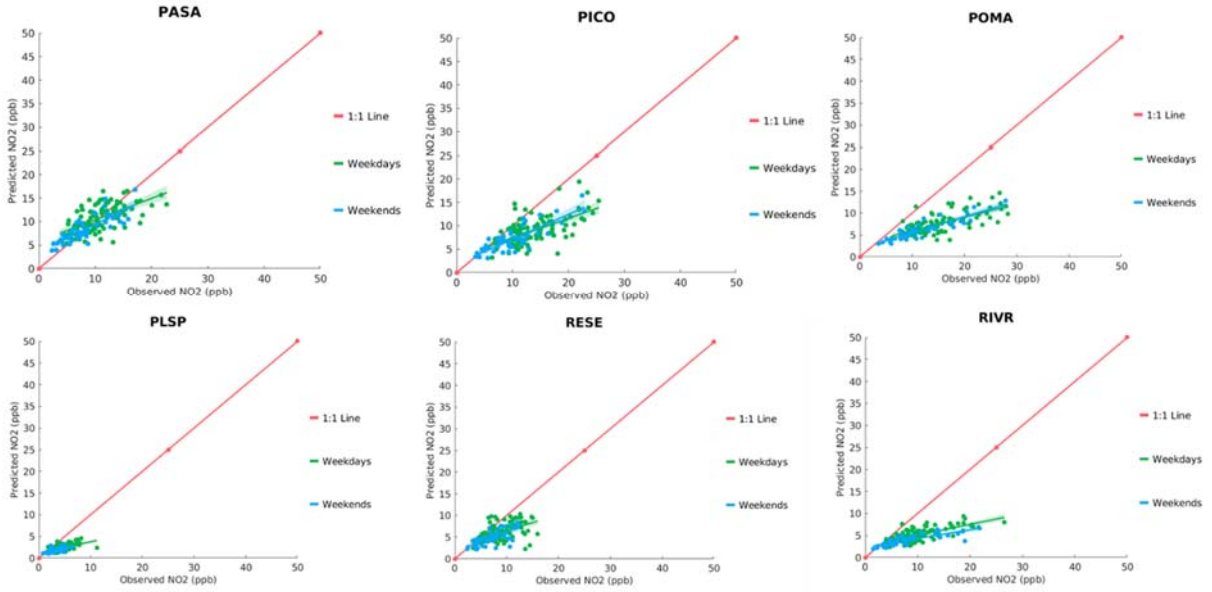

FIGURE M-3: SCATTER PLOT OF OBSERVED VS. PREDICTED DAILY AVERAGE NO2 DURING MAY 1ST TO SEPTEMBER 30TH, 2018, AT PASADENA (PASA), PICO RIVERO (PICO), POMONA (POMA), PALM SPRINGS (PLSP), RESEDA (RESE), AND RIVERSIDE (RIVR). GREEN AND BLUE LINES INDICATE GENERAL LINEAR MODEL FIT WITH 95% CONFIDENCE INTERVAL (SHADED AREA). THE RED LINE INDICATES 1:1 LINE.

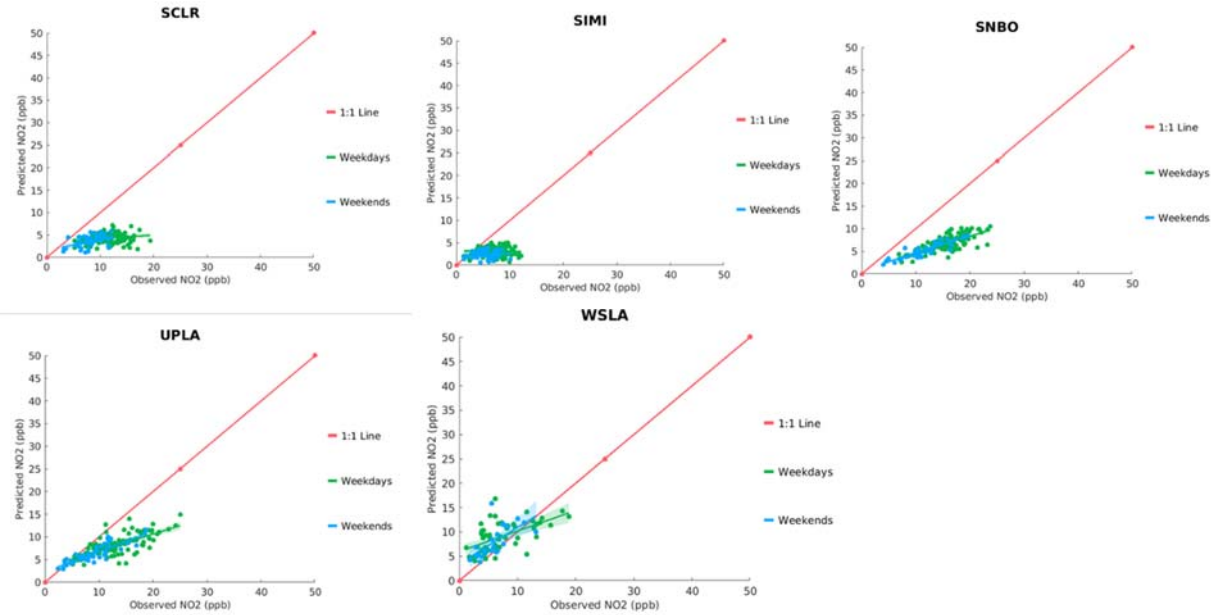

FIGURE M-4: SCATTER PLOT OF OBSERVED VS. PREDICTED DAILY AVERAGE NO2 DURING MAY 1ST TO SEPTEMBER 30TH, 2018, AT SANTA CLARIRA (SCLR), SIMI VALLEY (SIMI), SAN BERNARDION (SNBO), UPLAND (UPLA), AND WEST LOS ANGELES (WSLA). GREEN AND BLUE LINES INDICATE GENERAL LINEAR MODEL FIT WITH 95% CONFIDENCE INTERVAL (SHADED AREA). THE RED LINE INDICATES 1:1 LINE.

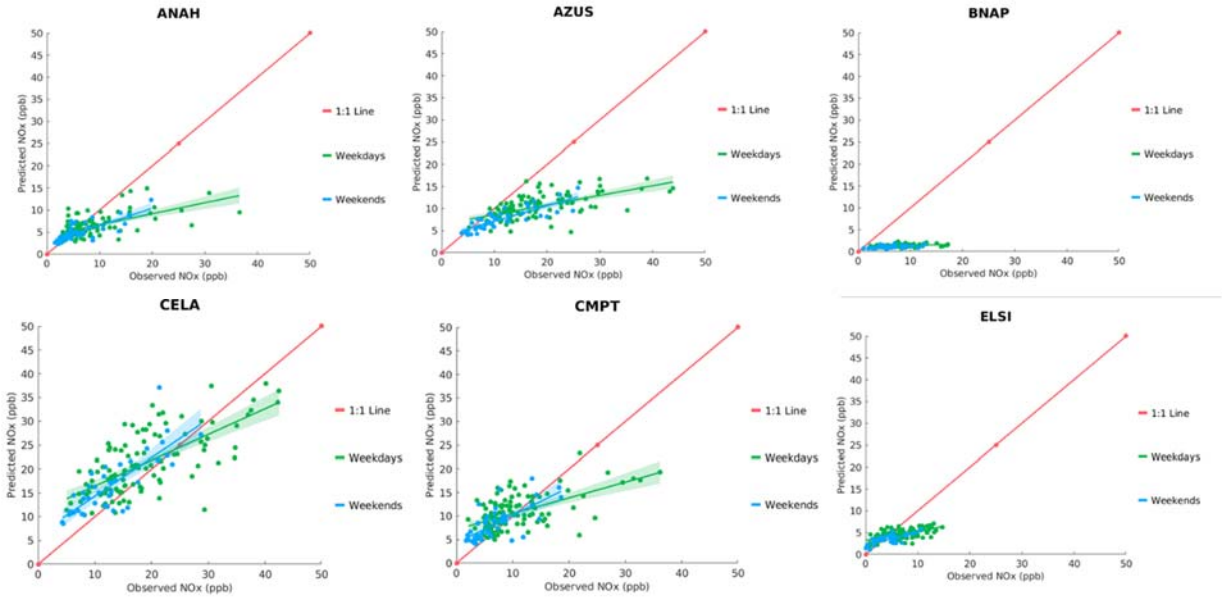

FIGURE N-1: SCATTER PLOT OF OBSERVED VS. PREDICTED DAILY AVERAGE NOX DURING MAY 1ST TO SEPTEMBER 30TH, 2018, AT ANEHIM (ANAH), AZUSA (AZUS), BANNING (BANP), COMPTON (CMPT), CENTRAL LOS ANGELES (CELA), AND LAKE ELSINORE (ELSI). GREEN AND BLUE LINES INDICATE GENERAL LINEAR MODEL FIT WITH 95% CONFIDENCE INTERVAL (SHADED AREA). THE RED LINE INDICATES 1:1 LINE.

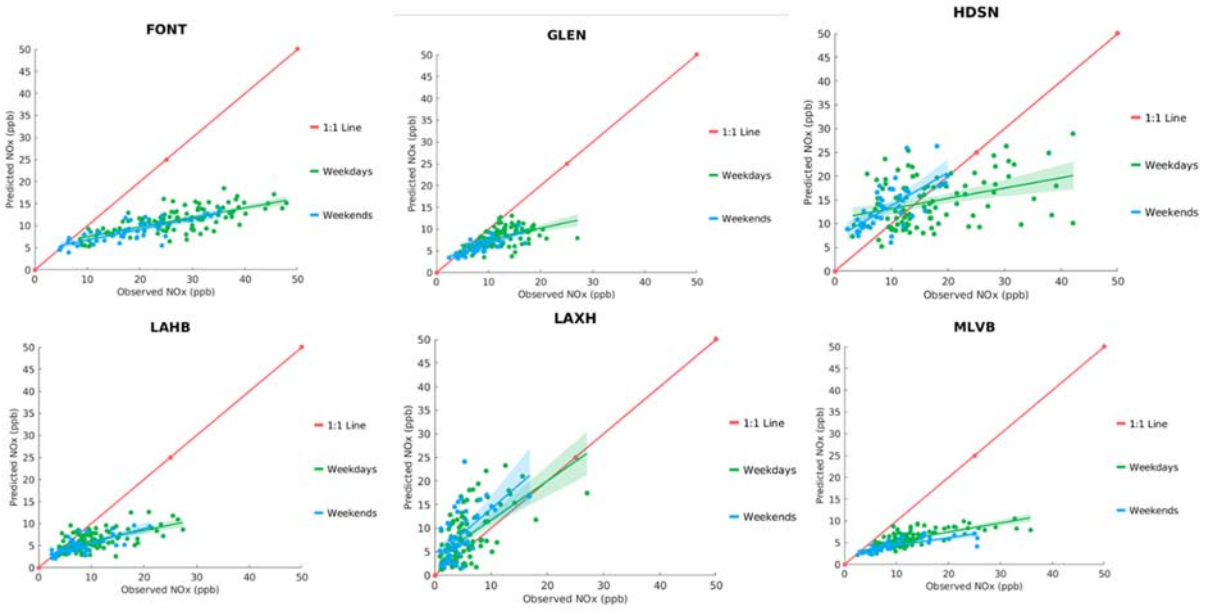

FIGURE N-2: SCATTER PLOT OF OBSERVED VS. PREDICTED DAILY AVERAGE NOX DURING MAY 1ST TO SEPTEMBER 30TH, 2018, AT FONTANA (FONT), GLENDORA (GLEN), HUDSON (HDSN), AND LA HABRA (LAHB), LAX (LAX), AND MIRA LOMA (MLVB). GREEN AND BLUE LINES INDICATE GENERAL LINEAR MODEL FIT WITH 95% CONFIDENCE INTERVAL (SHADED AREA). THE RED LINE INDICATES 1:1 LINE.

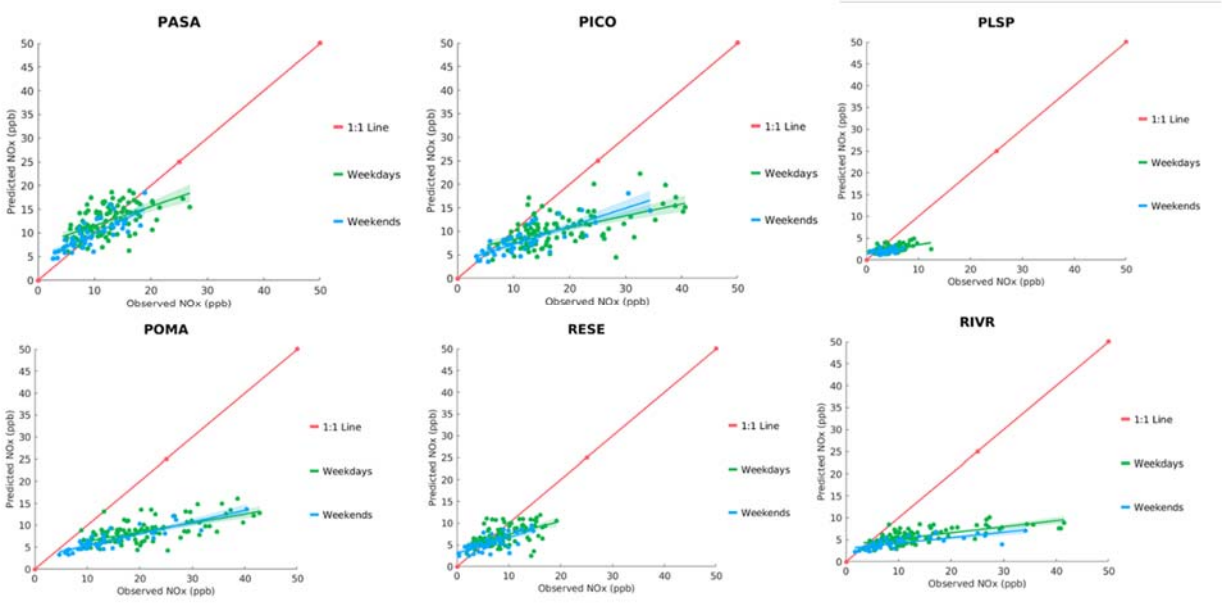

FIGURE N-3: SCATTER PLOT OF OBSERVED VS. PREDICTED DAILY AVERAGE NOX DURING MAY 1ST TO SEPTEMBER 30TH, 2018, AT PASADENA (PASA), PICO RIVERO (PICO), PALM SPRINGS (PLSP), POMONA (POMA), RESEDA (RESE), AND RIVERSIDE (RIVR). GREEN AND BLUE LINES INDICATE GENERAL LINEAR MODEL FIT WITH 95% CONFIDENCE INTERVAL (SHADED AREA). THE RED LINE INDICATES 1:1 LINE.

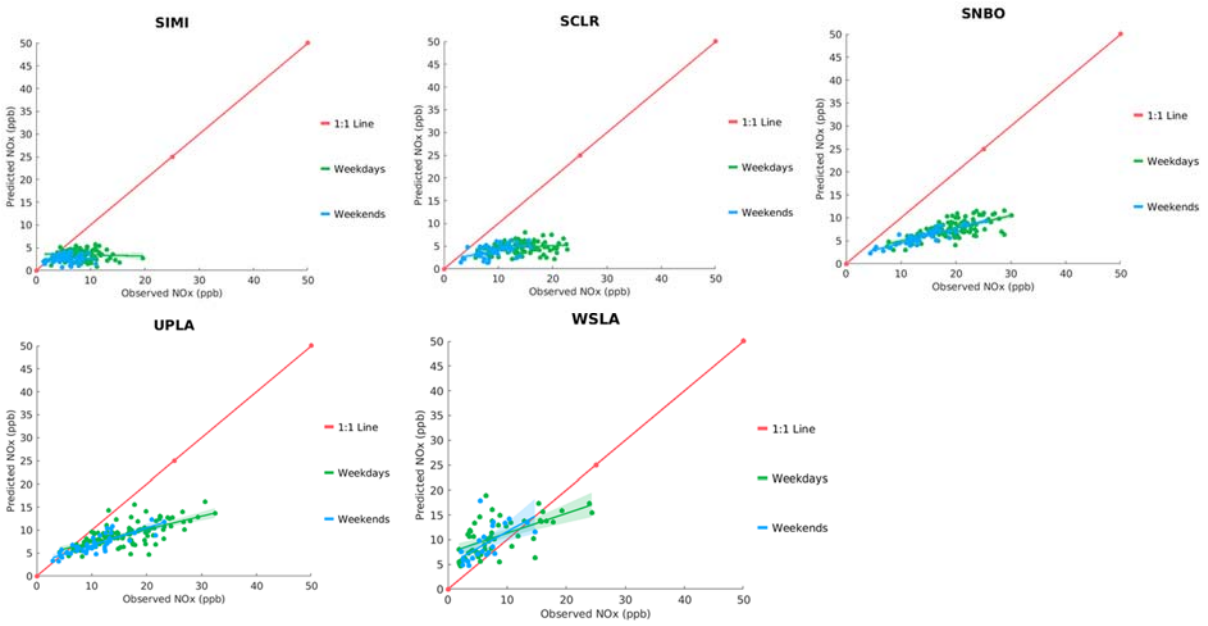

FIGURE N-4: SCATTER PLOT OF OBSERVED VS. PREDICTED DAILY AVERAGE NOX DURING MAY 1ST TO SEPTEMBER 30TH, 2018, AT SIMI VALLEY (SIMI), SANTA CLARITA (SCLR), SAN BERNARDION (SNBO), UPLAND (UPLA), AND WEST LOS ANGELES (WSLA). GREEN AND BLUE LINES INDICATE GENERAL LINEAR MODEL FIT WITH 95% CONFIDENCE INTERVAL (SHADED AREA). THE RED LINE INDICATES 1:1 LINE.

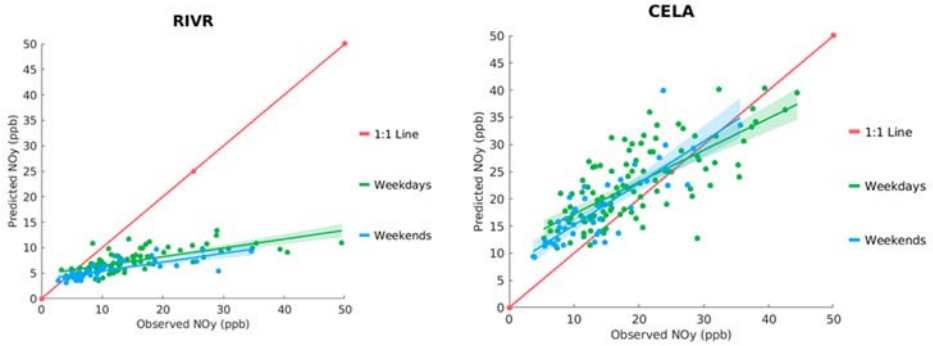

FIGURE O-1: SCATTER PLOT OF OBSERVED VS. PREDICTED DAILY AVERAGE NOY DURING MAY 1ST TO SEPTEMBER 30TH, 2018, AT RIVERSIDE (RIVR) AND CENTRAL LOS ANGELES (CELA). GREEN AND BLUE LINES INDICATE GENERAL LINEAR MODEL FIT WITH 95% CONFIDENCE INTERVAL (SHADED AREA). THE RED LINE INDICATES 1:1 LINE.

Attachment 3

EMISSIONS REDUCTIONS SUMMARY FOR FUTURE CONTROL SCENARIOS

TABLE 1. EMISSIONS REDUCTIONS FROM THE PROPOSED CONTROL MEASURES FOR THE 2037 ATTAINMENT SCENARIO

Control Measures	Average composite CF[1]			2037 planning control baseline (tons/day)			2037 planning remaining (tons/day)			2037 planning reduction (tons/day)		
	NOX	VOC	PM25	NOX	VOC	PM25	NOX	VOC	PM25	NOX	VOC	PM25
C-CMB-01: Commercial Water Heating	35.7%	100.0%	100.0%	0.42	0.08	0.13	0.15	0.08	0.13	0.28	0	0
C-CMB-02: Commercial Space Heating	29.4%	100.0%	100.0%	0.34	0.02	0.03	0.1	0.02	0.03	0.24	0	0
C-CMB-03: Commercial Cooking	34.7%	100.0%	100.0%	0.98	1.04	9.61	0.34	1.04	9.61	0.64	0	0
C-CMB-04: Small Internal Combustion Engines (Non-permitted)	34.9%	100.0%	100.0%	3.47	0.4	0.6	1.21	0.4	0.6	2.25	0	0
C-CMB-05: Miscellaneous Small Commercial Combustion Equipment (Non-permitted)	27.0%	100.0%	100.0%	7.05	1.86	0.58	1.9	1.86	0.58	5.14	0	0
L-CMB-01: NOx RECLAIM	55.1%	100.0%	100.0%	0.69	0.58	0.22	0.38	0.58	0.22	0.31	0	0
L-CMB-02: Large Boilers and Process Heaters	79.7%	100.0%	100.0%	2.36	0.34	0.44	1.88	0.34	0.44	0.48	0	0
L-CMB-03: Large Internal Combustion Prime Engines	68.0%	100.0%	100.0%	1.03	0.16	0.05	0.7	0.16	0.05	0.34	0	0
L-CMB-04: Large Internal Combustion Emergency Standby Engines	52.9%	64.3%	100.0%	4.54	0.28	0.17	2.4	0.18	0.17	2.04	0.1	0
L-CMB-05: Large Turbines	69.2%	100.0%	100.0%	0.26	0.18	0.2	0.18	0.18	0.2	0.07	0	0
L-CMB-06: Electric Generating Facilities	57.5%	100.0%	100.0%	2.14	0.2	0.37	1.23	0.2	0.37	0.91	0	0
L-CMB-07: Petroleum Refining	80.0%	100.0%	100.0%	4.44	1.89	2.14	3.55	1.89	2.14	0.89	0	0
L-CMB-08: Landfills and POTWs	74.8%	100.0%	100.0%	1.31	0.22	0.36	0.98	0.22	0.36	0.33	0	0
L-CMB-09: Incineration	25.0%	100.0%	100.0%	1.2	0.04	0.05	0.3	0.04	0.05	0.9	0	0
L-CMB-10: Miscellaneous Combustion	19.7%	100.0%	100.0%	1.27	7.4	1.69	0.25	7.4	1.69	1.01	0	0

TABLE 1. EMISSIONS REDUCTIONS FROM THE PROPOSED CONTROL MEASURES FOR THE 2037 ATTAINMENT SCENARIO (CONTINUED)

Control Measures	Average composite CF[1]			2037 planning control baseline (tons/day)			2037 planning remaining (tons/day)			2037 planning reduction (tons/day)		
	NOX	VOC	PM25	NOX	VOC	PM25	NOX	VOC	PM25	NOX	VOC	PM25
R-CMB-01: Residential Water Heating	21.3%	100.0%	100.0%	1.78	0.35	0.55	0.38	0.35	0.55	1.4	0	0
R-CMB-02: Residential Space Heating	34.8%	100.0%	100.0%	2.01	0.19	0.3	0.7	0.19	0.3	1.31	0	0
R-CMB-03: Residential Cooking	34.7%	100.0%	100.0%	1.21	0.06	0.1	0.42	0.06	0.1	0.79	0	0
R-CMB-04: Residential Other Combustion	28.0%	100.0%	100.0%	4.29	0.23	0.27	1.2	0.23	0.27	3.09	0	0
FUG-01: Improved Leak Detection and Repair	100.0%	86.4%	100.0%	0	4.42	0	0	3.82	0	0	0.6	0
CTS-01: Further Emission Reduction from Coatings, Solvents, Adhesives, and Sealants	100.0%	97.5%	100.0%	0	19.93	1.45	0	19.43	1.45	0	0.5	0
CARB Consumer Product	100.0%	93.9%	100.0%	0	131.79	0	0	123.79	0	0	8	0
TOTAL STATIONARY:	**44.8%**	**94.6%**	**100.0%**	**40.78**	**171.66**	**19.3**	**18.27**	**162.46**	**19.3**	**22.41**	**9.2**	**0**
Passenger Vehicles (ACC 2.0)	62.1%	84.5%	79.6%	13.12	24.64	7.60	8.15	20.81	6.05	4.97	3.84	1.54
Motorcycles (Motorcycle standards)	61.6%	77.4%	100.0%	2.16	9.19	0.02	1.33	7.11	0.02	0.83	2.08	0
Medium Duty Vehicles (ACT/ACF)	100.0%	100.0%	100.0%	1.35	0.72	0.26	1.35	0.72	0.26	0	0	0
Heavy Duty Vehicles (ACT/Omnibus/ACF/HD I&M)	27.9%	33.1%	62.7%	20.06	1.33	1.42	5.59	0.44	0.89	14.47	0.88	0.53
TOTAL CARB ONROAD:	**44.8%**	**81.0%**	**77.6%**	**36.69**	**35.88**	**9.3**	**16.42**	**29.08**	**7.22**	**20.27**	**6.8**	**2.07**
CHC 2020 MSS	43.9%	10.7%	41.7%	4.65	0.28	0.12	2.04	0.03	0.05	2.61	0.25	0.07
CHE Regulation	3.2%	11.6%	50.0%	0.63	0.43	0.04	0.02	0.05	0.02	0.61	0.39	0.02
Proposed Forklift LSI Regulation	39.4%	39.1%	40.0%	1.55	0.23	0.15	0.61	0.09	0.06	0.94	0.14	0.09
Amendment to In-Use Off-road Regulation	83.7%	66.4%	87.0%	6.03	1.28	0.23	5.05	0.85	0.2	0.99	0.43	0.02
Proposed In-Use Locomotive Reg	29.5%	23.0%	28.6%	15.5	0.61	0.28	4.57	0.14	0.08	10.94	0.47	0.2

TABLE 1. EMISSIONS REDUCTIONS FROM THE PROPOSED CONTROL MEASURES FOR THE 2037 ATTAINMENT SCENARIO (CONTINUED)

Control Measures	Average composite CF[1]			2037 planning control baseline (ton/day)			2037 planning remaining (tons/day)			2037 planning reduction (tons/day)		
	NOX	VOC	PM25	NOX	VOC	PM25	NOX	VOC	PM25	NOX	VOC	PM25
Pleasure Craft 2020 MSS	90.2%	100.0%	92.0%	3.37	10.76	0.5	3.04	10.76	0.46	0.33	0	0.04
Proposed Tier V Regulation	55.8%	89.3%	100.0%	9.73	1.87	0.31	5.43	1.67	0.31	4.3	0.2	0
TRU Phase 1 & 2	0.5%	1.4%	0.0%	5.51	0.72	0.18	0.03	0.01	0	5.48	0.71	0.18
ZE Manufacture Rule	87.0%	100.0%	100.0%	16.89	12.11	0.84	14.69	12.11	0.84	2.2	0	0
OGV (Cleaner Vessel Visit + More Stringent NOx Standard)	20.1%	100.0%	100.0%	30.65	9.97	0.78	6.17	9.97	0.78	24.48	0	0
Aircraft (Cleaner fuel and visit requirement + aviation emission cap)	30.6%	30.0%	30.1%	27.93	3.93	0.73	8.54	1.18	0.22	19.39	2.75	0.51
TOTAL CARB OFFROAD:	**41.0%**	**87.4%**	**72.6%**	**122.44**	**42.19**	**4.16**	**50.19**	**36.86**	**3.02**	**72.27**	**5.34**	**1.13**
MOB-11: On-Road HD Trucks	77.4%	100.0%	99.3%	5.91	1.05	0.98	4.57	1.05	0.97	1.34	0.00	0.01
MOB-05: Accelerated Retirement of Older Light-duty and Medium-duty Vehicles	98.7%	100.0%	100.0%	8.15	20.81	6.05	8.04	20.81	6.05	0.11	0.00	0.00
MOB-11: School Buses	22.1%	100.0%	98.7%	0.38	0.04	0.09	0.08	0.04	0.09	0.30	0.00	0.00
MOB-11: Agricultural	25.1%	100.0%	5.6%	0.11	0.11	0.02	0.03	0.11	0.00	0.08	0.00	0.02
MOB-11: Construction	20.5%	100.0%	80.2%	2.26	2.07	0.35	0.46	2.07	0.28	1.80	0.00	0.07
MOB-11: Industrial and CHE	93.3%	100.0%	98.2%	5.50	8.34	0.24	5.13	8.34	0.24	0.37	0.00	0.00
MOB-11: Commercial Harbor Crafts	35.9%	100.0%	44.0%	2.84	0.12	0.10	1.02	0.12	0.04	1.82	0.00	0.06
MOB-11: TRUs	73.2%	100.0%	100.0%	0.03	0.00	0.00	0.02	0.00	0.00	0.01	0.00	0.00
MOB-11: Locomotives	78.5%	100.0%	5.0%	4.57	0.18	0.06	3.59	0.18	0.00	0.98	0.00	0.06
TOTAL INCENTIVE:	**77.1%**	**100.0%**	**97.3%**	**29.75**	**32.72**	**7.89**	**22.95**	**32.72**	**7.68**	**6.80**	**0.00**	**0.21**
Further Deployment of Cleaner Technology from Stationary	83.7%	100.0%	100.0%	18.37	38.77	17.86	15.37	38.77	15.37	3	0	0
SIP Set Aside Account	103.3%	100.0%	100.0%	15.37	38.77	15.37	15.87	42.77	15.37	-0.5	-4	0
GRAND TOTAL:	**32.6%**	**94.9%**	**94.2%**	**184.46**	**338.68**	**58.58**	**60.21**	**321.34**	**55.17**	**124.25**	**17.34**	**3.41**

[1]Average Composite CF (control factor) for each measure defined as the ratio between remaining emission and baseline emission per pollutants

TABLE 2. EMISSIONS REDUCTIONS FROM THE PROPOSED CONTROL MEASURES FOR THE 2032 CONTROL SCENARIO

Control Measures	Average composite CF[1]			2032 planning control baseline (tons/day)			2032 planning remaining (tons/day)			2032 planning reduction (tons/day)		
	NOX	VOC	PM25	NOX	VOC	PM25	NOX	VOC	PM25	NOX	VOC	PM25
C-CMB-01: Commercial Water Heating	91.1%	100.0%	100.0%	0.45	0.09	0.14	0.41	0.09	0.14	0.04	0	0
C-CMB-02: Commercial Space Heating	91.7%	100.0%	100.0%	0.48	0.02	0.03	0.44	0.02	0.03	0.04	0	0
C-CMB-03: Commercial Cooking	79.8%	100.0%	100.0%	1.04	1.02	9.37	0.83	1.02	9.37	0.21	0	0
C-CMB-04: Small Internal Combustion Engines (Non-permitted)	100.0%	100.0%	100.0%	3.58	0.41	0.62	3.58	0.41	0.62	0	0	0
C-CMB-05: Miscellaneous Small Commercial Combustion Equipment (Non-permitted)	100.0%	100.0%	100.0%	7.04	1.81	0.59	7.04	1.81	0.59	0	0	0
L-CMB-01: NOx RECLAIM	100.0%	100.0%	100.0%	0.7	0.57	0.22	0.7	0.57	0.22	0	0	0
L-CMB-02: Large Boilers and Process Heaters	100.0%	100.0%	100.0%	2.45	0.33	0.43	2.45	0.33	0.43	0	0	0
L-CMB-03: Large Internal Combustion Prime Engines	100.0%	100.0%	100.0%	0.99	0.16	0.04	0.99	0.16	0.04	0	0	0
L-CMB-04: Large Internal Combustion Emergency Standby Engines	100.0%	100.0%	100.0%	4.48	0.28	0.17	4.48	0.28	0.17	0	0	0
L-CMB-05: Large Turbines	100.0%	100.0%	100.0%	0.25	0.17	0.2	0.25	0.17	0.2	0	0	0
L-CMB-06: Electric Generating Facilities	95.8%	100.0%	100.0%	2.15	0.2	0.37	2.06	0.2	0.37	0.09	0	0
L-CMB-07: Petroleum Refining	100.0%	100.0%	100.0%	4.7	1.89	2.14	4.7	1.89	2.14	0	0	0
L-CMB-08: Landfills and POTWs	100.0%	100.0%	100.0%	1.29	0.21	0.35	1.29	0.21	0.35	0	0	0
L-CMB-09: Incineration	100.0%	100.0%	100.0%	1.18	0.04	0.05	1.18	0.04	0.05	0	0	0
L-CMB-10: Miscellaneous Combustion	100.0%	100.0%	100.0%	1.27	7.47	1.68	1.27	7.47	1.68	0	0	0

TABLE 2. EMISSIONS REDUCTIONS FROM THE PROPOSED CONTROL MEASURES FOR THE 2032 CONTROL SCENARIO (CONTINUED)

Control Measures	Average composite CF[1]			2032 planning control baseline (tons/day)			2032 planning remaining (tons/day)			2032 planning reduction (tons/day)		
	NOX	VOC	PM25	NOX	VOC	PM25	NOX	VOC	PM25	NOX	VOC	PM25
R-CMB-01: Residential Water Heating	74.4%	100.0%	100.0%	1.8	0.36	0.56	1.34	0.36	0.56	0.46	0	0
R-CMB-02: Residential Space Heating	81.7%	100.0%	100.0%	2.4	0.19	0.3	1.96	0.19	0.3	0.44	0	0
R-CMB-03: Residential Cooking	76.4%	100.0%	100.0%	1.23	0.06	0.1	0.94	0.06	0.1	0.29	0	0
R-CMB-04: Residential Other Combustion	72.7%	100.0%	100.0%	4.21	0.23	0.26	3.06	0.23	0.26	1.15	0	0
FUG-01: Improved Leak Detection and Repair	100.0%	85.9%	100.0%	0	4.27	0	0	3.67	0	0	0.6	0
CTS-01: Further Emission Reduction from Coatings, Solvents, Adhesives, and Sealants	100.0%	97.5%	100.0%	0	19.82	1.46	0	19.32	1.46	0	0.5	0
TOTAL STATIONARY:	**93.5%**	**97.2%**	**100.0%**	**41.69**	**39.60**	**19.08**	**38.97**	**38.50**	**19.08**	**2.72**	**1.10**	**0.00**
Passenger Vehicles (ACC 2.0)	85.9%	94.2%	90.8%	14.93	29.79	7.59	12.83	28.06	6.89	2.1	1.73	0.7
Motorcycles (Motorcycle standards)	75.7%	87.6%	100.0%	2.1	8.8	0.02	1.59	7.71	0.02	0.52	1.09	0
Medium Duty Vehicles (ACT/ACF)	100.0%	100.0%	100.0%	2.25	1.15	0.28	2.25	1.15	0.28	0	0	0
Heavy Duty Vehicles (ACT/Omnibus/ACF/HD I&M)	58.4%	63.5%	81.4%	23.92	1.37	1.4	13.96	0.87	1.14	9.96	0.5	0.26
TOTAL CARB ONROAD:	**70.9%**	**91.9%**	**89.7%**	**43.21**	**41.11**	**9.29**	**30.63**	**37.8**	**8.33**	**12.57**	**3.31**	**0.96**
CHC 2020 MSS	53.2%	16.1%	46.2%	5.64	0.31	0.13	3	0.05	0.06	2.64	0.26	0.08
CHE Regulation	42.4%	16.7%	37.5%	1.77	0.48	0.08	0.75	0.08	0.03	1.02	0.41	0.05
Proposed Forklift LSI Regulation	52.7%	53.6%	53.3%	1.84	0.28	0.15	0.97	0.15	0.08	0.88	0.07	0.13
Amendment to In-Use Off-road Regulation	77.8%	61.3%	85.3%	7.78	1.42	0.34	6.05	0.87	0.29	1.73	0.55	0.05
Proposed In-Use Locomotive Reg	43.7%	31.0%	44.1%	17.75	0.71	0.34	7.75	0.22	0.15	10	0.48	0.19
Pleasure Craft 2020 MSS	97.7%	100.0%	100.0%	3.41	12.84	0.58	3.33	12.84	0.58	0.08	0	0.01

TABLE 2. EMISSIONS REDUCTIONS FROM THE PROPOSED CONTROL MEASURES FOR THE 2032 CONTROL SCENARIO (CONCLUDED)

Control Measures	Average composite CF[1]			2032 planning control baseline (tons/day)			2032 planning remaining (tons/day)			2032 planning reduction (tons/da)		
	NOX	VOC	PM25	NOX	VOC	PM25	NOX	VOC	PM25	NOX	VOC	PM25
Proposed Tier V Regulation	83.0%	97.0%	100.0%	11.06	1.98	0.44	9.18	1.92	0.44	1.88	0.06	0
TRU Phase 1 & 2	33.5%	9.1%	35.3%	5.1	0.66	0.17	1.71	0.06	0.06	3.39	0.6	0.11
TOTAL CARB OFFROAD:	**60.2%**	**86.7%**	**75.8%**	**54.35**	**18.68**	**2.23**	**32.74**	**16.19**	**1.69**	**21.62**	**2.43**	**0.62**
MOB-11: On-Road HD Trucks	93.0%	100.0%	99.2%	14.32	1.84	1.21	13.32	1.84	1.20	1.00	0.00	0.01
MOB-05: Accelerated retirement of older light-duty and medium-duty vehicles	98.4%	100.0%	100.0%	12.83	28.06	6.89	12.63	28.06	6.89	0.20	0.00	0.00
MOB-11: School Buses	73.8%	100.0%	98.1%	0.89	0.06	0.11	0.66	0.06	0.11	0.23	0.00	0.00
MOB-11: Agricultural	63.0%	100.0%	2.5%	0.26	0.15	0.02	0.16	0.15	0.00	0.10	0.00	0.02
MOB-11: Construction	49.0%	100.0%	80.8%	4.98	2.12	0.42	2.44	2.12	0.34	2.54	0.00	0.08
MOB-11: Industrial and CHE	93.2%	100.0%	95.8%	10.01	11.76	0.32	9.33	11.76	0.31	0.68	0.00	0.01
MOB-11: Commercial Harbor Crafts	41.7%	100.0%	48.9%	2.99	0.13	0.11	1.25	0.13	0.05	1.74	0.00	0.06
MOB-11: TRUs	98.6%	100.0%	99.7%	1.71	0.25	0.01	1.69	0.25	0.01	0.02	0.00	0.00
MOB-11: Locomotives	89.7%	100.0%	56.5%	7.75	0.31	0.11	6.96	0.31	0.06	0.79	0.00	0.05
TOTAL INCENTIVE:	**86.9%**	**100.0%**	**97.5%**	**55.74**	**44.68**	**9.20**	**48.43**	**44.68**	**8.97**	**7.31**	**0.00**	**0.23**
GRAND TOTAL:	**77.8%**	**98.0%**	**96.9%**	**198.88**	**344.88**	**58.13**	**154.66**	**338.04**	**56.32**	**44.22**	**6.84**	**1.81**

[1]Average Composite CF (control factor) for each measure defined as the ratio between remaining emission and baseline emission per pollutants

Attachment 4

2037 8-HOUR OZONE ISOPLETHS

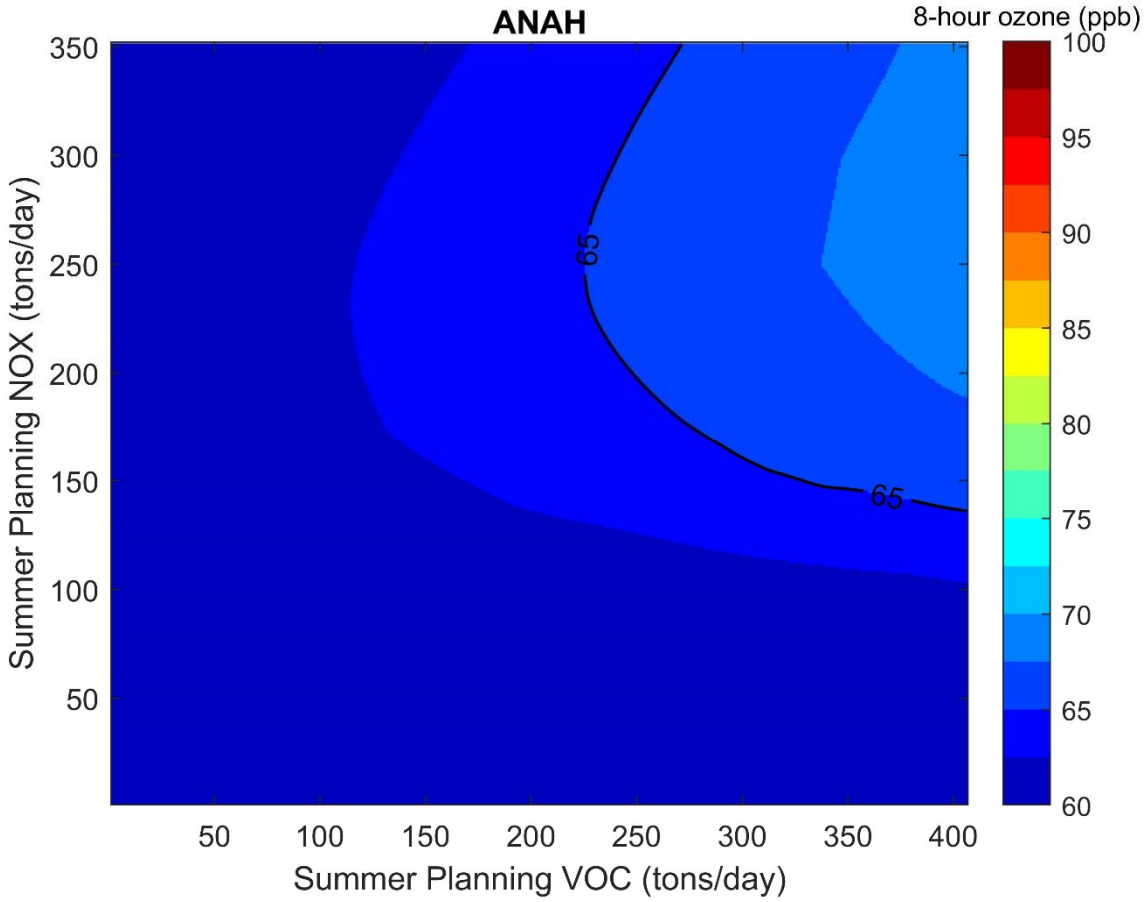
ANAH
8-hour ozone (ppb)
100
95
90
85
80
75
70
65
60
65
65
350
300
250
200
150
100
50
Summer Planning NOX (tons/day)
50
100
150
200
250
300
350
400
Summer Planning VOC (tons/day)

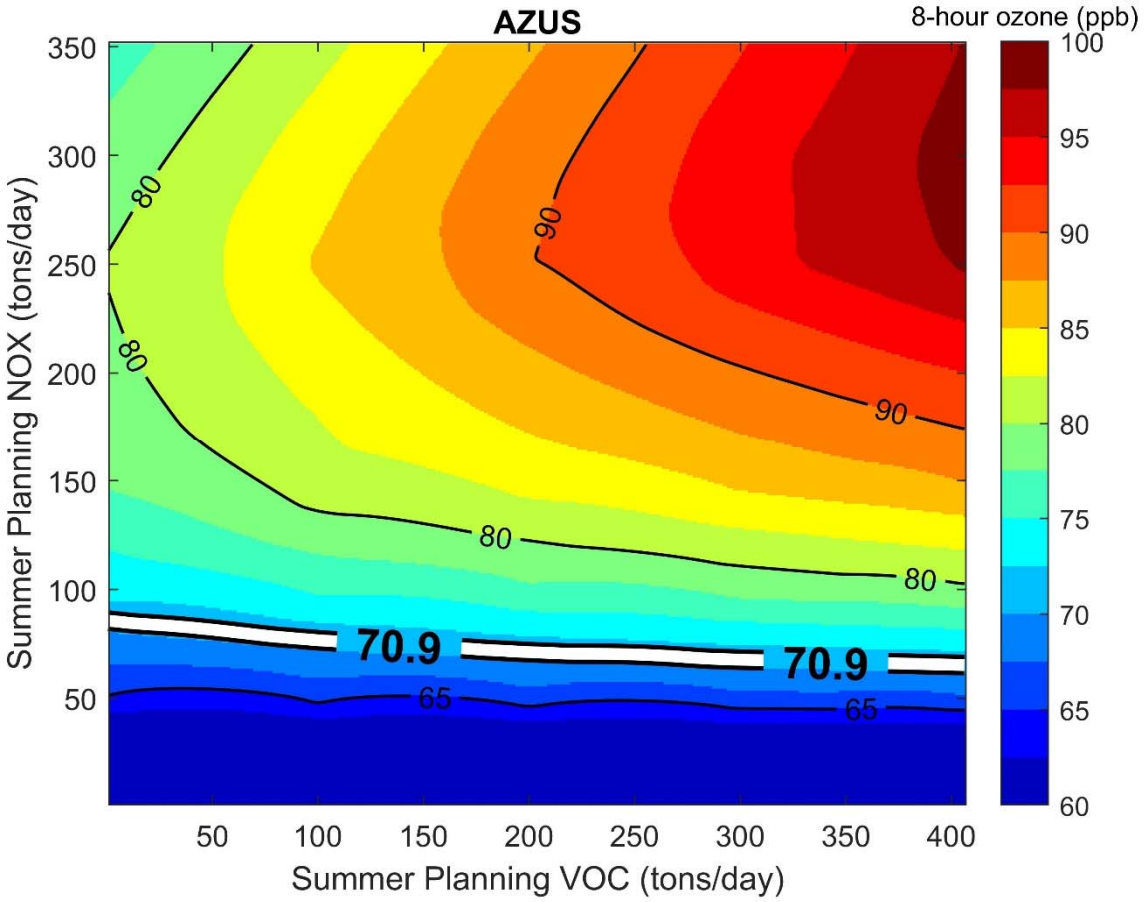
AZUS
8-hour ozone (ppb)
100
95
90
85
80
75
70
65
60
Summer Planning NOX (tons/day)
350
300
250
200
150
100
50
Summer Planning VOC (tons/day)
50
100
150
200
250
300
350
400
80
80
90
90
80
80
70.9
70.9
65
65

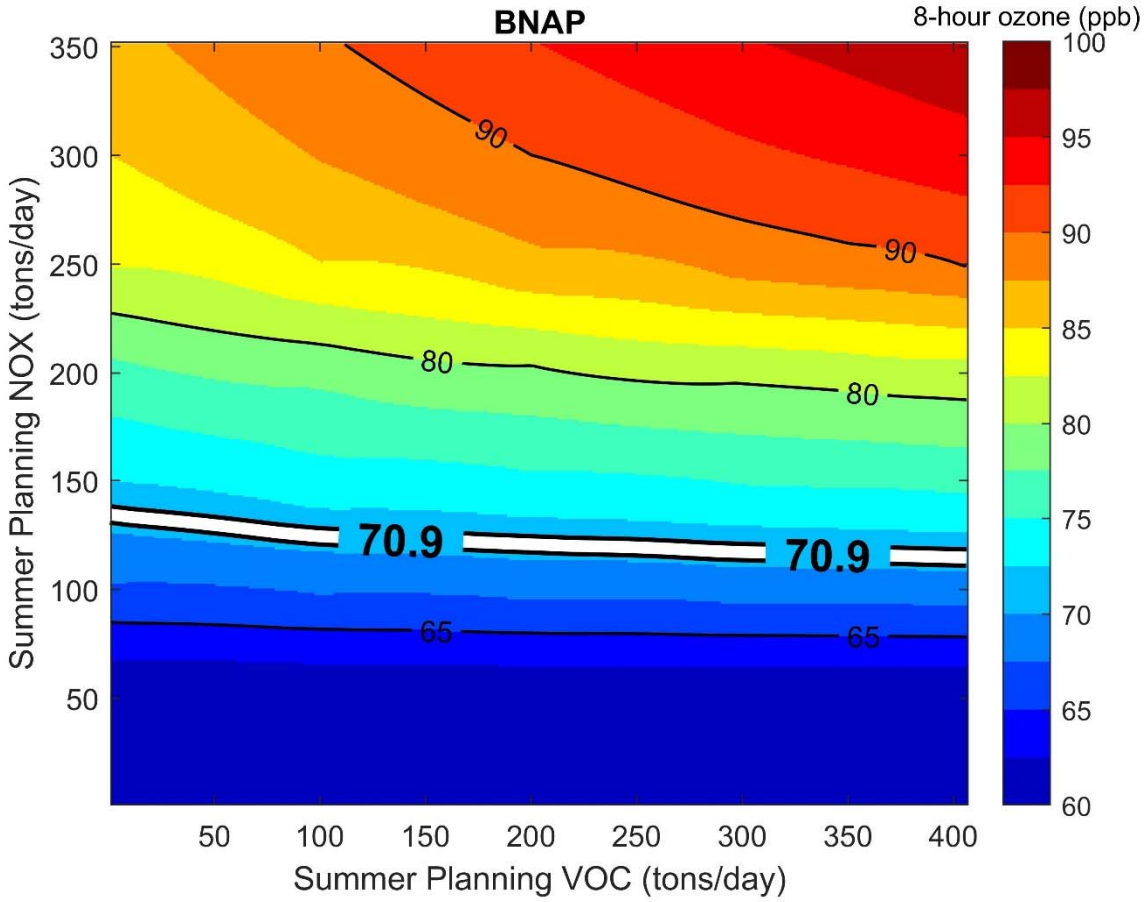
BNAP
8-hour ozone (ppb)
100
95
90
85
80
75
70
65
60
350
300
250
200
150
100
50
Summer Planning NOX (tons/day)
90
90
80
80
70.9
70.9
65
65
50
100
150
200
250
300
350
400
Summer Planning VOC (tons/day)

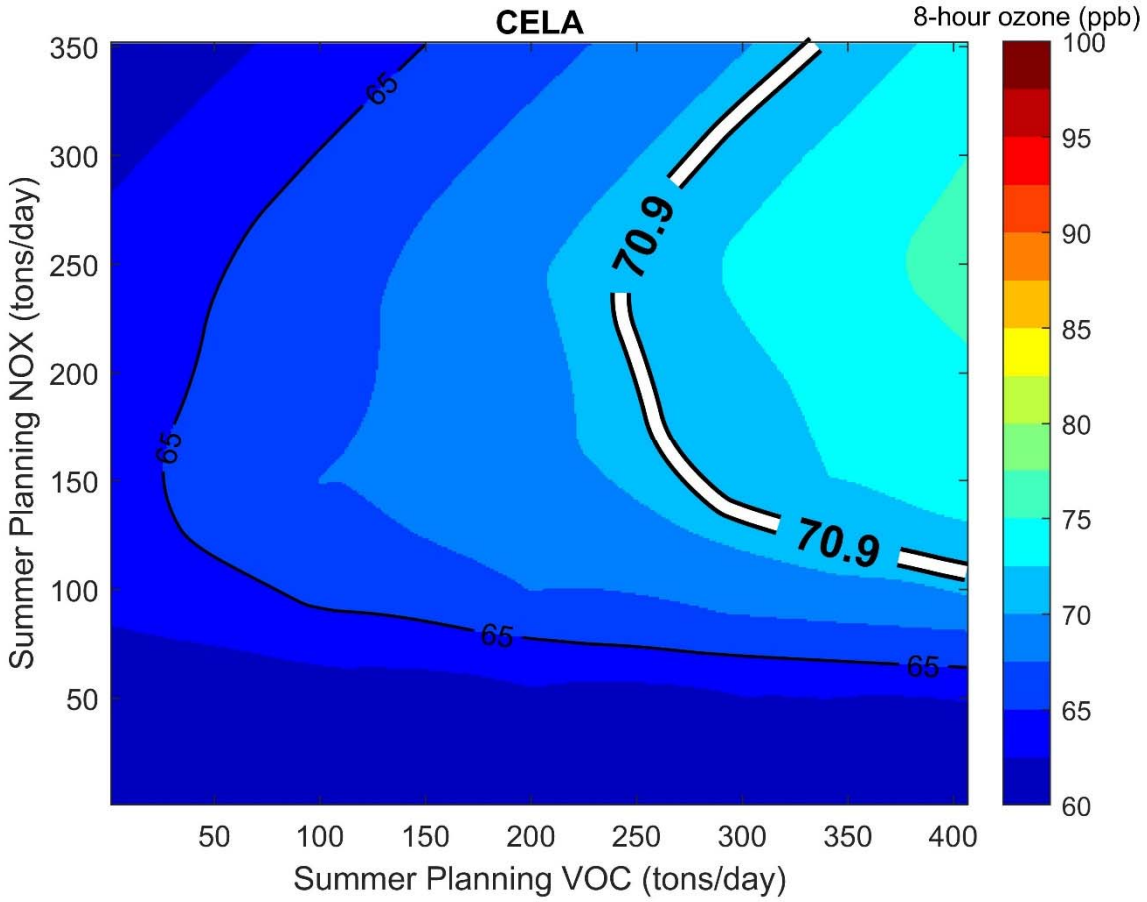
CELA
8-hour ozone (ppb)
100
95
90
85
80
75
70
65
60
Summer Planning NOX (tons/day)
350
300
250
200
150
100
50
Summer Planning VOC (tons/day)
50
100
150
200
250
300
350
400
65
65
65
65
70.9
70.9

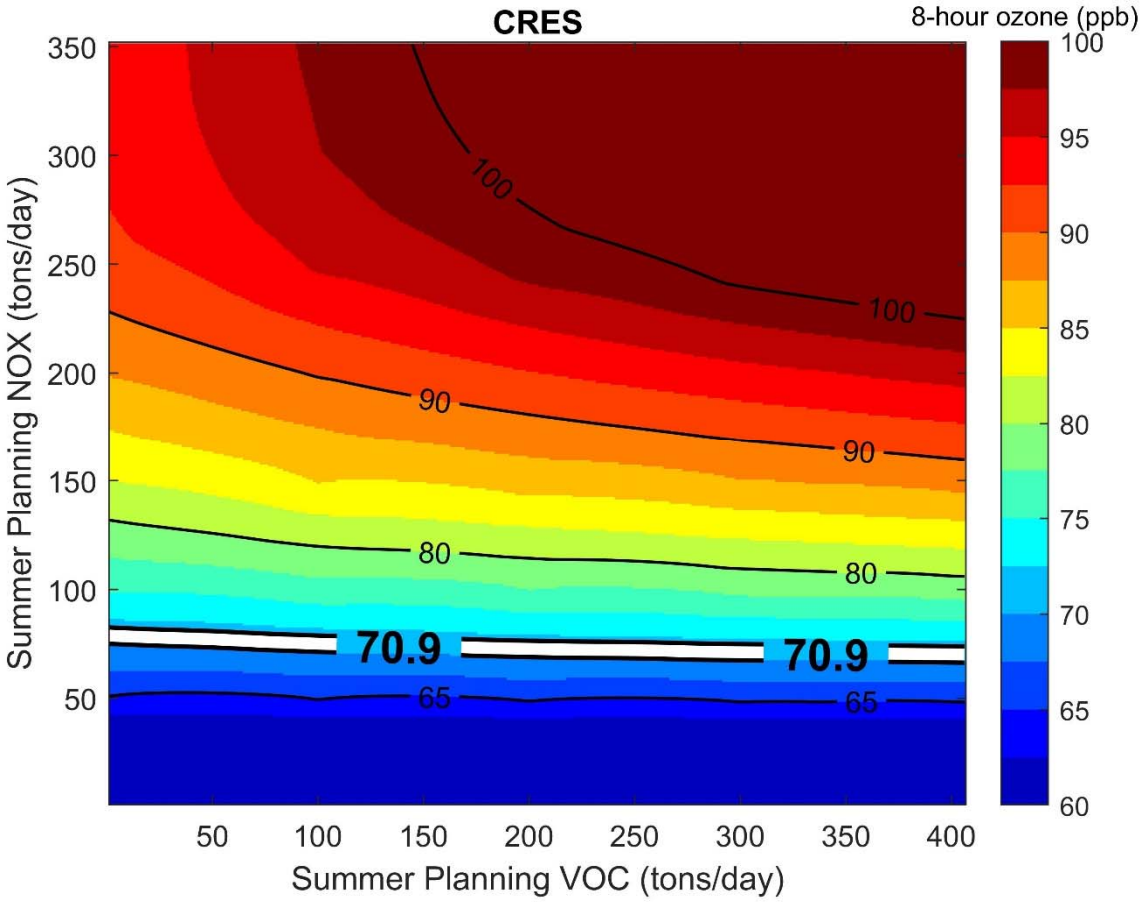
CRES
8-hour ozone (ppb)
100
95
90
85
80
75
70
65
60
Summer Planning NOX (tons/day)
350
300
250
200
150
100
50
Summer Planning VOC (tons/day)
50
100
150
200
250
300
350
400
100
100
90
90
80
80
70.9
70.9
65
65

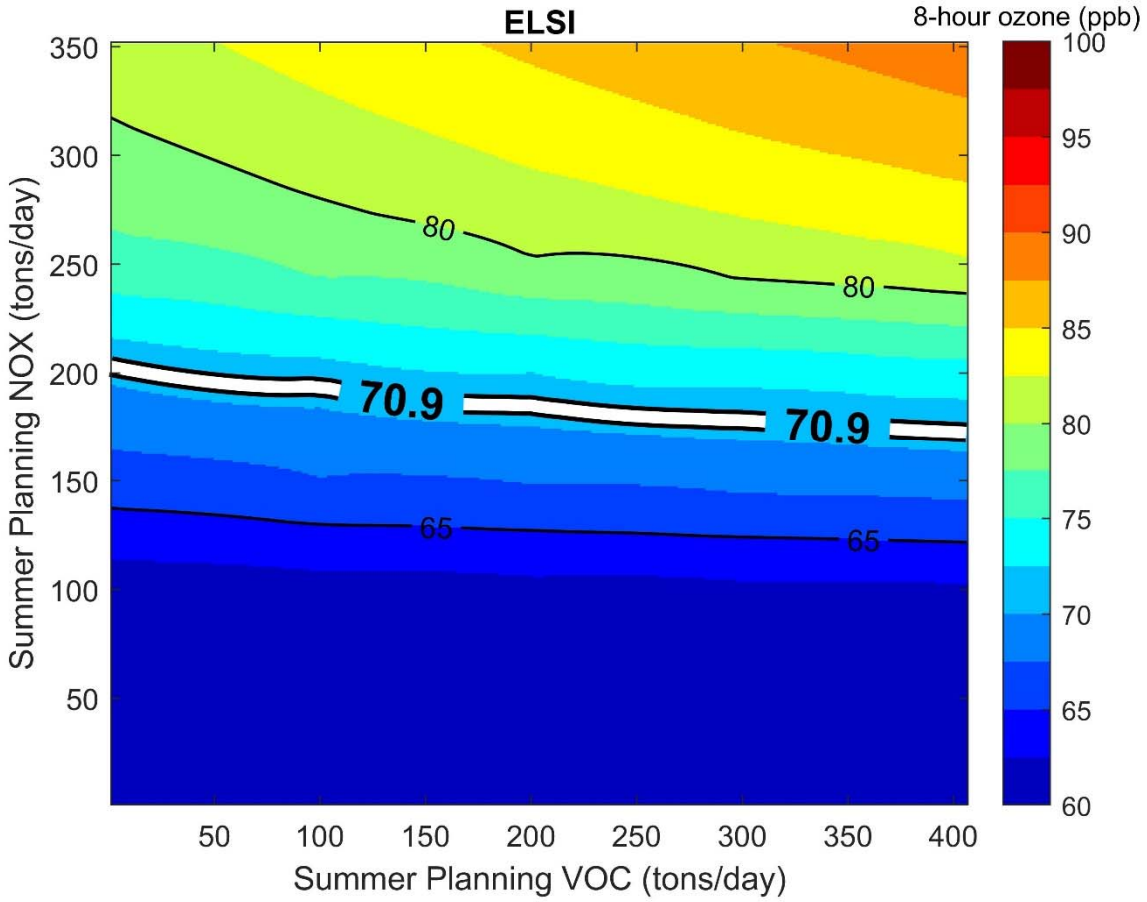
ELSI
8-hour ozone (ppb)
100
95
90
85
80
75
70
65
60
Summer Planning NOX (tons/day)
350
300
250
200
150
100
50
80
80
70.9
70.9
65
65
50
100
150
200
250
300
350
400
Summer Planning VOC (tons/day)

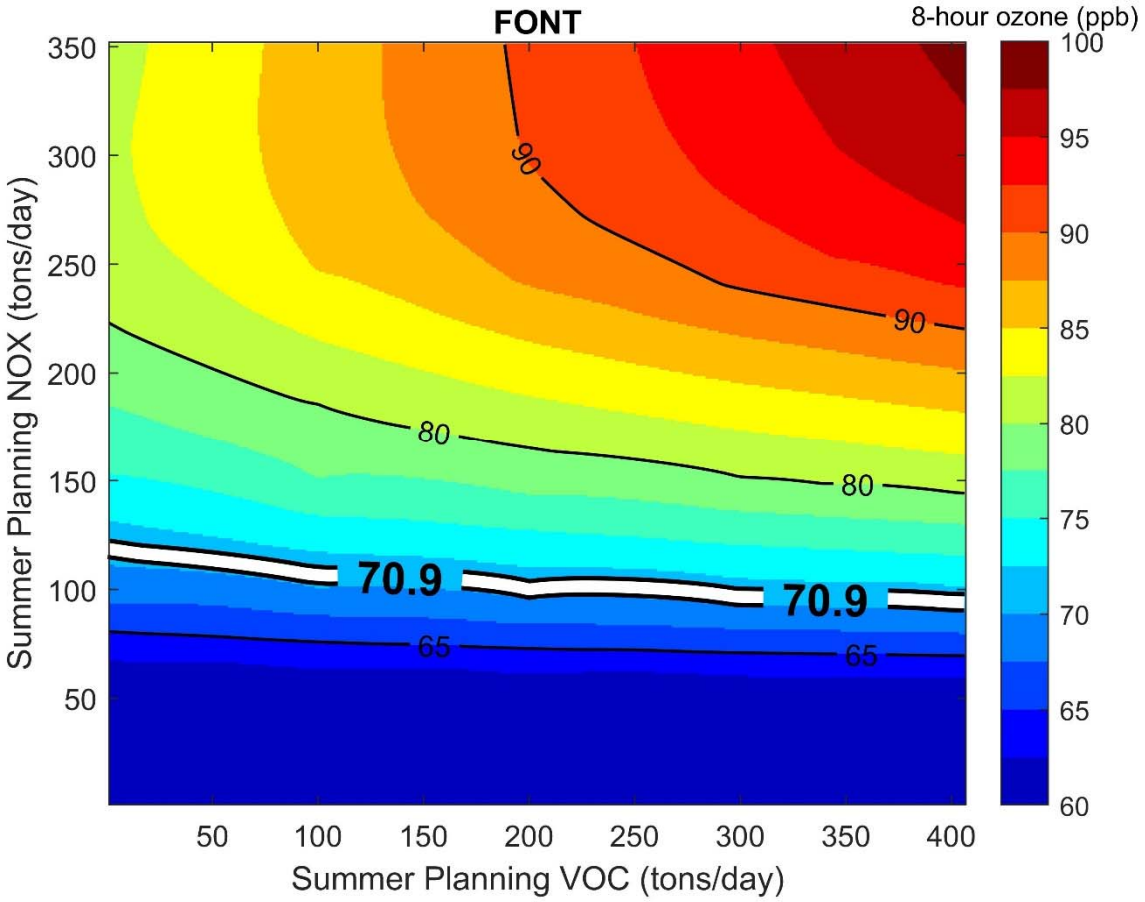
FONT
8-hour ozone (ppb)
100
95
90
85
80
75
70
65
60
Summer Planning NOX (tons/day)
350
300
250
200
150
100
50
90
90
80
80
70.9
70.9
65
65
50
100
150
200
250
300
350
400
Summer Planning VOC (tons/day)

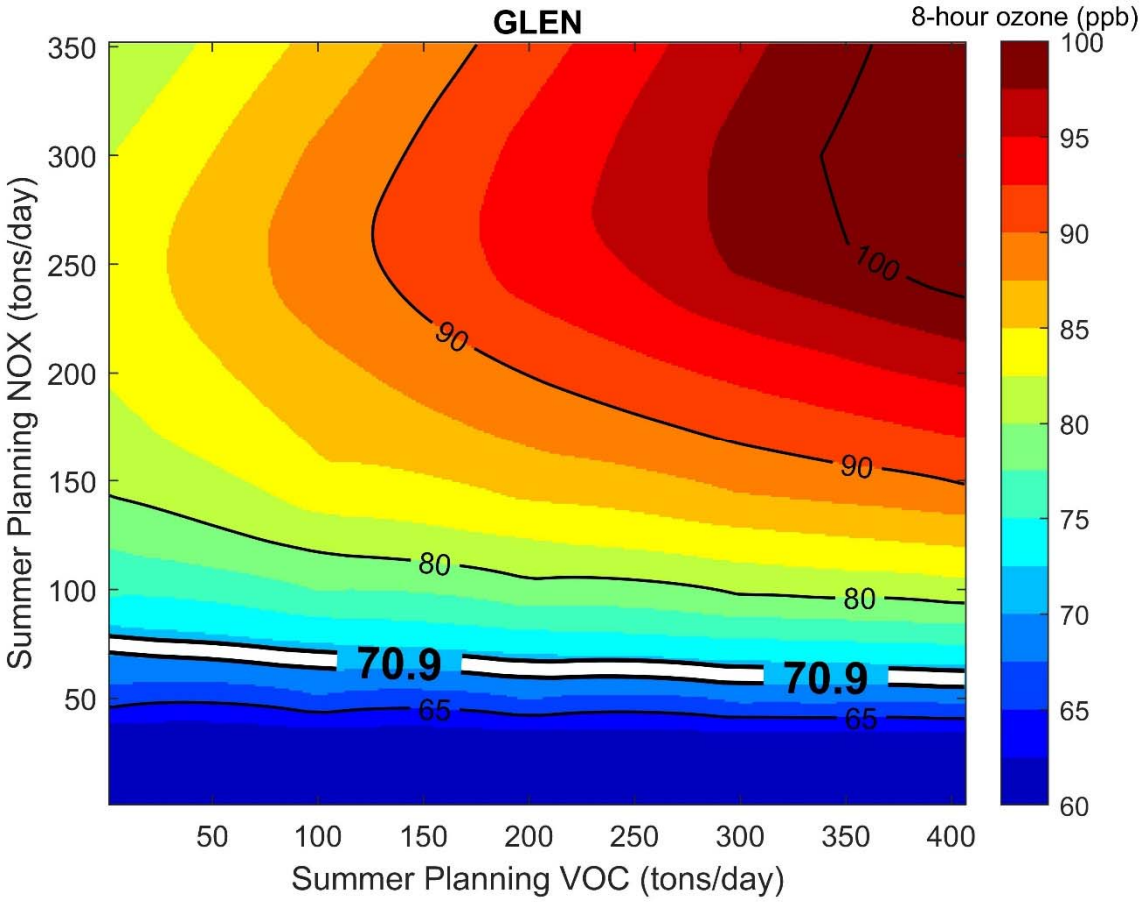
GLEN
8-hour ozone (ppb)
100
95
90
85
80
75
70
65
60
Summer Planning NOX (tons/day)
350
300
250
200
150
100
50
100
90
90
80
80
70.9
70.9
65
65
50
100
150
200
250
300
350
400
Summer Planning VOC (tons/day)

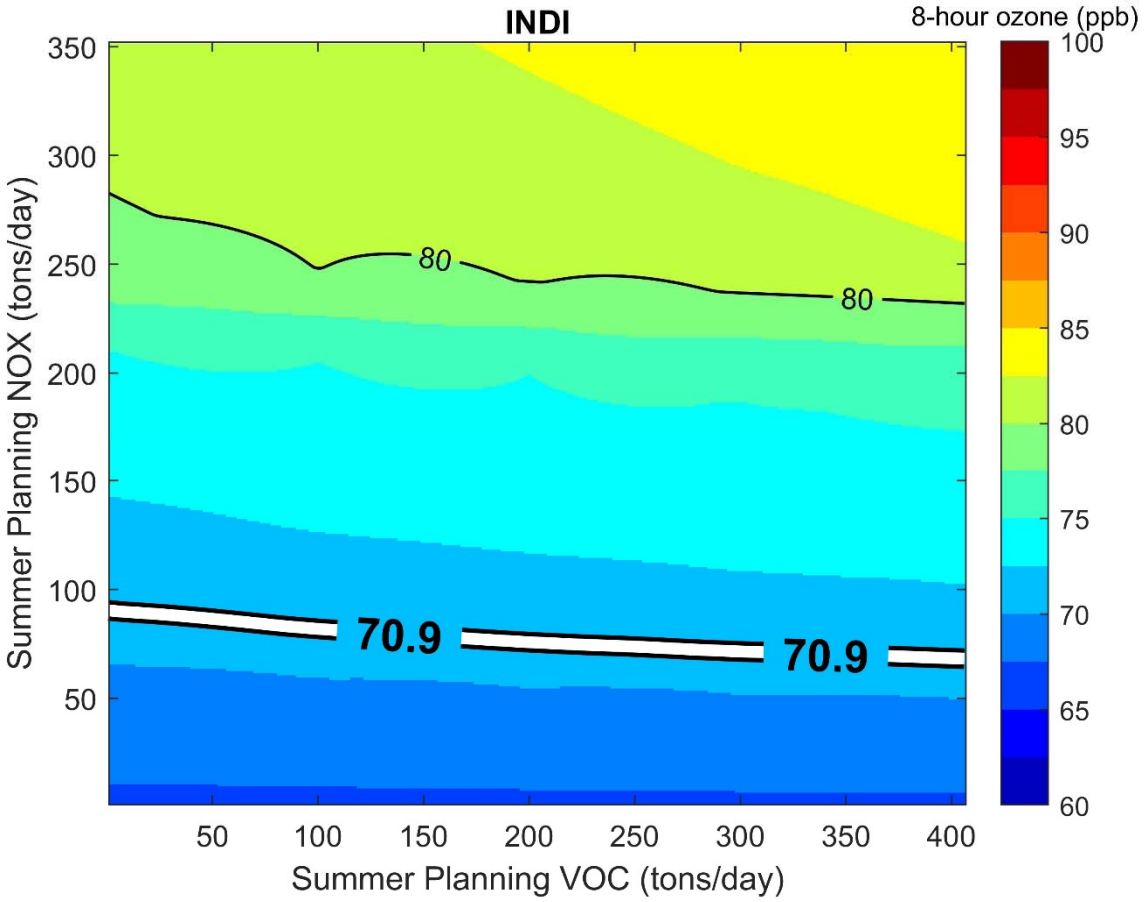
INDI
8-hour ozone (ppb)
100
95
90
85
80
75
70
65
60
350
300
250
200
150
100
50
Summer Planning NOX (tons/day)
80
80
70.9
70.9
50
100
150
200
250
300
350
400
Summer Planning VOC (tons/day)

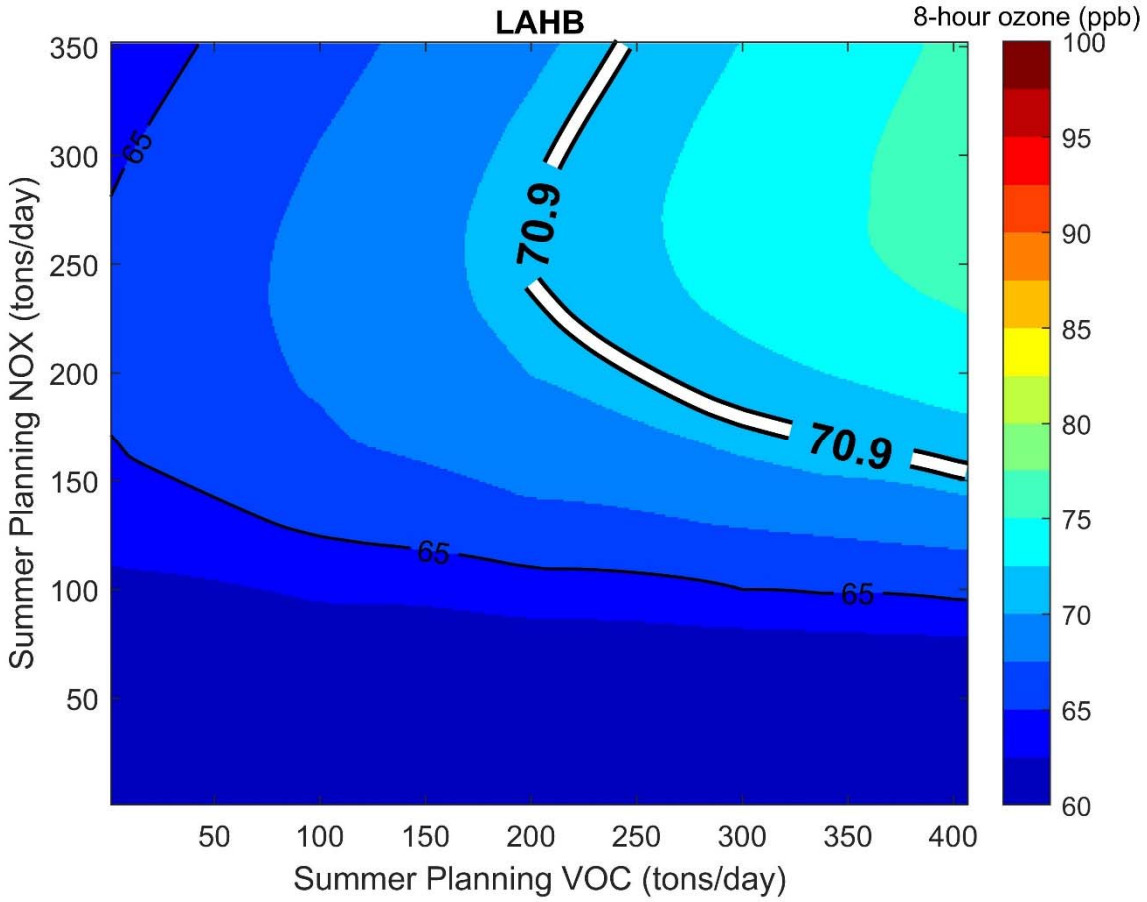
LAHB
8-hour ozone (ppb)
100
95
90
85
80
75
70
65
60
350
300
250
200
150
100
50
Summer Planning NOX (tons/day)
65
70.9
70.9
65
65
50
100
150
200
250
300
350
400
Summer Planning VOC (tons/day)

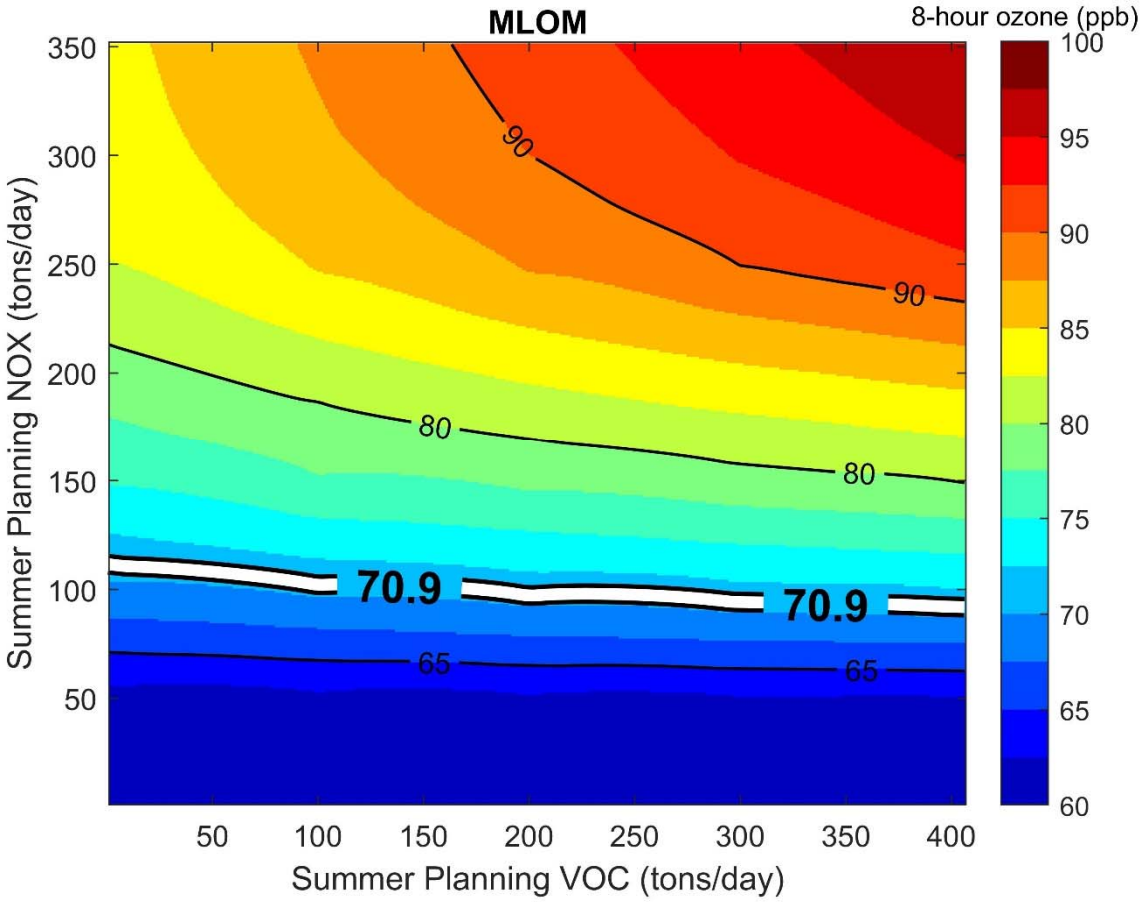
MLOM
8-hour ozone (ppb)
100
95
90
85
80
75
70
65
60
Summer Planning NOX (tons/day)
350
300
250
200
150
100
50
90
90
80
80
70.9
70.9
65
65
50
100
150
200
250
300
350
400
Summer Planning VOC (tons/day)

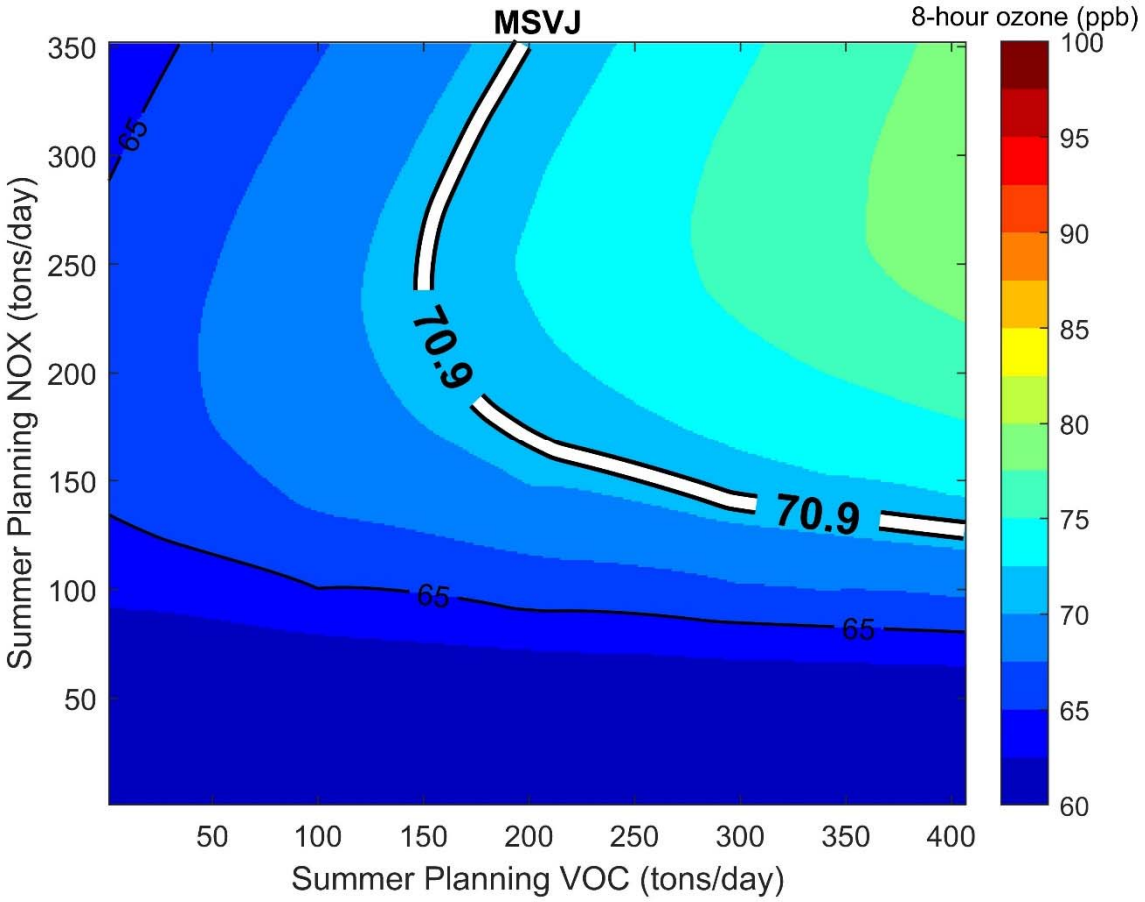
MSVJ
8-hour ozone (ppb)
100
95
90
85
80
75
70
65
60
Summer Planning NOX (tons/day)
350
300
250
200
150
100
50
Summer Planning VOC (tons/day)
50
100
150
200
250
300
350
400
65
70.9
70.9
65
65

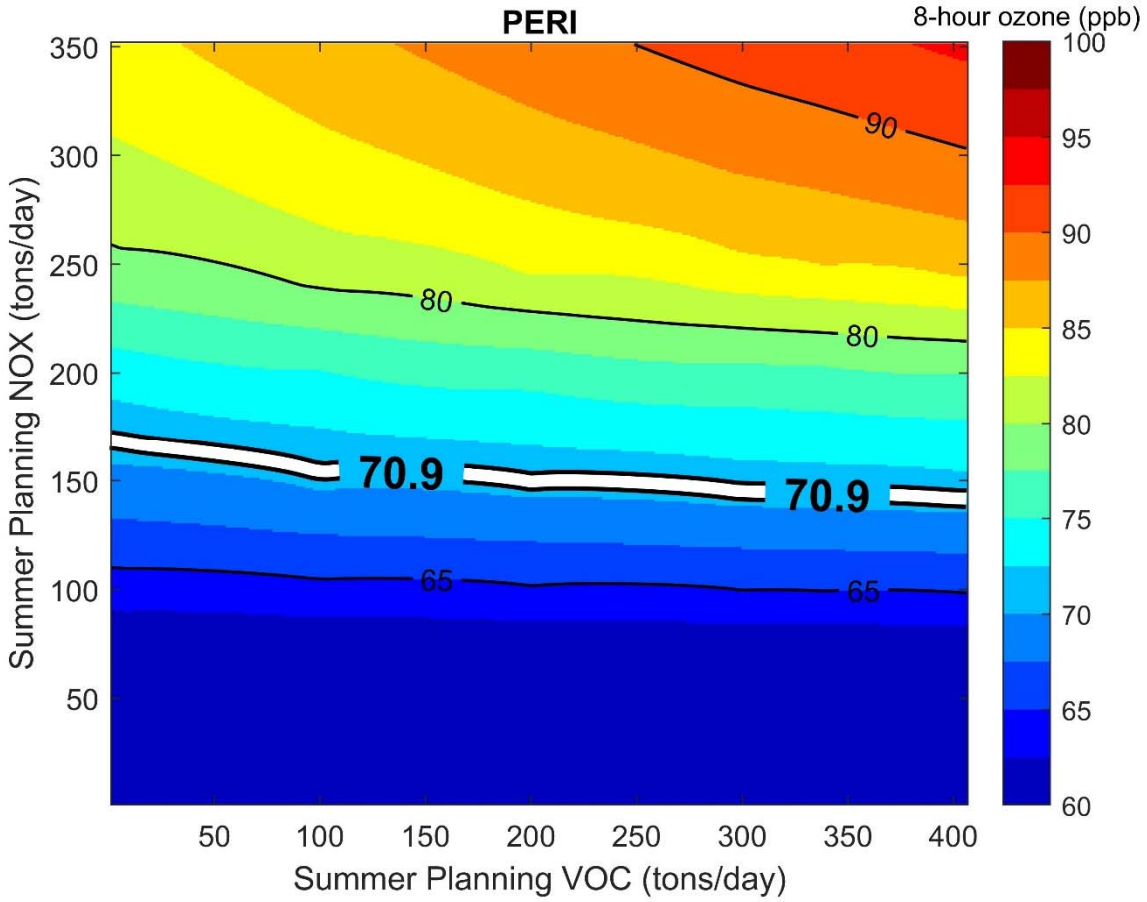
PERI
8-hour ozone (ppb)
100
95
90
85
80
75
70
65
60
350
300
250
200
150
100
50
Summer Planning NOX (tons/day)
90
80
80
70.9
70.9
65
65
50
100
150
200
250
300
350
400
Summer Planning VOC (tons/day)

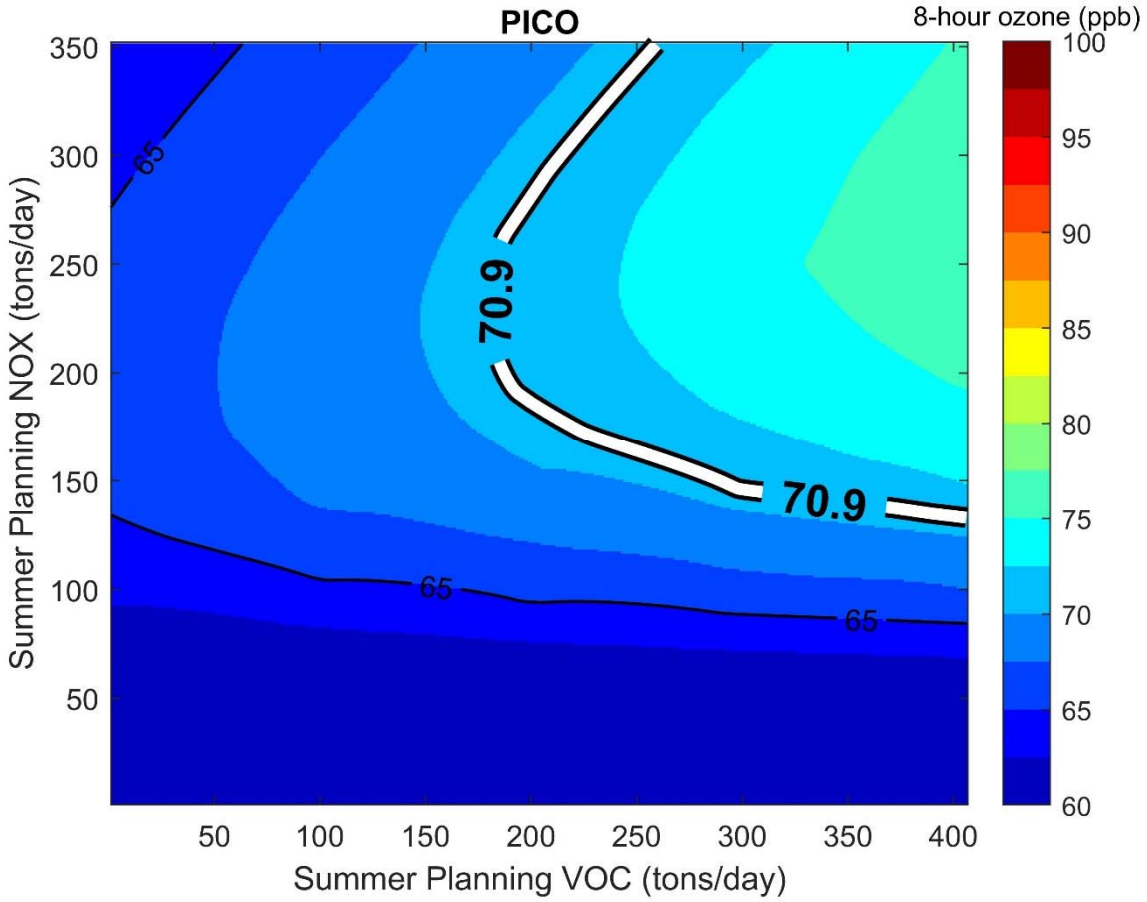
PICO
8-hour ozone (ppb)
100
95
90
85
80
75
70
65
60
Summer Planning NOX (tons/day)
350
300
250
200
150
100
50
65
70.9
70.9
65
65
50
100
150
200
250
300
350
400
Summer Planning VOC (tons/day)

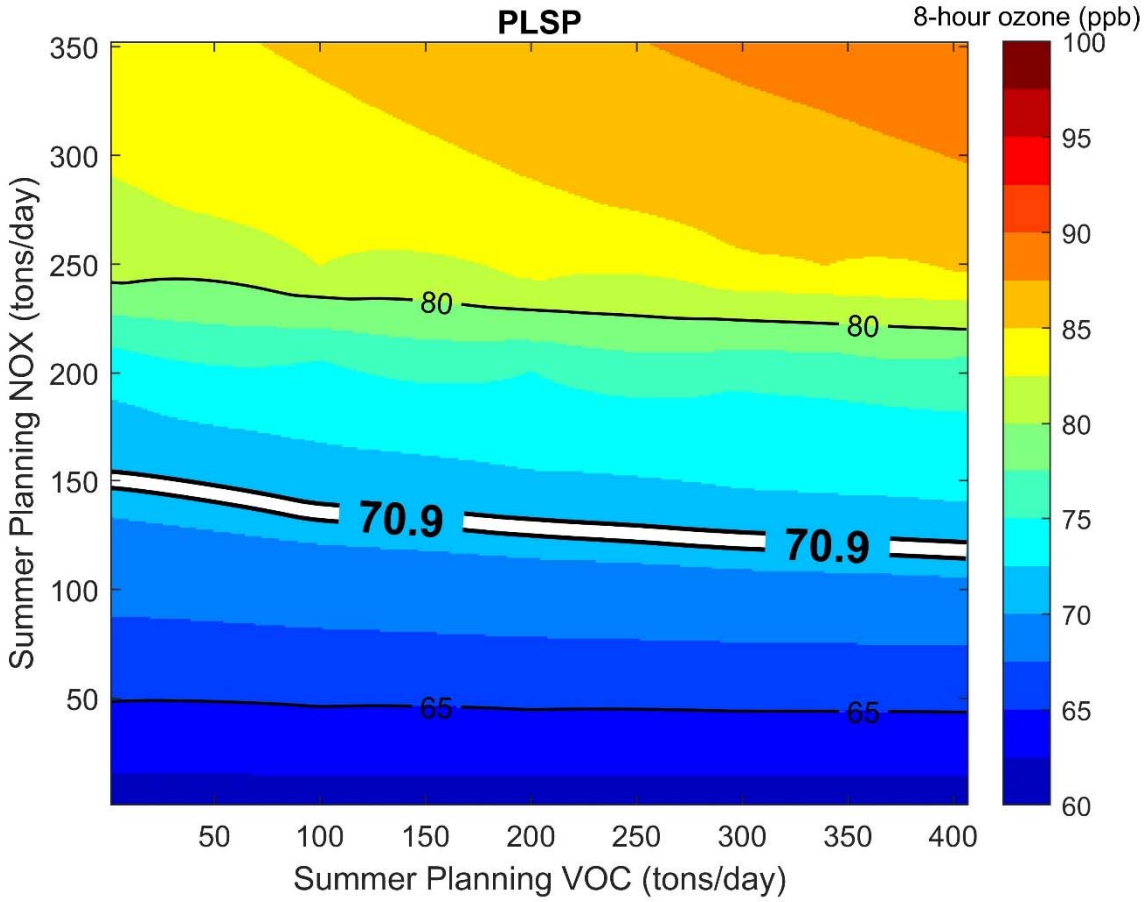
PLSP
8-hour ozone (ppb)
100
95
90
85
80
75
70
65
60
Summer Planning NOX (tons/day)
350
300
250
200
150
100
50
80
80
70.9
70.9
65
65
50
100
150
200
250
300
350
400
Summer Planning VOC (tons/day)

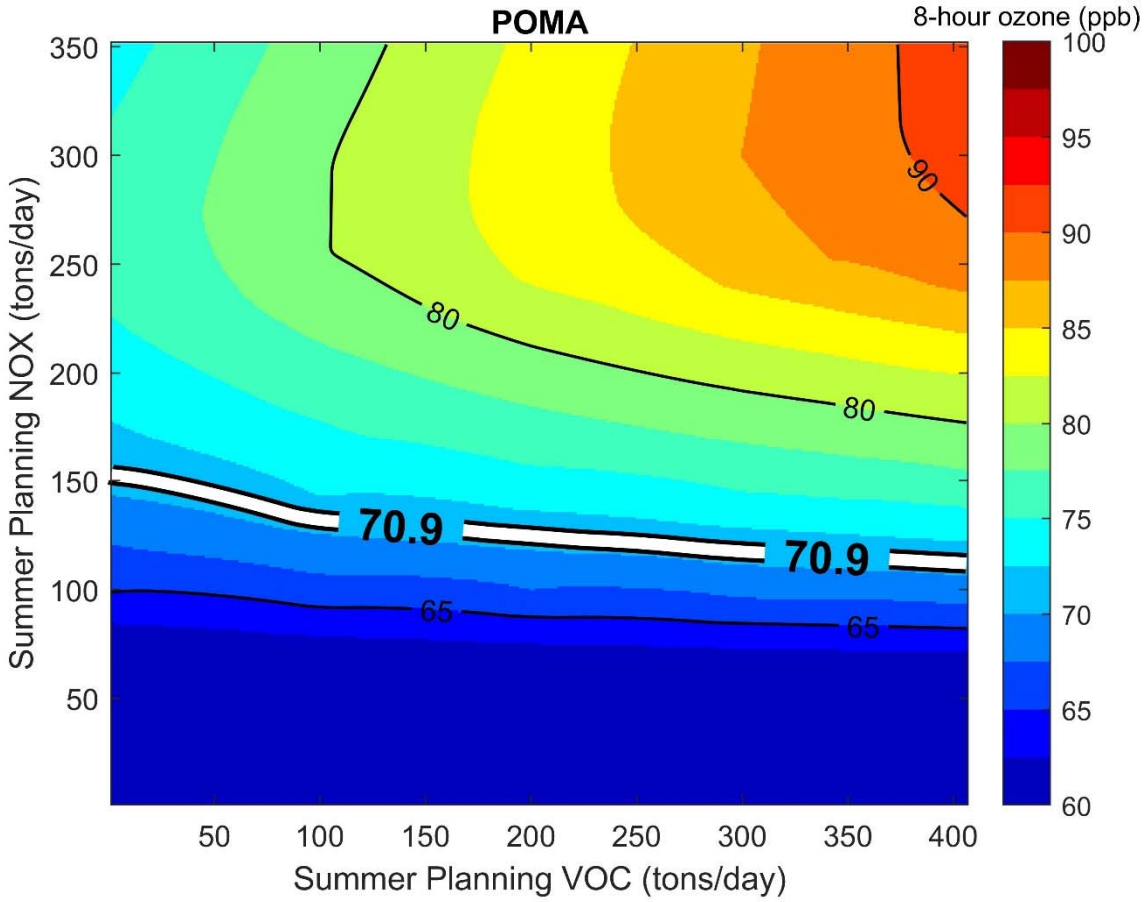
POMA
8-hour ozone (ppb)
100
95
90
85
80
75
70
65
60
Summer Planning NOX (tons/day)
350
300
250
200
150
100
50
90
80
80
70.9
70.9
65
65
50
100
150
200
250
300
350
400
Summer Planning VOC (tons/day)

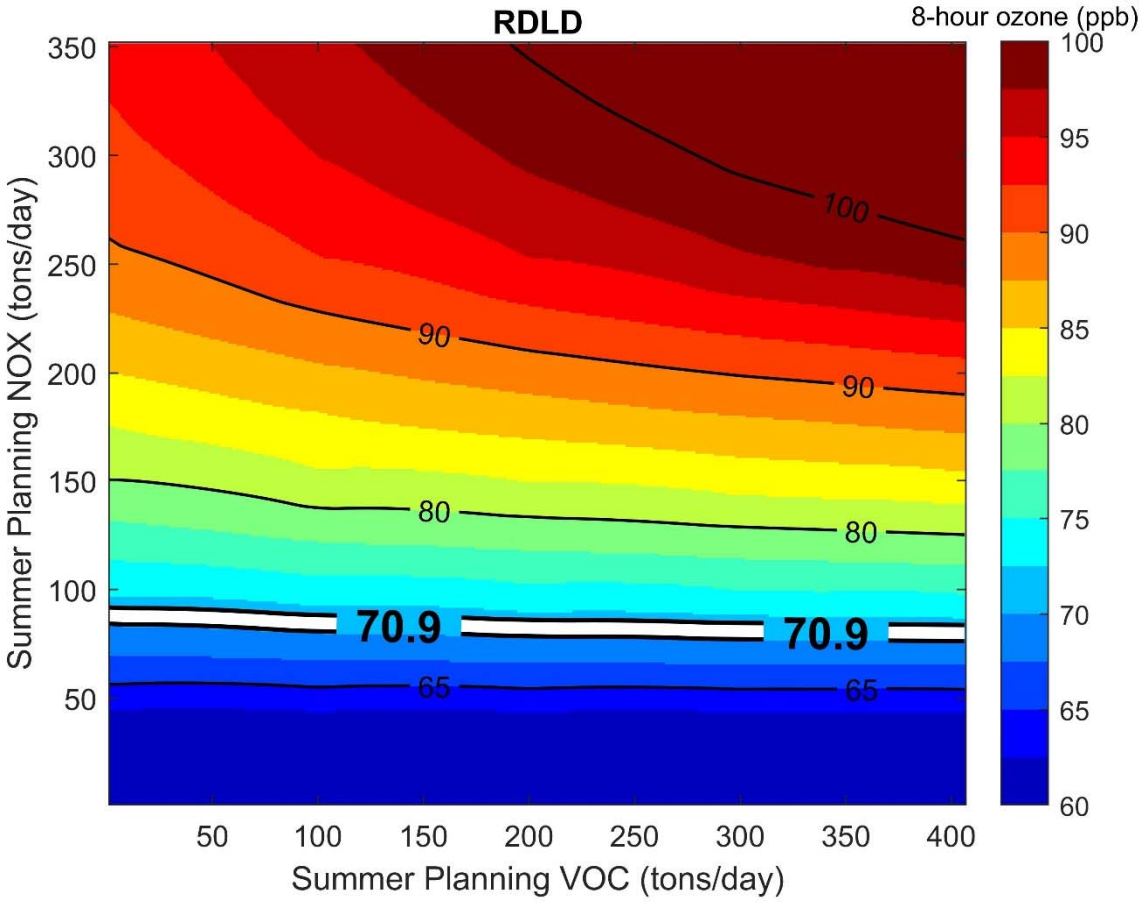
RDLD
8-hour ozone (ppb)
100
95
90
85
80
75
70
65
60
Summer Planning NOX (tons/day)
350
300
250
200
150
100
50
Summer Planning VOC (tons/day)
50
100
150
200
250
300
350
400
100
90
90
80
80
70.9
70.9
65
65

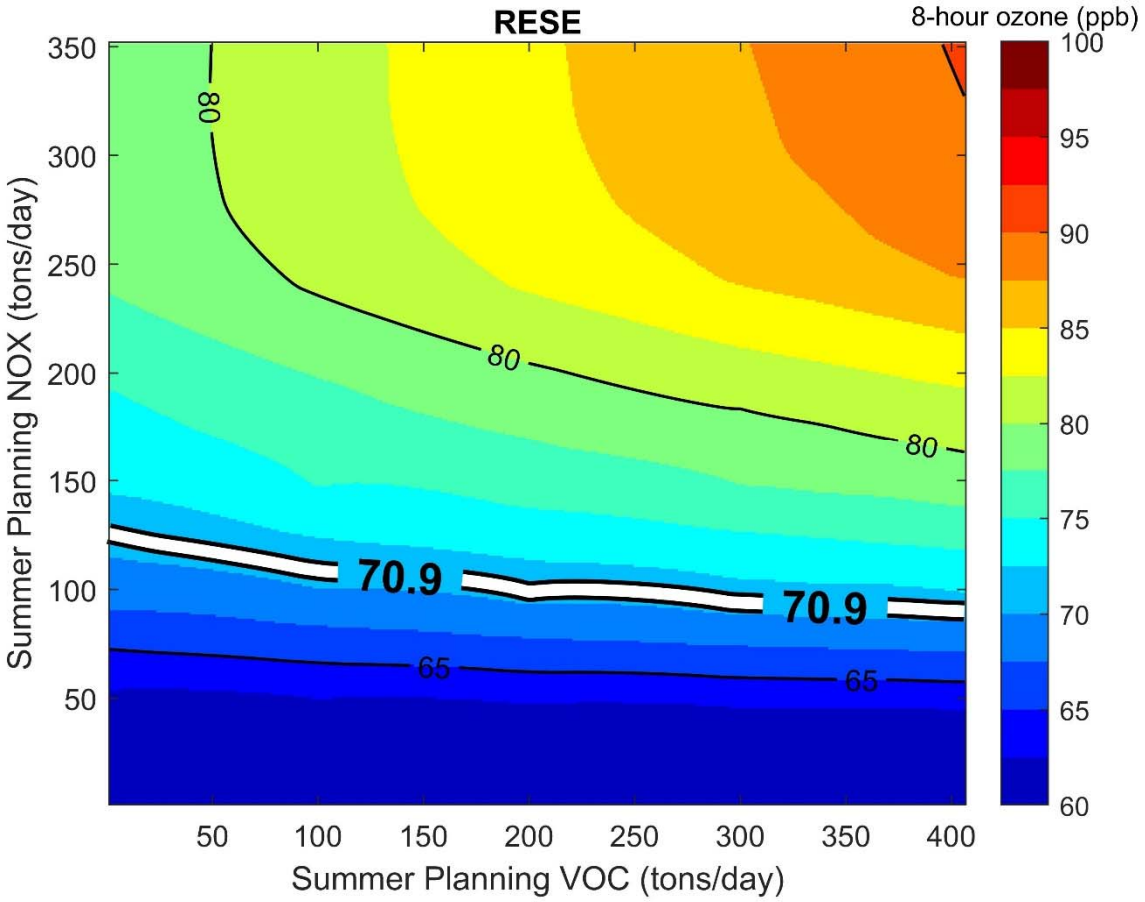
RESE
8-hour ozone (ppb)
100
95
90
85
80
75
70
65
60
Summer Planning NOX (tons/day)
350
300
250
200
150
100
50
80
80
80
70.9
70.9
65
65
50
100
150
200
250
300
350
400
Summer Planning VOC (tons/day)

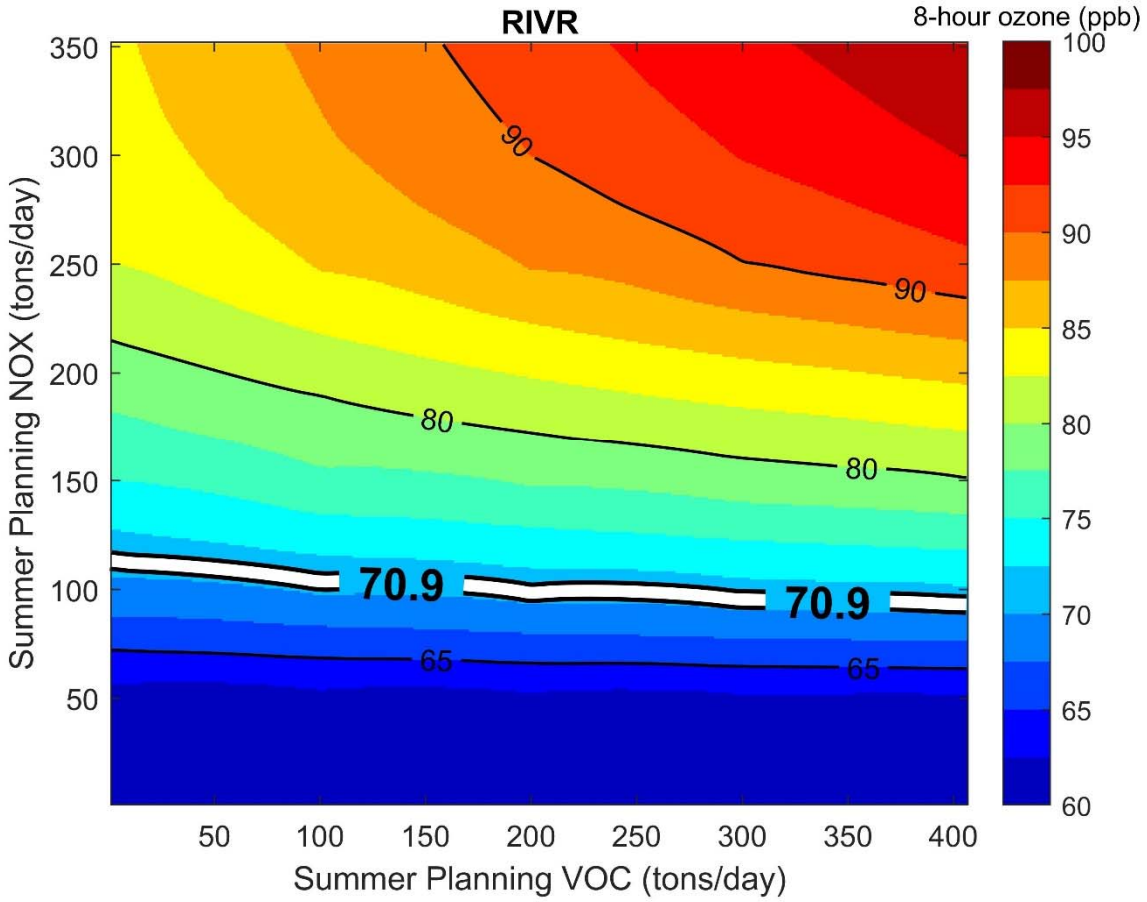
RIVR
8-hour ozone (ppb)
100
95
90
85
80
75
70
65
60
350
300
250
200
150
100
50
Summer Planning NOX (tons/day)
90
90
80
80
70.9
70.9
65
65
50
100
150
200
250
300
350
400
Summer Planning VOC (tons/day)

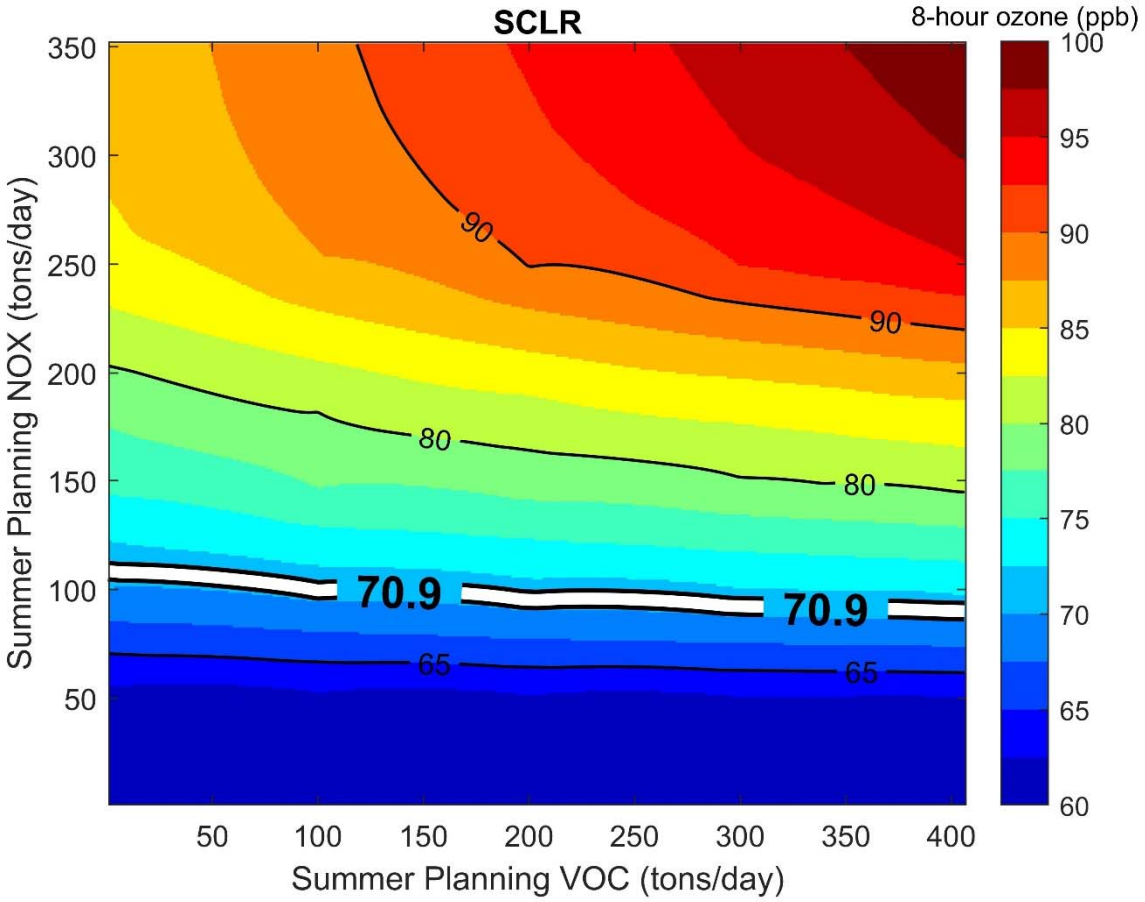
SCLR
8-hour ozone (ppb)
100
95
90
85
80
75
70
65
60
Summer Planning NOX (tons/day)
350
300
250
200
150
100
50
90
90
80
80
70.9
70.9
65
65
50
100
150
200
250
300
350
400
Summer Planning VOC (tons/day)

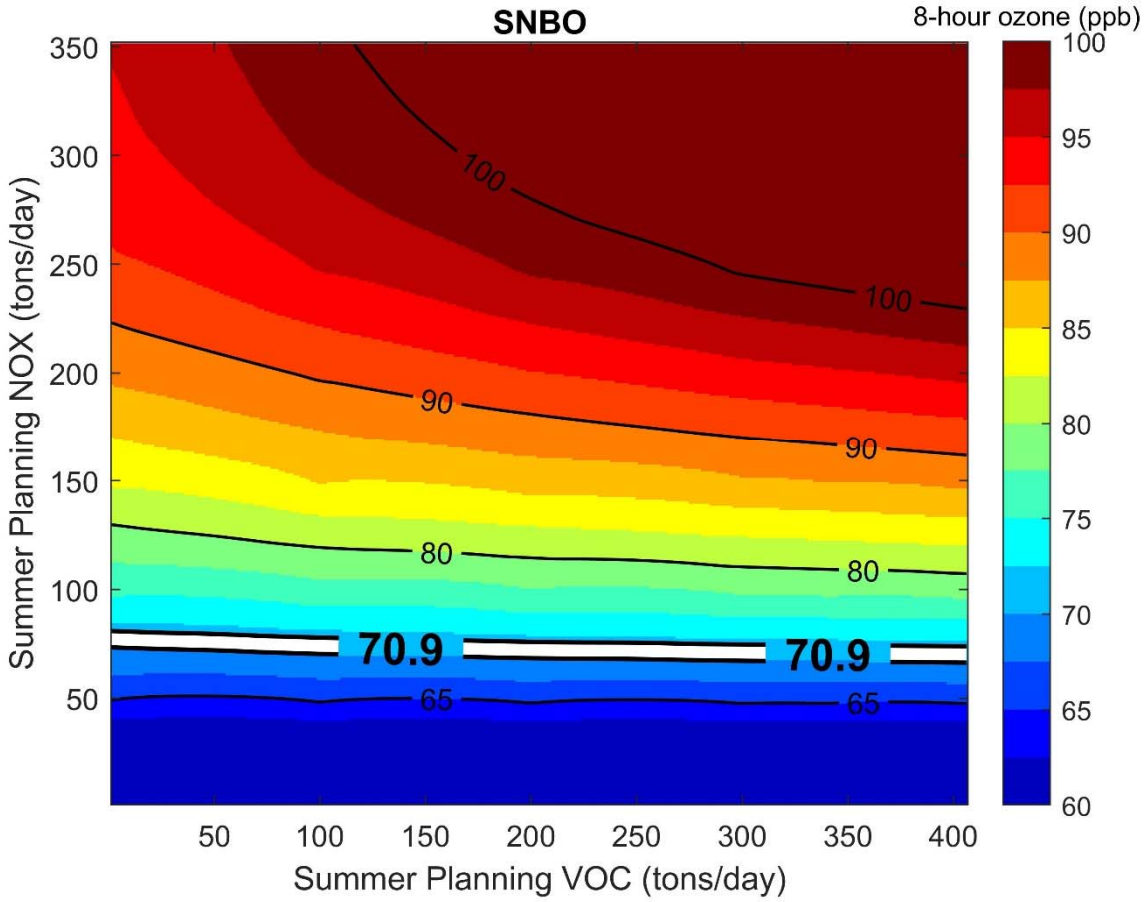
SNBO
8-hour ozone (ppb)
100
95
90
85
80
75
70
65
60
Summer Planning NOX (tons/day)
350
300
250
200
150
100
50
Summer Planning VOC (tons/day)
50
100
150
200
250
300
350
400
100
100
90
90
80
80
70.9
70.9
65
65

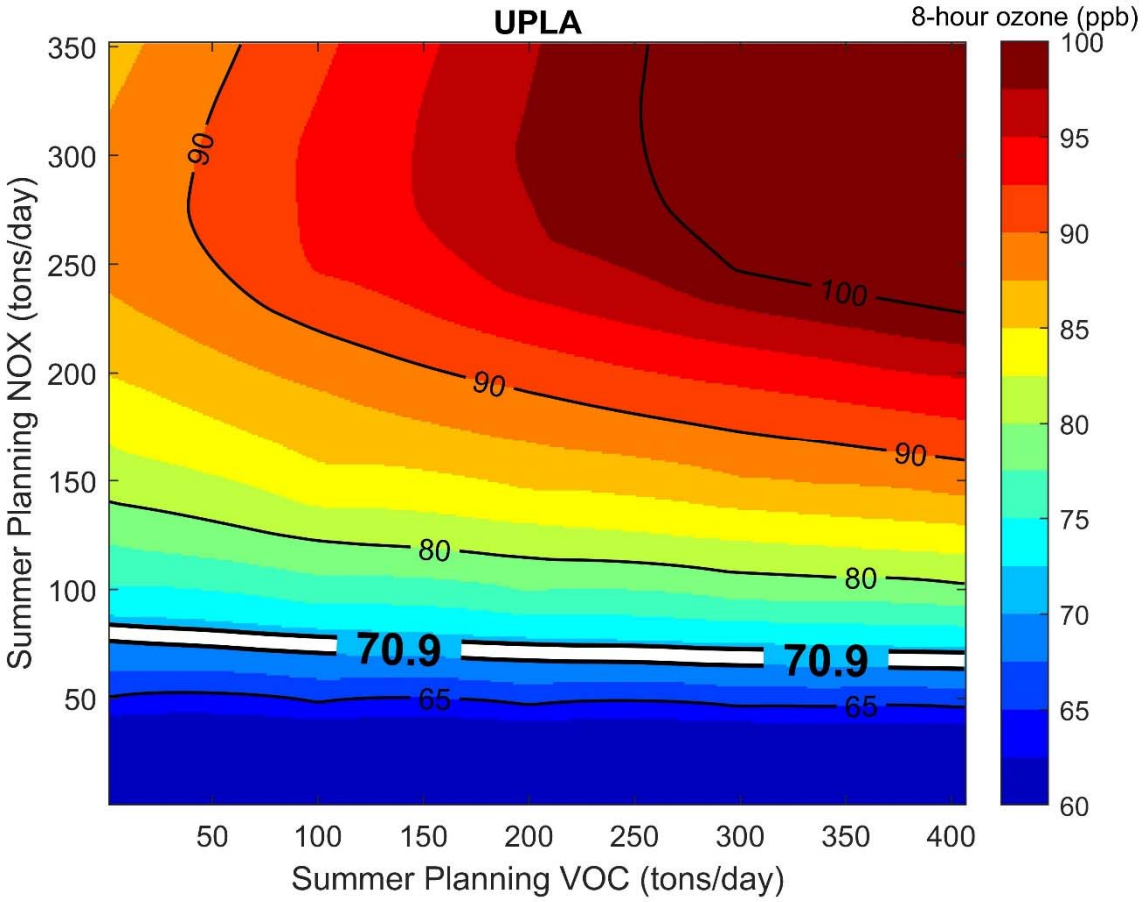
UPLA
8-hour ozone (ppb)
100
95
90
85
80
75
70
65
60
Summer Planning NOX (tons/day)
350
300
250
200
150
100
50
90
100
90
90
80
80
70.9
70.9
65
65
50
100
150
200
250
300
350
400
Summer Planning VOC (tons/day)

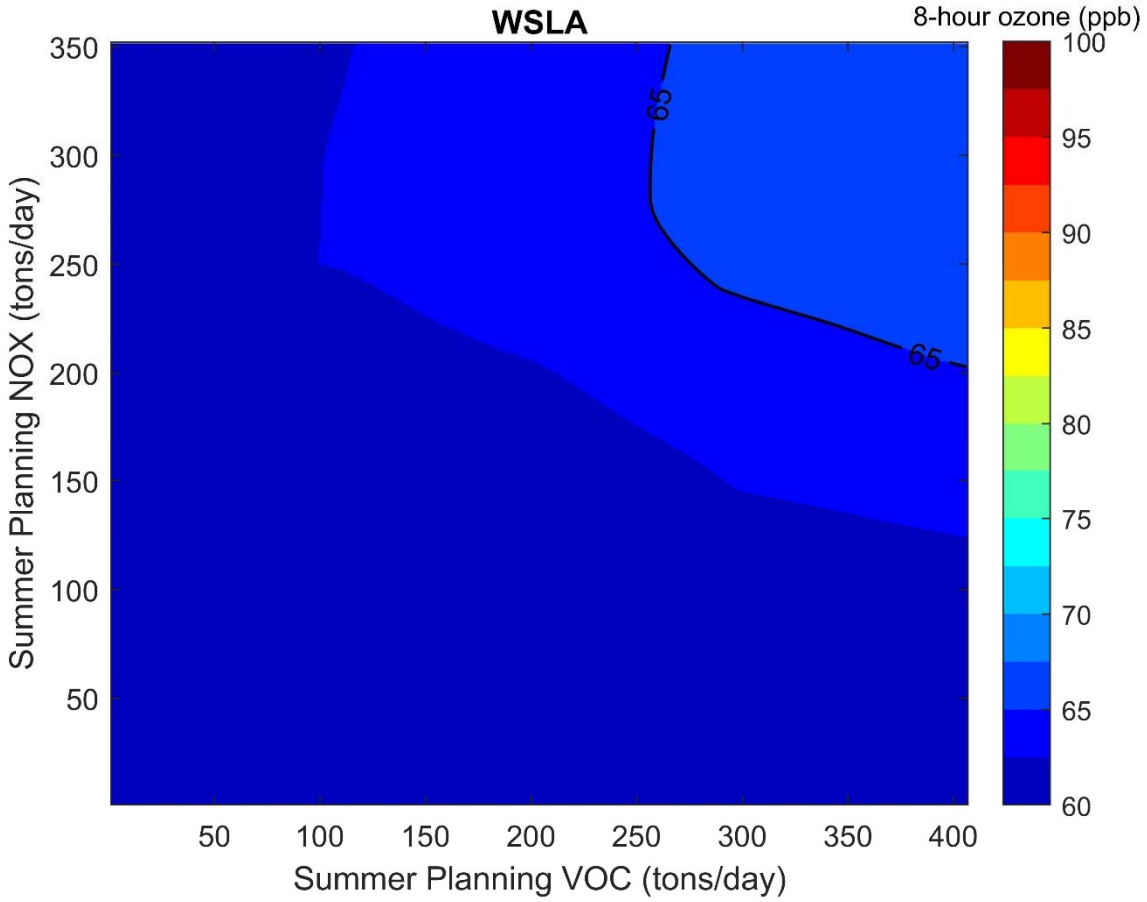
WSLA
8-hour ozone (ppb)
100
95
90
85
80
75
70
65
60
65
65
350
300
250
200
150
100
50
Summer Planning NOX (tons/day)
50
100
150
200
250
300
350
400
Summer Planning VOC (tons/day)

Attachment 5

Performance Evaluation of VOC Species

To assess model performance in simulating volatile organic carbon (VOC) concentrations across the Basin, modeled concentrations of total non-methane organic compounds (TNMOC) and individual VOC species during 2018 were compared to available measurements from South Coast AQMD stations. VOC measurements used for this analysis include measurements of toxic VOC species at seven stations as part of the Multiple Air Toxics Exposure Study V (MATES V) monitoring campaign[1] and measurements of carbonyl and hydrocarbon species at five stations in the Photochemical Assessment Monitoring Stations (PAMS) network. In 2018, both programs collected 24-hour samples on a 1-in-6 days schedule for VOC measurements.

Figures 1-14 show modeled vs. measured concentrations of TNMOC and selected individual VOC species. In general, modeled TNMOC and individual VOC concentrations were reasonably well correlated with measured values. However, in most cases, the model underpredicted measured ambient concentrations. There are two notable exceptions. First, predicted isoprene concentrations were higher than observed values. Unlike the other VOC species, the predominant source of isoprene is biogenic emissions. Second, modeled methyl ethyl ketone (MEK) concentrations were comparable with measured concentrations. However, in the current SPARC07tc chemical module formulation, MEK is not an explicit chemical species. Instead, the modeled MEK species includes ketones and some other non-aldehyde oxygenated products. Therefore, it is expected that modeled MEK concentrations will be higher than measured concentrations.

Figure 1. Scatter Plot of Predicted vs. Observed Concentrations

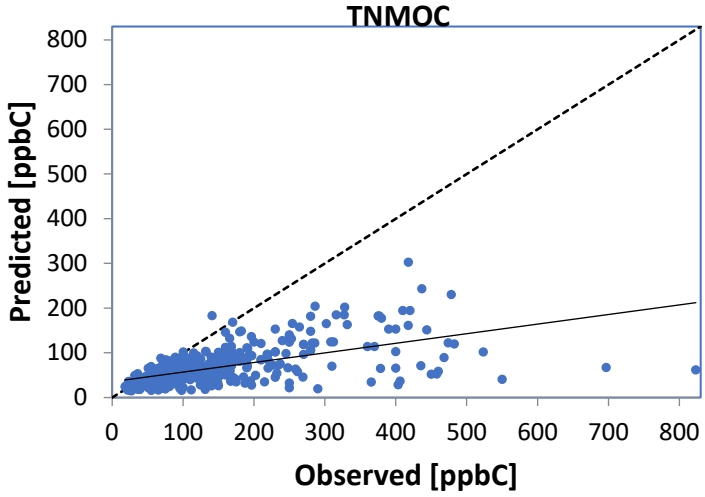

[1] The MATES V monitoring campaign was conducted from May 2018-April 2019, although measurements at some stations began several months earlier. All available data was included in this analysis.

Figure 2. Scatter Plot of Predicted vs. Observed Concentrations
Formaldehyde

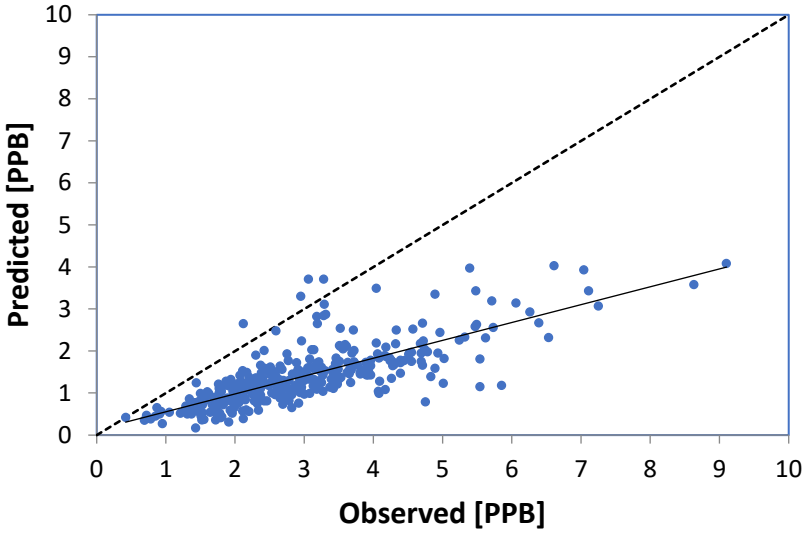

Figure 3. Scatter Plot of Predicted vs. Observed Concentrations
Acetylene

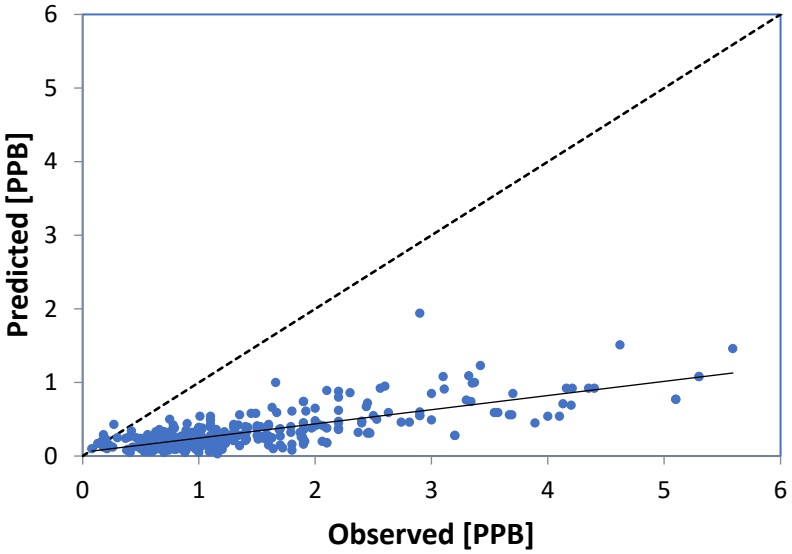

Figure 4. Scatter Plot of Predicted vs. Observed Concentrations
Touluene

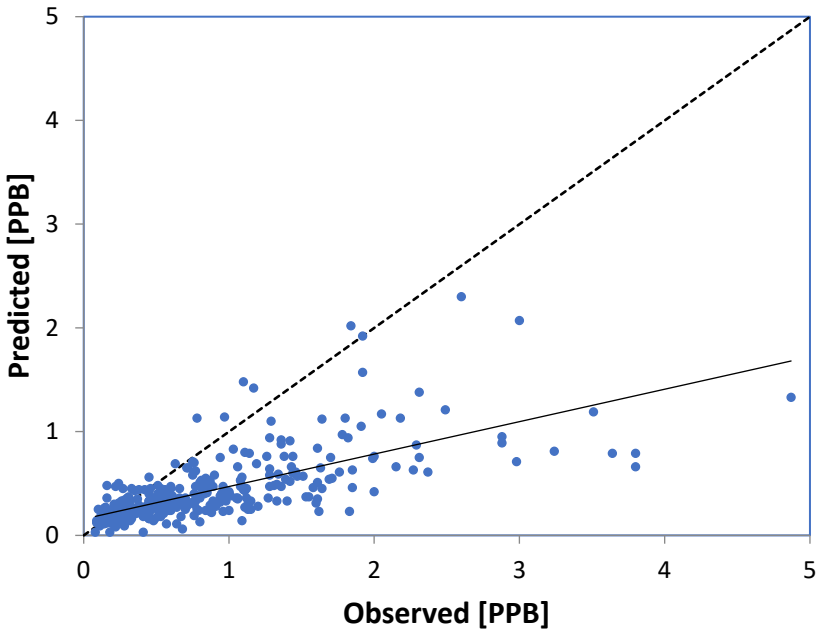

Figure 5. Scatter Plot of Predicted vs. Observed Concentrations
Isoprene

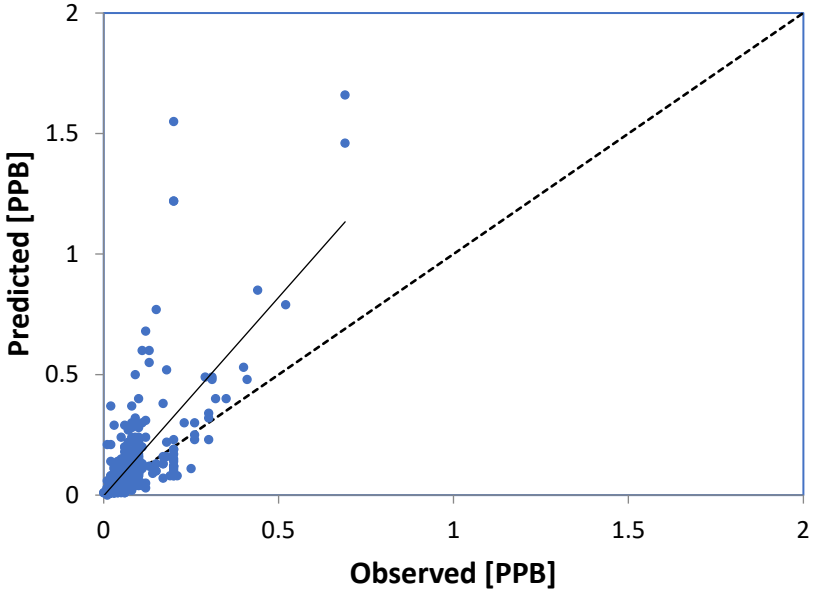

Figure 6. Scatter Plot of Predicted vs. Observed Concentrations
Benzene

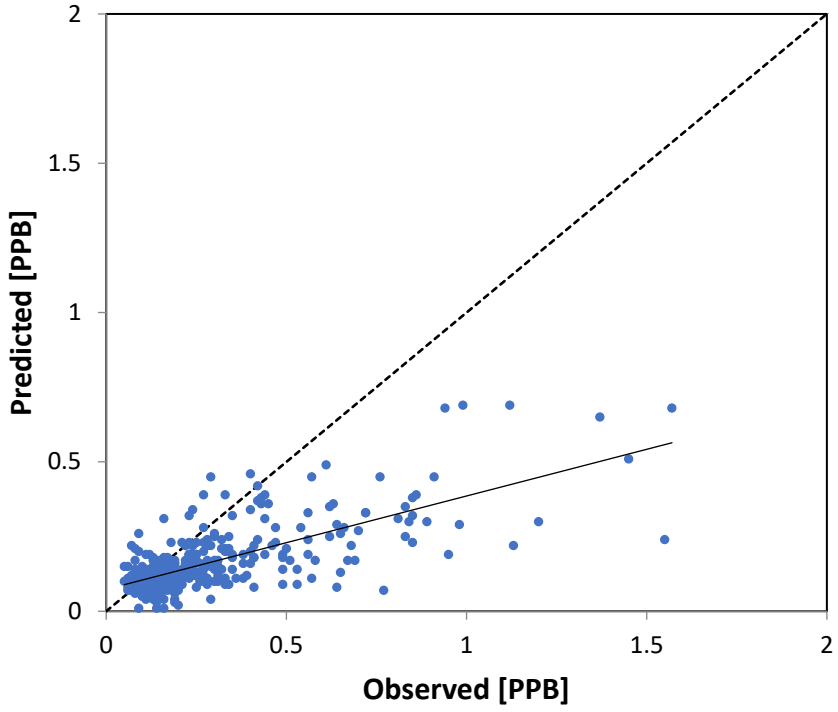

Figure 7. Scatter Plot of Predicted vs. Observed Concentrations
Acetaldehyde

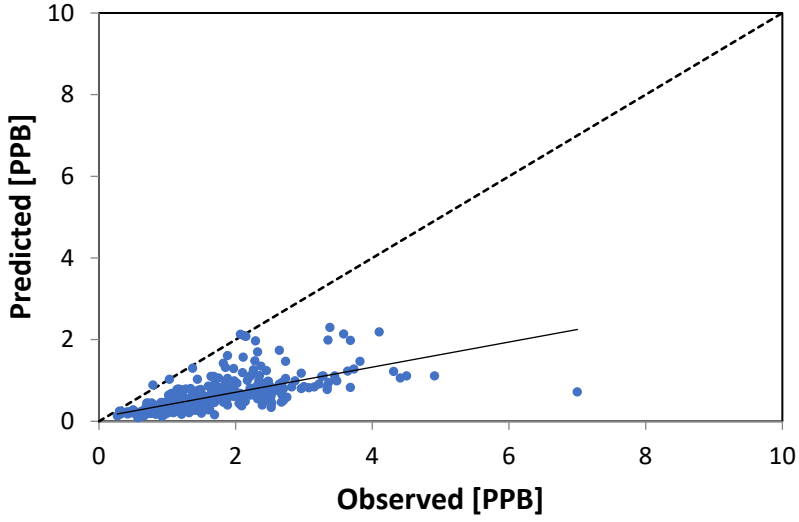

Figure 8. Scatter Plot of Predicted vs. Observed Concentrations
Acetone

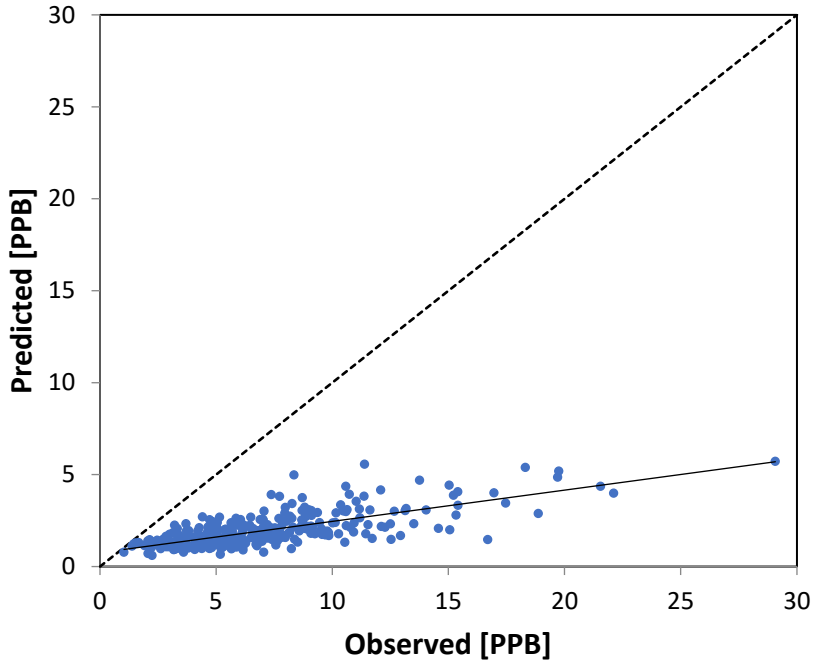

Figure 9. Scatter Plot of Predicted vs. Observed Concentrations
m&p-Xylene

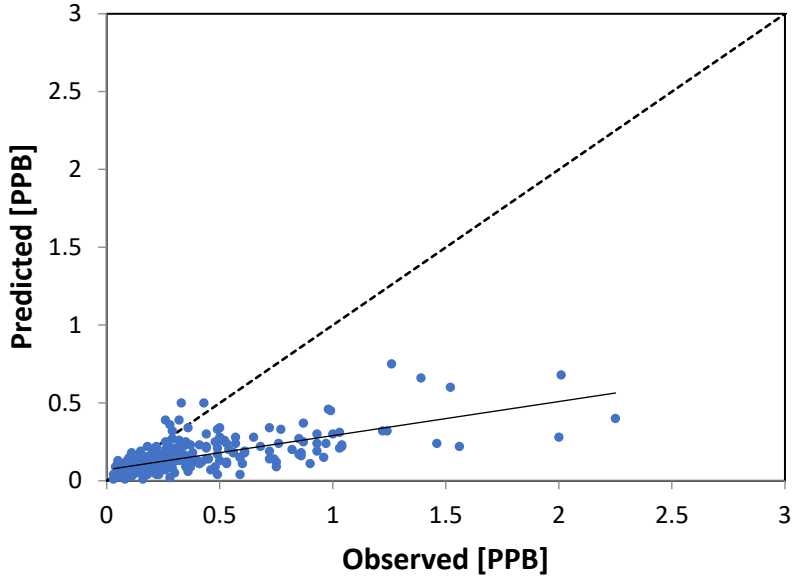

Figure 10. Scatter Plot of Predicted vs. Observed Concentrations
Propylene

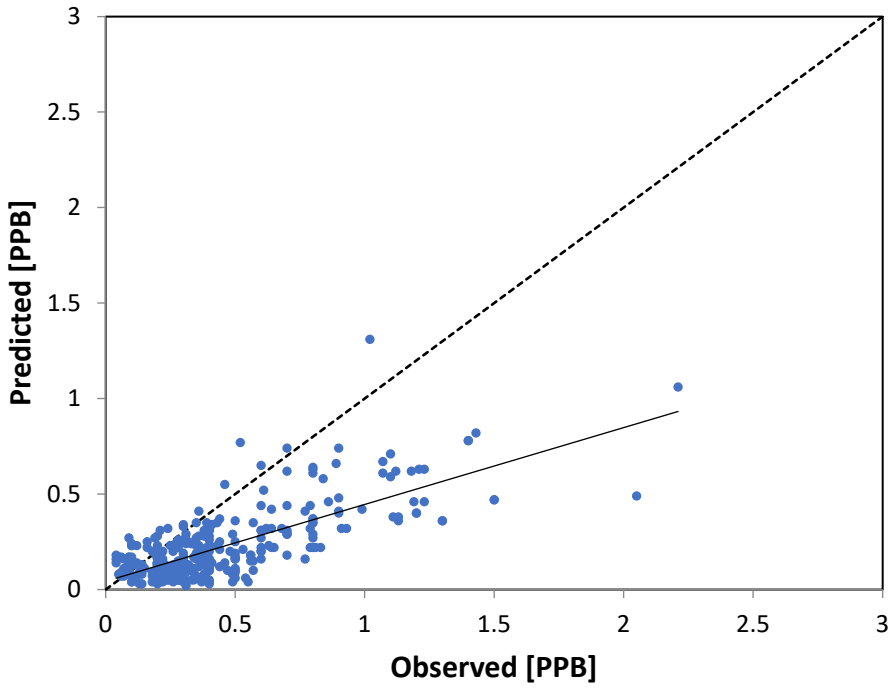

Figure 11. Scatter Plot of Predicted vs. Observed Concentrations
o-Xylene

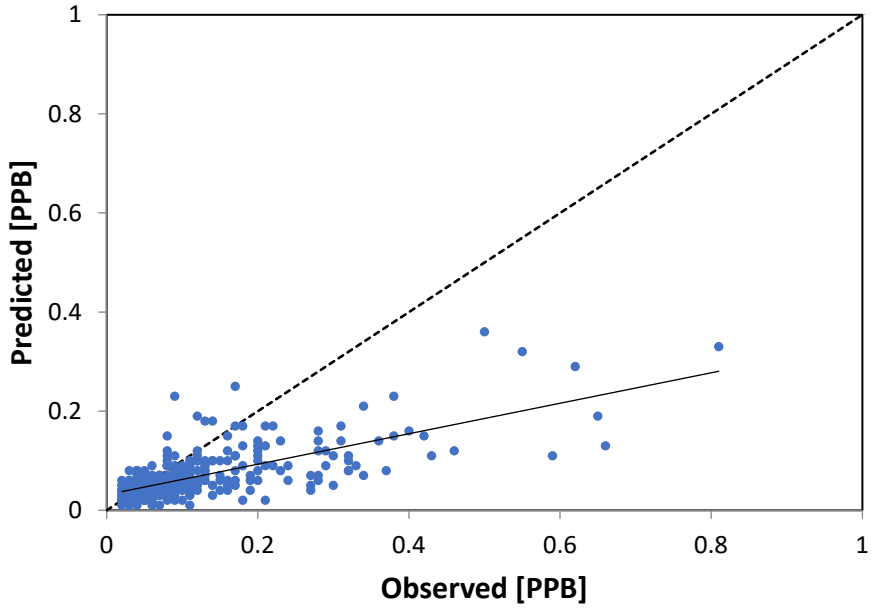

Figure 12. Scatter Plot of Predicted vs. Observed Concentrations
Ethylene

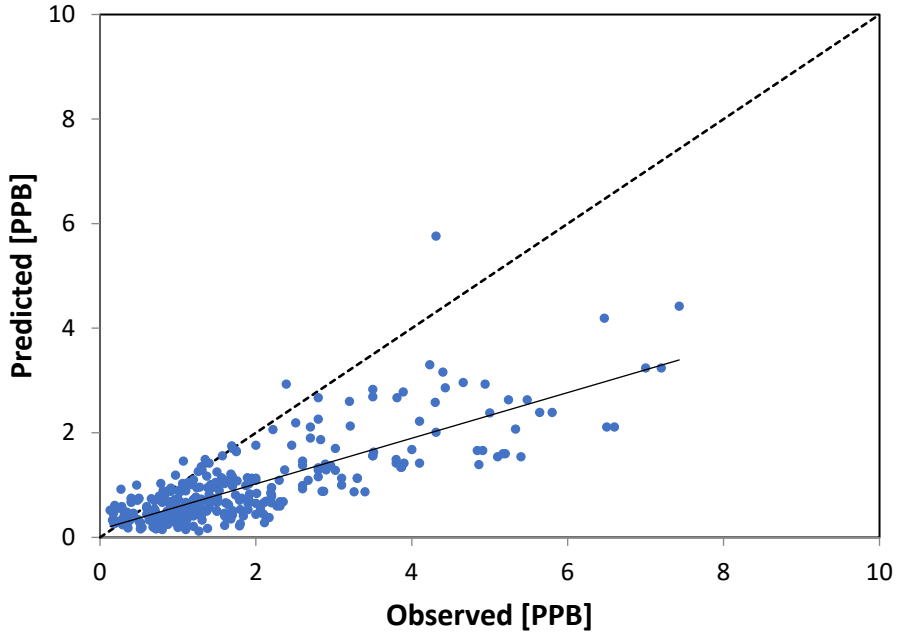

Figure 13. Scatter Plot of Predicted vs. Observed Concentrations
1,3-Butadiene

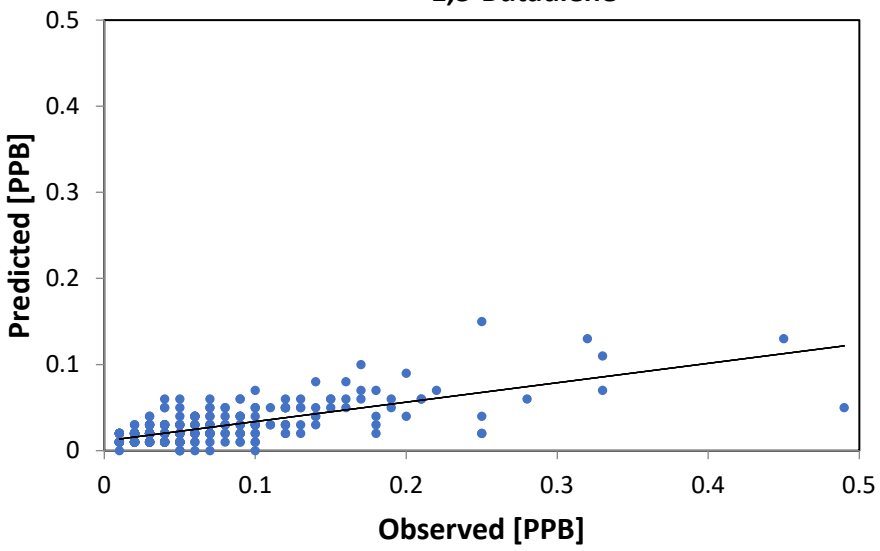

Figure 14. Scatter Plot of Predicted vs. Observed Concentrations

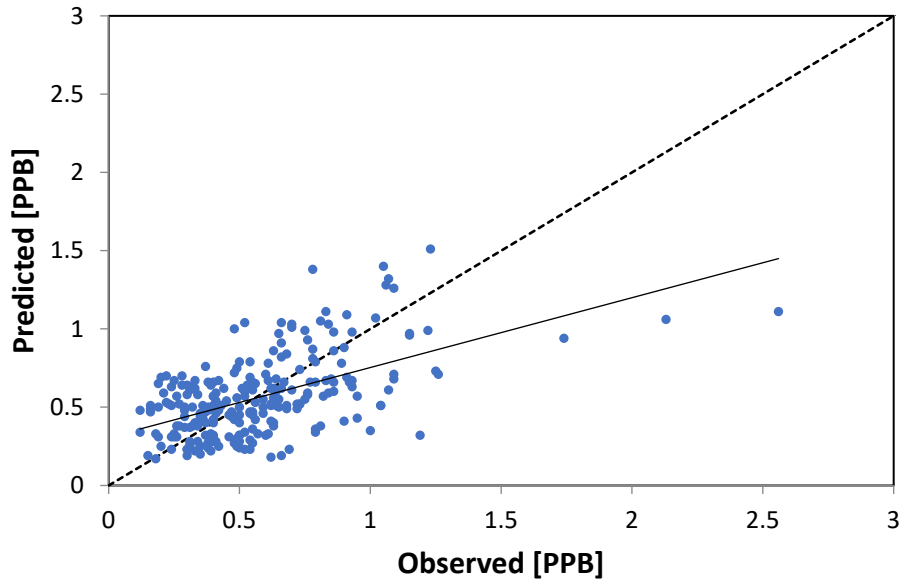

Figures 15-28 show modeled and measured quarterly and annual concentrations at various sites. TNMOC concentrations were higher in the first and fourth quarters compared to the second and third quarters of 2018. Differences between observed and modeled concentrations were also more pronounced during periods of higher TNMOC concentrations. These patterns prevail for all primary VOC species with predominantly anthropogenic sources. Isoprene, which is primarily derived from biogenic sources, showed higher concentrations and larger disparities between observed and modeled concentrations during the second and third quarters. This pattern is consistent with higher biogenic emissions during the spring and summer. Formaldehyde and acetaldehyde, which are mainly produced through secondary formation processes with minor contributions from direct emissions, also reached much higher concentrations in the second and third quarters when ambient conditions were more conducive to photochemical formation.

Figure 15. Measured and Modeled Quarterly and Annual TNMOC Concentrations

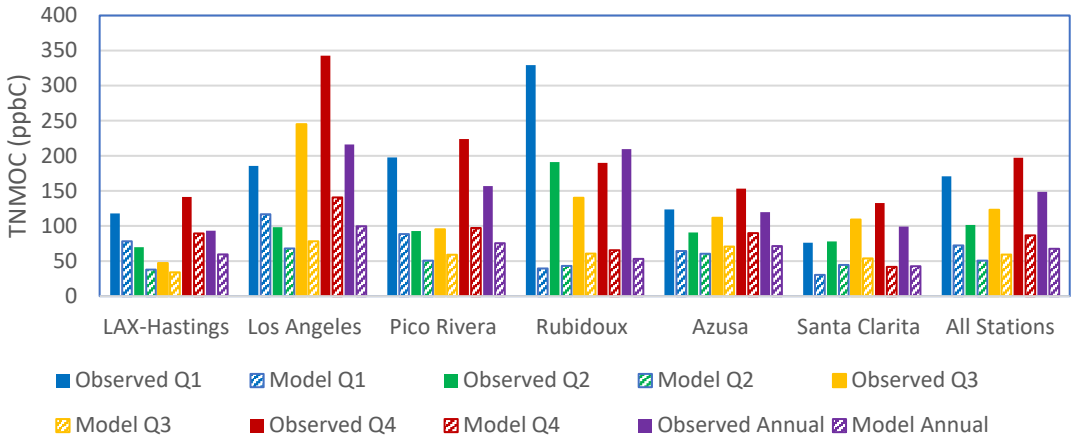

Figure 16. Measured and Modeled Quarterly and Annual Acetaldehyde Concentrations

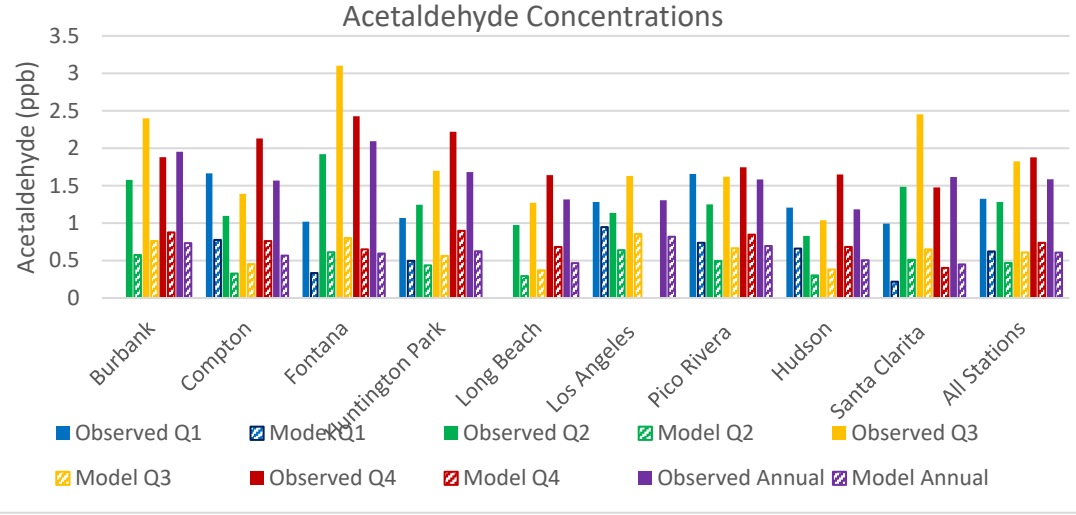

Figure 17. Measured and Modeled Quarterly and Annual Acetone Concentrations

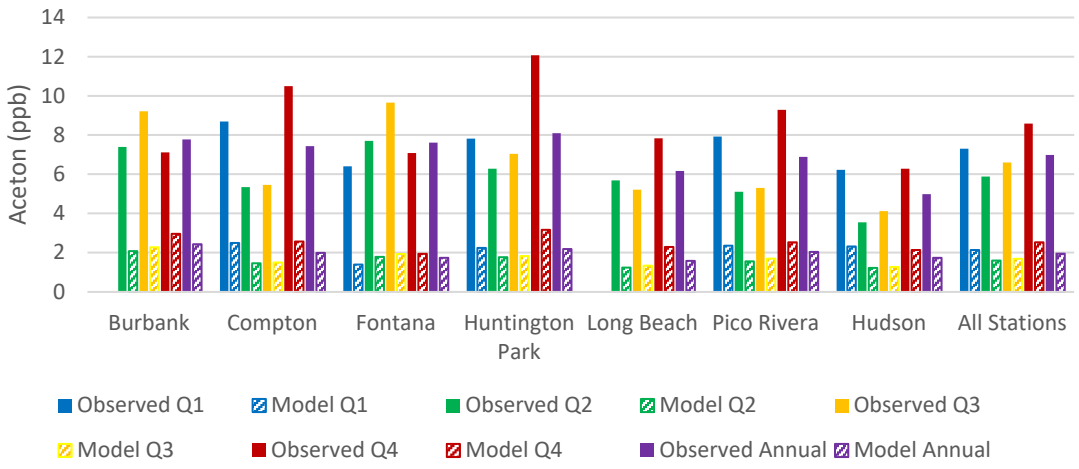

Figure 18. Measured and Modeled Quarterly and Annual Acetylene Concentrations

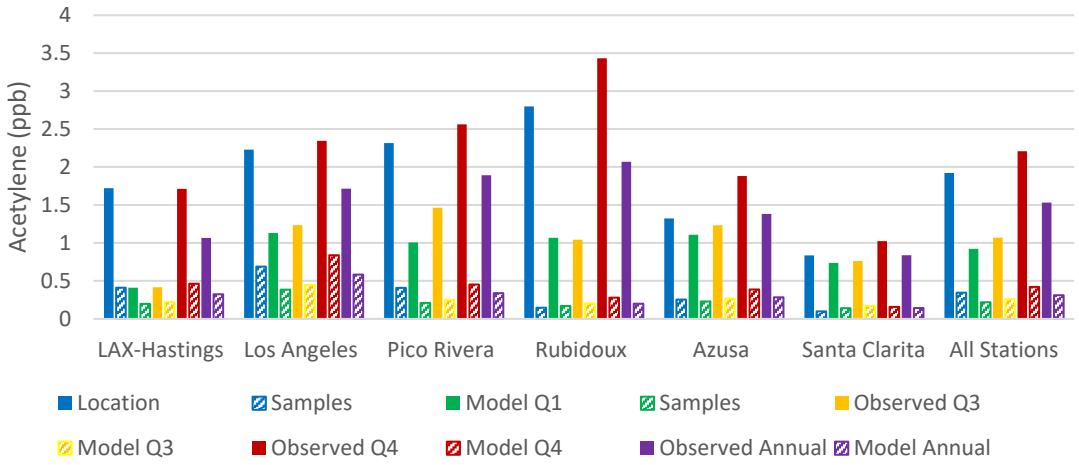

Figure 19. Measured and Modeled Quarterly and Annual Benzene Concentrations

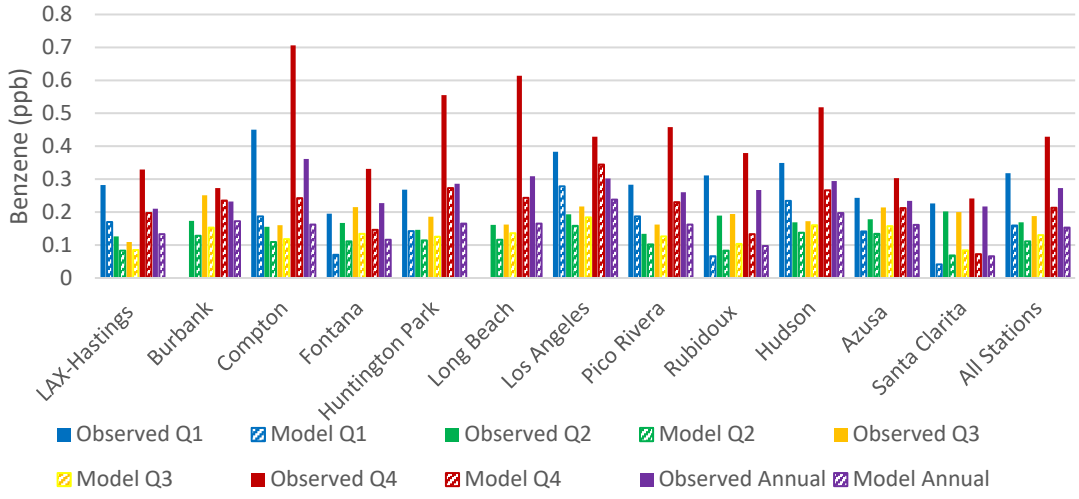

Figure 20. Measured and Modeled Quarterly and Annual 1,3-Butadiene Concentrations

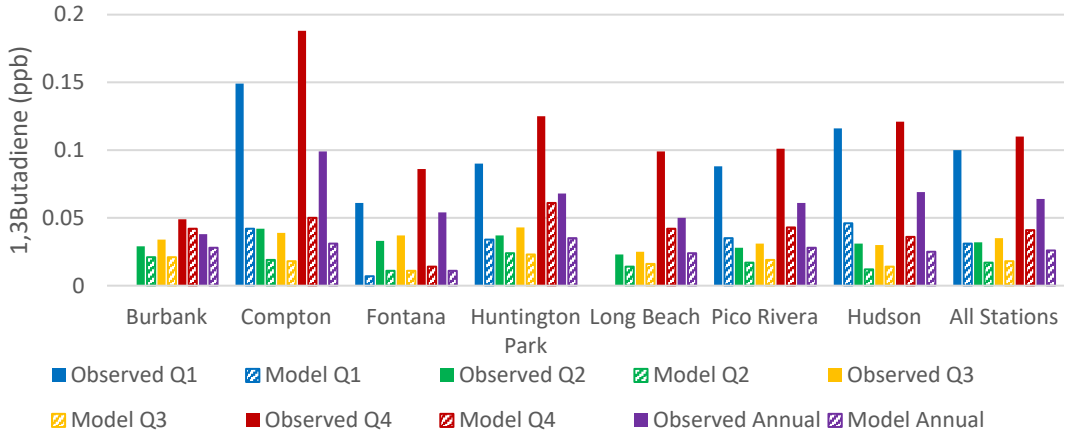

Figure 21. Measured and Modeled Quarterly and Annual Ethylene Concentrations

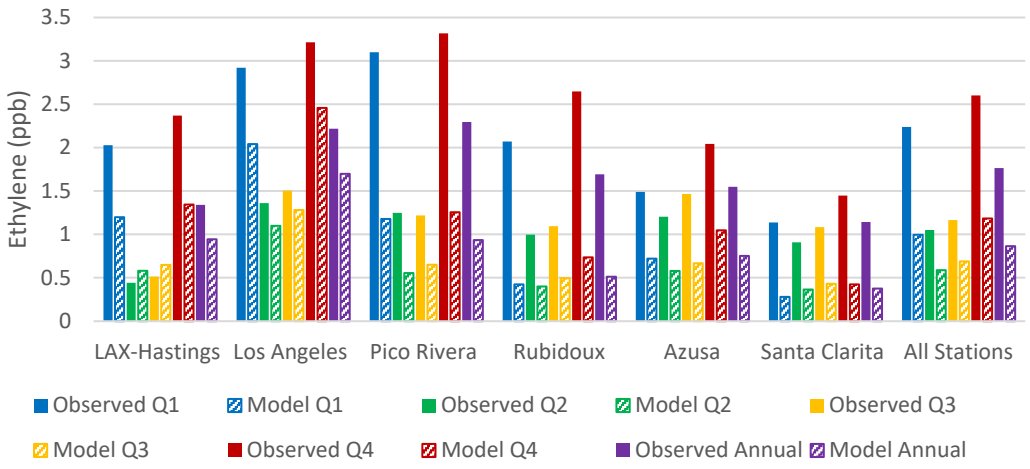

Figure 22. Measured and Modeled Quarterly and Annual Formaldehyde Concentrations

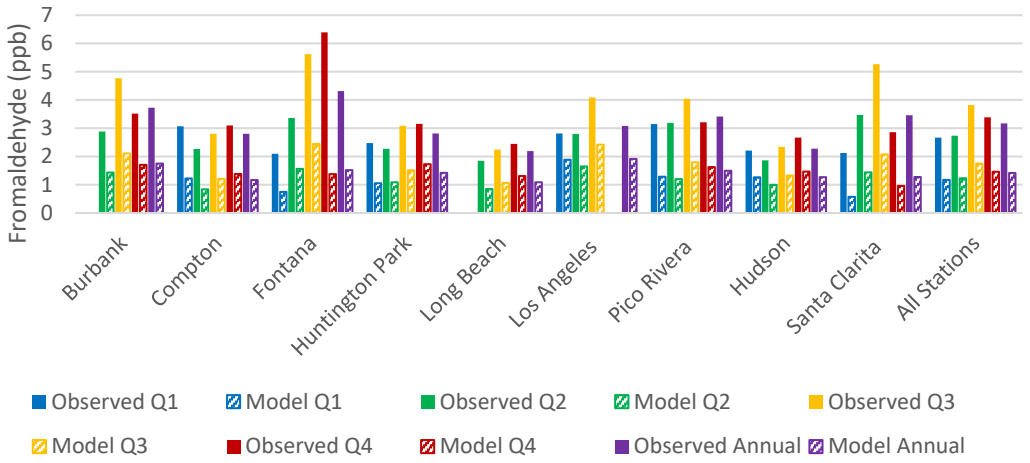

Figure 23. Measured and Modeled Quarterly and Annual Isoprene Concentrations

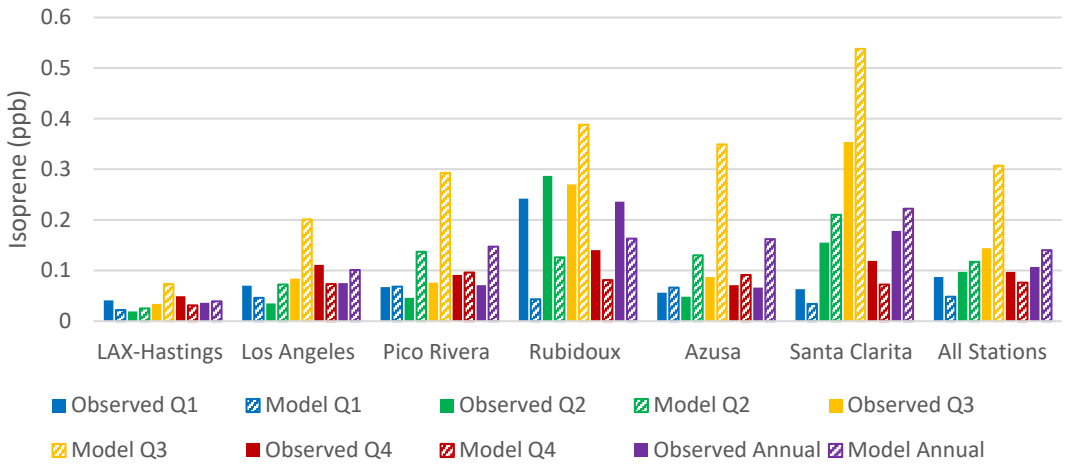

Figure 24. Measured and Modeled Quarterly and Annual MEK Concentrations

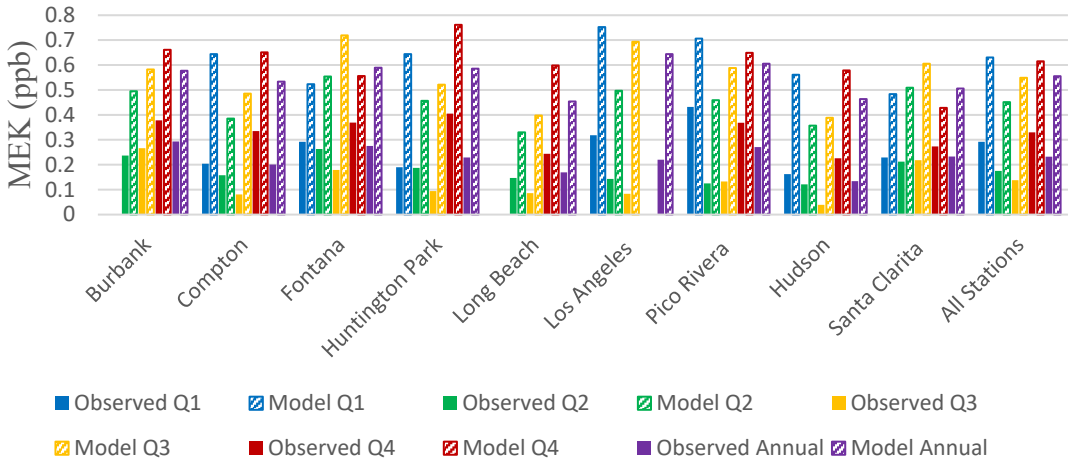

Figure 25. Measured and Modeled Quarterly and Annual m&p-Xylene Concentrations

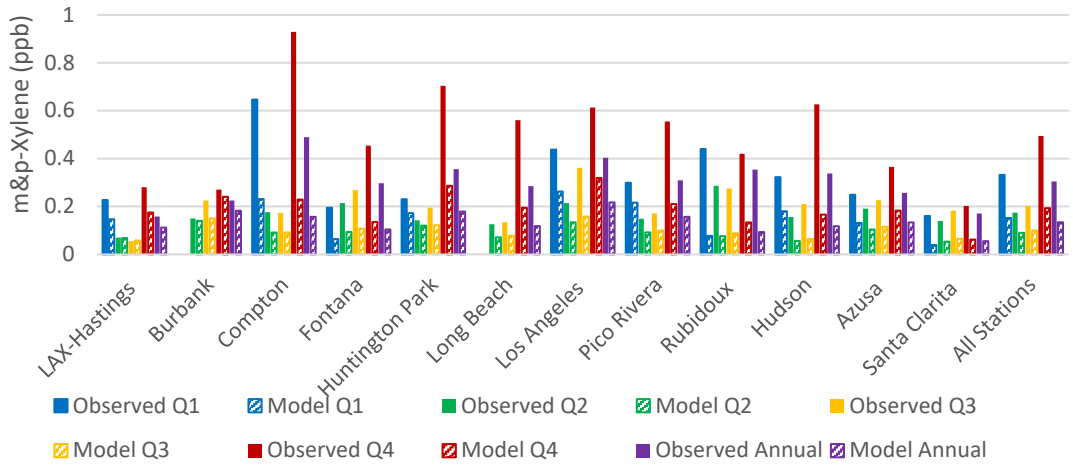

Figure 26. Measured and Modeled Quarterly and Annual o-Xylene Concentrations

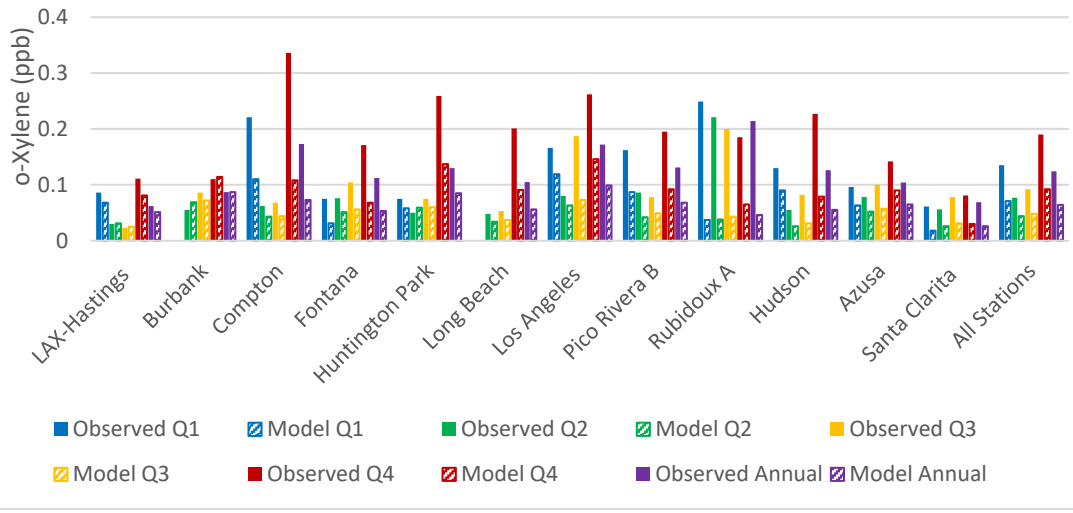

Figure 27. Measured and Modeled Propylene Quarterly and Annual Concentrations

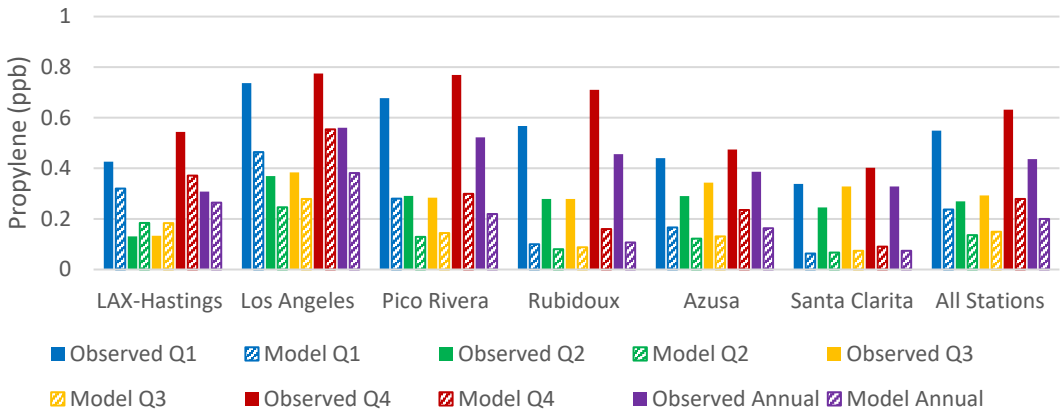

Figure 28. Measured and Modeled Toluene Quarterly and Annual Concentrations

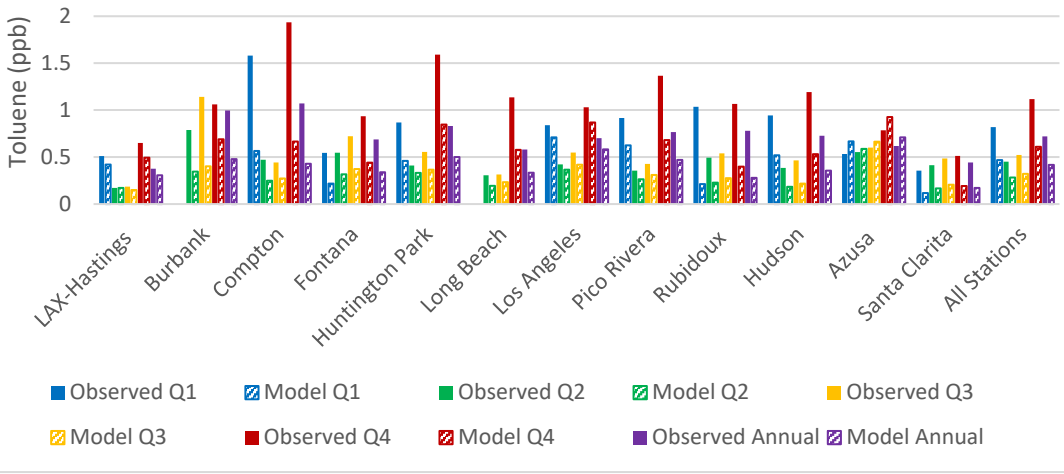

As shown in Figure 29, where predicted and observed daily average CO concentrations were plotted, predicted CO concentrations were also lower than observed values. However, compared to TNMOC and VOC species, CO underprediction was less severe. As shown in Figure 30, observed concentrations of TNMOC and CO were correlated. Modeled CO and TNMOC concentrations were also strongly correlated (Figure 31). Although modeled TNMOC/CO ratios were lower than observed values, model predictions were more accurate for TNMOC/CO ratios compared to predictions of TNMOC concentration alone.

Figure 29. Scatter Plot of Predicted vs. Observed Concentrations

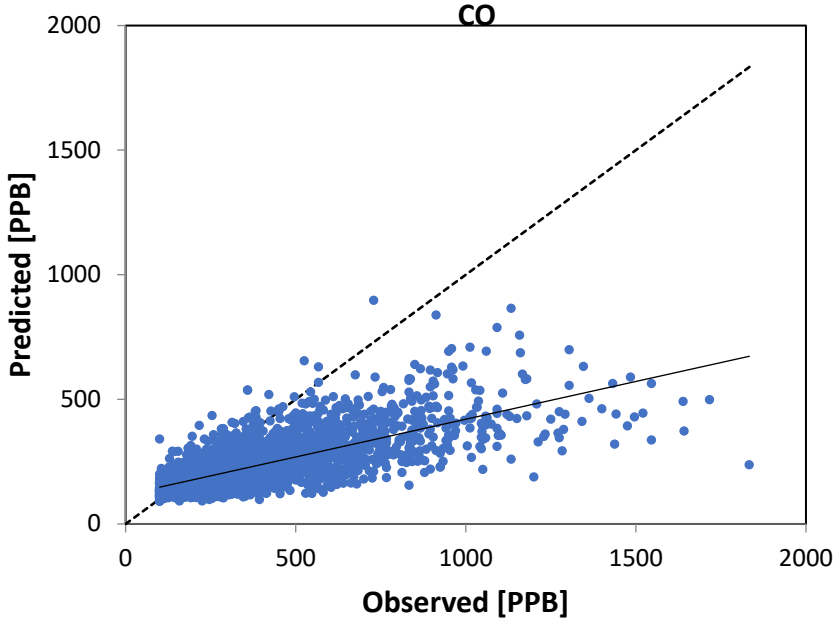

Figure 30. Observed TNMOC and CO Concentrations

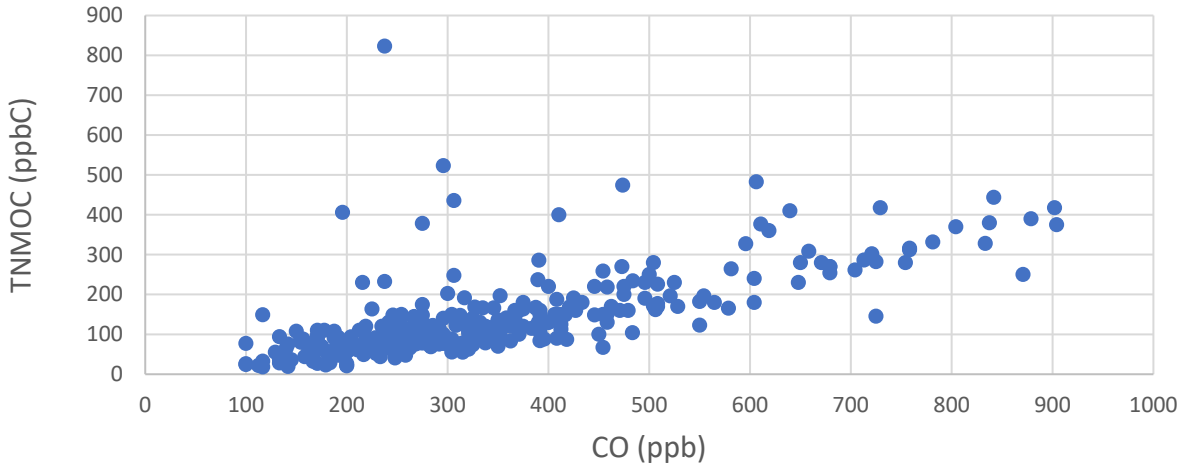

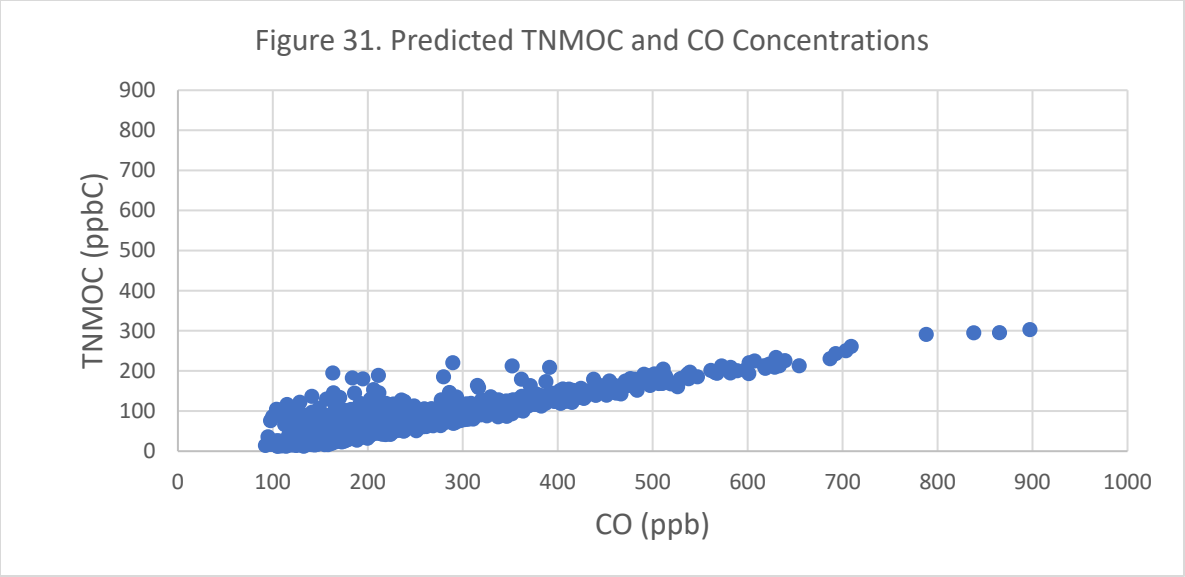

Gasoline combustion is the primary source of both CO and acetylene in the SCAB. As shown in Figures 32 and 33, concentrations of CO and acetylene were indeed well correlated for both observed and modeled values. Measured acetylene/CO ratios were much higher than modeled ratios, indicating acetylene emissions were lower in relation to CO. This could be due to underestimating total organic gas (TOG) emissions from gasoline combustion, underweighting of acetylene in speciation profiles, or a combination of both factors.

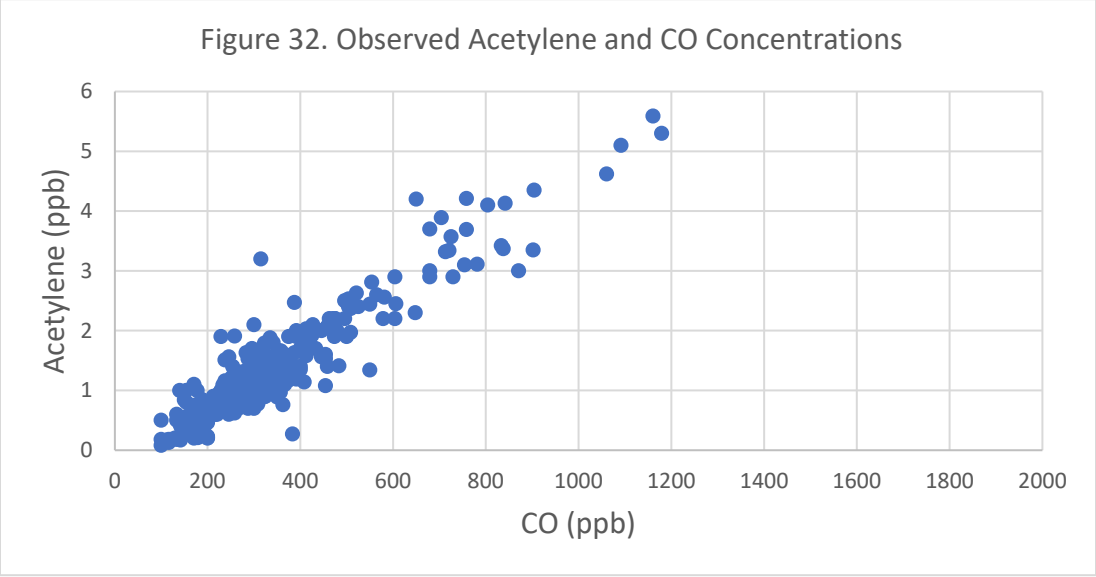

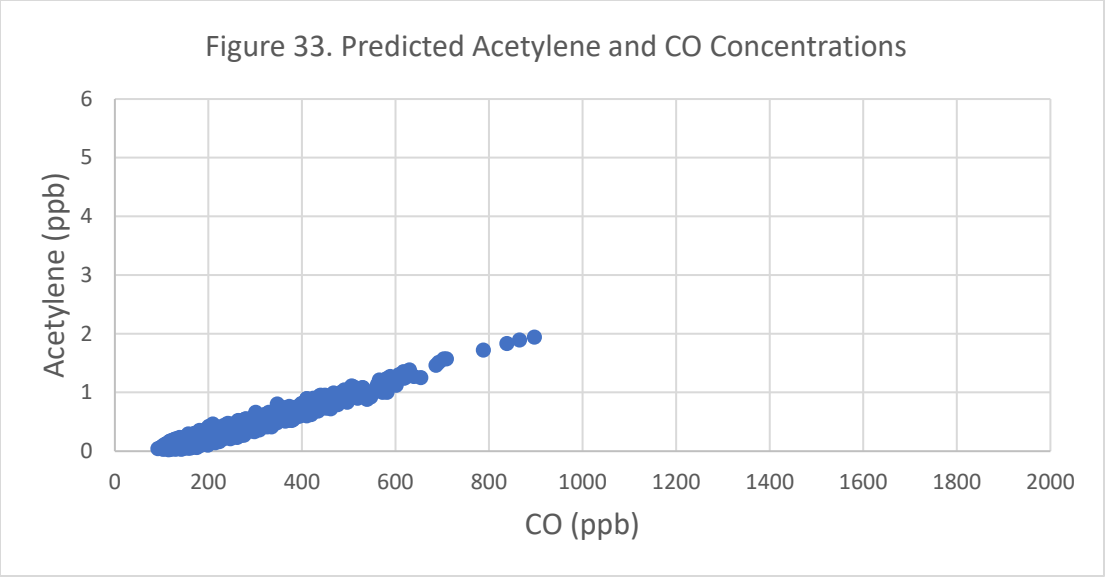

As shown in Figure 34, where predicted and observed daily average NOx concentrations were plotted, predicted NOx concentrations were also lower than observed values. There is known instrument bias in the measured NOx concentrations since NOx monitors detect other nitrogen containing species, such as N2O5, HONO, and PAN, etc.in addition to NO and NO2. Therefore, the observed TNMOC/NOx slope shown in Figure 35 should be considered a lower bound on the true ratio. Predicted TNMOC vs. NOx concentrations are shown in Figure 36. The model predicted TNMOC/NOx ratios were comparable to the observed lower bound TNMOC/NOx ratios.

Figure 34. Scatter Plot of Predicted vs. Observed Concentrations

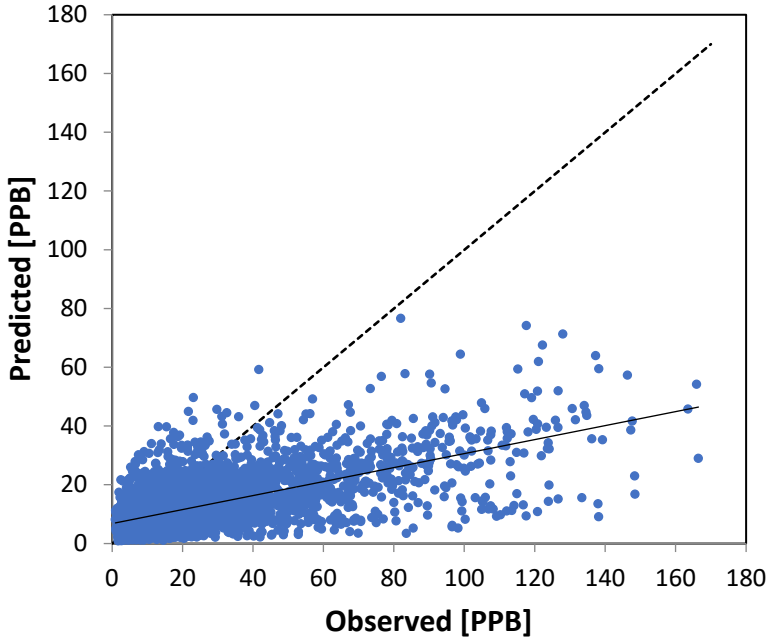

Figure 35. Observed TNMOC and NOx Concentrations

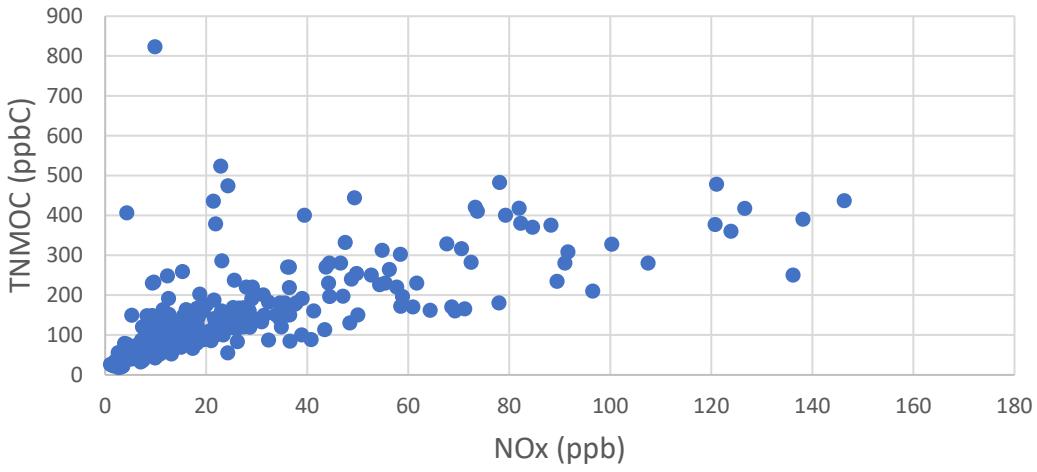

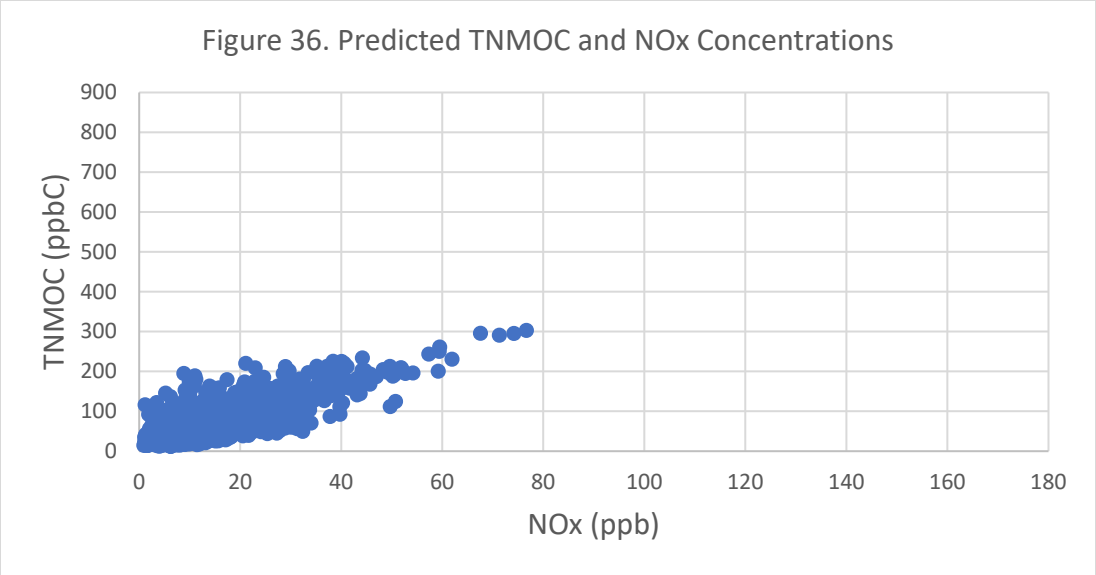

In summary, the model underpredicted TNMOC and most individual VOC concentrations in 2018. For secondary VOCs, such as formaldehyde and acetaldehyde, model underprediction was more pronounced in the second and third quarters while it was more severe in the first and fourth quarters for primary VOCs. The model overpredicted isoprene concentrations, particularly in the second and third quarters. Model underprediction was less severe for TNMOC/CO and TNMOC/NOx ratios, which were more comparable to observed values.

Attachment 6

CMAQ VERTICAL PROFILES

Base-Year Vertical Profiles

Vertical profiles are presented for several species including NO, NO2, HNO3, O3, and select VOCs. The profiles represent Basin averages for the month of July (i.e., all hours in July and all grid cells within the Basin were averaged) and extend from ground-level up to the highest modeling layer at approximately 16 km. Vertical cross-sections up to approximately 1 km are also presented.

July was chosen as it exhibited a combination of moderate and high ozone events. In the profiles, the tropopause is denoted by a dashed line and assumes a height of 11 km. The lack of vertically resolved measurements for these species precludes a comprehensive model performance evaluation. However, the profiles are consistent with a qualitative understanding of the atmosphere. For example, NOx emissions primarily occur at ground-level where the highest concentrations are expected, yet NOx also exists in higher concentrations in the stratosphere due to photolysis of N2O and commercial aircraft emissions. VOCs, which are also emitted at ground-level, are reactive species and therefore are unable to survive long enough to be transported to the stratosphere. Thus, their concentrations taper off rapidly. The profiles are consistent with these trends, demonstrating that CMAQ performs as expected.

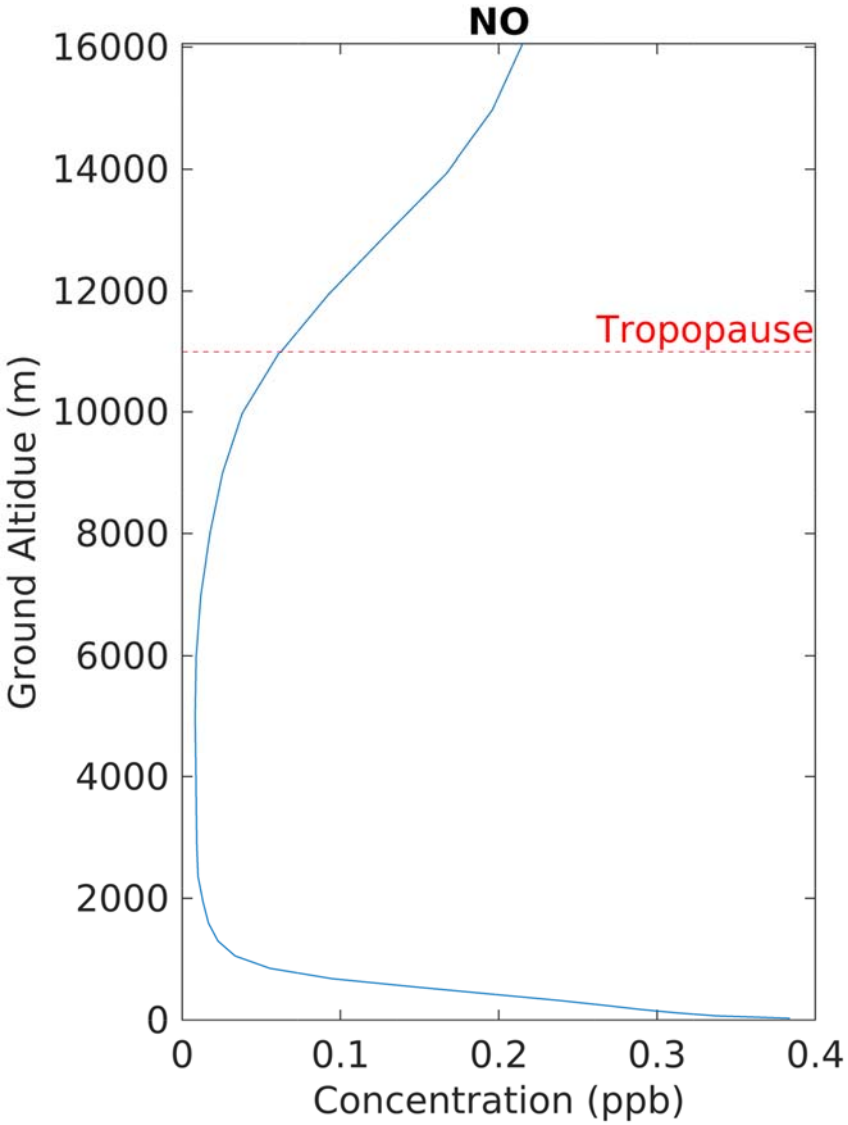

Figure 1: Vertical profile of NO averaged over the Basin during July 2018

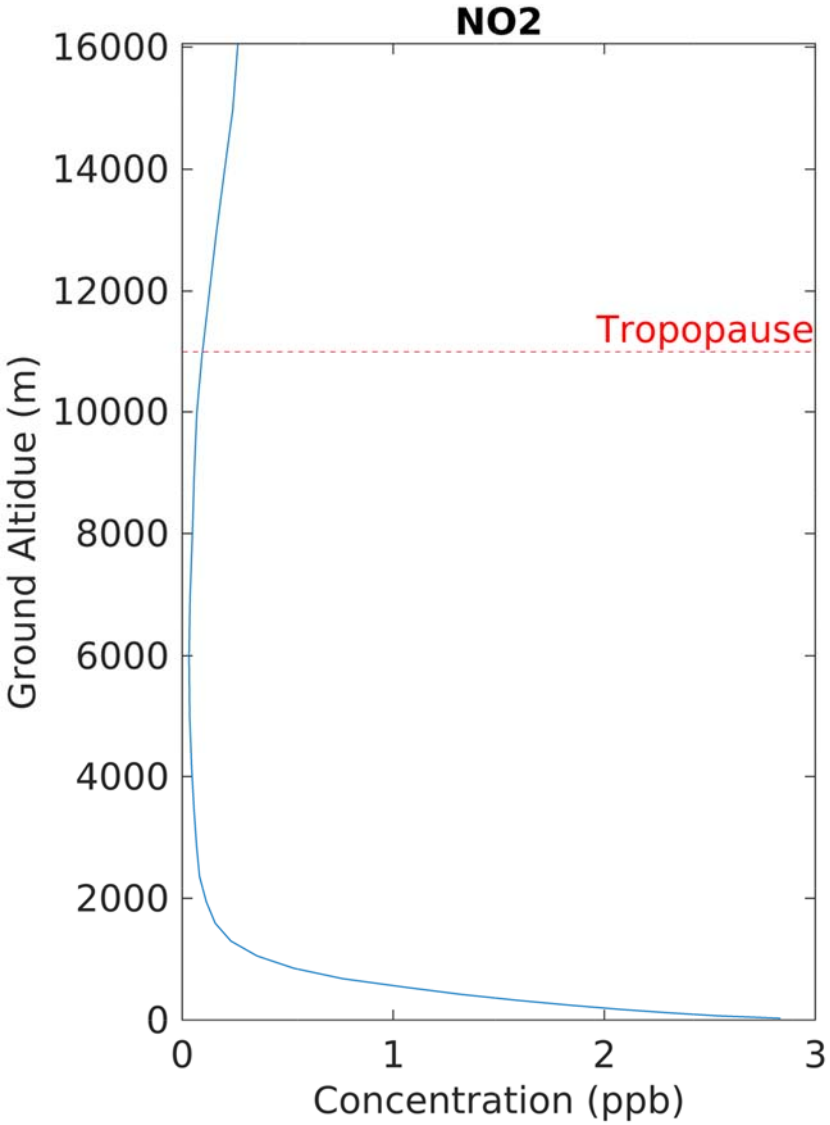

Figure 2: Vertical profile of NO2 averaged over the Basin during July 2018

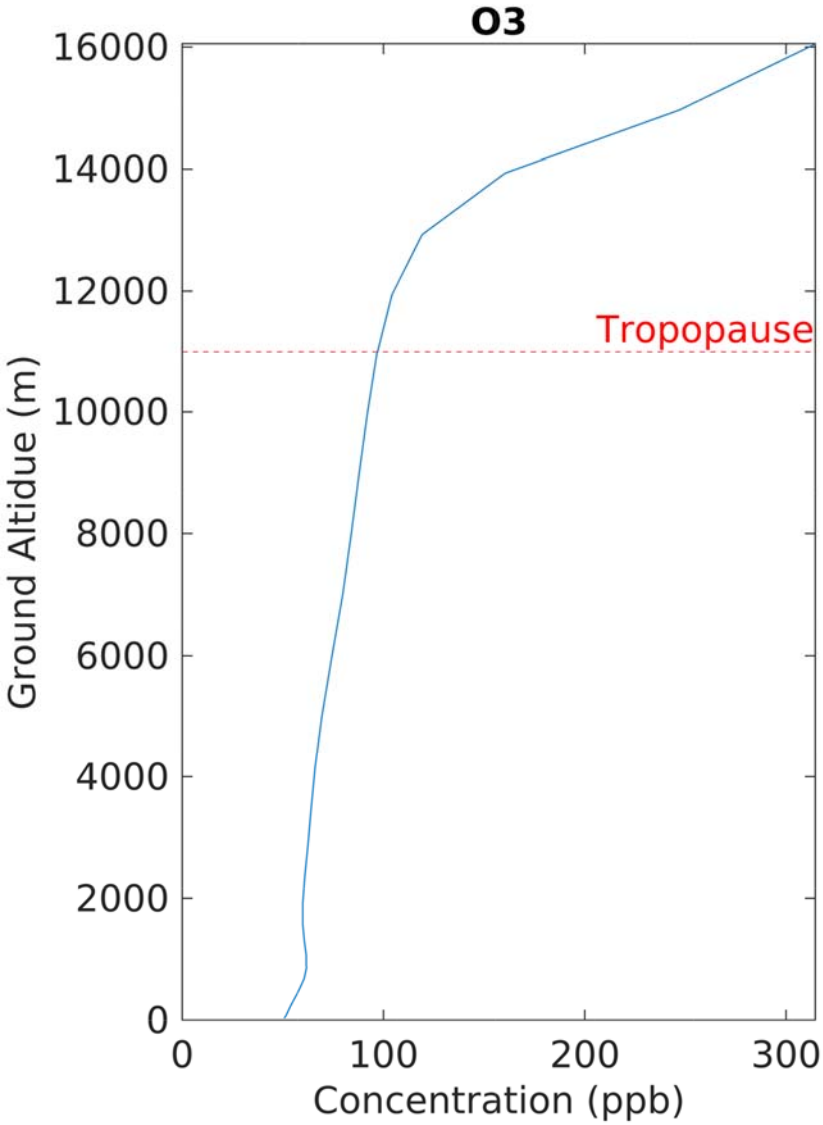

Figure 3: Vertical profile of O3 averaged over the Basin during July 2018

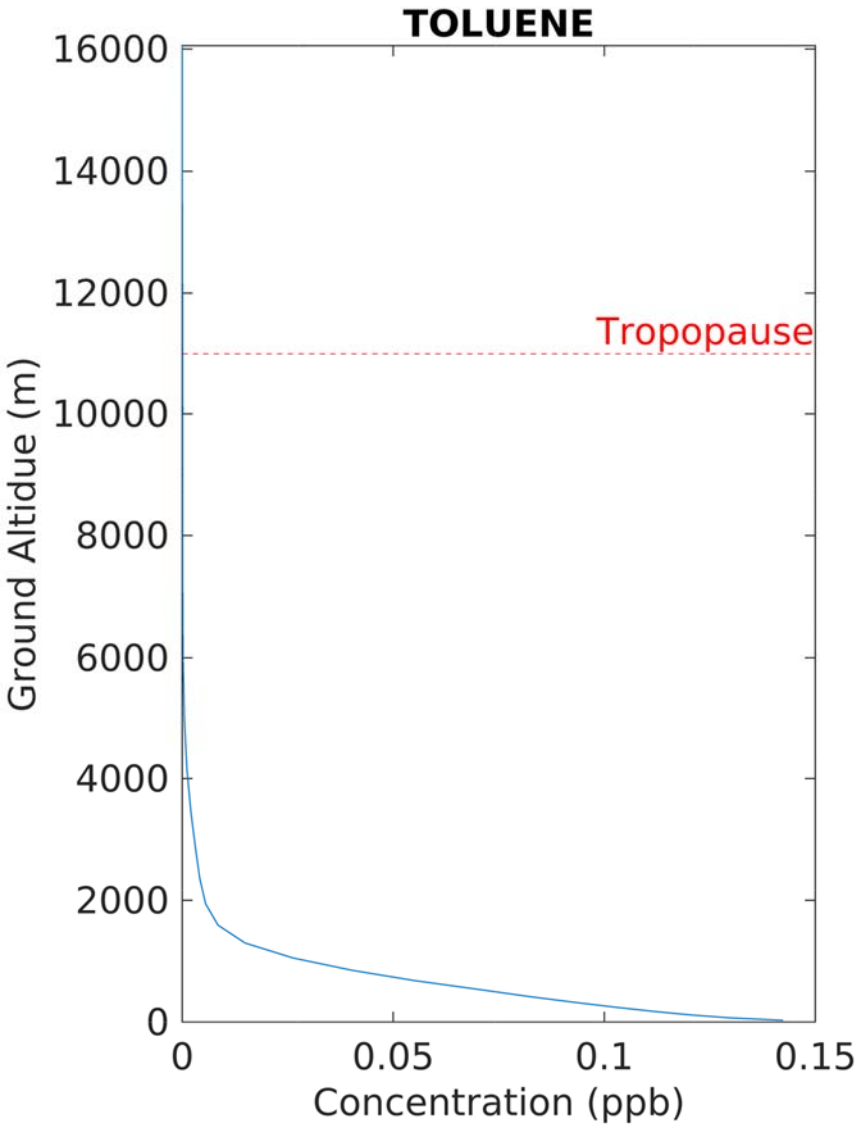

Figure 4: Vertical profile of toluene averaged over the Basin during July 2018

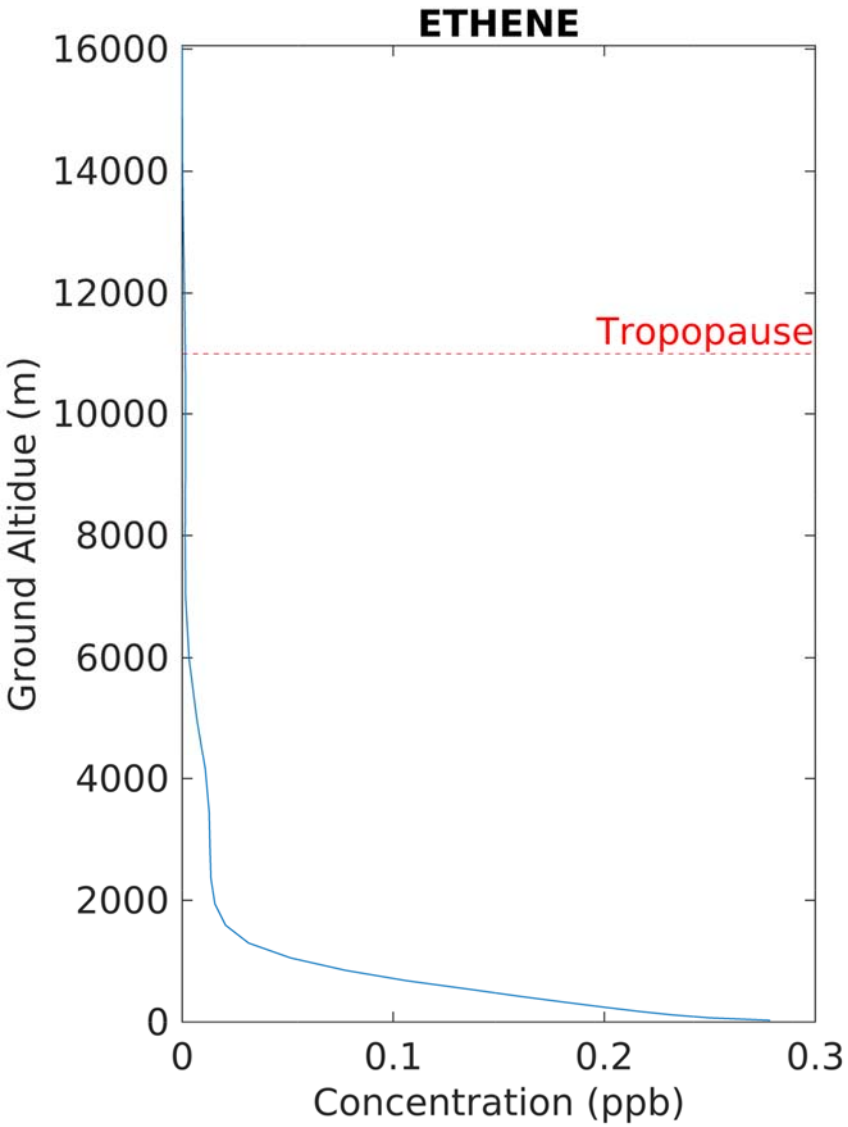

Figure 5: Vertical profile of ethene averaged over the Basin during July 2018

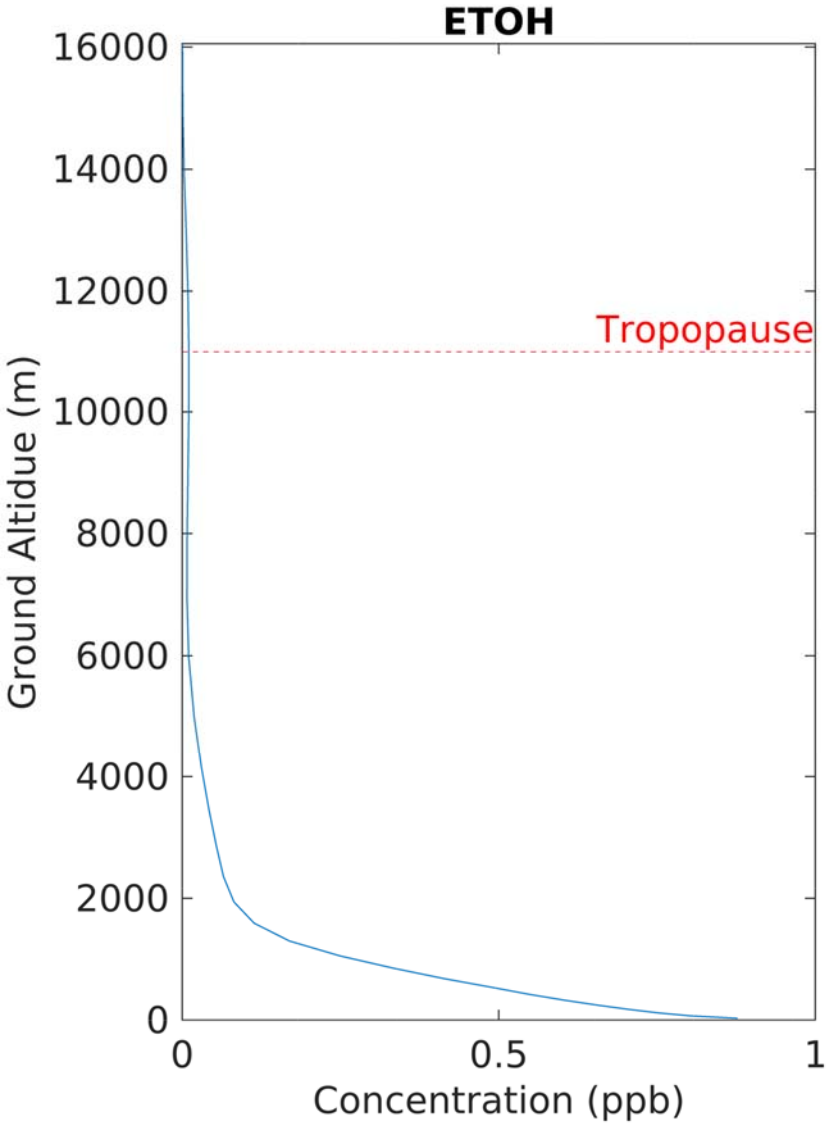

Figure 6: Vertical profile of ethanol averaged over the Basin during July 2018

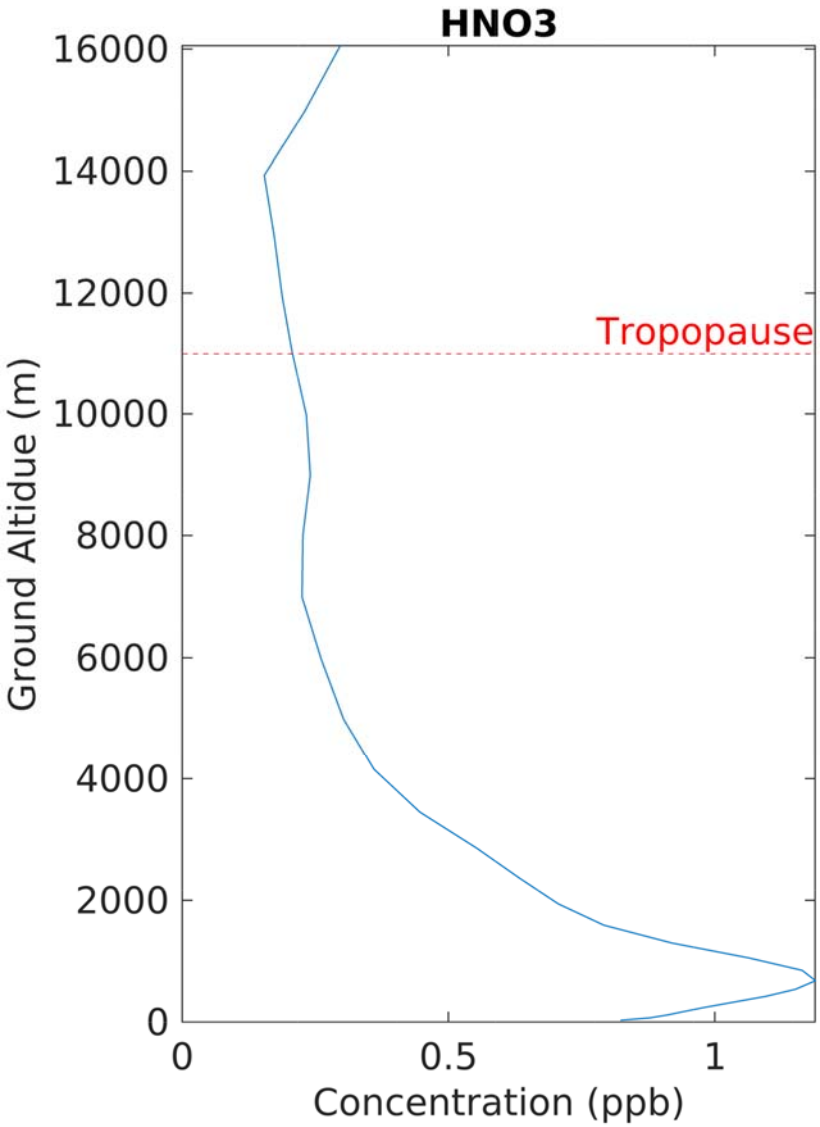

Figure 7: Vertical profile of HNO3 averaged over the Basin during July 2018

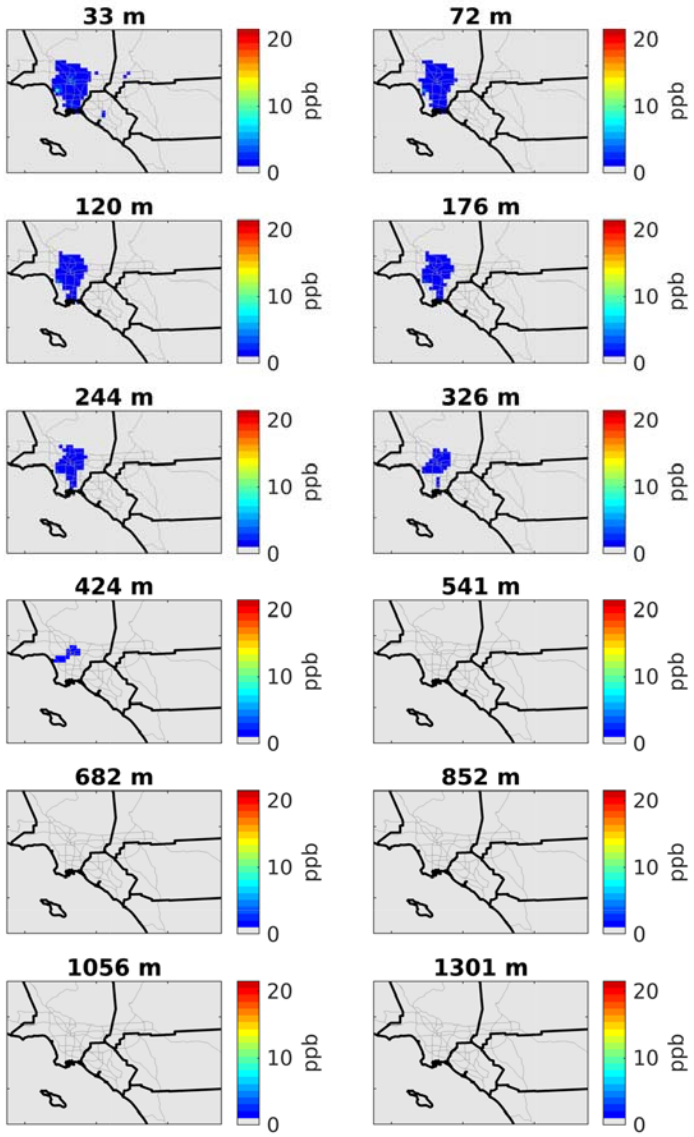

Figure 8: Vertical cross-sections of NO during July 2018. Heights correspond to the top of each layer.

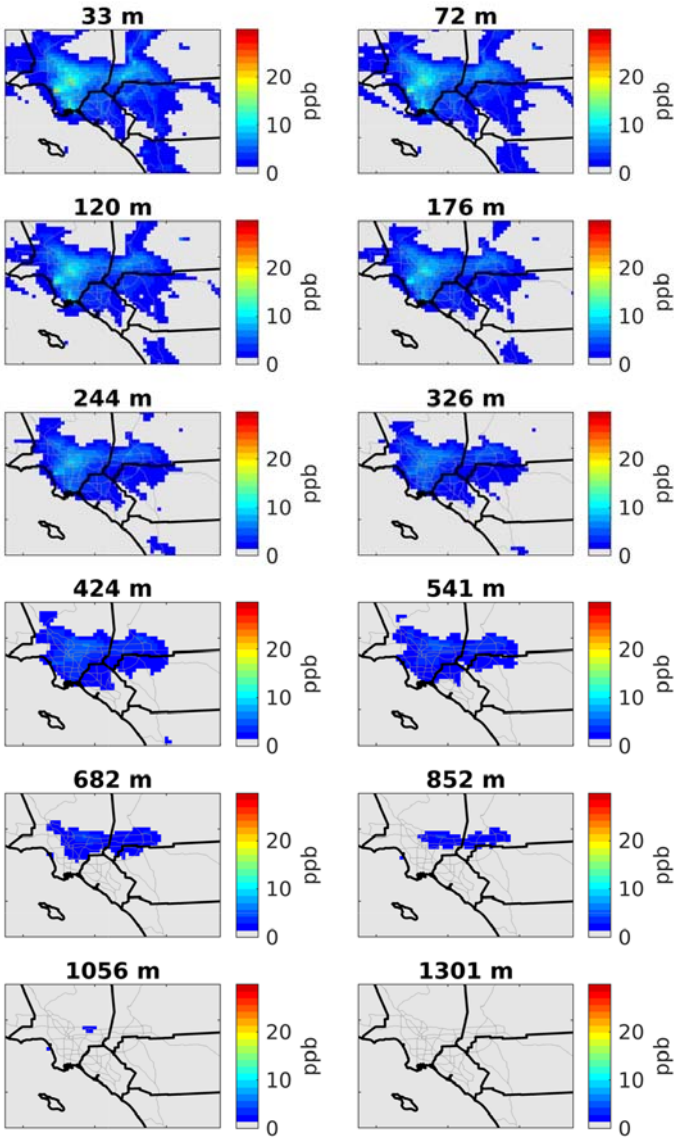

Figure 9: Vertical cross-sections of NO2 during July 2018. Heights correspond to the top of each layer.

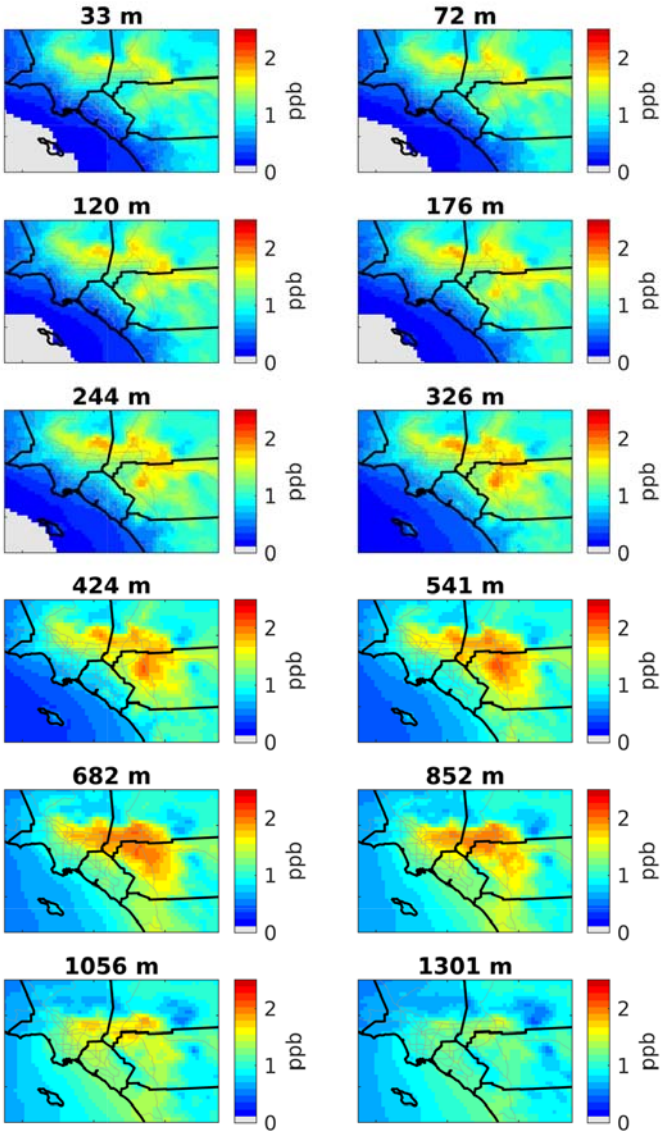

Figure 10: Vertical cross-sections of HNO3 during July 2018. Heights correspond to the top of each layer.

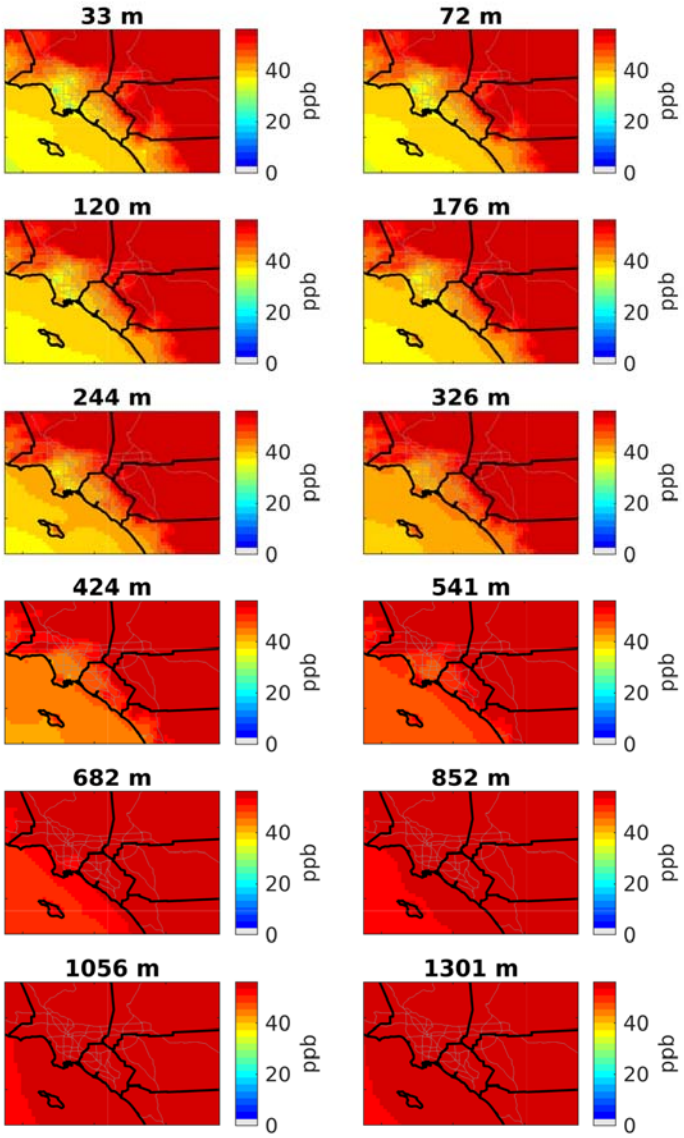

Figure 11: Vertical cross-sections of O3 during July 2018. Heights correspond to the top of each layer.

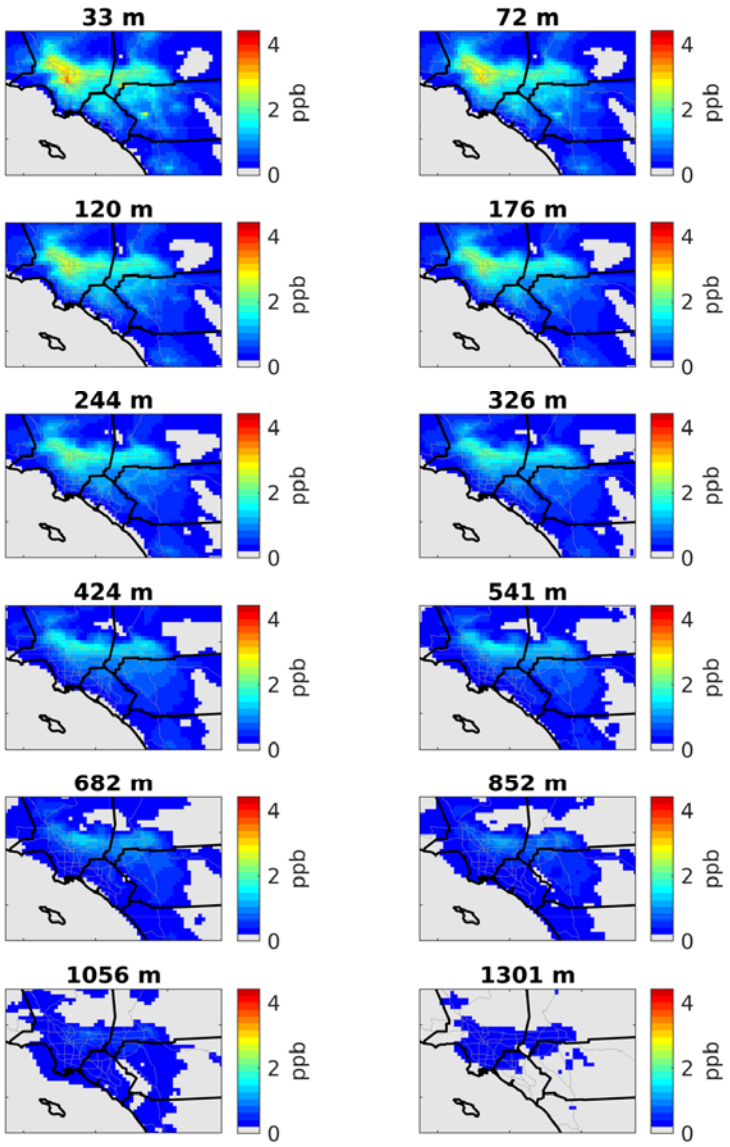

Figure 12: Vertical cross-sections of ethanol during July 2018. Heights correspond to the top of each layer.

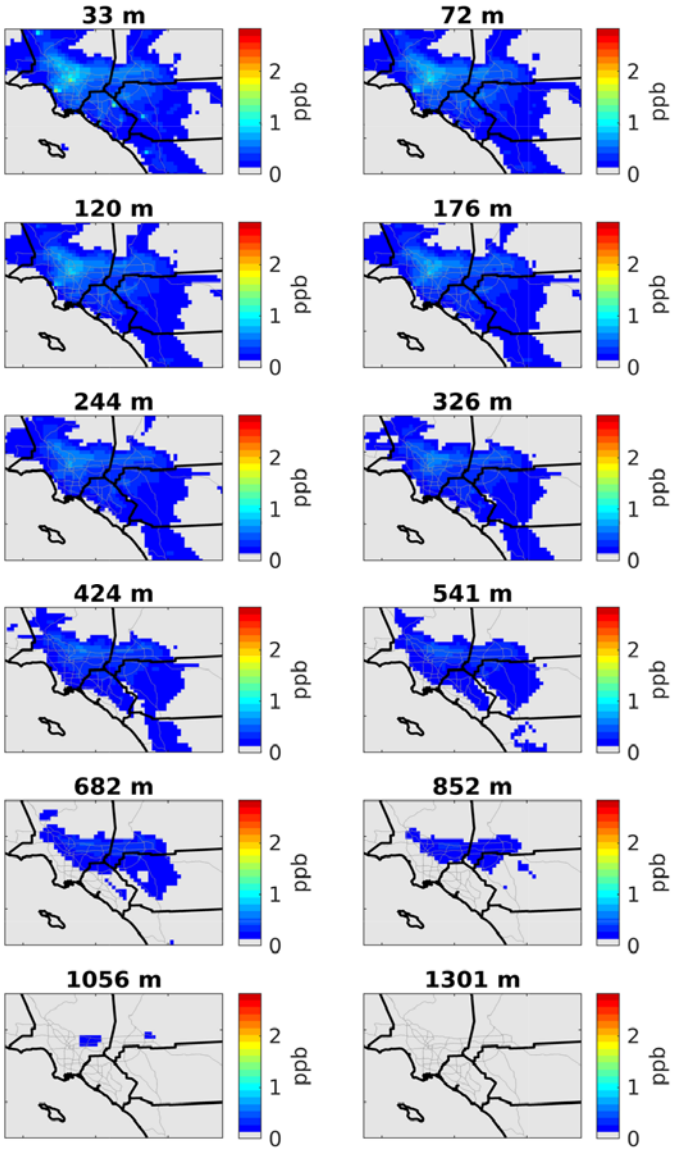

Figure 13: Vertical cross-sections of ethene during July 2018. Heights correspond to the top of each layer.

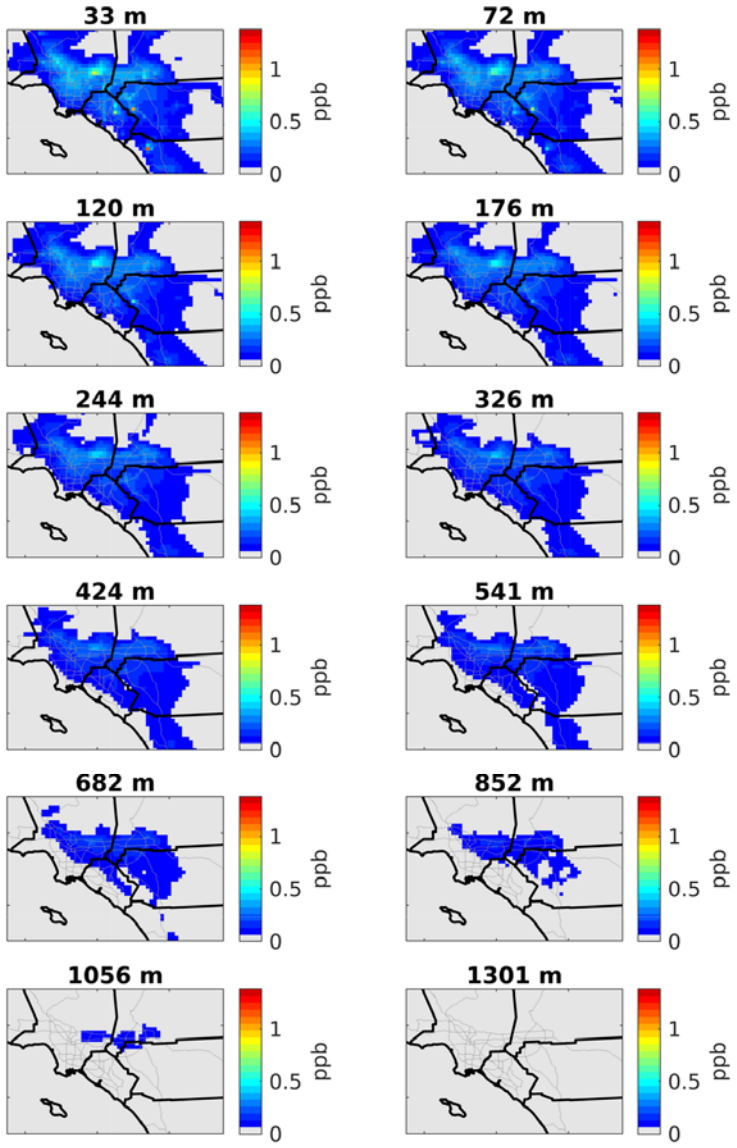

Figure 14: Vertical cross-sections of toluene during July 2018. Heights correspond to the top of each layer.